

Interaction of activation-repolarization coupling and restitution properties in two models of human ventricular tissue

Mahshid Bozorgizadeh

Supervisor: Dr R.H. Clayton

**Submitted in partial fulfilment of the requirements
for the degree of philosophy at
The University of Sheffield
Department of computer science**

December 2013

Acknowledgement

I would like to express my sincere acknowledgment to my supervisor Dr R.H. Clayton for providing programmes written in C, support, and valuable feedback. I am thankful to the University of Sheffield that awarded an EPSRC Doctoral Training Grant to undertake this research in the Department of Computer Science. I would like to say special thank you to Dr Michael K Griffith for his informative technical support. I am also very grateful to Drs. Patrick A. Helm and Raimond L. Winslow at the Centre for Cardiovascular Bioinformatics and Modelling, Johns Hopkins University, and Dr. Elliot McVeigh at the National Institute of Health for provision of the DT-MRI data used in this study.

This thesis is dedicated to my dear young cousin Miss Pariya who lost her life due to cardiovascular disease and has inspired me to continue researching on the heart.

Abstract

Dispersion of repolarization time (or recovery time) is known to be pro-arrhythmic, but not much is known about the rate-dependency of dispersion in repolarization time.

The aim of this thesis was to investigate how heterogeneity in structure and function influence the dispersion of repolarization time following normal and premature beats in simulated human left ventricular tissue. The modelling tools were (1) geometrical models of tissue and fibre; (2) two cell models including a simple and a biophysically detailed human ventricular cell models; and (3) a monodomain model of ventricular tissue. During decreasing stimulus (S1S2) intervals, dispersion in repolarization time remained constant for normal beats while changed greatly for premature beats.

In 2D tissue with structural discontinuities and no fibre orientation, the structural discontinuity was found to produce increased dispersion of repolarization, and slowing of propagation in the region between two structural discontinuities.

In 3D tissue with functional heterogeneity (including a linear or a non-linear change in fibre orientation), the dispersion of repolarization time produced at different S1S2 intervals depended on the differences in local restitution. Thus longer S1S2 intervals could produce greater dispersion of repolarization time than shorter S1S2 intervals. Speed of depolarization conduction was also depended on the differences in local restitution. Therefore, combination of anisotropy and fibrosis could suppress the speed of depolarization conduction for premature beats in the mid-myocardial region of heterogeneous tissues composed of three ventricular cell types. The results suggest that 3D cubes of anisotropic fibrosis heterogeneous tissue may promote tissue vulnerably to ventricular arrhythmia.

In an anatomically detailed left ventricular wedge with functional heterogeneity, long and short S1S2 intervals could produce greater dispersion of repolarization time than 3D cubes of tissues.

These simulations have implications for our understanding of arrhythmias in the whole heart. Restitution profiles of repolarization time and profiles of dispersion in repolarization time (not action potential duration) may be used for estimating abnormal changes in repolarization time of premature beats and arrhythmia risk.

Abbreviations

AP: action potential

APD: action potential duration

S1: sixth normal stimulus beat

S2: premature stimulate beat

S1S2: stimulus intervals between AP upstroke of sixth normal beats and AP upstroke of premature beats

aniso: anisotropic conduction

D: dimensional (i.e. 2D slabs, and 3D cubes)

Epi: epicardial cells in the epicardial region of left ventricular tissue

M: mid-myocardial cells in the middle region of left ventricular tissue

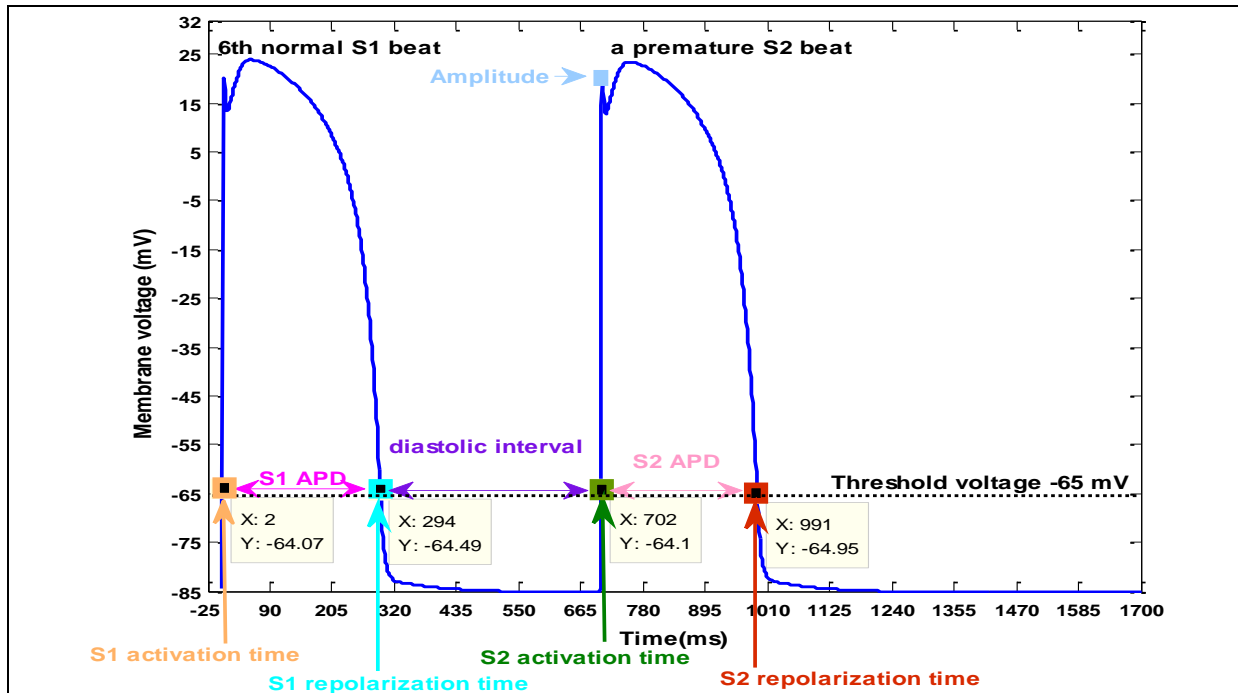
Endo: endocardial cells in the endocardial region of left ventricular tissue

FK4V model: the simple 4-variable phenomenological cell model

TP06 model: the biological detailed cell model with 21 variables

Definitions

The simulation results in this thesis are based on seven timings that were calculated at each S1S2 interval, and then were used to calculate other desired data (i.e. three measures of dispersion in activation time, repolarization time, and APD). For clarity, Figure below is provided as a reference figure that shows seven timings at S1S2 interval of 700 ms.



One: activation time that corresponds to indices of AP upstroke above the threshold voltage for normal S1 beat (highlighted in orange as **S1 activation time**);

Two: repolarization time that corresponds to indices of AP downstroke above the threshold voltage for normal S1 beat (highlighted in cyan as **S1 repolarization time**);

Three: APD as the difference between activation time and repolarization time for normal S1 beat (highlighted in magenta as **S1 APD**);

Four: activation time that corresponds to indices of AP upstroke above the threshold voltage for premature S2 beats (highlighted in green as **S2 activation time**);

Five: repolarization time that corresponds to indices of AP downstroke above the threshold voltage for premature S2 beats (highlighted in red as **S2 repolarization time**);

Six: APD for premature S2 beats (highlighted in pink as **S2 APD**);

Seven: diastolic interval as the difference between activation time of the premature S2 beat and repolarization time of the normal S1 beat (highlighted in violet).

Note 1: Amplitude of AP upstroke for premature S2 beats corresponds to the largest membrane voltage during AP depolarization.

Note 2: Normal S1 beats are referred to the sixth normal S1 beats followed by a premature S2 beat.

Note 3: Each S1S2 interval corresponds to the difference between indices of AP upstroke of premature S2 beats (S2 activation time) and normal S1 beats (S1 activation time).

Three measures of dispersion in activation time, repolarization time, and APD:

- Dispersion in activation time was the difference between the maximum and the minimum activation time at each S1S2 interval, for normal S1 and premature S2 beats.
- Dispersion in repolarization time was the difference between the maximum and the minimum repolarization time at each S1S2 interval, for normal S1 and premature S2 beats.
- Dispersion in APD was the difference between the maximum and the minimum APD at each S1S2 interval, for normal S1 and premature S2 beats.

These values were used to calculate:

- The largest dispersion in repolarization time: the largest value of measures of dispersion in repolarization time among all S1S2 intervals for premature S2 beats.
- The smallest dispersion in repolarization time: the smallest value of measures of dispersion in repolarization time among all S1S2 intervals for premature S2 beats.
- The largest and the smallest dispersion in activation time and APD were calculated similarly.

Regarding Figures, it is important to note that:

- all spatial profiles of data are referred to plots of data against transmural distance and restitution profiles of data are referred to plots of data against diastolic interval;
- all x-axis in spatial profiles corresponds to the percentage of transmural distance;
- the plots that compare profiles of two groups of tissue, the curves with similar colour but different markers usually correspond to the same S1S2 interval that was not written in the legend for the second group of tissue to avoid lengthening of legend;
- the last S1S2 interval corresponds to the shortest S1S2 interval that AP can propagate through tissue models;
- the rest of Figures were provided in the enclosed CD, Appendices 1 to 5.

Table of contents

Chapter 1	1
General thesis introduction	1
1.1 Introduction	1
1.2 Summary of chapters	5
1.3 References	7
Chapter 2	9
From biological system to computational models	9
2.1 Introduction	10
Part I: The heart	11
2.2 The heart membrane and myocardium	11
2.3 Coronary arteries	12
2.4 The cardiac cycle	12
2.4.1 Physiological sequence of ventricular function in a cardiac cycle	13
2.4.2 Sequential motion during ventricular filling and emptying	15
2.5 From cellular excitation to cardiac contraction	16
2.5.1 Cardiac conduction system	16
2.5.2 Cell membrane at rest	17
2.5.3 How an action potential arises in ventricular cells	17
2.5.4 Ventricular action potential phases	18
2.5.5 The absolute, effective, and relative refractory period	19
2.5.6 Action potential in different regions of the heart	19
2.5.7 Cardiac excitation-contraction coupling	20
2.6 Electrical disturbances in the human ventricles	21
Part II: Modelling the heart at cell and tissue level	22
2.7 Experimental and simulation studies	22
2.7.1 Limitation in experimental studies	22
2.7.2 Why computational modelling	24
2.8 A history of cardiac models	25
2.8.1 The historical background of the TP06 model	27
2.8.2 The historical background of the FK4V model	27
2.8.3 Bidomain and monodomain tissue models	27
2.9 Modelling of restitution and dispersion in repolarization time	30
2.9.1 Restitution	30
2.9.2 Dispersion in activation time and repolarization time	32
2.10 Challenging issues in modelling cardiac tissue	32
2.10.1 Tissue structure	32
2.10.2 Linear or non-linear change in fibre orientation	34
2.10.3 Mid-myocardial cells	35
2.10.4 Sharp or gradual increase in spatial APD profiles	36
2.11 Summary	36
2.12 References	36
Chapter 3	42
Aims, approaches, and modelling tools	42
3.1 Introduction	42
3.2 Activation and repolarization time and re-entry	42
3.2.1 Increase or decrease in dispersion of repolarization time	42
3.2.2 Reversal direction of ventricular activation	43
3.3 Restitution and re-entry	44
3.3.1 Homogenous tissues	45
3.3.2 Heterogeneous tissue	46
3.3.3 Transmural and apico-basal gradients	46
3.4 Myocardial structure and tissue geometry	49
3.4.1 Anisotropic and orthotropic conductions	49
3.4.2 Fibre structure	50
3.4.3 Effects of fibrosis	51
3.4.4 Effects of fibre-sheet structure	52
3.4.5 Effects of boundaries and geometries in homogenous tissue	52
3.5 Excitation, repolarization, and APD	54
3.6 Novelty of this research	54
3.7 Modelling tools in programs written in C	55
3.7.1 Why geometrical models	55

3.7.1-1 Tissue with 2D geometries	56
3.7.1-2 Tissue with 3D geometries	57
3.7.1-3 Left ventricular wedge model	60
3.7.1-4 Direction of conduction in tissues	61
3.7.2 Geometrical models of fibre structure	62
3.7.2-1 A linear change in fibre orientation in 3D cubes	62
3.7.2-2 A non-linear change in fibre orientation in 3D cubes	63
3.7.3 Cell models	64
3.7.3-1 A simple cell model	64
3.7.3-2 A detailed cell model	66
3.7.4 The monodomain tissue model	67
3.7.5 Numerical methods	71
3.8 Calculations in MATLAB	72
3.9 Testing stability of the numerical simulations	74
3.10 Summary	75
3.11 References	76
Chapter 4	82
Simulation results in 2D tissues	82
4.1 Introduction	82
4.2 Spatiotemporal profiles of normal and premature beats	83
4.2.1 Spatial APD profiles in five geometries	83
4.2.2 Rate dependent effects	85
4.2.3 Premature beats influence repolarization profiles	86
4.2.4 Profiles for premature beats at one S1S2 interval	88
4.2.5 Profiles for premature beats for long and short S1S2 intervals	91
4.2.5-1 Spatial profiles for premature beats	91
4.2.5-2 A new look to profiles of repolarization time	95
4.2.5-3 Restitution profiles for premature beats	97
4.2.6 Qualitative comparison with experimental studies	102
4.3 Three measures of dispersion for normal and premature beats	103
4.3.1 Profiles of measures of dispersion for premature beats	104
4.3.2 The largest and the smallest measures of dispersion	106
4.3.4 Quantitative comparison of measures of dispersion for normal and premature beats	107
4.4 Speed of depolarization conduction	109
4.4.1 Comparison among four regions of H-shape tissue	110
4.4.2 Comparison between slim tissue and slim region	113
4.4.3 Summary figures and link with simulation studies	114
4.5 Summary of results	116
4.6 References	116
Chapter 5	117
Simulation results in 3D tissues	117
5.1 Introduction	117
Part I: Simulation results with linear fibre structure	122
5.2 Spatiotemporal profiles of normal and premature beats	122
5.2.1 Spatial APD profiles in the five regions of tissue	122
5.2.2 Rate dependent effects	133
5.2.3 Profiles of premature activation time, repolarization time, and APD	134
5.2.4 Comparison with other studies	146
5.2.4-1 Quantitative comparisons	146
5.2.4-2 Qualitative comparisons	146
5.3 Three measures of transmural dispersion	148
5.3.1 Dispersion in activation time	149
5.3.1-1 Quantitative comparison between normal and premature beats	150
5.3.1-2 Profiles of dispersion in activation time for premature beats	152
5.3.1-3 The largest and the smallest dispersion	153
5.3.2 Dispersion in repolarization time	156
5.3.2-1 Quantitative comparison	156
5.3.2-2 The largest and the smallest dispersions	158
5.3.3 Dispersion in action potential duration	160
5.3.3-1 Normal and premature beats	160
5.3.3-2 The largest and the smallest measures of dispersion	162
5.3.4 Comparison with experimental studies	164
5.3.4-1 Left ventricular epicardium	164

5.3.4-2 Left ventricular epicardium and endocardium	164
5.3.4-3 Left ventricular endocardium	165
5.3.4-4 Relationship among three measures of dispersion in homogenous tissue	165
5.3.4-5 Relationship among three measures of dispersion in heterogeneous tissue	167
5.4 Speed of depolarization conduction	174
5.4.1 Homogenous tissue: 100%Epi, 100%Endo, and 100 %M	175
5.4.2 Heterogeneous tissue: 50% Endo-50%Epi	177
5.4.3 Heterogeneous tissue: 15% Endo-55%M-30%Epi	180
5.4.4 Heterogeneous tissue: 10% Endo-30%M-60%Epi	181
5.4.5 Heterogeneous tissue: 60% Endo-30%M-10%Epi	184
5.4.6 Summary of the speed of depolarization conduction	186
5.4.7 Comparison with previous studies	186
5.5 Vulnerability to ventricular arrhythmia	187
5.5.1 When	187
5.5.2 Which S1S2 intervals	200
5.5.3 Vulnerable regions fore wave break	201
5.5.4 Which spatial profiles	205
5.5.5 Restitution profiles of activation time	206
5.6 Summary of results in Part of this chapter	209
Part II: Supplementary simulations	210
5.7 Effects of changing proportion of cells & conductivity on spatial APD profiles	210
5.8 Effects of non-linear fibre orientation on spatial APD profiles	214
5.8.1 Tissue composed of 60% Endo-30%M-10%Epi	214
5.8.2 Summary figures	217
5.8.3 Four heterogeneous tissues	220
5.8.4 Numerical stability	229
5.8.5 Importance of fibre structure	229
5.9 Visualization of AP propagation	229
5.10 Summary of results	239
5.11 References	239
Chapter 6	242
Simulation results in the left ventricular wedge model	242
6.1 Introduction	242
6.2 Spatiotemporal profiles of normal and premature beats	243
6.2.1 Rate dependent effects	244
6.2.2 Profiles of premature activation time, repolarization time, and APD	244
6.2.2-1 Left ventricular wedge composed of homogeneous tissue	246
6.2.2-2 Left ventricular wedge composed of heterogeneous tissue	249
6.2.3 Qualitative comparison with experimental studies	252
6.3 Three measures of dispersion	253
6.3.1 Profiles of three measures of dispersion	254
6.3.2 Vulnerable regions for wave break	256
6.3.3 The smallest and the largest measures of dispersion and link to previous studies	257
6.4 Speed of depolarization conduction	258
6.5 Visualization of AP propagation	261
6.6 Summary of results	266
6.7 References	266
Chapter 7	267
Discussion, future studies, and conclusions	267
7.1 Introduction	267
7.2 Some research questions and answers	267
7.3 Limitation and future studies	275
7.3.1 Fibre-sheet structure and orthotropic conductivities	276
7.3.2 Fibroblast	277
7.3.3 Mechanics	277
7.3.4 Speed of depolarization conduction and speed of repolarization conduction	278
7.4 Conclusions	280
7.5 References	280

Chapter 1

General thesis introduction

1.1 Introduction

Understanding the sequence of ventricular repolarization is important, because any abnormality in repolarization and dispersion in repolarization may lead to arrhythmia [1, 2]. Cardiac arrhythmia is an irregularity of heartbeat which causes the heart to miss a beat, beat irregularly, or beat at the wrong speed [3] and is one of the contributors to cardiovascular disease morbidity and mortality in the world [4]. Abnormal dispersion of repolarization supports the initiation and maintenance of life-threatening re-entrant arrhythmias, which has been observed in both animal studies [5-7] and in the human heart [8]. If this finding is established in the human heart, a simple measure of dispersion in repolarization may be used as a clinical diagnostic tool to estimate the vulnerability of the heterogeneous tissue to re-entry (an excitation wave repeatedly propagates along a closed path). Investigating about the mechanism, initiation and maintenance of cardiac arrhythmias caused by re-entry have been the focus of numerous studies. The motivation of this study was to study the association between dispersion in repolarization and tissue heterogeneity in two models of human ventricular tissue to represent normal, scar, and fibrosis tissue.

The heart is a rhythmic electromechanical pump, where electrical activation initiates and synchronizes contraction. Cardiac tissue is where the electrical and mechanical activity occurs and contains cardiac cells with excitability, contractility, conductivity, and automaticity. Cardiac excitation is the result of the interplay between cell membrane dynamic processes and structural properties of the cardiac tissue. The cell membrane stays at a resting potential until it receives an over-threshold stimulus from its neighbouring cells that can depolarize the cell membrane. Then an action potential (AP) is generated and the cell membrane potential changes in separated phases. A typical human ventricular AP have phases including (1) AP depolarization; (2) AP early repolarization; (3) AP plateau; (4) AP final repolarization; and (5) AP rest. The electrical coupling or conduction of AP from one cell to another is provided through gap junctions. Action potential propagates as electrical waves in different regions of the heart with different shape, duration, and speed. Several dynamic processes modulate the timing and sequence of AP depolarization and AP repolarization that can influence dispersion of activation time and repolarization time, which may be important for initiation of ventricular arrhythmia.

First, when electrical activation propagates through tissue, action potential duration (APD) decreases progressively in tissue [9], animal and human hearts [8, 10-12] but activation time increases. The inverse relationship between APD and activation time may modulate the dispersion of repolarization under particular conditions, i.e. in patients with undergoing coronary artery bypass grafting (with upright T-wave) while dispersion in repolarization time increased in patients with aortic valve replacement (with T-inversion) [13]. The question is whether reducing dispersion in repolarization time is considered as a protective mechanism and can provide an intrinsic anti-arrhythmic property of ventricular tissue? In addition, reversing the direction of activation reduced ventricular heterogeneity of repolarization in

dilated cardiomyopathy patients [14] while increased the dispersion in transmural repolarization in human heart failure [15, 16]. So, why transmural heterogeneity of repolarization is amplified as a consequence of reversal of the normal activation sequence in some patients but not in other patients?

Second, APD restitution and conduction velocity restitution are also two important dynamic processes [17, 18] that may modulate the activation time and repolarization time as seen in simulation studies [18-21] and animal models [22-24]. Electrical restitution is often defined as a dynamic or rate dependent adaptation of cardiac electrophysiology associated with the ability of a cardiac cell to recover after excitation. During premature activation when the diastolic interval of a premature beat varies, both APD and conduction velocity for a premature beat change, i.e. AP conduction became slow for short diastolic intervals. It is generally believed that APD and conduction velocity restitutions are two important determinants for the stability of re-entrant arrhythmias [18, 19, 25-27]. The question is whether measures of APD and dispersion in APD are accurate enough or can be used to represent changes in ventricular AP repolarization for premature beats particularly for short stimulus intervals or not? In addition, does large dispersion in AP repolarization facilitate the development of the conduction delay?

Third, the electrical restitution curves are heterogeneous in shape and distribution [28, 29]. Heterogeneity in AP shape and duration in the ventricular wall may provide a substrate for arrhythmias. Specific shape of APD and conduction velocity restitution curves and steepness of APD restitution curves may be important for the mechanism underlying the breakup of excitation wave in a model of cardiac electrical activity [30]. A human study in two dimensional (2D) atrial myocytes [31] showed that abrupt changes in tissue geometry could affect premature spatial APD profiles. There are also evidences [32, 33] that the cell-tissue architecture can influence the direction and shape of electrical waves. The question is how cellular configurations in ventricular tissue with anisotropic (orthotropic) properties and fibre structure can influence the spatial and restitution profiles of activation time and repolarization time as well as measures of dispersion in activation time and repolarization time in tissue with and without structural discontinuities.

Fourth, increase in fibrosis formations after myocardial infarction are strongly correlated with an increase incidence of ventricular tachycardia (heart rhythm goes beyond the normal range of 120 to 200 beats per minute [3]) and sudden cardiac death [34]. In myocardial infarction, well-coupled, excitable, and contractile cardiac tissue may be replaced by poorly coupled, non-excitable, non-contractile scar tissue [35]. Myocardial scarring is fibrous tissue that can disrupt the cardiac electrical conduction system. Simulated fibrosis in 2D, 3D tissue and 3D voxel description of the human ventricular anatomy using a biophysically detail human ventricular cell model [36] showed that diffuse fibrosis can slow wave propagation and increase tissue susceptibility to wave break and spiral wave formation [37]. Engelman et al. [38] based on a modified Luo-Rudy I [39] model in isotropic conduction suggested that the structural heterogeneity caused by non-uniform discontinuities of resembling patchy fibrosis in the structural heart disease may be sufficient to increase tissue vulnerability to arrhythmia. The question is how fibrosis tissue may affect measures of dispersion in repolarization time in human tissue with fibre structure for long and short stimulus intervals?

Despite huge number of experimental and simulation studies, it is still not clear how activation-repolarization coupling and restitutions interact during premature activation in the human hearts and how this influences the spatiotemporal pattern of AP depolarization and AP repolarization. The aims of this study were to study the interaction of ventricular

activation-repolarization coupling, restitution properties, and fibre structure by characterizing four ideas that are believed that play an important role in initiation of re-entry including the regional differences in:

- (1) spatial and restitution profiles of activation time, repolarization time, and APD;
- (2) three measures of dispersion in activation time, repolarization time, and APD;
- (3) restitution profiles of speed of depolarization conduction;
- (4) AP propagation during depolarization time and repolarization time.

The novelty of the thesis was to study these four ideas (1) for long and short stimulus intervals; (2) for both normal stimulus (S1) and premature S2 beats; (3) for 2D isotropic tissues with and without structural discontinuities; (4) for 3D cubes of anisotropic homogenous and heterogeneous tissues with and without fibrosis, simulated with a linear and a non-linear change in fibre orientation, and with epicardial and endocardial pacing; (5) for an anatomically detailed the left ventricular wedge model composed of anisotropic homogenous and heterogeneous tissues; and (6) with two newly developed human ventricular cell models. Whereas, the previous simulation studies were often limited to animal models (i.e. Clayton and Holden [40] described in section 3.3.3), epicardial or endocardial region of the ventricles (i.e. Cates and Pollard [41] explained in Chapter 3, section 3.4.2), one type of heterogeneity (i.e. Engelman et al. [38] described in Chapter 3, section 3.4.3), homogenous tissues (i.e. Cherry and Fenton [31] described in section 3.4.5), or studied one or two of these issues (i.e. Colli Franzone et al. [42] explained in Chapter 3, section 3.5). Investigating these issues in the same study with two different models could increase current understanding about dynamics of depolarization and repolarization in the small scale of the heart (i.e. in 2D slices of tissue, 3D cubes of tissue, and the left ventricular wedge models).

Over three centuries ago, experimental studies were only way to study cardiovascular disease. After the discovery of bioelectricity in 1700s, the first mathematical model of cardiac AP was developed in 1962 [43] and then many cell models have been introduced from a low to a high degree of electrophysiological detail. Mathematical models of the cell membrane may be categorized in two groups: (1) one with a detailed description of ionic channels, pumps, and exchangers; and (2) the other with a simplified description of some macroscopic approximation of the average channel behaviour. In both groups, the gating processes of ionic channels, membrane potential, and other physical quantities are described by two or more than two variables. In addition, both groups represent dynamics that depend on parameters obtained from the latest available experimental animal and human data. The main differences between a simple cell model and a detailed cell model are:

- in a simple cell model, phenomenological currents quantitatively create restitution and do not show measured currents, and there is no relationship between model parameters and the cellular physiological mechanism while a detailed cell model is able to explain the ionic mechanism of cardiac AP;
- a simple cell model compared to a detailed cell model is computationally efficient particularly when it is used for studying a left ventricular wedge model.

An important advantage of mathematical models compared to experimental studies is that there are no practical and ethical restrictions. However, it was shown that there are differences in the behaviour of re-entry among the most human cell models [44].

This thesis used the monodomain tissue model [45] and two human cell models developed by:

- (1) Fenton-Karma with four variables [44] that is called the FK4V model as an example of a simple cell model;
- (2) ten-Tusscher and Panfilov with 21 variables [36] that is called the TP06 model as an example of a biologically detailed cell model with approximately realistic formulations of calcium dynamics.

The reasons for using these two models in this thesis were that these models were able to reproduce the shape of AP of epicardial, mid-myocardial, and endocardial human ventricular cells and their key dynamical properties i.e. APD restitution and conduction velocity restitution which play an important role in arrhythmogenesis and maintenance.

Electrophysiological studies, when coupled with mathematical and geometrical models provide useful information for appropriate diagnosis and interpretation of cardiac abnormalities including conduction disturbances. The cardiac structure affects orthotropic electrical and mechanical properties of cardiac muscle. Thus, using geometrical models close to real tissue structure and fibre orientation is necessary to study dynamics of AP depolarization and repolarization in both normal and diseased heart. This thesis focused on simplified geometrical models rather than a complex description of the ventricular tissue because (1) anatomical models of the heart require detailed information about geometry and structure that is still difficult to obtain; (2) obtaining an accurate solution of boundary conditions [46] on the voltage is still challenging in asymmetric geometries; and (3) the current knowledge about the interaction of activation-repolarization coupling and restitution properties in 2D, 3D, and left ventricular wedge models is not sufficient and it is required to be studied first to gain an insight into complex whole heart geometry. However, increasing levels of complexity was imposed gradually in:

- geometrical tissue models as 2D slabs of tissue geometries with and without structural discontinuities in the absence of fibre structure;
- geometrical tissue models as 3D cubes of tissue with seven cellular configurations with and without fibrosis, and geometrical fibre models based on a linear and a non-linear change in fibre orientation;
- the left ventricular wedge model including tissue and fibre geometries obtained experimentally from [47].

In this thesis, computational implementations were performed in three stages to:

First, create transmembrane voltage in tissues using programmes written in C;

Second, extract voltage from the central region of tissue to calculate seven timings including six timings for normal S1 and premature S2 beats (activation time, repolarization time, APD), and one timing of diastolic interval for premature beats, as well as three measures of dispersion in activation time, repolarization time, and APD for both normal and premature beats, and speed of depolarization conduction for premature beats during decreasing S1S2 intervals using programmes written in MATLAB;

Third, visualize data in MATLAB as images or frames.

All simulation results showed that (1) rate dependency of premature beats compared to normal beats can influence shape, duration, and speed of AP propagation as well as

dispersion in activation time, repolarization time, and APD during decreasing stimulus intervals; (2) APD and repolarization time only decrease with increasing distance for long S1S2 intervals but APD and repolarization time change for short S1S2 intervals; and (3) simulations results with both FK4V and TP06 models were qualitatively similar but quantitatively different, however, TP06 model was computationally expensive particularly when it is used for studying the left ventricular wedge models..

In total, it was concluded that dispersion in repolarization time (not APD) could be used clinically for estimating arrhythmia risk if it is addressed from a variety different angles including whether an increase or decrease in dispersion of repolarization time is due to:

- fibre structure with a linear or non-linear change in fibre orientation;
- short or long S1S2 intervals;
- structural discontinuities in tissue geometries or fibrosis;
- cellular configurations with and without mid-myocardial cells;
- anisotropic or orthotropic conduction;
- epicardial or endocardial pacing in transmural direction, or in apico-basal direction.

The results in this thesis emphasized that correct modelling of tissue structure particularly fibre organization with orthotropic conductivities is necessary for studying the changes in ventricular depolarization and repolarization in the normal and diseased human hearts.

1.2 Summary of chapters

Chapter 2 is organized in two parts to provide an association between the heart as a biological system and mathematical models of the heart as a virtual system. Part I describes the structure and function of the normal heart. Then, it is explained how excitable cells are electrically excited to initiate cardiac contraction. Next, electrical disturbances as one consequence of a myocardial infarction are described.

Part II initially highlights the current limitations in experimental and simulation studies and the need for cardiac modelling. Then, a historical review of a simple and a detailed cell models are provided before introducing modelling of restitution and dispersion in repolarization time. Next, challenging issues in modelling cardiac tissue are illustrated including (1) tissue structure based on functional syncytium or laminar structure; (2) linear or non-linear change in fibre organization; (3) presence of mid-myocardial cells; and (4) sharp or gradual transition between epicardial and sub-endocardial regions.

Chapter 3 initially provides a link between the previous results of experimental and simulation studies, and the gaps in knowledge that this thesis is going to fill. Next, it is explained how this thesis addresses these issues by introducing ventricular tissue with different aspects of heterogeneities using the geometrical, cell, and tissue models. Finally, the stability of the numerical schemes in programmes written in C are tested and the speed of depolarization conduction of 2D isotropic slim epicardial, endocardial, and mid-myocardial tissues with both FK4V and TP06 models are compared with other simulations.

Simulation results in 2D geometries, 3D cubes of tissue, and the left ventricular wedge model are provided in Chapter 4, 5, and 6 respectively. These chapters are organised in three to four sections to characterize (1) spatial and restitution profiles of activation time, repolarization time, and APD; (2) profiles of three measures of dispersion in activation time, repolarization time, and APD; (3) restitution profiles of speed of depolarization condition (conduction velocity) during decreasing S1S2 intervals for both normal and premature beats.

The simulation results at the end of each section are evaluated against experimental or other simulation studies. The last section visualizes AP propagation for normal and premature beats at the last S1S2 interval to find out whether wave break during AP depolarization and AP repolarization occurs or not.

Chapter 4 provides simulation results in two groups of 2D tissues with and without structural discontinuities composed of epicardial, mid-myocardial, and endocardial cells. These tissues were simulated with isotropic diffusion and no fibre structure to highlight the effects of scar tissues on (1) spatial and restitution profiles of activation time, repolarization time, and APD; (2) three measures of dispersion in activation time, repolarization time, and APD for normal and premature beats; and (3) restitution profiles of speed of depolarization conduction for premature beats. The results showed that during decreasing S1S2 intervals with both FK4V and TP06 models:

- Structural discontinuities could increase the largest and the smallest value of transmural dispersion in activation time, repolarization time, and APD among all S1S2 intervals around 1 to 7 ms compared to slim tissues without structural discontinuities.
- Structural discontinuities reduced the speed of depolarization conduction slightly in the middle region of H-shape tissues compared to slim tissues.

Chapter 5 is organized in two parts to describe simulation results based on geometrical models of tissue and fibre. Part I provides simulation results in detail for 3D cubes of tissue with a linear change in fibre orientation and sharp transition between regions of different cell types. It was shown that:

- In heterogeneous tissues composed of two or three ventricular cell types, dispersion of repolarization time for premature beats initially decreased for long S1S2 intervals and increased for short S1S2 intervals when (1) repolarization time in the epicardial region became close or greater than the largest repolarization time in the mid-myocardial region with endocardial pacing; and (2) when the largest repolarization time in the mid-myocardial region became close or greater than repolarization time in the endocardial region with epicardial pacing. These changes occurred in the transition regions with sharp APD or repolarization time (i.e. between endocardial and epicardial, endocardial and mid-myocardial, or mid-myocardial and epicardial tissue) where depolarization or repolarization waves may break.
- The combination of anisotropy and fibrosis in heterogeneous tissues could suppress the speed of depolarization conduction in the mid-myocardial region of tissues composed of three ventricular cell types and also in the epicardial region in tissue composed of 60%Endo-30%M-10%Epi during decreasing S1S2 intervals with both models. The reason is possibly due to combination of anisotropy, fibrosis, and the longer APD of mid-myocardial cells.

Part II of this Chapter introduces three approaches for creating gradual APD in the transition regions of heterogenous tissues. These approaches included (1) changing the proportion of different cell types; (2) changing anisotropic diffusion coefficients along and across the fibre axis; and (3) creating geometrical models of fibre based on a non-linear change in fibre orientation. The main result was that some simulated tissues with non-linear change in fibre orientation could reduce significantly the transmural gradient in APD and repolarization time and suppress the dome morphology on spatial APD and repolarization profiles in anisotropic tissues while in the same tissues with fibrosis, these changes were

compensated. In the latter, the speed of depolarization conduction in mid-myocardial region was suppressed similar to anisotropic fibrosis heterogeneous tissues with a linear change in fibre orientation.

Chapter 6 compares simulation results in a left ventricular wedge model and 3D cubes of tissue composed of anisotropic homogenous and heterogeneous tissue during decreasing S1S2 intervals and showed:

- qualitatively similar changes in spatial and restitution profiles of activation time, repolarization time, and APD for premature beats;
- greater measures of dispersion in activation time and repolarization time in the left ventricular wedge model due to greater size of tissue geometry ($3.5 \times 11 \times 6 \text{ cm}^3$) than 3D tissue geometries ($0.8 \times 0.8 \times 1.2 \text{ cm}^3$);
- the numerical values of speed of depolarization conduction was in the physiological range i.e. 0.265-0.18 m/s in the left ventricular wedge model.

Chapter 7 initially discusses a number of research questions based on the new findings in this thesis and links these to the literature. Then some limitations of this thesis are described, and a summary of further studies are suggested: (1) simulations of fibre-sheet structure with orthotropic conductivities; (2) using electromechanical models in parallel with electrical models since repolarization occurs during systole when the ventricular myocardium is mechanically contracting; (3) using cellular configurations with not only epicardial, mid-myocardial, and endocardial cells but also other cardiac cell types such as fibroblast; and (4) studying the speed of repolarization conduction. Finally, some conclusions are provided.

1.3 References

1. Ghanem RN and Burnes JE and Waldo AL and Rudy Y, Imaging dispersion of myocardial repolarization, II: noninvasive reconstruction of epicardial measures. *Circulation*, 2001. **104**: p. 1306–1312.
2. Burgess MJ and Green LS and Millar K and Wyatt R and Abildskov JA., The sequence of normal ventricular recovery. *Am. Heart J.* , 1972. **84**: p. 669–678.
3. The UK's leading independent health site. Available from: <http://www.patient.co.uk>.
4. World Health Organization (WHO). Available from: <http://www.who.int/mediacentre/factsheets/fs310/en/index2.html>.
5. Han J and Moe GK, Nonuniform recovery of excitability in ventricular muscle. *Circulation Research*, 1964. **14**: p. 44-60.
6. Kuo CS and Munkata K and Reddy P and Surawicz B, Characteristics and possible mechanism of ventricular arrhythmia dependent on the dispersion of action potential durations. *Circulation*, 1983. **67**: p. 1356-1367.
7. Gough W and Mehra R and Restivo M and Zeiler R and El-Sherif N., Reentrant ventricular arrhythmias in the late myocardial infarction period in the dog: Correlation of activation and refractory maps. *Circ Res*, 1985. **57**: p. 432-442.
8. Chauhan VS and Downar E and Nanthakumar k and Parker JD and Ross HJ and Chan W and Picton P., Increased ventricular repolarization heterogeneity in patients with ventricular arrhythmia vulnerability and cardiomyopathy: a human in vivo study. *Am J Physiol Heart Circ Physiol*, 2006. **290**: p. H79-H86.
9. Burgess MJ and Steinhaus BM and Spitzer KW and Green LS., Effects of activation sequence on ventricular refractory periods of ischemic canine myocardium. *J Electrocardiology*, 1985. **18**: p. 323–329.
10. Yuan S and Kongstad O and Hertvig E and Holm M and Grins E and Olsson B., Global repolarization sequence of the ventricular endocardium: monophasic action potential mapping in swine and humans. *Pacing Clin. Electrophysiol.* , 2001. **24**: p. 1479–1488.
11. Franz MR and Bargheer K and Rafflenbeul W and Haverich A and Lichtlen PL, Monophasic action potential mapping in human subjects with normal electrocardiograms: direct evidence for the genesis of the T wave. *Circulation*, 1987. **75**: p. 379-386.

12. Yue AM and Betts TR and Roberts PR and Morgan JM., Global dynamic coupling of activation and repolarization in the human ventricle. *Circulation*, 2005. **112**: p. 2592–2601.
13. Cowan JC and Hilton CJ and Griffiths CJ and Tansuphaswadikul S and Bourke JP and Murray A and Campbell RWF., Sequence of epicardial repolarisation and configuration of the T wave. *Eur. Heart J.* , 1988. **60**: p. 424–433.
14. Santangelo L and Ammendola E and Russo V and Cavallaro C and Vecchione F and Garofalo S and D'Onofrio A and Calabrò R., Influence of biventricular pacing on myocardial dispersion of repolarization in dilated cardiomyopathy patients. *Europace*, 2006. **8**: p. 502-5.
15. Medina-Ravell VA and Lankipalli RS and Yan GX and Antzelevitch C and Medina-Malpica NA and Medina-Malpica OA and Droogan C and Kowey PR., Effect of epicardial or biventricular pacing to prolong QT interval and increase transmural dispersion of repolarization. Does resynchronization therapy pose a risk for patients predisposed to long QT or torsade de pointes? *Circulation*, 2003. **107**: p. 740–746.
16. Fish JM and Brugada J and Antzelevitch C., Potential proarrhythmic effects of biventricular pacing. *J Am Coll Cardiol.*, 2005. **46**: p. 2340–2347.
17. Boyett MR and Jewell BR, A study of the factors responsible for rate-dependent shortening of the action potential in mammalian ventricular muscle. *J Physiol*, 1978. **285**: p. 359–380.
18. Qu Z and Weiss JN and Garfinkel A, Cardiac electrical restitution properties and stability of re-entrant spiral waves: a simulation study. *Am J Physiol Heart Circ Physiol*, 1999. **276**: p. H269–H283.
19. Karma A., Electrical alternans and spiral wave breakup in cardiac tissue. *Chaos*, 1994. **4**: p. 461–472.
20. Clayton RH and Taggart P, Regional differences in APD restitution can initiate wavebreak and re-entry in cardiac tissue: A computational study. *BioMedical Engineering*, 2005. **4**:54.
21. Keldermann RH and ten Tusscher KH and Nash MP and Hren R and Taggart P and Panfilov AV, Effect of heterogeneous APD restitution on VF organization in a model of the human ventricles. *Am J Physiol Heart Circ Physiol*, 2007. **294**: p. H764-H774
22. Laurita KR and Girouard SD., Modulation of ventricular repolarization by a premature stimulus. Role of epicardial dispersion of repolarization kinetics demonstrated by optical mapping of the intact guinea pig heart. *Circ Res*, 1996. **79**: p. 493–503.
23. Laurita KR and Girouard SD and Akar FG and Rosenbaum DS., Modulated dispersion explains changes in arrhythmia vulnerability during premature stimulation of the heart. *Circulation*, 1998. **98**: p. 2774–2780.
24. Huang J and Zhou X and Smith WM and Ideker RE., Restitution properties during ventricular fibrillation in the in situ swine heart. *Circulation*, 2004. **110**: p. 3161–3167.
25. Cao J and Qu Z and Kim Y and Wu T and Garfinkel A and Weiss JN and Karagueuzian HS and Chen P., Spatiotemporal heterogeneity in the induction of ventricular fibrillation by rapid pacing, importance of cardiac restitution properties. *Circ Res*, 1999. **84**: p. 1318–1331.
26. Garfinkel A and Kim YH and Voroshilovsky O and Qu Z and Kil JR and Lee MH and Karagueuzian HS and Weiss JN and Chen PS, Preventing ventricular fibrillation by flattening cardiac restitution. *Proc Natl Acad Sci USA*, 2000. **97**: p. 6061–6066.
27. Watanabe MA and Fenton FH and Evans SJ and Hastings HM and Karma A, Mechanism for discordant alternans. *J Cardiovasc Electrophysiol*, 2001. **12**: p. 196-206.
28. Yue AM and Franz MR and Roberts PR and Morgan JM, Global endocardial electrical restitution in human right and left ventricles determined by noncontact mapping. *J Am Coll Cardiol*, 2005. **46**.
29. Nash MP and Bradley CP and Sutton PM and Clayton RH and Kallis P and Hayward MP and Peterson DJ and Taggart P., Whole heart action potential duration restitution properties in cardiac patients: a combined clinical and modeling study. *Exp Physiol*, 2006. **91**: p. 339–354.
30. Fenton FH and Cherry EM and Hastings HM and Evans SJ, Multiple mechanisms of spiral wave breakup in a model of cardiac electrical activity. *Chaos*, 2002. **12**: p. 852–892.
31. Cherry EM and Fenton F, Effects of boundaries and geometry on the spatial distribution of action potential duration in cardiac tissue. *Journal of Theoretical Biology*, 2011. **285**: p. 164-176.
32. Kleber AG and James MJ and Fast VG, Normal and abnormal conduction in the heart: The hand book of physiology. 2002, New York: Oxford University Press.
33. Kleber AG and Rudy Y., Basic mechanisms of cardiac impulse propagation and associated arrhythmias. *Physiological Reviews*, 2004. **84**: p. 431-488.
34. Assomull RG and Prasad SK and Lyne J and Smith G and Burman ED and Khan M and Sheppard MN and Poole-Wilson PA and Pennell DJ, Cardiovascular Magnetic Resonance, Fibrosis, and Prognosis in Dilated Cardiomyopathy. *J Am Coll Cardiol*, 2006. **48**: p. 1977-1985.

35. Ertl G and Frantz S., Healing after myocardial infarction. *Oxford Journals*, 2005. **66**: p. 22-32.
36. ten Tusscher KH and Panfilov AV., Alternans and spiral breakup in a human ventricular tissue model. *Am J Physiol Heart Circ Physiol.*, 2006. **291**: p. H1088–H1100.
37. ten-Tusscher KH and Panfilov AV., Influence of diffuse fibrosis on wave propagation in human ventricular tissue. *Europace*, 2007. **9**.
38. Engelman ZJ and Trew ML and Smaill BH, Structural heterogeneity alone is a sufficient substrate for dynamic instability and altered restitution. *Circ Arrhythmia Electrophysiol*, 2010. **3**: p. 195-203.
39. Luo C and Rudy Y., A dynamic model of the cardiac ventricular action potential, I: simulations of ionic currents and concentration changes. *Circ Res*, 1994. **74**: p. 1071-1096.
40. Clayton RH and Holden AV, propagation of normal beats and reentry in a computational model of ventricular cardiac tissue with regional differences in action potential shape and duration. *Progress in Biophysics & Molecular Biology*, 2004. **85**.
41. Cates AW and Pollard A.E., A computer modeling study of the relationship between intramural fiber rotation and the spatial distribution of repolarization properties in ventricular myocardium. *IEEE-EMBC and CMBEC*, 1995. **1**: p. 79-80.
42. Colli Franzone P and Pavarino LF and Scacchi S and Taccardi B, Modeling ventricular repolarization: Effects of transmural and apex-to-base heterogeneities in action potential durations. *Math. Biosci.*, 2008. **214**: p. 140-152.
43. Noble D., A Modification of the Hodgkin-Huxley Equations Applicable to Purkinje Fibre Action and Pace-maker Potentials. *Journal of Physiology*, 1962. **160**: p. 317-352.
44. Bueno-Orovio A and Cherry EM and Fenton FH, Minimal model for human ventricular action potentials in tissue. *Journal of Theoretical Biology*, 2008. **235**: p. 544-560.
45. Keener JP and Sneyd J, *Mathematical Physiology*. 1998, Berlin: Springer, New York, Heidelberg.
46. Hunter PJ and Pullan AJ and Smaill BH, Modeling total heart function. *BioMedical Engineering*, 2003. **5**: p. 147-177.
47. The centre for cardiovascular bioinformatics and modelling of the Johns Hopkins University (CCBM). Available from: <http://www.ccbm.jhu.edu/reacerch>.

Chapter 2

From biological systems to computational models

2.1 Introduction

The human heart is cone shaped, with the size about a clenched fist. It is located within the mediastinum of the thorax and rests upon the diaphragm. It is located between the lungs, behind to the left sternum and in front of the vertebral column. The heart is composed of four chambers: two upper chambers are the right and left atria and two lower chambers are the right and left ventricles, separated by a wall of muscle called the septum, as shown in Figure 2-1. The two upper chambers are thin-walled chambers. The right atrium has multiple muscular trabeculations, responsible for expansion of the thin-walled right atrium. The left atrium is made of smooth tissue with no trabecular muscle bundles. The two lower chambers have thick walls compared to the atria. The right ventricle has a great number of coarse trabeculations. The left ventricle consists of papillary muscles and trabeculae which are muscular bundles that pervade the ventricle at the endocardium. The heart also has four valves, opening and closing in response to pressure changes as the heart contracts and relaxes.

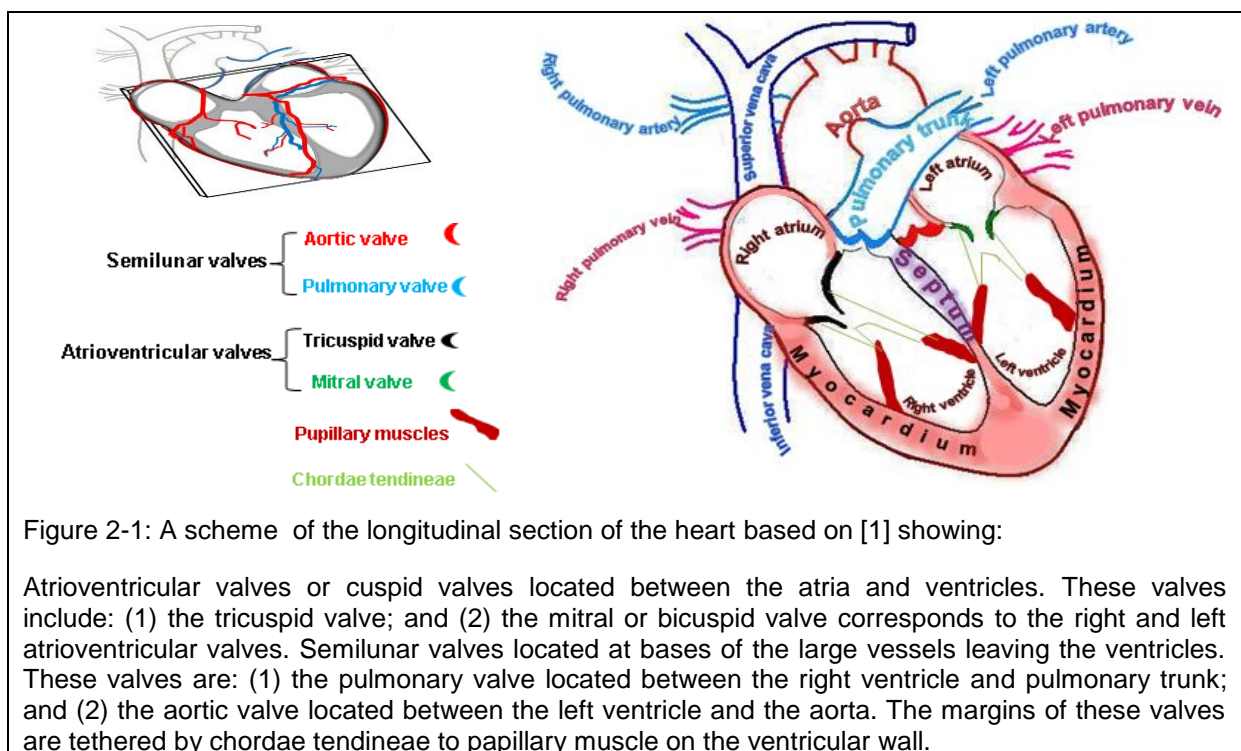


Figure 2-1: A scheme of the longitudinal section of the heart based on [1] showing:

Atrioventricular valves or cuspid valves located between the atria and ventricles. These valves include: (1) the tricuspid valve; and (2) the mitral or bicuspid valve corresponds to the right and left atrioventricular valves. Semilunar valves located at bases of the large vessels leaving the ventricles. These valves are: (1) the pulmonary valve located between the right ventricle and pulmonary trunk; and (2) the aortic valve located between the left ventricle and the aorta. The margins of these valves are tethered by chordae tendineae to papillary muscle on the ventricular wall.

This Chapter is organized in two parts. Part I provides a general background of the heart membrane, coronary arteries, physiological sequence of ventricular function in a cardiac cycle and sequential motions during ventricular filling and emptying, then explains how each cell is electrically excited to initiate contraction. Next, electrical disturbances or arrhythmias in the human ventricles are described. Part II initially highlights the current limitations in experimental and simulation studies and the need for cardiac modelling. Then, a historical

review of a simple cell model and a detailed cell model are provided before introducing modelling of restitution and dispersion in repolarization. Subsequently, challenging issues in modelling cardiac tissue are illustrated. These issues provide a foundation for the motivation of this study and the research plan that are introduced in the next Chapter.

Part I: The heart

2.2 The heart membrane and myocardium

The heart is surrounded with a membrane known as the pericardium. It is a triple-layered fluid-filled sac including:

The outer coat called the partial pericardium: it is the fibrous pericardium and made up of a thick layer of dense connective tissue, and it behaves as a tough outer coat that holds the heart in place and keeps it from overfilling with blood.

The inner coat called the visceral pericardium or epicardium: it is a double layered serous pericardium located after the fibrous pericardium: one layer is adherent to the inner surface of the fibrous pericardium, and the other layer is serous pericardium or epicardium that lines the inner surface of the outer coat.

The two layers of membrane are separated by a coating of pericardial fluid allowing the heart to move as it beats. Figure 2-2 shows a scheme of the distinct layers of the heart membrane from fibrosis layer to endocardium.

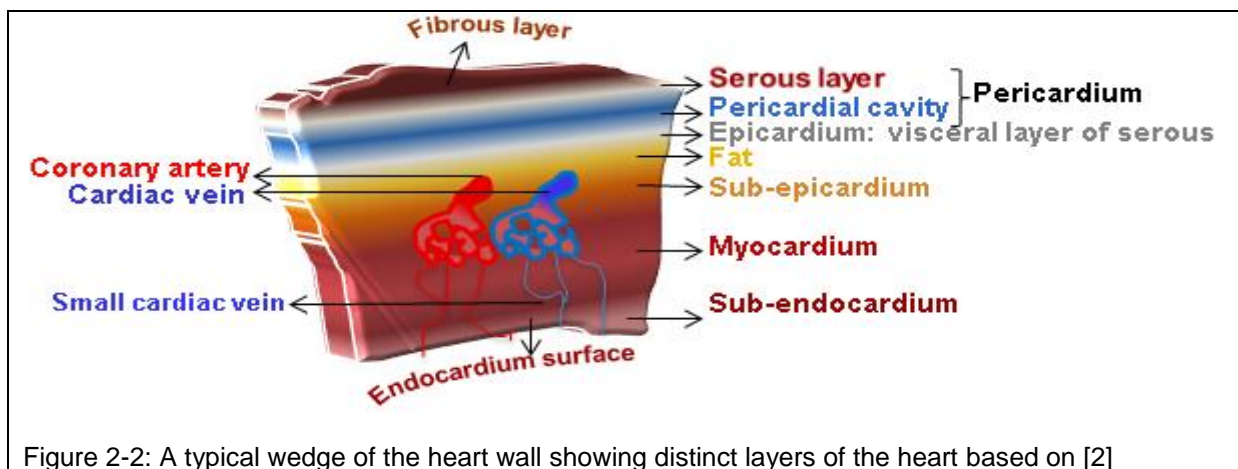


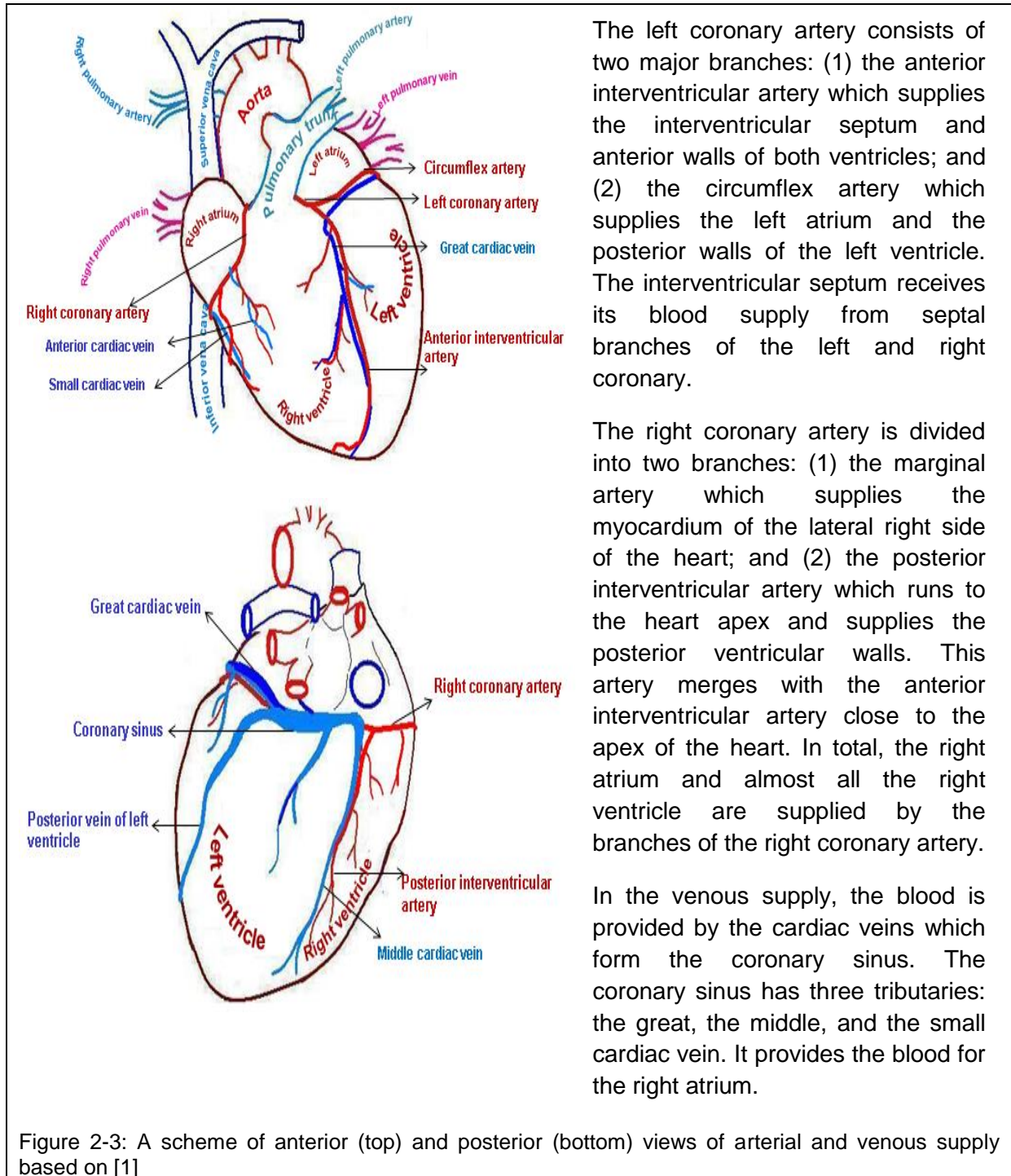
Figure 2-2: A typical wedge of the heart wall showing distinct layers of the heart based on [2]

The ventricular wall is usually divided into outer, middle, and inner regions:

- Epicardium is made up of a thin layer of connective tissue around the heart that gives the surface of the heart a smooth, slippery texture.
- Sub-epicardium is below the epicardium. Coronary arteries and blood veins are located in this region and send penetrating branches toward the endocardium to supply mid-myocardium and sub-endocardium.
- Myocardium or the middle muscular layer of the ventricular wall consists of transversely and longitudinally striated syncytium of cardiac cells (cell-to-cell coupling by intercellular channels).
- Sub-endocardial is the deepest region of the ventricular wall, made up of connective tissue. Purkinje fibres (impulse conducting fibres) are found in this layer.
- Endocardium or inner region of the ventricular wall lines the inner surface of the heart chambers and valves. It is thin, made up of single layer of endothelial cells.

2.3 Coronary arteries

The myocardium has two blood supplies including an arterial supply and a venous supply plus three major cardiac vessels. The first two cardiac vessels are left and right coronary arteries that carry oxygen and are responsible for nourishing the myocardium and lie in the epicardium, and the third is coronary sinus that carries deoxygenated blood and waste. For clarity, a brief description of the blood supply is given next to Figure 2-3.



The left coronary artery consists of two major branches: (1) the anterior interventricular artery which supplies the interventricular septum and anterior walls of both ventricles; and (2) the circumflex artery which supplies the left atrium and the posterior walls of the left ventricle. The interventricular septum receives its blood supply from septal branches of the left and right coronary.

The right coronary artery is divided into two branches: (1) the marginal artery which supplies the myocardium of the lateral right side of the heart; and (2) the posterior interventricular artery which runs to the heart apex and supplies the posterior ventricular walls. This artery merges with the anterior interventricular artery close to the apex of the heart. In total, the right atrium and almost all the right ventricle are supplied by the branches of the right coronary artery.

In the venous supply, the blood is provided by the cardiac veins which form the coronary sinus. The coronary sinus has three tributaries: the great, the middle, and the small cardiac vein. It provides the blood for the right atrium.

Figure 2-3: A scheme of anterior (top) and posterior (bottom) views of arterial and venous supply based on [1]

2.4 The cardiac cycle

The cardiac cycle includes the sequence of atrial and ventricular events associated with blood flow during one complete heartbeat. Since ventricular contraction is dynamically more

important, the cardiac cycle is often started with ventricular contraction. Accordingly, the cardiac cycle is divided into two phases: ventricular systole and ventricular diastole.

Ventricular systole is referred to the efficient ventricular emptying functions of the heart. The term systole was derived from the Greek word stello which means reduction or shortening. Ventricular diastole is referred to the efficient ventricular filling functions of the heart. The term diastole was derived from the Greek word diastello which means augmentation or lengthening.

Under normal conditions, atrial systole and diastole are followed by ventricular systole and diastole in a cardiac cycle.

2.4.1 Physiological sequence of ventricular function in a cardiac cycle

The relative temporal changes of sequential ventricular systole and diastole are subdivided into a physiological sequence of ventricular function in a cardiac cycle as follows:

- (1) Iso-volumetric contraction phase: In this phase, left ventricular contraction begins at the apex and proceeds up the ventricles.
- (2) Ejection: In the ejection phase, the blood is ejected from the ventricles.
- (3) Iso-volumetric relaxation: It is the period when no blood enters or leaves ventricles.
- (4) Passive ventricular filling: In this phase, the blood enters the ventricles rapidly and approximately 70% of the ventricular filling occurs during mid-diastole.
- (5) Active ventricular filling: It is a period when ventricle's widening continues by slower filling, before the atrium contracts prior to the next organized beat. Approximately 30% of both right and left ventricular filling is due to atrial contraction.

The first two phases occur during ventricular systole and the others during ventricular diastole. The contraction and relaxation of the heart produces blood pressure changes and results in opening and closing cardiac valves. Figure 2-4 provides a brief discretion with a scheme of changes in the cardiac valves and chambers during ventricular systole and diastole.

In a normal human adult heart that beats at a rate of 75 beats per minute, the approximate durations of the phases of the cardiac cycle in seconds is given in Table 2-1 obtained from [3].

A cardiac cycle length =0.8 s						
Total systole=0.31 s			Total diastole=0.49 s			
Iso-volumetric contraction (s)	Maximum ejection (s)	Reduced ejection (s)	Iso-volumetric relaxation (s)	Rapid filling (s)	Slow filling (Diastasis) (s)	Atrial systole (s)
0.05	0.09	0.17	0.08	0.11	0.19	0.11

Table 2-1: Estimation of durations of the phases of the cardiac cycle in a human adult's heart

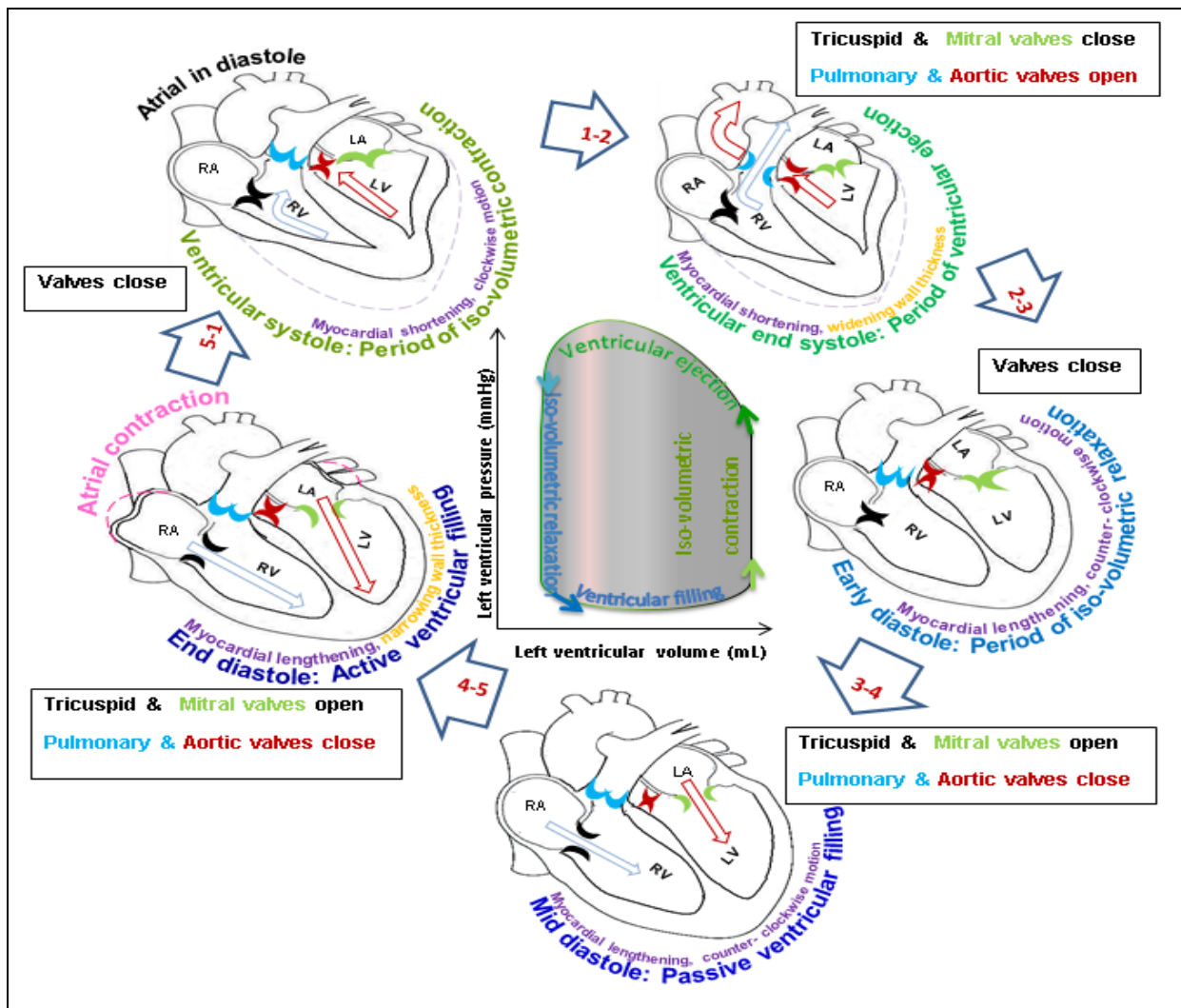


Figure 2-4: The scheme of changes in valves and chambers and a plot of pressure against left ventricular volume during a cardiac cycle based on [1]

At one set of the active phase, electrical stimulation causes the ventricular muscle to contract.

During the ventricular systole, the tricuspid and the mitral valves shut to prevent blood from returning to the atria; and (2) the volume of the ventricular cavities and the ventricular long axis decrease but the thickness of their wall increases (shown as dash line).

At early ventricular systole, atria are in diastole and ventricular pressure rises iso-volumetrically.

Late ventricular systole is a period of ventricular ejection. The aortic and pulmonary valves open when ventricular pressure become equal to the arterial pressure and blood is ejected from left ventricle into the aorta and from right ventricle to pulmonary trunk marked as a red and blue arrow respectively.

During ventricular diastole from early to late, (1) the pulmonary and aortic valves shut to prevent blood from flowing back into the heart from ventricles to arteries; and (2) the volume of ventricular cavities and the ventricular long axis increase but the thickness of their wall decreases.

When left ventricular pressure falls below the arterial pressure, the aortic valve closes and the heart relaxes iso-volumetrically. The mitral and tricuspid valves open when the intra-ventricular pressure drops below the atrial pressure and blood flows from the atrium into the ventricles until the late-diastole.

Ventricular filling is completed by atrial contraction marked as decreasing of atrial volume shown as pink dash.

Right and left atrium and ventricles were labelled as RA, LA, RV, and LV respectively.

2.4.2 Sequential motions during ventricular filling and emptying

During a cardiac cycle, there is a systolic twist and an early diastolic untwist of left ventricle about the ventricular long axis. In addition, apical rotation is the opposite of basal rotation. Figure 2-5 shows how the cavity's volume, valves, and wall thickness change during two phases of a cardiac cycle.

- The systolic phase of the cardiac cycle

In this phase, the myocardial muscle is active, ejecting the blood out of the ventricles, changes in fiber architecture is more apparent i.e. contraction, clockwise myocardial wall motion, and myocardial shortening. Interestingly, electrical repolarization occurs during mechanical systole when the ventricular myocardium is mechanically contracting.

- The diastolic phase of the cardiac cycle

During diastolic phase, the myocardial muscle is considered as a passive structure while narrowing wall thickness. From early to end ventricular diastolic, the myocardial expansion, counter-clockwise myocardial motion, and myocardial lengthening occur.

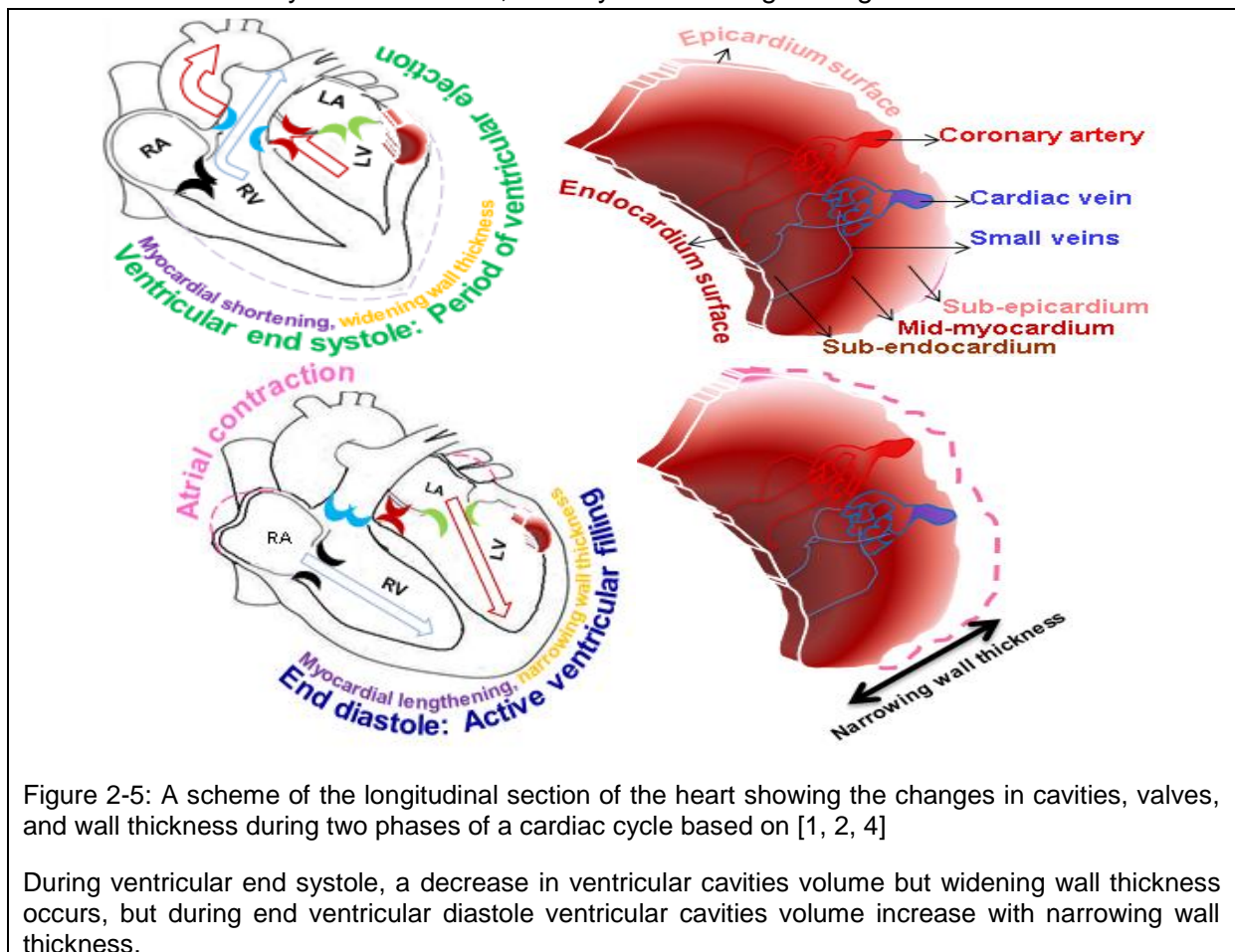
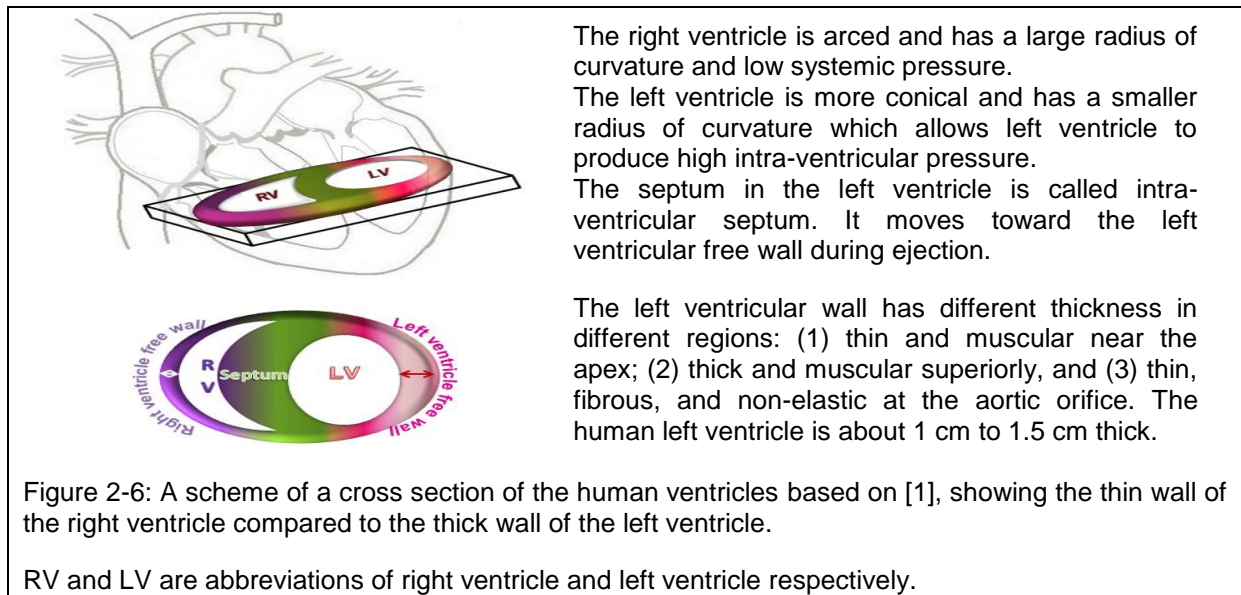


Figure 2-5: A scheme of the longitudinal section of the heart showing the changes in cavities, valves, and wall thickness during two phases of a cardiac cycle based on [1, 2, 4]

During ventricular end systole, a decrease in ventricular cavities volume but widening wall thickness occurs, but during end ventricular diastole ventricular cavities volume increase with narrowing wall thickness.

Furthermore, there is adoption of the ventricular shapes to the pressure developed in the cavities. The different wall thickness in ventricles may be due to variations in the myocardial mass, which corresponds to the force the chamber requires to pump the blood out of the heart. For example, during the left ventricular contraction, because the pressure in the systemic circulation is much higher than in the pulmonary circulation, the left ventricle

requires more pressure to pump out the blood. That might explain why the left ventricle is larger and stronger than right ventricle and its wall is roughly three times thicker than that of the right ventricle as shown in Figure 2-6.



2.5 From cellular excitation to cardiac contraction

The heart is an electromechanical pump, where contraction results from electrical excitation. Cardiac cells are often divided into four groups: (1) the primary cardiac cells including nodal cells i.e. sinoatrial node and atrioventricular node, Purkinje fibre cells, and myocardial cells; (2) vascular endothelial cells located in the inner lining of the heart's newly formed blood vessels; (3) smooth muscle cells located in the wall of the heart's blood vessels; and (4) fibroblasts interspersed between the layers of the heart, that appear as a spindle-shaped cell with an elliptic nucleus, and behave as a protein-secreting cell that is a well-developed rough endoplasmic reticulum and a golgi apparatus. The focus of this study is on myocardial cells in the left ventricle.

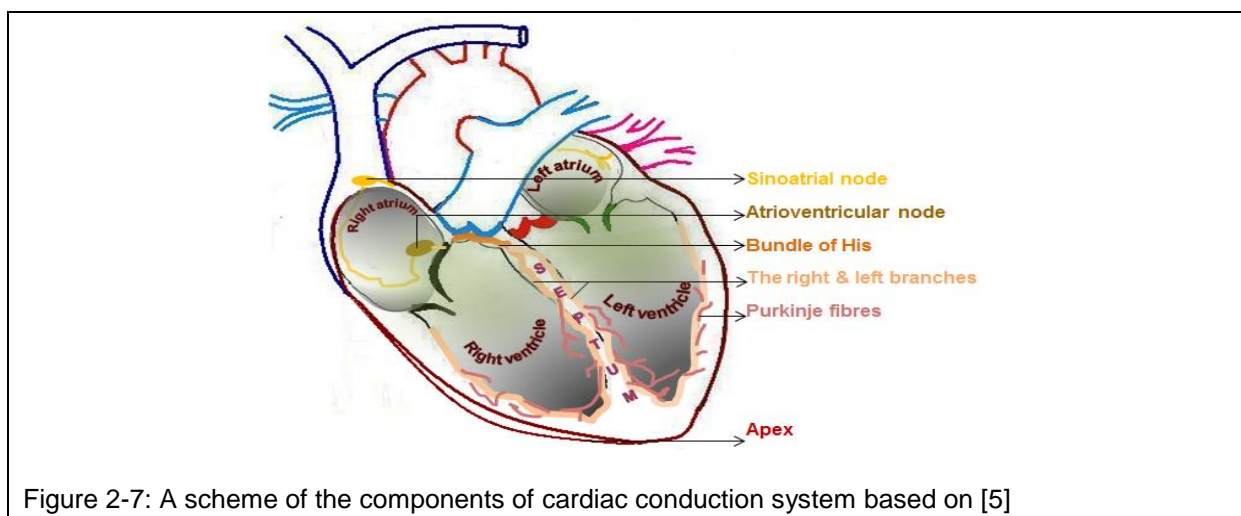
Cells in atria and ventricles exhibit both excitability and contractility properties. But the cells of the pacemaker system show only excitability. Excitability is the ability of the cardiac cells and tissue to respond to the over-threshold stimuli by generating and propagating electrical pulses known as action potentials (AP). Contractility is the ability of cell contractile elements (sarcomere) to shorten the cell length in response to an increase in the intracellular calcium concentration in the process of developing AP. Therefore, myocardial contraction occurs followed by the ejection of the blood. The generation of AP is the results of a sequence of rapidly occurring events that reverse the membrane potential and eventually restore it to the rest. These events are illustrated in the following sections.

2.5.1 Cardiac conduction system

For normal contraction to occur cardiac cells must first be excited and electrical impulses produced should be distributed as the electrical waves through the cardiac conduction system. Figure 2-7 shows a scheme of components of cardiac condition system. The impulse starts in a small bundle of specialized cells, called the sinoatrial node, located at the top of the right atrium. It is known as the heart's natural pacemaker because it sets the rate and rhythms of heartbeat i.e. about 70-80 beats per minute in an adult human heart.

Following the propagation of electrical impulses from sinoatrial node through the walls of the right and left atrium, the atrial contraction occurs and forces blood into the ventricles.

The atrio-ventricular node is located between the atria and ventricles. This cluster of cells, slows the electrical impulses before they spread through the right and left ventricles with a delay about 0.1-0.2 seconds (s). This delay gives the atria time to contract and allows the ventricles to fill completely. The intrinsic frequency of atrioventricular node is about 50 beats per minute. His-Purkinje network in the ventricular region consists of (1) the bundle of His; (2) the right and left branches; and (3) the Purkinje fibres. This network provides the pulse at relatively high speed to the ventricles through the pathway of fibres in which the electrical impulse spreads to the muscular wall of the ventricles on a cell-to-cell basis from endocardium to epicardium and from apex to base. This causes the ventricles to contract and pump blood out the heart to the lungs and body. After cardiac activation, de-activation occurs and cardiac muscles are ready for a new activation. This arrangement allows the coordination of atria and ventricles to be synchronised.



2.5.2 Cell membrane at rest

Many cells have a membrane potential which is the difference of the electrical charges between inside and outside of plasma membrane. When a cell is at rest or steady-state condition, the cell membrane is more permeable to potassium than other ions. A transmembrane protein in the cell membrane called sodium-potassium-exchange-pump transports three sodium ions out of the cell against its steep electrochemical gradient, and two potassium ions into the cell. It is based on an active transport mechanism as this pump acquires energy from the hydrolysis of adenosine three phosphates. Unequal concentration in potassium and sodium causes the membrane potential to push toward sodium equilibrium potential and ions move from the area of low concentration to the area of high concentration. Consequently, a difference in electrical potential across the cell membrane is created and cell is polarised with positive and negative charges on its external and internal surfaces.

2.5.3 How an action potential arises in ventricular cells

In ventricular cells, the transmembrane resting potential is approximately -90 mV, close to the potassium reversal potential. This negative potential across the plasma cell membrane is called the resting membrane potential. The cell membrane stays at rest until it receives a supercritical electrical stimulus from its neighbouring cells. A description about the cell-to-cell coupling is provided in section 2.5.7. Anything in the cell environment that can convert or change resting membrane potential is called a stimulus. If a stimulus can depolarize the cell

membrane at rest state and raise the resting membrane potential from -90 mV to the sodium threshold potential about -70 mV, then an AP arises. At the onset of AP, fast sodium channels are opened or activated for a few milliseconds and the sodium currents increase while potassium channels are still closed.

2.5.4 Ventricular action potential phases

When an AP is induced, the membrane potential rises above this level in four separate phases: (1) AP depolarization or rising phase or AP upstroke; (2) AP early repolarization; (3) AP plateau or slow repolarization; (4) AP final repolarization or AP downstroke; and (5) AP rest. Figure 2-8 provides a brief description with the scheme of the physiological processes responsible for the shape of a typical normal ventricular AP.

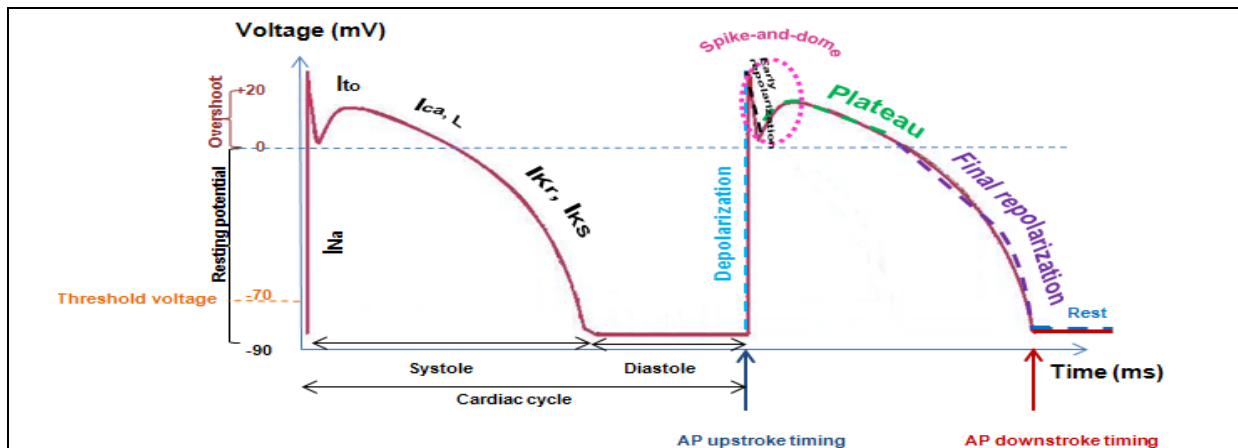


Figure 2-8: A typical normal shape of epicardial AP based on [6] and its dominant currents

AP upstroke or rising phase or rapid depolarization

The abundance of sodium current (I_{Na}) forms the upstroke of AP shape. The membrane potential responds quickly to a higher transmembrane potential around +20 mV and the interior of the cell transiently becomes positive compared to the exterior. The parts of AP in which a membrane potential raise from 0 to +20 mV is called AP overshoot. The fast sodium channels are both voltage and time dependent. The transmembrane potential stops at +20 mV, because sodium channels become voltage-inactivated by closure of inactivation gates.

AP early rapid repolarization

The AP upstroke is terminated by closing of the fast sodium channels and opening of potassium channels. Repolarization originates mainly from transient outward potassium currents (I_{to}) through potassium channels along with hyperpolarizing sodium-calcium exchangers and currents generated by sodium-potassium adenosine three phosphates (ATPase). In early repolarization phase, membrane potential is gradually decreased and **the spike-and-dome morphology** of the AP is formed.

AP plateau

An approximately horizontal plateau is formed mainly because of influx of the calcium currents via L-type calcium channels ($I_{ca,L}$) while sodium channels are inactivated and the delayed rectifying potassium outward current is decreased. The AP plateau in the left ventricle approximately prolongs 200-300 ms in the human heart because the slow calcium channels might remain open. The muscle contraction events are activated by calcium ions. At the end of the plateau, the transmembrane potential is still decreasing close to zero and the slow calcium-sodium channels are inactivated while the voltage gated potassium channels are activated.

AP final repolarization or AP downstroke

When all the potassium channels open, the final rapid repolarization is initiated by a fast increase of rapid and slow components of outward potassium currents (I_{Kr} and I_{Ks}). It is terminated when the transmembrane potential become equal to the voltage-gated potassium channels.

AP rest

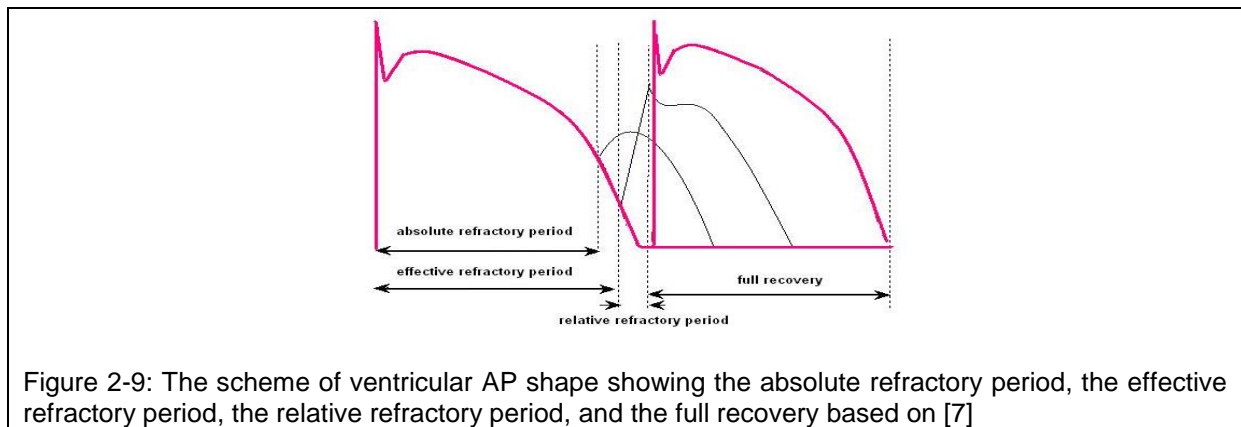
It is recognized by the resting membrane potential and when the ionic concentrations are restored.

2.5.5 The absolute, effective, and relative refractory period

Under normal condition, atria contracts and ventricles relax. Figure 2-9 shows the absolute, effective, and relative refractory period that emerges during the contraction phase of the cardiac cycle. The absolute refractory period is a time interval from an AP upstroke to around AP final repolarization. During this period generally no re-excitation can occur to trigger a new AP due to the inactivation of all fast sodium voltage dependent channels. During this time cardiac cells restore their ionic balance.

After this period, some of sodium and calcium channels recover, so that a stimulus can cause some cellular depolarization but the response will not propagate. The sum of this period and the absolute refractory period is called an effective refractory period. After an effective refractory period, there is a relative refractory period, in which a larger stimulus than normal stimuli depolarizes the membrane so the response will propagate.

Following the relative refractory period, a full recovery occurs and a normal stimulus will lead to a new AP. Diastole is the time when the cells rest from excitation and all the processes of the ionic channel gates return to their initial conditions.



2.5.6 Action potential in different regions of the heart

Figure 2-10 shows AP shapes in different regions of the heart. Under normal condition, pacemaker cells in sinoatrial node have the shortest spontaneous depolarization and so the highest frequency. As pacemaker cells do not have a stable diastole, a slow influx of sodium and or calcium produces slow depolarization. During slow depolarization of pacemaker fibres the membrane potential increases to the threshold potential and the cell automatically becomes depolarized and produces a spontaneous AP without external stimuli. This characteristic forms the basis of automaticity and induces repetitive activity. At termination of an AP, pacemaker fibres initiate a new AP.

Slow response fibres in sinoatrial and atrioventricular nodes have a lower resting membrane potential, slower AP upstroke, and little or no AP overshoot. The dominant current in the resting membrane potential, AP plateau, and AP repolarization phase is inward rectifier potassium current. The AP upstroke in both nodal cells depends on calcium currents.

The AP upstroke in fast response fibres such as atrial, ventricular and Purkinje fibres depends on the fast sodium currents. In addition, early rapid repolarization is resulted from the transient outward potassium currents. In the case of Purkinje fibres, they show the highest AP upstroke due to the higher density of sodium currents. The L-type calcium currents contribute to the later stage of depolarization phase.

Regarding atrial and ventricular AP, the latter has the longer action potential duration (APD), the higher plateau potential, a faster repolarization, and a more negative resting membrane potential because of inward rectifier potassium currents. In atrial AP, ultra-rapid delayed rectifier potassium current is dominant current in AP plateau.

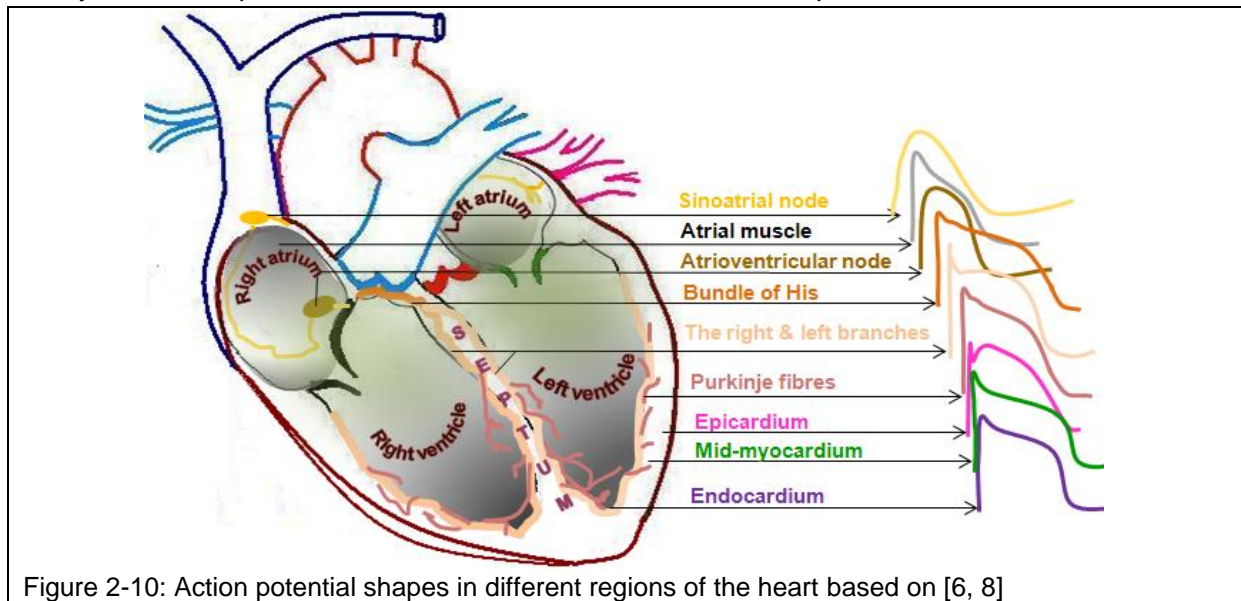


Figure 2-10: Action potential shapes in different regions of the heart based on [6, 8]

Electrocardiography is a method that records the normal and abnormal electrical activity during the cardiac cycle at body surface based on voltage differences in different regions of the heart. The three main graphical deflections that are seen on a typical electrocardiogram are (1) P-wave that reflects atrial depolarization; (2) QRS-wave that reflects the electrical activation of the ventricles caused by AP upstroke; and (3) T-wave that reflects the ventricular repolarization. In the human heart, the total activation time is around 80 ms and the total repolarization is approximately smaller than 400 ms at 1 HZ [9].

2.5.7 Cardiac excitation-contraction coupling

Cardiac tissue is where the electrical and mechanical activity occurs. The myocyte has a cytoplasm called sarcoplasm, with a width of about 20-30 μm plus a centrally positioned nucleus and atrial granules. Intercalated disks connect the cells in the bundles in an axial direction. Figure 2-11 provides a scheme showing how cardiac cells are joined end-to-end by intercalated disks. These disks are dense junctional complexes and cross the cardiac cells at uneven intervals in step-like fashion. The mechanical adhesion of the cells is provided by adhering junctions in the intercalated disk [10].

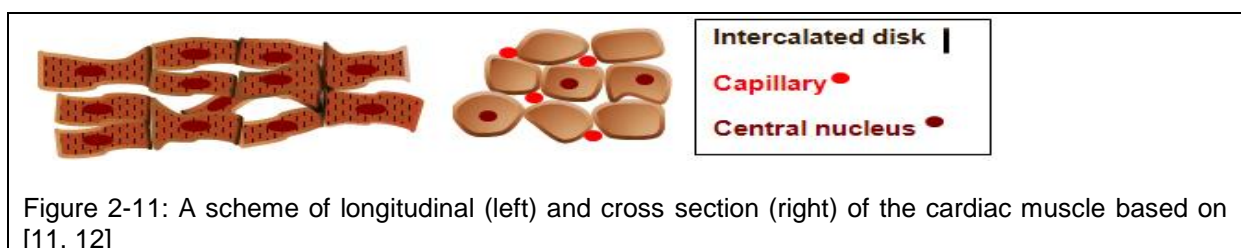


Figure 2-11: A scheme of longitudinal (left) and cross section (right) of the cardiac muscle based on [11, 12]

The electrical coupling of cells means impulse movement from one cell to another. The electrical coupling of cells is provided through tubular protein structures called gap junction located in intercalated disks. Gap junctions are cylinder intracellular channels and are permeable to large molecules such as ions, nutrient and metabolites. Cardiac contraction occurs when an AP triggers the rapid release of calcium from the sarcoplasmic reticulum by

a mechanism called the excitation-contraction coupling. The coupling between myocyte AP and contraction include a number of events that are summarized below:

- An AP activates membrane calcium channels allowing rapid influx of calcium during a prolonged AP but still insufficient for contraction.
- Additional calcium is provided by the initial inward movement of calcium that acts as an amplification signal for the larger release of calcium from the myocyte sarcoplasmic reticulum.
- The global increase in myoplasmic calcium activates myofilaments to initiate contraction.
- Under normal conditions, the same amount of calcium that entered the cell through the cell membrane (called sarcolemma) from the extracellular space is extruded from the cell. Similarly, the amount of calcium that was released from sarcoplasmic reticulum is re-sequestered in the sarcoplasmic reticulum. In both cases, the transport of calcium is against the electrochemical gradient.

2.6 Electrical disturbances in the human ventricles

Severe and prolong myocardial ischemia (state of inadequate blood supply to tissue) leads to myocardial infarction, a situation in which myocardium die and the excitability and the cellular coupling are disrupted.

Ischemia, injury, and myocardial infarction are three successive stages of increasing severity of myocardial cells electric dysfunction secondary to coronary under-perfusion. In this sense,

- ischemia refers to the earliest stage and preceding injury;
- injury termed to the phase of reversible changes;
- a myocardial infarction refers to irreversible cell injury and death [4].

Whether or not a person survives a myocardial infarction besides other factors depends on the extent and location of the damage. For extent of damage, the formation of an infarct may involve the (1) full thickness infarct extends from endocardial to epicardial and is called a transmural infarct; and (2) partially thickness of the ventricular wall that is called sub-endocardial and sub-epicardial infarct.

Regarding the location of damage, an infarction often involves the left ventricular muscle and septum and rarely the wall of atria or right ventricle. The left ventricle is more vulnerable to obstruction of its blood supply, which may be due to its much thicker wall than the right ventricle and its function as the systemic pump (that pumps blood under high pressure and requires great blood supply). Thus, if myocardial infarction occurs in the left ventricle, damage is more serious than other parts of the heart.

Clinically, the importance of the location of myocardial infarction is due to the different treatment and complications of structures in myocardial infarction. For clarity, two examples are described here.

- anterior wall infarction

An obstruction of the left anterior descending artery causes an infarction in the anterior wall and partially anterior inter-ventricular septum. Block of the circumflex artery may damage the lateral wall [13]. Any malfunction of the anterior wall (that pumps blood at high pressure) may lead to low blood pressure, high heart rate, shock, and in the longer term may

lead to heart failure. In heart failure, cardiac output which is the volume of blood ejected per minute from the left ventricle into aorta or from the right ventricle to pulmonary trunk is reduced.

- inferior wall infarction

An obstruction of the right coronary artery leads to an infarct of the back wall of the left ventricle and partially posterior inter-ventricular septum. The block of the main left coronary artery may damage both anterior and lateral wall of the left ventricle [13]. Any inferior wall infarction may lead to low heart rate because of involvement of the sinus node.

One of the consequences of a myocardial infarction is arrhythmia. The most serious cardiac rhythm disturbance is ventricular fibrillation in which the ventricles contract in a rapid unsynchronized way so that the heart quivers and pumps little. In arrhythmia caused by re-entry, the heart beats at a fast heart rate more than 100 beats per minute (tachycardia). In ventricular tachycardia, abnormal electrical activity in the ventricles interferes with normal electrical impulses coming from sinoatrial node. Therefore the ventricles do not have time to fill completely and heart cannot pump efficiently because of the rapid heart-beat. Another type of disturbance of cardiac rhythm occurs if conduction of impulse from atria to the ventricles is blocked. In addition, since adult muscles are essentially amitotic, most dead myocardial tissue is replaced by non-contractile scar tissue or collagen scar. Myocardial scarring is fibrous tissue that can disrupt the cardiac electrical conduction system, and may also irritate the surrounding viable ventricular myocytes making them more likely to depolarize spontaneously.

In the diseased heart, the consequence of most electrical disturbances is an abnormal decrease in the conduction velocity and plus prolongation or shortening of APDs that may increase vulnerability to arrhythmia.

Part II: Modelling the heart at cell and tissue level

2.7 Experimental and simulation studies

Investigating about the mechanism, initiation and maintenance of cardiac arrhythmias caused by re-entry have been the focus of numerous experimental and simulation studies as cardiac arrhythmias is one of the contributors to cardiovascular disease morbidity and mortality in the world [14]. This part of the Chapter explains why computational modelling is useful for studying electrical activities in the normal and diseased heart.

2.7.1 Limitations in experimental studies

The experimental and clinical possibilities for studying electrical abnormalities in the human heart are still limited. The major experimental problems are described here.

- Difficulties in experimental techniques

The traditional methods for mapping activation and repolarization were based on surface unipolar and bipolar electrograms measured with large arrays of recording electrodes [15]. However, it was difficult to interpret activation sequences [16] during fast synchronous depolarization (i.e. after electric shock application) and in ischemia due to slowly changing depolarization. In addition, repolarization time measured with these methods often does not coincide with the repolarization time at the recording sites [16, 17]. In 1991, Franz [18]

suggested that a monophasic AP technique may be a reliable method for measuring AP repolarization and APD but not for multisite mapping.

The sequence of AP repolarization can be measured by optical imaging using voltage-sensitive fluorescent dyes [19]. However, repolarization time points are not easy to determine because AP repolarization are often encumbered by drifting baselines and motion artifacts [20]. To suppress the motion artifacts, mechanical or pharmacological immobilization techniques should be used [19]. The other technical difficulties to dynamically map physiological processes in intact hearts using optical methods are cellular heterogeneities, spatial and temporal resolution, limitations of surface images, depth-of-field, and need for large fields of view (i.e. ranging from $2 \times 2 \text{ mm}^2$ to $3 \times 3 \text{ cm}^2$) [21].

- Uncertainties about reliable method

Uncertainties exist about the reliable method for measuring recovery time, while there is a reliable method for determining activation times directly from the heart. Spach and Dolber [22] in 1986, and Punske et al. in 2003 [23] established methods for determining activation times from unipolar electrograms recorded directly from the heart. However, a study by Scacchi et al. [24] in 2009 about the reliability analysis of cardiac repolarization time markers showed that the spatial distribution of activation recovery intervals may provide inaccurate estimates of spatial distribution of APD.

- Techniques of measurements and surface recordings

The great variability among experimental data may be due to variation in the experimental conditions and techniques of measurements. For example, transmural dispersion of repolarization measured by activation recovery intervals from unipolar plunge electrodes during coronary artery bypass surgery did not show any significant transmural heterogeneity of repolarization or presence of mid-myocardial cells in patients in the study by Taggart et al. in 2001 [25]. The endocardial region in the human heart has anterior wall depth around 9-11 mm, so it was possible that electrodes (spanning 6 mm from the first recording node to the last) could not probe the deep area in the left ventricular wall, as suggested by Antzelevitch [26]. In addition, the location of the epicardial electrode 0.85 mm from the surface may be another reason that did not allow recording of the briefest surface epicardial response [26].

- Data measured at basic cycle length

Data collected under controlled conditions do not show the full range of physiologically reasonable values or limited to some long or short stimulus intervals. For example, Hanson et al. [27] studied the interaction of activation–repolarization coupling and restitution properties in the human left ventricular endocardium without any information about transmural gradients or other regions of the left ventricle.

- Sparse human data

There are a few studies that determined cardiac activation and repolarization in the same heart. For example, the total activation of the normal human heart was described in detail by Durrer et al. [28] in 1970 with electrode-base techniques while the sequence of repolarization of the same human heart remained unknown. Moreover, the current knowledge about the sequence of ventricular repolarization in both normal and diseased tissue is largely based on animal studies because human data are sparse.

- Data measured from patient with different pathology

Epicardial and endocardial measurements may not be performed in the same patients and may be performed with different wedge preparation. For example, a human study by Drouin et al. [29] is one of the important study that compared the effects of chronic amiodarone therapy on transmembrane activity of epicardium, mid-myocardium, and endocardium in the left ventricle explanted from normal, heart failure and amiodarone-treated heart failure patients. They showed that amiodarone (an antiarrhythmic agent) acted to decrease significantly the heterogeneity of repolarization in ventricular tissues in patients than other groups. However, the data, from which the actions of amiodarone were deduced, were based on a heterogeneous mixture of diseased hearts [29].

- Lack of detailed measurement of data

There are limited number of studies that have made detailed measurements of the transmural variation of myocyte orientation in the ventricles i.e. the study in the pig heart by Streeter and Bassett [30], the canine heart by Streeter [31, 32], and the human heart by Greenbaum et al. [33].

2.7.2 Why computational modelling

Alternatively, computer simulations of the heart under normal and pathological conditions may overcome some of these problems by providing a realistic feedback allowing an experimental test to be performed on the computer copy of the heart, not on the patients. These models are scaled from cellular level to tissue level and to the whole organ structurally, functionally or combination of both. However, the limitations of cardiac modelling may be involved in validation, modifications, and implementations.

Validation of cardiac models for the human heart when the experimental data arises from animal experiments is one of the problems. Animal hearts may differ from human heart in the cases of AP profiles or vulnerability to arrhythmias. For example, a series of studies by Colli Franzone et al. [34-36] about the sequence of activation, repolarization, and APD was based on the phase I Luo–Rudy membrane ionic model of guinea pig [37]. This model did not describe the transient outward potassium current that play an important role in epicardial AP spike-and-dome morphology in the human left ventricle [38].

Second, some models may be designed primarily for use as isolated cells in one region of the heart or for specific pacing rate such as slow pacing rates, and it may not be able to reconstruct the properties of cells in tissue during rapidly paced tissue. In addition, models may reflect only one type of tissue heterogeneities. Modifying a model by changing variables or equations may compromise the original validation, Clayton et al. [39] in 2010.

Third, a large scale cardiac model involves solving high order equations, huge memory, and long running time. For example, the running time and maximum virtual memory for simulating tissue in the left ventricular wedge with size of $3.5 \times 11 \times 6 \text{ cm}^3$ in this thesis were around seven days and 5 Giga bytes at each stimulus interval using a simple human cell model [40].

Both experimental and simulation studies have a number of limitations, however, simulation studies may dominate experimental studies due to ethical problems in the human hearts.

The following section provides a background about the mathematical models which were used in this thesis.

2.8 A history of cardiac models

In 1928, Van der Pol and Van der Mark [41] introduced a mathematical model of the heart beat to simulate AP in the heart as a relaxation oscillator. The macroscopic model of the membrane ionic currents in a single nerve fibre was initially introduced by Hodgkin and Huxley [42] in 1952. They modelled the axon (a nerve fibre) as an electrical cable that has some capacitance and resistance, in which the uneven spread of ions across the cell membrane forms electromotive force. Figure 2-12 shows the scheme of a simple mathematical model of the cell membrane as an equivalent resistor-capacitance circuit based on the Hodgkin-Huxley model [42].

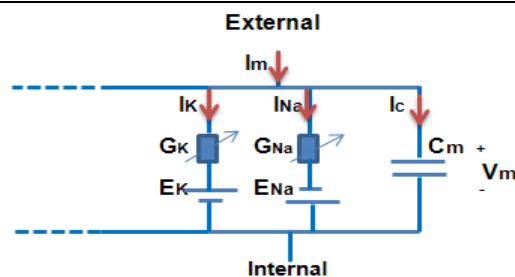


Figure 2-12: A model of a cell membrane as an equivalent resistor-capacitance circuit based on [42]

V_m : Transmembrane potential is like voltage stored in a battery and corresponds to the difference electrical charges between internal and external of the circuit

C_m : The phospholipid double-layer structure of the cell membrane modelled as a capacitor

G_{Na} and G_K : Voltage-gated sodium, potassium, and other ion channels modelled as variable resistors

E_{Na} and E_K : Sodium and potassium and other ion gradients modelled as voltage sources

I_m : Flow of ions across cell membrane and through pores of ion channels and was described based on Kirchhoff's law (the sum of currents into a point in a circuit equals the sum of currents out of that point)

$$I_m = I_K + I_{Na} + I_C + \dots$$

Sodium current I_{Na} and potassium current I_K were modelled as flow of electrical currents in the circuit and were given by:

$$I_K = (V_m - E_K) \cdot G_K$$

$$I_{Na} = (V_m - E_{Na}) \cdot G_{Na}$$

In an electrical circuit, the capacitor acts like a balloon to contain electrons and stores a charge proportional to the potential difference applied $Q = V_m \cdot C_m$.

As current is the rate of flow of charge, $I_c = \frac{dQ}{dt}$, so the instantaneous current I_c flowing through a capacitor is proportional to the instantaneous rate of change of voltage across it and is described by:

$$I_c = C_m \frac{dV_m}{dt}$$

It is important to note that Hodgkin and Huxley [42] described the potassium and sodium conductance by equations suggesting a physical meaning. For example, potassium conductance was described by following equations [42]:

$$g_k = \bar{g}_k n^4 \quad \text{and} \quad \frac{dn}{dt} = \alpha_n(1 - n) - \beta_n n$$

\bar{g}_k : Constant with dimension of conductance/cm²

α_n and β_n : Rate constants which vary with voltage and not with time with dimension of 1/ms

n : A variable with no dimension which varies between 0 and 1

n and $1 - n$: The proportion of the particle inside and outside of the membrane respectively

If it is assumed that potassium ions can only pass the membrane when four similar particles occupy a certain position inside or outside of the membrane, the α_n and β_n rate constants can determine the rate of transfer from outside to inside and the reverse respectively [42]. For a particle with a negative charge, α_n and β_n are expected to increase and decrease during AP depolarization.

Sodium conductance was described by equations given by [42]:

$$g_{Na} = \bar{g}_{Na} m^3 h \quad \text{and} \quad \frac{dm}{dt} = \alpha_m(1 - m) - \beta_m m \quad \text{and} \quad \frac{dh}{dt} = \alpha_h(1 - h) - \beta_h h$$

\bar{g}_{Na} : Constant with dimension of conductance/cm²

α_m and β_m : Rate constants which vary with voltage and not with time with dimension of 1/ms

m and h : Activation and inactivation variables

m and $(1 - m)$: The proportion of activating molecule on the inside and outside of the membrane

h and $(1 - h)$: The proportion of inactivating molecule on the outside and inside of the membrane

The α_m or β_h and β_m or α_h represent the transfer rate constants in the two directions, if it is assumed that sodium conductance is proportional to the number of inside sites in the membrane which are occupied by three activating molecules but are not blocked by an inactivating molecules [42]. In the cardiac cell model, many channels have been modelled as channels described by Hodgkin and Huxley [42] with different activation and inactivation variables based on available data.

Following the Hodgkin and Huxley [42] model, the models of the membrane currents may be categorized in two groups: (1) a detailed description of channels, pumps, and exchangers; and (2) a simple description of some macroscopic approximation of the average channel behaviour. The main difference between a biophysically detailed cell model and a simple cell model is that

1. in a detailed cell model the parameters of the model have biological definitions, while in a simple cell model there is no relationship between model parameters and the cellular physiological mechanism;
2. a detailed cell model is usually based on the available detailed experimental measurements of ion channels while a simple cell model quantitatively creates restitution and do not show measured currents. However, a simple model can mimic the most important AP properties and decrease the computing requirements.

The following two subsections provide a historical review of two human cell models, the FK4V model [40] and the TP06 model [43].

2.8.1 The historical background of the TP06 model

The first model of a cardiac cell was developed in 1962 by Noble [44] who adapted the Hodgkin and Huxley model [42] to describe the long lasting AP and pacemaker potentials of the Purkinje fibres of the heart. In the Noble model, the current membrane was the voltage gated inward current, I_{Na} with a clue that other ion currents are also present. The mammalian ventricular AP was reproduced by Beeler and Reuter in 1977 [45] in a model which represented ionic currents as follows: fast inward sodium current I_{Na} , slow inward calcium current I_{Ca} , time dependent outward potassium current I_k , and time independent transient outward potassium current I_{kt} . This model was updated by Lue and Rudy in 1991 [37] to describe depolarization, repolarization and their interaction in the guinea pig ventricles. They also used the Hodgkin and Huxley equations [42] to calculate ionic currents.

In 2004, ten Tusscher et al. [46] developed a ventricle model with 17 variables to model human ventricular cell based on mostly human data. Three gates for sodium current were modelled as Hodgkin-Huxley [42] equations and were characterized by a steady-state value and a time constant for reaching this steady-state value, both of which vary with membrane potential. The model of ten-Tusscher et al. [46] was improved by ten Tusscher and Panfilov [43] in 2006 by new formulations for some (not all details) description of intracellular calcium dynamics in order to obtain more realistic dynamical models of calcium transient, calcium current inactivation and the contraction staircase.

2.8.2 The historical background of the FK4V model

The time course of changes in nerve membrane potential was described using a simple model by Fitz Hugh [47] in 1961 and Nagumo et al. in 1967 [48]. They described the excitability, threshold, plateau and refractoriness with minimal number of equations in the axon. In 1994, this model was adapted for cardiac tissue by Rogers and McCulloch [49] to reproduce a cardiac AP by increasing the velocity of the upstroke and ignoring the large hyperpolarisation at the end of the recovery phase. Over the next two years, Aliev-Panfilov [50] modified their model to obtain a more realistic restitution period to study the re-entry.

In 1998, Fenton and Karma [51] developed a simple ionic model of ventricular AP which contains 3 variables: the membrane potential and two gating variables. This model consisted of three major transmembrane currents which correspond to the activation, inactivation and reactivation dynamics of the sodium I_{Na} , potassium I_K and calcium currents I_{Ca} . In this model, arbitrary APD and conduction velocity restitution curves were reproduced properly but AP shapes particularly spike-and-dome morphologies were not formed. Subsequently, Fenton in 1999 [52] modified this model by adding a fourth variable to the model. Following these studies, Bueno-Orovio et al. in 2008 [40] developed a minimal ventricle model with four variables that summarized inward and outward currents, together with a parameter set to reproduces the AP shapes and restitution of epicardial, mid-myocardial, and endocardial cells in the human left ventricle.

2.8.3 Bidomain and monodomain tissue models

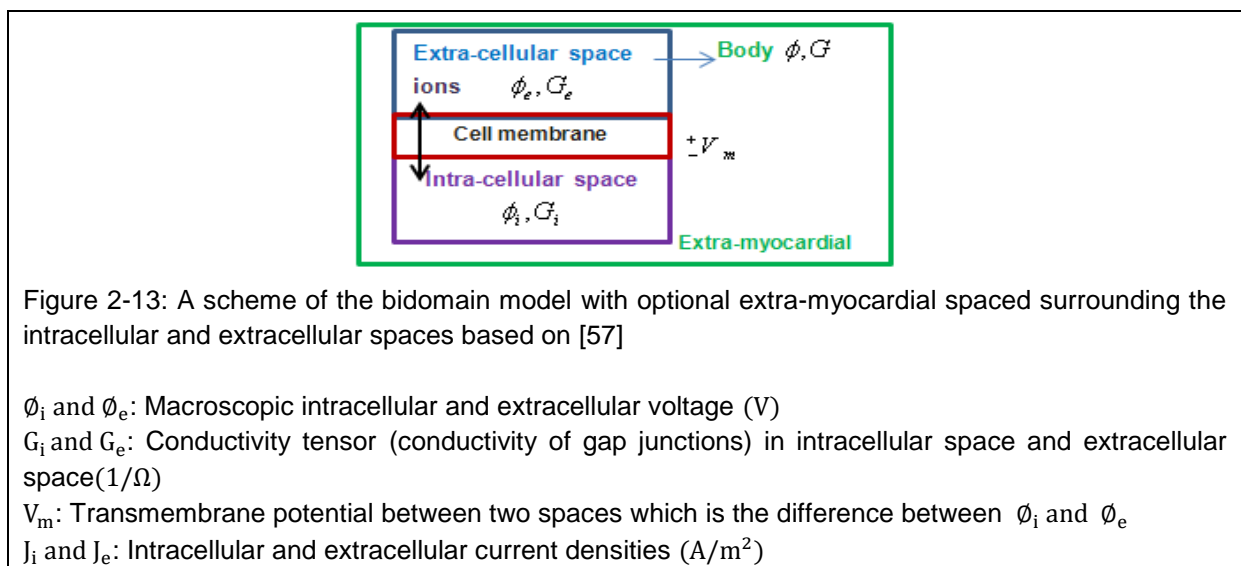
Basically, cardiac tissue consists of discrete cellular structure but the electrical behaviour of the tissue is generally modelled with a continuum approach that averages the electrical properties over a length scale larger than that of single cells. Continuum approximation of cardiac tissue, has been supported by experimental studies [53, 54]. Under normal

condition, intercellular channels couple each cell to its adjacent so that cardiac tissue behaves functionally as a syncytium at macroscopic scale.

The question is whether the continuum approximation of cardiac tissue is appropriate or not and at what point does it become inappropriate. From a macroscopic point of view, cardiac tissue can be modelled as a continuum based on the assumption of syncytial behaviour. Accordingly, intracellular space is continuous in the sense that moving ions from one cell to another do not require passing to the extracellular space [55]. But, at microscopic scales, the intracellular region of a cardiac cell is connected with the intracellular space of the neighbouring cells by low resistance gap junctions. In this sense, distribution of electrical potential is not continuous [55].

By conceptually dividing cardiac tissue into extracellular and intracellular spaces, a mathematical model can be constructed which describes AP propagation in the tissue. To model cardiac tissue with two domains that can represent cardiac cells with the space surrounding them, a bidomain model is used that models cardiac tissue as a syncytium composed of intracellular and extracellular spaces. This model assumed that both extracellular and intracellular spaces are overlapping and continuous, but separated by the cell membrane [39]. This model was first formulated by Tung in 1978 [56] and reviewed by many researchers (i.e. Pullan et al. [57]).

Figure 2-13 shows a scheme of a bidomain model in which intracellular and the extracellular domains are separated by a cell membrane and represents the regions inside the cells and the space between the cells.



To model cardiac tissue with bidomain model, three physiological processes are involved [58]:

- (1) Distribution of electrical potential to describe each space

The intracellular and extracellular current densities are described based on ohm's law in which electrical field, E is expressed as the gradient of a scalar potential field, ϕ . In addition, the resistance to intercellular and interstitial current flow (depends on the geometry of each region) is usually homogenized to have uniform continuous properties. Moreover, a conductivity tensor is assigned at each point to represent the local fibre orientation in both spaces with unequal anisotropy ratio. The two current densities are described by [39]:

$$J_i = \frac{1}{R_i} E_i = G_i \cdot E_i = G_i (-\nabla \phi_i)$$

$$J_e = \frac{1}{R_e} E_e = G_e \cdot E_e = G_e (-\nabla \phi_e)$$

R_i : Intercellular resistivity with unit of Ω

E : Electric field strength ($\frac{V}{m}$)

∇ : Gradient operator consists of spatial derivatives

(2) The conservation of charge and current to describe divergence equations [39]

$$\nabla \cdot J_i = -I_m$$

J_i : Intracellular current densities (A/m^2)

$$\nabla \cdot J_e = I_m$$

J_e : Extracellular current densities (A/m^2)

$$\nabla \cdot (J_i + J_e) = 0$$

(3) Current flow

$$I_m = S_v \left(C_m \frac{dV_m}{dt} + i_{ion} \right)$$

I_m : The current flows across the cell membrane (A/cm^3)

S_v : The cell membrane surface area to tissue volume ratio between the domains ($\frac{1}{cm}$)

i_{ion} : Total transmembrane current (A/cm^3)

C_m : The space membrane capacitance per unit area ($\mu F/cm^2$)

The bidomain equations are obtained based the equations that described three physiological processes. This model represents an anisotropic continuous approximation of 2D cardiac sheet with both intracellular and extracellular spaces, if the boundary conditions Γ are satisfied.

$$\Gamma: n \cdot (G_i \nabla \phi_i) = n \cdot (G_i \nabla (\phi_e + V_m)) = 0$$

Equation 2-1

$$\Gamma: n \cdot (G_e \nabla \phi_e) = 0$$

Equation 2-2

$$\nabla \cdot G_i (\nabla V_m + \nabla \phi_e) = S_v (C_m \frac{\partial V_m}{\partial t} + i_{ion})$$

Equation 2-3

$$\nabla \cdot ((G_i + G_e) \nabla \phi_e) = -\nabla \cdot (G_i \nabla V_m)$$

Equation 2-4

Note: No current flows from extracellular space to the adjacent spaces homogenous Neumann boundary conditions

n : (outward) unit vector normal to the boundary

The monodomain model [39] can be obtained from the bidomain model to describe current flow only in intracellular domain assuming that the conductivity in the extracellular domain is proportional to the conductivity in the intracellular domain:

$$G_e = \lambda G_i$$

Equation 2-5

λ : Ratio between intracellular and extracellular spaces

Substituting the Equation 2-5 into the bidomain Equation 2-4 gives:

$$\nabla \cdot (G_i \nabla \phi_e) = -\frac{1}{1+\lambda} \nabla \cdot (G_i \nabla V_m) \quad \text{Equation 2-6}$$

And substituting Equation 2-6 in bidomain Equations 2-3 gives:

$$\nabla \cdot \left(\frac{\lambda}{1+\lambda} G_i \nabla V_m \right) = S_v \left(C_m \frac{\partial V_m}{\partial t} + i_{ion} \right) \quad \text{Equation 2-7}$$

By introducing an effective conductivity $G = \frac{\lambda}{1+\lambda} G_i$, and diffusion tensor $D_i = \frac{1}{S_v C_m R_i}$ with unit of ($\text{cm}^2/\mu\text{s}$), and the assumption of no flux boundary condition $n \cdot (G \nabla V_m) = 0$, the monodomain equation [57] is obtained:

$$\frac{\partial V_m}{\partial t} = \nabla \cdot (D_i \nabla V_m) - \frac{i_{ion}}{C_m} = D_i \left(\frac{\partial^2 V_m}{\partial x^2} + \frac{\partial^2 V_m}{\partial y^2} \right) - \frac{i_{ion}}{C_m} \quad \text{Equation 2-8}$$

$-\frac{\partial V_m}{\partial t}$: Corresponds to depolarization or increasing V_m , resulted from $-i_{ions}$ which represent an inward flow of +ions into the cell membrane

$+\frac{\partial V_m}{\partial t}$: Corresponds to repolarization or decreasing V_m , resulted from $+i_{ions}$ which represent an outward flow of +ions out of the cell membrane

Note: The currents which cross a membrane from extracellular to intracellular domain are called inward currents and the reverse is called outward currents.

This thesis used the monodomain model to simulate AP propagation in ventricular tissues.

2.9 Modelling of restitution and dispersion in repolarization time

After describing a history of cardiac models, this section introduces modelling of restitution and dispersion in repolarization time to emphasize the requirement for clinical diagnostic tools that can assist doctors to identify patients at arrhythmia risk.

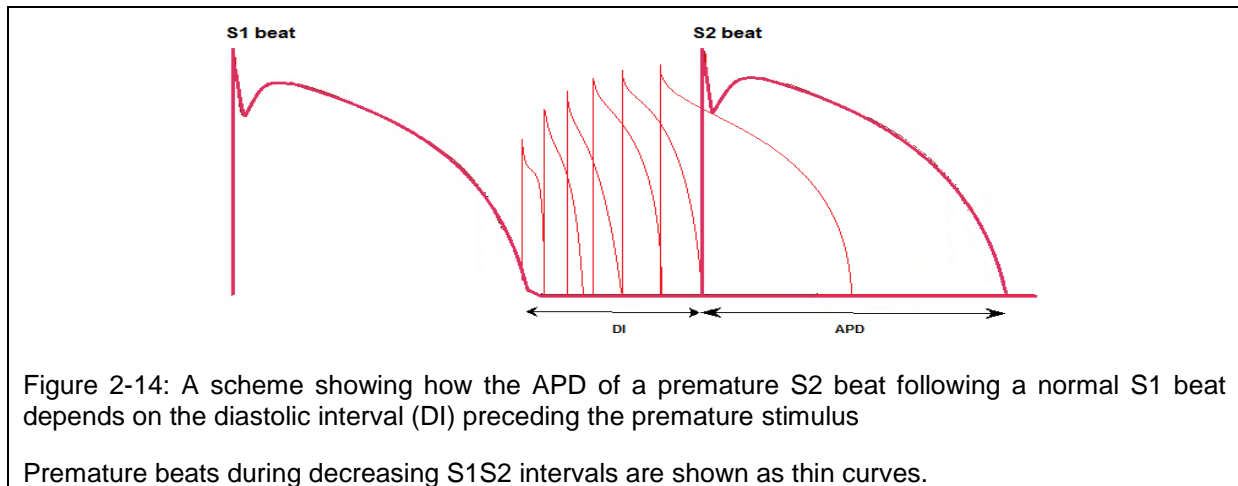
2.9.1 Restitution

Since the 1950s, many studies has focused on the dynamic modulation of APD following an abrupt change in the preceding diastolic intervals [59]. In the mammalian ventricular muscle, both APD and contractility vary with the preceding stimulus interval. Both are decreased in premature beats and increased for long stimulus interval. These phenomena termed as

- electrical restitution in 1958 [60];
- mechanical restitution in 1975a [61] and 1975b [62].

These restitutions represent recovery of membrane conductance [59, 63] and restoration of calcium into the myoplasm [64, 65]. Pidgeon et al. in 1982 [66] studied the time course of mechanical restitution in the human heart and then Franz et al. in 1983 [67] studied the time course of electrical restitution and its relation to the mechanical restitution in the human heart. It was shown that both electrical and mechanical restitution occur after AP repolarization, i.e. as a function of the electrical diastolic interval preceding a beat [67].

When the heart beats at a faster rate than normal, the cardiac systole and diastole are adjusted for efficient pumping of chambers (i.e. filling and ejection of blood). If for any reason the systole duration did not change, the diastole duration may decrease disproportionately. It is important to know that at high frequencies ventricular filling does not occur before contracting. In the meantime, if a next AP is initiated sooner after the first AP (when not all ionic processes have recovered fully to their rest states), the second APD is shorter than the first one. Figure 2-14 shows an example of a normal stimulus (S1) beat and a train of premature stimulus (S2) beats with shorter APD than the normal S1 beat.



The S1S2 protocol is usually used to stimulate a sequence of normal and premature beats during decreasing S1S2 intervals (difference between indices of AP upstroke of normal S1 beats and premature S2 beats). Pacing the tissue assigns APD restitution to individual ventricular cell in inner, middle, and outer regions of tissue.

It follows that an APD is not a unique function of the previous diastolic interval and is influenced by the excitation history [68]. In addition, when a sequence of propagating pulses are produced, the influence of the preceding pulse on the subsequent one is reflected not only in its APD but also in its speed of propagation [68]. For a premature S2 beat, when the diastolic interval vary, both APD and conduction velocity usually decrease with decreasing diastolic interval. Basically,

- APD restitution represents kinetics of recovery from inactivation of calcium channels and deactivation of potassium channels while the sodium channel has effects only at short diastolic interval.
- Conduction velocity restitution represents the recovery kinetics of sodium channels at short diastolic intervals.

APD and conduction velocity restitutions are two important determinants for the stability of re-entrant arrhythmias [69-73]. In addition, systematically analysed global repolarization data from the human right and left ventricles using noncontact mapping showed that under physiological conditions, conduction velocity restitution may be an important factor that maintains electrical stability despite heterogeneity of APD restitution [74]. This study suggested that global APD and conduction velocity restitution can be determined in the clinical setting [74]. For example, modification of APD and conduction velocity restitution characteristics may prevent spiral wave to break in simulated cardiac tissue, suggesting that drugs with similar effects in real cardiac tissue may prevent tachycardia from degenerating to fibrillation [74] in animals.

2.9.2 Dispersion in activation time and repolarization time

The other recent focus has been dispersion in activation and repolarization time across left ventricular wall. Difference in the activation time (indices of AP upstroke during propagation) in different regions of the ventricles is often called dispersion in the activation time. Difference in repolarization time (i.e. indices of AP downstroke during rapid final repolarization) in different regions of the heart is called dispersion in repolarization time. Dispersion in APD and repolarization time may be found between base and apex, the anterior and posterior side of the ventricles, right and left ventricles, and from epicardium to endocardium in the left ventricular free wall, de Bakker et al. 2002 [75].

Experimental studies in canine myocardium by Burgess et al. [76], human [77-79], and swine and human hearts [80] have shown that when ventricular activation propagates, APDs decrease and this inverse relationship may act as a protective mechanism at a basic cycle length (i.e. from 1000 to 600 ms) that can reduce dispersion in repolarization time. These studies are usually limited to (1) one region of the ventricles without considering regional differences in intrinsic electrophysiological properties; (2) some S1S2 intervals; and (3) patients with different pathophysiology. Table 2-2 provides a number of researches that have shown variable in vivo dispersion in repolarization time in human diseased hearts.

Researchers	Years	Regions of the ventricles
Franz et al. [77]	1987	Left ventricular epicardium
Cowan et al. [81]	1988	Left ventricular epicardium
Yuan [80]	2001	Left ventricular endocardium
Yue et al. [78]	2005	Left and right ventricles
Chauhan et al. [79]	2006	Along left ventricular epicardium and right ventricular endocardium
Hanson et al. [27]	2009	Left ventricular endocardium

Table 2-2: Studies of dispersion in APD and repolarization in human hearts

Understanding the sequence of ventricular repolarization is important, because any abnormality in AP repolarization and large dispersion in repolarization time may lead to lead to arrhythmia [82, 83].

Following the previous studies, the motivation of this thesis was to providing a guideline for estimating arrhythmia risk by understanding dispersion in activation time, repolarization time, and APD for both normal and premature S2 beats during progressively decreasing S1S2 intervals.

2.10 Challenging issues in modelling cardiac tissue

Not surprisingly, insufficient current knowledge about the human heart has led to many controversies in modelling cardiac tissue. Some important issues that are relevant to this thesis are illustrated in the following sections.

2.10.1 Tissue structure

From a general point of view, normal ventricular myocardium behaves as a functional syncytium in which side-to-side electrical coupling between neighbours is uniform as suggested by Streeter et al. in 1969 [32] (supporting AP depolarization and AP repolarization propagation in studies by Saffitz in 1994 [84] in canine ventricular myocardium and by Kleber et al. in 2004 [85] in the canine and human atrial trabecular). In this sense, it is assumed that electrical properties of ventricular myocardium of free wall are axially anisotropic with maximum velocity in the myofiber direction and in plane transverse to it [84, 85].

Saffitz et al. [84] and Luke et al. [86] showed that on average, a single ventricular myocyte is connected to about 11 neighbours via gap junctions, (about half to side-to-side and half to end-to-end orientation) in 3D reconstructions of the canine ventricular myocardium. They categorized cell-to-cell connections according to the degree of side-to-side and end-to-end orientations. This pattern of intercellular connections suggests a uniform sheet of ventricular myocardium in which cardiac activation wave propagates in both longitudinal and transverse direction, Saffitz in 2005 [87].

On the contrary to the functional syncytium, studies on the discontinuities in the ventricular wall suggest that the intramural architecture of myocardial fibres is laminar. An animal study by LeGrice et al. [88] in canine ventricular myocardium showed that syncytial myocardium is not true opposite to the study by Streeter et al. [32] who suggested a true syncytial myocardium. The laminar organization involves branching and discontinuous sheets that contains the fibre structure, and may be regionally different within the ventricular wall.

According to the concept of laminar structure that initially reported in the canine left ventricle [88], 3D muscle fibres forms a helical pattern and are arranged in sheet bundles. The term sheet is used to describe the planar feature of the myocardial wall. In dogs, the myocardial sheets lie radial to the ventricular surfaces, and tangential to the epicardial surface. In tangential sections, the plane of the laminae coincides with local fibre orientation. Figure 2-15 shows a view of macroscopic arrangement of sheets that are forming roughly 4 to 6 cells thick and separated by the gaps between the sheets called cleavage planes. These sheets create a laminar structure of the fibres oriented transversally to the heart wall, running radially from epicardial to endocardial region within the ventricular wall.

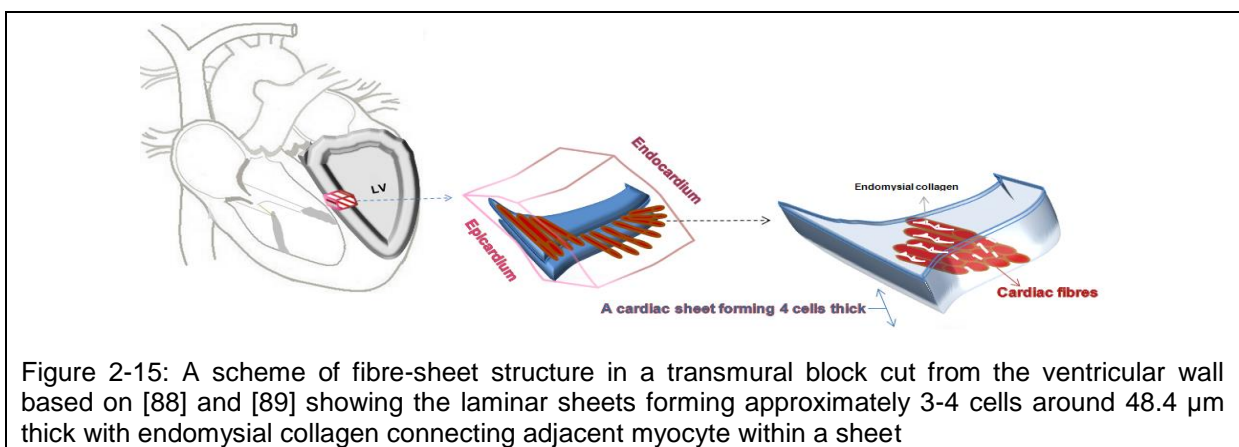


Figure 2-15: A scheme of fibre-sheet structure in a transmural block cut from the ventricular wall based on [88] and [89] showing the laminar sheets forming approximately 3-4 cells around 48.4 μm thick with endomyxial collagen connecting adjacent myocyte within a sheet

The concept of laminar structure in the left ventricular of mammal's heart has been developing since 1990s i.e. in the anatomical study by LeGrice et al. [90] and microscopic [90, 91], and macroscopic studies by Hort [92]. It has been supported by using cardiac models based on mechanical function [93], the magnetic resonance diffusion-tensor imaging (MRI-DT) study [94], and in vivo 3D diffusion tensor imaging [95]. Laminar structure still have not been verified experimentally in the human ventricles however, it has been accepted in the human heart by Anderson et al. [96] based on a histological study.

Furthermore, according to anatomical knowledge of Lunkenheimer et al. [97], the concept of laminar structure is deficient in detail when set against the known variability in the overall alignment of the fascicles of myocardial fibres. In addition, it is incompatible with the evidence concerning global ventricular structure.

All ventricular tissues simulated in this study were based on functional syncytium [32].

2.10.2 Linear or non-linear change in fibre orientation

Physically, the left ventricle has directional and twisting sequential motions during emptying and filling of the beating heart. The term fibre denotes a continuous axial sequence of individual human ventricular cells [98]. The term fibre orientation is used to denote the changes in shapes of ventricular chambers and movement of specific points of the ventricular wall [99]. In the ventricular wall across species, a local fibre orientation can be defined along the principal axis of the myocyte that smoothly rotate between endocardium and epicardium. For more than a century, there have been anatomical and histological studies which support regional variations in fibre arrangement in the form of (1) longitudinal myocardial fibres; (2) fibres spiralling clockwise or counter clockwise; and (3) circular fibres within the ventricular mass in both human ventricles. Table 2-3 summarized a number of important studies on the fibre orientation in mammals and human hearts.

Researchers	Concepts/assumptions	The heart
Pettigrew [100, 101]	The concept of the two populations of fibres: longitudinal and circular fibres within the left ventricular walls	Sheep
Rushmer et al. [99] (functional point of view)	Two sets of myocardial bundles for the ventricles: First, the spiral muscle (initially noted by Ludwig [99]) which forms the internal and external investment spiralling in the opposite direction (clockwise or counter-clockwise). Second, the middle circular layer behaves as a constrictor, lies between the inner and outer layers of the ventricular myocardium.	Dogs
Streeter et al. [32] Histological study	The concept of syncytial myocardium based on visual inspection of myofiber orientation in the left ventricular wall	Dogs
Streeter [31]	The uniform arrangement of fibres throughout the various regions of the ventricular wall: the myocardial fibres were aligned parallel to the epicardium, with only a minor proportion of the fibres extending in transmural direction.	Dogs
Greenbaum et al. [33] (anatomical study unlike the studies by Streeter et al. [33])	The longitudinal myocardial fibres in sub-endocardium and sub-epicardium of the left ventricular wall run parallel to the equatorial plane in the ventricles with different angle when measured on a radial axis	Human
Hunter et al. [102]	Smooth transmural variation in fibre angle up to 180°	Pigs, dogs, and human
Anderson et al. [96] Histological study	Anatomical arrangement of myocardial cells making up ventricular mass, but they rejected the anatomical concept of a unique ventricular myocardial band	Human

Table 2-3: Historical review of studies for tissue and fibre structure

There is evidence that myocardial fibre orientation is uniform between and within species based on the histological study [103], the optical study [104], and a study using magnetic resonance imaging [105]. However, cardiac sheet structure may be different within species [105]. Fibre orientation, has been confirmed using optical techniques [106] and diffusion tensor magnetic resonance imaging [107]. But the linearity or non-linearity of fibre rotation within the ventricular wall is still not clear. For example,

- Streeter and Nielsen et al. [31, 108] suggested the smooth rotation of cardiac fibres from endocardial to epicardial region in the ventricular wall;
- Streeter-Bassett [30] and Vetter et al. [109] showed the non-linear change in fibre rotation in the swine right ventricle.

Accordingly, 3D simulations of this thesis were based on geometrical fibre models with a linear and a non-linear change in fibre orientation.

2.10.3 Mid-myocardial cells

Cardiac tissue has different types of heterogeneities. Some studies indicate the presence of different cell types within the ventricular wall showing different dynamic properties [38, 110-112] and heterogeneity due to structural components i.e. regional distribution of gap junctions in human ventricles [113-116].

From the definition proposed in the early 1990s, mid-myocardial cells are distinguished from other ventricular cell types due to the ability of their APD to prolong prominently at slow pacing rate and or exposure to a drug that prolong APD [117]. The position of mid-myocardial cells within the ventricular wall is not fixed, as suggested by Antzelevitch et al. [26]. Mid-myocardial cells with the longest APD, appears to shift from the deep sub-endocardium to the deep sub-epicardium as one move from the anterior wall to the lateral and posterior wall of the left ventricle in the canine heart. These regions might be (1) in the deep sub-endocardium to mid-myocardium in the anterior wall of the canine left ventricular wedge preparation [111]; (2) throughout the wall in the region of the canine right ventricle [117, 118]; and (3) in the deep cell layers of endocardial structures, including papillary muscles, trabeculae, and the interventricular septum in the canine left ventricular free wall [119], and in the anterior wall of the canine left ventricular wedge preparation [120]. However, the involvement of mid-myocardial cells in transmural ventricular activation and repolarization is still not clear for the human heart.

- Evidences of presence of mid-myocardial cells

For the human heart, the evidence of mid-myocardial cells was supported by Drouin in 1995 and 1998 [29, 121], and Pereon in 2000 [122] in the left ventricular wall using standard microelectrode techniques and in the right ventricle based on enzymatically dissociated cells from normal and failing human heart by Li et al. [123].

Furthermore, Glukhov et al. [124] in 2010 used optical mapping technique to record AP in the coronary-perfused left ventricular wedge preparation isolated from normal and failing human heart. They found mid-myocardial cells clustering in an isolated island (rather than forming a contiguous layer) in 60% of non-failing ventricular wedge preparations and no evidence of mid-myocardial cells in failing human hearts [124]. It is important to note that Glukhov et al. [124] data were based on left ventricle wedges without prominent scar and fibrosis (i.e. structural remodelling as a factor that may contribute to increase in dispersion of repolarization in failing heart).

- No mid-myocardial cells

On the other hand, some studies identified no mid-myocardial cells in the left ventricular free wall in guinea pig [125] or any significant transmural heterogeneity of repolarization in the human study by Taggart et al. [25]. This may be due to the electrotonic cancellation effect by intercellular coupling through gap junctions [126, 127], experimental artefact [26], or the plunge electrode technique that cannot probe the deep area in the left ventricular wall [25, 26]. The other possible explanation might be the regional variation in left ventricular structure i.e. fibre orientation during systolic and diastolic phases of the cardiac cycle. Therefore, due to the limitations of conventional recording techniques, dynamic changes in cardiac repolarization and the role of mid-myocardial cells in heterogeneity of repolarization within the ventricular wall are continues topics [128].

2.10.4 Sharp or gradual increase in spatial APD profiles

Experimental and simulation studies in the human and animals have created AP shapes with or without notch or spike-and-dome appearance due to describing different gate variables, transmembrane voltage and ionic concentrations, and ion currents. For example, a prominent notch in the AP shape in the canine ventricular epicardial and mid-myocardial regions and no prominent notch in the ventricular endocardial regions was created, mainly due to the greater transient outward potassium current in the epicardial and mid-myocardial regions and smaller one in endocardial region, as suggested by Antzelevitch in 2001 [26].

In the human heart [129], a clear notch was only observed in the AP of sub-epicardial myocytes isolated from the left ventricle suggesting the presence of a prominent transient potassium outward current. In 1995 and 1998, a prominent notch for human AP of mid-myocardial cells did not observed by Drouin et al. [29, 121] and Li et al. [123].

Furthermore, there are evidences of sharp and gradual increase in APD between regions of different cell types in left ventricular tissue. For example,

- in the human heart, Taggart et al. [126] observed gradual increase in APD in transmural direction of the left ventricle;
- in the canine heart, there is evidence of a sharp increase in APD between the epicardium and sub-epicardium in arterially perfused canine left ventricular wedge preparations in the study by Yan et al. [111] and between mid-myocardium and sub-epicardium in intact canine heart preparations in the study by Poelzing et al. [130].

2.11 Summary

The heart is a rhythmic electromechanical pump, where electrical activation initiates and synchronizes contraction. The electrical excitation of the cardiac cells through the process of excitation-contraction coupling leads to a series of events which results in cardiac contraction and generation of many heart-beats. Fundamentally, cardiac excitation is the result of the interplay between membrane dynamic process and structural properties of the cardiac tissue. Cardiac cells communicate electrically through gap junctions to facilitate propagation of AP within tissue. The cardiac tissue is where the electrical and mechanical activity occurs. Not surprisingly, ventricular tissue structure with different heterogeneity and spatial arrangement of the myocardial fibres influence AP activation and repolarization time.

This thesis concentrated on measures of dispersion in repolarization time in tissues simulated with different structure that are described next.

2.12 References

1. Marieb EN., Human anatomy and physiology. 6 ed. 2004: Pearson Benjamin Cummings.
2. Agur AMR and Dalley AF, Grant's atlas of anatomy. 12 ed. 2009: Lippincott Williams & Wilkins.
3. Wiggers CJ, Physiology in health and disease. 5 ed. 1949: Lea & Febiger.
4. Randall DC and El-Wazir YM, ECG Interpretation. 2004: Hayes Barton Press.
5. The Internet encyclopedia of science Available from: <http://www.daviddarling.info/encyclopedia/H/heart.html>.
6. Zipes J, Cardiac electrophysiology from cell to bedside. 4 ed. 2004: Saunders.
7. Kusumoto FM, Cardiovascular Pathophysiology. 2004: Hayes Barton Press.
8. Malmivuo J and Plonsey R, Bioelectromagnetism: principles and applications of bioelectric and biomagnetic fields. 1995: Oxford University Press.
9. Opthof T, In vivo dispersion in repolarization and arrhythmias in the human heart. Am J Physiol Heart Circ Physiol, 2006. **290**: p. h77-h78.

10. Keener JP and Sneyd J, *Mathematical Physiology*. 1998, Berlin: Springer, New York, Heidelberg.
11. The World Health Organization (WHO). Available from: www.e-heart.org.
12. Cardiac Muscle. Available from: http://www.mhhe.com/biosci/ap/histology_mh/strimusc.html#cardiac.
13. Leonard VC., *An Introduction to Human Disease: Pathology and Pathophysiology Correlations*. 2009: Jones & Bartlett Learning.
14. World Health Organization (WHO). Available from: <http://www.who.int/mediacentre/factsheets/fs310/en/index2.html>.
15. Garfinkel and Chen and Walter and Karagueuzian and Kogan and Evans and Karpoukhin and Hwang and Uchida and Gotoh and Nwasokwa and Sager and Weiss, Quasiperiodicity and chaos in cardiac fibrillation. *J Clin Invest*, 1997. **15**: p. 305–314.
16. Haws CW and Lux RL., Correlation between in vivo transmembrane action potential durations and activation-recovery intervals from electrograms: effects of interventions that alter repolarization time. *Circulation Research*, 1990. **81**: p. 281–288.
17. Steinhaus BM., Estimating cardiac transmembrane activation and recovery times from unipolar and bipolar extracellular electrograms: a simulation study. *Circ Res*, 1989. **64**: p. 449–462.
18. Franz MR., Method and theory of monophasic action potential recording. *Prog Cardiovasc Dis*, 1991. **33**: p. 347–368.
19. Efimov IR and Huang DT and Rendt JM and Salama G., Optical mapping of repolarization and refractoriness from intact hearts. *Circulation*, 1994. **90**: p. 1469–1480.
20. Witkowski FX and Leon LJ and Penkoske PA and Clark RB and Spano ML and Ditto WL and Giles WR., A method for visualization of ventricular fibrillation: Design of a cooled fiberoptically coupled image intensified CCD data acquisition system incorporating wavelet shrinkage based adaptive filtering. *Chaos*, 1998. **1**: p. 94-102.
21. Efimov IR and Nikolski VP and Salama G, Optical Imaging of the Heart. *Circulation Research* 2004(95): p. 21-33.
22. Spach MS and Dolber PC, Relating extracellular potentials and their derivatives to anisotropic propagation at a microscopic level in human cardiac muscle. Evidence for electrical uncoupling of side-to-side fiber connections with increasing age. *Circ Res*, 1986. **58**.
23. Punske BB and Ni Q and Lux RL and MacLeod RS and Ershler PR and Dustman TJ and Allison MJ and Taccardi B., Spatial methods of epicardial activation time determination in normal hearts. *Biomedical Engineering*, 2003. **31**: p. 781-792.
24. Scacchi S and Franzone PC and Pavarino LF and Taccardi B, A reliability analysis of cardiac repolarization time markers. *Math Biosci*, 2009: p. 113-128.
25. Taggart P and Sutton PM and Opthof T and Coronel R and Trimlett R and Pugsley W and Kallis P, Transmural repolarisation in the left ventricle in humans during normoxia and ischaemia. *Cardiovasc Res*, 2001. **50**: p. 454–462.
26. Antzelevitch C., Transmural dispersion of repolarization and the T wave. *Cardiovasc Res.*, 2001. **50**: p. 426-431.
27. Hanson B and Sutton P and Elameri N and Gray M and Critchley H and Gill JS and Taggart P., Interaction of Activation–Repolarization Coupling and Restitution Properties in Humans. *Circulation: Arrhythmia and Electrophysiology*, 2009. **2**: p. 162-170.
28. Durrer D and van Dam RT and Freud GE and Janse MJ and Meijler FL and Arzbacher RC, Total excitation of the isolated human heart. *Circulation*, 1970. **41**.
29. Drouin E and Lande G and Charpentier F, Amiodarone reduces transmural heterogeneity of repolarization in the human heart. *J Am Coll Cardiol*, 1998. **32**: p. 1063-1067.
30. Streeter DDJ and Bassett DL, An Engineering Analysis of Myocardial Fiber Orientation in Pig's Left Ventricle in Systole. *Anat Rec*, 1966. **155**: p. 503–511.
31. Streeter DDJ, Gross morphology and fiber geometry of the heart, in *Handbook of Physiology. The Cardiovascular System*, Berne RM and Sperelakis N and Greger SR, Editor. 1979, Baltimore, Maryland, Williams & Wilkins Co.
32. Streeter DDJ and Spotnitz HM and Patel DP and Ross JJ and Sonnenblick EH, Fiber orientation in the canine left ventricle during diastole and systole. *Circulation Research*, 1969. **24**: p. 339–347.
33. Greenbaum RA and Ho SY and Gibson DG and Becker AE and Anderson RH, Left ventricular fibre architecture in man. *Br Heart J* 1981. **45**: p. 248-263.
34. Colli Franzone P and Pavarino L and Taccardi B, Simulating patterns of excitation, repolarization and action potential duration with cardiac Bidomain and Monodomain models. *Mathematical Biosciences*, 2005. **197**: p. 35-66.

35. Colli Franzone P and Pavarino LF and Taccardi B, Effects of transmural heterogeneity and electrotonic interactions on the dispersion of cardiac repolarization and action potential duration: a simulation study. *Math Biosci*, 2006. **204**: p. 132–165.
36. Colli Franzone P and Pavarino LF and Scacchi S and Taccardi B, Modeling ventricular repolarization: Effects of transmural and apex-to-base heterogeneities in action potential durations. *Math Biosci*, 2008. **214**: p. 140-152.
37. Luo CH and Rudy Y., A Model of the ventricular cardiac action potential: depolarisation, repolarisation and their Interaction. *Circulation Research*, 1991. **68**: p. 1501-1526.
38. Antzelevitch C and Fish J, Electrical heterogeneity within the ventricular wall. *Basic Res. Card.*, 2001. **96**: p. 517–527.
39. Clayton RH and Bernus O and Cherry EM and Dierckx H and Fenton FH and Mirabella L and Panfilov AV and Sachse FB and Seemann G and Zhang H., Models of cardiac tissue electrophysiology: Progress, challenges and open questions. *Progress in Biophysics and Molecular Biology*, 2010. **104**: p. 22-48.
40. Bueno-Orovio A and Cherry EM and Fenton FH, Minimal model for human ventricular action potentials in tissue. *Journal of Theoretical Biology*, 2008. **235**: p. 544-560.
41. Van der Pol B and Van der Mark J, The heartbeat considered as a relaxation oscillation and an electrical model of the heart. *The London, Edinburgh and Dublin Physiological Magazine and Journal of Science*, 1928. **6**: p. 763-775.
42. Hodgkin AL and Huxley AF, A quantitative description of membrane current and its application to conduction and excitation in nerve. *Journal of Physiology*, 1952. **119**: p. 500-544.
43. ten Tusscher KH and Panfilov AV, Alternans and spiral breakup in a human ventricular tissue model. *Am J Physiol Heart Circ Physiol*, 2006. **291**: p. H1088–H1100.
44. Noble D., A Modification of the Hodgkin-Huxley Equations Applicable to Purkinje Fibre Action and Pace-maker Potentials. *Journal of Physiology*, 1962. **160**: p. 317-352.
45. Beeler GW and Reuter H, Reconstruction of the action potential of ventricular myocardial fibres. *Journal of Physiology*, 1977. **268**: p. 177-210.
46. ten-Tusscher KH and Noble D and Noble PJ and Panfilov AV, A model for human ventricular tissue. *Am J Physiol*, 2004. **286**: p. H1573–H1589.
47. FitzHugh RA, Impulses and physiological states in theoretical models of nerve membrane. *Biophys J*, 1961. **1**: p. 445-466.
48. Nagumo J and Arimoto S and Yoshizawa S, An active pulse transmission line simulating nerve axon. *Proc Inst Radio Engineers*, 1962. **50**: p. 2061-2070.
49. Rogers JM and McCulloch AD, A collocation-Galerkin finite element model of cardiac action potential propagation. *IEEE Trans. Biomed. Eng*, 1994. **41**: p. 743-757.
50. Aliev RR and Panfilov AV, A simple two-variable model of cardiac excitation. *PubMed ID*, 1996. **7**: p. 293-301.
51. Fenton F and Karma A, Vortex dynamics in three-dimensional continuous myocardium with fiber rotation: Filament instability and fibrillation. *Chaos*, 1998. **20**.
52. Fenton F., Theoretical Investigation of Spiral and Scroll Wave Instabilities Underlying Cardiac Fibrillation. 1999, Northeastern University.
53. Weidmann S., Electrical constants of trabecular muscle from mammalian heart. *J physiol*, 1970. **210**: p. 1041-1054.
54. Chapman RA and Fry CH, An analysis of the cable properties of frog ventricular myocardium. *J physiol*, 1978. **283**: p. 263-282.
55. Misra JC., *Biomathematics: modelling and simulation*. 2006: World Scientific.
56. Tung L., A bidomain model for describing ischemic myocardial D.C. potentials. 1978, MIT: Cambridge.
57. Pullan AJ and Cheng LK and Buist ML, Mathematically modeling the electrical activity of the heart: from cell to body surface and back again. 2005: World scientific.
58. Henriquez CS., Simulating the electrical behavior of cardiac tissue using the bidomain model. *Crit Rev Biomed Eng*, 1993. **21**: p. 1–77.
59. Boyett MR and Jewell BR, A study of the factors responsible for rate-dependent shortening of the action potential in mammalian ventricular muscle. *J Physiol*, 1978. **285**: p. 359–380.
60. Braveny P and Kruta V, Dissociation de deux facteurs: restitution et potentiation dans l'action de l'intervalle sur l'amplitude de la contraction du myocarde. *Arch Intern Physiol Biochem*, 1958. **66**: p. 633-652.
61. Bass BG, Enhanced contractility during relaxation of cat papillary muscle. *Am J Physiol* 1975a. **228**: p. 1708-1716.
62. Bass BS, Restitution of the action potential in cat papillary muscle. *Am J Physiol*, 1975b. **228**: p. 1717-1724.

63. Trautwein W and McDonald TF and Tripathi O, Calcium conductance and tension in mammalian ventricular muscle. *Pfluegers Arch*, 1975. **534**: p. 55-74.
64. Fozzard HA and Gibbons WR, Action potential and contraction of heart muscle. *Am J Cardiol* 1973. **31**: p. 182-192.
65. Edman KAP and Johannsson M, The contractile state of rabbit papillary muscle in relation to stimulation frequency. *J Physiol(Lond)*, 1976. **254**: p. 565-581.
66. Pidgeon J and Miller GAH and Noble MIM and Papadoyannis D and Seed WA, The relationship between the strength of the human heart beat and the interval between beats. *Circulation*, 1982. **65**: p. 1404-1410.
67. Franz MR and Schaefer J and Schottler M and Seed WA and Noble MI, Electrical and mechanical restitution of the human heart at different rates of restitution. *Circulation*, 1983. **53**: p. 815-822.
68. Fenton FH and Cherry EM and Hastings HM and Evans SJ, Multiple mechanisms of spiral wave breakup in a model of cardiac electrical activity. *Chaos*, 2002. **12**: p. 852–892.
69. Cao J and Qu Z and Kim Y and Wu T and Garfinkel A and Weiss JN and Karagueuzian HS and Chen P., Spatiotemporal heterogeneity in the induction of ventricular fibrillation by rapid pacing, importance of cardiac restitution properties. *Circ Res*, 1999. **84**: p. 1318–1331.
70. Garfinkel A and Kim YH and Voroshilovsky O and Qu Z and Kil JR and Lee MH and Karagueuzian HS and Weiss JN and Chen PS, Preventing ventricular fibrillation by flattening cardiac restitution. *Proc Natl Acad Sci USA*, 2000. **97**: p. 6061–6066.
71. Karma A., Electrical alternans and spiral wave breakup in cardiac tissue. *Chaos*, 1994. **4**: p. 461–472.
72. Qu Z and Weiss JN and Garfinkel A, Cardiac electrical restitution properties and stability of re-entrant spiral waves: a simulation study. *Am J Physiol Heart Circ Physiol*, 1999. **276**: p. H269–H283.
73. Watanabe MA and Fenton FH and Evans SJ and Hastings HM and Karma A, Mechanism for discordant alternans. *J Cardiovasc Electrophysiol*, 2001. **12**: p. 196-206.
74. Yue AM and Franz MR and Roberts PR and Morgan JM, Global endocardial electrical restitution in human right and left ventricles determined by noncontact mapping. *J Am Coll Cardiol*, 2005. **46**.
75. de Bakker JMT and Tobias O, Is the Apico-basal Gradient Larger Than the Transmural Gradient? *Journal of Cardiovascular Pharmacology*, 2002. **39**: p. 328-331.
76. Burgess MJ and Steinhaus BM and Spitzer KW and Green LS., Effects of activation sequence on ventricular refractory periods of ischemic canine myocardium. *J Electrocardiology*, 1985. **18**: p. 323–329.
77. Franz MR and Bargheer K and Rafflenbeul W and Haverich A and Lichtlen PL, Monophasic action potential mapping in human subjects with normal electrocardiograms: direct evidence for the genesis of the T wave. *Circulation*, 1987. **75**: p. 379-386.
78. Yue AM and Betts TR and Roberts PR and Morgan JM, Global dynamic coupling of activation and repolarization in the human ventricle. *Circulation*, 2005. **112**: p. 2592–2601.
79. Chauhan VS and Downar E and Nanthakumar k and Parker JD and Ross HJ and Chan W and Picton P., Increased ventricular repolarization heterogeneity in patients with ventricular arrhythmia vulnerability and cardiomyopathy: a human in vivo study. *Am J Physiol Heart Circ Physiol*, 2006. **290**: p. H79-H86.
80. Yuan S and Kongstad O and Hertvig E and Holm M and Grins E and Olsson B, Global repolarization sequence of the ventricular endocardium: monophasic action potential mapping in swine and humans. *Pacing Clin Electrophysiol*, 2001. **24**: p. 1479–1488.
81. Cowan JC and Hilton CJ and Griffiths CJ and Tansuphaswadikul S and Bourke JP and Murray A and Campbell RWF, Sequence of epicardial repolarisation and configuration of the T wave. *Eur Heart J*, 1988. **60**: p. 424–433.
82. Ghanem RN and Burnes JE and Waldo AL and Rudy Y, Imaging dispersion of myocardial repolarization, II: noninvasive reconstruction of epicardial measures. *Circulation*, 2001. **104**: p. 1306–1312.
83. Burgess MJ and Green LS and Millar K and Wyatt R and Abildskov JA, The sequence of normal ventricular recovery. *Am Heart J*, 1972. **84**: p. 669–678.
84. Saffitz JE and Kanter HL and Green KG and Tolley TK and Beyer EC, Tissue-specific determinants of anisotropic conduction velocity in canine atrial and ventricular myocardium. *Circulation Research*, 1994. **74**.
85. Kleber AG and Rudy Y, Basic mechanisms of cardiac impulse propagation and associated arrhythmias. *Physiological Reviews*, 2004. **84**: p. 431-488.
86. Luke RA and Saffitz JE, Remodeling of ventricular conduction pathways in healed canine infarct border zones. *J Clin Invest* 1991. **87**: p. 1594–1602.

87. Saffitz JE, The pathology of sudden cardiac death in patients with ischemic heart disease arrhythmology for anatomic pathologists. *Cardiovasc Pathol*, 2005. **14**: p. 195-203.
88. LeGrice IJ and Smaill BH and Chai LZ and Edgar SG and Gavin JB and Hunter PJ, Laminar structure of the heart: ventricular myocyte arrangement and connective tissue architecture in the dog. *Am J Physiology.*, 1995. **269**: p. H571-H582.
89. Smaill BH and LeGrice IJ and Hooks DA and Pullan AJ and Caldwell BJ and Hunter PJ, Cardiac structure and electrical activation: Models and measurement. *Proceedings of the Australian Physiological and Pharmacological Society*, 2004. **34**: p. 141-149.
90. Hort W, Micrometric examination of guinea pig hearts of different width. *Verh Dtsch Ges Kreislaufforsch* 1957a. **23**: p. 343-346.
91. Hort W, Research on muscle fiber dilation and the structure of the right heart chamber wall in a guinea pig. *Virchows Archiv*, 1957b. **329**: p. 694-731.
92. Hort W, Macroscopic and micrometric research on the myocardium of the left ventricle filled to varying degrees. *Virchows Archives of Pathology Anatomy and Physiology and Clinical Medicine*, 1960. **333**: p. 523-564.
93. LeGrice IJ and Takayama Y and Covell JW, Transverse shear along myocardial cleavage planes provides a mechanism for normal systolic wall thickening. *Circ Res.*, 1995. **77**: p. 182-193.
94. Chen J and Liu W and Zhang H and Lacy L and Yang X and Song SK and Wickline SA and Yu X., Regional ventricular wall thickening reflects changes in cardiac fiber and sheet structure during contraction: quantification with diffusion tensor MRI. *Am J Physiology Heart Circ Physiol.*, 2005. **289**.
95. Helm PA and Tseng HJ and Younes L and McVeigh ER and Winslow RL, Vivo 3D diffusion tensor imaging and quantification of cardiac laminar structure. *Magnetic Resonance in Medicine*, 2005. **54**: p. 850-859.
96. Anderson RH and Ho SY and Redmann K and Sanchez-Quintana D and Lunkenheimer PP, The anatomical arrangement of the myocardial cells making up the ventricular mass. *Eur J Cardiothorac Surg* 2005. **28**: p. 517-525.
97. Lunkenheimer PP and Redmann K and Anderson RH, The architecture of the ventricular mass and its functional implications for organ-preserving surgery. *Eur J Cardiothorac Surg*, 2005. **27**: p. 183-190.
98. Fernandez-Teran MA and Hurle JM, Myocardial fiber architecture of the human heart ventricles. *Anat Rec*, 1982. **204**: p. 137-147.
99. Rushmer RF and Crystal DK and Wagner C, The functional anatomy of ventricular contraction. *Circ Res*, 1953. **1**: p. 162-170.
100. Pettigrew JB, On the arrangement of the muscular fibres of the ventricular portion of the heart of the mammal. *Proc Roy Soc Lond*, 1860. **10**: p. 433-440.
101. Pettigrew JB, On the arrangement of the muscle fibres in the ventricles of the vertebrate heart, with physiological remarks. *Phil Trans Roy Soc*, 1865. **154**: p. 445-500.
102. Hunter PJ and Pullan AJ and Smaill BH, Modeling total heart function. *BioMedical Engineering*, 2003. **5**: p. 147-177.
103. Scollan DF and Holmes A and Winslow R and Forder J, Histological validation of myocardial microstructure obtained from diffusion tensor magnetic resonance imaging. *Am J Physiol*, 1998. **275**: p. H2308-H2318.
104. Jouk PS and Usson Y and Michalowicz G and Grossi L, Three-dimensional cartography of the pattern of the myofibres in the second trimester fetal human heart. *Anat Embryol (Berl)*, 2000. **202**: p. 103-118.
105. Helm PA and Beg FM and Miller MI and Winslow RL, Measuring and Mapping Cardiac Fiber and Laminar Architecture Using Diffusion Tensor MR Imaging. *Proceedings Fairberg Cardiac Workshop Annals NY Acad. Sci.*, 2005. **1047**: p. 296-307.
106. Smith RM and Matiukas A and Zemlin CW and Pertsov AM, Nondestructive optical determination of fiber organization in intact myocardial wall. *Microsc Res Tech*, 2008. **71**: p. 510-516.
107. Gilbert SH and Benson AP and Li P and Holden AV, Regional localisation of left ventricular sheet structure: integration with current models of cardiac fibre, sheet and band structure. *Euro. J. of Cardio-thoracic Surgery*, 2007. **32**: p. 231-249.
108. Nielsen PMF and LeGrice IJE and Smaill BH and Hunter PJ, Mathematical model of geometry and fibrous structure of the heart. *American Journal of Physiology (Heart and Circulatory Physiology)* 1991. **260**: p. H1365-H1378.
109. Vetter FJ and Simons SB and Mironov S and Hyatt CJ and Pertsov AM, Epicardial fiber organization in swine right ventricle and its impact on propagation. *Circulation research*, 2005. **96**: p. 244-251.

110. Antzelevitch C, Electrical Heterogeneity, Cardiac Arrhythmias, and the Sodium Channel Cric. Res, 2000. **87**: p. 964-965.
111. Yan GX and Shimizu W and Antzelevitch C, Characteristics and distribution of M-cells in arterially perfused canine left ventricular wedge preparations. Circulation, 1998. **98**: p. 1921-1927.
112. Sampson KJ and Henriquez CS, Simulation and prediction of functional block in the presence of structural and ionic heterogeneity. Am J Physiol Heart Circ Physiol, 2001. **281**: p. H2597-H2603.
113. Panfilov AV and Keener JP, Re-entry in three-dimensional Fitzhugh-Nagumo medium with rotational anisotropy. Physica D, 1995. **84**: p. 545–552.
114. Fenton F. and Karma A., Vortex dynamics in three-dimensional continuous myocardium with fiber rotation: Filament instability and fibrillation. Chaos, 1998. **20**.
115. Rappel WJ, Filament instability and rotational tissue anisotropy: a numerical study using detailed cardiac models. Chaos 2001. **11**: p. 71–80
116. Engelman ZJ and Trew ML and Smail BH, Structural heterogeneity alone is a sufficient substrate for dynamic instability and altered restitution. Circ Arrhythmia Electrophysiol, 2010. **3**: p. 195-203.
117. Antzelevitch C and Sicouri S and Litovsky SH and Lukas A and Krishnan SC and Di Diego JM and Gintant GA and Liu DW, Heterogeneity within the ventricular wall. Electrophysiology and pharmacology of epicardial, endocardial, and M cells. Circ. Res., 1991. **69**: p. 1427–1449.
118. Antzelevitch C and Shimizu W and Yan GX and Sicouri S and Weissenburger J and Nesterenko VV and Burashnikov A and Di Diego JM and Saffitz J and Thomas GP, The M cell: its contribution to the ECG and to normal and abnormal electrical function of the heart. J Cardiovasc Electrophysiol., 1999. **10**: p. 1124–1152.
119. Sicouri S and Antzelevitch C, Electrophysiologic characteristics of M cells in the canine left ventricular free wall. J Cardiovasc Electrophysiol, 1995. **6**: p. 591–603.
120. Sicouri S and Glass A and Ferreiro M and Antzelevitch C., Transseptal dispersion of repolarization and its role in the development of torsade de pointes arrhythmias. J Cardiovasc Electrophysiol, 2010. **21**: p. 441-447.
121. Drouin E and Charpentier F and Gauthier C and Laurent K and Le Marec H, Electrophysiologic characteristics of cells spanning the left ventricular wall of human heart: evidence for presence of M cells. J Am Coll Cardiol, 1995. **26**: p. 185-192.
122. Pereon Y and Demolombe S and Baro I and Drouin E and Charpentier F and Escande D, Differential expression of KvLQT1 isoforms across the human ventricular wall. Am J Physiol Heart Circ Physiol, 2000. **278**: p. H1908– H1915.
123. Li GR and Feng J and Yue L and Carrier M, Transmural heterogeneity of action potentials and Ito1 in myocytes isolated from the human right ventricle. Am J Physiol, 1998. **275**: p. H369–H377.
124. Glukhov AV and Fedorov VV and Qing L and Ravikumar VK and Kalish PW and Schuessler RB and Moazami N and Efimov IR, Transmural dispersion of repolarization in failing and nonfailing human ventricle. Circ Res, 2010. **106**: p. 981-991.
125. Bryant SM and Wan X and Shipsey SJ and Hart G., Regional differences in the delayed rectifier current (IKr and IKs) contribute to the differences in action potential duration in basal left ventricular myocytes in guinea-pig. Cardiovasc. Res., 1998. **40**: p. 322–331.
126. Taggart P and Sutton P and Opthof T and Coronel R and Kallis P, Electrotonic cancellation of transmural gradients in the left ventricle in man. Biophysics and Mol Biol, 2003. **82**: p. 243-254.
127. Conrath CE and Wilders R and Coronel R and de Bakker JMT and Taggart P and de Groot JR and Opthof T., Intercellular coupling through gap junctions masks M cells in the human heart. Cardiovasc. Progress in Biophysics & Molecular Biology, 2004a. **62**: p. 407–414.
128. Conrath CE and Opthof T., Ventricular repolarization: An overview of (patho)physiology, sympathetic effects and genetic aspects. Progress in Biophysics & Molecular Biology, 2006. **92**: p. 269-307.
129. Nabauer M and Beuckelmann DJ and Uberfuhr P and Steinbeck G, Regional differences in current density and rate-dependent properties of the transient outward current in subepicardial and subendocardial myocytes of human left ventricle. Circulation, 1996. **93**: p. 168–177.
130. Poelzing S and Akar FG and Baron E and Rosenbaum DS., Heterogeneous connexin43 expression produces electrophysiological heterogeneities across ventricular wall. Am J Physiol Heart Circ Physiol, 2004. **286**: p. H2001-H2009.

Chapter 3

Aims, approaches, and modelling tools

3.1 Introduction

The presence of a transmural repolarization gradient in the ventricular wall is well established in mammalian and human hearts. There have been a large number of studies that have investigated whether transmural repolarization across the left ventricular wall is uniform or heterogeneous, how transmural and apico-basal dispersion of repolarization influence the T-wave morphology, how the dispersion in repolarization is increased as a consequence of reversing the normal activation sequence and its relation to ventricular arrhythmias, and how the findings may apply to patients.

This Chapter summarizes some of these experimental and simulation studies to highlight what these studies showed and what the gaps in knowledge are that this thesis is going to fill. Next, the approaches and modelling tools for achieving this purpose are described with evidences. Finally, the stability of the numerical schemes is established with the FK4V and the TP06 models [1, 2].

3.2 Activation and repolarization time and re-entry

Activation time and repolarization time as well as dispersion of repolarization play an important role in initiation and maintenance of re-entrant arrhythmia. This finding has been shown in animal studies i.e. in the ventricular surface of dog heart (Han et al. in 1964, Kuo et al. in 1983, and Gough et al. in 1985 [3-5]), in the uniform layer of epicardium on the anterior left ventricular surface of intact guinea pig hearts (Laurita et al. [6, 7]), and the anterior right ventricular wall in pig hearts [8]. Two current uncertainties about dispersion in repolarization are described here.

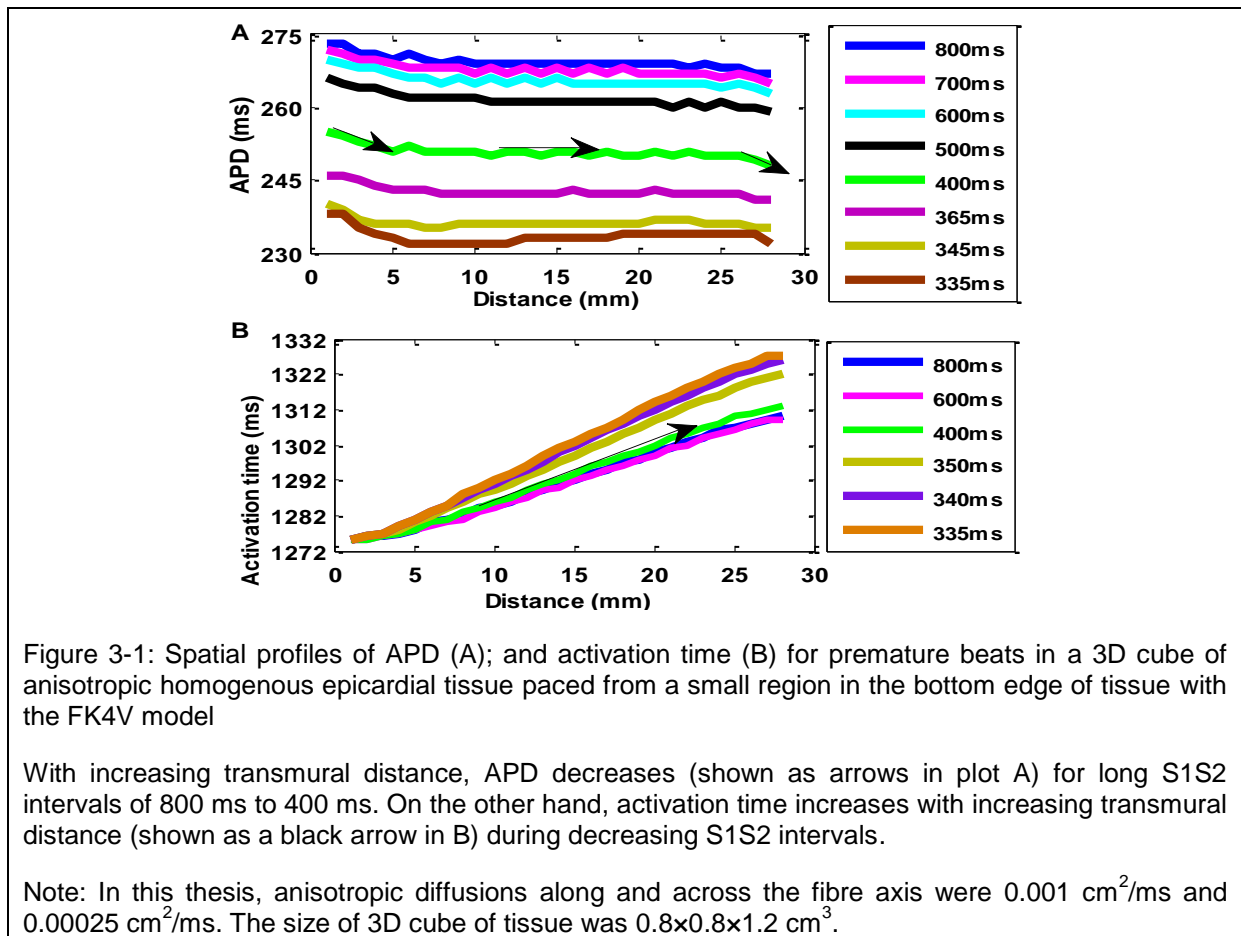
3.2.1 Increase or decrease in dispersion of repolarization time

An inverse relationship between APD and activation time has been shown in a number of in vivo studies. Some examples were in the left ventricle free wall in pentobarbital anesthetized dogs (Burgess et al. [9] in 1972), in patients with upright or inverted T-waves in the left ventricular epicardium (Cowan et al. [10] in 1988), on the epicardial surface of the normal human left ventricle (Franz et al. [11] in 1988), in the ventricular endocardium (Yuan et al. [12] in 2001), in the human ventricles (Yue et al. [13] in 2005), in patients with and without positive microvolt T-wave alternans (Chauhan et al. [14] in 2006), and on the endocardial surfaces of normal left ventricle (Hanson et al. [15] in 2009).

This relationship may reduce the dispersion of repolarization time in some conditions. For example, Cowan et al. [10] studied two groups of patients and showed this inverse relation in one group of patients with undergoing coronary artery bypass grafting (upright T-wave). If reducing dispersion in repolarization is considered as a protective mechanism, this relationship may provide an intrinsic anti-arrhythmic property of ventricular tissue, while this

relationship was not true in the other group of patients with aortic valve replacement (with T-inversion), where the dispersion of repolarization increased [10].

The results in this thesis with the FK4V [1] and the TP06 [2] models showed that the inverse relationship between APD and activation time is only true for homogenous epicardial, endocardial, and mid-myocardial tissues for long S1S2 intervals (i.e. S1S2 intervals of 800 ms to 400 ms). However, spatial profiles of APD and repolarization time for premature S2 beats change for shorter S1S2 intervals than around 400 ms due to boundary and rate dependent effects. This issue is explained in detail in Chapters 4, 5, and 6. For clarity, examples of spatial profiles of APD and activation time for premature beats in 3D cubes of anisotropic epicardial tissue with the FK4V model are shown in Figure 3-1.



3.2.2 Reversal direction of ventricular activation

Over a 3-year period from 2003 to 2005, clinical studies in human heart failure [16, 17] and arterially perfused canine left ventricle wedge preparations [18] have shown that reversing the direction of activation in electrically heterogeneous ventricular myocardium prolongs the QT interval and greatly increases the dispersion in transmural repolarization. Consequently, the delayed activation and repolarization of the mid-myocardial cells when coupled with earlier repolarization of epicardium may create a substrate for re-entrant arrhythmia.

On the other hand, a human study [19] in 2006 showed that reversing the direction of activation reduced significantly ventricular heterogeneity of repolarization and had an electrophysiological anti-arrhythmic influence on the arrhythmogenic substrate of dilated

cardiomyopathy. In the dilated cardiomyopathy, the left ventricle becomes stretched and heart muscles become weak and the heart cannot pump blood efficiently.

Further studies are required to assess the influence of left-ventricular pacing on dispersion in repolarization and to evaluate whether left ventricular pacing affects the initiation of ventricular arrhythmias. In addition, whether repolarization across the ventricular wall is uniform or heterogeneous is still a matter of controversy [20-25].

The new findings in this thesis showed that reversing direction of normal activation sequence in heterogeneous tissues composed of two or three ventricular cell types may increase or decrease dispersion of repolarization during decreasing S1S2 intervals. For example, dispersion in repolarization time in a 3D cube of anisotropic heterogeneous tissue composed of 50%endo-50%epi increased with endocardial pacing and decreased with epicardial pacing for long S1S2 intervals of 700 ms to 400 ms as shown in Figure 3-2, plot A. On the other hand, dispersion in repolarization time was amplified with epicardial pacing in a 3D cube of anisotropic heterogeneous tissue composed of 10%endo-30%M-60%epi for long S1S2 intervals of 700 ms to 470 ms as highlighted in magenta in Figure 3-2, plot B. This issue is discussed in detail in Chapter 7.

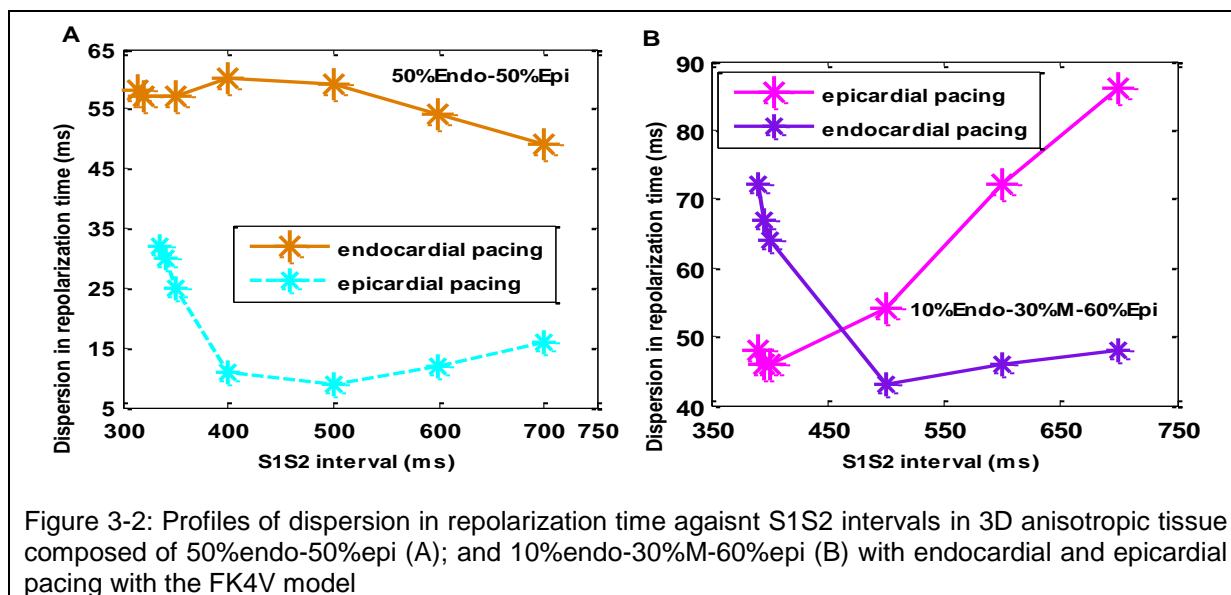


Figure 3-2: Profiles of dispersion in repolarization time against S1S2 intervals in 3D anisotropic tissue composed of 50%endo-50%epi (A); and 10%endo-30%M-60%epi (B) with endocardial and epicardial pacing with the FK4V model

Another factor that is important for understanding dynamic properties of the heart suggested by numerical [26] and experimental [27-30] studies is the electrical restitution that is discussed in the following section.

3.3 Restitution and re-entry

During AP depolarization and AP final repolarization several dynamic processes are engaged, such as conduction velocity restitution as suggested by Boyett-Jewel [31] in 1978 and Qu et al. [32] in 1999 in mammalian ventricles. Steepness and specific shape of APD restitution curves and conduction velocity restitution curves as well as many other factors can be important for some breakup mechanisms to occur in a model of cardiac electrical activity [33]. This part of the Chapter summarizes some simulation studies using animal and human models that showed how the restitution properties modulate the activation and repolarization time in both 2D homogenous and 3D heterogeneous tissues and how it is important in the development of an arrhythmia.

3.3.1 Homogenous tissues

When slope of APD restitution curve became greater than 1, steep APD restitution may lead to unstable re-entry in a 2D sheet. In this case, small changes in diastolic interval may cause larger changes in APD, whereas changes in APD due to changes in diastolic interval are damped out at smaller slopes, and then a conduction block may occur because a long APD created by the oscillations may demand a diastolic interval below the minimum diastolic interval [33].

However, the effects of steepness of the APD restitution curve on spiral wave stability and initiation of re-entry are not straightforward. For example, Karma [27] showed that increasing steepness of APD restitution curves may lead to unstable re-entry and wave breakup in a 2D sheet using the 2-variable Karma model [34] including a fast variable related to the membrane voltage and a slow gate variable. On the other hand, Courtemanche [35] showed that the maximum steepness of APD restitution curve due to speeding the kinetics of calcium (slow inward current) can prevent spiral wave breakup in a 2D sheet based on the Beeler-Reuter AP model [36]. This model has four currents including potassium transient outward current as time-independent function of voltage and three currents of outward potassium current, fast inward sodium current, and slow inward calcium current that are time-dependent gating variables.

Qu et al. [32] studied the role of APD and conduction velocity restitution in the stability of spiral wave re-entry in a 2D isotropic homogenous sheet of tissue using the modified phase I Luo-Rudy model [37] to eliminate the restitution properties caused by potassium, calcium, and sodium currents. They [32] suggested that (1) for developing spiral wave breakup, the maximum steepness is less important compared to the range of diastolic intervals over which the slope of APD restitution curve is steep; and (2) promoting spiral wave breakup by conduction velocity restitution may be independent of APD restitution.

Clayton and Taggart [38] studied whether the regional differences in APD restitution can act as a potent substrate for initiating re-entrant arrhythmias. They simulated a 2D sheet of isotropic tissue using a 3-variable model of cellular electrophysiology [39] that produced the APD and conduction velocity restitution based on animal data. Their main findings were that (1) regional differences in repolarization may be concealed at normal heart rates but may be created by a premature stimulus; and (2) wave break and re-entry can be initiated during further premature stimulus independent of the steepness of the APD restitution curve.

All of these studies were limited to spiral wave behaviour based on animal data in 2D sheets and did not take into account anisotropy, electrophysiological heterogeneity, anatomic obstacles, and the scroll wave behaviour in a 3D tissue model and its relation to the spiral wave behaviour in a 2D tissue model. However, there are some animal studies in 2D suggested that the anisotropy can create re-entrant pattern [40, 41].

In 3D simulations with rotational anisotropy but in homogenous tissue, Fenton and Karma [39] showed that the rotation of fibre orientation from endocardium to epicardium may induce breakup of re-entrant scroll waves by inducing filament twist. They approximated the restitution properties and spiral wave behaviours based on a simple ionic model [39] with three phenomenological currents including the (1) fast inward current that corresponds to the sodium current responsible for AP depolarization; (2) slow outward current that corresponds to the potassium current responsible for AP repolarization; and (3) slow inward current that corresponds to the calcium current responsible of AP plateau.

Furthermore, Panfilov and Keener [42] used a modified FitzHugh-Nagumo model [43, 44] in two studies based on 3D simulations and showed that (1) for premature S2 beats, rotational anisotropy may create wave break in the 3D excitable tissue; and (2) rotational anisotropy can destabilize re-entry (breakdown of re-entry from a stable scroll wave) [45]. In the latter, they could not relate the results to real myocardium tissue because of setting a grid space of 1 mm to correlate with anisotropic refractoriness that lead to a large jump in angles between small numbers of layers. In total, they suggested that the region in the left ventricle with the largest thickness and rotation of fibres is the most probable region for the breakup even in re-entrant waves.

3.3.2 Heterogeneous tissues

The association between APD dispersion and susceptibility to re-entry was studied by Clayton and Holden [46] using the phase I Luo–Rudy model [37]. They introduced 2D heterogeneous sheets of tissue by decreasing maximum potassium conductance in a square region located in central region of simulated tissues. They showed that larger spatial scale of heterogeneity, decreasing cell-to-cell coupling, and greater electrophysiological heterogeneity may increase APD dispersion and susceptibility to re-entrant arrhythmia.

Keldermann et al. [47] studied effects of the heterogeneous restitution properties on multiple wavelet re-entry in a 3D human model. Regional differences in restitutions were based on data from measurements by Nash et al. [48] in different patients. The biophysically detailed cell model of ten-Tusscher et al. [49] and a tissue model coupled with ventricular anatomy and fibre direction anisotropy were used. Similar to studies by Clayton-Holden [46] and Clayton-Taggart [38], they showed that APD restitution heterogeneity is important for the initiation of wave break and re-entry.

The simulated tissues in these studies were homogenous or heterogeneous in terms of ionic properties and were limited to epicardium and did not take into account fibrosis.

After observation of mid-myocardial cells with the longer APD than epicardial and endocardial cells in response to slowing of the heart rate, or in response to agents that increase APD in the early 1990's [20, 21, 50], many researchers have started to simulate ventricular tissues with additional layers of mid-myocardial cells. Combining mid-myocardial cells with other ventricular cells within left ventricular wall thickness has advanced the current understanding of the transmural voltage gradient and its effects on T-wave morphology. Two studies that highlighted the involvement of mid-myocardial cells in transmural ventricular repolarization are summarized here.

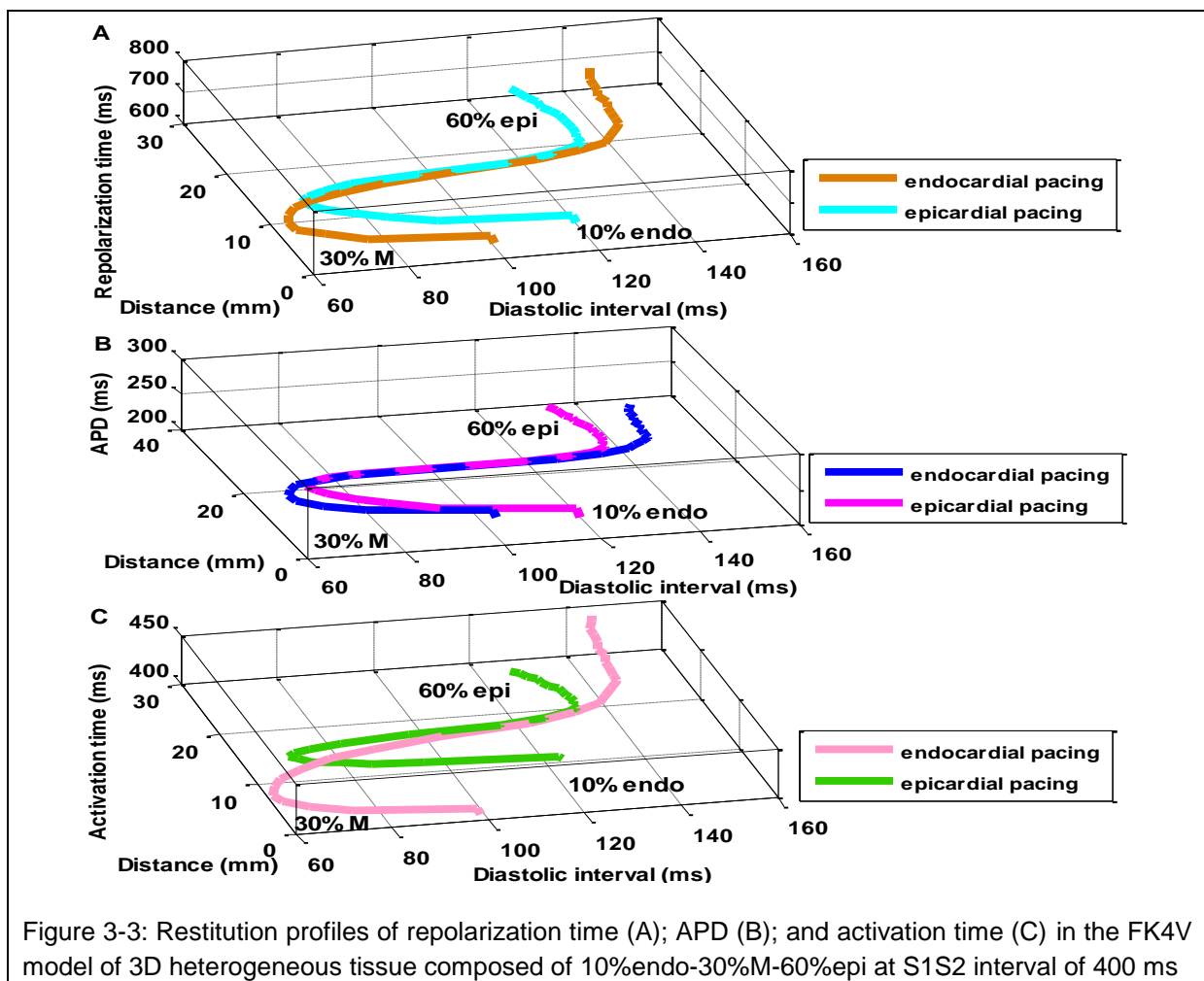
3.3.3 Transmural and apico-basal gradients

In 2004, Clayton and Holden [51] studied the propagation of both normal beats and re-entry on 2D isotropic tissues of $40 \times 12 \text{ mm}^2$ with different cellular configurations: (1) equal layers of endocardial, mid-myocardial, and epicardial cells; (2) equal layers of endocardial and epicardial cells with three circular regions of mid-myocardial cells; and (3) equal layers of endocardial and epicardial cells and a tapered mid-myocardial cell layer with different thickness. They used a biophysically detailed phase II Luo–Rudy dynamic model of guinea pig ventricular myocytes [52] including a detailed model of Ca^{2+} sequestration and release within the myocytes. They showed that in uniform tissues, a small transmural APD gradient exists during normal paced activity. Mid-myocardial layers with different thickness and configuration may affect repolarization sequence and may underlie apex-base differences in repolarization.

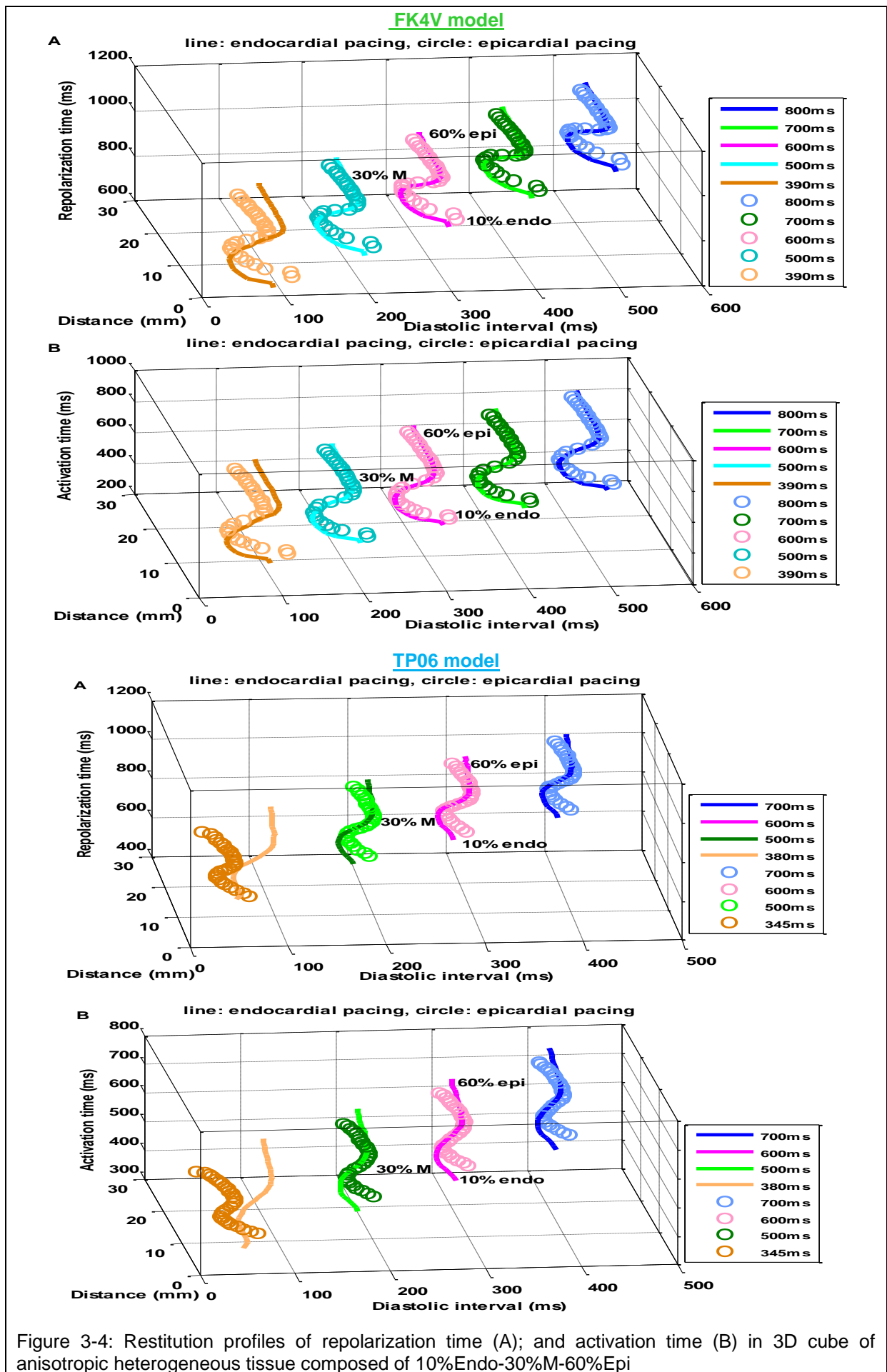
In 2011, Okada et al. [53] examined the effect of APD distribution in both transmural and apico-basal directions on T-wave morphology using (1) a human heart model with the conduction system based on finite element method; (2) a torso model with distinct organ structures to obtain the standard electrocardiography leads; and (3) a biophysically detailed human model of ten-Tusscher [49] that was modified to introduce apico-basal gradient by changing ion channel parameters. They changed the APD distribution in the transmural direction by locating the mid-myocardial cells in the endocardial and epicardial regions. The main finding was that the transmural distribution of APD in the region between endocardium and mid-myocardium is important for origination of positive T-wave however, the apico-basal gradient may be required to attain the physiological waveform.

Yet, many factors should be included in these models for further improvement, including the anisotropic (orthotropic) properties, fibre structure, and using new ventricular cell models in both normal and diseased tissues.

The new findings in this thesis showed the involvements of mid-myocardial cells not only in restitution profiles of repolarization time and APD but also in restitution profiles of activation time with endocardial and epicardial pacing with the FK4V and the TP06 models (described in Chapters 5 and 6). Figure 3-3 shows examples of these profiles in the 3D cube of anisotropic tissue composed of 10%endo-30%M-60%epi with endocardial and epicardial pacing at S1S2 interval of 400 ms.



This result was also true during decreasing S1S2 intervals with the FK4V and the TP06 models as shown in Figure 3-4.



3.4 Myocardial structure and tissue geometry

Simulation studies have shown that the cardiac architecture plays an important role in the electrical and mechanical function of the heart. From a mechanical viewpoint, the complex structure of fibres and sheets are responsible for the orthotropic mechanical properties of cardiac muscle [54, 55]. From an electrical viewpoint, fibre arrangement and sheet structure enable the spread of excitation through the heart. Fibre structure significantly affects both the excitation and repolarization, and may be a main factor of the anisotropic conductivity in cardiac tissue [56]. There is evidence [57, 58] that the cell-tissue architecture can influence the direction and shape of electrical waves.

Some examples of experimental and simulated tissues with fibre and fibre-sheet structure are described in the following sections.

3.4.1 Anisotropic and orthotropic conductions

Generally, electrical coupling is assumed to be longitudinal in the direction of the fibre's long axis and transverse in the direction perpendicular to the long axis of the fibres [58, 59]. The electrical coupling is more in longitudinal direction and less in transverse direction [59, 60]. An experimental study by Saffitz et al. [61] showed that there are more gap junctions in the transverse direction (roughly two third) than in the intercalated disks in the longitudinal direction (around one third) over an equivalent distance in the canine ventricle. Thus, the low electrical resistance pathway provided by gap junctions allows rapid longitudinal conduction through a uniform tissue. In transverse direction, since cells are rod shaped and gap junctions are usually located at the ends of cardiac cells, electrical activation waves need to passing through more gap junctions per unit distance, and so that resulting in greater resistance. That is why conduction in transverse direction occurs more slowly than that of in longitudinal direction.

In 1981 and 1982, Spach and colleagues classified tissue with electrical anisotropy as having uniform anisotropy [40] or non-uniform anisotropy [62].

- Uniform anisotropy

In both longitudinal and transverse directions, the tight electrical coupling between cells and normal arrangement of gap junctions may lead to continuous impulse propagation in all directions. But, the apparent conduction velocity alters monotonically from fast to slow, as the direction of propagation changes between longitudinal direction and transverse direction.

- Non-uniform anisotropy

In the longitudinal direction, there is still a tight electrical coupling between cells while in the transverse direction, a recurrent area is defined in which there is no side to side electrical coupling of unit bundles of parallel fibres. In this case, the spatial distribution or function of gap junctions is changed to such an extent that transvers conduction is interrupted and become significantly slower than longitudinal conduction so that muscle fibres are activated asynchronously.

The non-uniform anisotropy conductivity may occur not only in diseased tissue i.e. in area of occurrence of myocardial infarction but also in real cardiac tissue due to variability of the fibre orientations.

Furthermore, there is some evidence of electrical orthotropy in the animal [63] and human hearts [64] but still has not been established. For example, in 2009, Caldwell et al. [63] by the use of high-density intramural electrical mapping showed that the wave propagation in

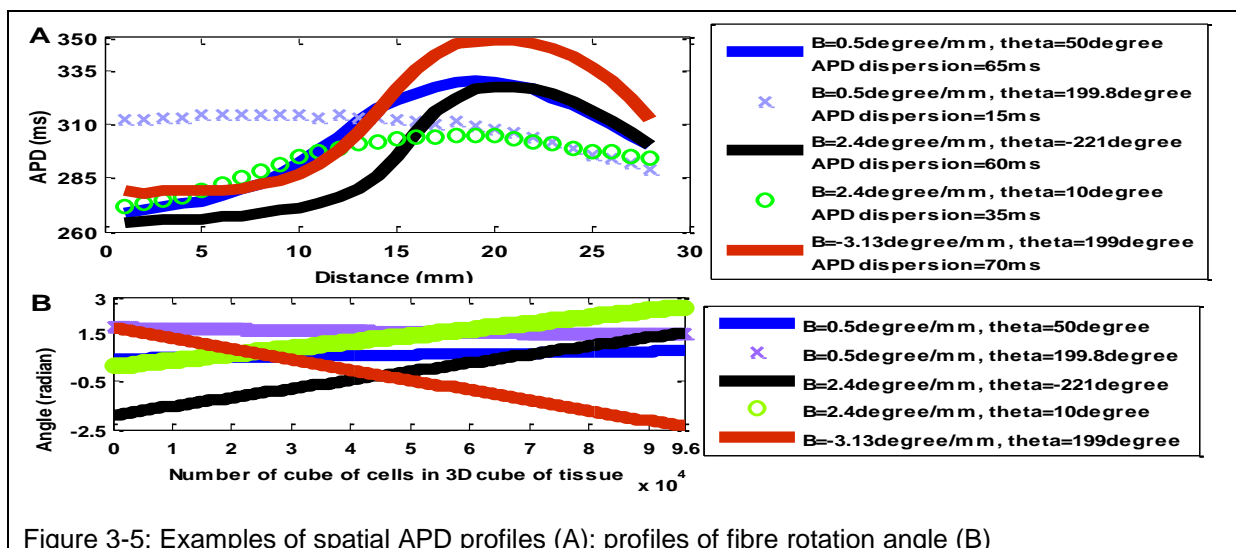
porcine left ventricular myocardium is orthotropic. This finding may imply that the electrical properties of ventricular myocardium are not axially anisotropic, and are not uniform transverse to the local myofiber axis. The three distinct velocities of propagation at any point within ventricular myocardium are: fast in the direction of myofiber, and fast and slow within and across microscopic laminar groupings of the myocyte with local conduction velocity of 0.67, 0.3, and 0.17 m/s in a ratio of 4.3:1.8:1.0. They [63] showed that the conductivity of ventricular tissue is determined by the direction of fibres, and rapid longitudinal propagation of currents and spatial changes of fibre orientation may influence conduction properties in the porcine left ventricle myocardium.

3.4.2 Fibre structure

Cates and Pollard [65] studied the effect of an abrupt, 90° intramural fibre rotation on the spatial distribution of repolarization in a 2D slice of tissue with size of 7.2 × 3.5 mm² with two fibre orientations: (1) an isotropic region with fibre orientation perpendicular to the plane of the slice; and (2) an uniformly anisotropic region with fibre orientation parallel with the plane of the slice. They used the phase I Luo-Rudy membrane model [37] and showed that with certain stimuli, fibre rotation can create non-uniform spatial APD distributions. The simulated tissues in this study were limited to epicardium and endocardium.

Whether fibre rotation varies linearly or non-linearly within the left ventricle wall is still not clear. In 2005, Vetter et al. [66] studied the epicardial fibre organization in isolated coronary-perfused right ventricular free wall preparations using optical mapping. For modelling the electrical propagation, they used a monodomain model with a simplified description of ionic current developed by Fenton and Karma [39]. They showed that the free wall of swine right ventricle has a thin epicardial layer around 110 to 930 μm with no depth-dependant fibre rotation and with distinctly different fibre orientation. This layer can influence propagation and give rise to unusually shaped activation waves. In 2008, Taccardi et al. [67] showed that myocardial structure plays an important role in distinct patterns of epicardial excitation in the canine heart using electrode arrays and transmural plunge electrodes.

New findings in this thesis showed the effects of non-linear change in fibre orientation on spatial APD profiles and APD dispersion (described in Chapter 5 part II). Figure 3-5 shows examples of spatial APD profiles in 3D cubes of anisotropic tissue composed of 60%endo-30%M-10%epi simulated with different fibre structure with epicardial pacing at S1S2 interval of 1000 ms with the FK4V model.



3.4.3 Effects of fibrosis

In myocardial infarction, well-coupled, excitable, and contractile cardiac tissues may be replaced by poorly coupled, non-excitable, non-contractile scar tissue, containing mainly fibroblasts and accumulating extracellular matrix [68]. Fibrosis in myocardial infarction and diseased hearts often form isolating barriers and discontinuities. The consequence is disruption in both electrical and mechanical activation of myocardium particularly in the left ventricle that affects cardiac function and reduces cardiac output. Cardiac output is the product of heart rate defined as the number of beats per minute and stroke volume defined as the amount of blood ejected by left ventricle during each beat or in one contraction. A normal adult's heart for a 70 kg man can easily pump 5 litres per minute of blood at rest (70 beats/min \times 70 ml/beats). Increased fibrosis formations after myocardial infarction are strongly correlated with an increase incidence of ventricular tachycardia and sudden cardiac death [69].

In 2001, a histologic human study by Kawara et al. [70] showed that architecture of fibrosis plays an important role in conduction delay after premature beats in the chronically diseased myocardium. They suggested three types of fibrosis with regard to architecture in chronically diseased human myocardium including:

- Patchy fibrosis: It is referred to non-uniform anisotropic fibrosis with long, compact groups of strands [70]. This type of fibrosis leads to a progressive increase of conduction delay at long coupling intervals of premature beats. This conduction delay significantly depended on the direction of the wave-front curvature and had more effect in transverse direction.
- Diffuse fibrosis: It is randomly distributed fibrosis with short strands [70]. This type only marginally affected conduction delay even at high density of fibrosis.
- Stringy fibrosis: It is homogeneously distributed fibrosis with long, single strands [70]. Stringy fibrosis caused more conduction disturbance than diffuse fibrosis and may lead to more arrhythmogenic disease.

Clinically, it is desirable to influence healing of the cardiac scar to maintain structure and function of the heart particularly in patients with large infarction and severe left ventricular dysfunction [68]. In addition, it is important to distinguish between non-transmural and transmural necrosis after myocardial infarction, because if the degree of infarct increases, the number of infarct-related complications will rise [71].

In 2007, the role of diffuse fibrosis on wave propagation, the development of an arrhythmia, and arrhythmia mechanism in homogenous tissue was studied by ten-Tusscher and Panfilov [72]. They simulated diffuse fibrosis that randomly distributed across 2D and 3D tissues and 3D voxel description of human ventricular anatomy using a biophysically detail human ventricular cell model [2]. They showed that diffuse fibrosis (1) slows down wave propagation and increases tissue susceptibility to wave break and spiral wave formation; (2) prolongs the period of re-entrant arrhythmias and may suppress the spiral break-up caused by steep APD restitution.

In 2010, Engelman et al. [73] showed that the non-uniform discontinuities of resembling patchy fibrosis in structural heart disease has less effect on activation at low rate and great effect on activation time, conduction velocity, and APD restitution at high rate. They suggested that this structural heterogeneity may be sufficient to increase vulnerability to arrhythmias. It is important to note that the structural heterogeneity was simulated in the

absence of regional variation of the cellular properties using a modified Luo-Rudy I [74] model and the bidomain model [75] with isotropic diffusion.

Still, further studies are needed to evaluate the influence of simulated fibrosis tissues on (1) the sequence of cardiac activation and repolarization and; (2) the dispersion in repolarization in anisotropic heterogeneous tissues in the human heart.

Chapter 5 of this thesis address this issue in two groups of 3D cubes of anisotropic heterogeneous tissues with and without fibrosis and showed that combined effect of anisotropy and fibrosis could suppress the speed of depolarization conduction in the mid-myocardial region of heterogeneous tissue with the FK4V and the TP06 models.

3.4.4 Effects of fibre-sheet structure

Dos Santos et al. [76] studied the effect of a sea anemone toxin (ATX-II) on location of mid-myocardial cells in the left ventricular wedge using the bidomain tissue model and the human cell model of ten-Tusscher et al. [49] including epicardial, mid-myocardial, and endocardial cells. For fibre-laminar model, they used a local tensor based on histological data in the normal adult dog ventricle measured by Costa et al. [77] to specify the myocardial fibre orientation, the sheet direction, and the normal orientation of the overall sheet structure. They assumed that fibre angle varied linearly from $+60^\circ$ at the endocardium to -60° at the epicardium and sheet angle changed linearly from $+30^\circ$ at the endocardium to -10° at sub-epicardium [77].

They [76] showed that the combination of intercellular electrotonic interactions (which tend to decrease transmural APD distribution) and the heterogeneous effects of ATX-II (that slows inactivation of I_{Na} and thus prolongs APD of mid-myocardial cells) can shift the location of the ventricular myocytes. Consequently, the transmural APD profiles, the localized refractory period, and excitability significantly changed, that may change the overall substrates for conduction and may cause rhythm disturbances.

3.4.5 Effects of boundaries and geometries in homogenous tissue

In cardiac tissue, diffusive electrotonic currents from one cell to its neighbouring cells allow wave propagation. Simulation studies have shown that boundaries and overall tissue geometries may affect spatial profiles of APD, i.e. in 1D fibre [78] using a simple two current ionic model of Karma [34] and the model of Mitchell-Schaeffer [79], in 2D homogenous tissues [80] (with a simple AP model of Fenton et al. [33] and the canine ventricular myocytes model of Fox et al. [81] as an example of more detailed description of ion currents), and in the 2D homogenous canine tissue [82] (with a canine ventricular cell model [81] in most cases and a 3-variable phenomenological model of Cherry-Fenton [83]).

These studies assessed the effects of boundary and tissue geometry on only APD distribution in isotropic homogenous tissue mostly based on animal models and some S1S2 intervals.

The effects of tissue boundaries can be described by qualitative analysis of physiological process (i.e. the current flows across the cell membrane, I_m and the total transmembrane current, I_{ion}) such as the study by van Oosterom and Jacquemet [84] in a realistically-shape model of human atrial tissue. The possible explanation for prolongation and shortening of APD close to the boundaries based on previous studies [83, 84] is:

- positive large current that flow across the cell membrane at tissue boundary close to stimulations sites yields higher repolarization time because of electrotonic effects from neighbouring region of tissue;
- negative large current that flow across the cell membrane at the opposite tissue boundary yields lower repolarization time and electrotonic effects act to accelerate AP repolarization.

The new findings in Chapter 4 of this thesis highlight the effects of boundaries and rate dependency on spatial and restitution profiles of not only APD and repolarization time but also on restitution profiles of activation time. Figure 3-6 shows examples of spatial profiles of APD for premature beats in two groups of 2D isotropic epicardial tissues with structural discontinuities (i.e. H-shape tissue geometry) and without structural discontinuities (i.e. slim rectangular tissue geometry) with the FK4V model. Plots A and B show the effect of boundaries at long S1S2 interval of 800 ms. However, spatial APD profiles changed during decreasing S1S2 intervals, i.e. for short S1S2 interval of 320 ms as shown in plots C and D. The restitution in speed of depolarization conduction (conduction velocity restitution) may also act to change the spatial profiles of APD and repolarization time. This issue is discussed for different geometrical tissue models in next Chapters.

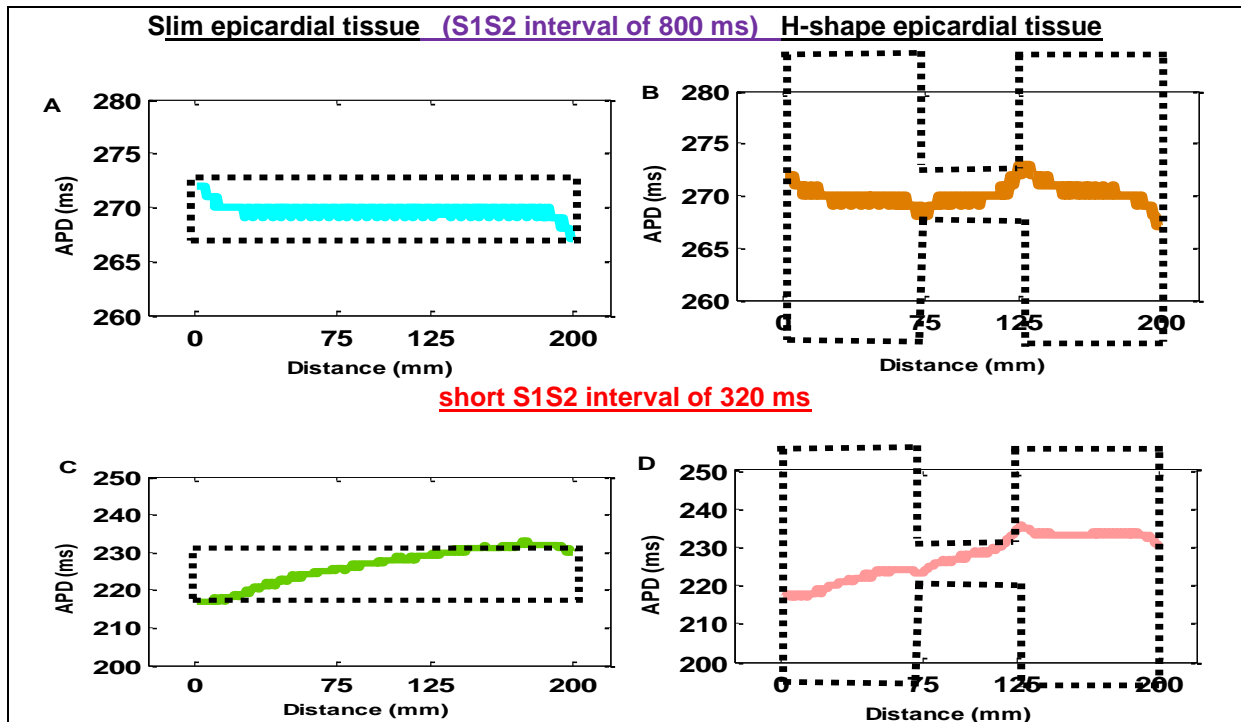


Figure 3-6: Examples of spatial profiles of APD in isotropic slim (A and C); and H-shape (B and D) epicardial tissues at S1S2 interval of 800 ms and 320 ms with the FK4V model

Plots A and B show the prolongation and shortening of APD close to the edges of slim tissue (200×4 grid points) and H-shape tissue (200×200 grid points) due to the effect of tissue boundaries.

The dip and peak in plots B and D correspond to the abrupt changes in the middle of H-shape tissue close to structural discontinuities at grid points 75 and 125 in H-geometry.

Note: The scheme of slim and H-shape tissue geometries are shown as black dots. The membrane voltage was extracted from middle of tissue.

So far, there are a few studies that tested the pattern of excitation, repolarization, and APD distribution in the same simulated tissues that are described here.

3.5 Excitation, repolarization, and APD

Recently, a series of 3D simulations were performed to study one or combined effects of heterogeneities on the patterns of excitation, repolarization, and APD as well as APD dispersion using the phase I Luo–Rudy membrane ionic model [37].

In 2005, Colli Franzone et al. [85] simulated 3D slabs of homogenous epicardial tissue with orthotropic or axisymmetric anisotropic conductivities in the presence of intramural fibre rotation using both the bidomain and monodomain models. They showed that APD patterns present a definite spatial dispersion even with the homogenous cellular membrane properties.

In 2006, the same group of researchers [86] incorporated both homogenous and heterogeneous tissue properties in 3D slabs of tissue in orthotropic anisotropy condition with transmural fibre rotation using the monodomain model. They showed that the repolarization pathway follows the activation sequence in a homogenous slab while this is not true in a heterogeneous slab of tissue. In another words, the transmural heterogeneity affected both the sequence of repolarization and APD dispersion.

In 2008, the previous simulations were performed in ventricular wall, shaped as an ellipsoidal volume with heterogeneity along both transmural and apex-to-base direction by Colli Franzone et al. [87]. Their results showed that the heterogeneities in transmural direction and along apex to base direction had a slight effect on the sequence of repolarization on myocardial layers parallel to the epicardium. In ellipsoidal walls, the sequence of repolarization was possibly independent of transmural heterogeneity because of insufficient anisotropic diffusion currents to mask the intrinsic repolarization differences in the normal cardiac tissue.

In 2009, Scacchi et al. [88] assessed the extracellular markers in 3D slabs of normal homogenous and heterogeneous ventricular tissue using the bidomain model and focused only on the repolarization sequence of endocardium, epicardium, and in the thickness of ventricular wall. They showed that the spatial distribution of activation-recovery intervals may provide an inaccurate estimate of the APD dispersion.

These series of studies used the phase I Luo–Rudy membrane ionic model of guinea pig [37] which shows a realistic AP based on animal data but does not consider the transient outward current that play an important role in ventricular AP spike and dome morphology during early repolarization phase [89].

3.6 Novelty of this research

In humans, there are gaps in the current knowledge about how activation-repolarization coupling and the restitution properties interact, and how this affects the dynamic aspects of activation and repolarization at premature stimulations [15].

The novelty of this thesis is study of the interaction of ventricular activation-repolarization coupling and the restitution properties

- (1) during progressively decreasing S1S2 intervals;
- (2) for normal and premature beats;
- (3) for two groups of 2D isotropic tissues with and without structural discontinuities;

- (4) for 3D cubes of homogenous and heterogeneous anisotropic tissues with and without fibrosis, simulated with a linear and a non-linear change in fibre orientation, and with endocardial and epicardial pacing;
- (5) for an anatomically detailed the left ventricular wedge model composed of anisotropic homogenous and heterogeneous tissues obtained from [90];
- (6) using more advanced models based on newer descriptions of the individual ventricular cells obtained from human data not animal data;

The results of this study are based on four major spatiotemporal profiles including:

- spatial and restitution profiles of activation time, repolarization time, and APD in tissues;
- profiles of three measures of dispersion in activation time, repolarization time, and APD against S1S2 interval;
- restitution profiles of speed of depolarization conduction;
- profiles of AP propagation during depolarization time and repolarization time.

3.7 Modelling tools in programs written in C

For computational simulations in this thesis, initially programs written in C were used to produce patterns of transmembrane voltage in whole tissues. The next parts of computational implementations were run in MATLAB to extract transmembrane potential from the central region of tissues in order to calculate and visualize desired data. This part of the Chapter illustrates the geometrical models of tissue and fibre, two cell models, and the monodomain tissue model that were used in programs. A brief description of programs is provided in the enclosed CD, Appendix.

3.7.1 Why geometrical models

Reaction–diffusion mathematical models of cardiac electrophysiology require not only dynamic excitation models that create the AP but also datasets of cardiac geometry and fibre structure that provide the electrical diffusion tensor which determine the conductivities of ventricular tissue [64]. The realistic considerations of the cardiac fibre organization [91, 92] can influence the electrical propagation and force development in tissue possibly due to the anisotropic (orthotropic) electrical and mechanical properties.

In 2010, Bishop et al. [93] used a geometry of a rabbit heart obtained from magnetic resonance imaging technique (MRI) and a mathematical model based on the canine data [94]. They compared the normal and arrhythmic excitation patterns in the high-resolution and simplified smoothed geometries. Both geometries showed qualitatively the same behaviours while the detailed geometry could change the development and the duration of re-entrant arrhythmias, suggesting that cardiac geometries are necessary for the quantitative prediction of arrhythmias in hearts with normal and pathological electrophysiology [94].

For the human heart, simulations of human tissue and fibre structure are necessary for highlighting the roles of anisotropic or orthotropic architecture in the initiation of arrhythmias. However, the current limitations are:

1. Anatomical models of the heart require detailed information about geometry and fibre structure that is still difficult to obtain. One reason is human heart has a 3D asymmetric geometric form with complex structural organization which require the high angular resolution diffusion imaging techniques to estimate diffusion within a

voxel. The current diffusion tensor-magnetic resonance imaging technique (DT-MRI) cannot resolve heterogeneity within a voxel and can approximate the anisotropy content of a voxel by an ellipsoid shape [64]. In addition, if the voxel size decreases less than 100 μm , the signal strength decreases according to the voxel volume [64].

2. An accurate solution of boundary conditions [91] on the voltage that can represent the correct interface between tissue and surrounding medium in different conditions is still challenging in asymmetric geometries.
3. There is the lack of knowledge about interaction of activation-repolarization coupling and the restitution properties in 2D slabs, 3D cubes of tissue, and the left ventricular wedge model that should be considered first before studying this interaction in the real complex tissue and fibre geometries.

Consequently, the current thesis focused on simple geometrical models rather than a complex description of the ventricular models of tissue and fibre. However, increasing levels of complexity was imposed gradually to simulations using 2D tissue geometries with different shapes, 3D tissue geometries with seven cellular configurations and different fibre structure, and a real left ventricular wedge model including tissue and fibre geometries obtained from imaging techniques. This approach may (1) highlight the role of geometrical models on interaction of activation-repolarization coupling and restitution properties in two human ventricular tissue models; and (2) explain whether the simulations results in simple geometrical models can be applied to the whole heart or not. The following sections describe geometrical models that were used in this thesis.

3.7.1-1 Tissue with 2D geometries

Infarct scars contain complex branching structures of viable myocardium. These strands of surviving ventricular tissue vary in both width and length, may branch, and often form narrow paths for impulse propagation through areas of infarct scars. A study by Kogan et al. [95] showed that specific geometric configurations (tapered shape) may cause unidirectional conduction failure, slow conduction velocity, and re-entry to occur even with uniform properties. They used a simplified ventricular membrane model of the modified FitzHugh-Nagumo equations [43] with APD restitution properties [96] and theoretical considerations.

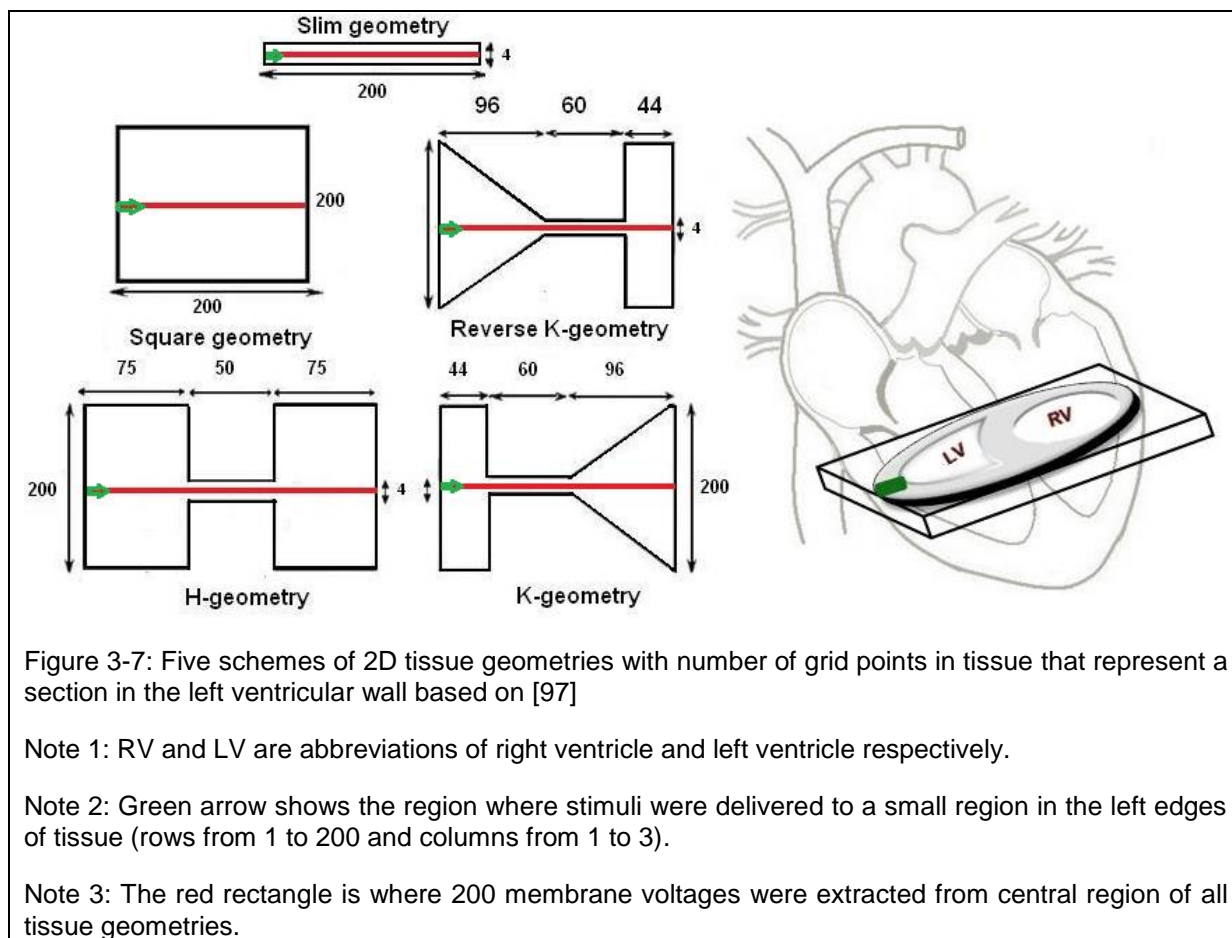
Similarly, the 2D simulations in this thesis introduce two groups of tissues with five idealized tissue geometries with particular types of border geometry to represent a section through the left ventricular free wall with and without structural discontinuities. Figure 3-7 shows

1. Two tissues with slim and square geometry as examples of tissues without structural discontinuities with size of $5 \times 0.1 \text{ cm}^2$ and $5 \times 5 \text{ cm}^2$. These tissue geometries contained 1s that correspond to excited cells.
2. One H-shape tissue geometry with parallel borders, and two K-shape and the reverse K-shape tissue geometries with combinations of parallel and tapered borders as examples of tissues with structural discontinuities (or scar tissues) with size of $5 \times 5 \text{ cm}^2$. These tissue geometries contained 1s and 0s that correspond to excited cells within parallel and tapered boundaries and inexcited cells outside the boundaries.

An example of the slim geometry and H-geometry is provided in Appendix, Figures 1 and 2.

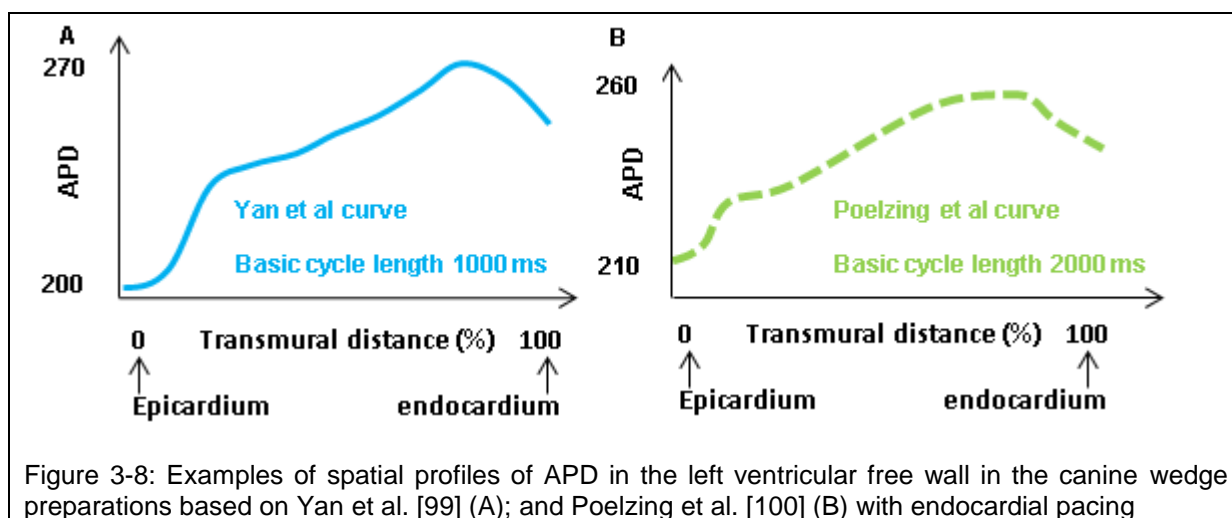
All 2D tissues were isotropic to highlight the effect of structural discontinuities created by abrupt changes in tissue geometry on (1) spatial and restitution profiles of activation time, repolarization time, and APD; (2) three measures of dispersion in activation time,

repolarization time, and APD; and (3) speed of depolarization conduction. These tissues were composed of 100% epicardial cells (epi), 100% mid-myocardial cells (M), and 100% endocardial cells (endo).



3.7.1-2 Tissue with 3D geometries

The real ventricular mass is formed by the anatomical arrangements of the myocardial cells in 3D geometry. A human study showed that increase in APD is relatively gradual in transmural direction [98]. However, a sharp increase in APD has been observed between the epicardium and sub-epicardium in arterially perfused canine left ventricular wedge preparations [99] and between mid-myocardium and sub-epicardium in intact canine heart preparations [100] as shown in Figure 3-8.



To address these issues, two groups of 3D cubes of homogenous and heterogeneous tissue were simulated. Homogenous tissues were introduced with a linear change in fibre orientation. Heterogeneous tissues were introduced with initially sharp and then gradual APD. Three approaches were used to create gradual APD in the transition regions with different cell type: (1) changing the proportion of different cell types; (2) changing anisotropic diffusion coefficients along and across the fibre axis; and (3) creating fibre structure with a linear or a non-linear change in fibre orientation.

Currently, there is no complete and detailed data that specifies the composition of the human ventricular wall. Therefore, 3D cubes of tissue were simulated with different combinations of epicardial, mid-myocardial, and endocardial cells, close to previous experimental or simulation studies in the human left ventricle. In total, 3D tissues were simulated with seven cellular configurations as shown in Figure 3-9.

- Three cubes of homogenous tissue composed of one ventricular cell type

To represent a homogenous section through the left ventricular free wall, three cubes of tissue were simulated with one ventricular cell type composed of 100% epicardial cells, 100% mid-myocardial cells, and 100% endocardial cells, (Figure 3-9, schemes 1 to 3).

- One cube of heterogeneous tissue composed of two ventricular cell type

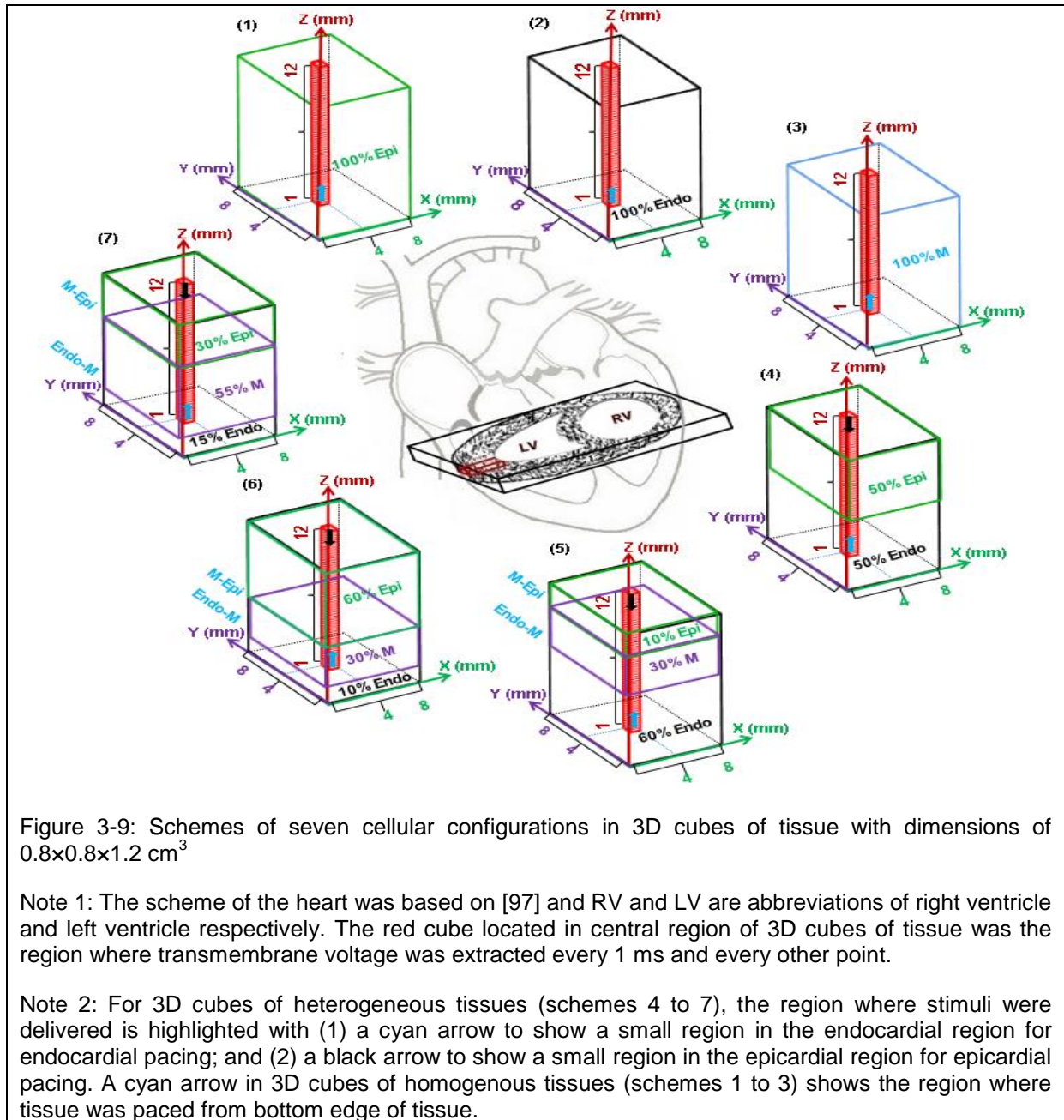
To represent a heterogeneous section through the left ventricular free wall without mid-myocardial cells (Figure 3-9, scheme 4), a cube of tissue was simulated with two ventricular cell type composed of 50% epicardial and 50% endocardial cells close to a modelling study by Cates et al. [65] and Okada et al. [53].

- Three cubes of heterogeneous tissue composed of three ventricular cell type

To represent a heterogeneous section through the left ventricular free wall with mid-myocardial cells, three cubes of tissue were simulated composed of three ventricular cell types. For the first two simulated tissues, the mid-myocardial cellular population was kept 30% of the total cellular populations in 3D cubes of tissue based on human experimental study by Drouin et al. [101]. Since currently there was no clear evidence to place mid-myocardial cells close to endocardium or epicardium, two configurations of epicardial and endocardial cells were used close to the human model by Okada et al. [53] with 60%endo-30%m-10%epi cells and 10%endo-30%m-60%epi cells as shown in Figure 3-9, schemes 5 and 6.

The third tissue was simulated with mid-myocardial cells placed between endocardial and epicardial cells but with greater numbers of cellular populations than epicardial and endocardial cells. This tissue was composed of 15%endo-55%mid-30%epi as shown in Figure 3-9, scheme 7. This cellular configuration was previously used by a number of combined clinical and modelling studies for different objectives, i.e. (1) testing the effect of sea anemone toxin, ATX-II on the location of mid-myocardial cells in the human left ventricular wedge using the human ventricular cell model of ten-Tusscher et al. [49] and the bidomain model including idealized fibre-sheet structure [76]; (2) studying whether abnormalities of calcium cycling explain AP oscillation and arrhythmic vulnerability in the human heart failure [102]; and (3) studying the effects of fast and slow pacing rate on alternans in AP voltage and whether calcium handling explains the rate dependant AP alternans in human heart failure [103]. The latter two studies were based on the human ventricular cell model [2] and the bidomain model.

All 3D cubes of tissue had $40 \times 40 \times 60$ grid points and dimensions of $0.8 \times 0.8 \times 1.2 \text{ cm}^3$ close to the size of human left ventricular wedge preparation in the experimental study by Drouin et al. [7]. Numerical values that were used to specify the heterogeneous of expression of ion channels in the epicardial, mid-myocardial, and endocardial regions within 3D cubes of tissue are provided in Appendix, Table 1.



The electrical anisotropy or discontinuous propagation is referred to the dependence of conduction properties (i.e. velocity, and other electrical parameters) on direction of impulse propagation in which they are measured and electrical isotropic is referred to the uniform electrical properties in all directions. All 3D cubes of simulated tissue were categorized as:

- isotropic tissue simulated with isotropic diffusion coefficients;
- anisotropic tissue without fibrosis simulated with anisotropic diffusion coefficients;
- anisotropic tissue with fibrosis.

In this thesis, fibrosis was simulated by reproducing randomly 0s as in-excitabile and 1s as excitable cells in geometrical tissue models with seven cellular configurations. For all cellular configurations in 3D cube of tissue, the amount of simulated excitable cells was 56% of the total number of grid points in tissue and the amount of inexcitable cells was 44% of the total number of grid points in tissue.

Table 3-5 provides diffusion coefficients for isotropic and anisotropic tissues. Comparison between simulation results with isotropic and anisotropic diffusions highlights the effects of isotropic and anisotropic conduction on the shape and duration of AP, speed of depolarization conduction, and three measures of dispersion in activation time, repolarization time, and APD in 3D cubes of homogenous and heterogeneous tissue. Moreover, simulation results of 3D cubes of anisotropic fibrosis tissue highlight how structural discontinuities created by fibrosis combined with tissue anisotropy can promote electrical disturbances and wave break from isotropic to anisotropic fibrosis tissue. It is important to note that for consistency, the cellular configurations in 3D cubes of isotropic, anisotropic, and anisotropic fibrosis tissue were kept similar.

3.7.1-3 Left ventricular wedge model

The last part of simulations in this study introduces the left ventricular wedge model including tissue and fibre geometries obtained from the centre for cardiovascular bioinformatics and modelling of the Johns Hopkins University [90] using a diffusion tensor-magnetic resonance imaging (DT-MRI) [104]. The left ventricular wedge with dimensions of $3.5 \times 11.0 \times 6.0 \text{ cm}^3$ is shown in Figure 3-10, plot A. This tissue geometry is explained in detail in Chapter 6.

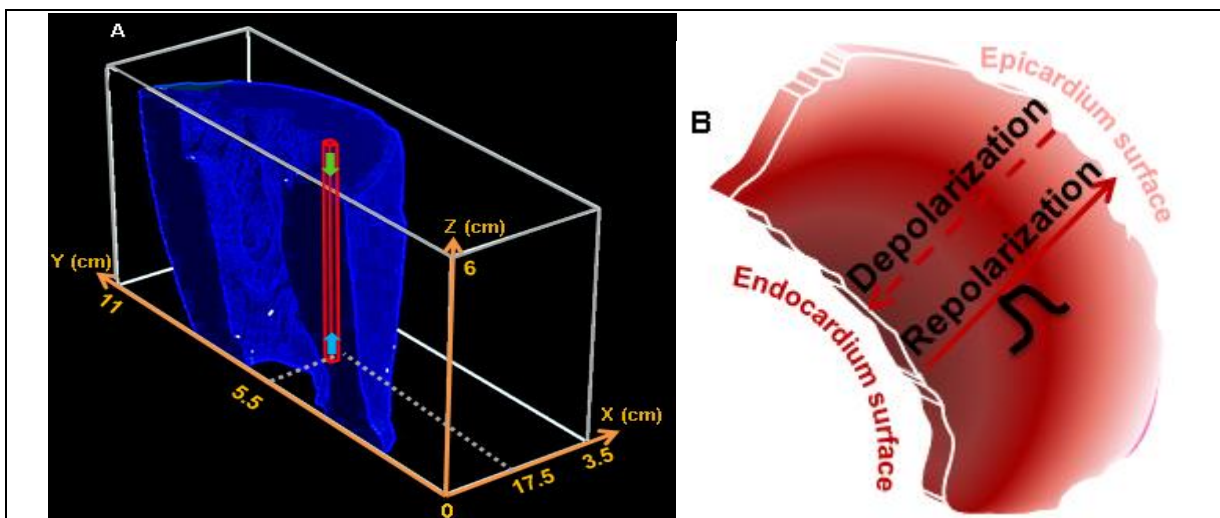


Figure 3-10: A scheme of left ventricular wedge model with dimensions of $3.5 \times 11.0 \times 6.0 \text{ cm}^3$ in this thesis (A); and a scheme of a slice of the left ventricular wedge model with different ventricular cell type showing direction of ventricular AP depolarization and AP repolarization based on [105]

Note: Stimuli were delivered to a small region in epicardial region of the wedge model shown as a cyan arrow for apex to base conduction and a green arrow for base to apex conduction.

Comparison the simulation results of left ventricular wedge model and 3D cubes of tissue may highlight the effect of real tissue and fibre structure on spatial and restitution profiles of activation time, repolarization time, and APD as well as three measures of dispersion in activation time, repolarization time, and APD. It is important to note that all 3D simulations run in the absence of the sheet structure due to current lack of data in detail.

3.7.1-4 Direction of conduction in tissues

In the healthy human myocardium, ventricular depolarization and repolarization occur in opposite direction as shown in Figure 3-10, plot B. The ventricular activation starts from terminal branches of the right and left bundle branches in endocardial region and propagates through the ventricular wall. Although the epicardium is activated last, it is repolarized first, producing a repolarization sequence that is spread from the sub-epicardium toward the sub-endocardium. In this thesis, the region where stimuli were delivered in 2D tissue geometries, 3D cubes of tissue, and the left ventricular wedge model are described here.

- 2D tissue geometries shown in Figure 3-7

All homogenous tissues composed of one ventricular cell type (i.e. 100% epicardial cells, 100% mid-myocardial cells, and 100% endocardial cells) were paced only in one direction to assign the APD restitution to the individual cell. The region was in the left edge of 2D tissue geometries (rows from 1 to 200 and columns from 1 to 3).

- 3D cubes of tissue shown in Figure 3-9

In 3D cubes of heterogeneous tissue composed of two or three ventricular cell types, stimuli were delivered to:

1. a small region in the endocardial region (rows and columns from 28 to 32 and layers 3 and 4) in order to create the sequence of ventricular activation from the endocardial to the epicardial region (endocardial pacing);
2. a small region in the epicardial region (rows and columns from 28 to 32 and layers 58 and 59) to create the reverse sequence of ventricular activation from the epicardial to the endocardial region (with epicardial pacing).

For 3D cubes of homogenous tissue composed of one ventricular cell type (100% epicardial cells, 100% mid-myocardial cells, and 100% endocardial cells), tissue was paced from a small region (rows and columns from 28 to 32 and layers 3 and 4) in the bottom edge of tissue.

- Left ventricular wedge model shown in Figure 3-10

For the left ventricular wedge model composed of heterogeneous tissue, the focus was on epicardial pacing and stimuli were delivered to:

1. a small region in the epicardial region (with rows from 85 to 88, columns from 77 to 80, and layers 3 and 4) to create apex to base conduction;
2. a small region in the epicardial region (with rows from 85 to 88, columns from 77 to 80, and 292 and 293) to create base to apex conduction.

For the homogenous left ventricular wedge model composed of 100% epicardial cells, 100% mid-myocardial cells, and 100% endocardial cells, tissue was paced from epicardial region (with rows from 85 to 88, columns from 77 to 80, and layers 3 and 4) to create apex to base conduction.

This approach may highlight the effects of reversing the direction of ventricular activation on the shape and duration of AP, speed of depolarization conduction, and three measures of dispersion in activation time, repolarization, and APD in heterogeneous tissues. For clarity, Table 3-1 provides numerical values of geometrical tissue models.

Geometry	Space step (cm)	Time step (ms)	Dimensions (grid points)	Tissue size	Paced region (grid points)
2D slim geometry	0.025	0.1	200×4	5×0.1 cm ²	200×2
2D H-geometry and other 2D geometries	0.025	0.1	200×200	5×5 cm ²	200×3
3D cube	0.02	0.05	40×40×60	0.8×0.8×1.2 cm ³	4×4×2
A left ventricular wedge model	0.02	0.05	175×550×300	3.5×11×6 cm ³	4×4×2

Table 3-1: Numerical values for geometrical tissue models

3.7.2 Geometrical models of fibre structure

The helically orientated myocardial fibres create left ventricular motion. For example, in the transmural region of the left ventricular wall, longitudinal epicardial fibres run clockwise from apex to base, in the mid-myocardial region fibres have circular geometry, and fibres spiralling anti-clock wise close to the epicardial region [106].

The dependence of fibre rotation on ventricular depth is well established. However, the current knowledge about whether the change in fibre orientation is linear [55, 107] or non-linear [66, 108] is not sufficient. In many multidimensional propagation models, it is often assumed that cardiac tissues are comprised of a collection of parallel fibres and are formulated in a spatial coordinate system in which an average myocytes direction (or fibre orientation) at each point can be defined. In this thesis, tissues were simulated

- in the absence of fibre geometry for 2D slabs of tissue;
- with fibre structure that was created for 3D cubes of tissue based on two assumptions: firstly, rotation of fibres are linear function of the transmural coordinate and the fibres run parallel to the inner and outer surfaces, and secondly, rotation of fibres are not linear;
- with fibre structure that was obtained from experimental measurement [90].

Fibre structure significantly affects both the excitation and repolarization [56]. Comparison of results for tissues with and without fibre structure may provide a new insight about the interaction of activation-repolarization coupling and restitution properties with two human ventricular tissues. In 3D simulations, geometrical fibre models were created based on equations that are briefly described in the following sections.

3.7.2-1 Linear change in fibre orientation in 3D cubes

To represent the spatial orientation of ventricular cell (the fibre orientation), the fibre geometry in this thesis specified three fibre components a_1 , a_2 , and a_3 in X, Y, and Z direction for each cell in tissues as shown in Figure 3-11, scheme B. In 3D cubes of tissue geometry, each cell had a position defined by n_x , n_y , and n_z that corresponds to number of rows, columns, and layers in tissue. The term layers was used by Greenbaum et al. [106] to describe regions of little change in fibre orientation in contrast to the region of rapid change in fibre orientation.

If it is assumed that the fibre rotation is linear with changing ventricular wall depth in z , then the fibre rotation angle θ is a linear function of depth, $\theta(z)$, and is given by Equation 3-1 used by Hyatt et al. in 2003 [109]:

$$\theta(z) = 90^\circ + (\text{layer} - 1) \times \frac{120^\circ}{z} \quad \text{Equation (3-1)}$$

After integration of Equation 3-1:

- Total transmural rotation of 120° over z range is produced between endocardial and epicardial regions from $+60^\circ$ to -60° based on the experimental study. For example, Streeter [55] established roughly 60° helical angular orientations of myocytes around the ventricular equator (that was confirmed by diffusion-tensor magnetic-resonance imaging in the rat heart [110]). In the canine hearts, LeGrice et al. [111] and Helm et al. [26] measured the total transmural fibre rotation of 180° from $+90^\circ$ at the epicardium to -90° at the endocardium.
- Fibre rotation angle increases linearly with layers from 90° to 210° .
- Fibres rotate counter-clockwise with increasing layers (i.e. as observed in a human experimental study by Greenbaum et al. [106] and [112]).

Figure 3-11 shows the fibre rotation in five selected layers of the 3D cube of tissue.

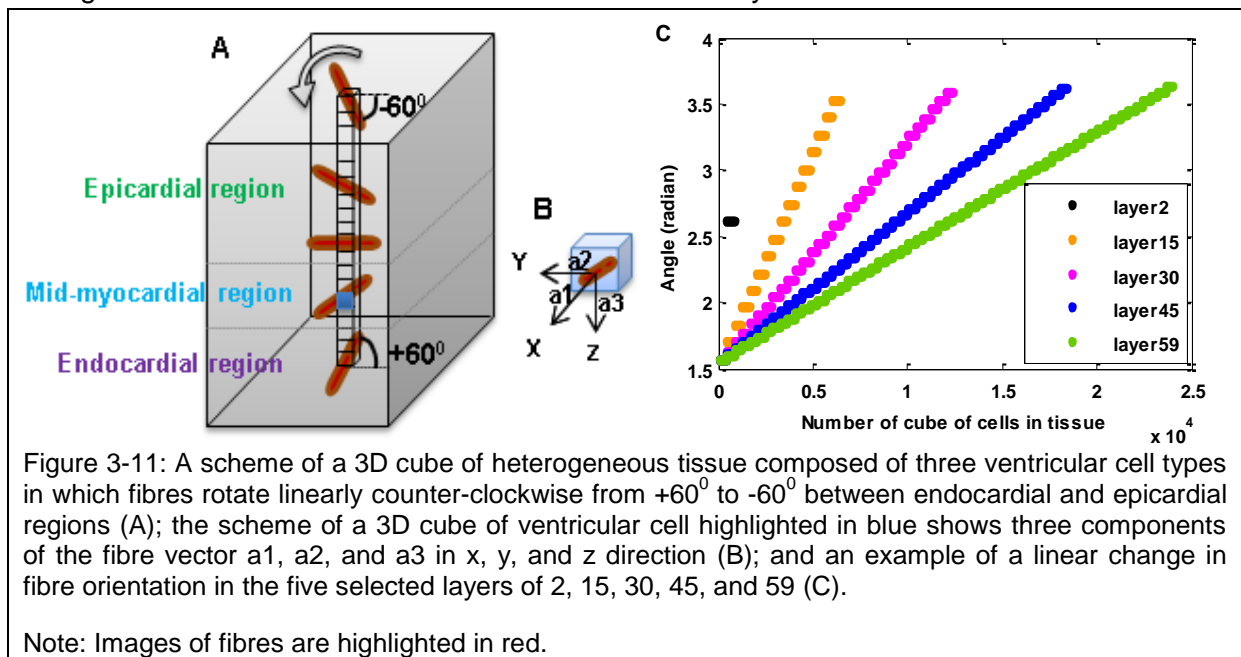


Figure 3-11: A scheme of a 3D cube of heterogeneous tissue composed of three ventricular cell types in which fibres rotate linearly counter-clockwise from $+60^\circ$ to -60° between endocardial and epicardial regions (A); the scheme of a 3D cube of ventricular cell highlighted in blue shows three components of the fibre vector a_1 , a_2 , and a_3 in x , y , and z direction (B); and an example of a linear change in fibre orientation in the five selected layers of 2, 15, 30, 45, and 59 (C).

Note: Images of fibres are highlighted in red.

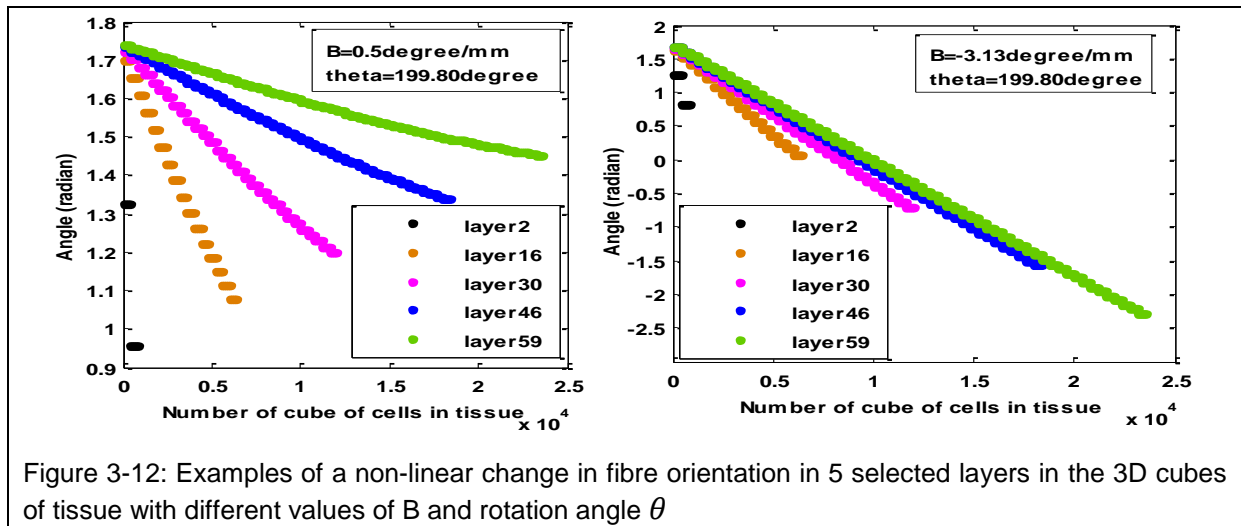
3.7.2-2 Non-linear change in fibre orientation in 3D simulations

Since a linear change in fibre orientation may be wrong, the Equation 3-2 based on the Boltzmann equation [66] was used to produce a non-linear fibre rotation.

$$\theta(z) = B \times layer + \frac{\theta}{1 + e^{-\frac{layer}{z}}} \quad \text{Equation (3-2)}$$

B is a variable in degree/mm and θ is fibre rotation angle in degree.

It is important to note that Boltzmann equation was used by Vetter et al. [66] to study an abrupt change in local fibre orientation in swine right ventricular sub-epicardium. Figure 3-12 shows examples of a non-linear change in fibre orientation in the five selected layers against number of cells in the 3D cubes of tissue.



The following sections describe the cell models and the tissue model that were used in this thesis and justifications for choosing them.

3.7.3 Cell models

Nowadays, there are a variety of cardiac cell models in [113] based on animal data. However, there are only seven human ventricular cell models that were developed by: (1) Priebe-Beuckelmann in 1998 with 17 variables [114] (the PB model), then Bernus et al. [115] reduced the model variables to six in 2002; (2) ten Tusscher-Noble-Noble-Panfilov [49] with 17 variables in 2004 (the TNNP model); (3) Iyer-Mazhari-Winslow [116] with 67 variables in 2004 (the IMW model); (4) ten Tusscher-Panfilov [2] with 21 variables in 2006 (the TP06 model); (5) Bueno-Orovio-Cherry-Fenton [1] with 4 variables in 2008 (the FK4V model); (6) Grandi-Pasqualini [117] in 2010; (7) O'Hara-Virág-Varró-Rudy [118] with 41 variables in 2011 (the ORD model).

The comparison among these models (except the ORD model) by Bueno-Orovio et al. [1] showed differences in the behaviour of re-entry among the PB model [114], the TNNP model [49], and the IMW model [116]. The APD and conduction velocity rate adoption were quantitatively different among these models because these models (1) may represent properties associated with different regions of the epicardium i.e. between apex to base or between anterior and posterior differences; and (2) may be designed for use as isolated myocytes or for slow pacing rates, and may not be suitable for rapidly paced tissue [1].

In this thesis, the human ventricular cell was described using the FK4V model [1] and the TP06 model [2] because:

- both models are able to reproduce the reliable spatial and restitution profiles of epicardial, mid-myocardial, and endocardial cells in the human left ventricle which play an important role in arrhythmias and the profiles agreed with experimental studies;
- simulation results can be compared with the TP06 model with more realistic formulations of calcium dynamics and the FK4V model with a simple description of calcium currents.

3.7.3-1 A simple cell model

The main advantages of the FK4V model [1] compared to the TP06 model are:

- Computationally cheap

The FK4V model compared to the TP06 model is cheaper to compute because this model is mathematically less complex and faster particularly for simulations with the wedge models. Table 3-2 provides examples of running time and memory for simulated tissues in this thesis. The maximum running time for the left ventricular wedge model at only one S1S2 interval was around 7 days with the FK4V model [1] and more than seven days with the TP06 model [2]. Therefore, this thesis used FK4V model to simulate tissue with the wedge. In addition, it was not possible to simulate a wedge model with the TP06 model in the serial method.

	2D slim geometry with at least 12 S1S2 intervals		2D H-geometry with at least 12 S1S2 intervals		3D cube of tissue with at least 12 S1S2 intervals		Left ventricular wedge model at one S1S2 interval	
	Time	Maximum memory	Time	Maximum memory	Time	Maximum memory	Time	Maximum memory
FK4V model	5 minute	135 GigaByte	2 hours & half	138 GigaByte	14 hours	170 GigaByte	7 days	5 GigaByte
TP06 model	30 minute	136 GigaByte	22 hours	144 GigaByte	2 days & 16 hours	181 GigaByte		

Table 3-2: Running time and virtual memory for simulations in this thesis with both models

- Smaller number of variables

The small number of variables in this model allows the role of individual parameters in generating AP shapes, and APD and conduction velocity restitution curves to be specified.

- Three phenomenological currents

One limitation of the FK4V model is that variation of model parameters may produce results with no physiological interpretation. Nevertheless the AP profiles during repolarization are faithfully reproduced for epicardial, mid-myocardial, and endocardial tissue by the FK4V model as shown in Figure 3-13, and so this model can be used for tissue scale simulations.

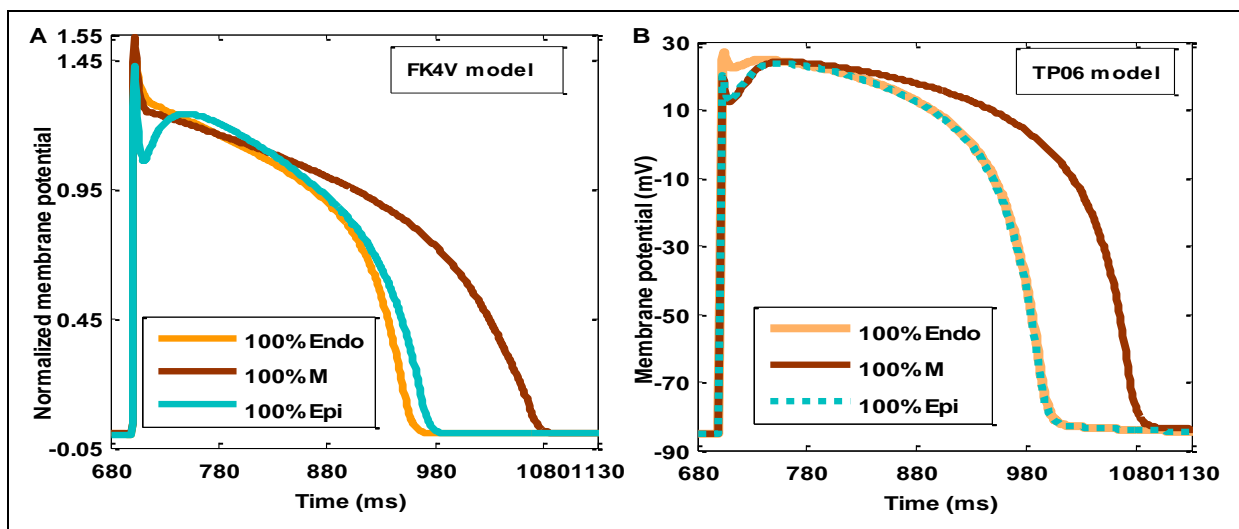


Figure 3-13: Profiles of AP of endocardial, mid-myocardial, and epicardial tissues at S1S2 interval of 700 ms with the FK4V model (A); and the TP06 model (B).

Plot A shows the spike-and dome morphology in AP profile of the simulated isotropic epicardial tissue, the longer APD of mid-myocardial tissue than endocardial and epicardial tissues, the notch appearance in the AP profile of endocardial tissues. Plot B shows that APD of epicardial and endocardial tissues with the TP06 model are roughly equal.

Three phenomenological currents quantitatively are described by equations [1] that are provided in Table 3-3 to estimate the dynamic concentration changes of three ions including sodium Na^+ , potassium K^+ , and calcium Ca^{2+} .

3 phenomenological currents	4 gate variables and the time parameters as functions of the voltage variable u
$J_{fi} = -vH(u - \theta_v)(u - \theta_v)(u_u - u) / \tau_{fi}$ <p>J_{fi}: A fast inward current that corresponds to the sodium current I_{Na} responsible for AP depolarization of the cell membrane and depends on inactivation-reactivation gate v</p>	<p>u: The membrane voltage</p> <p>v: The gating variable that regulates inactivation-reactivation of the fast inward sodium I_{Na}</p>
$J_{so} = (u - u_o)(1 - H(u - \theta_w)) / \tau_o + H(u - \theta_w) / \tau_{so}$ <p>J_{so}: A slow, time-independent, outward current that corresponds to the potassium current I_K responsible for repolarization of the membrane u</p>	<p>The gating variable w regulates inactivation-reactivation of the slow inward calcium I_{Ca} currents</p> $\tau_o = (1 - H(u - \theta_o))\tau_{o1} + H(u - \theta_o)\tau_{o2}$ $\tau_{so} = \tau_{so1} + (\tau_{so2} + \tau_{so1})(1 + \tanh(k_{so}(u - u_{so}))) / 2$
$J_{si} = -H(u - \theta_w)ws / \tau_{si}$ <p>J_{si}: A slow inward current that corresponds to the I_{Ca}, activated during the plateau phase of AP and depends on inactivation-reactivation gate w</p>	<p>s: Surface area of human ventricular cells that adjusts the inward current for shape of AP</p> $\tau_s = (1 - H(u - \theta_w))\tau_{s1} + H(u - \theta_w)\tau_{s2}$ <p>w: The gating variable regulates inactivation-reactivation of I_{Ca}</p>
<p>Ordinary differential equations describe the rates of changes of state variables</p>	
$\frac{\partial v}{\partial t} = (1 - H(u - \theta_v)) - (v_\infty - v) / \tau_v^- - H(u - \theta_v)v / \tau_v^+$ <p>with infinity values of $v_\infty = \begin{cases} 1, u < \theta_v^- \\ 0, u \geq \theta_v^- \end{cases}$</p>	$\tau_v^- = (1 - H(u - \theta_v^-))\tau_{v1}^- + H(u - \theta_v^-)\tau_{v2}^-$
$\frac{\partial w}{\partial t} = (1 - H(u - \theta_w)) - (w_\infty - w) / \tau_w^- - H(u - \theta_w)w / \tau_w^+$ <p>with infinity value of</p> $w_\infty = (1 - H(u - \theta_o))(1 - u / \tau_{w_\infty}) + H(u - \theta_o)w_\infty^*$	$\tau_w^- = \tau_{w1}^- + (\tau_{w2}^- + \tau_{w1}^-)(1 + \tanh(k_w^-(u - u_w^-))) / 2$
<p>Note: $H(x)$ is the standard Heaviside step function defined by 1 and 0 for x greater than zero and otherwise</p>	

Table 3-3: Current equations, ordinary differential equations, and gate variables in the FK4V model [1]

The FK4V model parameters are provided in Appendix, Table 3.

3.7.3-2 A detailed cell model

The main difference between the TP06 model [2] and the FK4V model is that the TP06 model is a biophysically detailed description of the individual ventricular cells and describes more realistic formulations of calcium dynamics. In addition, the TP06 model [2] is able to explain the ionic mechanism of cardiac AP particularly the effects of sodium current recovery dynamics in combination with APD restitution on spiral breakup.

In this model, the formulation for some description of intracellular calcium dynamics was improved in order to: (1) control the dynamics of the L-type calcium current and the ryanodine receptor current by including subspace calcium dynamics; (2) model calcium-induced calcium release with a reduced version of the Markov-state model [119] for the ryanodine receptor; and (3) reproduce L-type calcium current dynamics that agree better with experimental data using both fast and slow voltage-gated inactivation of the L-type calcium current.

This model has 21 variables (including 12 gate variables and 9 other variables) and 14 currents provided that are provided in Table 3-4. The 14 currents in the TP06 model [2] were mainly based on previous version of the model of ten-Tusscher et al. [49] except for new formulation of slow delayed rectifier potassium current, L-type calcium current, and adenosine three phosphate dependent potassium current. It is important to note that three ventricular cells were distinguished by (1) the steady-state value of gates and the time constant of gates for transient outward current; and (2) the parameters for slow delayed rectifier current (Appendix, Table 4). The equations for integrating the gating variables were in the form of Hodgkin-Huxley equations [120] and were described by the ordinary differential equations.

14 currents	21 variables
Fast sodium current $I_{Na} = G_{Na} m^3 h j (V - E_{Na})$	m: an activation gate h: a fast inactivation gate j: a slow inactivation
Transient outward current differ for three ventricular cells type $I_{to} = G_{to} r s (V - E_K)$	r: a voltage-dependent activation gate S: a voltage-dependent inactivation gate
Rapid delayed rectifier current $I_{Kr} = G_{Kr} \sqrt{\frac{k_0}{5.4}} x_{r1} x_{r2} (V - E_K)$	x_{r1} : an activation gate x_{r2} : an inactivation gate
Slow delayed rectifier current differ for three ventricular cell type $I_{Ks} = G_{Ks} x_s^2 (V - E_{Ks})$	x_s : an activation gate
L-type calcium current $I_{CaL} = G_{CaL} d f_2 f_{cass} \cdot 4 \frac{(V - 15) F^2}{RT} \frac{0.25 Ca_{ss} e^{2(V-15)F/RT} - Ca_0}{e^{2(V-15)F/RT} - 1}$	d: a voltage-dependent activation gate f: a slow voltage inactivation gate f_2 : a fast voltage inactivation gate f_{cass} : a fast subspace calcium inactivation gate Ca_{ss} : free dyadic subspace calcium concentration
Inward rectifier potassium $I_{K1} = G_{K1} \sqrt{\frac{k_0}{5.4}} x_{K1\infty} (V - E_K)$	K_i : intracellular potassium concentrations
Sodium/calcium exchanger current $I_{NaCa} = k_{NaCa} \frac{e^{\gamma VF/RT} Na_i^3 Ca_0 - e^{(\gamma-1)VF/RT} Na_0^3 Ca_i \alpha}{(k_{mNa_i}^3 + Na_0^3)(K_{mCa} + Ca_0)(1 + K_{ss1} e^{(\gamma-1)VF/RT})}$	Ca_i : free cytoplasmic calcium concentration Na_i : intracellular sodium concentrations
Plateau calcium current $I_{PCa} = G_{PCa} \frac{Ca_i}{K_{PCa} + Ca_i}$	$CaSR$: free sarcoplasmic reticulum calcium concentration
Plateau potassium current $I_{PK} = G_{PK} \frac{V - E_K}{1 + e^{(25-V)/5.98}}$	X_{mem} : memory
Background currents $I_{bNa} = G_{bNa} (V - E_{Na})$ $I_{bCa} = G_{bCa} (V - E_{Ca})$	V: transmembrane potential
Adenosine three phosphate (ATP) dependent potassium current $I_{katp} = \overline{G}_{katp} \cdot (U[V] - E_K)$ \overline{G}_{katp} : Conductance of the ATP-sensitive K channel (nS/ μ F)	oo: open conducting state rr: resting closed state

Table 3-4: Current equations and gate variables in the TP06 model [2]

3.7.4 The monodomain tissue model

This thesis modelled the continuous approximation of the cardiac tissue using the monodomain model because it has been shown that:

- the monodomain model is likely a proper tool for modelling cardiac tissue as in this model the preparation lies in a large volume conductor so that extracellular potential field is small enough to be negligible, suggested by Henriquez and Tranquillo [121];
- the patterns of AP propagation in the absence of external stimuli (Potse et al. [122]) as well as the spiral wave tip trajectories (Roth [123]) were almost similar using monodomain and bidomain models;
- the patterns of AP propagation in the absence of injection of current into the extracellular space in both models were almost close to each other even under unequal anisotropy ratio in the intracellular and extracellular spaces (Colli Franzone et al.[85]).

Monodomain equations are non-linear partial differential equations that are known as the reaction-diffusion equations [124]. The reaction term describes the total current flow through ion channels, pumps, and exchangers in the cardiac cell membrane. Diffusive term gives current flow due to the gradients in transmembrane potential. In diffusive term, a diffusion tensor can determine the dependence of electrical isotropy and anisotropy to the direction of impulse propagation in which they are measured. A brief description of the diffusive and reaction terms in 2D and 3D monodomain equations that were used in this thesis are provided here.

- Diffusive term in 2D isotropic monodomain equation

In 2D simulations, the membrane voltage u follows the standard continuous monodomain reaction-diffusion equation [75] described by Equation (3-3) with a no-flux boundary condition at each edge. In another words, there is zero current flow normal to the tissue boundaries where the tissue is electrically isolated ($\frac{\partial u}{\partial x} = 0$ and $\frac{\partial u}{\partial y} = 0$). In this case, the diffusion of neighbouring cells D is constant. Diffusion of ionic currents through gap junctions between adjacent cells can be described by the diffusive term [59].

the diffusive term the reaction term

$$\frac{\partial u}{\partial t} = D \left(\frac{\partial^2 u}{\partial y^2} + \frac{\partial^2 u}{\partial x^2} \right) - \frac{I_{ion}}{C_m} \quad \text{Equation (3-3)}$$

$\frac{\partial u}{\partial t}$: Rate of change of transmembrane potential u

D : The intracellular diffusion tensor (cm^2/ms)

I_{ion} : The total transmembrane ionic current determined by cell models ($\mu\text{A}/\text{cm}^3$)

C_m : The space membrane capacitance per unit area of 1 ($\mu\text{F}/\text{cm}^2$)

- Diffusive term in 3D anisotropic monodomain equation

Equation (3-4) from [124] was used to describe the axially symmetric anisotropic monodomain model in 3D cubes of tissue and the left ventricular wedge model. The ventricular conductivity tensor in diffusive term is described by Equation (3-5) and Equation

(3-6) [45]. The assumption was that transverse conductivity is the same in all directions orthogonal to the direction of the fibre axis.

the diffusive term **the reaction term**

$$\frac{\partial u}{\partial t} = \nabla \cdot (D_{3 \times 3} \nabla u) - \frac{I_{ion}}{C_m} \quad \text{Equation (3-4)}$$

u: The transmembrane potential (mV)

I_{ion} : The total transmembrane ionic current determined by cell models ($\mu A/cm^3$)

C_m : The space membrane capacitance per unit area of $1 \mu F/cm^2$

∇ : The 3D gradient operators consists of spatial derivatives

$D_{3 \times 3}$: The 3×3 diffusion matrix with elements given by (Panfilov-Keener [45]):

$$d_{ij} = D_2 I_{ij} + (D_1 - D_2) f_i f_j^T$$

$$d_{ij} = \begin{cases} D_2 + (D_1 - D_2) \times f_i f_j & i = j \\ (D_1 - D_2) \times f_i f_j & i \neq j \end{cases} \quad \text{Equation (3-5) and Equation (3-6)}$$

D_1 and D_2 : Diffusion coefficients along and across the fibre axis

i and j: Number of rows and columns in the matrix

f and f^T : A unit vector in the muscle fibre direction and transpose of it

I_{ij} : Identity matrix

- Reaction term based on cell models

In this thesis, the reaction term that describes the total current in the ventricular cell membrane was obtained based on the FK4V model [1] and TP06 [2] model. Examples of APD restitution profiles of 2D isotropic slim epicardial, mid-myocardial, and endocardial tissues with size of $5 \times 0.1 \text{ cm}^2$ at S1S2 interval of 800 ms are shown in Figure 3-14 and Figure 3-15. The shape of APD restitution curves with both model with a diffusion coefficient of $0.001171 \text{ cm}^2/\text{ms}$ were roughly similar.

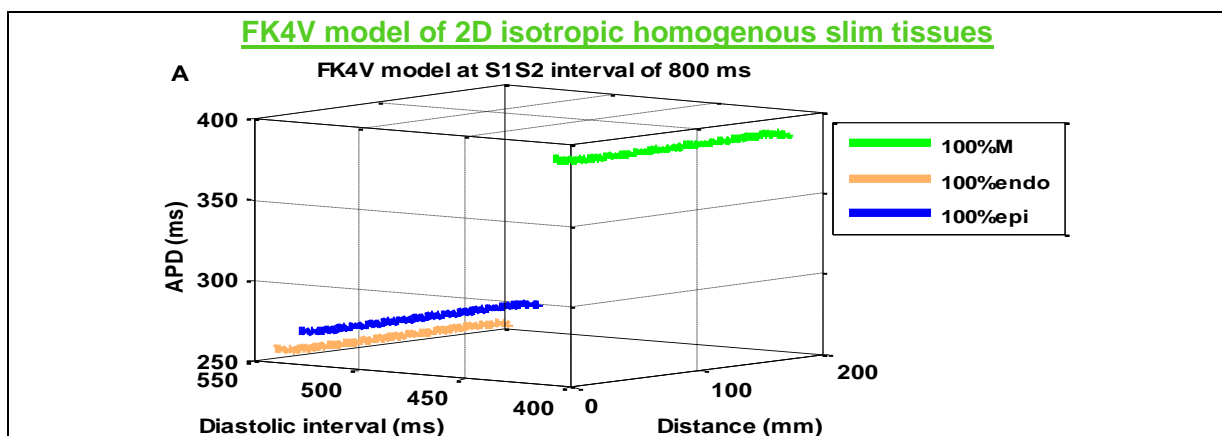


Figure 3-14: Restitution profiles of APD in 2D isotropic slim epicardial, mid-myocardial, and endocardial tissue with the FK4V model

The reaction term in the monodomain tissue model with the FK4V model [1] is based on three phenomenological currents (1) a fast inward current J_{fi} ; (2) a slow time-independent outward current J_{so} ; and (3) a slow inward current J_{si} (given by: Total current = $J_{fi} + J_{so} + J_{si}$)

TP06 model of 2D isotropic homogenous slim tissues

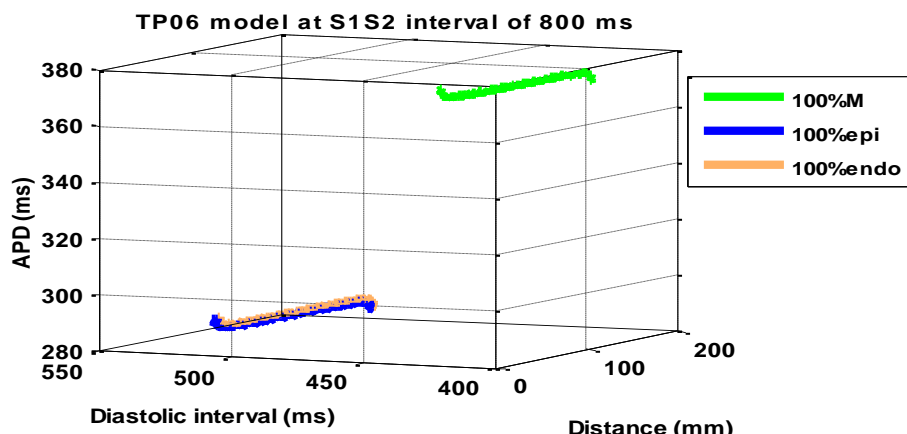


Figure 3-15: Restitution profiles of APD in 2D isotropic slim epicardial, mid-myocardial, and endocardial tissue with the TP06 model based on the reaction term given by:

$$I_{ion} = I_{Na} + I_{K1} + I_{to} + I_{Kr} + I_{Ks} + I_{CaL} + I_{NaCa} + I_{NaK} + I_{PCa} + I_{PK} + I_{bCa} + I_{bK} + I_{KatP} + I_{sim}$$

Fast sodium current I_{Na} , inward rectifier potassium current I_{K1} , transient outward current I_{to} , rapid delayed rectifier current I_{Kr} , slow delayed rectifier current I_{Ks} , L-type calcium current I_{CaL} , sodium/calcium exchanger current I_{NaCa} , sodium/potassium pump current I_{NaK} , plateau calcium current I_{PCa} , plateau potassium current I_{PK} , background currents I_{bCa} and I_{bK} , adenosine three phosphate (ATP) dependent potassium current I_{KatP} , and stimulus current I_{sim} set to -52 $\mu A/\mu F$.

The FK4V model [1] used the general description of calcium current for the reaction term while the TP06 model [2] was based on the experimental restitution data from [48] plus an improved description of intracellular calcium dynamics. The calcium ions and its components play an important role in cardiac excitation-contraction coupling. In addition, the reaction term in the monodomain tissue model with the TP06 model [2] and the FK4V model [1] was with and without stimulus current respectively. The reason was that in the TP06 model, the stimulus current was used in the formulation of intracellular potassium kinetic in order to match the transient time scales and equilibrium concentrations to the range of experimental measurements [125]. However, stimulus current had no effect on the phenomenological currents in the simple FK4V model [1].

The ventricular wall has the anisotropic (orthotropic) properties. From available data, diffusion in the longitudinal direction is 2 to 10 times greater than transvers direction [95]. The diffusion coefficients that were used in this thesis and examples of the speed of depolarization conduction at S1S2 interval of 700 ms are provided in Table 3-5. Diffusion 1 and Diffusion 2 defined the diffusion along and across the fibre axis.

These diffusion coefficients were previously used by Taggart et al. [2] to match the maximum conduction velocity of paced depolarization wave 70 cm/s along fibre direction (Taggart et al. [126]) and minimum conduction velocity of 41 cm/s across the fibre direction (Nanthakumar et al. [127]) in the human ventricular tissue. A brief discretion of obtaining isotropic diffusion coefficients based on experimental studies is provided in enclosed CD, appendix.

	Diffusion 1 (cm ² /ms)	Diffusion 2 (cm ² /ms)	Speed of depolarization conduction (m/s) at S1S2 interval of 700 ms
isotropic 2D tissues	0.001171	0.001171	0.65 for endocardial, 0.64 for epicardial, and 0.73 for mid-myocardial slim tissue with the FK4V model
			0.60 for endocardial, epicardial, and mid-myocardial slim tissue with the TP06 model
isotropic 3D tissues	0.001	0.001	0.31 for endocardial, 0.30 for epicardial, and 0.70 for mid-myocardial tissue with the FK4V model
			0.49 for endocardial, epicardial, and mid-myocardial tissue with the TP06 model
anisotropic 3D tissues	0.001	0.00025	0.28 for endocardial, 0.26 for epicardial, and 0.29 for mid-myocardial tissue with the FK4V model
			0.225 for endocardial, epicardial, and mid-myocardial tissue with the TP06 model
anisotropic wedge models	0.001	0.00025	0.42 for endocardial, 0.39 for epicardial, and 0.45 for mid-myocardial tissue with the FK4V model

Table 3-5: Numerical values of the diffusion coefficient along and across the fibre axis and speed of depolarization conduction with the FK4V model and the TP06 model

3.7.5 Numerical methods

The monodomain model is a system of partial differential equations. To model the propagation of the electrical activity in the human heart, the ordinary differential equations are coupled with the system of partial differential equations. Therefore, the efficiency of solutions of the monodomain equation depends on the efficiency of the ordinary differential equation solvers [75]. Similar to the original FK4V model [1] and the TP06 [2] model, the solutions to the model equations in this thesis were based on (1) the forward Euler method for solution in time; (2) the finite difference method to approximate the differential in space; and (3) the Rush and Larsen method to solve equations for the gating parameters.

- The forward Euler method

In general, the ordinary differential equations can be solved using the explicit or the implicit methods. The forward Euler method is a first-order explicit method and can be used to integrate through time due to its ease of implementation. Assuming a constant rate of change of function $f(t, u)$ over small interval h (i.e. 0.02 ms), the ordinary differential equations can be intergraded as follows:

$t_{n+1} = t_n + h$	and	$u_{n+1} = u_n + hf(t_n, u_n)$
---------------------	-----	--------------------------------

On the other hand, the forward Euler method can be limited by stability constrains if the stiffness is not captured by dating equations [128]. In another words, numerical solution of the monodomain equation can be unstable if the step size is too large. In linear cases, stability of the numerical solution of the monodomain equation depends on the appropriate chose of time step and space step in order to satisfy:

$\frac{\text{time step}}{(\text{space step})^2} < 0.5$
--

For non-linear cases, the stability of numerical solution can be tested by comparing the convergence of solutions with a constant time step but different space step.

- Finite difference method

The spatial derivatives can be approximated with finite difference method. For a cell at x_i and time t_n , the solution is given by:

$$\frac{\partial u}{\partial x}(x_i, t_n) \approx \frac{u(x_{i+1}, t_n) - u(x_{i-1}, t_n)}{2(\Delta x)} \quad \text{and} \quad \frac{\partial^2 u}{\partial x^2}(x_i, t_n) \approx \frac{u(x_{i+1}, t_n) + u(x_{i-1}, t_n) - 2u(x_i, t_n))}{(\Delta x)^2}$$

- The Rush and Larsen method

The Rush and Larsen method [129] solves the equations for the gating variables with an exponential integrator. For a typical gating variable n , the Rush and Larsen method assumed a constant transmembrane potential, u (mV), over each step.

So, the solution of the ordinary differential equation of $\frac{dn}{dt} = \frac{n_\infty - n}{\tau_n}$ is given by:

$$n = n_\infty - (n_\infty - n_0) \times e^{\frac{-t}{\tau_n}}$$

$$n_\infty = \frac{\alpha_m}{\alpha_m + \beta_m} \quad \text{and} \quad \tau_n = \frac{1}{\alpha_m + \beta_m}$$

τ_n & n_0 : The time constant in ms^{-1} and steady-state value of each gate variable n

α_m & β_m : Constants parameters over a small time step

Consequently, the next value of n can be calculated as:

$$n(t + \Delta t) = n_\infty - (n_\infty - n(t)) \times e^{\frac{-\Delta t}{\tau_n}}$$

Δt : Time step

For the TP06 model, n_∞ and $e^{\frac{-dt}{\tau_n}}$ were calculated for the transmembrane potential u from -100 mV to +100 mV with a step of 0.1 mV (in the create-TNNPv2-lookup-OpSplit file described in Appendix).

- Finite element method

The finite element method is used to incorporate tissue and fibre geometries, fibrous structure, and boundary conditions of the heart wall, and the non-linear anisotropic material properties of the myocardium into a mathematical model. The detail description of this method for cardiac geometry modelling was provided by Panfilov and Holden [130], Hunter and Smaill [131], and Nielsen et al. [107].

3.8 Calculations in MATLAB

In programmes written in C, the S1S2 stimulus protocol was used to simulate six normal S1 beats at a fixed cardiac cycle length 1000 ms in the 2D and 800 ms in the 3D cubes and the left ventricular wedge model close to the normal human sinus rhythm. Following six normal S1 beats, a consistent APD profiles was obtained. Then a single premature S2 beat was delivered and tissue was restored to its initial state before the subsequent S1S2 sequence. This process was repeated for progressively decreasing S1S2 coupling intervals.

The transmembrane voltage was

- created every 1 ms in the whole tissue in the 2D geometries, 3D cubes and the wedge and the precision of transmembrane voltage was three decimal places;
- sampled for every grid points in 2D tissues (200 voltage) and every other point along the line in 3D tissues (30 voltage) and the left ventricular wedge model to prevent the creation of huge number of output files after completing simulations (150 voltage).

The second part of computational implementation was run in MTALAB to initially extract transmembrane voltages from a desired region in tissues (i.e. the central region of tissues where the spatial and restitution profiles of repolarization and APD changes more than other regions). Next, the indices of AP upstroke and AP downstroke for normal S1 beats and premature S2 beats were used to calculate seven valuable timing at each S1S2 interval as shown in Figure 3-16. These seven timings are:

1. activation time that corresponds to indices of AP upstroke above the threshold voltage for normal S1 beat (highlighted in orange as **S1 activation time**);
2. repolarization time that corresponds to indices of AP downstroke above the threshold voltage for normal S1 beat (highlighted in cyan as **S1 repolarization time**);
3. APD as the difference between activation time and repolarization time for normal S1 beat (highlighted in magenta as **S1 APD**);
4. activation time that corresponds to indices of AP upstroke above the threshold voltage for premature S2 beats (highlighted in green as **S2 activation time**);
5. repolarization time that corresponds to indices of AP downstroke above the threshold voltage for premature S2 beats (highlighted in red as **S2 repolarization time**);
6. APD for premature S2 beats (highlighted in pink as **S2 APD**);
7. diastolic interval as the difference between activation time of the premature S2 beat and repolarization time of the normal S1 beat (highlighted in violet).

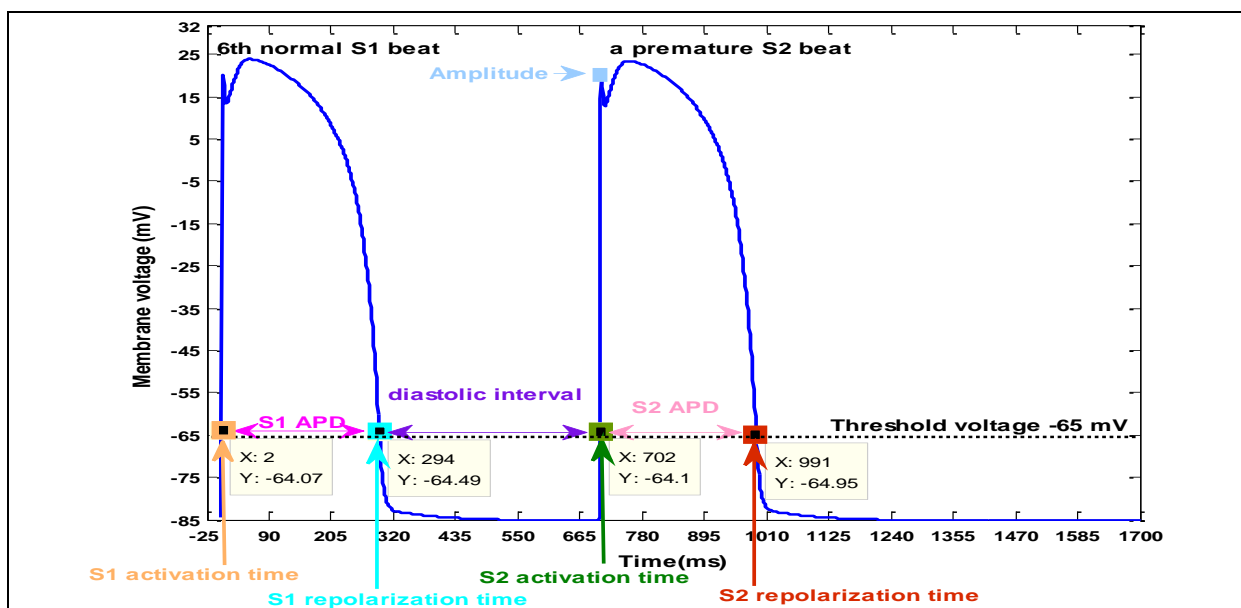


Figure 3-16: An example of AP shape for the sixth normal S1 beat and premature S2 beat in 2D slim epicardial tissue at S1S2 interval of 700 ms with the TP06 model showing seven timings

Note 1: Square markers are extracted data in which X corresponds to the indices of AP upstroke and AP downstroke and Y corresponds to membrane voltage above the threshold voltage -65 mV.

Note 2: Amplitude of AP upstroke for premature S2 beats corresponds to the largest membrane voltage during AP depolarization.

For the FK4V model [1], the normalized threshold voltage was 0.15 in 2D tissues, and 0.1 in the 3D cubes and the wedge model. For the TP06 model [2], the threshold voltage was -65 mV in all tissues to characterize APD based on experimental studies i.e. [101, 132]. It is important to note that in this thesis, for all tissues (1) normal S1 beats are referred to the sixth normal S1 beats followed by a premature S2 beat; (2) each S1S2 interval corresponds to the difference between indices of AP upstroke of premature S2 and normal S1 beats.

3.9 Testing stability of the numerical simulations

To test the accuracy and stability of the numerical simulations, both the time step and space steps of integration were changed as:

- space step was kept as constant value, 0.25 mm, while time step was decreased;
- time step was kept as constant, 0.1 ms, while space step was decreased.

For different space steps and time steps, the speed of depolarization conduction in a 2D slim epicardial tissue at S1S2 interval of 800 ms with the FK4V model and TP06 model are shown in Table 3-6.

The change in the speed of depolarization conduction was approximately similar to the original models [1, 2]. For constant value of space step 0.25 mm, speed of depolarization conduction increased a little with decreasing time step from 0.1 ms to 0.04 ms using the FK4V and TP96 models. However, with constant value of time step at 0.1 ms, speed of depolarization conduction increased around 0.2 m/s with decreasing space step from 0.25 mm to 0.2 mm using the FK4V model and approximately 0.3 m/s with decreasing space step from 0.25 mm to 0.17 mm using the TP06 model.

Speed of depolarization conduction at S1S2 interval of 800 ms in 2D slim epicardial tissue				
FK4V model		Time step 0.1 ms	Time step 0.05 ms	Time step 0.04 ms
	Space step 0.25 mm	0.641 m/s	0.685 m/s	0.694 m/s
		Space step 0.2 mm	Space step 0.19	Space step 0.17
	Time step 0.1 ms	0.833 m/s	0.99 m/s	0.99 m/s
TP06 model		Time step 0.1 ms	Time step 0.05 ms	Time step 0.04 ms
	Space step 0.25 mm	0.602 m/s	0.6098 m/s	0.6111 m/s
		Space step 0.2 (mm)	Space step 0.18 (mm)	Space step 0.17 (mm)
	Time step 0.1 ms	0.781 m/s	0.877 m/s	0.943 m/s

Table 3-6: Numerical accuracy of the speed of depolarization conduction for different space step and time step in 2D slim epicardial tissue at S1S2 interval of 800 ms with the FK4V and the TP06 models

After testing the numerical stability, some simulations were run for 2D slim tissues with the maximum space step of 0.25 mm and time step of 0.1 ms to test the reliability of restitution profiles of speed of depolarization conduction by comparing with the original models [1, 2]. For this purpose, 2D isotropic epicardial, mid-myocardial, and endocardial tissue were simulated with the FK4V and TP06 models.

There was agreement between FK4V model of tissues with size of $5 \times 0.1 \text{ cm}^2$ in this thesis and 1D-2 cm cable with the original FK4V model [1]. For example, premature S2 beats had the largest speed of depolarization conduction around 73 cm/s in 2D isotropic mid-myocardial tissue with a diffusion coefficient of $0.001171 \text{ cm}^2/\text{ms}$ close to the original FK4V model [1] and the experimental human data by Taggart et al. [126]. The range of speed of depolarization conduction for premature S2 beats in 2D isotropic epicardial and endocardial tissues varied in physiological range from 32 cm/s to 70 cm/s during progressive decreasing S1S2 intervals as shown in Figure 3-17.

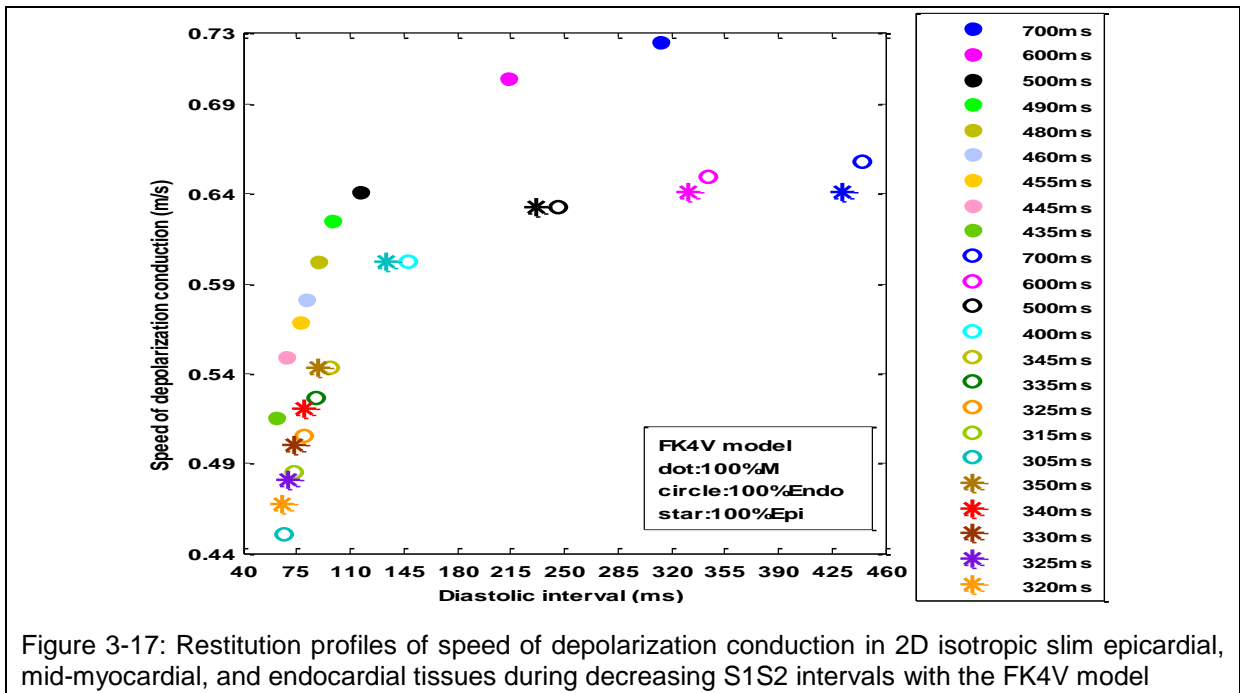


Figure 3-17: Restitution profiles of speed of depolarization conduction in 2D isotropic slim epicardial, mid-myocardial, and endocardial tissues during decreasing S1S2 intervals with the FK4V model

Furthermore, the simulation results of TP06 model of tissue with size of $5 \times 0.1 \text{ cm}^2$ in this thesis were in agreement with those of tissue with size of $25 \times 25 \text{ cm}^2$ using the original TP06 model [2]. For three isotropic slim epicardial, endocardial, and mid-myocardial tissues with diffusion coefficient of $0.001171 \text{ cm}^2/\text{ms}$, the speed of depolarization conduction for premature S2 beats changed similarly around 39 cm/s to 60 cm/s during decreasing S1S2 intervals as shown in Figure 3-18. These values were close to a maximum planar conduction velocity of 68 cm/s produced in the original TP06 model [2] (with diffusion coefficient of $0.00154 \text{ cm}^2/\text{ms}$) and to the human experimental data [126].

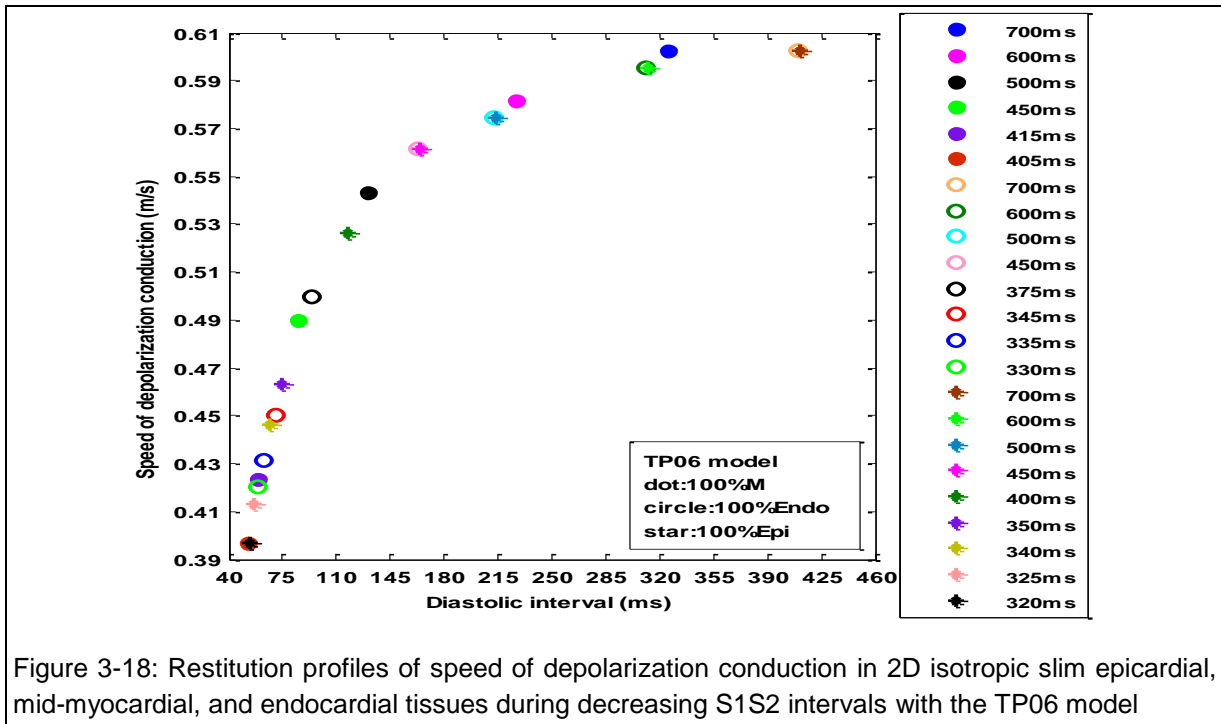


Figure 3-18: Restitution profiles of speed of depolarization conduction in 2D isotropic slim epicardial, mid-myocardial, and endocardial tissues during decreasing S1S2 intervals with the TP06 model

3.10 Summary

This thesis introduced three groups of geometrical models including: first, 2D slabs of tissue with and without structural discontinuities; second, 3D cubes of tissue with and without

fibrosis tissue with seven cellular configurations; and third, the left ventricular wedge model including tissue and fibre geometries. All heterogeneous tissues were simulated with epicardial and endocardial pacing in 3D cubes of tissue and with epicardial pacing with conduction from apex to base and base to apex in the wedge model. Two human ventricular cell models (a simple model and a biophysically detailed cell model) and the monodomain tissue model were used to implement the models equations and create transmembrane voltage. Numerical stabilities were tested and AP shape and speed of depolarization conduction were in agreement with previous simulations.

For all tissues, seven timings were calculated including activation time, repolarization time, and APD for both normal S1 and premature S2 beats as well as diastolic interval prior to premature beats for each S1S2 interval. These data were used to study how interaction of activation-repolarization coupling and restitution in tissue models can change (1) spatial and restitution profiles of activation time, repolarization time, and APD; (2) three measures of dispersion in activation time, repolarization time, and APD; (3) speed of depolarization conduction; and (4) AP propagation during depolarization and repolarization.

The simulation results in the 2D slabs, 3D cubes, and the left ventricular wedge model are illustrated in Chapters 4, 5, and 6 respectively.

3.11 References

1. Bueno-Orovio A and Cherry EM and Fenton FH, Minimal model for human ventricular action potentials in tissue. *Journal of Theoretical Biology*, 2008. **235**: p. 544-560.
2. ten Tusscher KH and Panfilov AV, Alternans and spiral breakup in a human ventricular tissue model. *Am J Physiol Heart Circ Physiol*, 2006. **291**: p. H1088–H1100.
3. Han J and Moe GK, Nonuniform recovery of excitability in ventricular muscle. *Circulation Research*, 1964. **14**: p. 44-60.
4. Kuo CS and Munkata K and Reddy P and Surawicz B, Characteristics and possible mechanism of ventricular arrhythmia dependent on the dispersion of action potential durations. *Circulation*, 1983. **67**: p. 1356-1367.
5. Gough W and Mehra R and Restivo M and Zeiler R and El-Sherif N., Reentrant ventricular arrhythmias in the late myocardial infarction period in the dog: Correlation of activation and refractory maps. *Circ Res*, 1985. **57**: p. 432-442.
6. Laurita KR and Girouard SD., Modulation of ventricular repolarization by a premature stimulus. Role of epicardial dispersion of repolarization kinetics demonstrated by optical mapping of the intact guinea pig heart. *Circ Res*, 1996. **79**: p. 493–503.
7. Laurita KR and Girouard SD and Akar FG and Rosenbaum DS., Modulated dispersion explains changes in arrhythmia vulnerability during premature stimulation of the heart. *Circulation*, 1998. **98**: p. 2774–2780.
8. Huang J and Zhou X and Smith WM and Ideker RE., Restitution properties during ventricular fibrillation in the in situ swine heart. *Circulation*, 2004. **110**: p. 3161–3167.
9. Burgess MJ and Green LS and Millar K and Wyatt R and Abildskov JA, The sequence of normal ventricular recovery. *Am Heart J*, 1972. **84**: p. 669–678.
10. Cowan JC and Hilton CJ and Griffiths CJ and Tansuphaswadikul S and Bourke JP and Murray A and Campbell RWF, Sequence of epicardial repolarisation and configuration of the T wave. *Eur Heart J*, 1988. **60**: p. 424–433.
11. Franz MR and Swerdlow CD and Liem LB and Schaefer J, Cycle length dependence of human action potential duration in vivo. *J Clin Invest*, 1988. **82**: p. 972–979.
12. Yuan S and Kongstad O and Hertvig E and Holm M and Grins E and Olsson B, Global repolarization sequence of the ventricular endocardium: monophasic action potential mapping in swine and humans. *Pacing Clin Electrophysiol*, 2001. **24**: p. 1479–1488.
13. Yue AM and Betts TR and Roberts PR and Morgan JM, Global dynamic coupling of activation and repolarization in the human ventricle. *Circulation*, 2005. **112**: p. 2592–2601.
14. Chauhan VS and Downar E and Nanthakumar k and Parker JD and Ross HJ and Chan W and Picton P., Increased ventricular repolarization heterogeneity in patients with ventricular arrhythmia vulnerability and cardiomyopathy: a human in vivo study. *Am J Physiol Heart Circ Physiol*, 2006. **290**: p. H79-H86.

15. Hanson B and Sutton P and Elameri N and Gray M and Critchley H and Gill JS and Taggart P., Interaction of Activation–Repolarization Coupling and Restitution Properties in Humans. *Circulation: Arrhythmia and Electrophysiology*, 2009. **2**: p. 162-170.
16. Medina-Ravell VA and Lankipalli RS and Yan GX and Antzelevitch C and Medina-Malpica NA and Medina-Malpica OA and Droogan C and Kowey PR, Effect of epicardial or biventricular pacing to prolong QT interval and increase transmural dispersion of repolarization. Does resynchronization therapy pose a risk for patients predisposed to long QT or torsade de pointes? *Circulation*, 2003. **107**: p. 740–746.
17. Fish JM and Brugada J and Antzelevitch C., Potential proarrhythmic effects of biventricular pacing. *J Am Coll Cardiol.*, 2005. **46**: p. 2340–2347.
18. Fish JW and Di Diego JM and Nesterenko VV and Antzelevitch C., Epicardial activation of left ventricular wall prolongs QT interval and transmural dispersion of repolarization implications for biventricular pacing. *Circulation*, 2004. **109**: p. 2136–2142.
19. Santangelo L and Ammendola E and Russo V and Cavallaro C and Vecchione F and Garofalo S and D'Onofrio A and Calabrò R., Influence of biventricular pacing on myocardial dispersion of repolarization in dilated cardiomyopathy patients. *Europace*, 2006. **8**: p. 502-5.
20. Antzelevitch C and Shimizu W and Yan GX and Sicouri S and Weissenburger J and Nesterenko VV and Burashnikov A and Di Diego JM and Saffitz J and Thomas GP, The M cell: its contribution to the ECG and to normal and abnormal electrical function of the heart. *J Cardiovasc Electrophysiol.*, 1999. **10**: p. 1124–1152.
21. Anyukhovskiy EP and Sosunov EA and Gainullin RZ and Rosen MR, The controversial M cell. *J Cardiovasc Electrophysiol*, 1999. **10**: p. 244–260.
22. Taggart P and Sutton PM and Opthof T and Coronel R and Trimlett R and Pugsley W and Kallis P, Transmural repolarisation in the left ventricle in humans during normoxia and ischaemia. *Cardiovasc Res*, 2001. **50**: p. 454–462.
23. Antzelevitch C., Transmural dispersion of repolarization and the T wave. *Cardiovasc Res.*, 2001. **50**: p. 426-431.
24. Opthof T and Coronel R and Janse MJ, Controversies in Arrhythmia and Electrophysiology. Is there a significant transmural gradient in repolarization time in the intact heart? Repolarization Gradients in the Intact Heart. *Circulation: Arrhythmia and Electrophysiology*, 2009. **2**: p. 89-96.
25. Patel C and Burke JF and Patel H and Gupta P and Kowey PR and Antzelevitch C and Yan G., Is there a significant transmural gradient in repolarization time in the intact heart? Cellular Basis of the T Wave: A Century of Controversy. *Circ Arrhythm Electrophysiol.*, 2009. **2**: p. 80–88.
26. Helm PA and Tseng HJ and Younes L and McVeigh ER and Winslow RL, Vivo 3D diffusion tensor imaging and quantification of cardiac laminar structure. *Magnetic Resonance in Medicine*, 2005. **54**: p. 850-859.
27. Karma A., Electrical alternans and spiral wave breakup in cardiac tissue. *Chaos*, 1994. **4**: p. 461–472.
28. Courtemanche M and Glass L and Keener JP., Instabilities of a propagating pulse in a ring of excitable media. *Physiological Reviews*, 1993. **70**: p. 2182–2185
29. Karma A and Levine H and Zou X, Theory of pulse instabilities in electrophysiological models of excitable tissues. *Physica D*, 1994. **73**: p. 113–127.
30. Ito H and Glass L, Theory of reentrant excitation in a ring of cardiac tissue. *Physica D*, 1992. **56b**: p. 84–106.
31. Boyett MR and Jewell BR, A study of the factors responsible for rate-dependent shortening of the action potential in mammalian ventricular muscle. *J Physiol*, 1978. **285**: p. 359–380.
32. Qu Z and Weiss JN and Garfinkel A, Cardiac electrical restitution properties and stability of re-entrant spiral waves: a simulation study. *Am J Physiol Heart Circ Physiol*, 1999. **276**: p. H269–H283.
33. Fenton FH and Cherry EM and Hastings HM and Evans SJ, Multiple mechanisms of spiral wave breakup in a model of cardiac electrical activity. *Chaos*, 2002. **12**: p. 852–892.
34. Karma A, Spiral breakup in model equations of action potential propagation in cardiac tissue. *Physical Review Letters*, 1993. **71**: p. 1103-1107.
35. Courtemanche M., Complex spiral wave dynamics in a spatially distributed ionic model of cardiac electrical activity. *Chaos*, 1996. **6**: p. 579–600.
36. Beeler GW and Reuter H, Reconstruction of the action potential of ventricular myocardial fibres. *Journal of Physiology*, 1977. **268**: p. 177-210.
37. Luo CH and Rudy Y., A Model of the ventricular cardiac action potential: depolarisation, repolarisation and their Interaction. *Circulation Research*, 1991. **68**: p. 1501-1526.

38. Clayton RH and Taggart P, Regional differences in APD restitution can initiate wavebreak and re-entry in cardiac tissue: A computational study. *BioMedical Engineering*, 2005. **4:54**.
39. Fenton F and Karma A, Vortex dynamics in three-dimensional continuous myocardium with fiber rotation: Filament instability and fibrillation. *Chaos*, 1998. **20**.
40. Spach MS and Miller WT and Geselowitz DB and Barr RC and Kootsey JM and Johnson EA, The discourteous nature of propagation in normal canine cardiac muscle. Evidenced for recurrent discontinuities of intracellular resistance that affect the membrane current. *Cardiovascular Research*, 1981. **48**: p. 39-54.
41. Keener JP., A mathematical model for the vulnerable phase in myocardium. *Mathematical Biosciences*, 1988. **90**: p. 3-18.
42. Panfilov AV and Winfree AT., Generation of re-entry in anisotropic myocardium. *Physica D* 1985. **17**: p. 323–330.
43. FitzHugh RA, Impulses and physiological states in theoretical models of nerve membrane. *Biophys J*, 1961. **1**: p. 445-466.
44. Nagumo J and Animoto S and Yoshizawa S, An active pulse transmission line simulating nerve axon. *Proc Inst Radio Engineers*, 1962. **50**: p. 2061-2070.
45. Panfilov AV and Keener JP, Re-entry in three-dimensional Fitzhugh-Nagumo medium with rotational anisotropy. *Physica D*, 1995. **84**: p. 545–552.
46. Clayton RH and Holden AV, Dispersion of cardiac action potential duration and the initiation of re-entry: A computational study. *Biomedical Engineering, OnLine* 2005. **4**: p. 4-11.
47. Keldermann RH and ten Tusscher KH and Nash MP and Hren R and Taggart P and Panfilov AV, Effect of heterogeneous APD restitution on VF organization in a model of the human ventricles. *Am J Physiol Heart Circ Physiol*, 2007. **294**: p. H764-H774
48. Nash MP and Bradley CP and Sutton PM and Clayton RH and Kallis P and Hayward MP and Peterson DJ and Taggart P., Whole heart action potential duration restitution properties in cardiac patients: a combined clinical and modeling study. *Exp Physiol*, 2006. **91**: p. 339–354.
49. ten-Tusscher KH and Noble D and Noble PJ and Panfilov AV, A model for human ventricular tissue. *Am J Physiol*, 2004. **286**: p. H1573–H1589.
50. Sicouri S and Antzelevitch C, A subpopulation of cells with unique electrophysiological properties in the deep subepicardium of the canine ventricle: The M cell. *Circ Res*, 1991. **68**: p. 1729-1741.
51. Clayton RH and Holden AV, propagation of normal beats and reentry in a computational model of ventricular cardiac tissue with regional differences in action potential shape and duration. *Progress in Biophysics & Molecular Biology*, 2004. **85**.
52. Luo CH and Rudy Y., A dynamic model of the cardiac ventricular action potential. II. After depolarizations, triggered activity, and potentiation. *Circ Res*, 1994. **74**: p. 1097–1113.
53. Okada J and Washio T and Maehara A and Momomura Sh and Sugiura S and Hisada T, Transmural and apicobasal gradients in repolarization contribute to T-wave genesis in human surface ECG. *Am J Physiol Heart Circ Physiol*, 2011. **301**: p. H200-H208.
54. Ursell PC and Gardner PI and Albala A and Fenoglio JJ Jr and Wit AL, Structural and electrophysiological changes in the epicardial border zone of canine myocardial infarcts during infarct healing. *Circ Res*, 1985. **56**.
55. Streeter DDJ, Gross morphology and fiber geometry of the heart, in *Handbook of Physiology. The Cardiovascular System*, Berne RM and Sperelakis N and Greger SR, Editor. 1979, Baltimore, Maryland, Williams & Wilkins Co.
56. Colli Franzone P and Pavarino L.F and Savare G, Computational electrocardiology: mathematical and numerical modeling, in *Complex systems in biomedicine*, Quarteroni A and Formaggia L and Veneziani A, Editor. 2006, Springer.
57. Kleber AG and James MJ and Fast VG, Normal and abnormal conduction in the heart: The hand book of physiology. 2002, New York: Oxford University Press.
58. Kleber AG and Rudy Y., Basic mechanisms of cardiac impulse propagation and associated arrhythmias. *Physiological Reviews*, 2004. **84**: p. 431-488.
59. Saffitz JE and Kanter HL and Green KG and Tolley TK and Beyer EC, Tissue-specific determinants of anisotropic conduction velocity in canine atrial and ventricular myocardium. *Circulation Research*, 1994. **74**.
60. Kleber AG and Rudy Y, Basic mechanisms of cardiac impulse propagation and associated arrhythmias. *Physiological Reviews*, 2004. **84**: p. 431-488.
61. Saffitz JE and Hoyta RH and Lukea RA and Kantera HL and Beyera EC, Cardiac myocyte interconnections at gap junctions: Role in normal and abnormal electrical conduction *Trends in Cardiovascular Medicine*, 1992. **2**: p. 56-60.
62. Spach MS and Miller WT and Dolber PC and Kootsey JM and Sommer JR and Mosher CE Jr, The functional role of structural complexities in the propagation of demilitarisation in the

- atrium of the dog. Cardiac conduction disturbances due to discontinuities of effective axial resistivity. *Cardiovascular Research*, 1982. **50**: p. 175-191.
63. Caldwell BJ and Trew ML and Sands GB and Hooks DA and LeGrice IJ and Smaill BH., Three distinct directions of intramural activation reveal nonuniform side-to-side electrical coupling of ventricular myocytes. *Circ Arrhythmia Electrophysiol*, 2009. **2**.
 64. Benson A and Bernus O and Dierckx and Gilbert S and Greenwood and Holden and Mohee and Plein and Radjenovic and Ries M and Smith and Sourbron and Walton., Construction and validation of anisotropic and orthotropic ventricular geometries for quantitative predictive cardiac electrophysiology. *Interface Focus*, 2011. **1**: p. 101-116
 65. Cates AW and Pollard A.E., A computer modeling study of the relationship between intramural fiber rotation and the spatial distribution of repolarization properties in ventricular myocardium. *IEEE-EMBC and CMBEC*, 1995. **1**: p. 79-80.
 66. Vetter FJ and Simons SB and Mironov S and Hyatt CJ and Pertsov AM, Epicardial fiber organization in swine right ventricle and its impact on propagation. *Circulation research*, 2005. **96**: p. 244-251.
 67. Taccardi B and Punske BB and Macchi E and MacLeod RS and Ershler PR, Epicardial and intramural excitation during ventricular pacing: effect of myocardial structure *American Journal of Physiology - Heart and Circulatory Physiology*, 2008. **294**: p. H1753-H1766
 68. Ertl G and Frantz S., Healing after myocardial infarction. *Oxford Journals*, 2005. **66**: p. 22-32.
 69. Assomull RG and Prasad SK and Lyne J and Smith G and Burman ED and Khan M and Sheppard MN and Poole-Wilson PA and Pennell DJ, Cardiovascular Magnetic Resonance, Fibrosis, and Prognosis in Dilated Cardiomyopathy. *J Am Coll Cardiol*, 2006. **48**: p. 1977-1985.
 70. Kawara T and Derksen R and De Groot JR and Coronel R and Tasseron S and Linnenbank AC and Hauer RNW and Kirkels H and Janse MJ and de Bakker JMT, Activation delay after premature stimulation in chronically diseased human myocardium relates to the architecture of interstitial fibrosis. *Circulation*, 2001. **104**: p. 3069-3075.
 71. Libby P and Bonow RO and Zipes DP and Mann DL, *Braunwald's Heart Disease: A Textbook of Cardiovascular Medicine*. 7th ed. 2005: Philadelphia, Saunders.
 72. ten-Tusscher KH and Panfilov AV, Influence of diffuse fibrosis on wave propagation in human ventricular tissue. *Europace*, 2007. **9**: p. 38-45.
 73. Engelman ZJ and Trew ML and Smaill BH, Structural heterogeneity alone is a sufficient substrate for dynamic instability and altered restitution. *Circ Arrhythmia Electrophysiol*, 2010. **3**: p. 195-203.
 74. Luo C and Rudy Y, A dynamic model of the cardiac ventricular action potential, I: simulations of ionic currents and concentration changes. *Circ Res*, 1994. **74**: p. 1071-1096.
 75. Clayton RH and Bernus O and Cherry EM and Dierckx H and Fenton FH and Mirabella L and Panfilov AV and Sachse FB and Seemann G and Zhang H., Models of cardiac tissue electrophysiology: Progress, challenges and open questions. *Progress in Biophysics and Molecular Biology*, 2010. **104**: p. 22-48.
 76. Dos Santos RW and Otaviano Campos F and Neumann Ciuffo L and Nygren A and Giles W and Koch H., ATX-II Effects on the Apparent Location of M Cells in a Computational Model of a Human Left Ventricular Wedg. *J Cardiovasc Electrophysiol.*, 2006. **17**: p. S86–S95.
 77. Costa KD and Takayama Y and McCulloch AD and Covell JW., Lamellar fiber architecture and the three-dimensional systolic mechanics in canine ventricular myocardium. *Am J Physiol Heart Circ Physiol*, 1999. **276**: p. H595-H607.
 78. Cain JW and Schaeffer DG, Shortening of cardiac action potential duration near an insulating boundary. *Mathematical Medicine and Biology*, 2008. **25**: p. 21-36.
 79. Mitchell CC and Schaeffer DG, A two-current model for the dynamics of cardiac membrane. *Bull Math Biol*, 2003. **65**: p. 767-793.
 80. Siso-Nadal F and Otani NF and Gilmour RF and Fox JJ, Boundary-induced reentry in homogeneous excitable tissue. *Phys Rev E.*, 2008. **78**: p. 031925-031955.
 81. Fox JJ and McHarg JL and Gilmour RF Jr, Ionic mechanism of electrical alternans. *Am J Physiol Heart Circ Physiol*, 2002. **282**: p. H516–H530.
 82. Cherry EM and Fenton F, Effects of boundaries and geometry on the spatial distribution of action potential duration in cardiac tissue. *Journal of Theoretical Biology*, 2011. **285**: p. 164-176.
 83. Cherry EM and Fenton F, Suppression of alternans and conduction blocks despite steep APD restitution: electrotonic, memory, and conduction velocity restitution effects. *Am J Physiol Heart Circ Physiol* 2004. **286**: p. H2332–H2341.
 84. van Oosterom A and Jacquemet V, The effect of tissue geometry on the activation recovery interval of atrial myocytes. *Physica D*, 2009. **238**: p. 962-968.

85. Colli Franzone P and Pavarino L and Taccardi B, Simulating patterns of excitation, repolarization and action potential duration with cardiac Bidomain and Monodomain models. *Mathematical Biosciences*, 2005. **197**: p. 35-66.
86. Colli Franzone P and Pavarino LF and Taccardi B, Effects of transmural heterogeneity and electrotonic interactions on the dispersion of cardiac repolarization and action potential duration: a simulation study. *Math Biosci*, 2006. **204**: p. 132–165.
87. Colli Franzone P and Pavarino LF and Scacchi S and Taccardi B, Modeling ventricular repolarization: Effects of transmural and apex-to-base heterogeneities in action potential durations. *Math Biosci*, 2008. **214**: p. 140-152.
88. Scacchi S and Franzone PC and Pavarino LF and Taccardi B, A reliability analysis of cardiac repolarization time markers. *Math Biosci*, 2009: p. 113-128.
89. Antzelevitch C and Fish J, Electrical heterogeneity within the ventricular wall. *Basic Res. Card.*, 2001. **96**: p. 517–527.
90. The centre for cardiovascular bioinformatics and modelling of the Johns Hopkins University (CCBM). Available from: <http://www.ccbm.jhu.edu/reacerch>.
91. Hunter PJ and Pullan AJ and Smaill BH, Modeling total heart function. *BioMedical Engineering*, 2003. **5**: p. 147-177.
92. Sachse FB, *Computational cardiology: modeling of anatomy, electrophysiology, and mechanics*. 2004: Springer.
93. Bishop MJ and Plank G and Burton RAB and Schneider JE and Gavaghan DJ and Grau V and Kohl P, Development of an anatomically detailed MRI-derived rabbit ventricular model and assessment of its impact on simulations of electrophysiological function. *Am J Physiol*, 2010. **298**: p. H699–H718.
94. Streeter DDJ and Spotnitz HM and Patel DP and Ross JJ and Sonnenblick EH, Fiber orientation in the canine left ventricle during diastole and systole. *Circulation Research*, 1969. **24**: p. 339–347.
95. Kogan BY and Karplusa WJ and Billetta BS and Stevensonb WG, Excitation wave propagation within narrow pathways: Geometric configurations facilitating unidirectional block and reentry. *Physica D*, 1992. **59**.
96. Kogan BY and Karplus WJ and Billett BS and Pang AT and Karagueuzian HS and Khan SS, The simplified FitzHugh-Nagumo model with action potential duration restitution: Effects on 2D wave propagation. *Physica D: Nonlinear Phenomena*, 1991. **50**: p. 327-340.
97. Marieb EN., *Human anatomy and physiology*. 6 ed. 2004: Pearson Benjamin Cummings.
98. Taggart P and Sutton P and Ophof T and Coronel R and Kallis P, Electrotonic cancellation of transmural gradients in the left ventricle in man. *Biophysics and Mol Biol*, 2003. **82**: p. 243-254.
99. Yan G and Shimizu W and Antzelevitch ch., Characteristics and Distribution of M Cells in Arterially Perfused Canine Left Ventricular Wedge Preparations. *Circulation*, 1998. **98**: p. 1921-1927.
100. Poelzing S and Akar FG and Baron E and Rosenbaum DS., Heterogeneous connexin43 expression produces electrophysiological heterogeneities across ventricular wall. *Am J Physiol Heart Circ Physiol*, 2004. **286**: p. H2001-H2009.
101. Drouin E and Charpentier Fand Gauthier C and Laurent K and Le Marec H, Electrophysiologic characteristics of cells spanning the left ventricular wall of human heart: evidence for presence of M cells. *J Am Coll Cardiol*, 1995. **26**: p. 185-192.
102. Narayan SM and Bayer JD and Lalani G and Trayanova NA., Action potential dynamics explain arrhythmic vulnerability in human heart failure: a clinical and modeling study implicating abnormal calcium handling. *J Am Coll Cardiol.*, 2008. **52**: p. 1782-1792.
103. Bayer JD and Narayan SM and Lalani GG and Trayanova NA., Rate-dependent action potential alternans in human heart failure implicates abnormal intracellular calcium handling. *Heart Rhythm*, 2010. **7**: p. 1093-1101.
104. Harrington KB and Rodriguez F and Cheng A and Langer F and abd George HA and Criscione JC and Ingels NB and Miller DC, Direct measurement of transmural laminar architecture in the anterolateral wall of the ovine left ventricle: New implications for wall thickening mechanics. *American Journal of Physiology. Heart and Circulatory*, 2005. **288**: p. 1324–1330.
105. Baltazar RF., *Basic and Bedside Electrocardiography*. 2009: Lippincott Williams & Wilkins.
106. Greenbaum RA and Ho SY and Gibson DG and Becker AE and Anderson RH, Left ventricular fibre architecture in man. *Br Heart J*, 1981. **45**: p. 248-263.
107. Nielsen PMF and LeGrice IJE and Smaill BH and Hunter PJ, Mathematical model of geometry and fibrous structure of the heart. *American Journal of Physiology (Heart and Circulatory Physiology)*, 1991. **260**: p. H1365-H1378.

108. Streeter DDJ and Bassett DL, An Engineering Analysis of Myocardial Fiber Orientation in Pig's Left Ventricle in Systole. *Anat Rec*, 1966. **155**: p. 503–511.
109. Hyatt CJ and Wellner M and Berenfeld O and Popp AK and Weitz DA and Jalife J and Pertsov AM, Synthesis of voltage-sensitive fluorescence signals from three-dimensional myocardial activation patterns. *Biophys J*, 2003. **85**: p. 2673-2683.
110. Chen J and Liu W and Zhang H and Lacy L and Yang X and Song SK and Wickline SA and Yu X., Regional ventricular wall thickening reflects changes in cardiac fiber and sheet structure during contraction: quantification with diffusion tensor MRI. *Am J Physiology Heart Circ Physiol.*, 2005. **289**.
111. LeGrice IJ and Smaill BH and Chai LZ and Edgar SG and Gavin JB and Hunter PJ, Laminar structure of the heart: ventricular myocyte arrangement and connective tissue architecture in the dog. *Am J Physiology.*, 1995. **269**: p. H571-H582.
112. Robb JS and Robb RC, The normal heart : anatomy and physiology of the structural units. *Am Heart J*, 1942. **23**: p. 455-467.
113. The CellML project. Available from: <http://www.cellml.org/>.
114. Priebe L and Beuckelmann DJ, Simulation study of cellular electric properties in heart failure. *Circ Res*, 1998. **82**: p. 1206–1223.
115. Bernus O and Wilders R and Zemlin CW and Verscheide H and Panfilov AV., A computationally efficient electrophysiological model of human ventricular cells. *Am J Physiol Heart Circ Physiol*, 2002. **282**: p. H2296-H2308.
116. Iyer V and Mazhari R and Winslow RL, A computational model of the human leftventricular epicardial myocytes. *Biophys J*, 2004. **87**: p. 1507–1525.
117. Grandi E and Pasqualini FS., A novel computational model of the human ventricular action potential and Ca transient. *J Mol Cell Cardiol*, 2010. **48**.
118. O'Hara Th and Virág L and Varró A and Rudy y, Simulation of the Undiseased Human Cardiac Ventricular Action Potential: Model Formulation and Experimental Validation. *PLoS Comput Biol*, 2011. **e1002061**.
119. Shannon TR and Wang F and Puglisi J and Weber C and Bers DM., A mathematical treatment of integrated Ca dynamics within the ventricular myocyte. *Biophys J*, 2004. **87**: p. 3351–3371.
120. Hodgkin AL and Huxley AF, A quantitative description of membrane current and its application to conduction and excitation in nerve. *Journal of Physiology*, 1952. **119**: p. 500-544.
121. Henriquez CS and Tranquillo JVT, Modelling the impact of cardiac tissue structure on current flow and wavefront propagation, in *Quantitative cardiac electrophysiology*, Cabo C and Rosenbaum DS, Editor. 2002, CRC Press.
122. Potse M and Dube B and Richer J and Vinet A and Gulrajani RM., A comparison of monodomain and bidomain reaction-diffusion models for action potential propagation in the human heart. *IEEE Transactions on Biomedical Engineering*, 2006. **53**: p. 2425-2435.
123. Roth BJ., Meandering of spiral waves in anisotropic cardiac tissue. *Physica D*, 2001. **150**: p. 127-136.
124. Keener J and Sneyd J, *Mathematical Physiology*. Vol. 8. 1998: Springer.
125. Hund TJ and Kucera JP and Otani NF and Rudy Y., Ionic charge conservation and long-term steady state in the Luo-Rudy dynamic cell model. *Biophys .J.*, 2001. **81**: p. 3324–3331.
126. Taggart P and Sutton PMI and Opthof T and Coronel R and Trimlett R and Pugsley W and Kallis P, Inhomogeneous transmural conduction during early ischemia in patients with coronary artery disease. *J Mol Cell Cardiol*, 2000. **32**: p. 621–639.
127. Nanthakumar K and Jalife J and Massé S and Downar E and Pop M and Asta J and Ross H and Rao V and Mironov S and Dhopeswarkar R, Optical mapping of Langendorff perfused human hearts: establishing a model for the study of ventricular fibrillation in humans. *Am J Physiol*, 2007. **293**: p. H875–H880.
128. Marsh M and Torabi Ziaratgahi S and Spiteri R., The Secrets to the Success of the Rush–Larsen Method and its Generalizations. *Transactions on biomedical engineering*, 2012. **59**.
129. Rush S and Larsen H., A practical algorithm for solving dynamic membrane equations. *IEEE Trans Biomed Eng*, 1978. **25**: p. 389–392.
130. Panfilov AV and Holden AV., *Computational Biology of the Heart*. 1997: Wiley.
131. Hunter PJ and Smaill BH., The analysis of cardiac function: A continuum approach. *Progress in Biophysics and Molecular Biology*, 1988. **52**: p. 101-164.
132. Taggart P and Sutton PM and Boyett MR and Lab M and Swanton H, Human ventricular action potential duration during short and long cycles. Rapid modulation by ischemia. *Circulation*, 1996. **94**: p. 2526–2534.

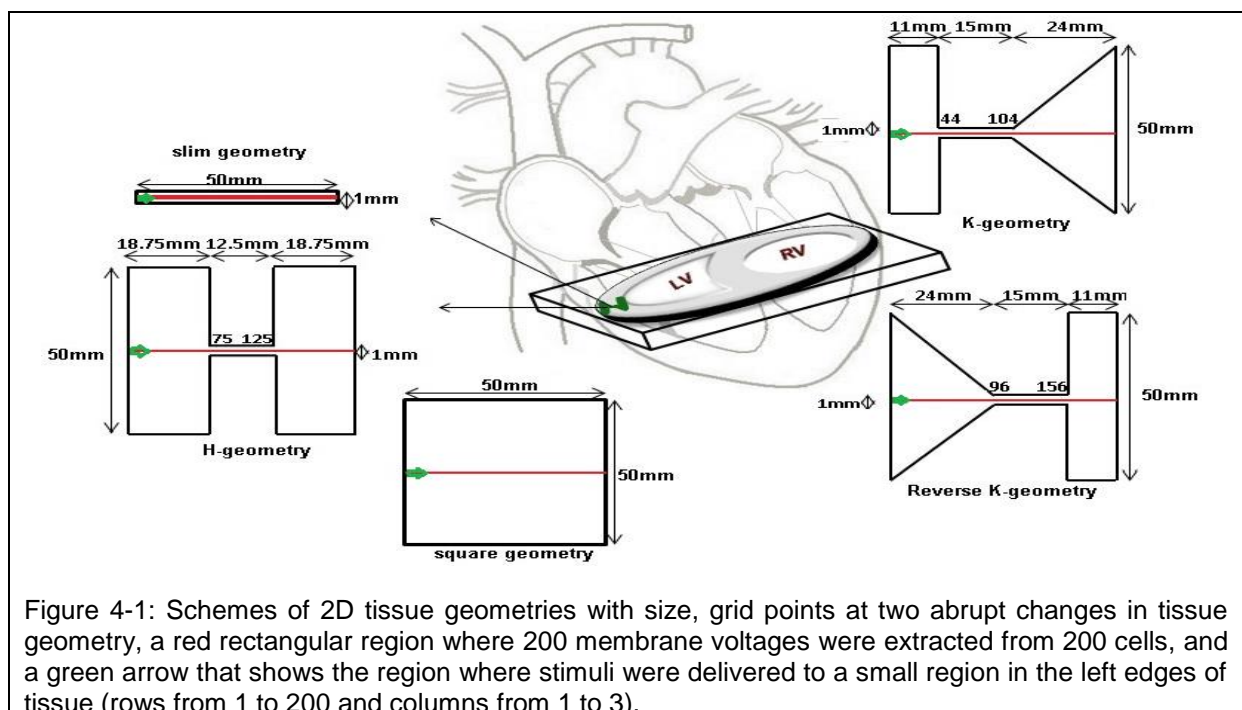
Chapter 4

Simulation results in 2D tissues

4.1 Introduction

The main research question addressed in this Chapter is the impact that regional or structural discontinuities have on AP depolarization and repolarization, for normal and premature activations. Abrupt changes in tissue geometry may be involved in the formation of unidirectional conduction block and re-entry even in the uniform tissue [1]. To address this issue, two groups of isotropic epicardial, mid-myocardial, and endocardial tissues were simulated with and without structural discontinuities using (1) a simple model of human cell FK4V model [2]; and (2) a detailed biological human TP06 cell model [3].

This Chapter is organized in three sections. The aim of the first section is to examine how structural discontinuities influence the spatial and restitution profiles of activation time, repolarization time, and APD. First, a number of tissues were simulated with five geometries to represent 2D isotropic tissues with and without structural discontinuities in the human left ventricle with sizes shown in Figure 4-1. Tissues with K-geometry, the reversed K-geometry and H-geometry (used by Kogan et al. [1]) were examples of tissues with structural discontinuities, including two abrupt changes where an isthmus of tissue bridges two large areas of ventricular tissue. An example of such structure is where surviving cell strands connect regions of intact tissue in infarcted myocardium [4, 5]. The 2D slim and square geometries were used as examples of tissues without structural discontinuities. All tissues were simulated with no-flux boundary conditions and paced from the left edge of tissue. The red rectangle in tissue geometries shows the region where 200 membrane voltages were extracted from 200 cells in the central region of 2D tissues.



The comparison of spatial APD profiles for both normal S1 and premature S2 beats in these five geometries provides a foundation for the rest of the current study. Then, the spatial and restitution profiles of activation time, repolarization time, and APD for premature S2 beats with the FK4V and TP06 models are compared in the isotropic slim and H-shape tissues for one S1S2 intervals and then during decreasing S1S2 intervals. A new approach for visualizing the relationship between data is introduced next. Last but not least, the spatial APD profiles are evaluated against experimental curves.

The aim of the second section is to study the effects of tissue with and without structural discontinuities on three measures of dispersion in activation time, repolarization time, and APD, for both normal S1 and premature S2 beats. The profiles of three measures of dispersion against S1S2 interval highlight the relationship among these measures of dispersion in epicardial, mid-myocardial, and endocardial tissues with slim and H-shape. Then, a summary figure is provided to show how much structural discontinuities increase or decrease the largest and the smallest values of three measures of dispersion in all simulated tissues and whether these values are similar to the available experimental data.

The third section highlights the role of structural discontinuities in slowing wave propagation in H-shape tissues by comparing the profiles of speed of depolarization conduction against diastolic interval in tissues with and without structural discontinuities. Finally, a summary of results is provided. For clarity, spatial and restitution profiles for premature S2 beats with both FK4V and TP06 models during decreasing S1S2 intervals were organized as follows:

- Group A (Figures A1-A18): Spatial profiles of activation time, repolarization time, and APD in slim and H-shape tissues;
- Group B (Figures B1-B6): A new look to the profiles of repolarization time against APD and distance in slim and H-shape tissues;
- Group C (Figures C1-C18): Restitution profiles of activation time, repolarization time, and APD in slim and H-shape tissues.

4.2 Spatiotemporal profiles of normal and premature beats

This section is organized in four subsections to study the effect of structural discontinuities on the profiles for normal S1 and premature S2 beats. The first two subsections characterize the spatial APD profiles and the rate dependency for both normal S1 and premature S2 beats in isotropic epicardial tissue with five tissue geometries using the FK4V model. The next subsection establishes that the premature S2 beats influence repolarization profiles. Then, for premature S2 beats, the effects of structural discontinuities on spatial and restitution profiles of activation time, repolarization time, and APD are described in isotropic epicardial, mid-myocardial, and endocardial tissues with and without regional discontinuities in tissue during decreasing S1S2 intervals using both FK4V and TP06 models. The new approaches for plotting data in order to represent the true information are provided next. The last subsection compares the spatial profiles in this thesis against experimental studies.

4.2.1 Spatial APD profiles in five geometries

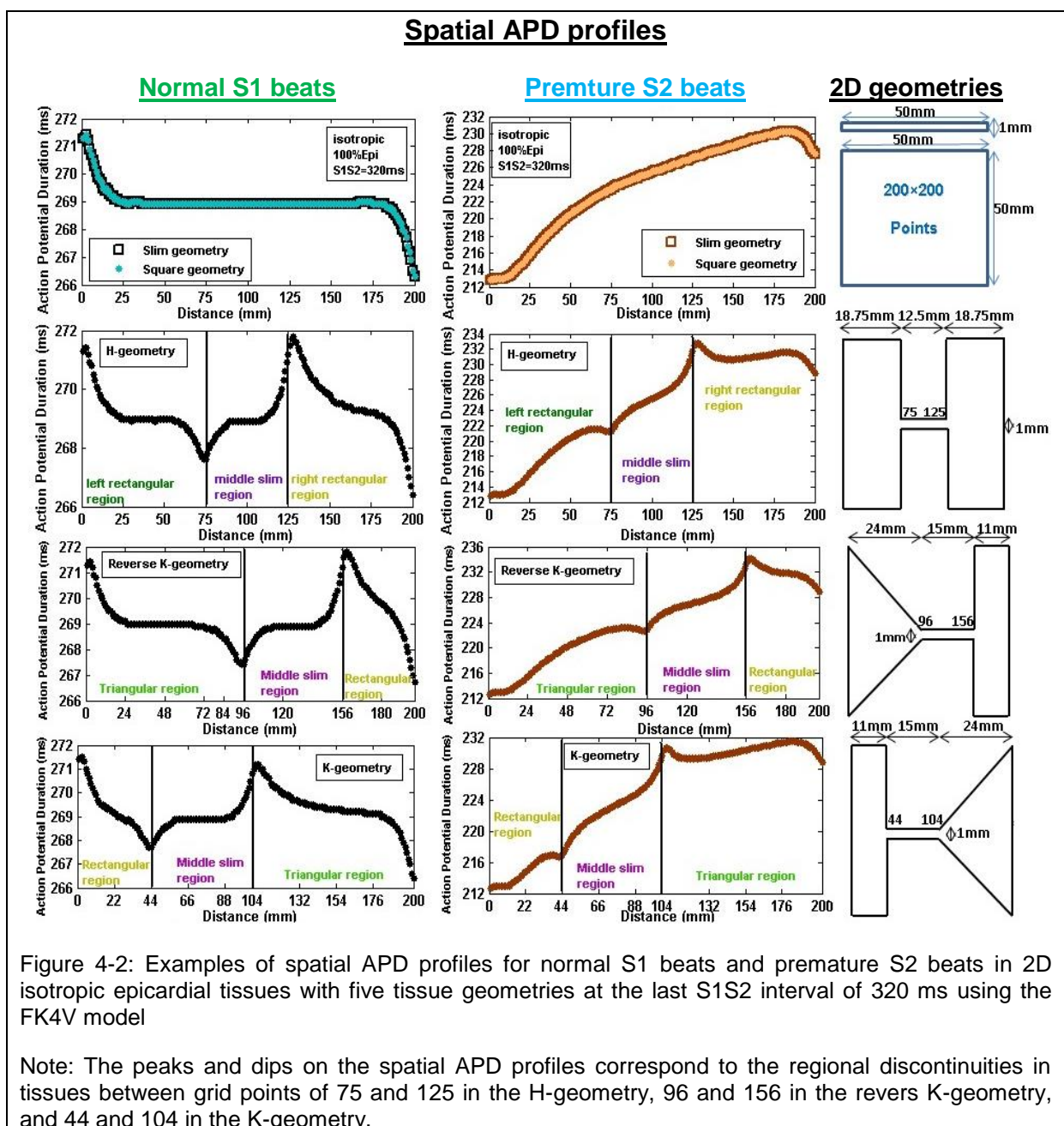
Figure 4-2 shows examples of spatial APD profiles for both normal S1 and premature S2 beats in two isotropic epicardial tissues without regional discontinuities in tissue (slim and

square geometry) and three epicardial tissues with regional discontinuities in tissue (H-geometry, k-geometry and the reverse K-geometry) at the last S1S2 interval of 320 ms with the FK4V model.

For isotropic epicardial tissues without regional discontinuities in tissue, spatial APD profiles were characterized with a stretched S-shape curve displaced up and down at edges of tissues for normal S1 beats and a disrupted S-shape curve for premature S2 beats.

For isotropic epicardial tissues with regional discontinuities in tissue,

1. spatial APD profiles for both normal and premature S2 beats were characterized with three S-shape curves;
2. the slim region between two regional discontinuities in these tissues acted to reverse the orientation of S-shape curve with respect to the APD axis, i.e. the region in the middle of tissue geometries between grid points of 75 and 125 in H-geometry, 96 and 156 in the revers K-geometry, and 44 and 104 in the K-geometry.

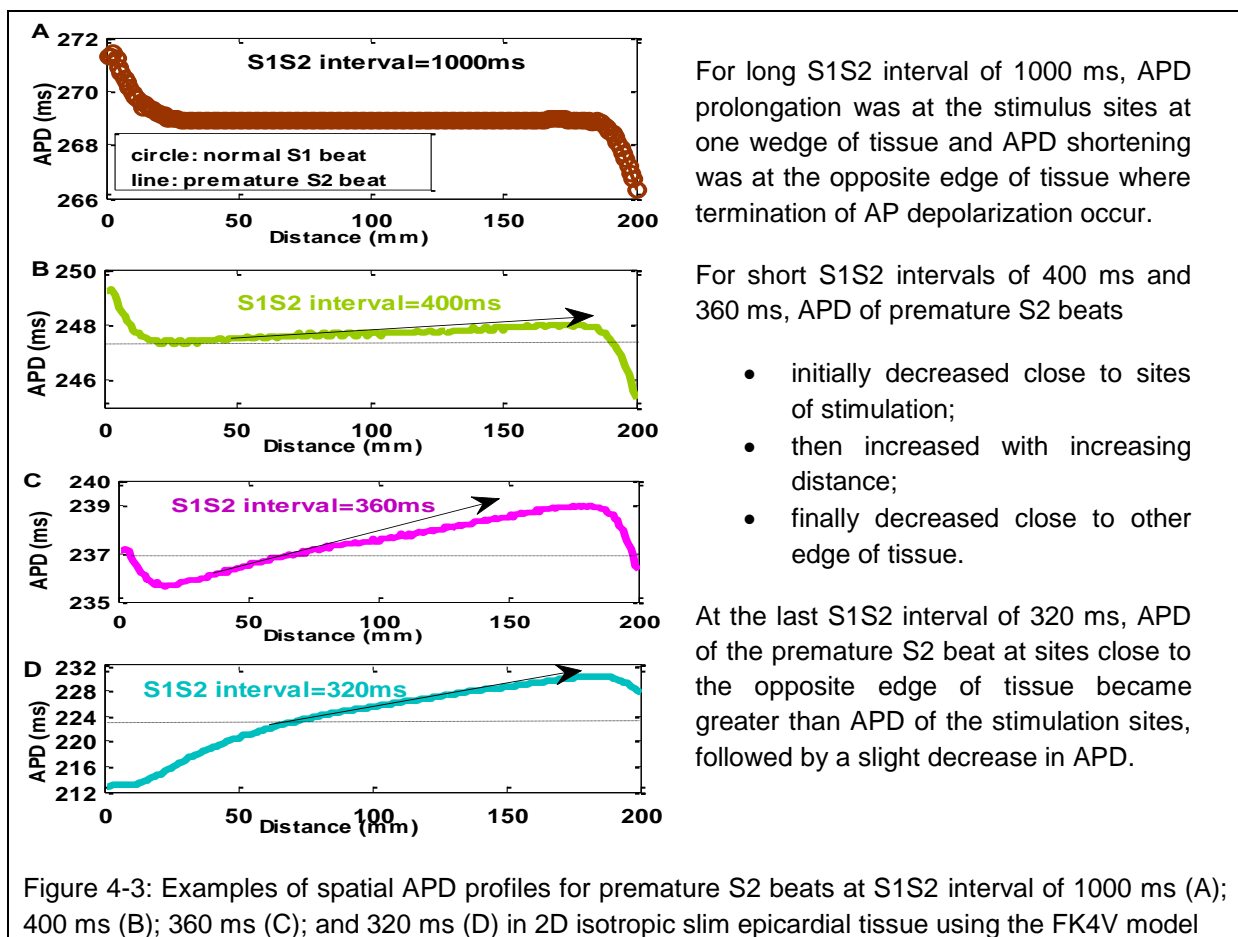


Comparison of the profiles of normal and premature beats in Figure 4-2 suggested rate dependency of premature S2 beats that is explained in detail in the following subsection.

4.2.2 Rate dependent effects

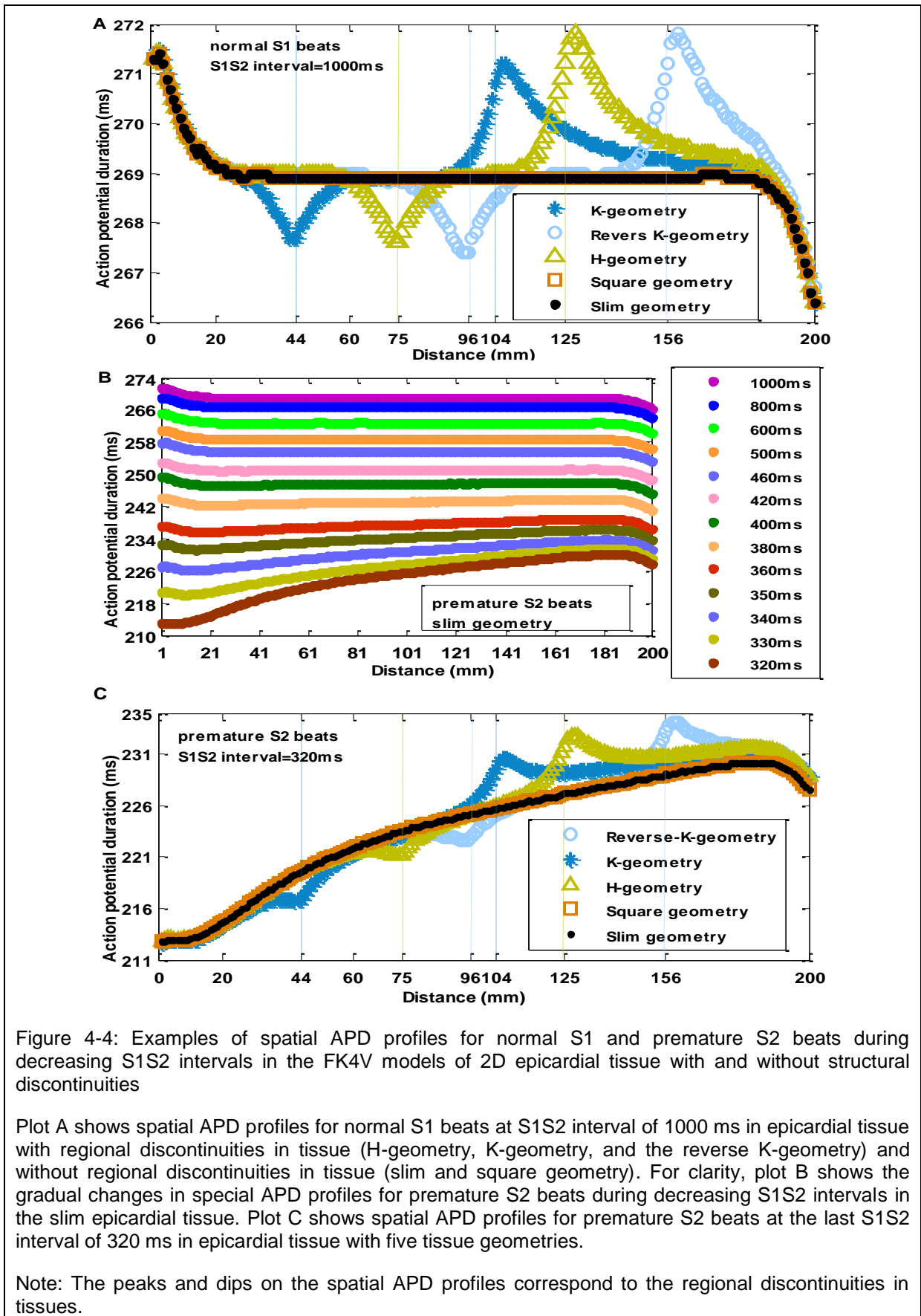
Figure 4-3 shows examples of spatial APD profiles for premature S2 beats at four S1S2 intervals in the isotropic slim epicardial tissue using the FK4V model. For both normal and premature beats, APD prolongation and shortening at tissue boundaries are possibly due to effects of boundaries (explained in Chapter 3, section 3.4.5). The APD of both normal S1 and premature S2 beat decreased gradually with increasing transmural distance at S1S2 interval of 1000 ms as shown in Figure 4-3, plot A. However, the spatial APD profiles for normal S1 beats did not change during decreasing S1S2 intervals. The reason was that normal S1 beats were no rate dependent compared to premature S2 beats.

For premature S2 beats, the stretched S-shape curve at S1S2 interval of 1000 ms became disrupted and rotated counter-clockwise with decreasing S1S2 intervals as explained next to Figure 4-3. These effects may represent the engagement of conduction velocity restitution that are explained in section 4.4. During the rotation of the spatial APD curve for premature S2 beats, an interesting finding was the shift in the APD prolongation and shortening during decreasing S1S2 intervals.



Spatial APD profiles of the FK4V model of isotropic epicardial tissues with H-geometry, K-geometry, and the reverse K-geometry in Figure 4-4 shows:

1. the effects of tissue boundaries for both normal S1 and premature S2 beats;
2. the effect of rate dependency for premature beats during decreasing S1S2 intervals.

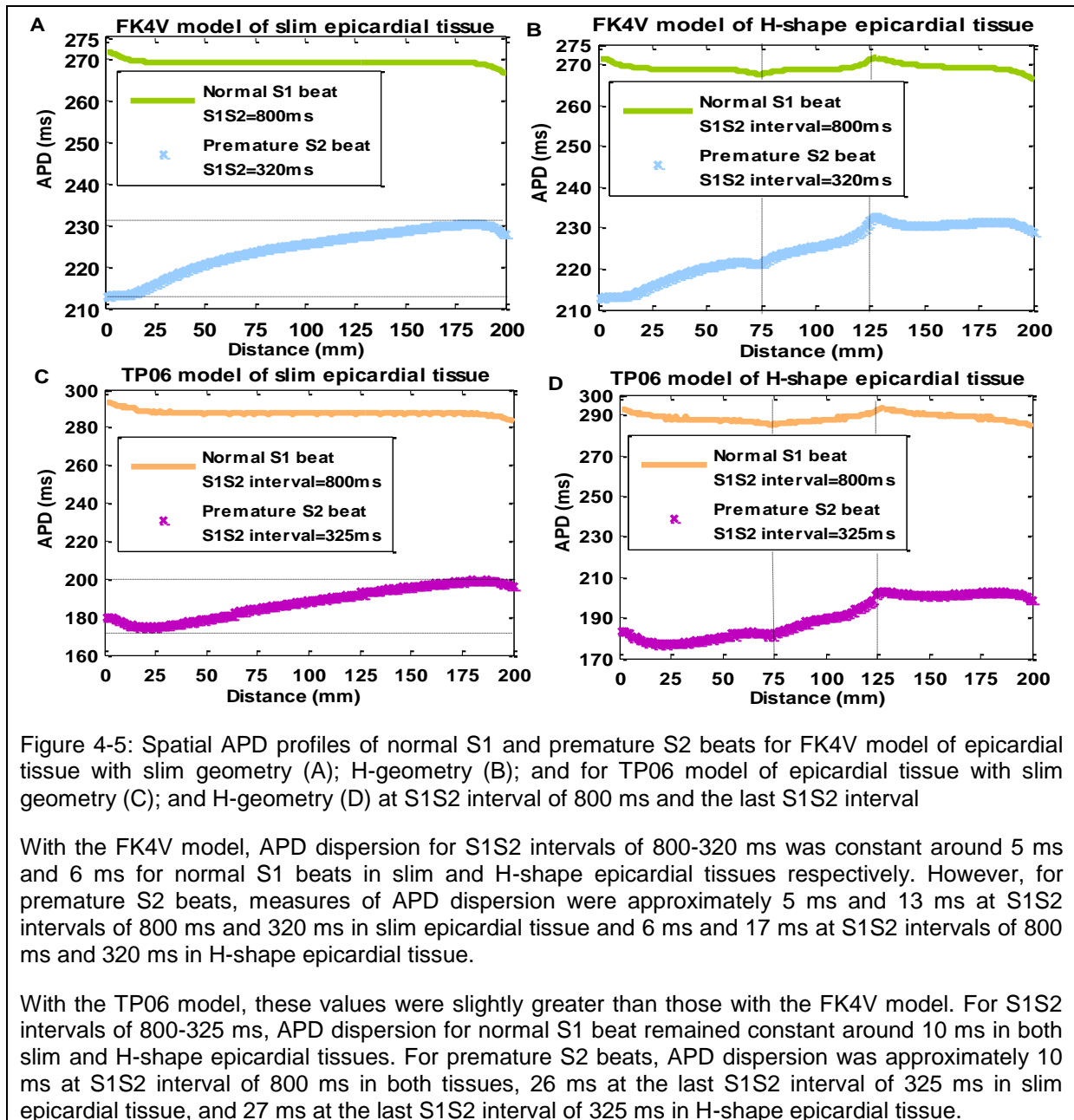


4.2.3 Premature beats influence repolarization profiles

After characterizing normal and premature profiles in epicardial tissue with five tissue geometries, this part of the Chapter plots the spatial APD profiles for normal S1 and

premature S2 beats on the same graph to emphasize the fact that APD dispersion for normal S1 beats was tiny whereas for S2 beats it was much bigger. Dispersion in APD was defined as the difference between the largest and the smallest APD measured across the tissue. Figure 4-5 shows examples of spatial APD profiles for normal S1 and premature S2 beats in the isotropic slim and H-shape epicardial tissue at S1S2 interval of 800 ms and the last S1S2 interval, using the FK4V and TP06 models.

Nevertheless, the overall profile of APD was similar. The descriptions of three measures of dispersion for normal and premature beats are provided in section 4.3.



The current results suggest that the premature S2 beats change the spatial profile of repolarization time using both FK4V and TP06 models. Thus, the model dependent effect is small. The following subsections focus on the profiles for premature S2 beats in three isotropic 2D tissues with slim geometry and H-geometry. The reason for choosing these two geometries was the similarity between spatial APD profiles of slim and square tissues and

among tissues with H-geometry, K-geometry, and the reverse K-geometry as shown in Figure 4-2.

4.2.4 Profiles for premature beats at one S1S2 interval

The previous subsections illustrated the differences between spatial APD profiles associated with normal S1 and premature S2 beats in 2D isotropic epicardial tissues with five shapes during decreasing S1S2 interval. Since APD was the difference between repolarization time and activation time, it was expected that structural discontinuities influenced the profiles of activation time and repolarization time for normal and premature beats.

In this part of the Chapter, initially six plots were provided for premature S2 beats to show how activation time, repolarization time, and APD change against (1) transmural distance; and (2) diastolic interval. To spatial profiles among epicardial, mid-myocardial, and endocardial tissues with and without structural discontinuities, these profiles were plotted on the same graph at S1S2 interval of 500 ms as shown in Figure 4-6. Restitution profiles of these tissues are shown in Figure 4-7.

For three ventricular tissues without regional discontinuities (slim geometry), the six spatial and restitution profiles of activation time, repolarization time, and APD were characterized with one S-shape curve.

The new finding was that regional discontinuities changed

- spatial and restitution profiles of repolarization time and APD;
- restitution profiles of activation time.

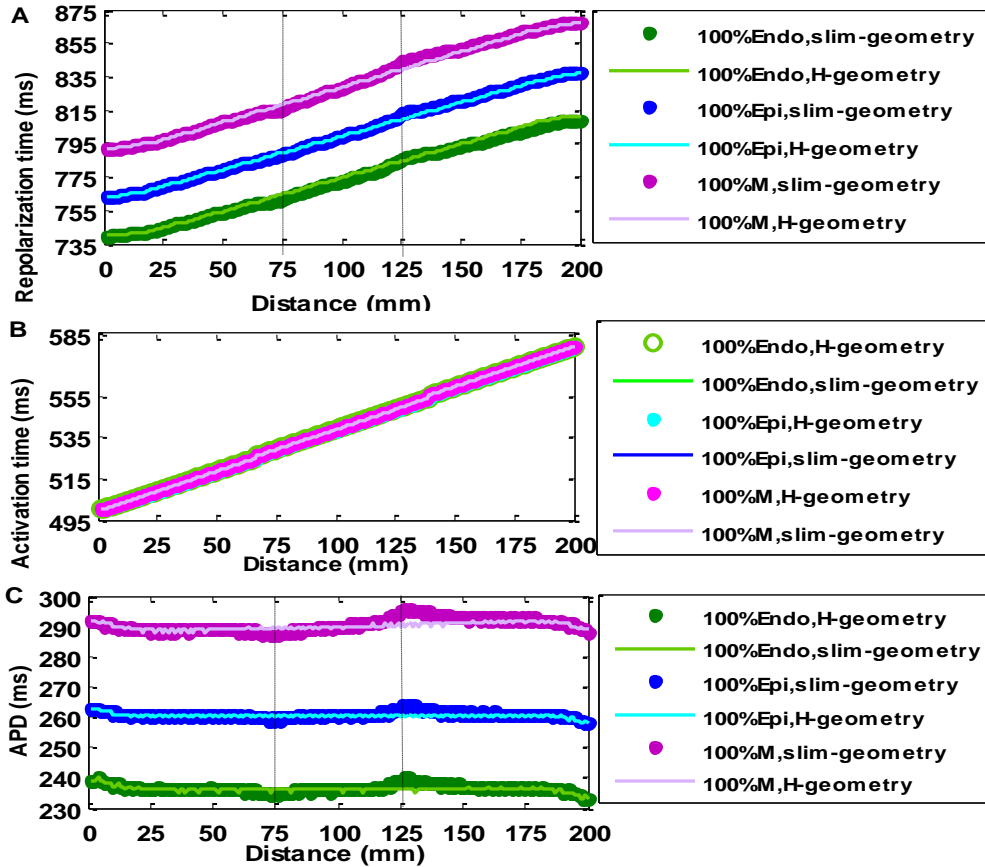
These profiles,

1. were characterized with three S-shape curves;
2. the two regional discontinuities in H-shape tissues reversed the direction of propagation and consequently the orientation of S-shape curve in the middle of profiles with respect to the x axis (activation time, repolarization time, and APD);
3. the dip and peak correspond to the abrupt changes in the middle of tissues (between grid points 75 and 125 in H-geometry as shown in Figure 4-2);
4. were qualitatively similar with both FK4V and TP06 models.

However, all six spatiotemporal profiles were quantitatively different due to description of epicardial, endocardial, and mid-myocardial cells for the FK4V model and TP06 model. For example, distinct spatial and restitution profiles were created for epicardial, mid-myocardial, and endocardial tissue with the FK4V model as described in the original paper [2]. Conversely, there was no significant difference between six profiles of epicardial and endocardial tissues with and without abrupt changes in tissue using the TP06 model, due to similarities between restitution properties of these two ventricular cell type in the original paper [3]. Moreover, with both FK4V and TP06 models, mid-myocardial tissues were characterized with longer repolarization time and APD than epicardial and endocardial tissue similar to the original papers [2, 3].

Spatial profiles at S1S2 interval of 500 ms

FK4V model of slim & H-shape endocardial, epicardial, & mid-myocardial tissues



TP06 model of slim & H-shape endocardial, epicardial, & mid-myocardial tissues

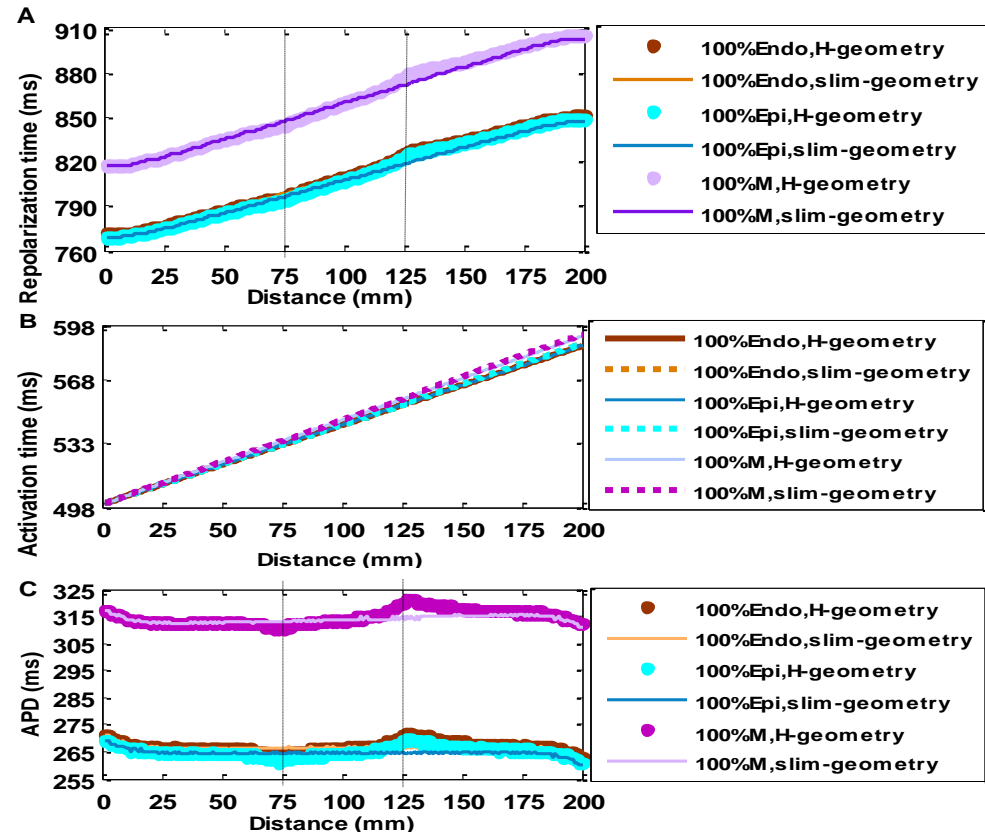
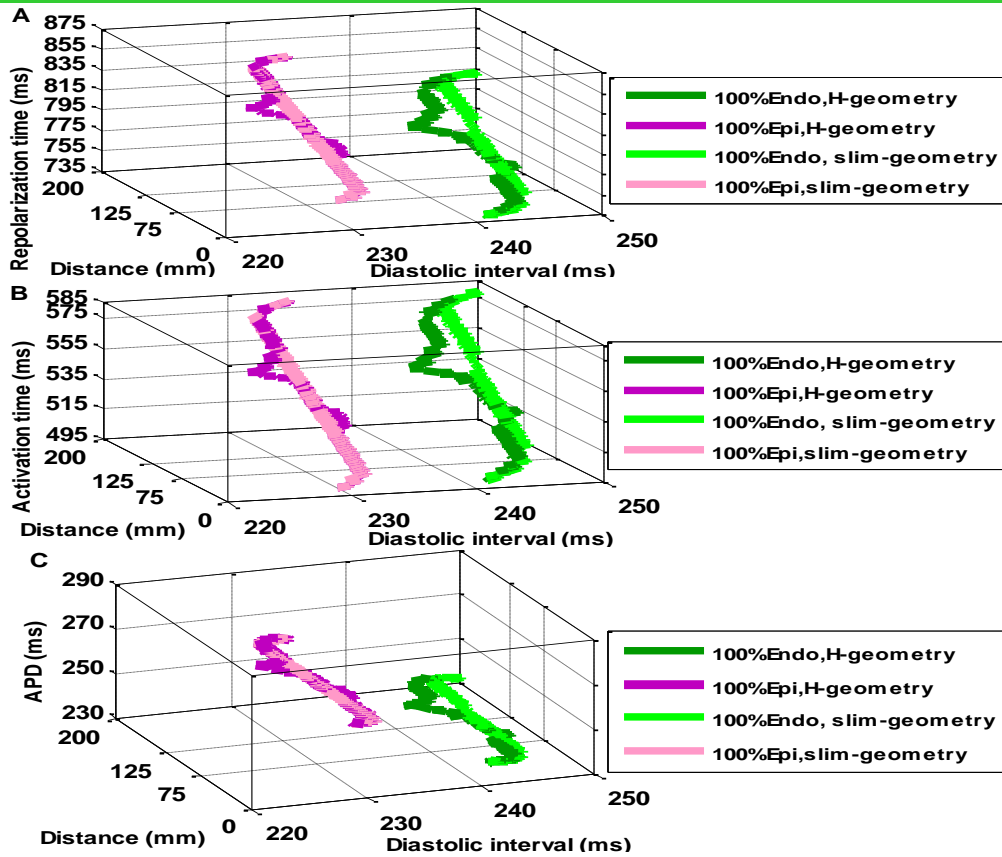


Figure 4-6: Spatial profiles of repolarization time (A); activation time (B); and APD (C) in 2D isotropic slim and H-shape tissues at S1S2 interval of 500 ms with the FK4V and the TP06 models

Restitution profiles at S1S2 interval of 500 ms

FK4V model of isotropic slim & H-shape endocardial & epicardial tissues



TP06 model of isotropic slim & H-shape endocardial & epicardial tissues

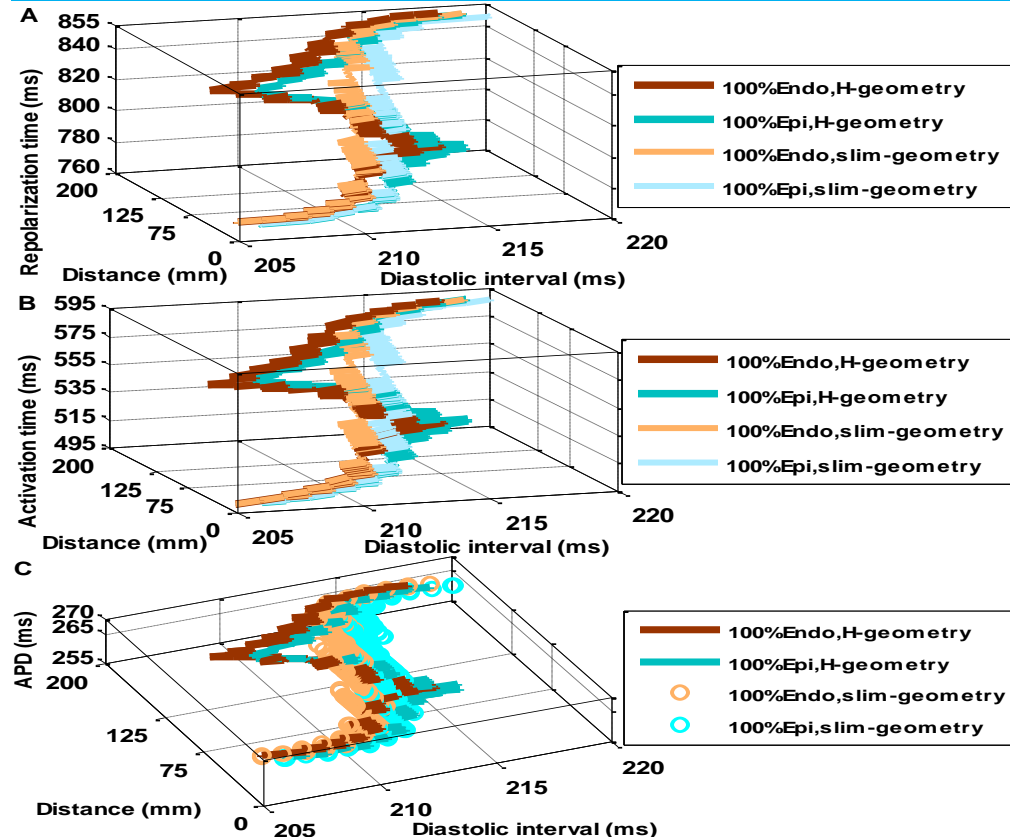


Figure 4-7: Restitution profiles of repolarization time (A); activation time (B); and APD (C) in 2D isotropic slim and H-shape tissues at S1S2 interval of 500 ms with the FK4V and the TP06 models

4.2.5 Profiles for premature beats for long and short S1S2 intervals

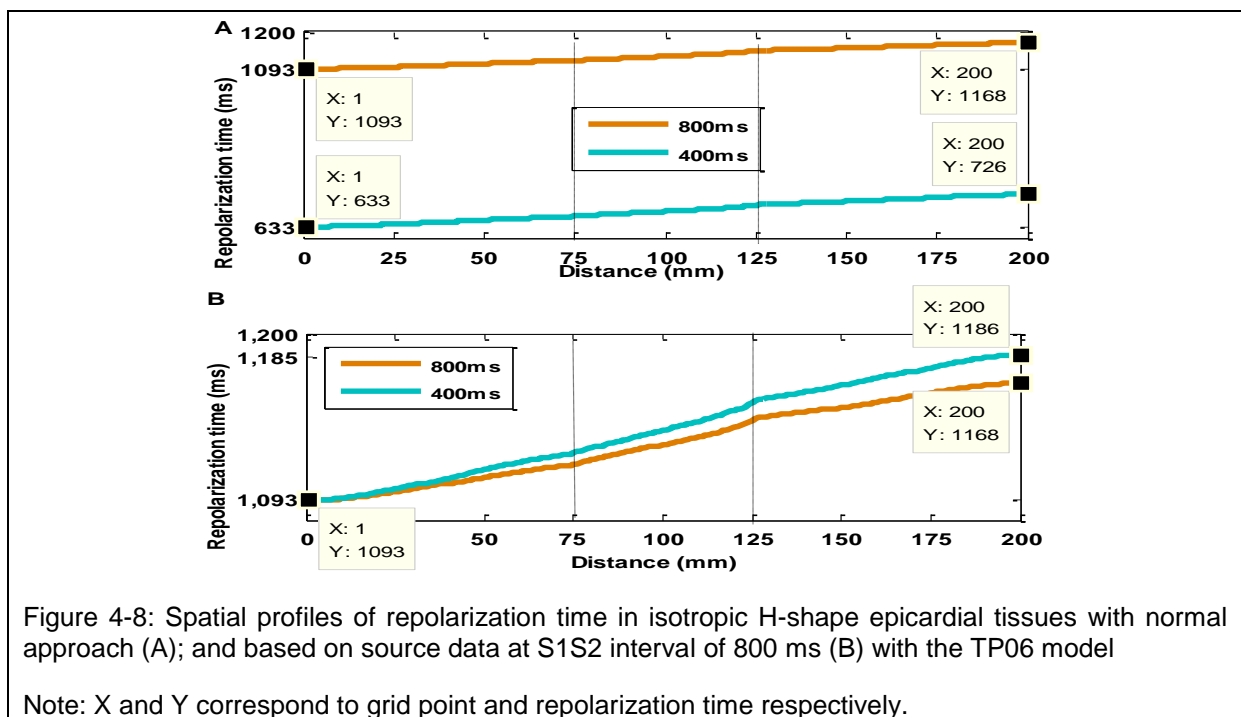
The features of spatial and restitution profiles (described in section 4.2.4) were not only true at a single S1S2 interval but also during progressively decreasing S1S2 intervals that are describe in the following sections.

4.2.5-1 Spatial profiles for premature beats

For premature S2 beats, plotting spatial profiles of activation time, repolarization time, and APD during decreasing S1S2 intervals in the same graph can hide the effects of structural discontinuities on the shape of the curves. To highlight these effects, the first numerical values of the activation time, the repolarization time, and the APD at S1S2 interval of 800 ms was used as the source data. Then the rest of data at other S1S2 intervals were plotted based on the source data. Organized Figures in Group A (Figures A1-A18) show the spatial profiles of activation time, repolarization time, and APD based on source data at S1S2 interval of 800 ms in 2D H-shape epicardial, mid-myocardial, and endocardial tissues with both FK4V and TP06 models.

For clarity, Figure 4-8 shows examples of spatial profiles of repolarization time for H-shape epicardial tissue with two approaches using the TP06 model. To plot spatial profiles of repolarization time at S1S2 interval of 400 ms based on data at S1S2 interval of 800 ms,

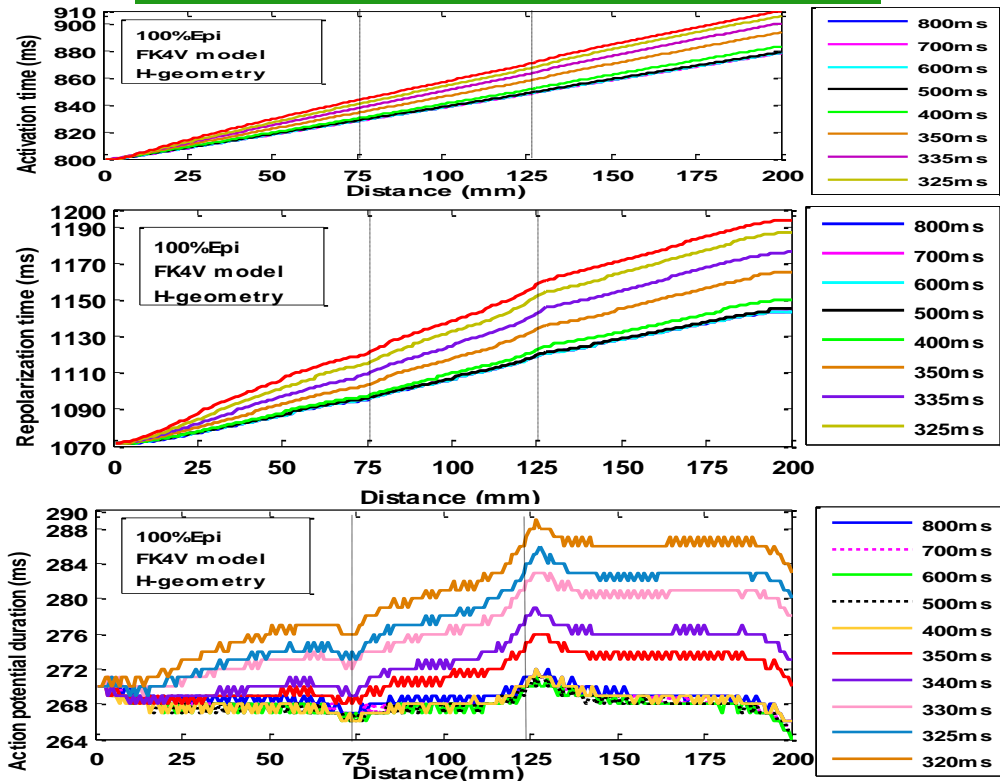
- the difference between the repolarization time at the first grid point at S1S2 intervals of 800 ms and 400 ms was calculated (i.e. 1093 ms-633 ms=460 ms, plot A);
- this difference value was added to the repolarization time of grid points 1 to 200 at S1S2 interval of 400 ms (i.e. repolarization time at grid point 200 at S1S2 interval of 400 ms became 726+460=1186 ms, plot B)



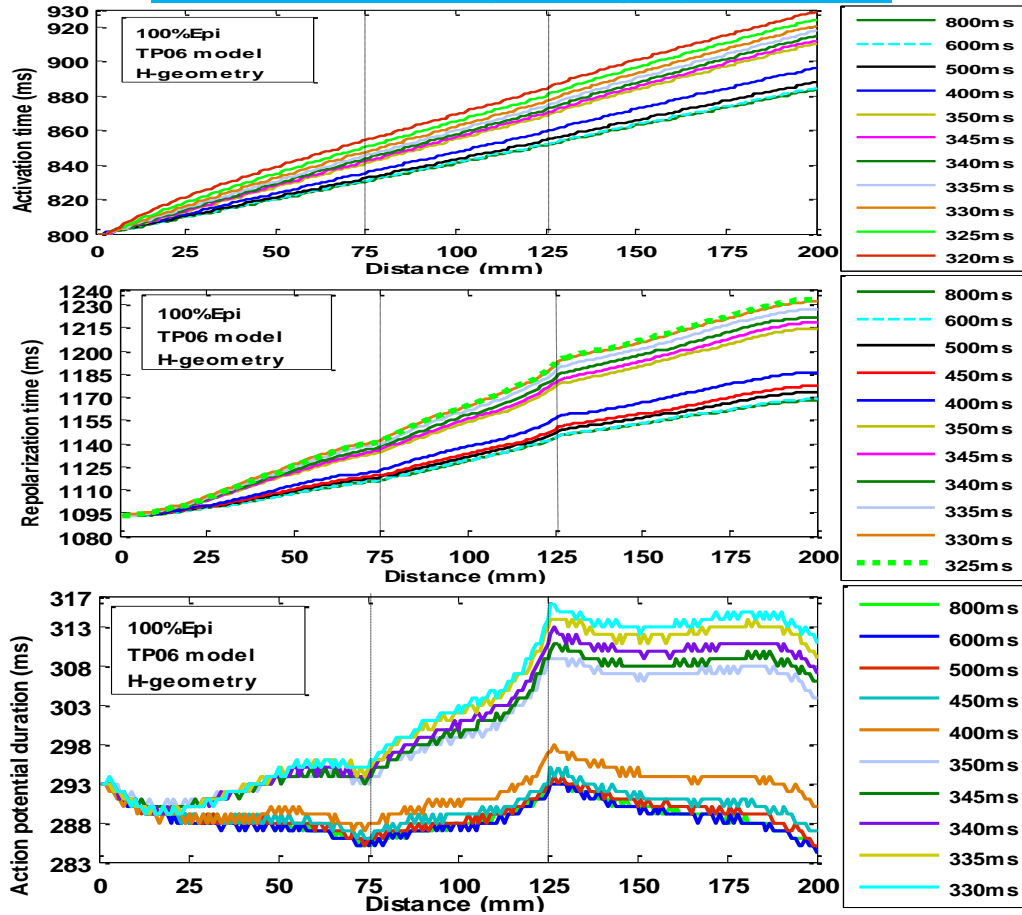
This approach was practically time consuming but clearly shows how structural discontinuities can change spatial profiles of activation time, repolarization time, and APD for premature S2 beats during decreasing S1S2 intervals.

Group A: Spatial profiles of epicardial tissues

FK4V model of 2D isotropic H-shape epicardial tissue



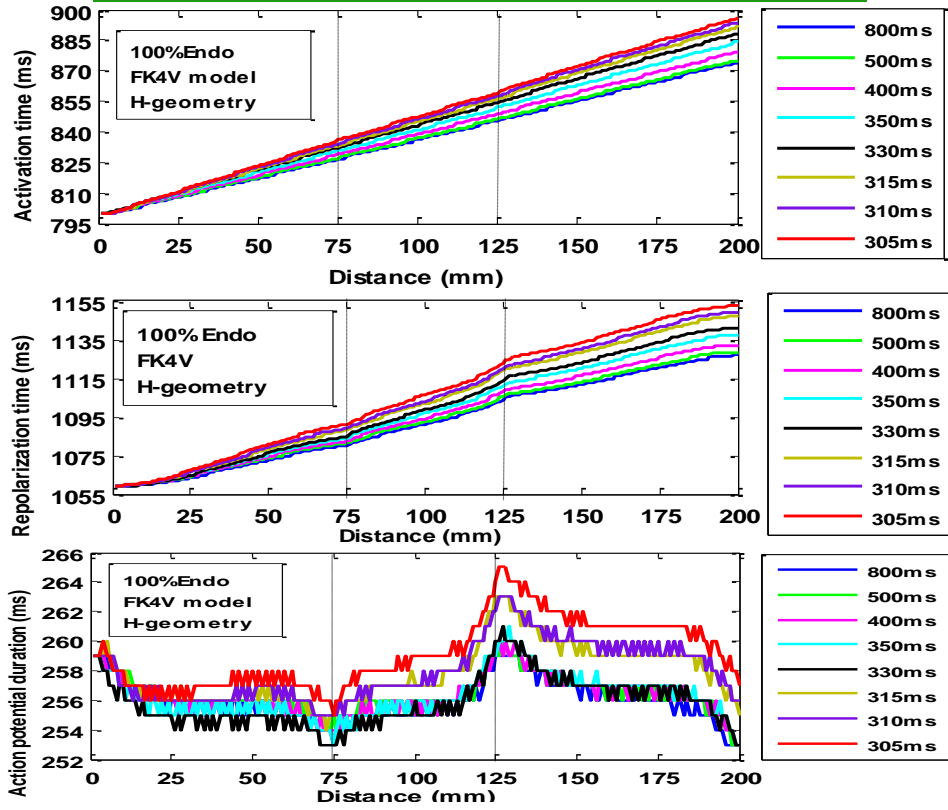
TP06 model of 2D isotropic H-shape epicardial tissue



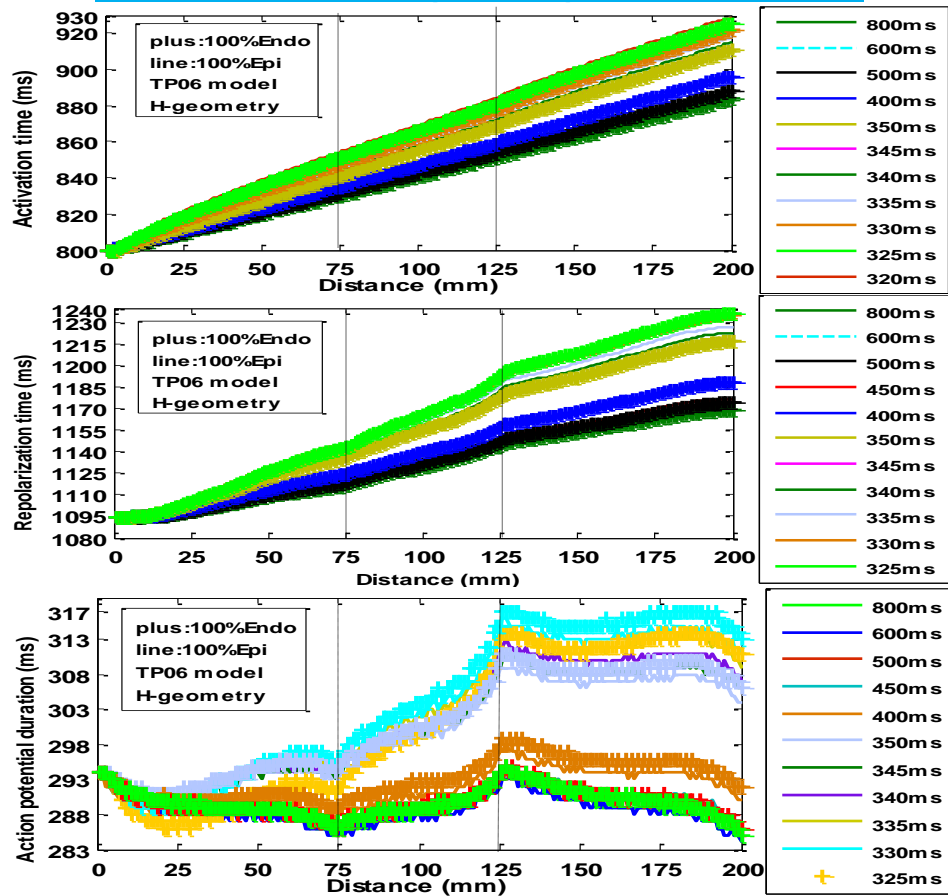
Figures A1-A6: Spatial profiles of activation time, repolarization time, and APD for epicardial tissues

Group A: Spatial profiles of endocardial tissues

FK4V model of 2D isotropic H-shape endocardial tissue



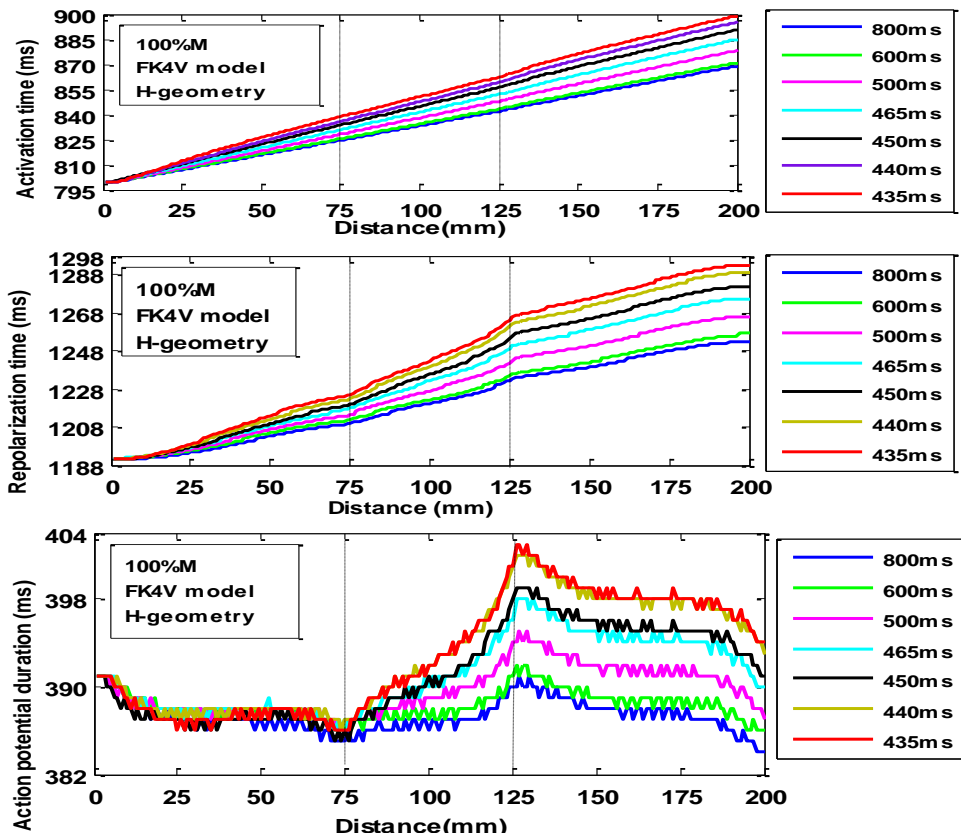
TP06 model of 2D isotropic H-shape endocardial tissue



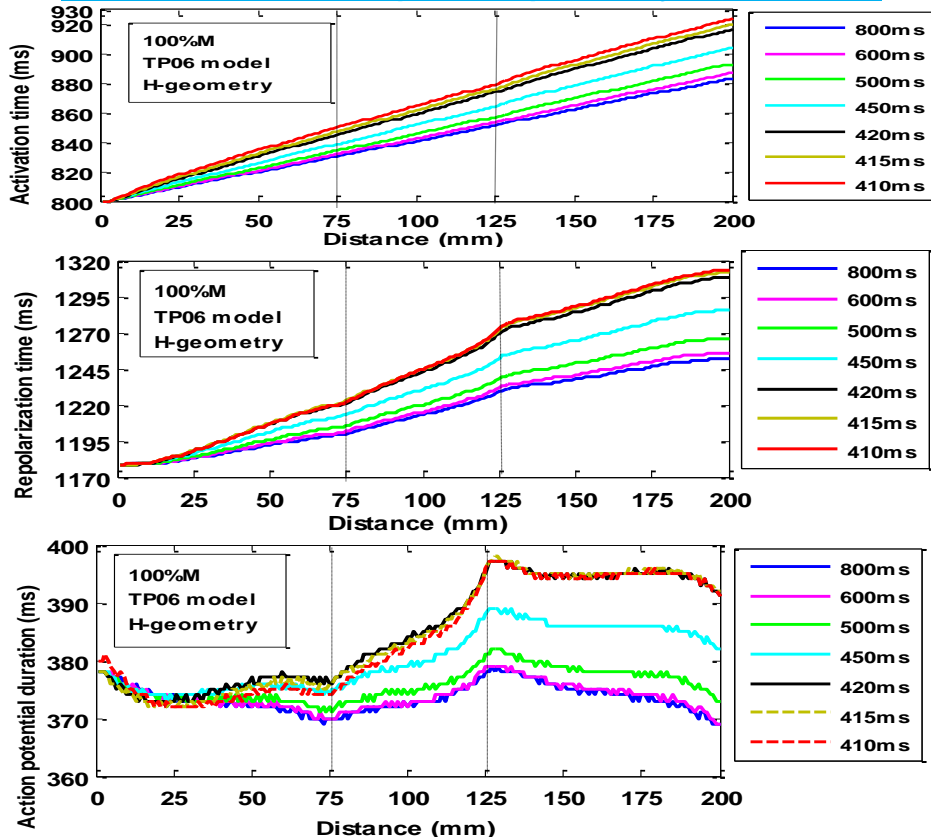
Figures A7-A12: Spatial profiles of activation time, repolarization time, and APD of endocardial tissues

Group A: Spatial profiles of mid-myocardial tissues

FK4V model of 2D isotropic H-shape mid-myocardial tissue



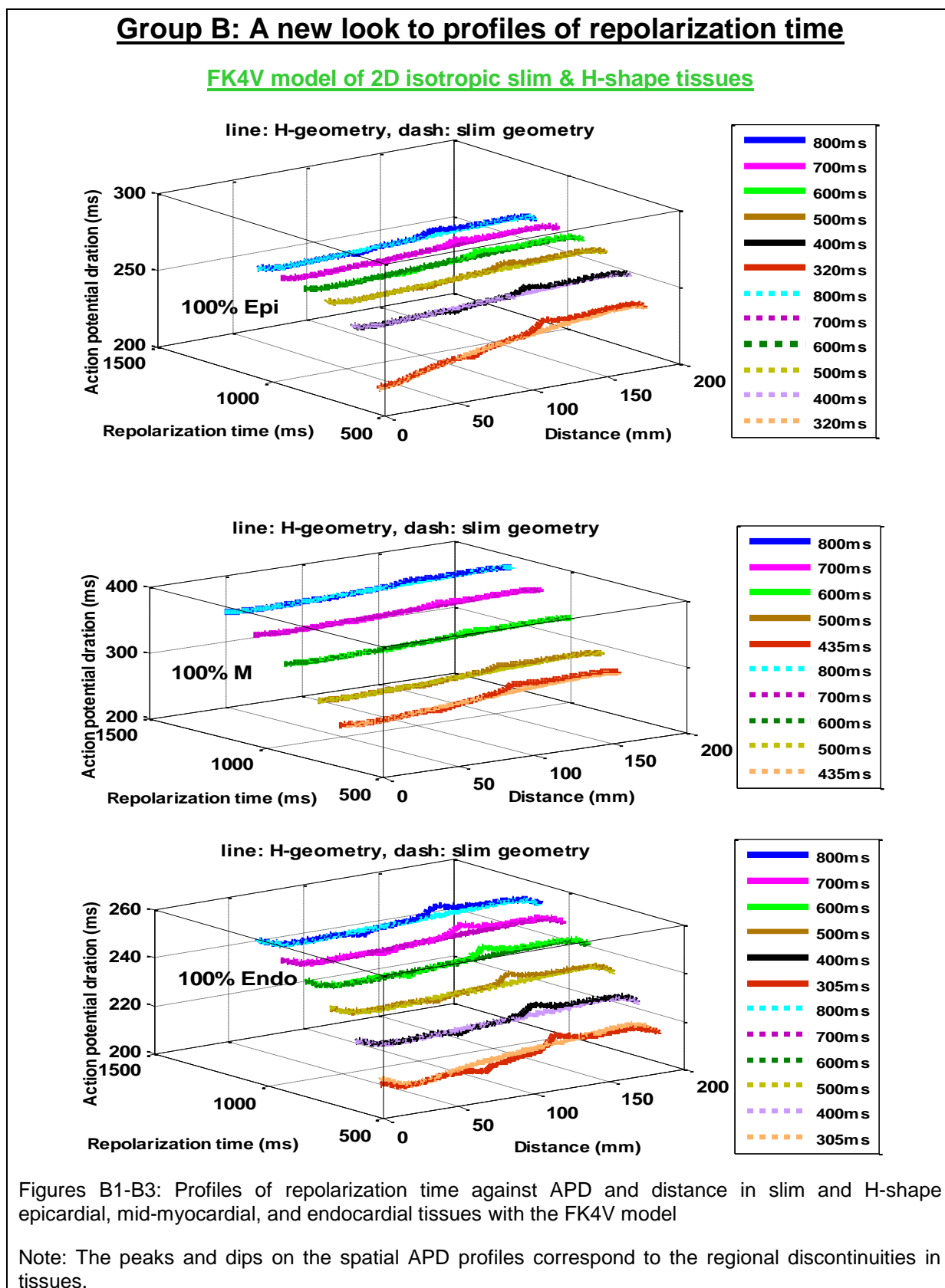
TP06 model of 2D isotropic H-shape mid-myocardial tissue



Figures A13-A18: Spatial profiles of activation time, repolarization time, and APD of mid-myocardial tissue

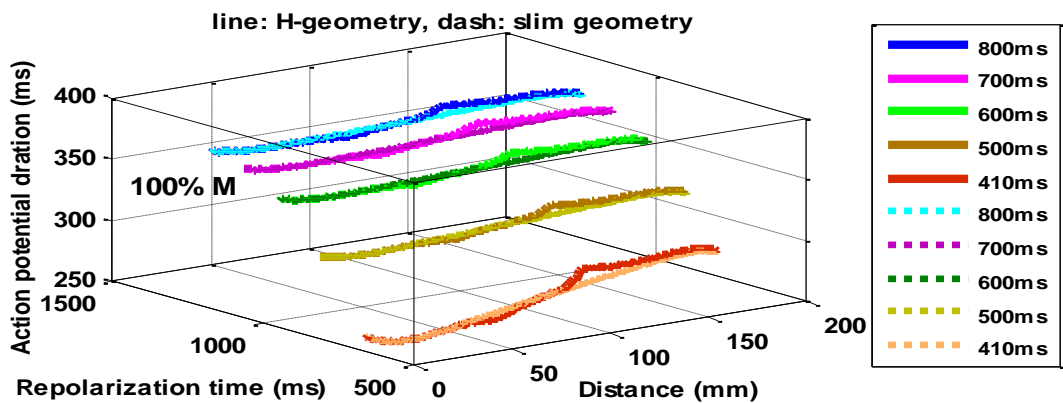
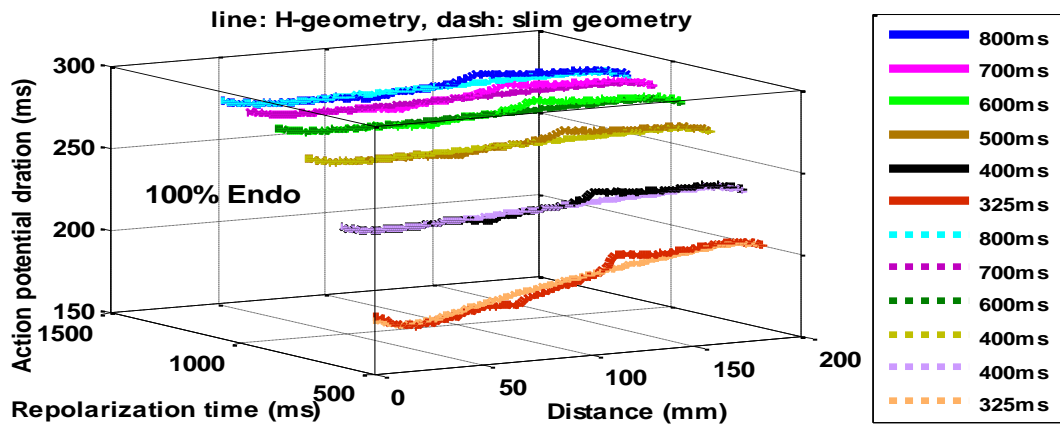
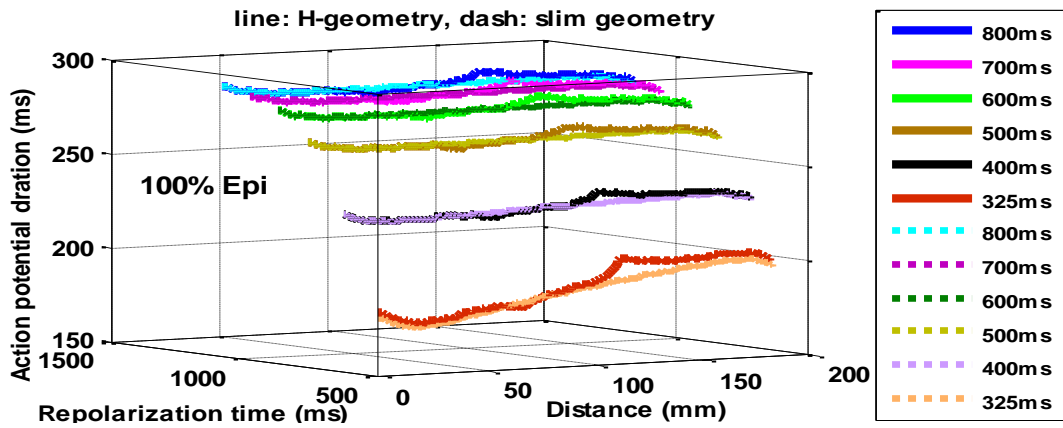
4.2.5-2 A new look to profiles of repolarization time

Figures B1 to B6 organized in Group B show a novel approach to observe the effects of structural discontinuities on the profiles of repolarization time for premature S2 beats. In this approach, repolarization time was plotted based on time (APD) and space (distance) in 3D plots for long and short S1S2 intervals.



Group B: A new look to profiles of repolarization time

TP06 model of 2D isotropic slim & H-shape tissues



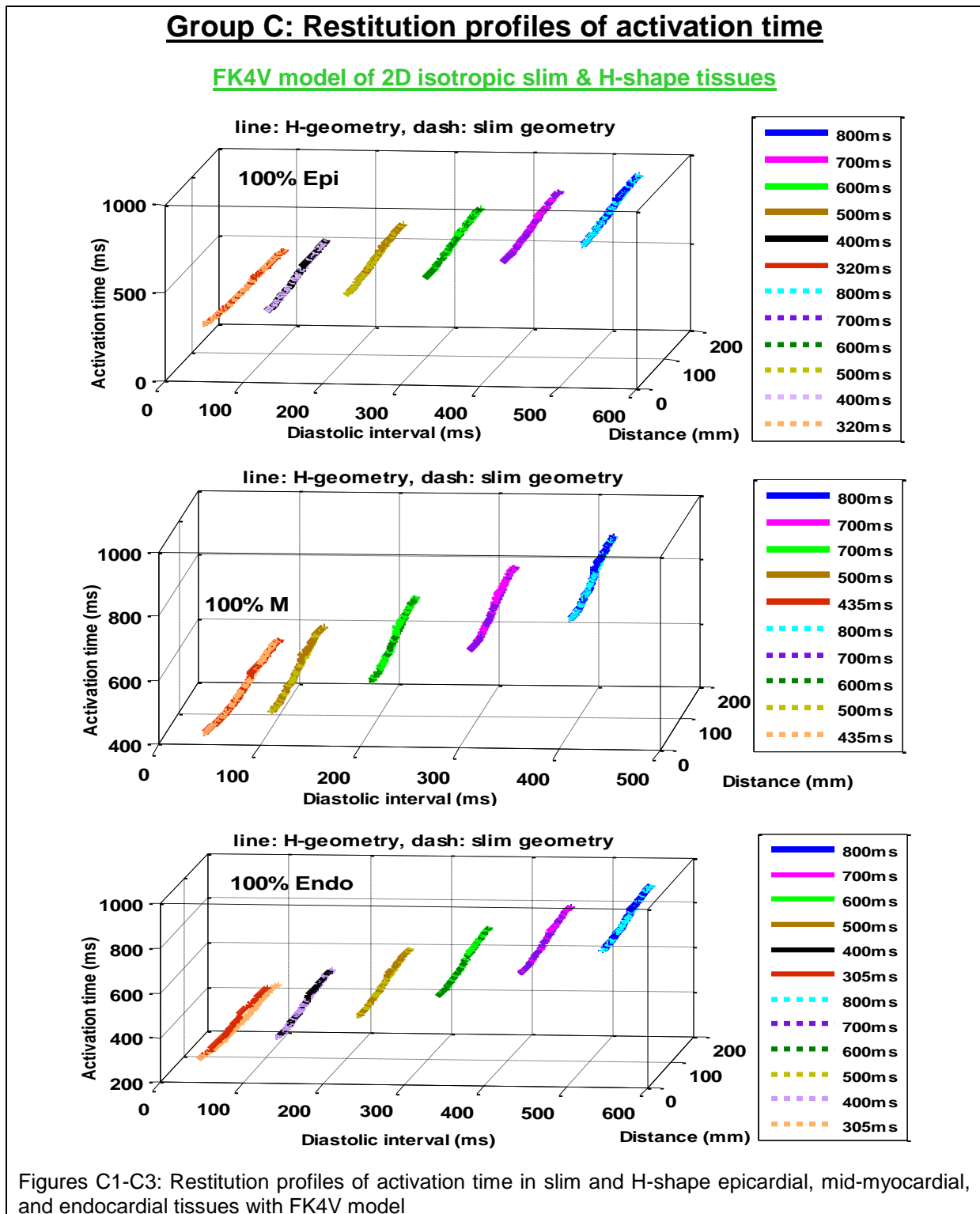
Figures B4-B6: Profiles of repolarization time against APD and distance in slim and H-shape epicardial, mid-myocardial, and endocardial tissues with the TP06 model

Note: The peaks and dips on the spatial APD profiles correspond to the regional discontinuities in tissues.

4.2.5-3 Restitution profiles for premature beats

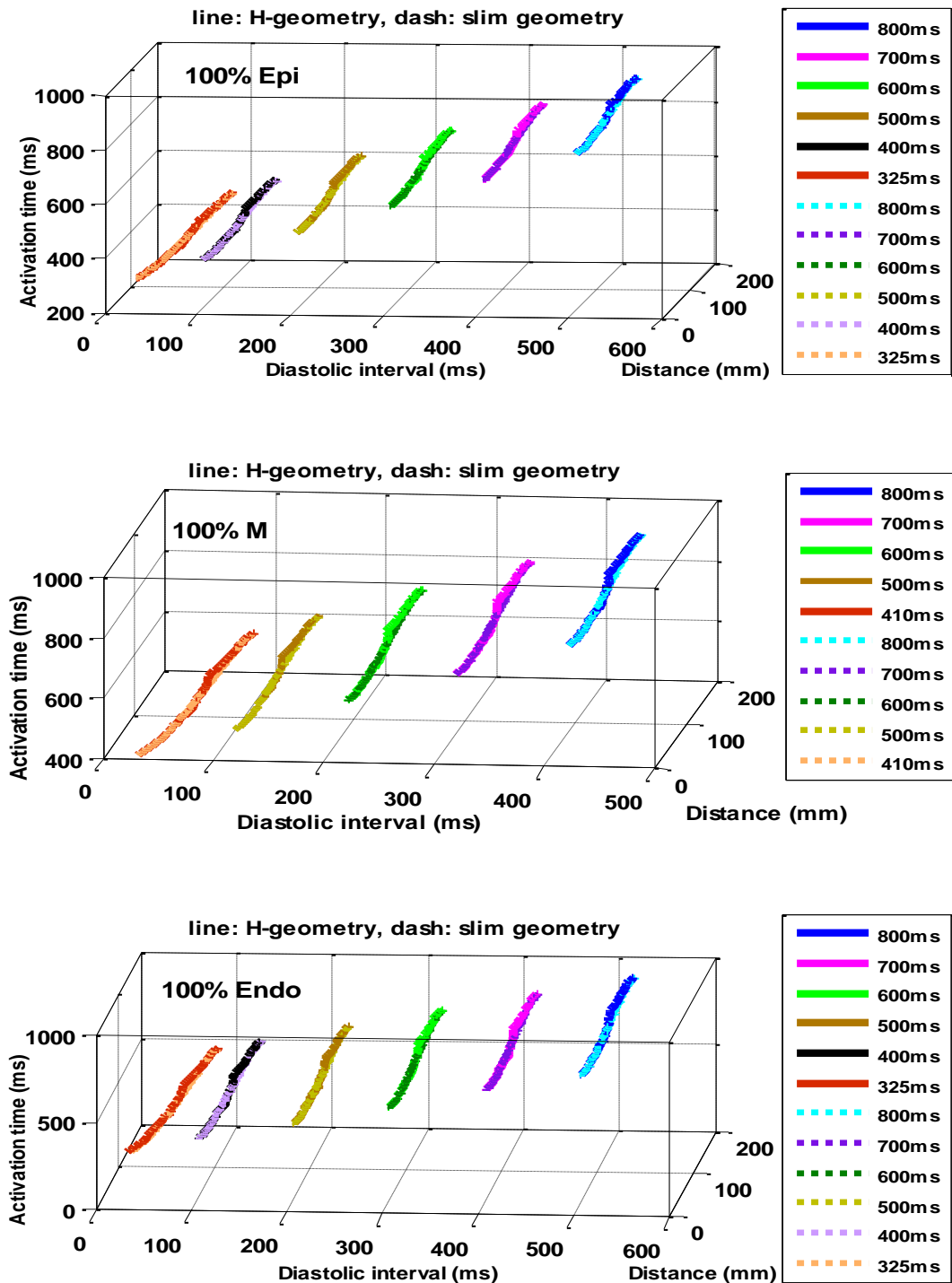
Figures C1 to C18 organised in Group C show restitution profiles of activation time, repolarization time, and APD during decreasing S1S2 intervals with the FK4V and the TP06 models. These 3D restitution profiles highlight the effects of structural discontinuities (as dips and peaks) on the shape of the curves for premature S2 beats.

Figures C1 to C6 show the restitution profiles of activation time (activation time against diastolic interval and distance) and emphasize that restitution profiles of activation time are quantitatively similar to restitution profiles of APD and repolarization time with both models.



Group C: Restitution profiles of activation time

TP06 model of 2D isotropic slim & H-shape tissues

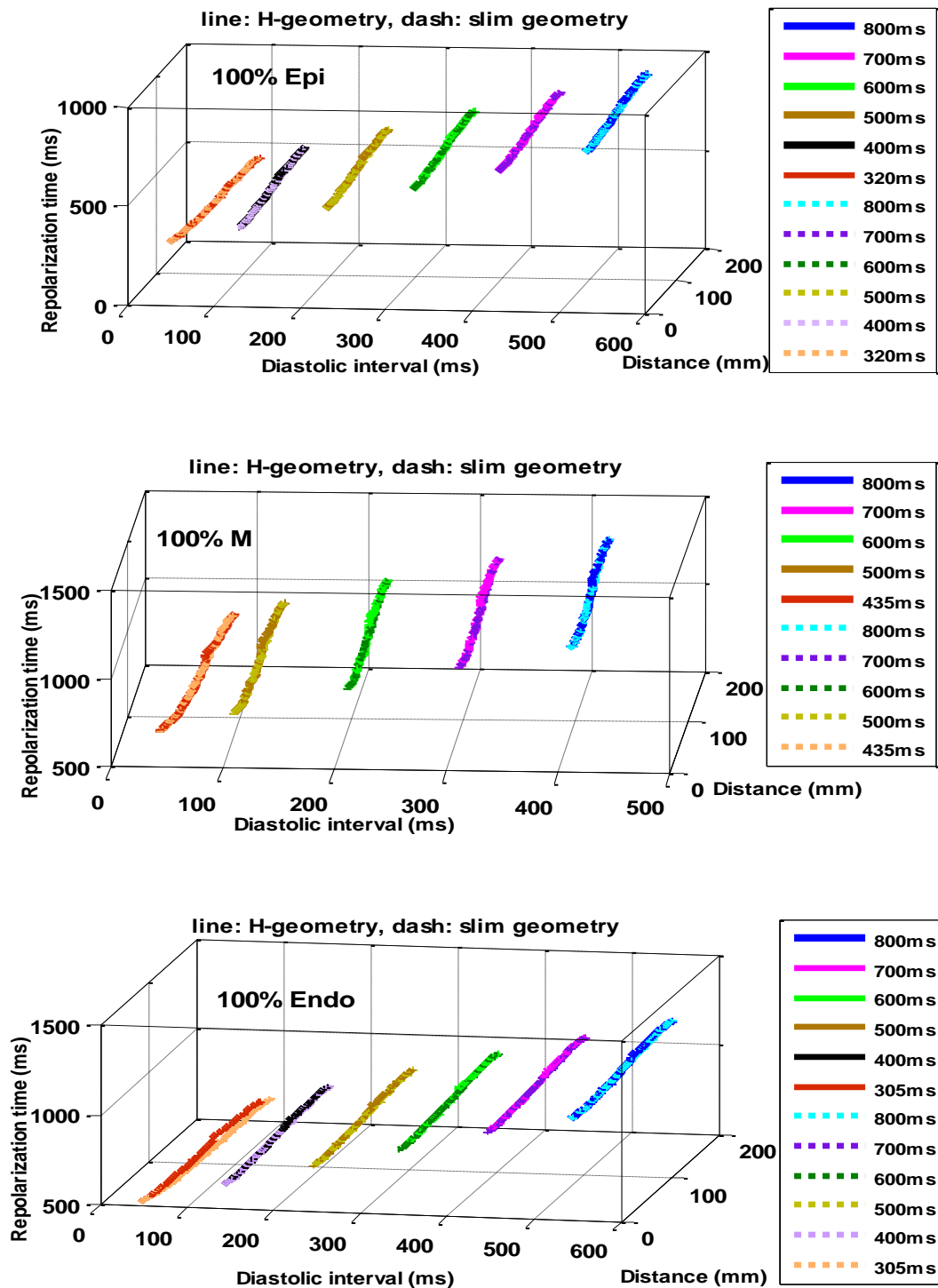


Figures C4-C6: Restitution profiles of activation time in slim and H-shape epicardial, mid-myocardial, and endocardial tissues with the TP06 model

Note: The peaks and dips on the spatial APD profiles correspond to the regional discontinuities in tissues.

Group C: Restitution profiles of repolarization time

FK4V model of 2D isotropic slim & H-shape tissues

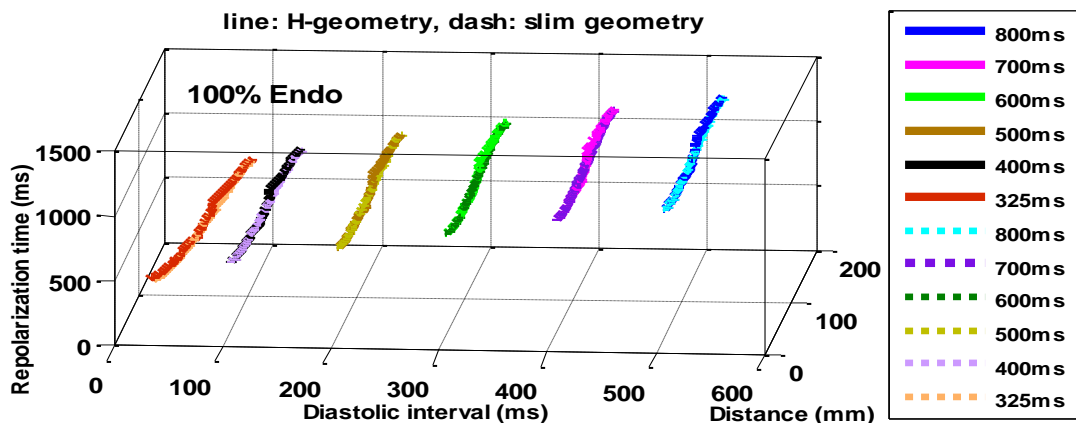
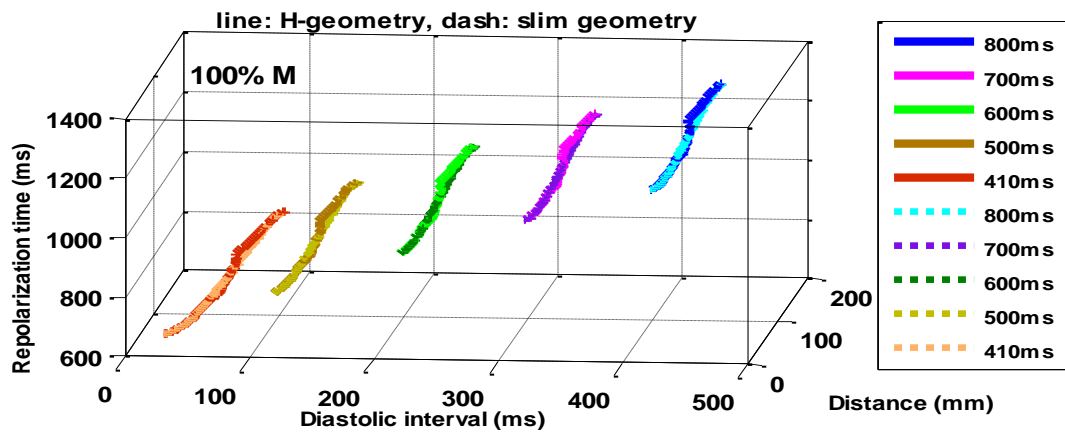
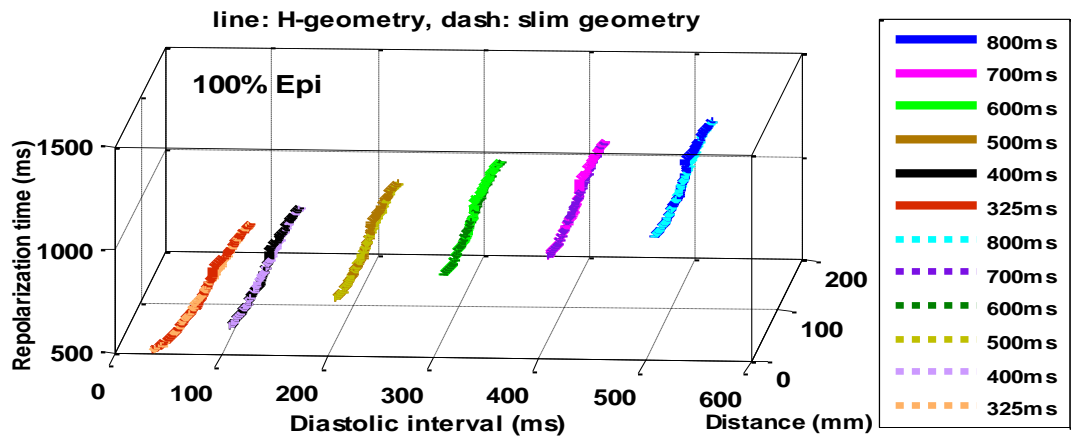


Figures C7-C9: Restitution profiles of repolarization time in slim and H-shape epicardial, mid-myocardial, and endocardial tissues with the FK4V model

Note: The peaks and dips on the spatial APD profiles correspond to the regional discontinuities in tissues.

Group C: Restitution profiles of repolarization time

TP06 model of 2D isotropic slim & H-shape tissues

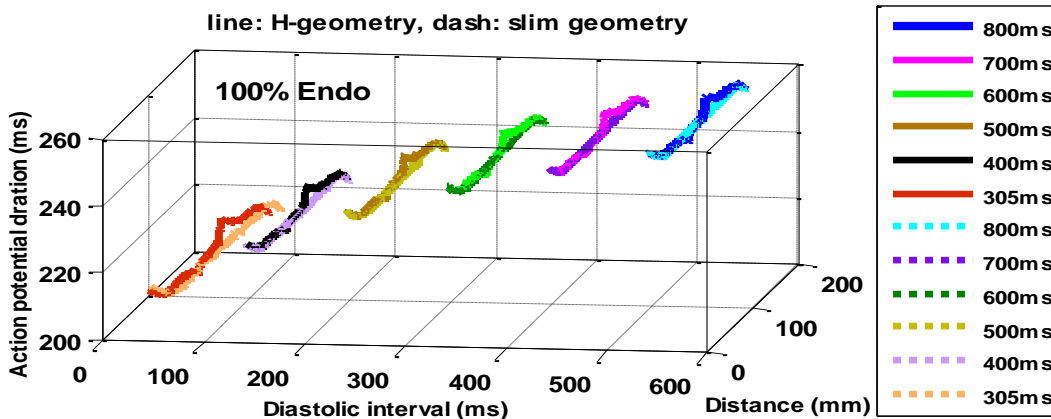
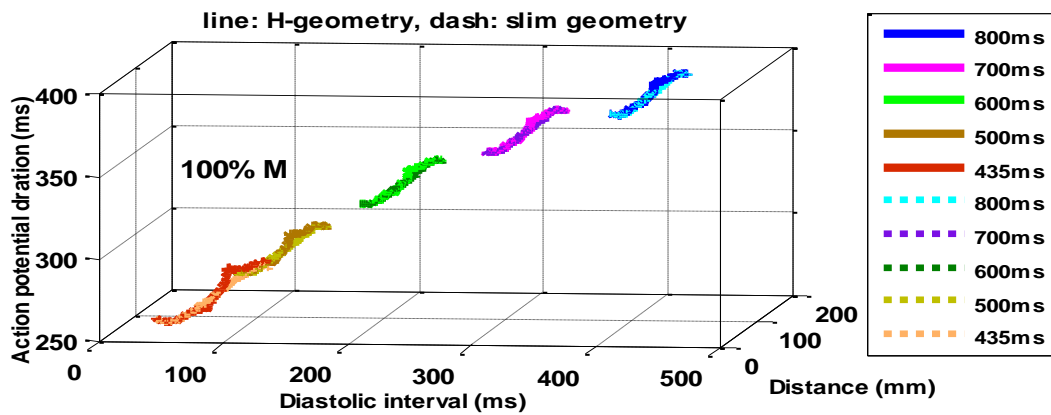
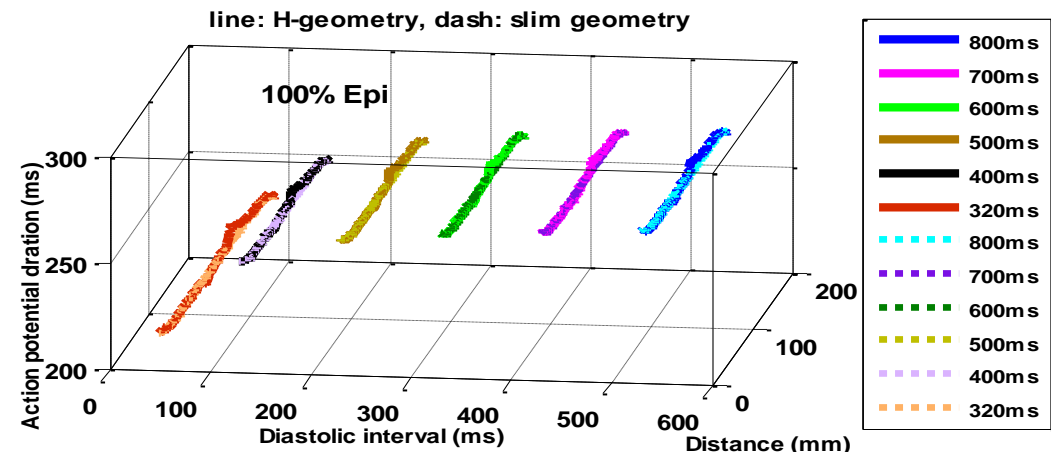


Figures C10-C12: Restitution profiles of repolarization time in slim and H-shape epicardial, mid-myocardial, and endocardial tissues with the TP06 model

Note: The peaks and dips on the spatial APD profiles correspond to the regional discontinuities in tissues.

Group C: Restitution profiles of APD

FK4V model of 2D isotropic slim & H-shape tissues

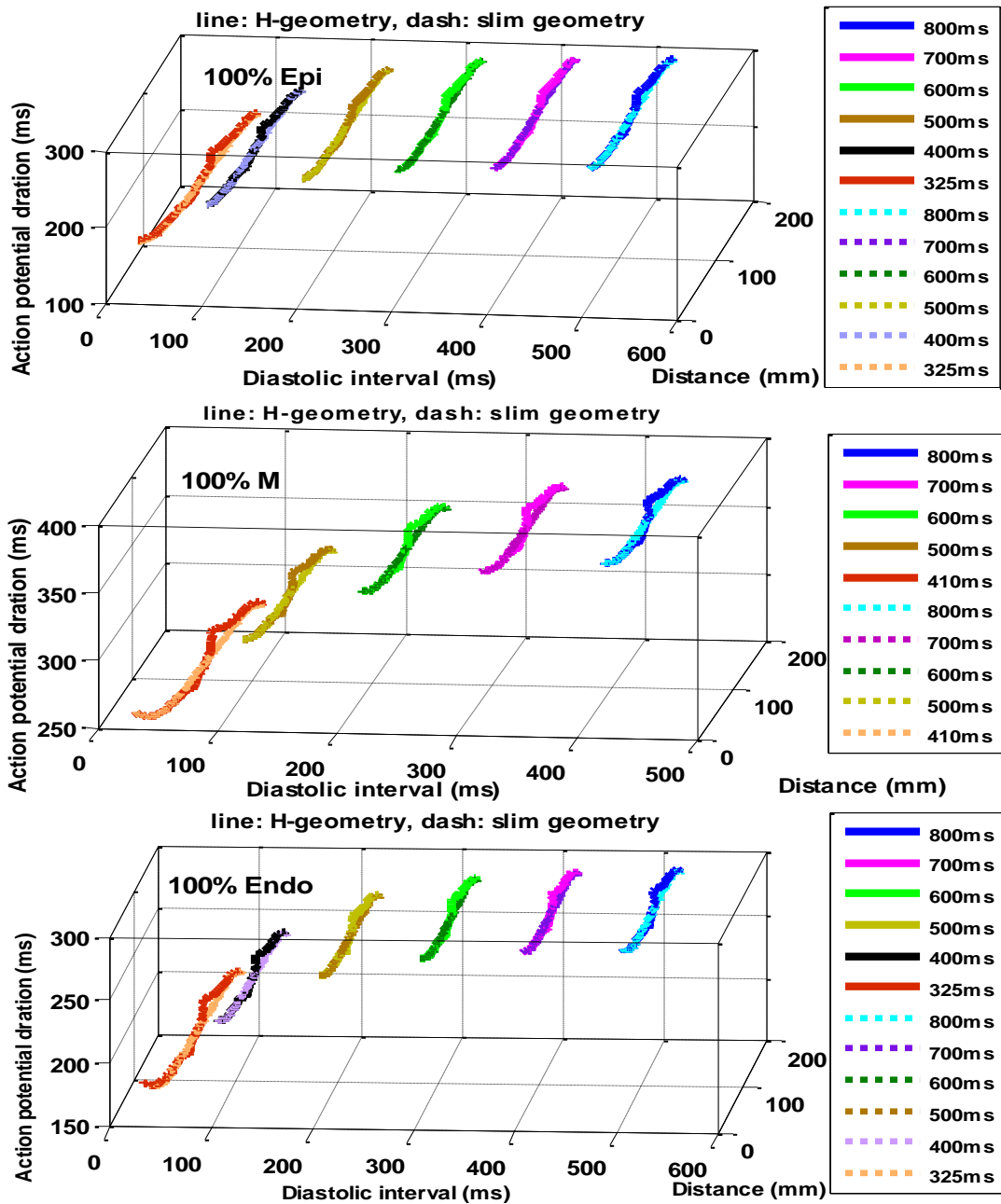


Figures C13-C15: Restitution profiles of APD in slim and H-shape epicardial, mid-myocardial, and endocardial tissues with the FK4V model

Note: The peaks and dips on the spatial APD profiles correspond to the regional discontinuities in tissues.

Group C: Restitution profiles of APD

TP06 model of 2D isotropic slim & H-shape tissues



Figures C16-C18: Restitution profiles of APD in slim and H-shape epicardial, mid-myocardial, and endocardial tissues with the TP06 model

Note: The peaks and dips on the spatial APD profiles correspond to the regional discontinuities in tissues.

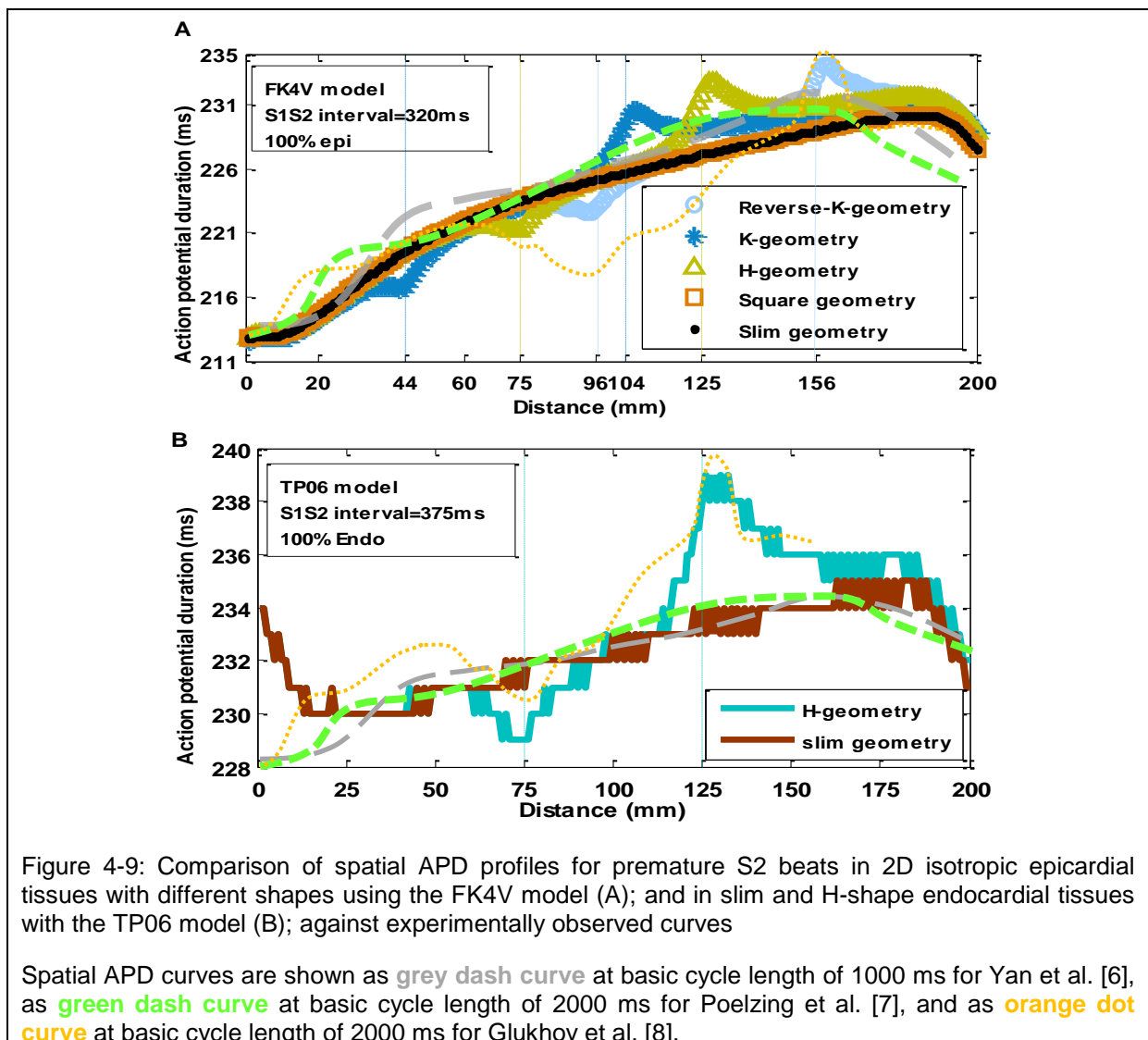
4.2.6 Qualitative comparison with experimental studies

Despite huge number of experimental studies, validation of simulation results requires high attention mainly due to the extensive variability among experimental data and limited availability of human data. Not surprisingly, there were similarities between APD spatial profiles for premature S2 beats in 2D simulated isotropic slim tissues in this thesis and in the left ventricular wedge preparation in experimental studies. It is possibly due to the techniques of measurements and surface recordings in experimental studies.

Figure 4-9 compares the simulated spatial APD profiles with the FK4V model in plot A, and the TP06 model in plot B in this thesis with experimentally observed APD profiles in canine left ventricular wedge preparation by Yan et al. [6] and Poelzing et al. [7] and in human left ventricular wedge preparation by Glukhov et al. [8]. In comparison,

- For slim shape isotropic epicardial tissue, spatial APD profiles at short S1S2 interval of 320 ms with the FK4V model was approximately similar to spatial APD profiles at basic cycle length of 1000 ms by Yan et al. [6], and at basic cycle length of 2000 ms by Poelzing et al. [7].
- For H-shape isotropic epicardial tissue, spatial APD profiles at short S1S2 interval 320 ms with the FK4V model was broadly similar to spatial APD profiles at basic cycle length 2000 ms by Glukhov et al. [8]. It is important to note that the peaks in spatial APD profiles of H-shape epicardial tissue correspond to structural discontinuities in tissue while the peak in the experimental curve [8] corresponded to an isolated island of the mid-myocardial region.

The same was true for simulated tissues with the TP06 model. However, there were differences in the initial part of spatial APD profiles for simulated tissues with the TP06 model and experimental curves.



4.3 Three measures of dispersion for normal and premature beats

The previous section illustrated how regional discontinuities influenced the spatial and restitution profiles of activation time, APD, and repolarization time during progressively decreasing S1S2 intervals for premature S2 beats in 2D tissues. There is evidence that increase in repolarization dispersion may increase vulnerability to cardiac arrhythmia in human [9, 10]. It was interesting to find out the effects of regional discontinuities on not only dispersion in repolarization time and APD but also dispersion in activation time for both normal S1 and premature S2 beats.

This part of the Chapter is based on three measures of dispersion including:

1. dispersion in activation time as the difference between the maximum and the minimum activation time at each S1S2 interval;
2. dispersion in repolarization time as the difference between the maximum and the minimum repolarization time at each S1S2 interval;
3. dispersion in APD as the difference between the maximum and the minimum APD at each S1S2 interval.

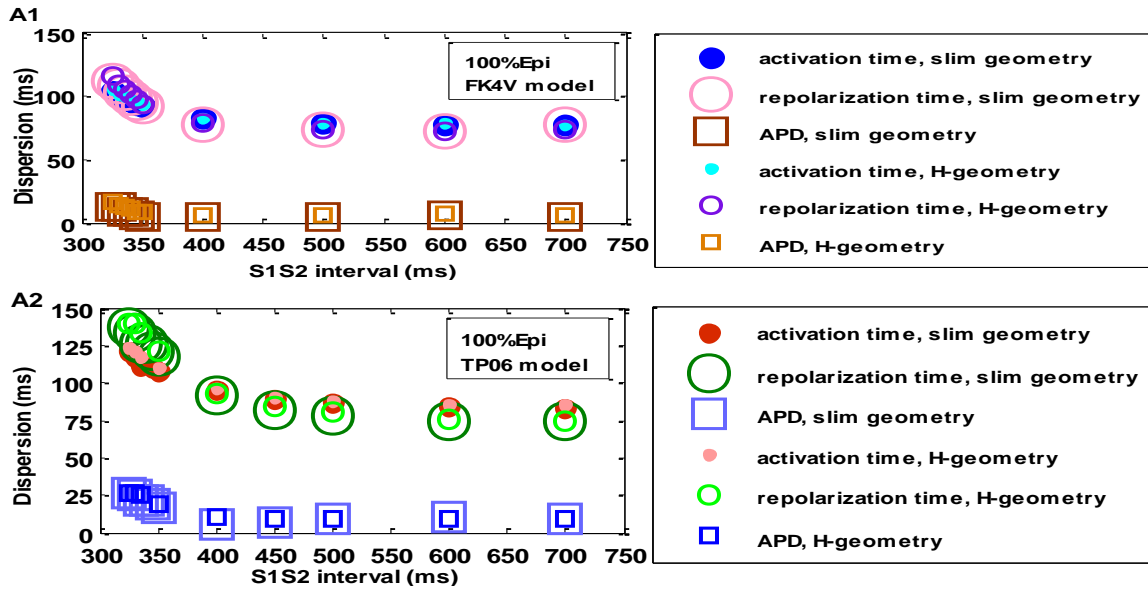
4.3.1 Profiles of measures of dispersion for premature beats

To study how tissues with and without structural discontinuities affect three measures of dispersion in activation time, APD, and repolarization time, these measures were plotted against S1S2 interval. Figure 4-10 shows these profiles for premature S2 beats in 2D isotropic epicardial, mid-myocardial, and endocardial tissue with slim and H-shape using both models.

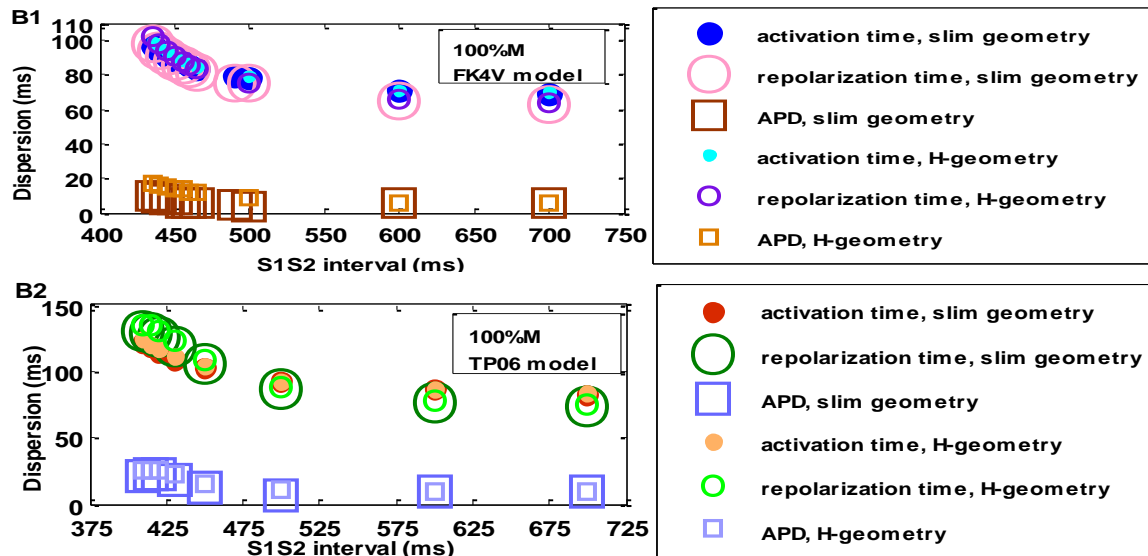
In these 2D tissues, three measures of dispersion

- gradually increased during decreasing S1S2 intervals;
- were slightly smaller for tissues with structural discontinuities than tissues without structural discontinuities;
- with the TP06 models were greater than the FK4V model.

Three measures of dispersion for premature beats in epicardial tissues



Three measures of dispersion for premature beats in mid-myocardial tissues



Three measures of dispersion for premature beats in endocardial tissues

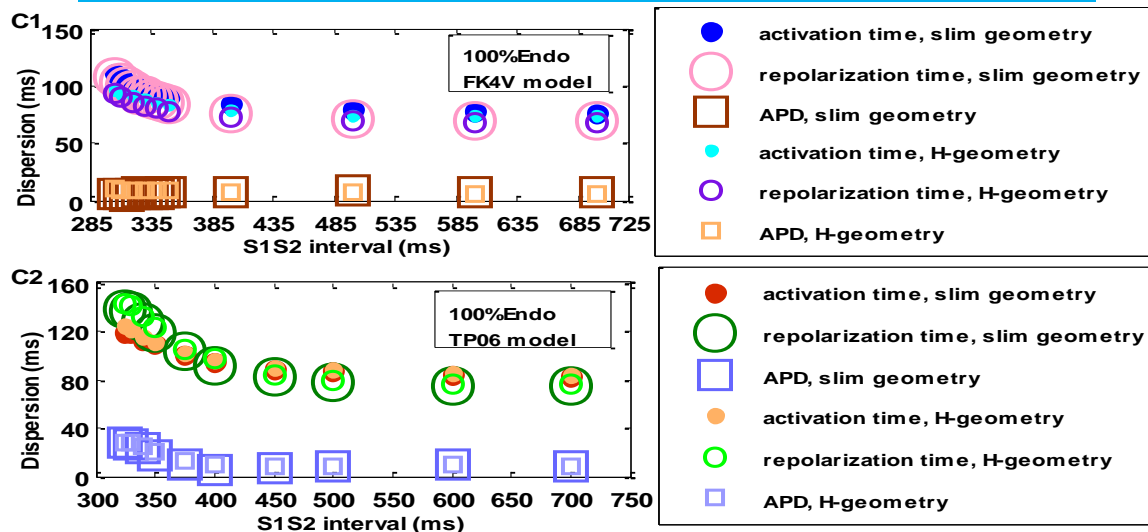


Figure 4-10: Profiles of dispersion in activation time, repolarization, and APD against S1S2 interval with the FK4V and TP06 models for isotropic slim and H-shape epicardial tissue (A1 and A2); mid-myocardial tissue (B1 and B2); and endocardial tissue (C1 and C2)

4.3.2 The largest and the smallest measures of dispersion

This part of the Chapter compares the smallest and the largest values of three measures of dispersion for epicardial, mid-myocardial, and endocardial tissues with and without structural discontinuities. For premature S2 beats,

- the smallest dispersion in repolarization time was the smallest value of measures of dispersion in repolarization time among all S1S2 intervals;
- the largest dispersion in repolarization time was the largest value of measures of dispersion in repolarization time among all S1S2 intervals.

The same was true for dispersion in activation time and APD. Summary Figure 4-11 compares the largest and the smallest value of three measures of dispersion in 2D isotropic slim and H-shape epicardial, mid-myocardial, and endocardial tissues with both models.

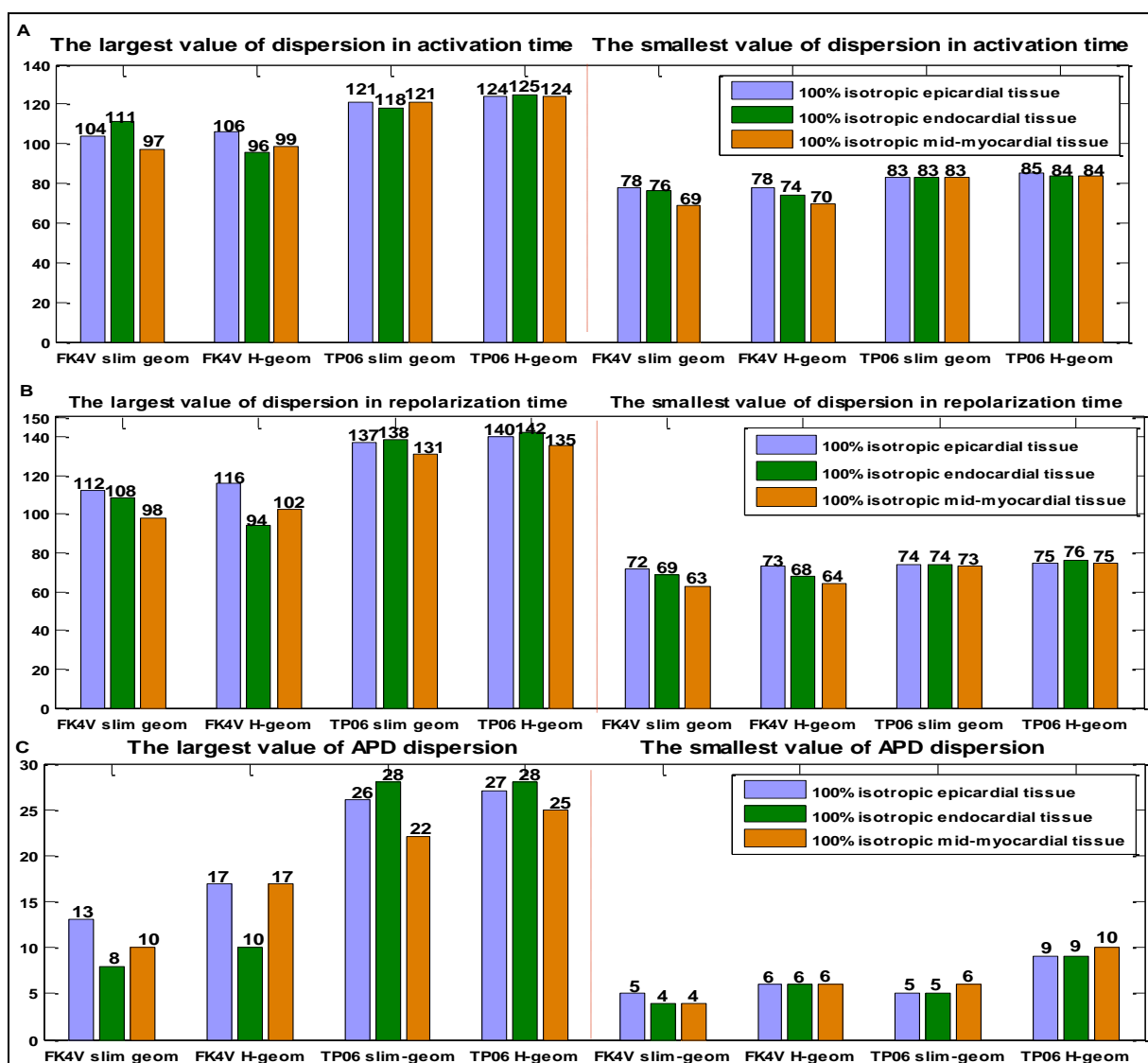


Figure 4-11: The largest and smallest value of measures of dispersion in activation time (A); repolarization time (B); and APD (C) for premature S2 beat in slim and H-shape tissues with both FK4V and TP06 models

The smallest and the largest three measures of dispersion in all H-shape tissues were greater than those in the slim tissues using both models.

Note: Geom is the abbreviation of geometry.

Comparison between tissues with and without structural discontinuity with both models showed that:

First, the structural discontinuities in the most H-shape tissues increased the largest and the smallest value of three measures of dispersion around 1 to 7 ms compared to slim tissues without structural discontinuities. On the contrary, for endocardial tissues with the FK4V model, structural discontinuities decreased the smallest and the largest dispersion in activation time and repolarization time possibly due to the model dependency i.e. 15 ms for the largest and 2 ms for the smallest value of dispersion in activation time as shown in Figure 4-11, plot A.

Second, the largest value of dispersion in repolarization at short S1S2 interval (i.e. shorter than 450 ms) became greater than the largest value of dispersion in activation time for all tissues (except in slim and H-shape endocardial tissue with the FK4V model as shown in Figure 4-11, plots A and B). The dispersion in repolarization of normal myocardium adjust to diseased myocardium is considered highly arrhythmogenic [11].

Third, the largest value of dispersions in repolarization time and activation time in this thesis are greater than those of animal and human experimental studies in the literature review. However, the smallest value of dispersion in repolarization time (varied from 63 ms to 76 ms shown in Figure 4-11, plot B) was in agreement with dispersion in repolarization of 66 ms along the left ventricular epicardium and 73 ms along right ventricular endocardium in patients with ventricular tachycardia or positive microvolt T-wave alternans by Chauhan et al. [9]. This issue is discussed in detail for homogenous and heterogeneous tissues in 3D cubes of tissue and a left ventricular wedge model in Chapters 5 and 6 respectively.

4.3.3 Quantitative comparison of measures of dispersion for normal and premature beats

Table 4-1 provides numerical values of three measures of dispersion with precision of 1 ms for both normal S1 and premature S2 beats during decreasing S1S2 intervals in 2D isotropic slim and H-shape epicardial, mid-myocardial, and endocardial tissues using FK4V and TP06 models.

For normal S1 beats, three measures of dispersion remained approximately constant for long and short S1S2 intervals.

For premature S2 beats, during decreasing S1S2 intervals from 700 ms to the last S1S2 interval, three measures of dispersion compared to normal S1 beats increased to around

- 22-41 ms for dispersion in activation time;
- 26-66 ms for repolarization time;
- 4-19 ms for APD dispersion.

Three measures of dispersion (in ms) for normal S1 and premature S2 beats during decreasing S1S2 intervals (S1S2) in ms				
	Activation time (ms)	Repolarization time (ms)	APD (ms)	
E P I	FK4V model, slim geometry S1S2 intervals of 700-325ms Normal S1 beats	77	72-74	4-5
	Premature S2 beats	78-104	78 at S1S2 700 72-112 (S1S2 600-325)	5-6 (S1S2 700-350) 13 at S1S2 325
	TP06 model, slim geometry S1S2 intervals of 700-325 ms Normal S1 beats	82-83	74	8-10
	Premature S2 beats	83-21	74-137	10-5 (S1S2 700-400) 17-26 (S1S2 350-325)
	FK4V model, H-geometry S1S2 intervals of 700-325 ms Normal S1 beats	77-78	73-74	6
	Premature S2 beats	78-106	78 at 700 72-116 (S1S2 600-325)	6-7 (S1S2 700-400) 17 at S1S2 325
	TP06 model, H-geometry S1S2 intervals of 700-325 ms Normal S1 beats	83	75-76	9-10
	Premature S2 beats	85-124	75-140	9-27
E N D O	FK4V model, slim geometry S1S2 intervals of 700-305ms Normal S1 beats	75-76	69-70	6-7
	Premature S2 beats	76-111	69-108	4-8
	TP06 model, slim geometry S1S2 intervals of 700-325 ms Normal S1 beats	82	73-74	8-9
	Premature S2 beats	83-118	74-138	7-10 (S1S2 700-450) 5-25 (S1S2 400-325)
	FK4V model, H-geometry S1S2 intervals of 700-305 ms Normal S1 beats	73-74	67-68	6-7
	Premature S2 beats	74-96	68-94	6-10
	TP06 model, H-geometry S1S2 intervals of 700-325 ms Normal S1 beats	83	75-76	9-10
	Premature S2 beats	84-125	76-142	9-10 (S1S2 700-400) 13-28 (S1S2 375-325)
M	FK4V model, slim geometry S1S2 intervals of 700-435 ms Normal S1 beats	68	62	6-7
	Premature S2 beats	69-97	63-98	6-7(S1S2 700-600) 4-10 (S1S2 500-435)
	TP06 model, slim geometry S1S2 intervals of 700-410 ms Normal S1 beats	81-82	71-73	9-11
	Premature S2 beats	83-121	73-131	10-6 (S1S2 700-500) 12-22 (S1S2 450-415) 21 at S1S2 of 410
	FK4V model, H-geometry S1S2 intervals of 700-435 ms Normal S1 beats	68-69	62-63	7-8
	Premature S2 beats	70-99	64-102	6-4 (S1S2 700-600) 9-17 (S1S2 500-435)
	TP06 model, H-geometry S1S2 intervals of 700-410 ms Normal S1 beats	82-83	73-74	10-11
	Premature S2 beats	85-124	75-135	10-26 (S1S2 700-415) 25 at S1S2 410

Table 4-1: Three measures of dispersion for normal and premature beats

4.4 Speed of depolarization conduction

Similar to a human study in 2D atrial myocytes [12], in this thesis, tissue geometry influenced the shapes of spatial profiles of activation time, repolarization time, and APD in 2D isotropic ventricular tissues with the FK4V and TP06 models.

Furthermore, simulation studies in 1D fibre [13], 2D homogenous tissue [12, 14] using animal models suggested that dependence of APD on distance, and prolongation and shortening of APD near a non-conducting boundary is because of the boundary effect. This thesis showed that the shapes of spatial profiles of repolarization time and APD for premature S2 beats changed during decreasing S1S2 intervals. This change is possibly a result of speed of depolarization conduction or rate dependent (dynamic) effects. Conduction velocity reduces with high excitation rate [15] i.e. velocity in atrial myocardium decreased around 2-fold at the shortest interval [16].

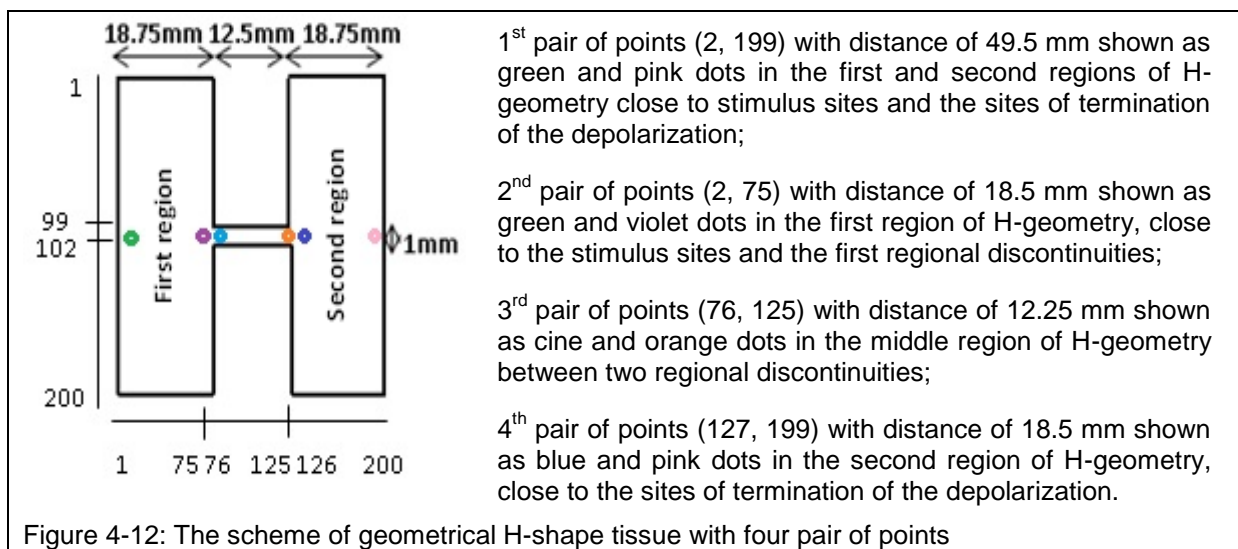
This part of the Chapter focuses on the speed of depolarization conduction for premature S2 beats from long to short S1S2 intervals in 2D tissues with slim and H-shape tissues. The speed of depolarization conduction between two cells (A and B) in tissue is given by:

$$\text{speed of depolarization conduction} = \frac{\text{distance between points A and B (mm)}}{\text{activation time at point B (ms)} - \text{activation time at point A (ms)}}$$

To study how the speed of depolarization conduction for premature S2 beat speeds up, speed of depolarization conduction was plotted against the average diastolic interval at points A and B. In this thesis, conduction velocity is called speed of depolarization conduction to highlight the difference between speed as a scalar quantity (that does not represent direction) and velocity as a vector quantity.

For slim tissues with 4×200 grid points, the membrane potential was created for all cells in tissue and then was extracted from middle of tissue from row 3 and columns from 1 to 200. In this region of tissue, one pair of points (1, 200) was selected close to the stimulus sites and sites of termination of depolarization. The distance between these points was 50 mm that was the product of space step 0.025 cm and the number of grid points, 200.

For H-shape tissues with 200×200 grid points, the membrane potential was extracted from the middle of tissue from row 100 and columns from 1 to 200. In this region, six points were selected as shown in Figure 4-12.



Section 4.2.5 showed that spatial and restitution profiles of repolarization time and APD as well as restitution profiles of activation time became reversed between two regional discontinuities in tissues. To find out how the profiles of speed of depolarization conduction between two regional discontinuities change, two approaches were used that are described in following subsections.

4.4.1 Comparison among four regions of H-shape tissue

First approach compares the speed of depolarization conduction in four regions of H-shape endocardial, epicardial, and mid-myocardial tissues as shown in Figures 4-13 to 4-15.

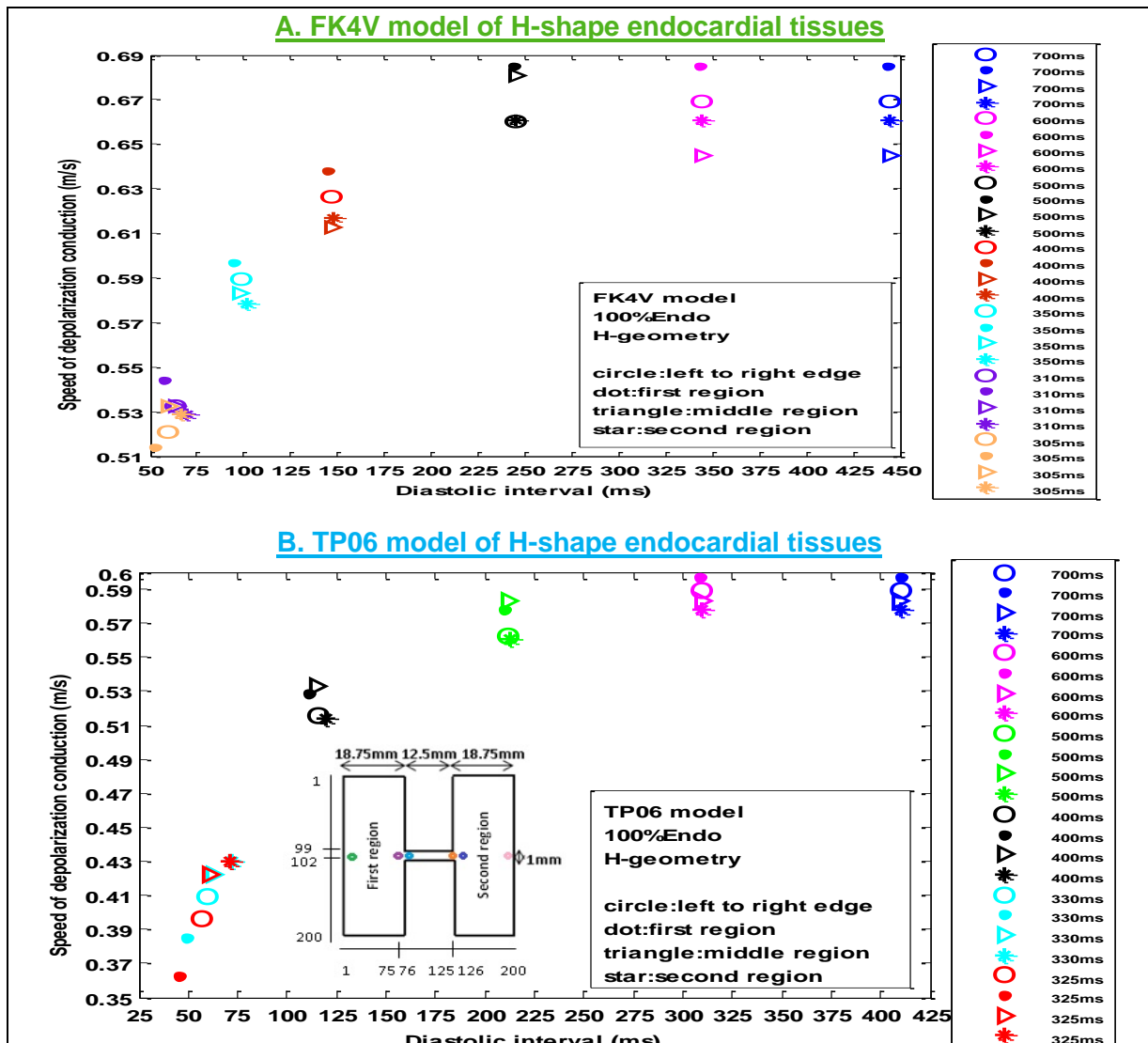
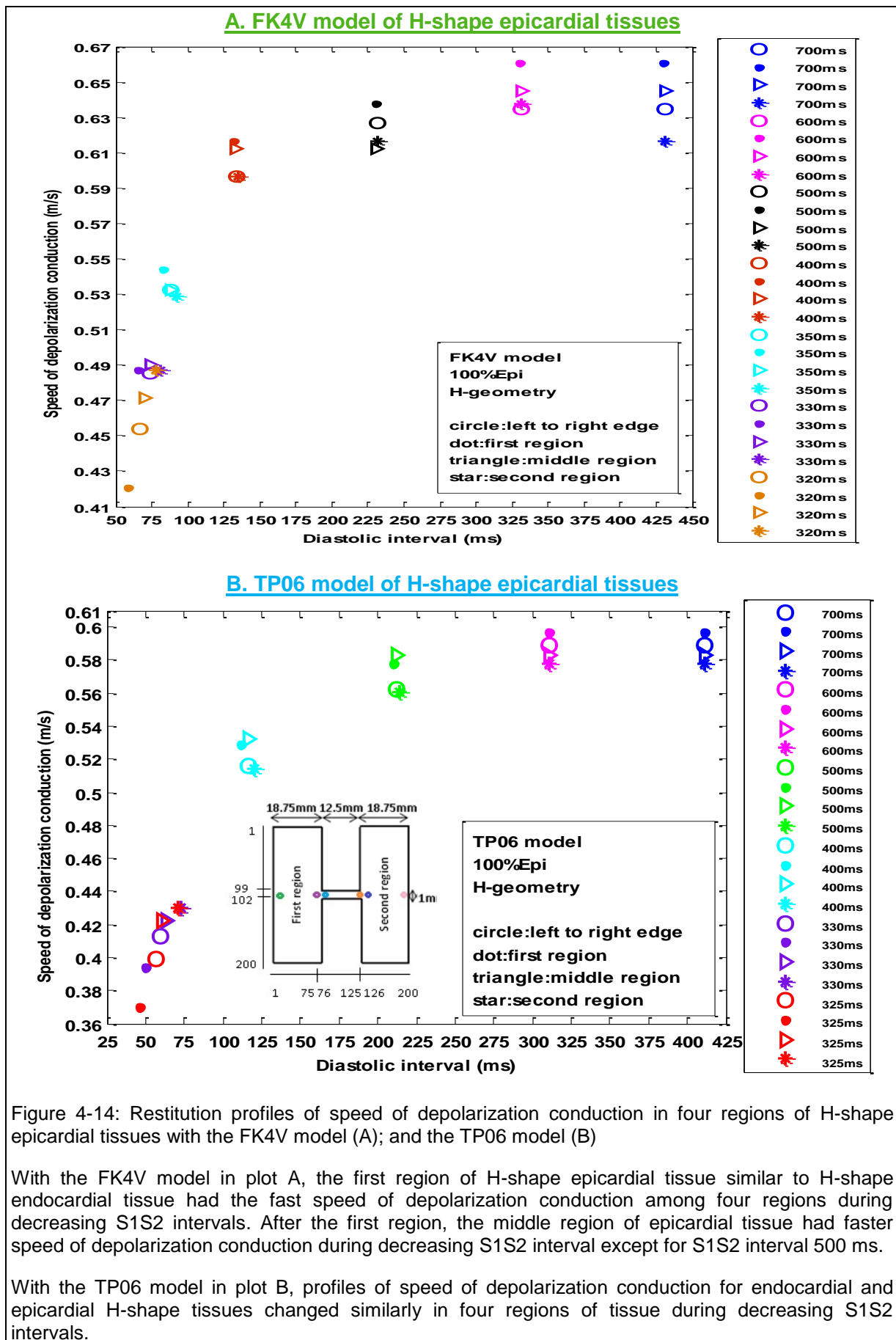
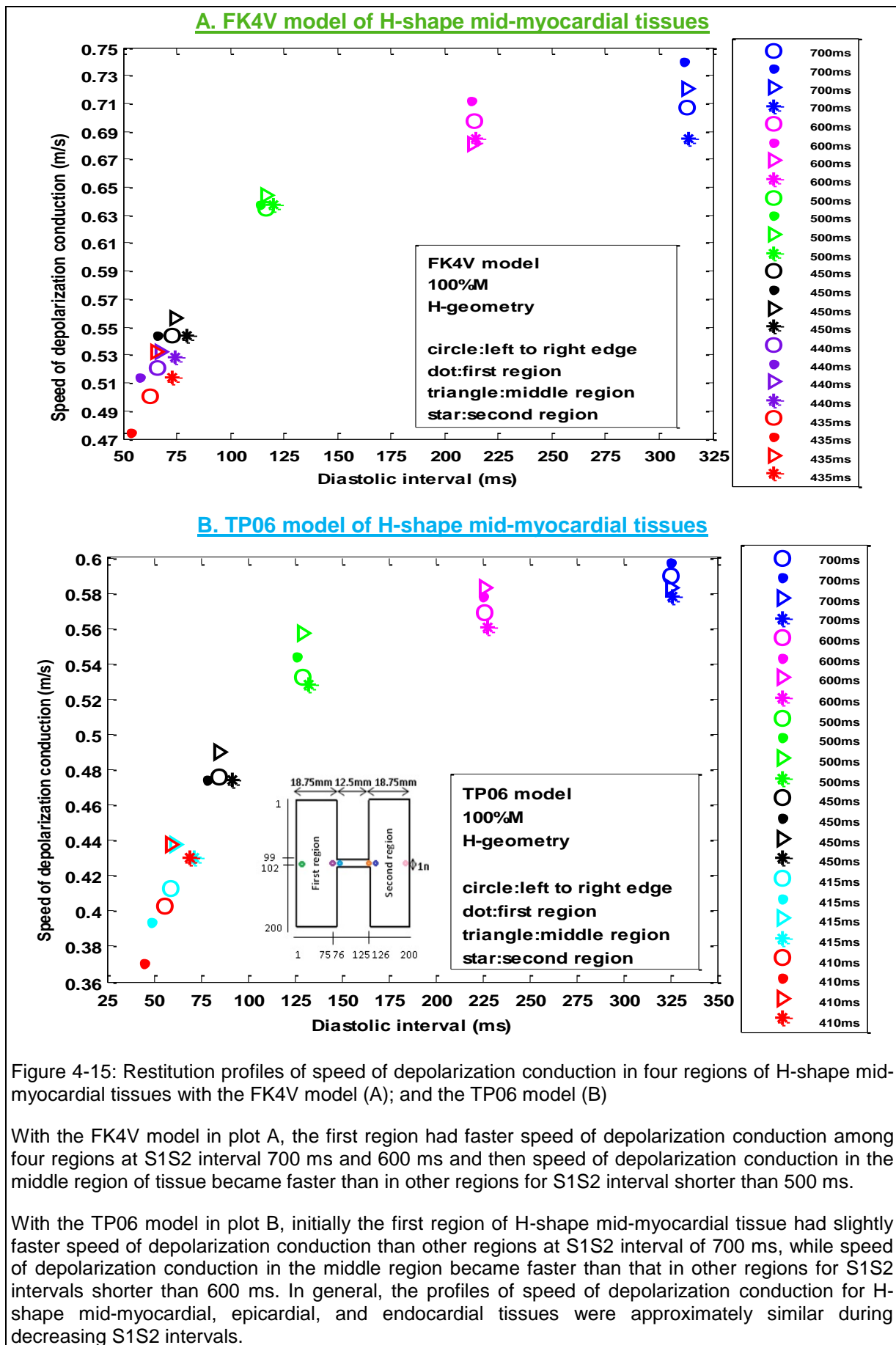


Figure 4-13: Restitution profiles of speed of depolarization conduction in four regions of H-shape endocardial tissues with the FK4V model (A); and the TP06 model (B)

With the FK4V model in plot A, the first region of H-shape endocardial tissue had the fast speed of depolarization conduction among four regions during decreasing S1S2 interval. Speed of depolarization conduction in the middle region of H-shape endocardial tissue was slower than other four regions for long S1S2 intervals of 700 ms and 600 ms shown as triangle.

With the TP06 model in plot B, initially the first region of H-shape endocardial tissue had slightly faster speed of depolarization conduction than other regions at S1S2 intervals of 700 ms and 600 ms while the speed of depolarization conduction in the middle region became faster than in other regions for S1S2 intervals shorter than 500 ms. Speed of depolarization conduction in the second region was slightly slower than other regions during decreasing S1S2 intervals.



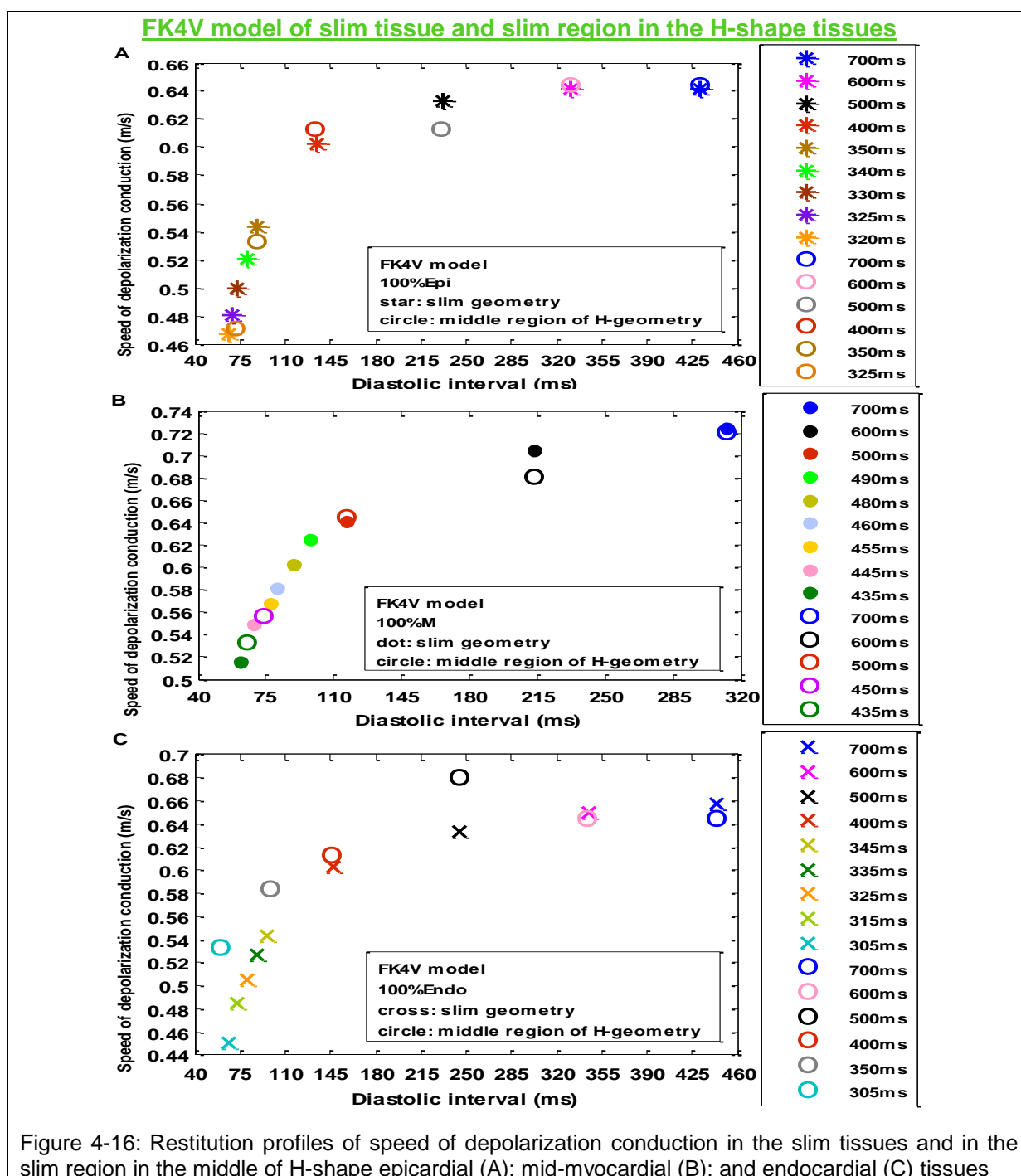


4.4.2 Comparison between slim tissue and slim region

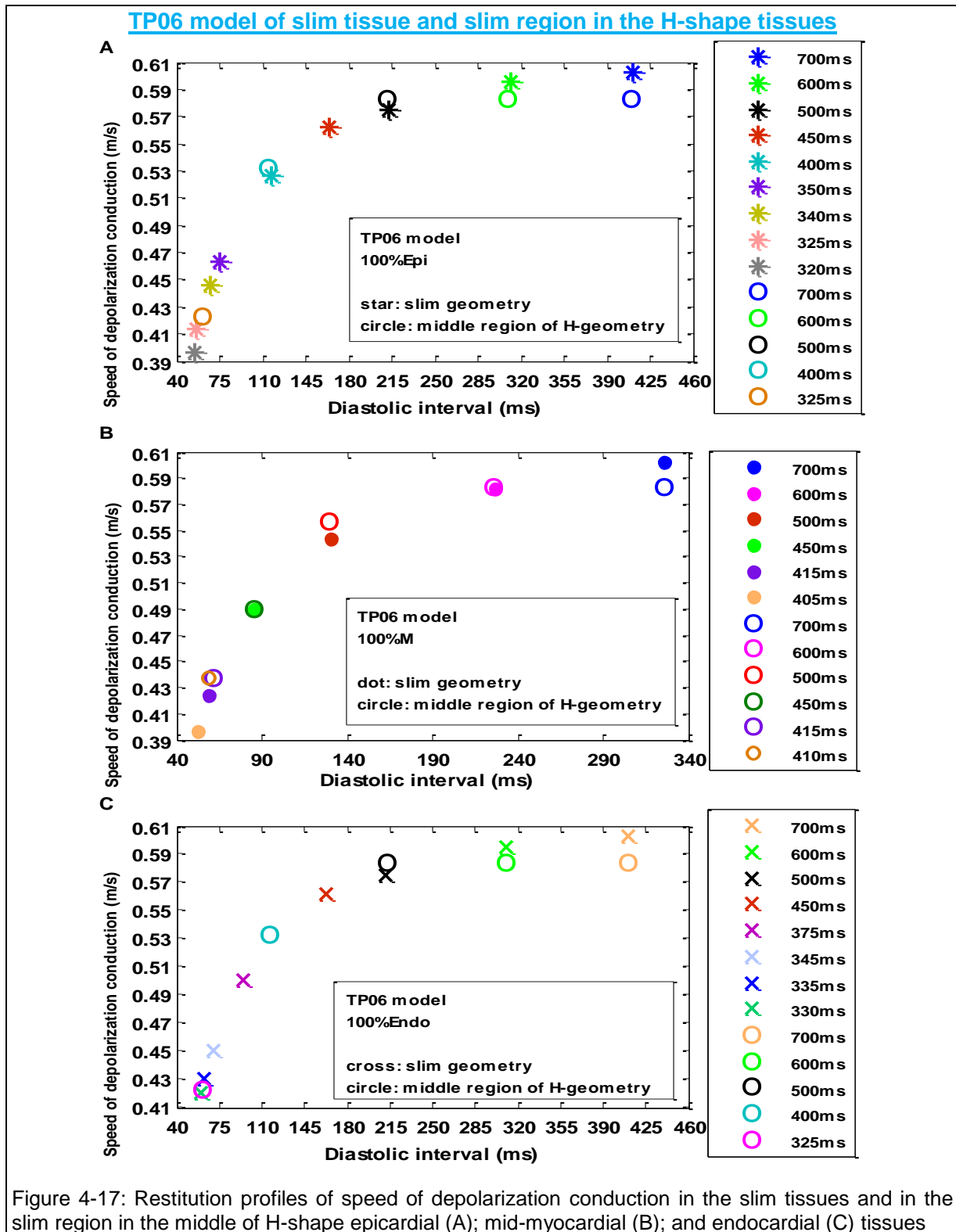
The second approach compares the speed of depolarization conduction in the middle region of H-shape tissues (slim region between points 76 and 125 with distance of 12.25 mm) and in the slim tissues (between points 1 and 200 with distance of 50 mm).

With the FK4V model, the speed of depolarization conduction in the middle region of all H-shape tissues was slightly slower than that in the slim tissues for S1S2 intervals of 700-600 ms as shown in Figure 4-16. However, for S1S2 intervals of 500-305 ms, the speed of depolarization conduction in the middle of H-shape endocardial tissue

- but changed similarly for epicardial and mid-myocardial tissues in plots A and B;
- became faster than that of slim endocardial tissue in plot C.



The same was true for the TP06 model as shown in Figure 4-17.

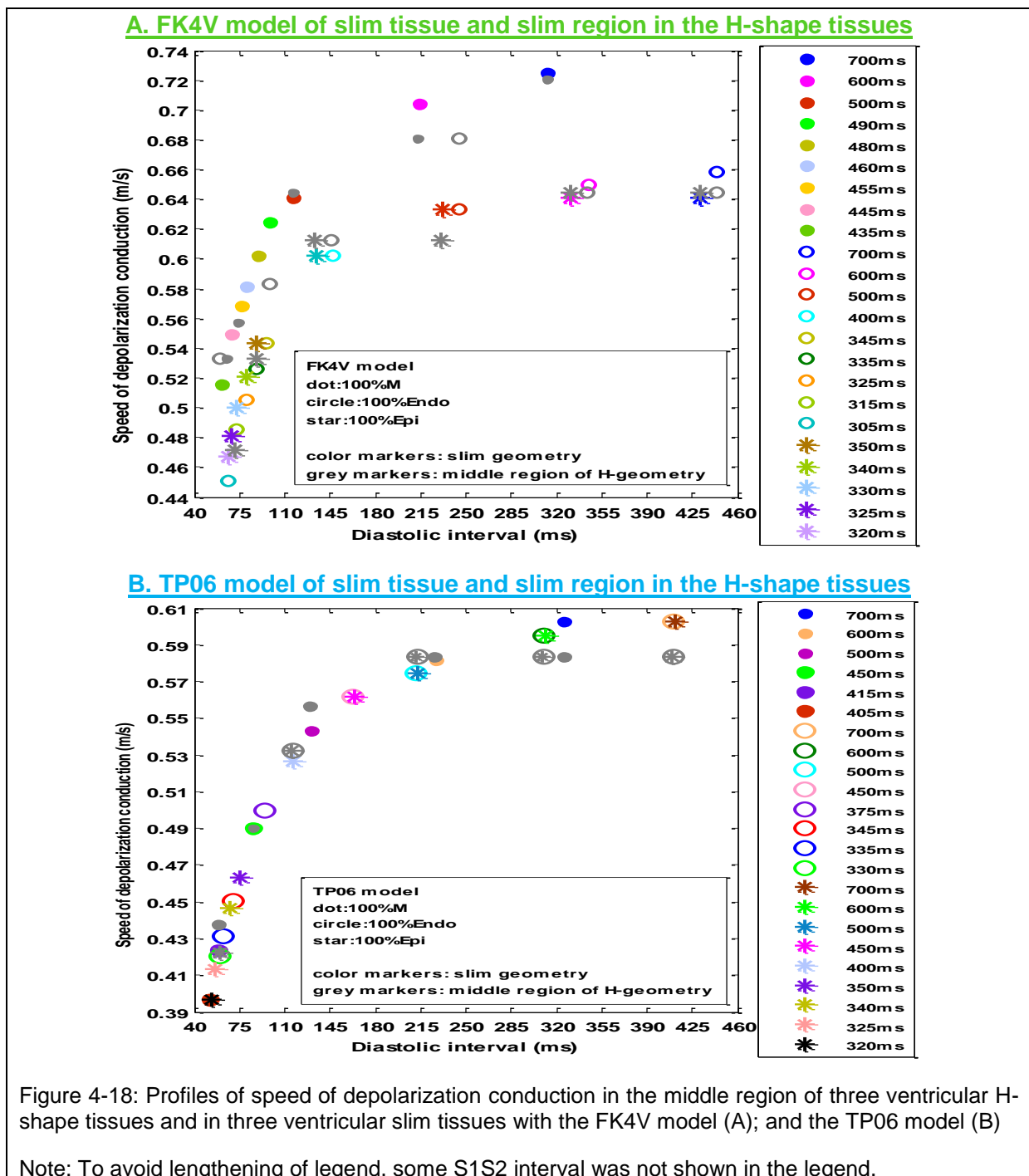


4.4.3 Summary figures and link with simulation studies

Summary Figure 4-18 shows profiles of speed of depolarization conduction in middle of H-shape three tissues and in three slim tissues in the same graph with the FK4V and the TP06 models.

In comparison, restitution profiles of speed of depolarization conduction for premature S2 beats in 2D simulated tissues with the FK4V and TP06 models were similar to the original models [2, 3] and the numerical values changed in the physiological range i.e. 0.7 m/s to 0.4 m/s during decreasing S1S2 intervals. With the FK4V model, both slim and H-shape mid-myocardial tissues had faster speed of depolarization conduction than other tissues. Speed of depolarization conduction in the slim endocardial tissue was slightly faster than slim epicardial tissue during long S1S2 intervals 700-600 ms and was fairly similar during S1S2 interval shorter than 500 ms.

With the TP06 model, the speed of depolarization conduction in three ventricular tissues with both slim and H-geometry changed similarly during decreasing S1S2 intervals. Moreover, the regional discontinuities reduced slightly the speed of depolarization conduction in the middle of H-shape tissues compared to other regions and slim tissues with both models.



4.5 Summary of results

Two groups of isotropic tissues with and without structural discontinuities were introduced in the absence of tissue heterogeneity and fibre-sheet structure. Both FK4V and TP06 models showed quantitatively similar behaviours i.e. two regional discontinuities in tissues, (1) changed the shape of spatial and restitution profiles of activation time, repolarization time, and APD; (2) increased the largest and the smallest value of three measures of dispersion around 1 to 7 ms compared to slim tissues without structural discontinuities; and (3) slowed the speed of depolarization conduction slightly in the middle region of H-shape tissues compared to slim tissues. The results suggest that the region between two structural discontinuities may increase tissue vulnerability to wave break and re-entry.

The role of structural discontinuities in 3D tissues with fibre structure are discussed next.

4.6 References

1. Kogan BY and Karplusa WJ and Billetta BS and Stevensonb WG, Excitation wave propagation within narrow pathways: Geometric configurations facilitating unidirectional block and reentry. *Physica D*, 1992. **59**.
2. Bueno-Orovio A and Cherry EM and Fenton FH, Minimal model for human ventricular action potentials in tissue. *Journal of Theoretical Biology*, 2008. **235**: p. 544-560.
3. ten Tusscher KH and Panfilov AV, Alternans and spiral breakup in a human ventricular tissue model. *Am J Physiol Heart Circ Physiol*, 2006. **291**: p. H1088–H1100.
4. Smith JH and Green CR and Peters NS and Rothery S and Severs NJ, Altered patterns of gap junction distribution in ischemic heart disease. An immunohistochemical study of human myocardium using laser scanning confocal microscopy. *Am J Pathol.*, 1991. **139**.
5. de Bakker JM and Capelle FJ van and Janse MJ and Tasseron S and Vermeulen JT and De Jonge N and Lahpor JR, Slow conduction in the infarcted human heart. 'Zigzag' course of activation. *Circulation*, 1993. **88**: p. 567-573.
6. Yan GX and Shimizu W and Antzelevitch C, Characteristics and distribution of M-cells in arterially perfused canine left ventricular wedge preparations. *Circulation*, 1998. **98**: p. 1921-1927.
7. Poelzing S and Akar FG and Baron E and Rosenbaum DS., Heterogeneous connexin43 expression produces electrophysiological heterogeneities across ventricular wall. *Am J Physiol Heart Circ Physiol*, 2004. **286**: p. H2001-H2009.
8. Glukhov AV and Fedorov VV and Qing L and Ravikumar VK and Kalish PW and Schuessler RB and Moazami N and Efimov IR, Transmural dispersion of repolarization in failing and nonfailing human ventricle. *Circ Res*, 2010. **106**: p. 981-991.
9. Chauhan VS and Downar E and Nanthakumar k and Parker JD and Ross HJ and Chan W and Picton P., Increased ventricular repolarization heterogeneity in patients with ventricular arrhythmia vulnerability and cardiomyopathy: a human in vivo study. *Am J Physiol Heart Circ Physiol*, 2006. **290**: p. H79-H86.
10. Hanson B and Sutton P and Elameri N and Gray M and Critchley H and Gill JS and Taggart P., Interaction of Activation–Repolarization Coupling and Restitution Properties in Humans. *Circulation: Arrhythmia and Electrophysiology*, 2009. **2**: p. 162-170.
11. Ramdat Misier AR and Opthof T and Van Hemel NM and Vermeulen JT and de Bakker JMT and Defauw JJAM and Van Capelle FJL and Janse MJ., Dispersion of refractoriness in noninfarcted myocardium of patients with ventricular tachycardia or ventricular fibrillation after myocardial infarction. *Circulation*, 1995. **91**: p. 2566–2572.
12. Cherry EM and Fenton F, Effects of boundaries and geometry on the spatial distribution of action potential duration in cardiac tissue. *J of Theoretical Biology*, 2011. **285**: p. 164-176.
13. Cain JW and Schaeffer DG, Shortening of cardiac action potential duration near an insulating boundary. *Mathematical Medicine and Biology*, 2008. **25**: p. 21-36.
14. Siso-Nadal F and Otani NF and Gilmour RF and Fox JJ, Boundary-induced reentry in homogeneous excitable tissue. *Phys Rev E.*, 2008. **78**: p. 031925-031955.
15. Fast VG and Kléber AG, Role of wavefront curvature in propagation of cardiac impulse. *Cardiovascular Research*, 1997. **33**: p. 258-271.
16. Smeets JL and Alessie MA and Lammers WJ and Bonke FI and Hollen J., The wavelength of the cardiac impulse and reentrant arrhythmias in isolated rabbit atrium. The role of heart rate, autonomic transmitters, temperature, and potassium. *Circ Res.*, 1986. **58**: p. 96-108.

Chapter 5

Simulation results in 3D tissues

5.1 Introduction

Dispersion of repolarization plays an important role in initiation of ventricular re-entrant arrhythmias in animal [1-3] and human [4]. In the presence of pathologies that slow repolarization, mid-myocardial cells with longer APD than epicardial and endocardial cells may provide a substrate for arrhythmias [5] that leads to the development of unidirectional block and re-entry because of the large APD dispersion [6]. For example, in real ventricular tissue, fibrosis after myocardial infarction may lead to cardiac conduction disturbances by forming isolating barriers and discontinuities [7-10]. To address this issue, three groups of 3D cubes of tissue were simulated with (1) isotropic diffusion; (2) anisotropic diffusion; and (3) anisotropic diffusion with fibrosis. All cubes (40 rows, 40 columns, and 60 layers) had dimensions of $0.8 \times 0.8 \times 1.2 \text{ cm}^3$, which is human left ventricular wall thickness [11].

To highlight the involvement of mid-myocardial cells in AP propagation, seven 3D cubes of tissue models were used to represent the homogenous and heterogeneous tissues within human left ventricular wall. Three homogenous geometrical tissue models were composed of 100% epicardial, 100% endocardial, and 100% mid-myocardial cells as shown in Figure 5-1, schemes 1 to 3. Four heterogeneous geometrical tissue models were:

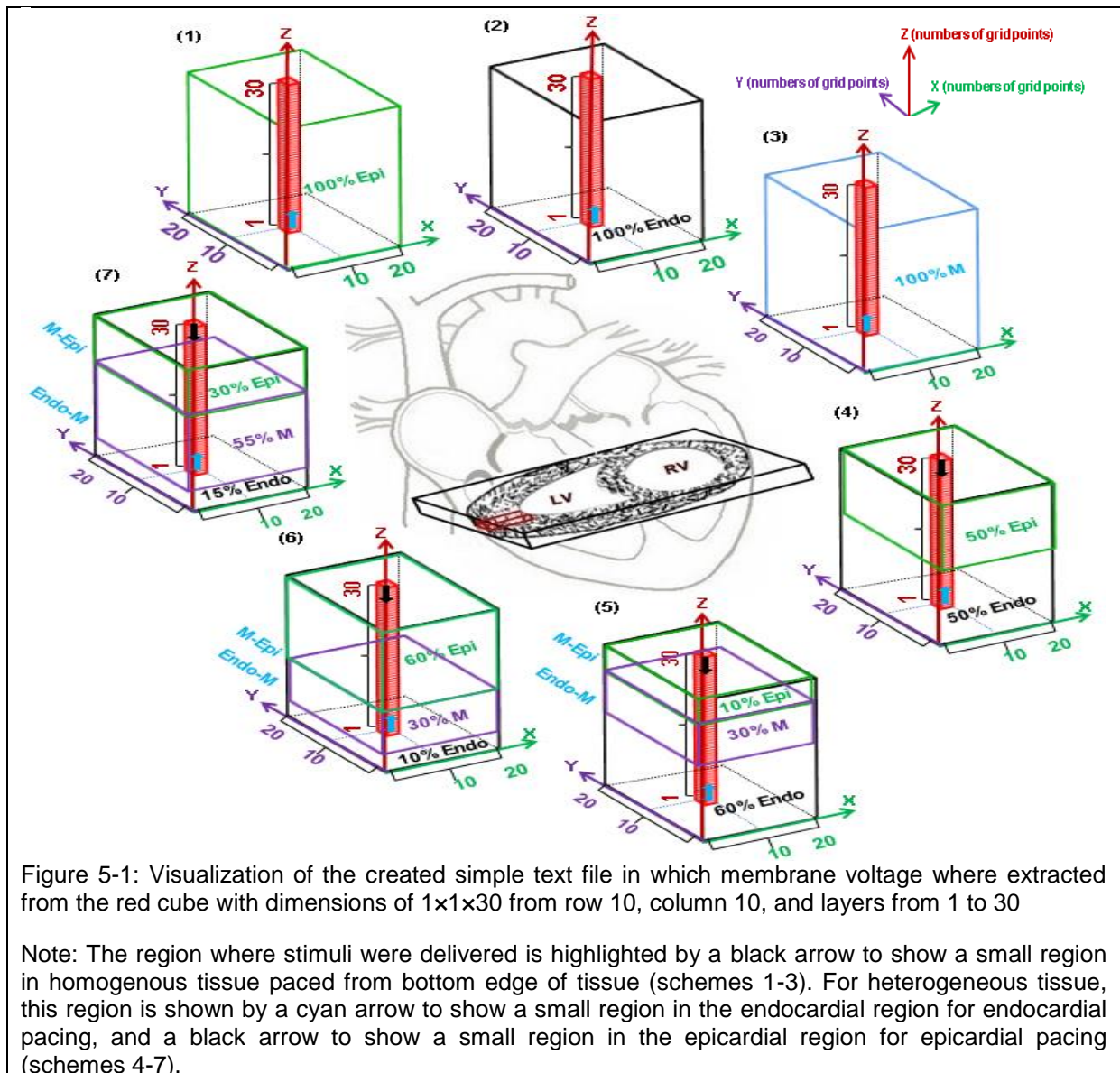
- 50%endo-50%epi (Figure 5-1, scheme 4): this tissue model was composed of equal cellular populations of epicardial and endocardial cells with no mid-myocardial cells;
- 60%endo-30%M-10%epi and 10%endo-30%M-60%epi (Figure 5-1, schemes 5 and 6): these two tissue models were composed of a fixed amount of mid-myocardial cells (30%) based on human experimental study [12] while the amount of epicardial and endocardial cells were 10% and 60% and the reverse close to a human model [13];
- 15%endo-55%M-30%epi (Figure 5-1, scheme 7): this tissue model was composed of greater amount of mid-myocardial cells than other cell types close to human studies [14-16].

There is evidence that reversing the direction of activation in electrically heterogeneous ventricular myocardium increases measures of dispersion in transmural repolarization in some patients [17, 18], but decreases it in others [19]. To study this phenomenon, two groups of heterogeneous tissues were simulated including (1) tissue models with endocardial pacing in which tissues were paced from a small region in the endocardium; and (2) tissue models with epicardial pacing in which tissues were paced from a small region in the epicardium as shown in Figure 5-1, schemes 4 to 7. For three homogenous tissue models, stimuli were delivered to a small region in the bottom edge of epicardial, endocardial and mid-myocardial tissue models as shown in Figure 5-1, schemes 1 to 3. The detailed description of the region was illustrated in Chapter 3, section 3.7.1-4.

For 3D simulations, the previous software was modified to simulate two groups of ventricular tissues with a monodomain model in which epicardial, mid-myocardial, and

endocardial cells were described using (1) a simple FK4V model [20] and; (2) a biophysically detailed TP06 cell model [21]. These two models created transmembrane voltage for every other point in 3D cubes of tissue with $40 \times 40 \times 60$ grid points to avoid creation of huge number of output files. Therefore, each output file had $20 \times 20 \times 30$ transmembrane voltage in which layers 1 and 30 with $20 \times 20 \times 1$ transmembrane voltage were boundary layers and contained 0s while the layers from 2 and 29 contained the created numerical values of the transmembrane voltage within 3D cubes of tissue.

Next, 30 transmembrane voltage were extracted from central region of 3D cubes of tissue. In order to show clearly the regions where transmembrane voltages were extracted from the created output files, a figure was used in which the simple text file was imaged as a 3D cube containing transmembrane voltage with dimensions of $20 \times 20 \times 30$ in which X corresponds to the number of rows in the simple text file, Y corresponds to the number of columns in the simple text file, and Z corresponds to the number of layers in the simple text file. This approach provided a clear visualization of the regions that were selected for comparing the spatial APD profiles in section 5-2-1. Visualization of the simple text file is shown in Figure 5-1 in which transmembrane voltage where extracted from row 10, column 10, and layers from 1 to 30 highlighted as red.



For both normal S1 and premature S2 beats, 28 transmembrane voltages were extracted above AP threshold voltage of -65 mV for the TP06 model and normalized AP threshold of 0.1 for the FK4V model. These thresholds correspond to 90% repolarization, which is used to characterize APD in experimental data i.e. [12, 22]. Indices of AP upstroke correspond to activation time and indices of AP downstroke correspond to repolarization time. For clarity, Figure 5-2 show profiles of 28 normal S1 and premature S2 beats at S1S2 interval of 700 ms (A); schemes of 28 extracted voltages above the threshold voltage of -65 mV from AP upstroke (B); AP downstroke (C) for premature beats in the TP06 model of epicardial tissue.

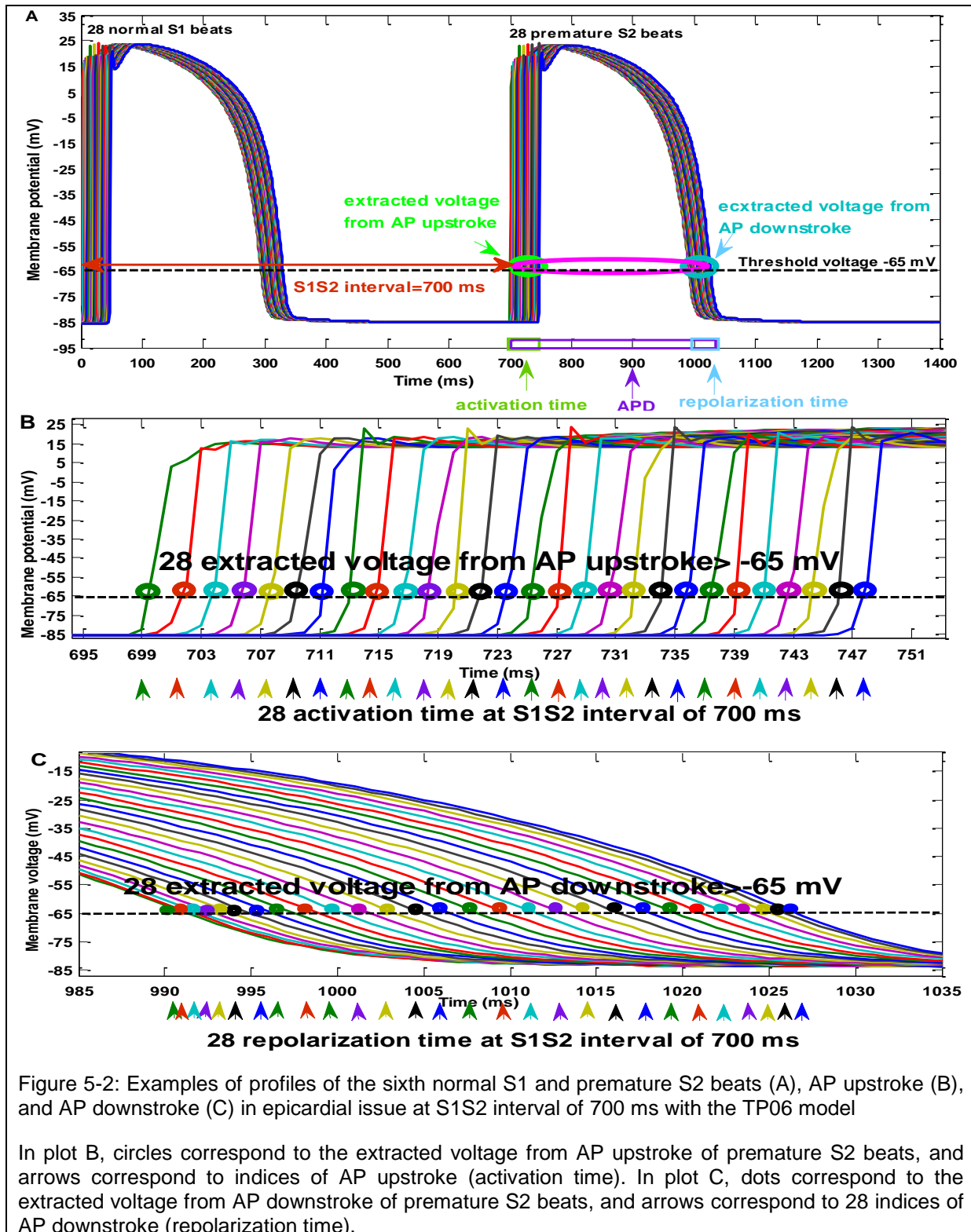


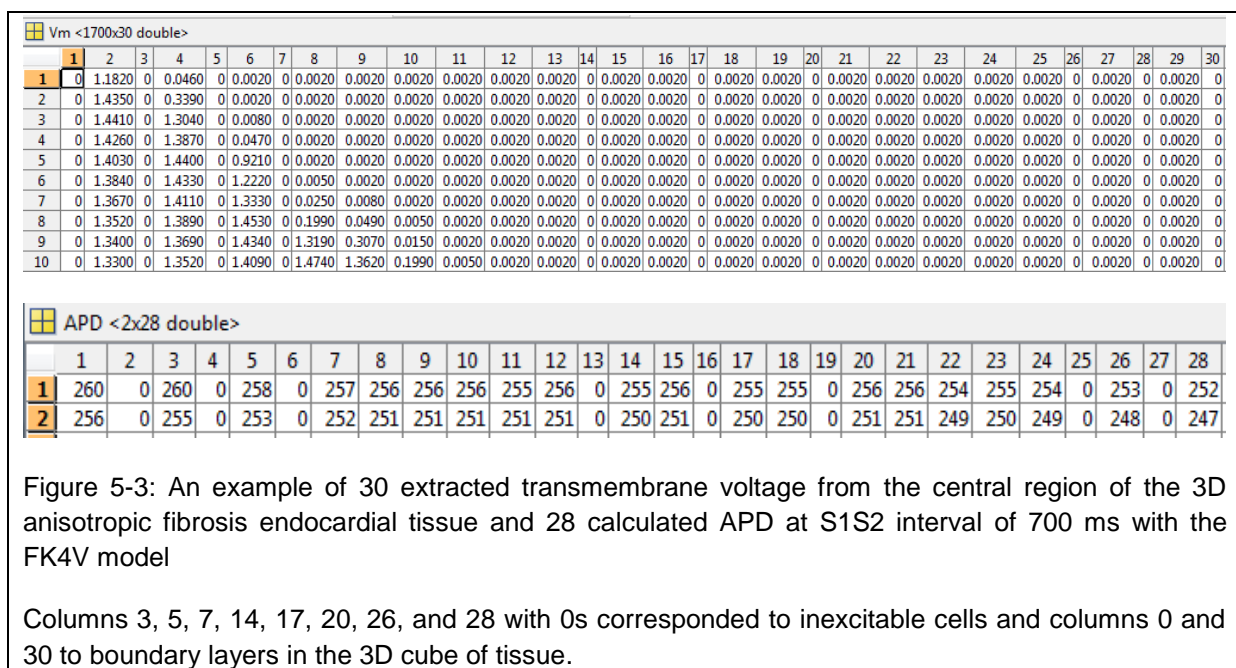
Figure 5-2: Examples of profiles of the sixth normal S1 and premature S2 beats (A), AP upstroke (B), and AP downstroke (C) in epicardial issue at S1S2 interval of 700 ms with the TP06 model

In plot B, circles correspond to the extracted voltage from AP upstroke of premature S2 beats, and arrows correspond to indices of AP upstroke (activation time). In plot C, dots correspond to the extracted voltage from AP downstroke of premature S2 beats, and arrows correspond to 28 indices of AP downstroke (repolarization time).

To study the effects of diffusion of ionic currents along and across ventricular fibres on the interaction between activation-repolarization coupling and restitution properties, two groups of tissue were introduced with isotropic and anisotropic diffusions. For isotropic tissues, the diffusion coefficient was 0.001 cm²/ms along and across fibre direction. For both anisotropic tissues and anisotropic fibrosis tissues, the diffusion coefficient was 0.001 cm²/ms along ventricular fibre and 0.00025 cm²/ms across ventricular fibre.

Furthermore, to study the combined effects of anisotropy and simulated fibrosis on interaction between activation-repolarization coupling and restitution properties, the other group of anisotropic tissues were simulated with fibrosis. The 3D geometrical tissue models were modified to simulate fibrosis by randomly allocating grid points to be either excitable or in-excitable. The proportion of excitable and in-excitable cells was 56% and 44%. These percentages were the largest amount of fibrosis that could produce an AP propagation using both FK4V and TP06 models.

Figure 5-3 shows an example of extracted transmembrane voltage from the central region of 3D anisotropic fibrosis endocardial tissue at S1S2 interval 700 ms. In this example, columns 3, 5, 7, 14, 17, 20, 26, and 28 correspond to inexcitable cells. Consequently, the calculated APD was zero in these cells and in boundaries (columns 1 and 30) as shown in the second plot in Figure 5-3. In total, 2x28 APD was created in the central region of the 3D cube of tissue for a normal S1 beat (row 1) and a premature S2 beat (row 2). The same was true for other calculations.



Fibre organization is another aspect of heterogeneity in tissue. The fibre structure within the human left ventricle is well characterized [23], but is variable and plays a major role in electromechanical function of the heart. In diseased hearts, fibre organization may change as a result of remodelling. This Chapter is organized in two parts to provide 3D simulation results based on two assumptions about fibre organization. Part I assumes that fibre rotated linearly and counter-clockwise from +60° in endocardium to -60° in epicardium. Part II assumes a non-linear change in fibre orientation in all heterogeneous tissues.

Part I presented 28 calculated activation time, repolarization time, and APD for normal S1 beats and premature S2 beats at each S1S2 interval to study the rate dependent effects in

(1) profiles of these data against transmural distance (spatial profiles) and against diastolic interval prior to premature beats (restitution profiles) in section 5.2; and (2) three measures of dispersion in activation time, repolarization time, and APD in section 5.3. Next, the effects of combination of anisotropy and fibrosis on the speed of depolarization conduction in regions of different cell type in heterogeneous tissues are highlighted in section 5.4. At the end of each section, the results are evaluated by comparing with experimental and simulation studies. The last section discusses how the changes in AP shape and duration, speed of depolarization conduction, and measures of dispersion in repolarization may increase tissue vulnerability to ventricular arrhythmia. The last section of Part II visualizes AP propagation at the last S1S2 interval for normal and premature beats to highlight the wave break that may occur during AP depolarization and repolarization in all simulated tissues. The figures that were plotted during decreasing S1S2 intervals with both models are organized in Groups (except for Group J and Group X for one S1S2 interval) as follows:

- Group J (Figures J1-J22): Spatial APD profiles in the five selected regions of 3D cubes of anisotropic tissue at one S1S2 interval;
- Group R (Figures R1-R20): Restitution profiles of speed of depolarization conduction and restitution profiles of activation time for heterogeneous tissues using the TP06 model;
- Group S (Figures S1-S33): Spatial profiles of repolarization time for isotropic and anisotropic tissues and profiles of dispersion of repolarization time against S1S2 interval for anisotropic tissues with and without fibrosis;
- Group T (Figures T1-T8): Restitution profiles of (1) repolarization time; and (2) activation time in anisotropic heterogeneous tissues with both models;
- Group X (Figures X1-X8): Examples of profiles of AP propagation during AP depolarization and repolarization at the last S1S2 interval for mid-myocardial tissue and tissues composed of 50%Endo-50%Epi and 10%Endo-30%M-60%Epi.
- Group V (Figures V1 to V18): Spatial profiles of APD and repolarization time in the FK4V models of isotropic, anisotropic, and anisotropic fibrosis heterogeneous tissues simulated with fibre structure (setting of $\theta=89^0$ and $B=1.7$ degree/mm) in Part II

The rest of figures are provided in the enclosed CD, Appendix 1.

- Group P (Figures P1-P43): Spatial profiles of (1) activation time; (2) repolarization time; (3) APD; and (4) profiles of APD against repolarization time in anisotropic tissues with and without fibrosis, with the TP06 model;
- Group Q (Figures Q1-Q38): Restitution profiles of speed of depolarization conduction and spatial profiles of activation time for tissues with isotropic and anisotropic diffusions using both models;
- Group R (Figures R21-R26): The rest of restitution profiles of speed of depolarization conduction for anisotropic heterogeneous tissues with and without fibrosis, with the FK4V model;
- Group U (Figures U1-U24): Profiles of (1) spatial APD for anisotropic heterogeneous tissues; and (2) APD dispersion against S1S2 interval in anisotropic heterogeneous tissues with and without fibrosis using both models.

The figures in Group X (Figures X8-X22) are provided in the CD, Appendix 2.

- Group X (Figures X8-X22): The rest of examples of profiles of AP propagation during AP depolarization and repolarization at the last S1S2 interval using both models for epicardial tissues, endocardial tissue, and tissues composed of 60%Endo-30%M-10%Epi, and 15%Endo-55%M-30%Epi cells.

All images of AP propagation for both normal S1 and premature S2 beats at the last S1S2 interval are provided in the enclosed CD (Appendix 3 for the FK4V model and Appendix 4 for the TP06 model).

Part I: Simulation results with linear fibre structure

This Part of the Chapter describes the simulation results for tissues with a geometrical fibre model created based on Equation 5-1 [24] in which the fibre angle rotation changes as a linear function of transmural distance (z) with total fibre rotation of 120° .

$$\theta(z) = 90^\circ + (\text{layer} - 1) \times \frac{120^\circ}{z} \quad \text{Equation (5-1)}$$

5.2 Spatiotemporal profiles of normal and premature beats

The global electrical restitution curve are heterogeneous in shape and distribution [25, 26]. Heterogeneity in AP shape and duration in the left ventricular wall may provide a substrate for arrhythmias.

The first part of this Chapter is organized in four subsections to assess normal and premature profiles of activation time, APD, and repolarization time in 3D simulations. The first subsection compares the spatial APD profiles for premature S2 beats in five regions within the 3D cube of tissue with anisotropic diffusion to specify the region in which spatial APD profiles change more than other regions with endocardial and epicardial pacing. The repolarization profiles of premature S2 beats change during decreasing S1S2 intervals are established next. The third subsection highlights the effects of tissue heterogeneity on spatial and restitution profiles of activation time, repolarization time, and APD for premature S2 beats in tissues with isotropic and anisotropic diffusions at one S1S2 interval and then over a broad range of S1S2 intervals. Then these profiles are compared for anisotropic tissues with and without fibrosis during decreasing S1S2 intervals. Finally, these profiles are compared with experimental and simulation studies.

5.2.1 Spatial APD profiles in the five regions of tissue

Since it was time consuming to plot data for the whole tissue, initially seven regions close to the edges and the central region of tissue were selected. Figure 5-4 shows examples of the selected transmembrane voltage from the visualization of the created simple text file in plot A.

To compare spatial APD profiles for premature S2 beats in the selected regions, these profiles were plotted in the same graph as shown in Figure 5-4, Plot B. These profiles show how APD for premature S2 beats changed in the 3D cube of anisotropic tissue composed of 60%Endo-30%M-10%Epi with endocardial pacing at S1S2 interval 400 ms using the FK4V model [20].

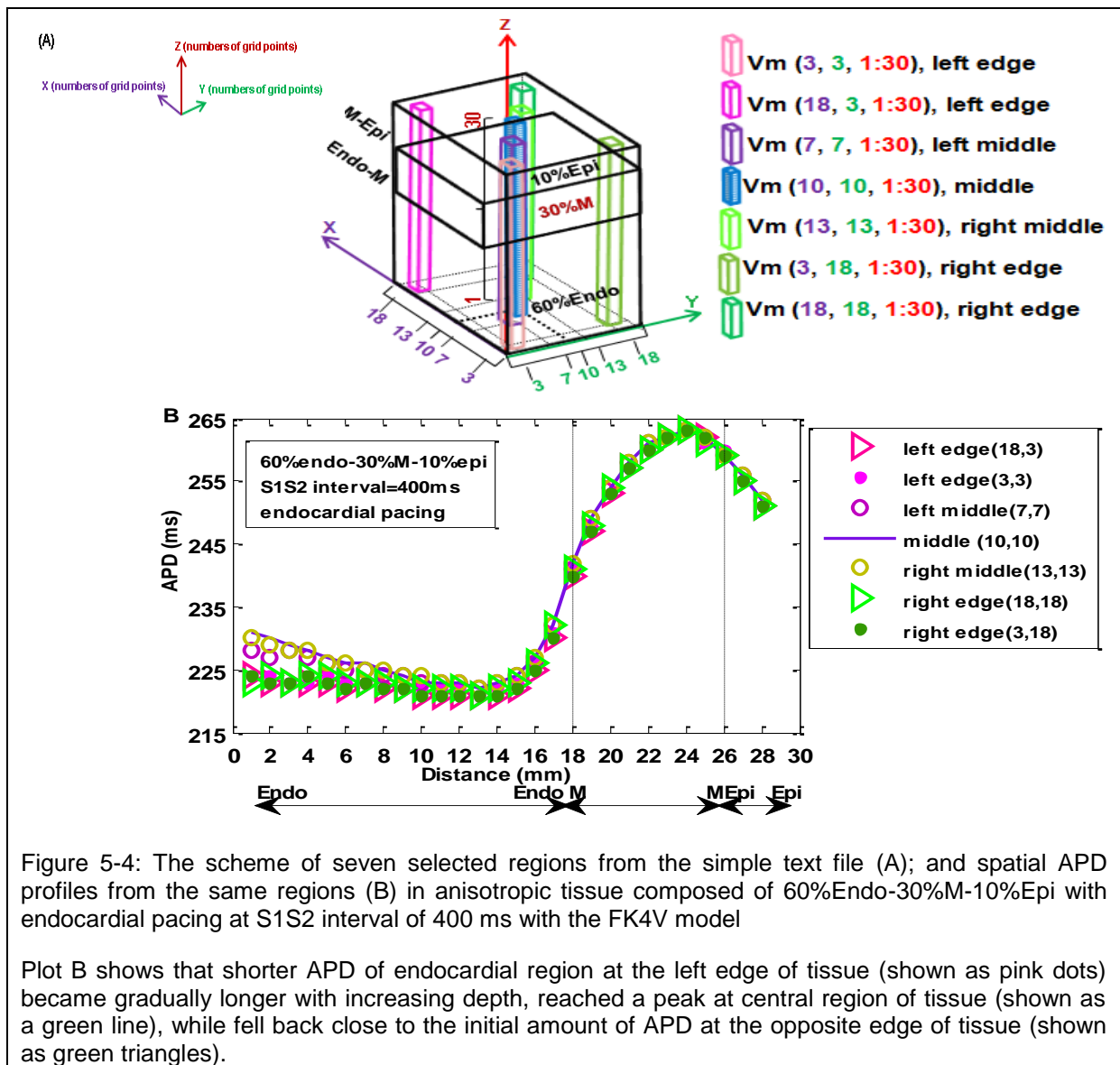


Figure 5-4: The scheme of seven selected regions from the simple text file (A); and spatial APD profiles from the same regions (B) in anisotropic tissue composed of 60%Endo-30%M-10%Epi with endocardial pacing at S1S2 interval of 400 ms with the FK4V model

Plot B shows that shorter APD of endocardial region at the left edge of tissue (shown as pink dots) became gradually longer with increasing depth, reached a peak at central region of tissue (shown as a green line), while fell back close to the initial amount of APD at the opposite edge of tissue (shown as green triangles).

Since there was no great difference among the spatial APD profiles for premature S2 beats in the regions close to the edges of tissue (shown as violet and green triangles and dots), the rest of this section focused on the five selected regions as shown in Figure 5-5.

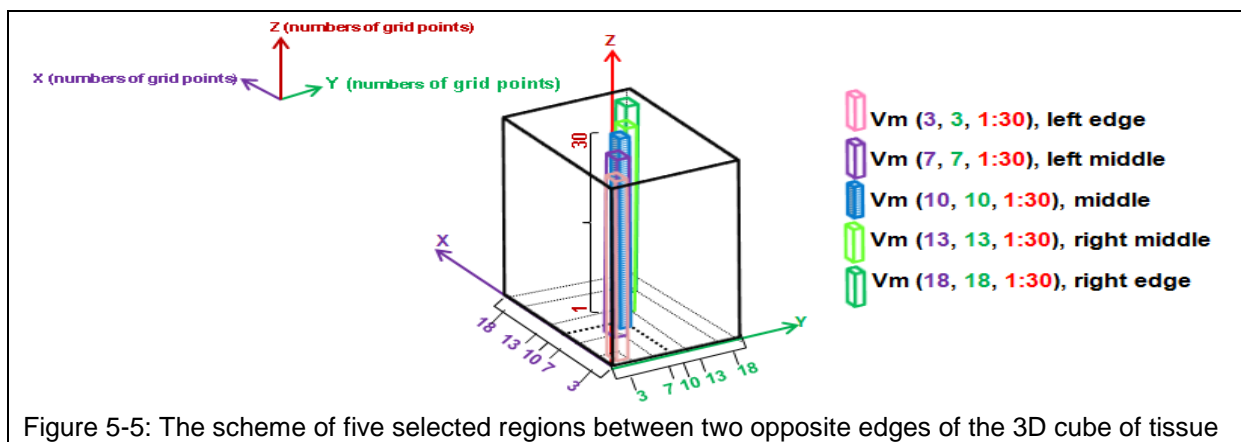
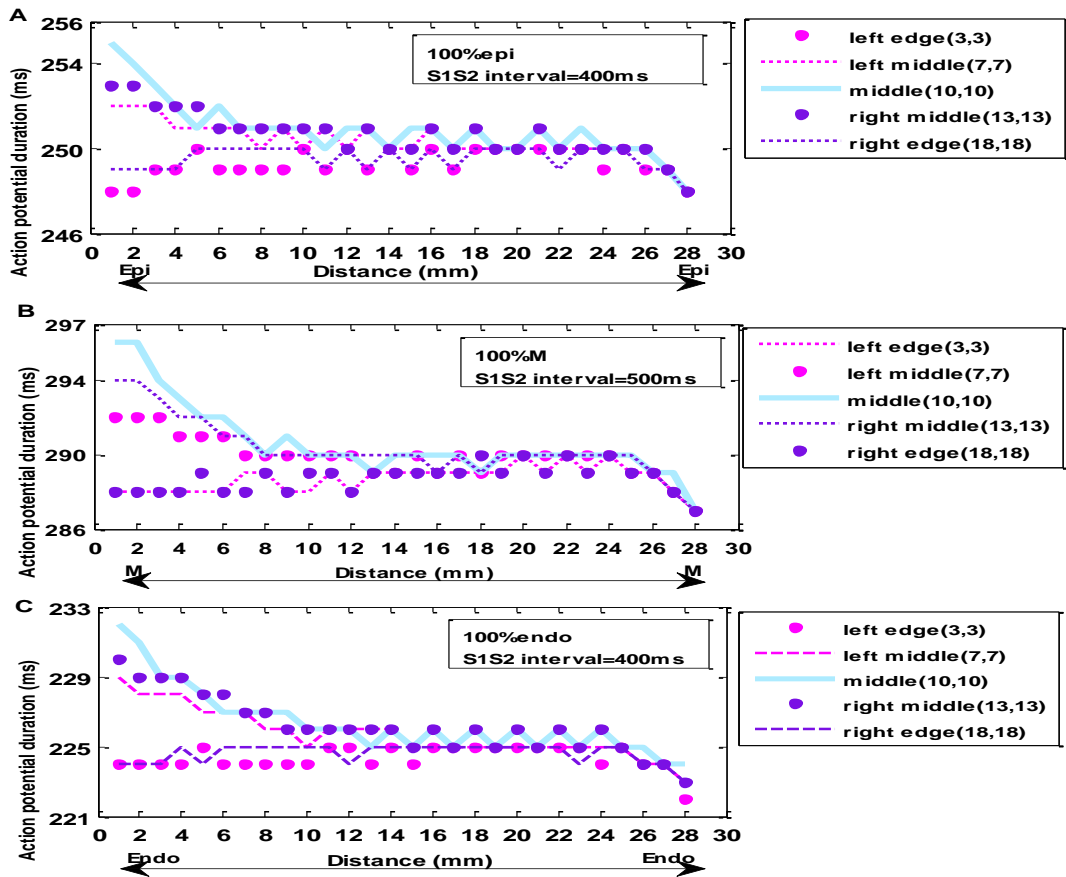


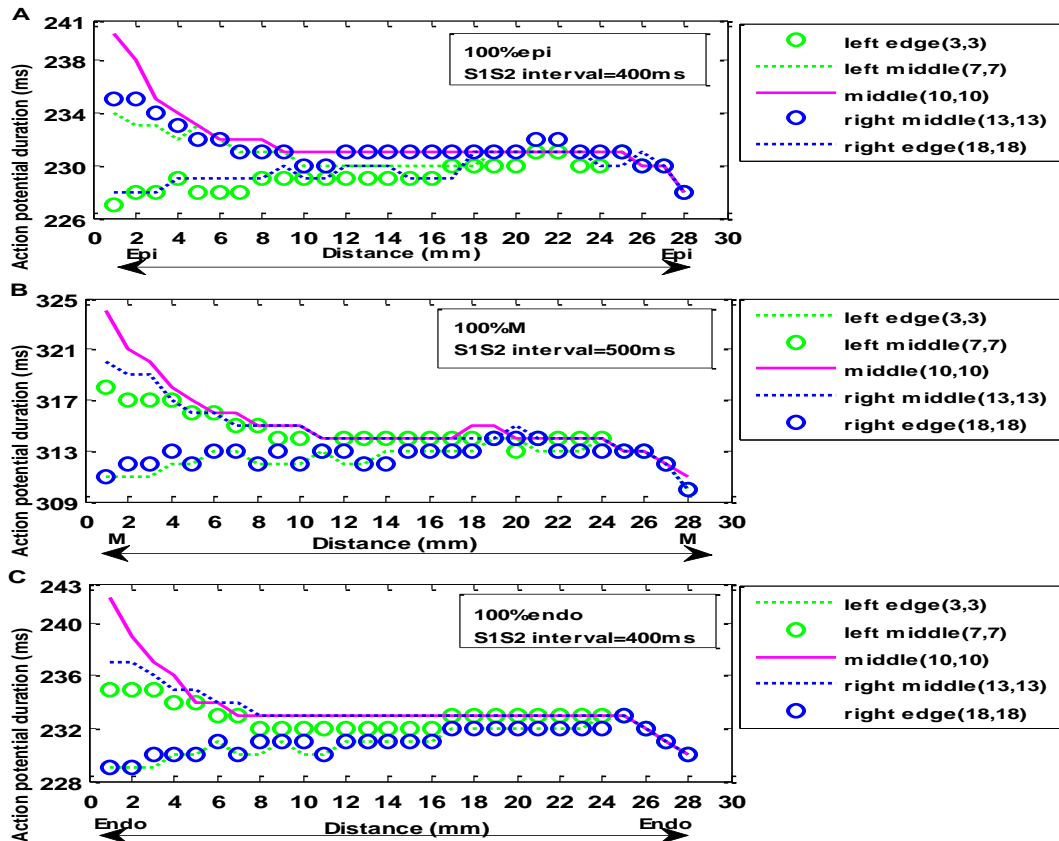
Figure 5-5: The scheme of five selected regions between two opposite edges of the 3D cube of tissue

Figures organized in Group J (Figures J1 to J22) show spatial APD profiles for premature S2 beats in the five selected regions of 3D cubes of tissue with anisotropic diffusion at one S1S2 interval using the FK4V [20] and the TP06 [21] models.

Group J: FK4V model of anisotropic homogenous tissues

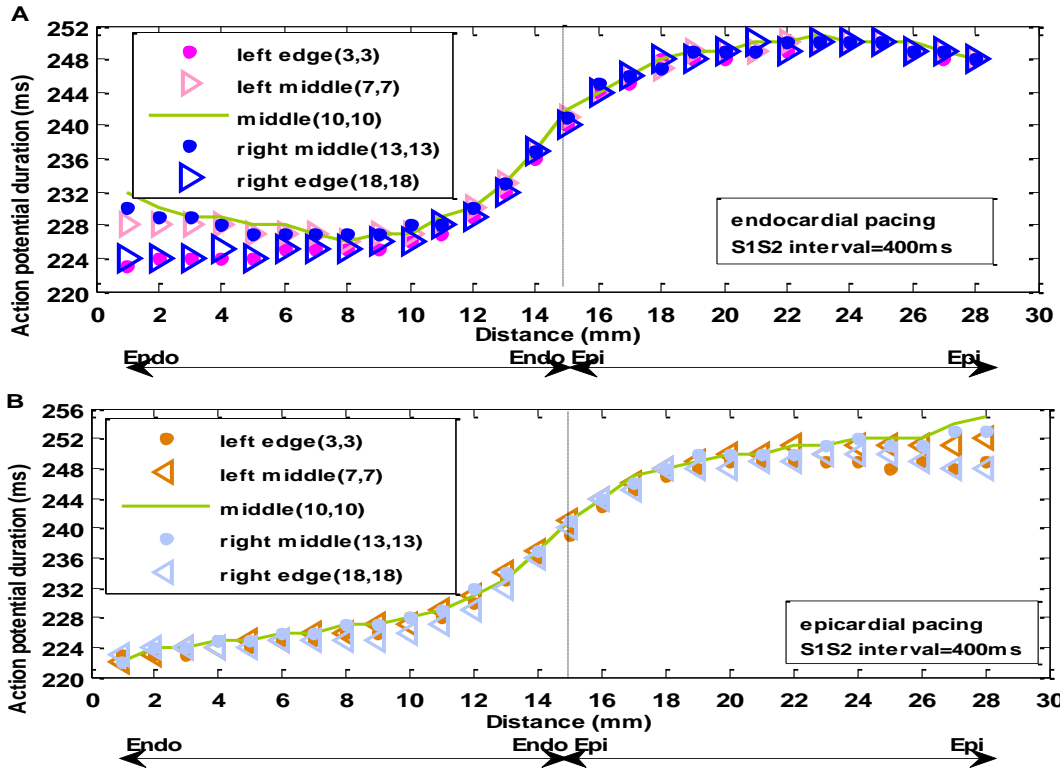


TP06 model

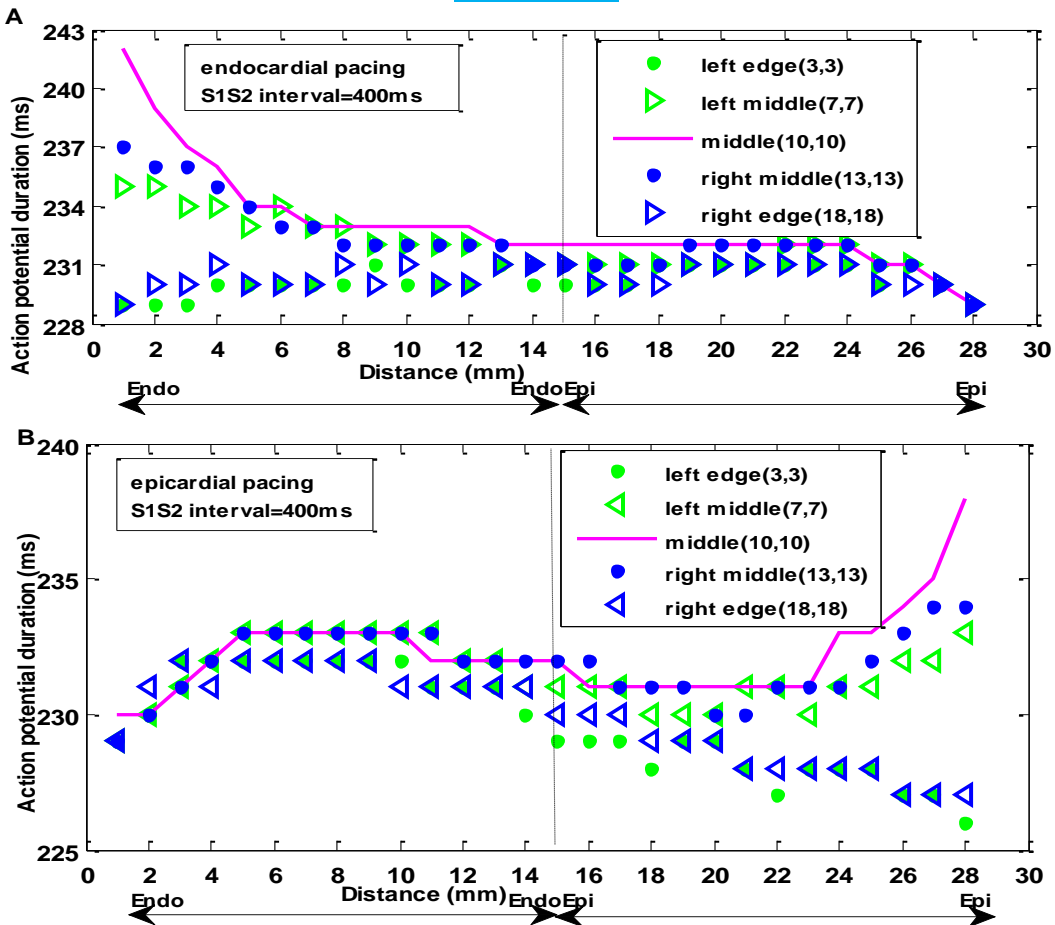


Figures J1-J6: Spatial APD profiles of homogenous epicardial (A); mid-myocardial (B); and endocardial (C) tissues paced from the bottom edge of tissue at S1S2 intervals of 400 ms and 500 ms

Group J: FK4V model of anisotropic heterogenous tissues with 50%Endo-50%Epi

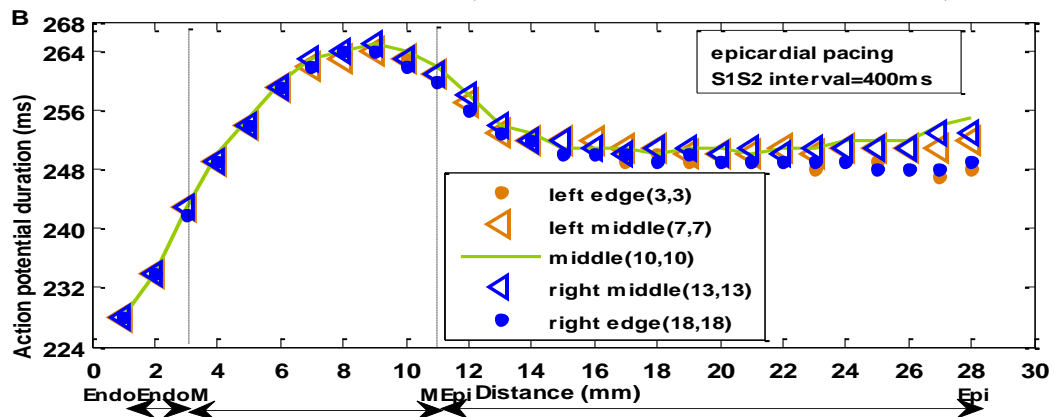
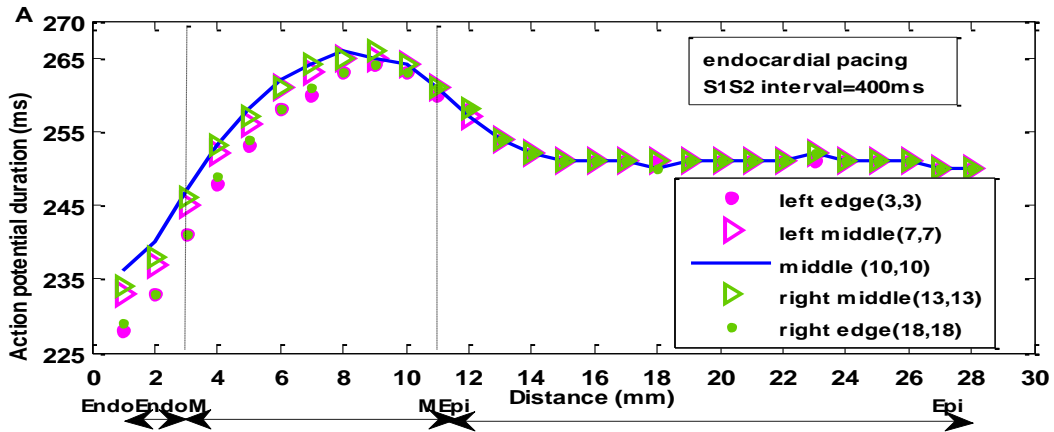


TP06 model

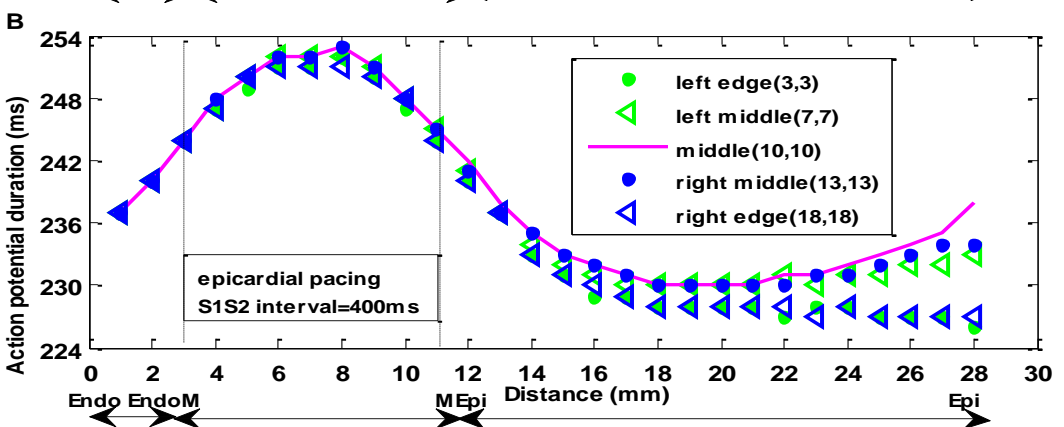
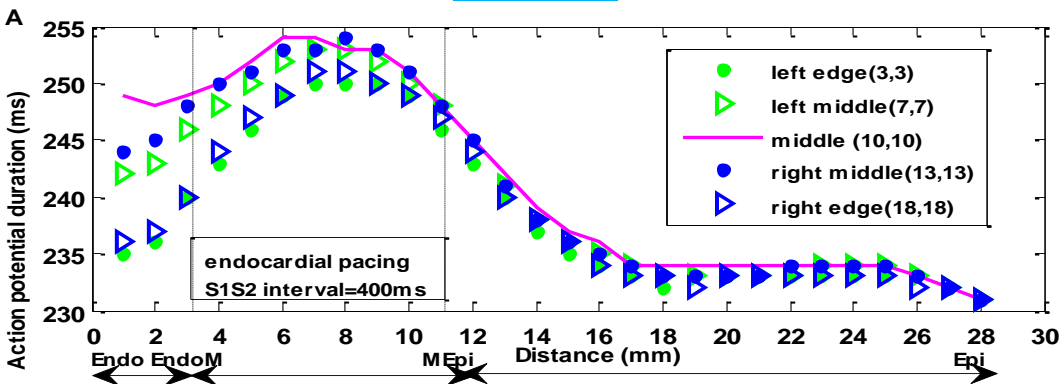


Figures J7-J10: Spatial APD profiles of heterogeneous tissue composed of 50%endo-50%epi cells with endocardial (A); and epicardial (B) pacing at S1S2 interval of 400 ms

Group J: FK4V model of anisotropic tissues with 10%Endo-30%M-60%Epi

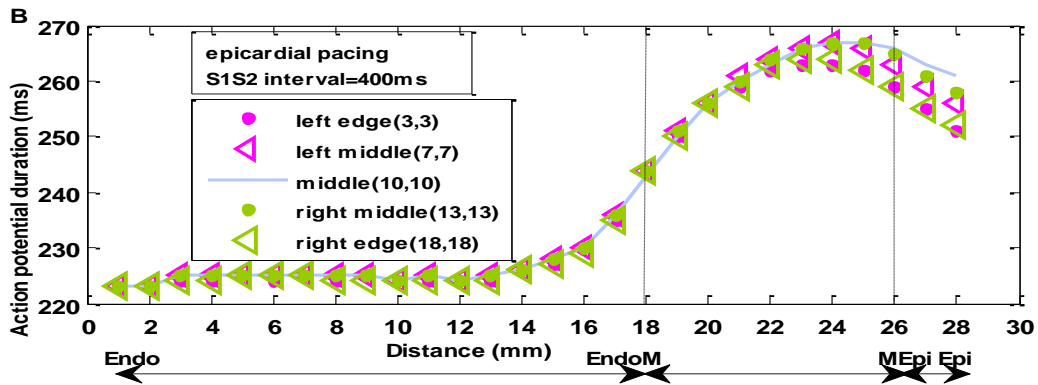
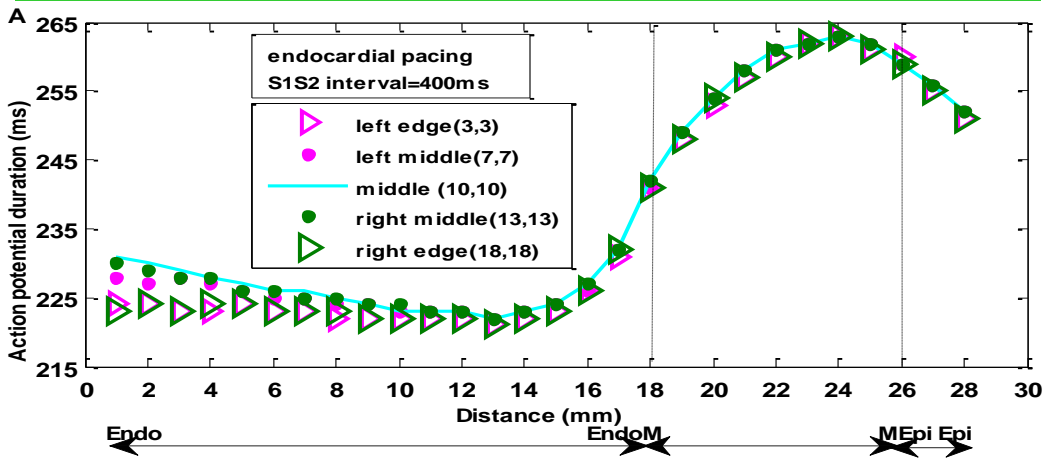


TP06 model

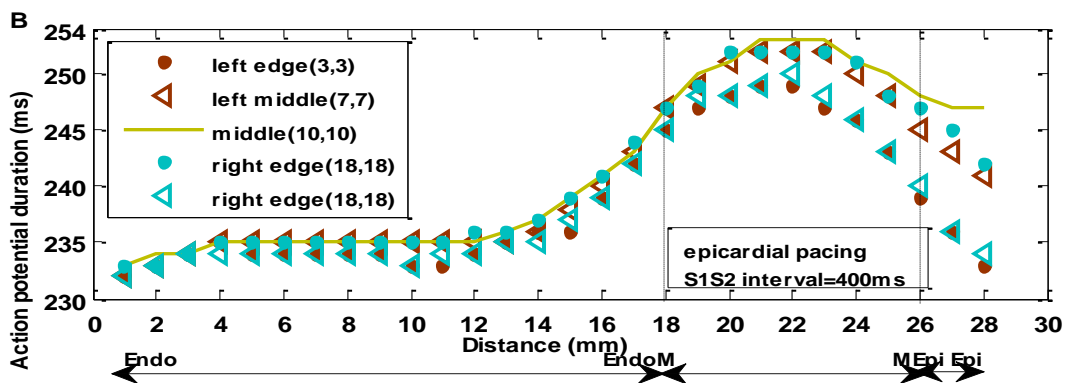
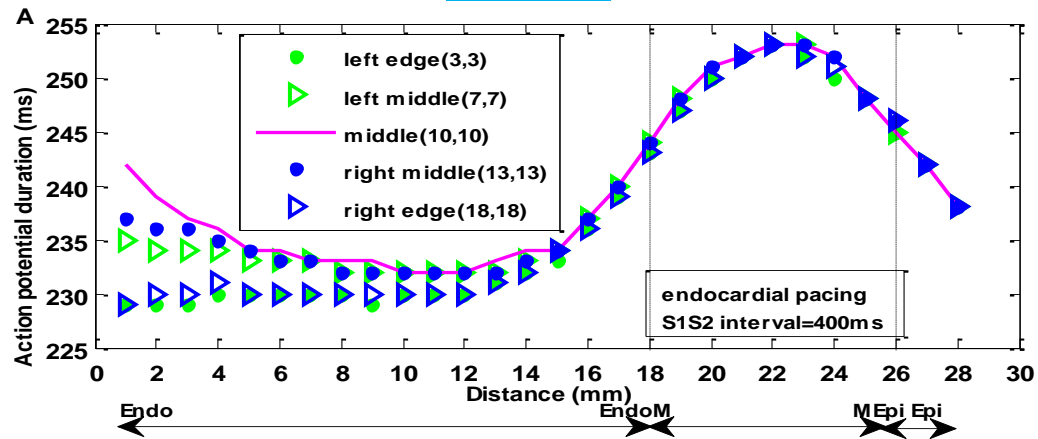


Figures J11-J14: Spatial APD profiles of heterogeneous tissue composed of 10%endo-30%M-60%epi cells with endocardial (A); and epicardial (B) pacing at S1S2 interval of 400 ms

Group J: FK4V model of anisotropic tissues with 60%Endo-30%M-10%Epi

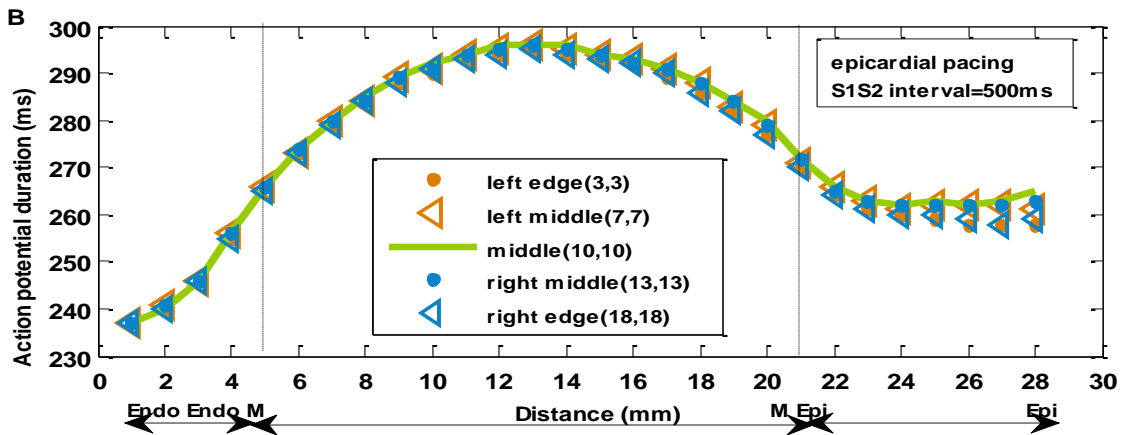
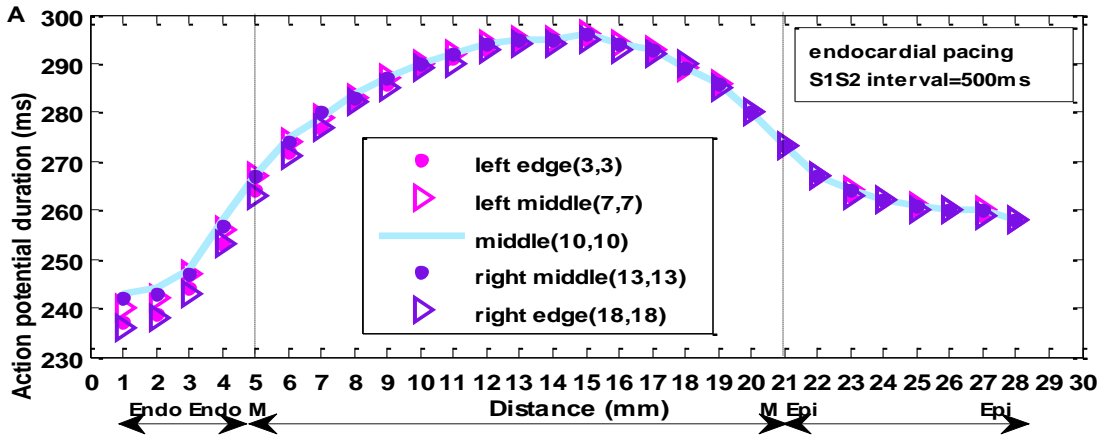


TP06 model

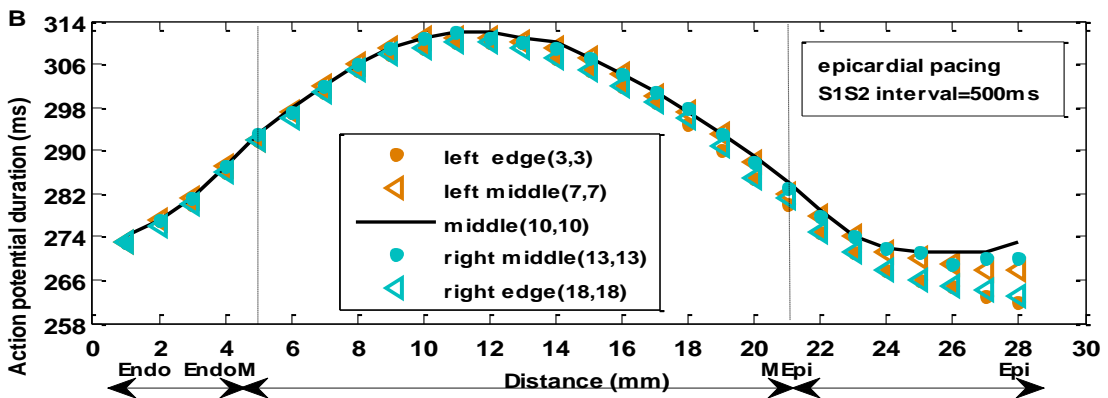
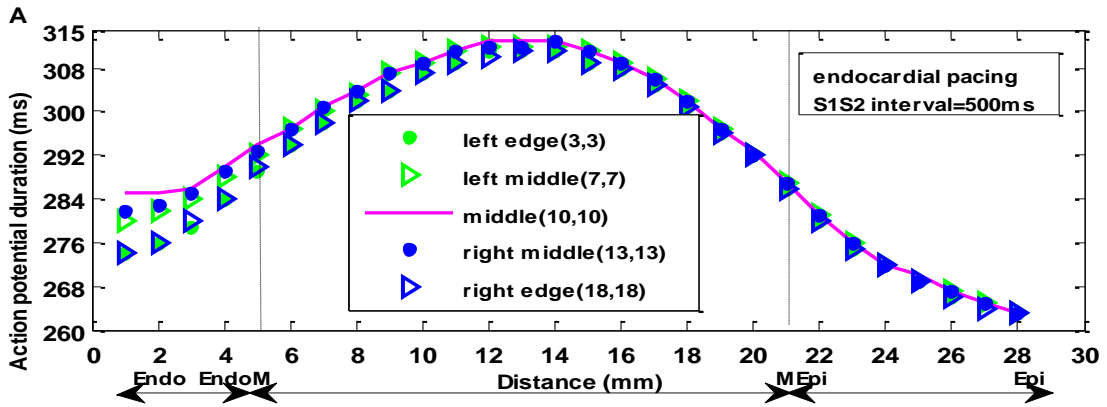


Figures J15-J18: Spatial APD profiles of heterogeneous tissue composed of 60%endo-30%M-10%epi cells with endocardial (A); and epicardial (B) pacing at S1S2 interval of 400 ms

Group J: FK4V model of anisotropic tissues with 15%Endo-55%M-30%Epi



TP06 model



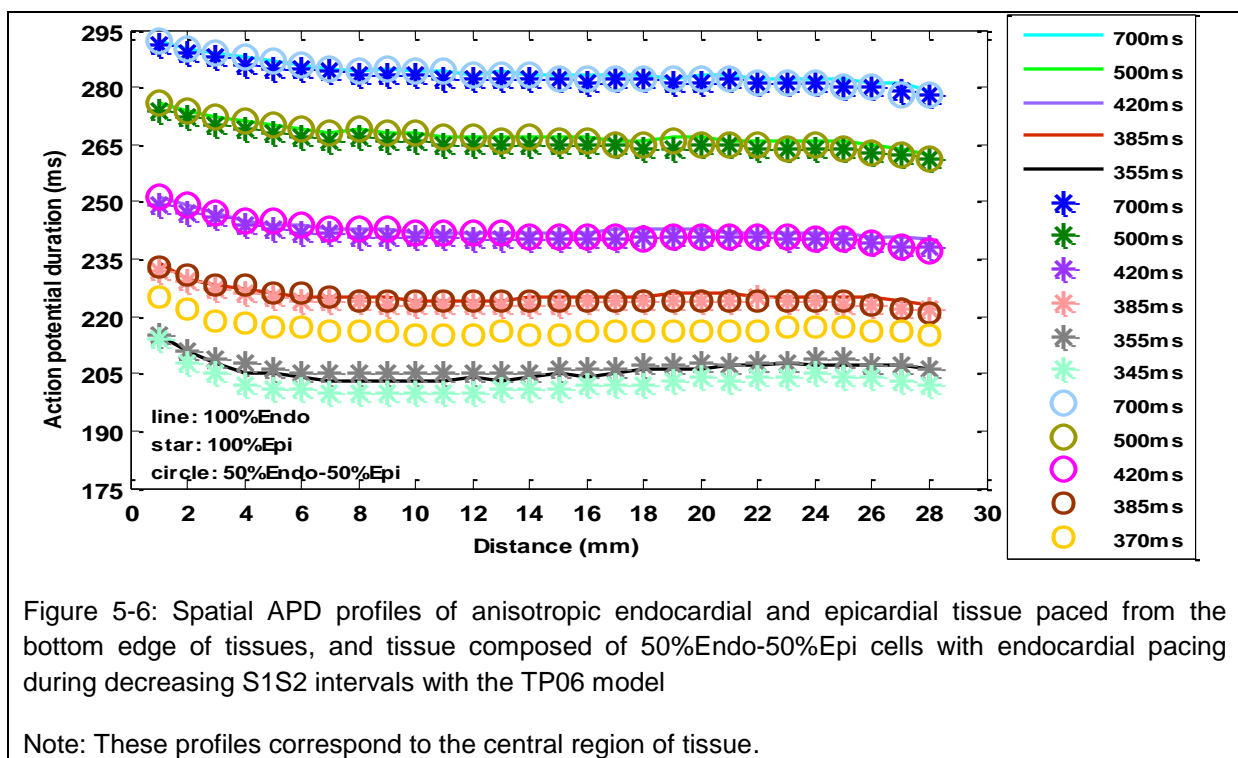
Figures J19-J22: Spatial APD profiles of heterogeneous tissue composed of 15%endo-55%M-30%epi cells with endocardial (A); and epicardial (B) pacing at S1S2 interval of 500 ms

The features of these curve depended on the type of cell model that are explained as follows.

- Homogenous tissues

The FK4V and TP06 models of anisotropic homogenous epicardial, endocardial, and mid-myocardial tissues, resulted in a stretched S-shape curve of APD against transmural distance displaced up and down the APD axis close to the edge of tissues due to the effect of boundaries, Figures J1 to J6.

With the TP06 model [21], the spatial APD profiles were fairly similar in (1) tissues composed of 50%Endo-50%Epi with endocardial pacing; (2) homogenous tissues composed of 100% epicardial; and (3) homogenous tissues composed of 100% endocardial tissues paced from the bottom edge of tissues during decreasing S1S2 intervals as shown in Figure 5-6.



- Tissue with 50%Endo-50%Epi

Figure 5-7 shows how the epicardial and endocardial properties of the FK4V and the TP06 models influenced the spatial APD profiles in 3D cubes of tissue composed of 50%Endo-50%Epi with endocardial and epicardial pacing.

With the FK4V model, the spatial APD profile was characterized by an S-shape curve with endocardial pacing, and a stretched S-shape curve with epicardial pacing in heterogeneous tissue composed of 50%Endo-50%Epi cells at five selected regions in tissue, at S1S2 interval 400 ms as shown in Figure 5-7, plot A.

However, the TP06 model of heterogeneous tissue composed of 50%endo-50%epi behaved as the TP06 model of homogenous epicardial or endocardial tissue because of small difference between the restitution properties of epicardial and endocardial cells as shown in Figure 5-7, plot B.

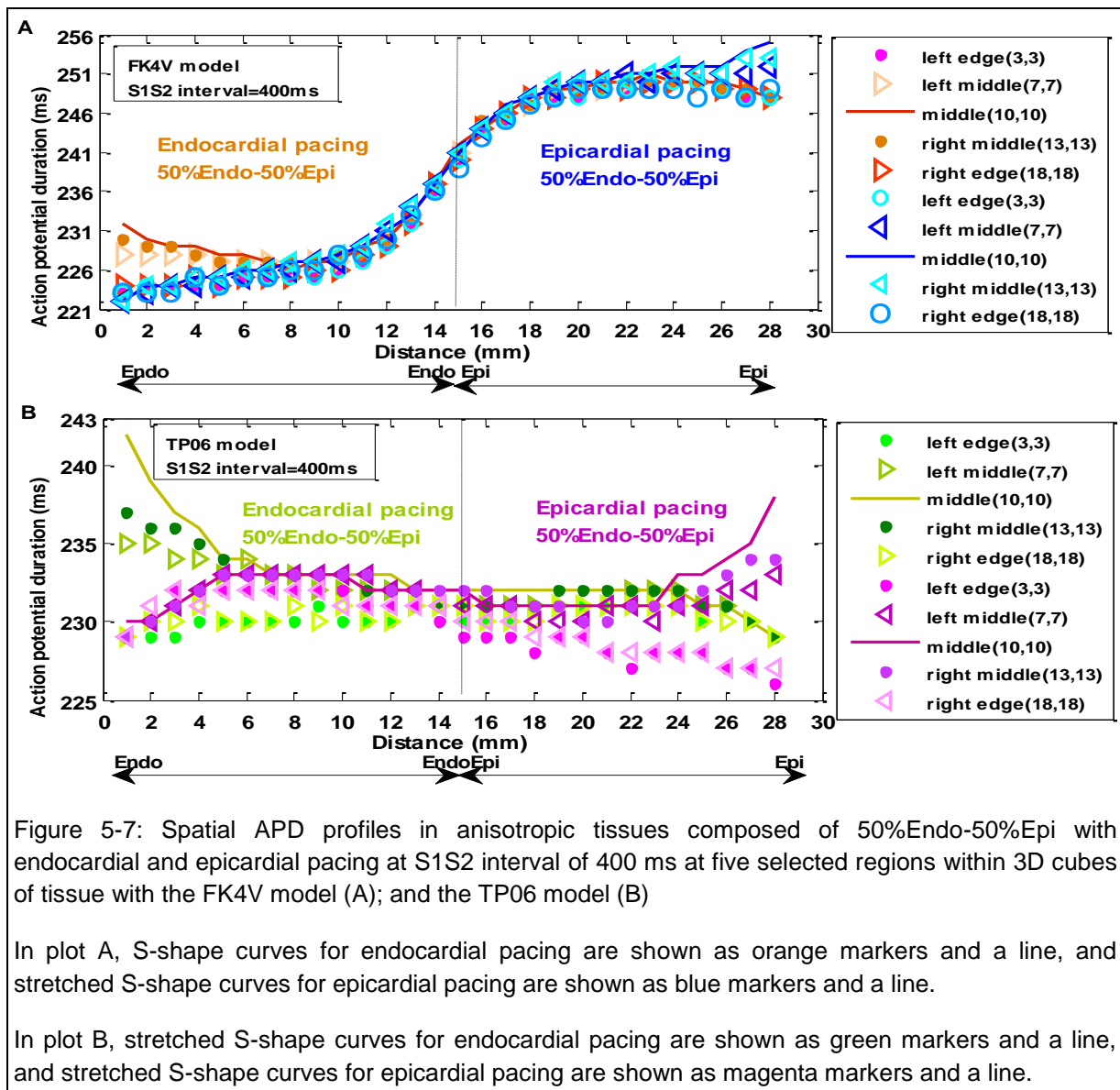


Figure 5-7: Spatial APD profiles in anisotropic tissues composed of 50%Endo-50%Epi with endocardial and epicardial pacing at S1S2 interval of 400 ms at five selected regions within 3D cubes of tissue with the FK4V model (A); and the TP06 model (B)

In plot A, S-shape curves for endocardial pacing are shown as orange markers and a line, and stretched S-shape curves for epicardial pacing are shown as blue markers and a line.

In plot B, stretched S-shape curves for endocardial pacing are shown as green markers and a line, and stretched S-shape curves for epicardial pacing are shown as magenta markers and a line.

Furthermore, opposite to the TP06 model, epicardial regions showed longer APD than endocardial regions in the five selected regions of tissue with both pacing using the FK4V model. One question was how spatial APD profiles change if the epicardial region possesses a shorter APD than the endocardial region with the FK4V model. To answer this question, the endocardial and epicardial parameters (in fk4v.c file explained in Appendix) were exchanged and two new tissues were simulated composed of 50%Epi-50%Endo with endocardial and epicardial pacing using the FK4V model. The created transmembrane voltages were extracted from the central region of tissues.

Exchanging epicardial and endocardial model parameters produced symmetrical APD profiles at S1S2 intervals of 1000 ms and 800 ms as shown in Figure 5-8. For example, the spatial APD curve in tissue with exchanging epicardial and endocardial model parameters with epicardial pacing and in tissue without exchanging but with endocardial pacing were symmetric with respect to APD axis and distance axis.

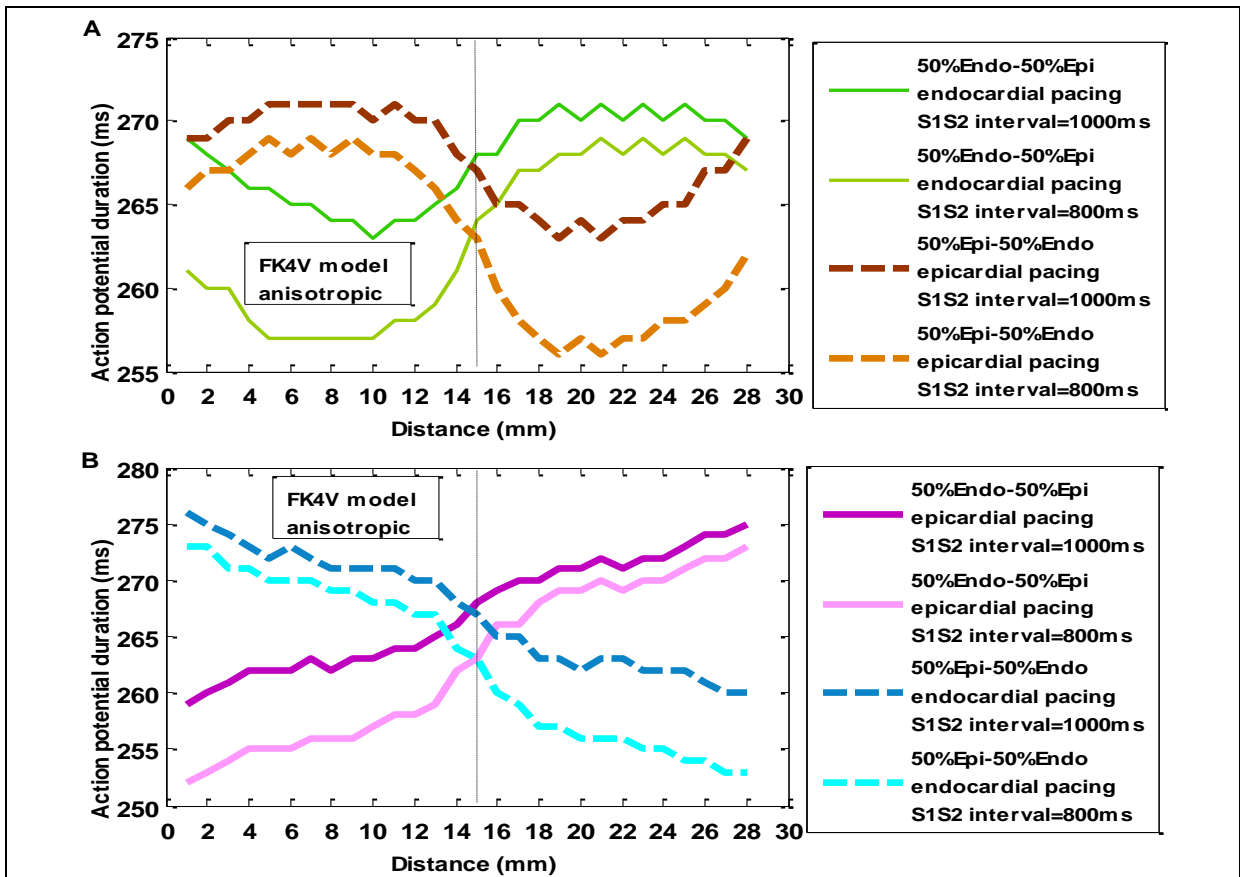


Figure 5-8: Spatial APD profiles in anisotropic tissues composed of two cell types using the FK4V model showing symmetrical profiles at S1S2 intervals of 1000 ms and 800 ms for

(A) 50%Endo-50%Epi with endocardial pacing and 50%Epi-50%Endo with epicardial pacing
 (B) 50%Endo-50%Epi with epicardial pacing and 50%Epi-50%Endo with endocardial pacing

Note: These profiles correspond to the central region of tissue.

- Tissue composed of 15%Endo-55%M-30%Epi

With an additional layer of mid-myocardial cells with longer APD than other cell types, a dome morphology in the middle of the spatial APD profile was formed with both endocardial and epicardial pacing using both models as shown in Figure 5-9. However, the epicardial region had longer APD than the endocardial region using the FK4V model while the reverse was true with the TP06 model.

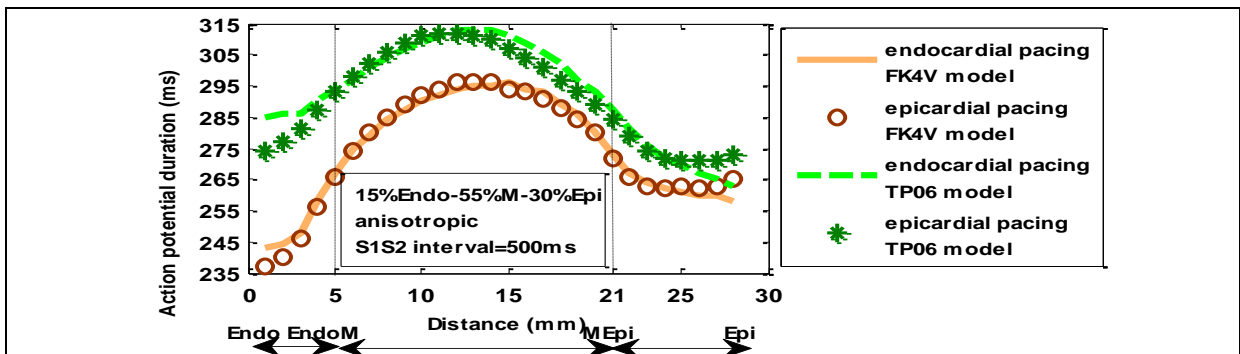


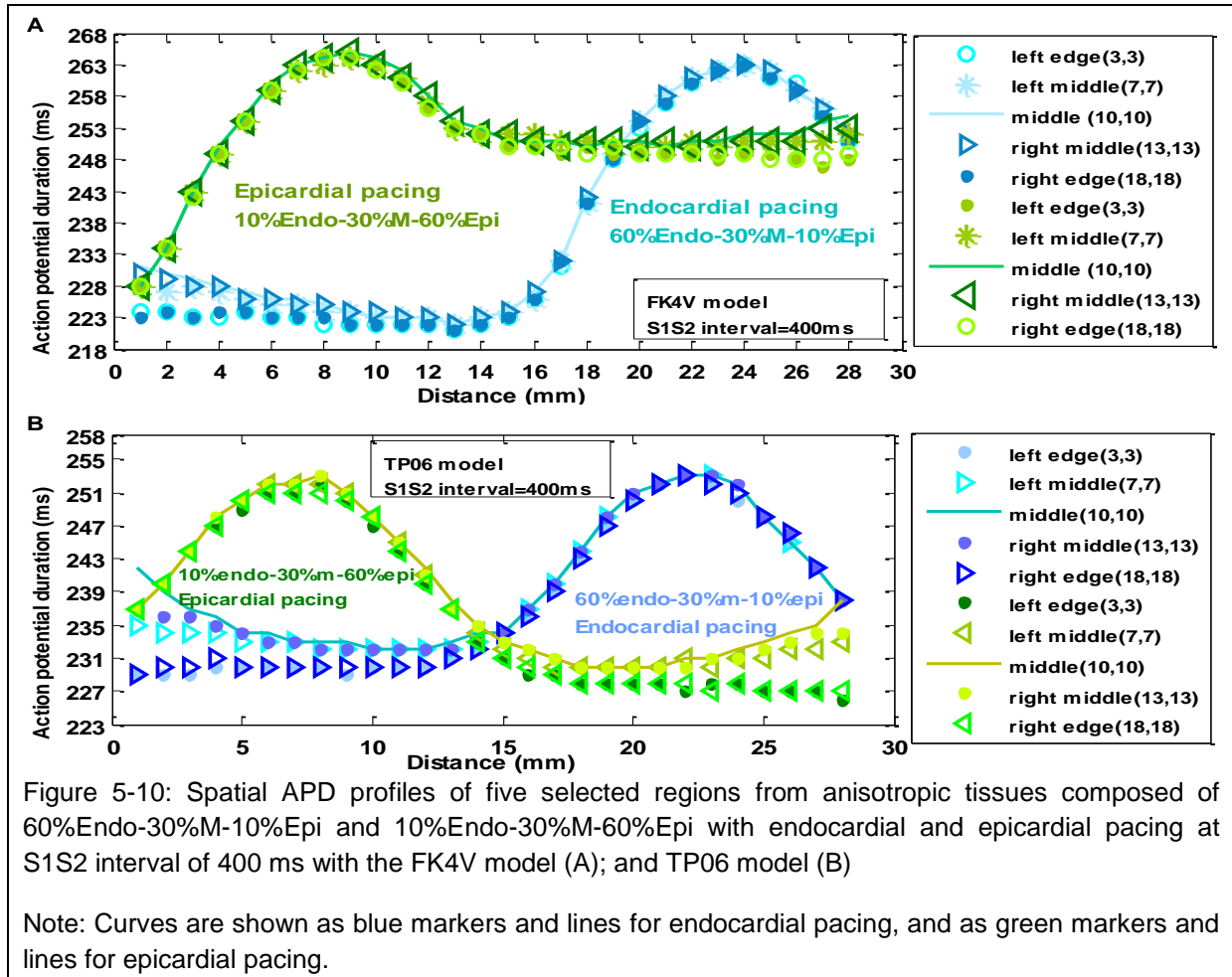
Figure 5-9: Comparison the spatial APD profile of anisotropic tissues composed of 15%Endo-55%M-30%Epi with endocardial and epicardial pacing at S1S2 interval of 500 ms showing a dome morphology in the mid-myocardial region using the FK4V and TP06 models

Note: These profiles correspond to the central region of tissue.

- Tissues with 60%Endo-30%M-10%Epi cells and 10%Endo-30%M-60%Epi cells

Similar to tissue composed of 15%Endo-55%M-30%Epi, a dome morphology in the spatial APD profiles was formed that shifted toward endocardial or epicardial region in two simulated tissues with the FK4V and the TP06 models as shown in Figure 5-10. These tissues were composed of the fixed populations of mid-myocardial cells and different populations of epicardial and endocardial cells.

Interestingly, with the TP06 model, the spatial APD profiles at five selected regions in tissue compose of 60%Endo-30%M-10%Epi with endocardial pacing and in tissue composed of 10%Endo-30%M-60%Epi with epicardial pacing were mirror of each other. Examples of these profiles at S1S2 interval of 400 ms are shown in Figure 5-10, plot B.



In summary, spatial APD profiles at five selected regions using both models changed with:

- ❖ local arrangement of cardiac cells in tissues, i.e. any amount of mid-myocardial layers prolonged the APD of layers between endocardial and epicardial regions;
- ❖ endocardial and epicardial pacing i.e. shorter APD close to the stimulus sites became greater with increasing depth in the transmural direction of ventricular tissue particularly at central region of the 3D cube of tissue, and then became shorter at opposed sites with both endocardial and epicardial pacing;
- ❖ tissue boundaries because boundaries acted to prolong APD close to sites of earliest activation, and to shorten APD at sites of latest activation.

The following sections focus on data obtained from central region of the 3D cubes of tissue (as shown in Figure 5-1 as a red cub) in which endocardial and epicardial pacing influenced the spatial APD profiles more than other regions in tissues.

5.2.2 Rate dependent effects

Similar to findings in 2D isotropic tissues with and without abrupt changes in tissue geometries, spatial APD profiles and APD dispersion for premature S2 beats changes during decreasing S1S2 intervals in the FK4V and TP06 models of 3D cubes of isotropic, anisotropic, and anisotropic fibrosis tissues.

Figure 5-11 shows examples of spatial APD profiles for normal S1 and premature S2 beats for long and short S1S2 intervals in the FK4V models of tissues composed of 50%Endo-50%Epi with endocardial (A); and epicardial (B) pacing. The Figure emphasizes that spatial profiles of premature APD change during decreasing S1S2 intervals possibly due to the rate dependent effects while spatial profiles of normal APD did not changed for long and short S1S2 intervals. This was true for activation time and repolarization time using both models but the plots are not shown.

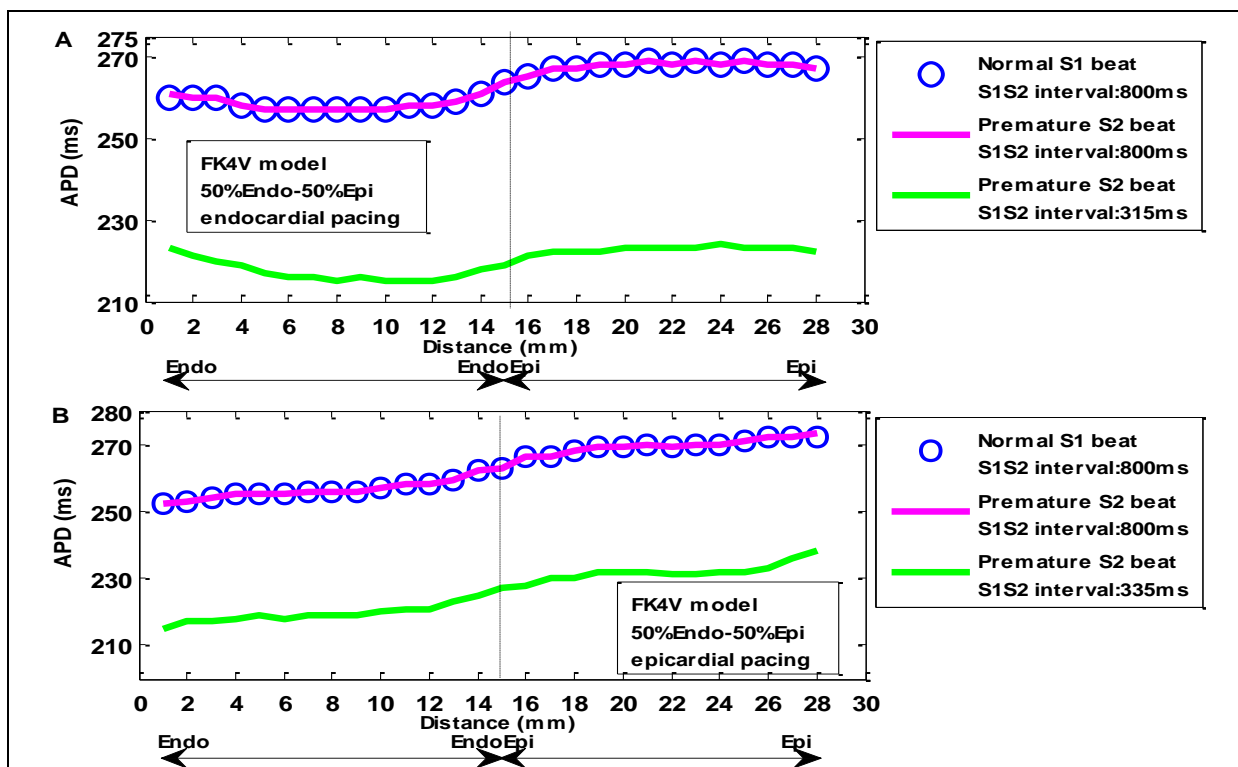


Figure 5-11: Examples of spatial APD profiles for normal S1 and premature S2 beats in the FK4V models of anisotropic tissues composed of 50%Endo-50%Epi with endocardial (A); and epicardial (B) pacing at S1S2 interval of 800 ms and the last S1S2 interval

For normal S1 beats, measures of APD dispersion remained approximately constant between S1S2 interval of 800 ms and the last S1S2 interval (i.e. 12 ms with endocardial pacing in plot A and 20 ms with epicardial pacing in plot B).

For premature S2 beats, APD dispersion varied from 12 ms at S1S2 interval of 800 ms to 9 ms at S1S2 interval of 315 ms with endocardial pacing in plot A, and from 21 ms at S1S2 interval of 800 ms to 23 ms at S1S2 interval of 335 ms with epicardial pacing in plot B.

Figure 5-12 compares spatial APD profiles for normal and premature beats for tissues composed of 10%Endo-30%M-60%Epi cells with endocardial (A); and epicardial (B) pacing.

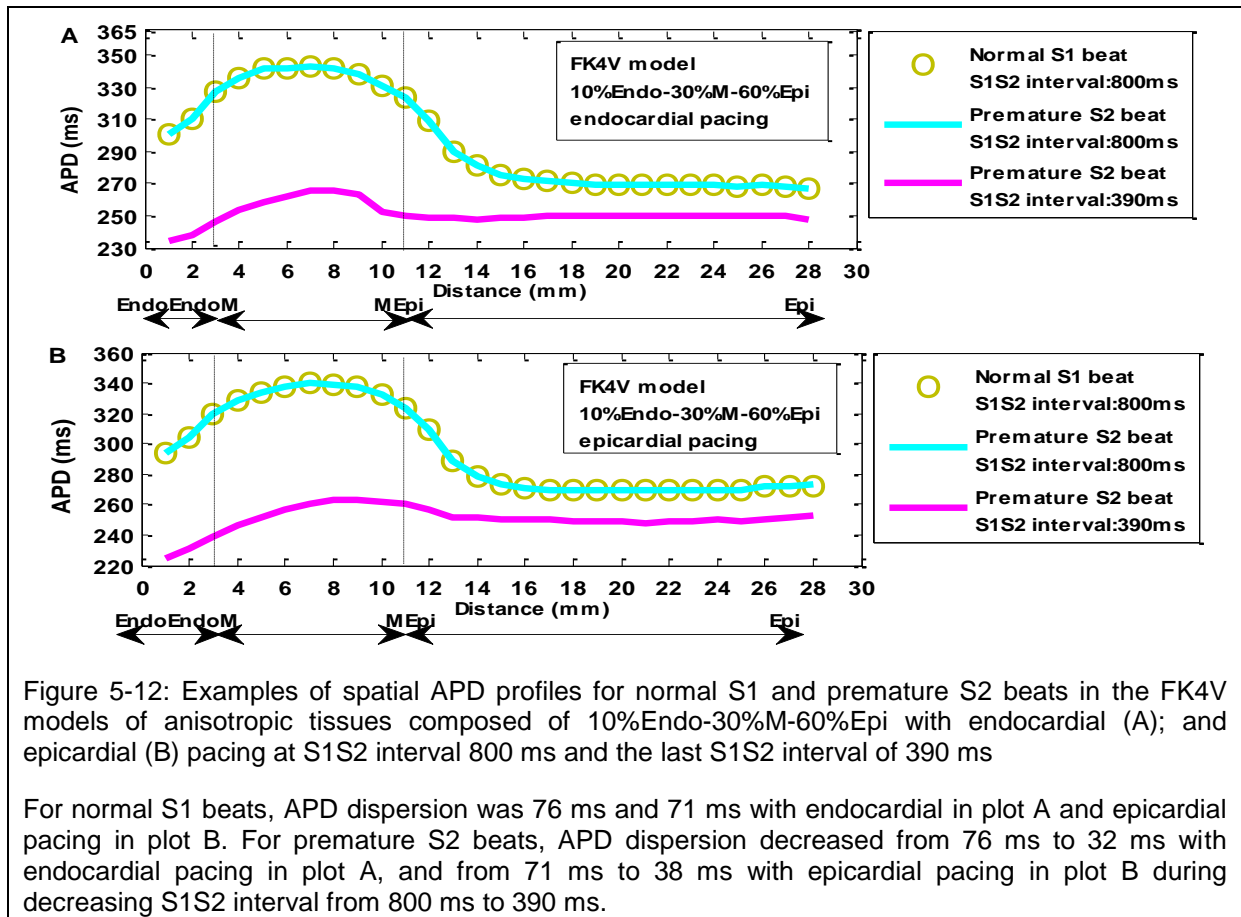


Figure 5-12: Examples of spatial APD profiles for normal S1 and premature S2 beats in the FK4V models of anisotropic tissues composed of 10%Endo-30%M-60%Epi with endocardial (A); and epicardial (B) pacing at S1S2 interval 800 ms and the last S1S2 interval of 390 ms

For normal S1 beats, APD dispersion was 76 ms and 71 ms with endocardial in plot A and epicardial pacing in plot B. For premature S2 beats, APD dispersion decreased from 76 ms to 32 ms with endocardial pacing in plot A, and from 71 ms to 38 ms with epicardial pacing in plot B during decreasing S1S2 interval from 800 ms to 390 ms.

5.2.3 Profiles of premature activation time, repolarization time, and APD

This part of the Chapter concentrates on the profiles of activation time, repolarization time, and APD for premature S2 beats in the FK4V and the TP06 models of homogenous and heterogeneous tissues to study how

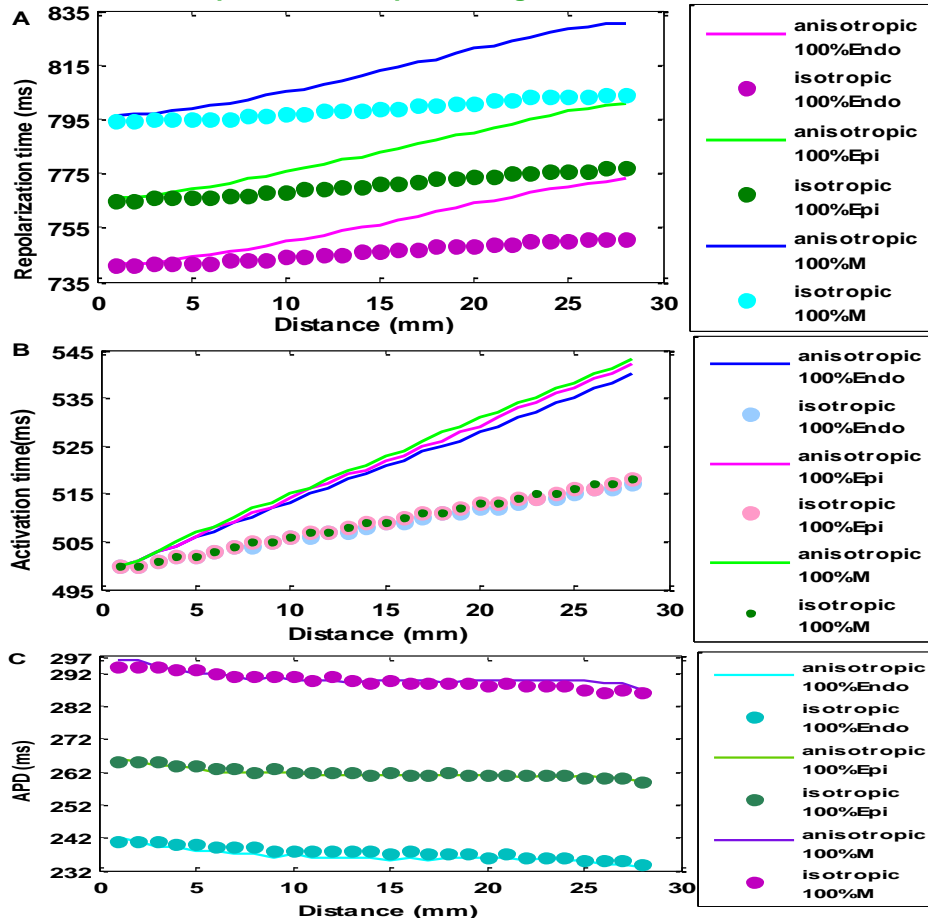
- (1) activation time, repolarization time, and APD change against transmural distance;
- (2) activation time, repolarization time, and APD change against diastolic interval.

To achieve this purpose, initially six plots for each simulated tissue are provided to compare the shape of curves in tissues with isotropic and anisotropic diffusions at one S1S2 interval in the same graph. Next, the effect of broad range of S1S2 interval on these profiles is assessed by plotting these data during progressively decreasing S1S2 intervals. Finally, anisotropic tissues with fibrosis are compared with anisotropic tissues without fibrosis by providing some examples.

For homogenous tissues composed of 100% endocardial, 100% epicardial cells, and 100% mid-myocardial paced from the bottom edge of tissue,

- the six profiles were characterised by a single curve using the FK4V and TP06 models as shown in Figure 5-13 for spatial profiles and Figure 5-14 for restitution profiles;
- the FK4V model produced distinct profiles for these homogenous tissues while the TP06 model created similar profiles for epicardial and endocardial tissues.

FK4V model of isotropic & anisotropic homogenous tissues at S1S2 interval 500ms



TP06 model of isotropic & anisotropic homogenous tissues at S1S2 interval 600 ms

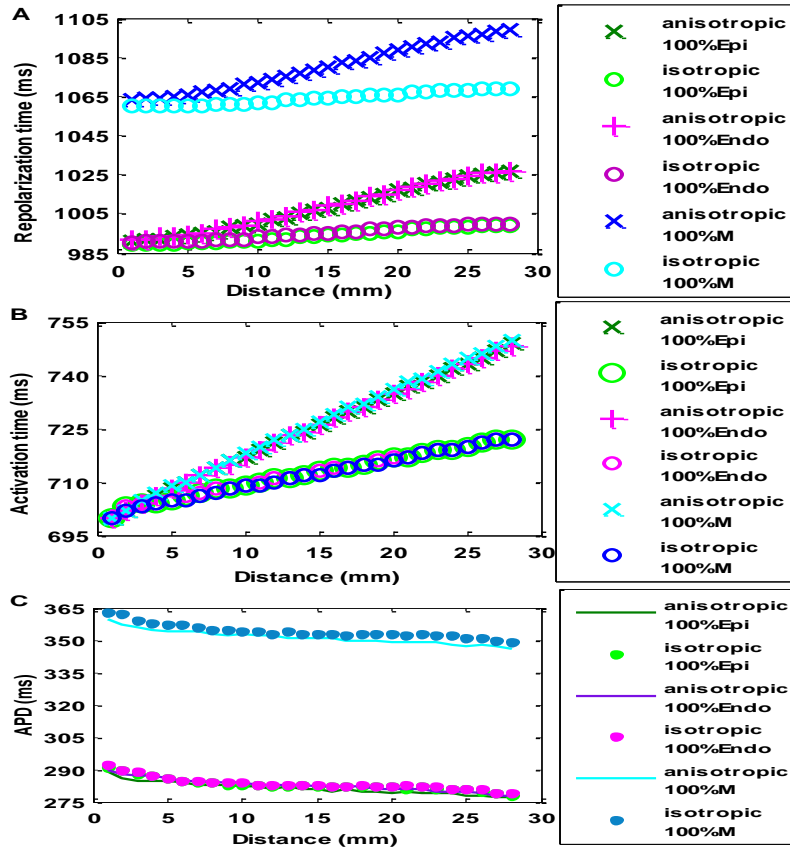
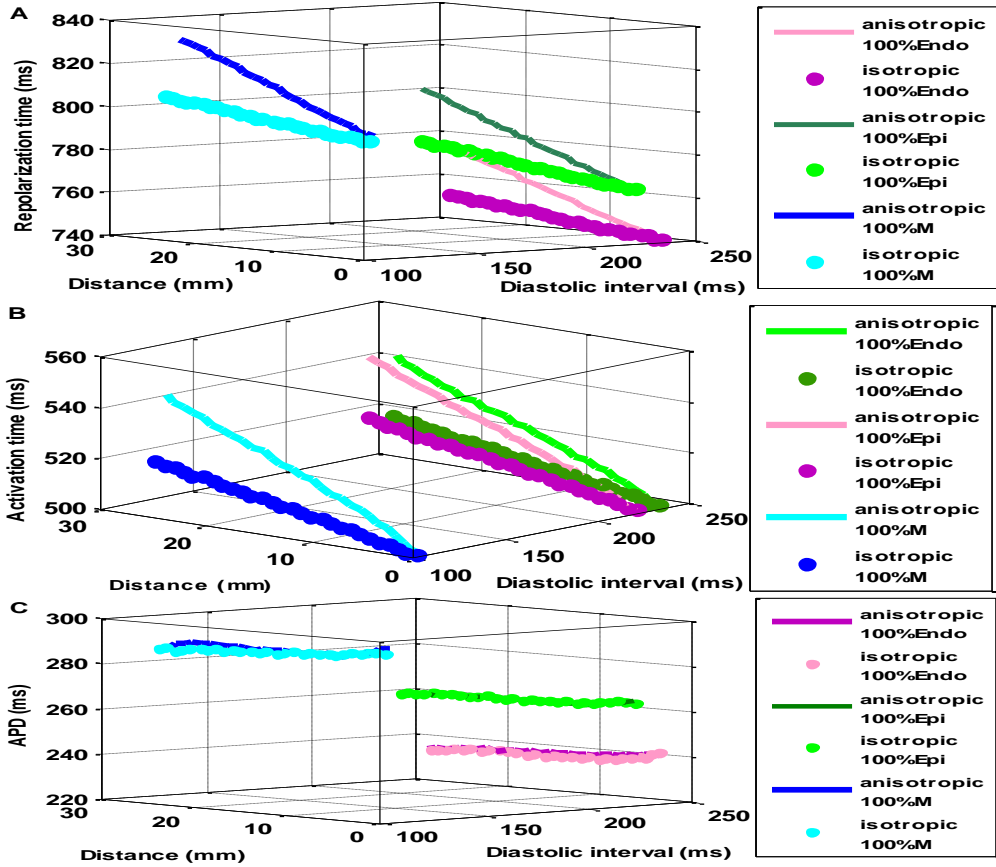


Figure 5-13: Spatial profiles of repolarization time (A); activation time (B); and APD (C)

FK4V model of isotropic & anisotropic homogenous tissues at S1S2 interval 500 ms



TP06 model of isotropic & anisotropic homogenous tissues at S1S2 interval 600 ms

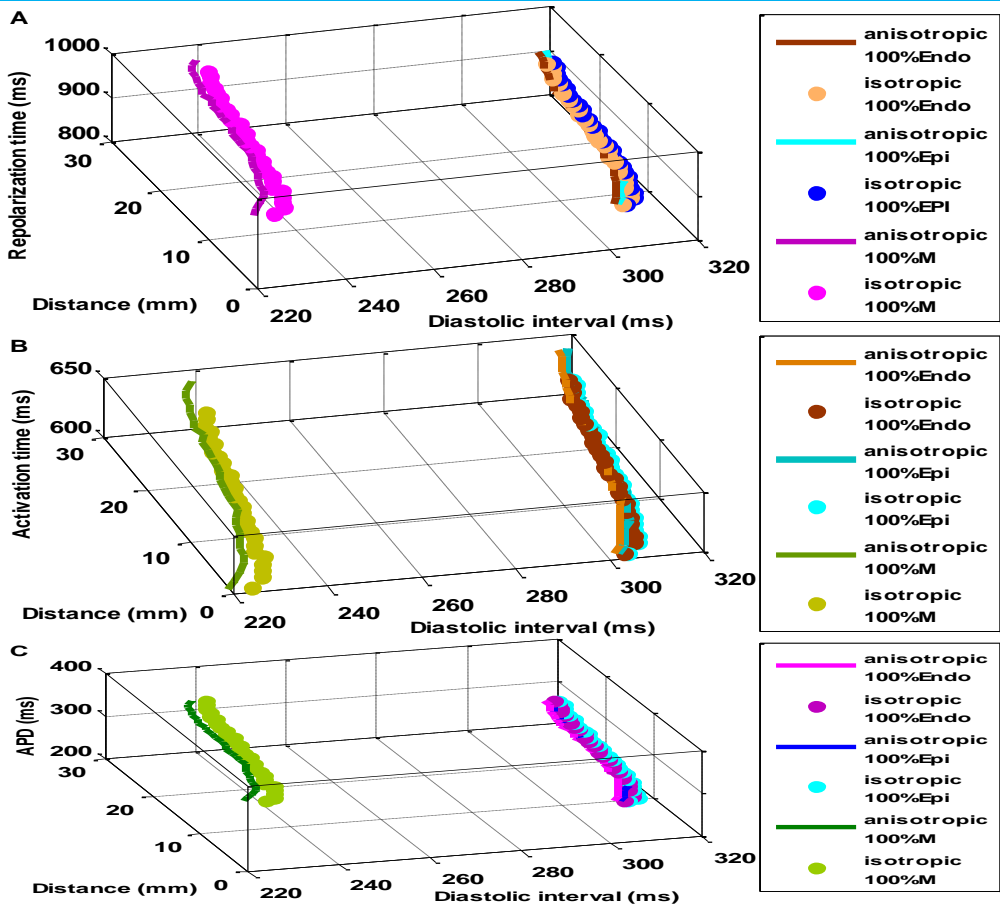


Figure 5-14: Restitution profiles of repolarization time (A); activation time (B); and APD (C)

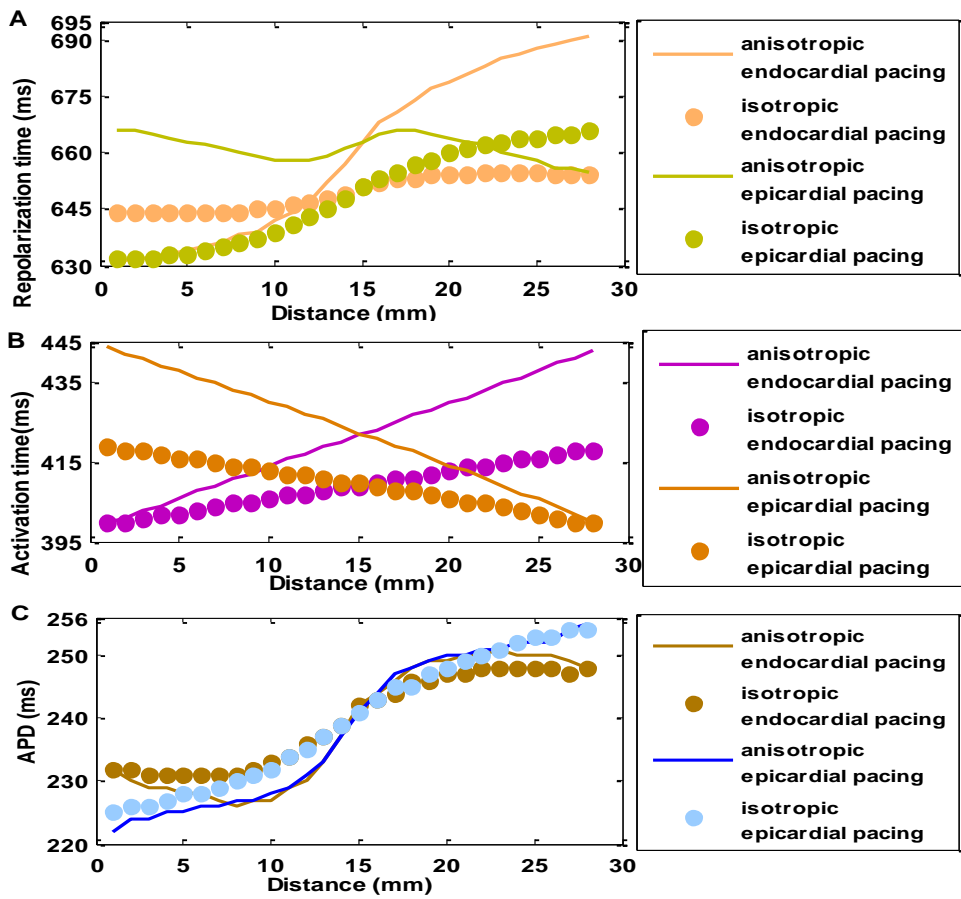
The heterogeneity in ventricular tissue influenced the shape and duration of premature activation time, APD and repolarization time with the FK4V and the TP06 models. Figure 5-15 to Figure 5-22 show six spatial and restitution profiles of activation time, APD and repolarization time at one S1S2 interval for each 3D cube of tissue. For heterogeneous tissues composed of more than one cell type with endocardial and epicardial pacing,

- these six profiles were characterized by a family of S-shape curves rather than a single curve;
- similar to spatial and restitution profiles of APD and repolarization time, a dome-morphology in restitution profiles of activation time in the mid-myocardial region of three heterogeneous tissues (10%Endo-30%M-60%Epi, 60%Endo-30%M-10%Epi, and 15%Endo-55%M-30%Epi) was created (shown in restitution profiles in plots B);
- the dome-morphology was tiny in the spatial profile of activation time in these tissues because this profile reflects the activation and inactivation of ion channels during AP depolarization (shown in spatial profiles in plots B);
- spatial profiles of activation time with endocardial and epicardial pacing was approximately symmetric with respect to activation time axis (shown in spatial profiles in plots B);
- these six profiles with the FK4V model were qualitatively similar to those with the TP06 model in isotropic, anisotropic, and anisotropic fibrosis tissues.

These features were also true during progressively decreasing S1S2 intervals using both models that emphasized the rate dependency of premature repolarization time and APD as well as premature activation time when it is plotted against diastolic interval.

Figures organized in Group P (Figures P1 to P43) in Appendix 1 provides examples of (1) spatial profiles of activation time; (2) repolarization time; and (3) APD; and (4) profiles of APD against repolarization time in anisotropic tissues with and without fibrosis during decreasing S1S2 intervals with the TP06 model. In most tissues, the significant change in the curves was at the last S1S2 interval with both models. However, the last S1S2 interval in isotropic tissue with the TP06 model was significantly shorter than with the FK4V model and was approximately 500 ms.

FK4V model of isotropic & anisotropic tissues with 50%Endo-50%Epi at S1S interval 400 ms



TP06 model of isotropic & anisotropic tissues with 50%Endo-50%Epi at S1S2 interval 600 ms

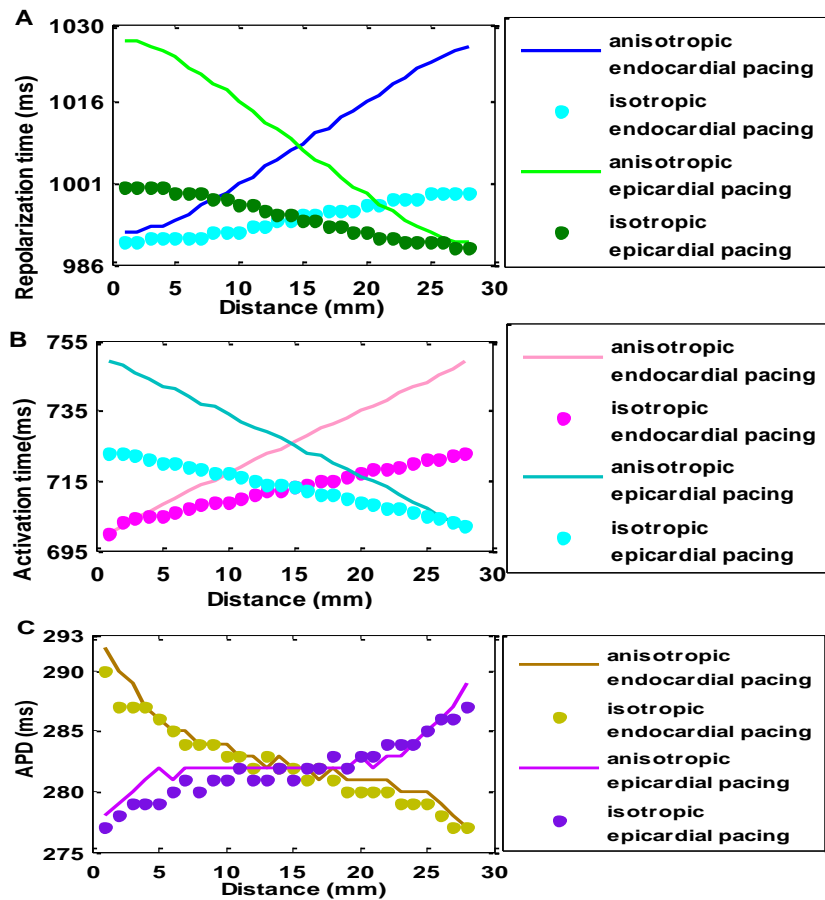
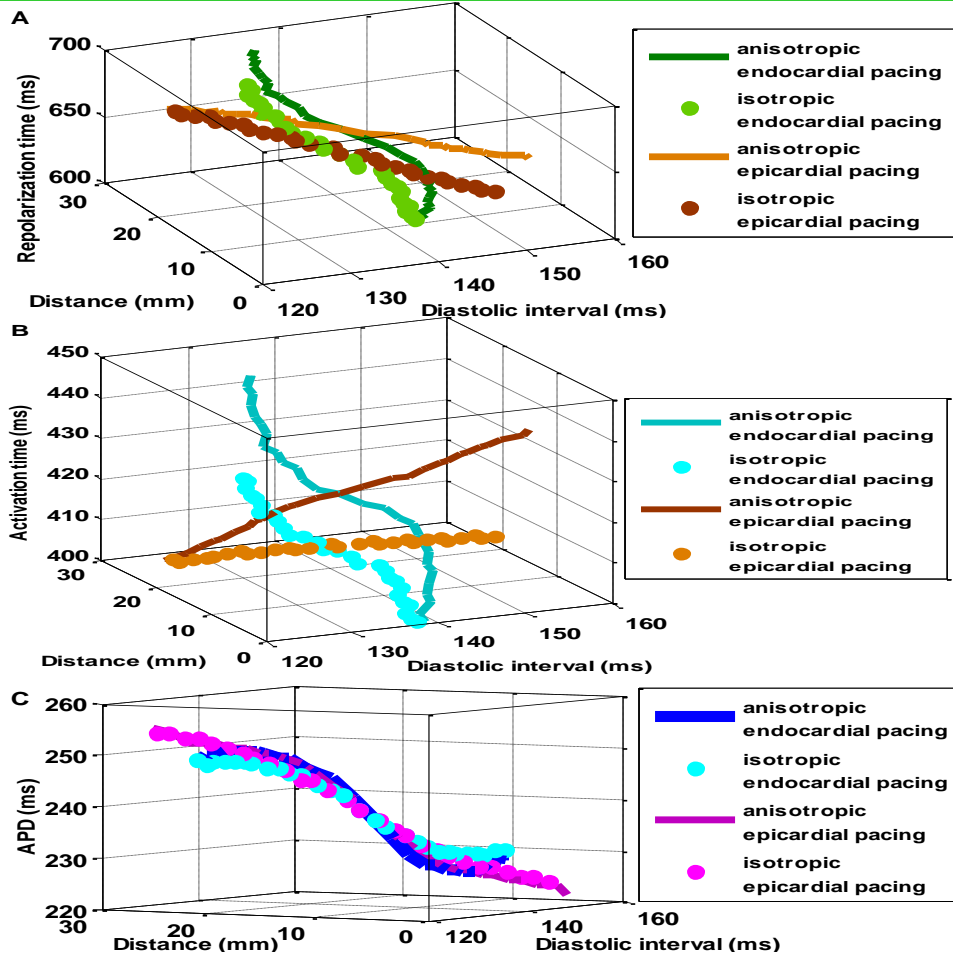


Figure 5-15: Spatial profiles of repolarization time (A); activation time (B); and APD (C)

FK4V model of isotropic & anisotropic tissues 50%Endo-50%Epi at S1S2 interval 400 ms



TP06 model of isotropic & anisotropic tissues 50%Endo-50%Epi at S1S2 interval 600 ms

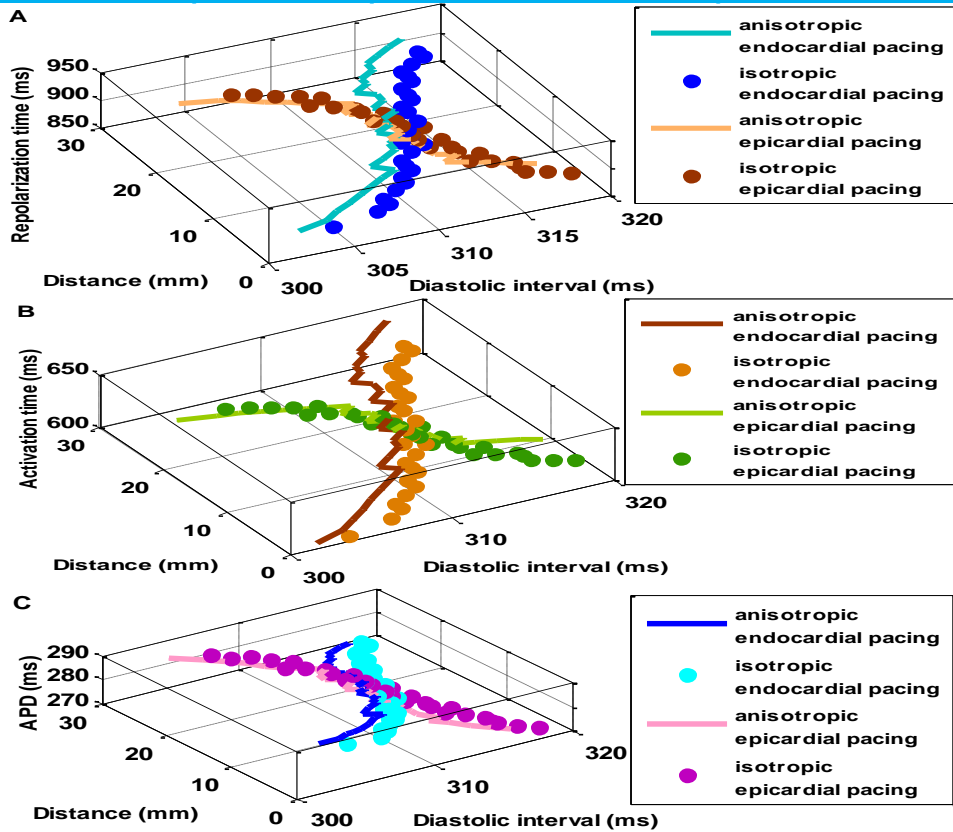
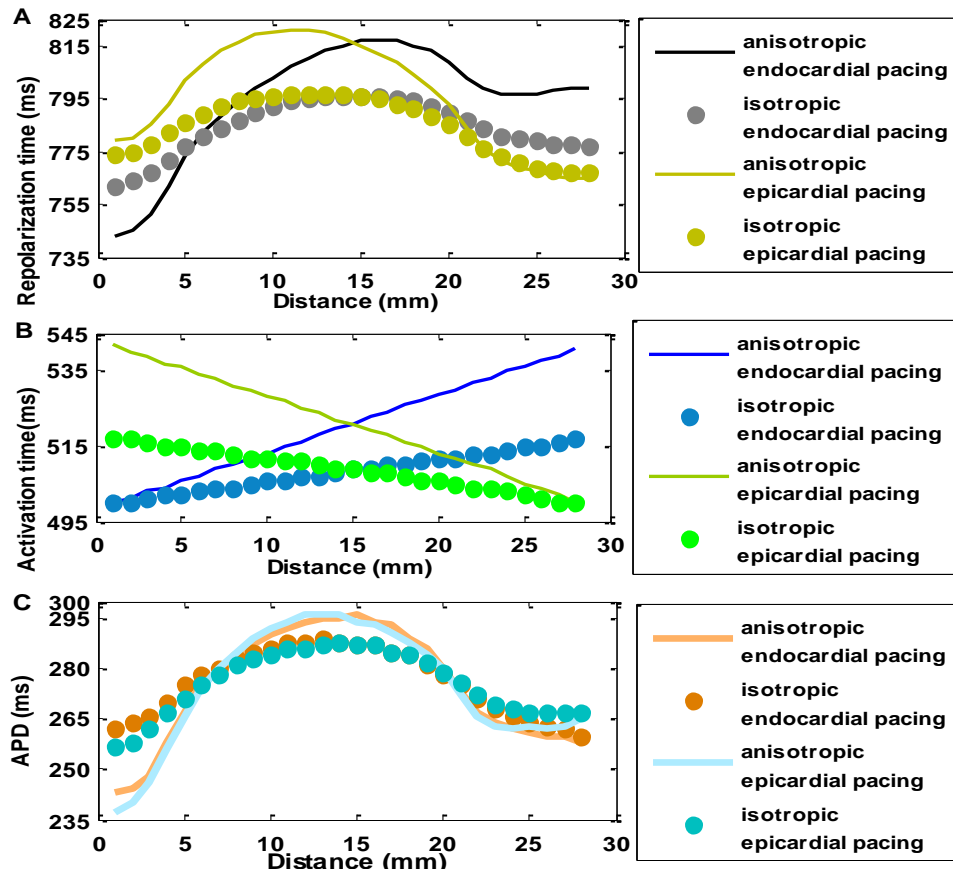


Figure 5-16: Restitution profiles of repolarization time (A); activation time (B); and APD (C)

FK4V model of isotropic & anisotropic tissue 15%Endo-55%M-30%Epi at S1S2 interval 500 ms



TP06 model of isotropic & anisotropic tissue 15%Endo-55%M-30%Epi at S1S2 interval 600 ms

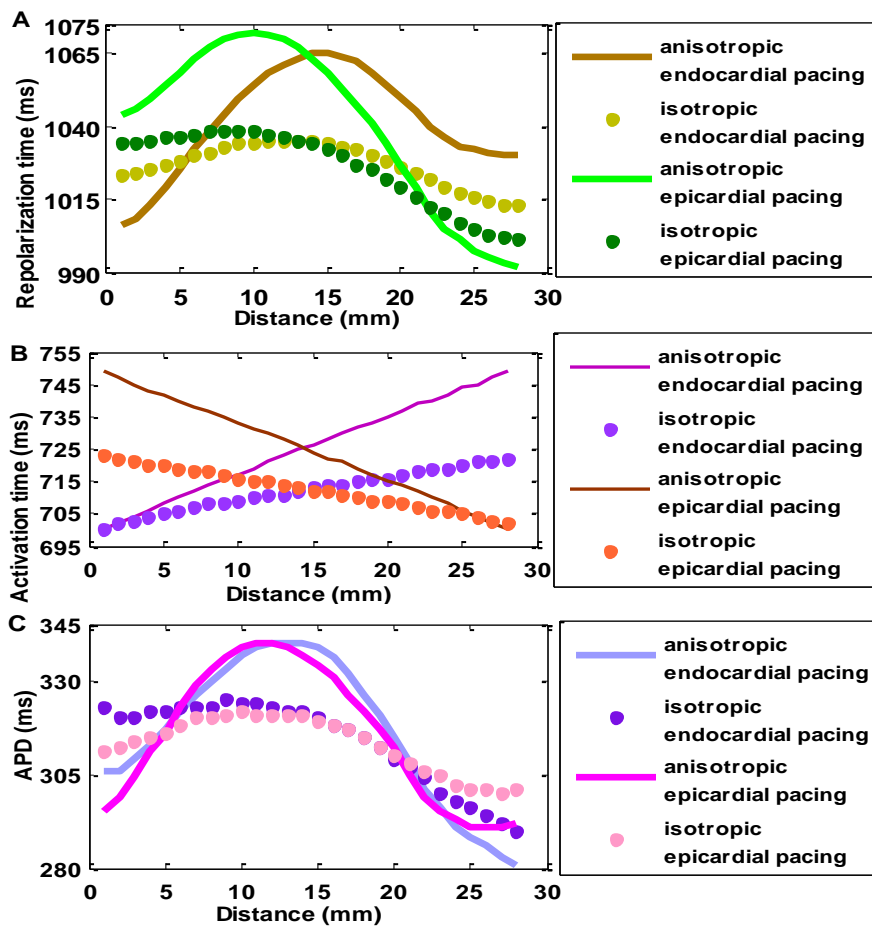
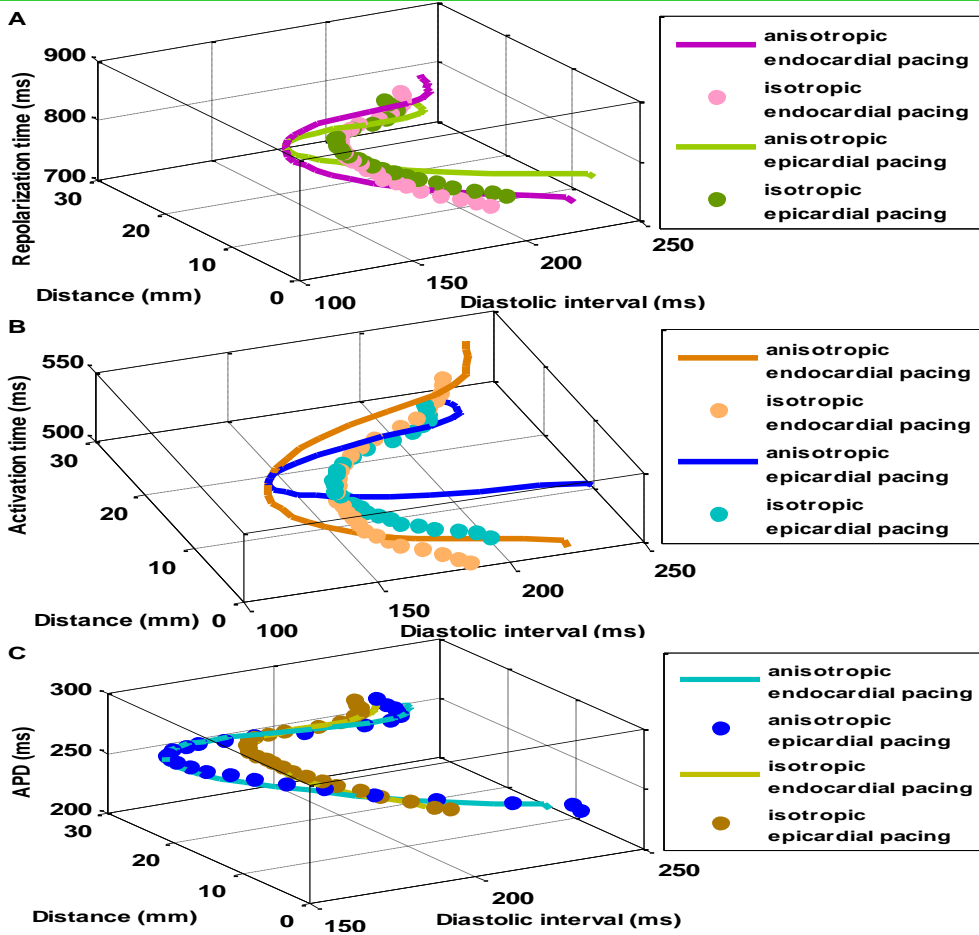


Figure 5-17: Spatial profiles of repolarization time (A); activation time (B); and APD (C)

FK4V model of isotropic & anisotropic tissue 15%Endo-55%M-30%Epi at S1S2 interval 500 ms



TP06 model of isotropic & anisotropic tissue 15%Endo-55%M-30%Epi at S1S2 interval 600 ms

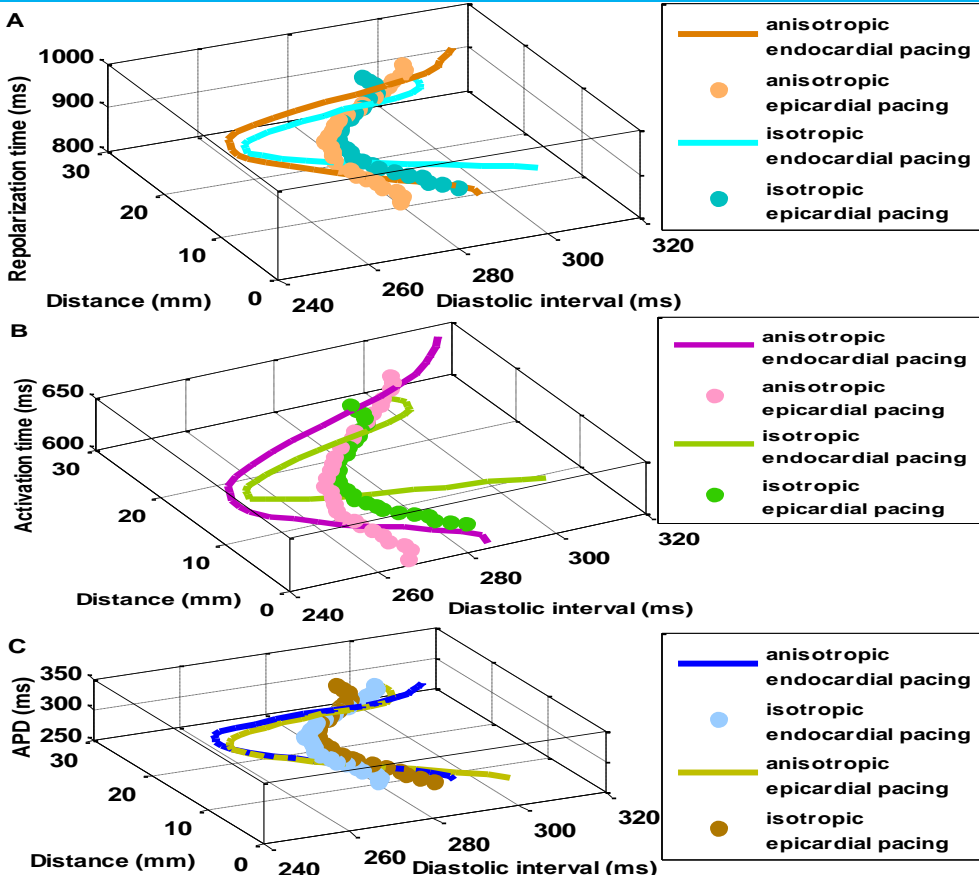
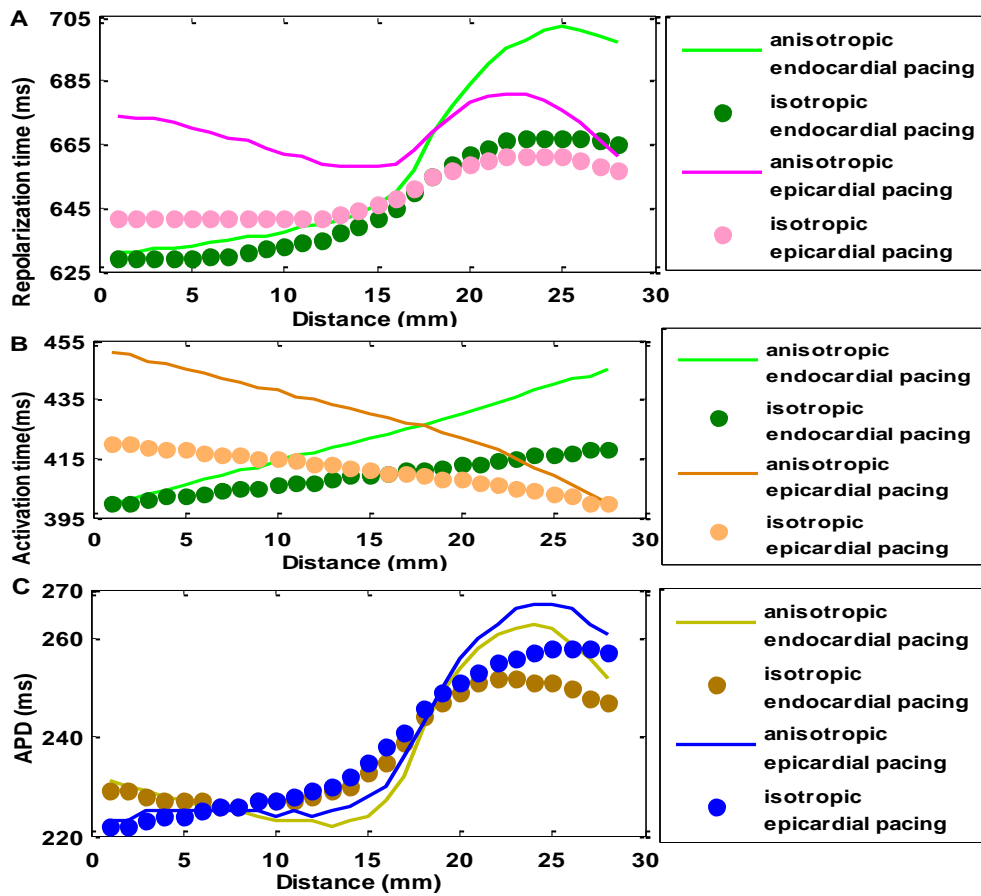


Figure 5-18: Restitution profiles of repolarization time (A); activation time (B); and APD (C)

FK4V model of isotropic & anisotropic tissue 60%Endo-30%M-10%Epi at S1S2 interval 400 ms



TP06 model of isotropic & anisotropic tissue 60%Endo-30%M-10%Epi at S1S2 interval 600 ms

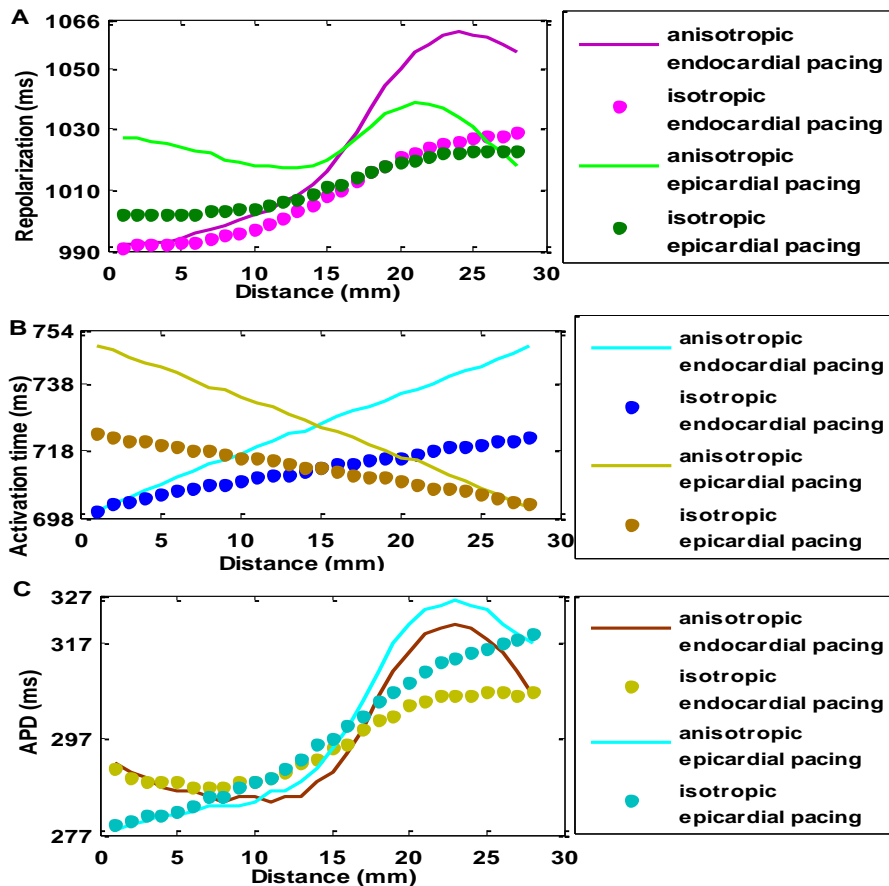
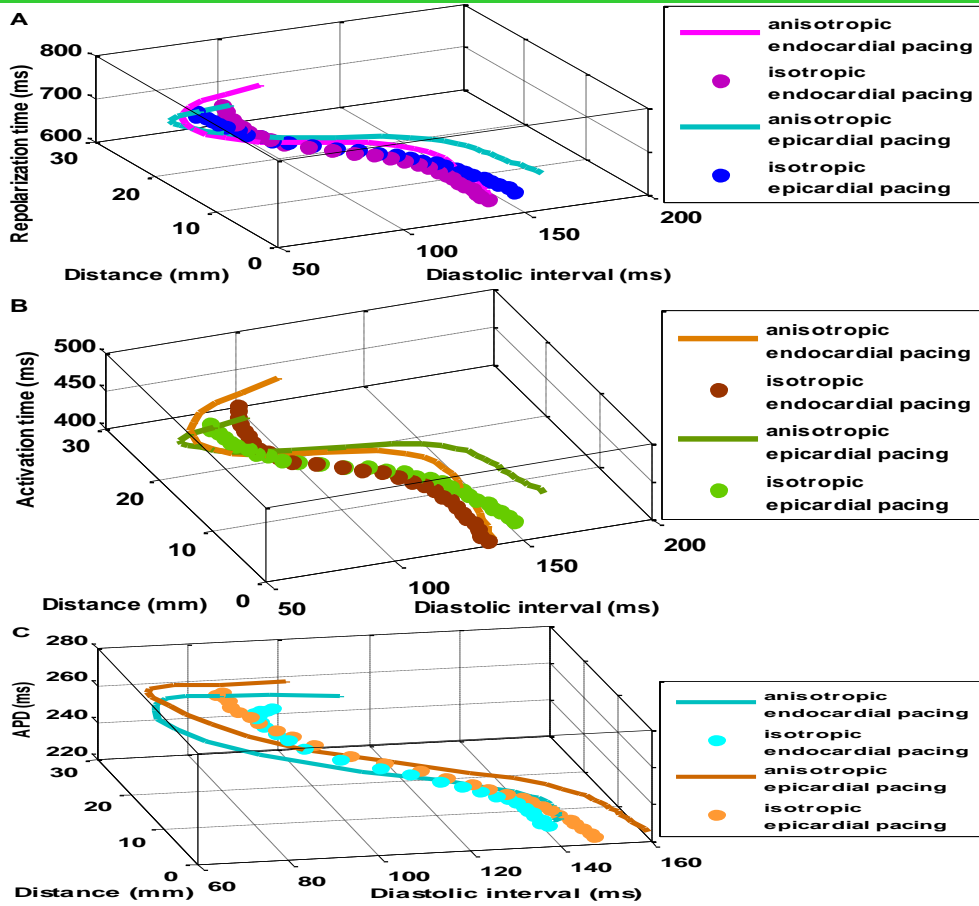


Figure 5-19: Spatial profiles of repolarization time (A); activation time (B); and APD (C)

FK4V model of isotropic & anisotropic tissue 60%Endo-30%M-10%Epi at S1S2 interval 400 ms



TP06 model of isotropic & anisotropic tissue 60%Endo-30%M-10%Epi at S1S2 interval 600 ms

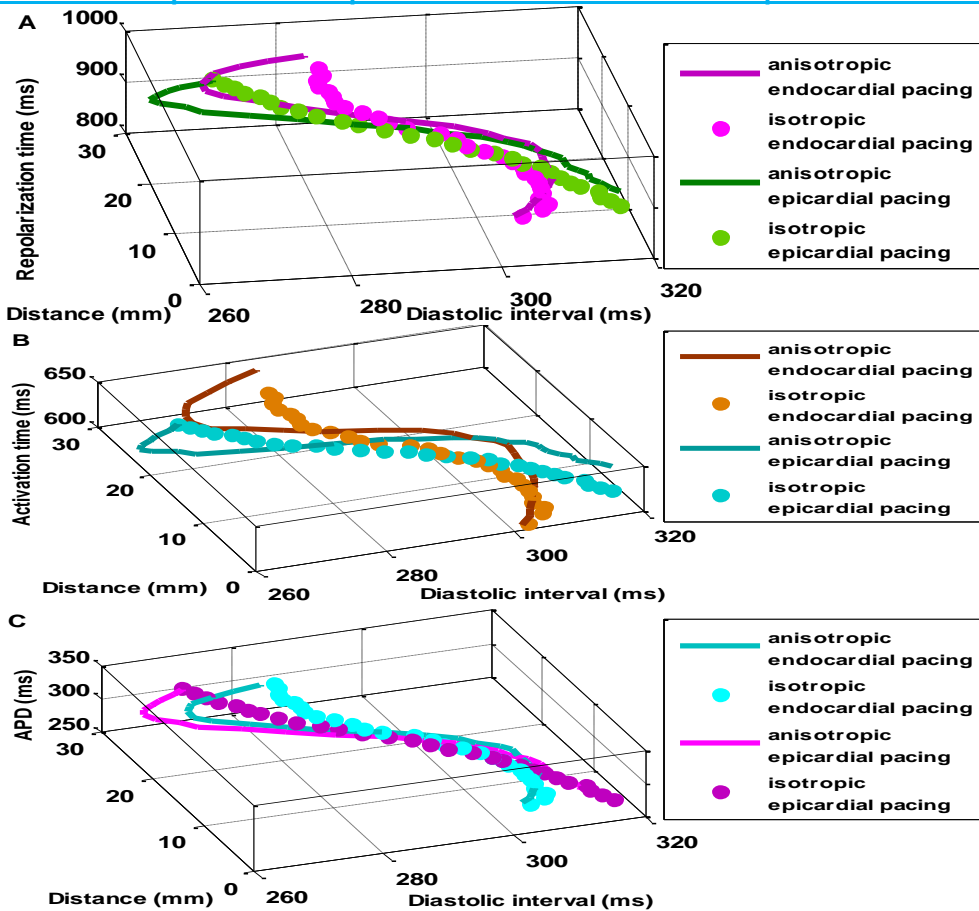
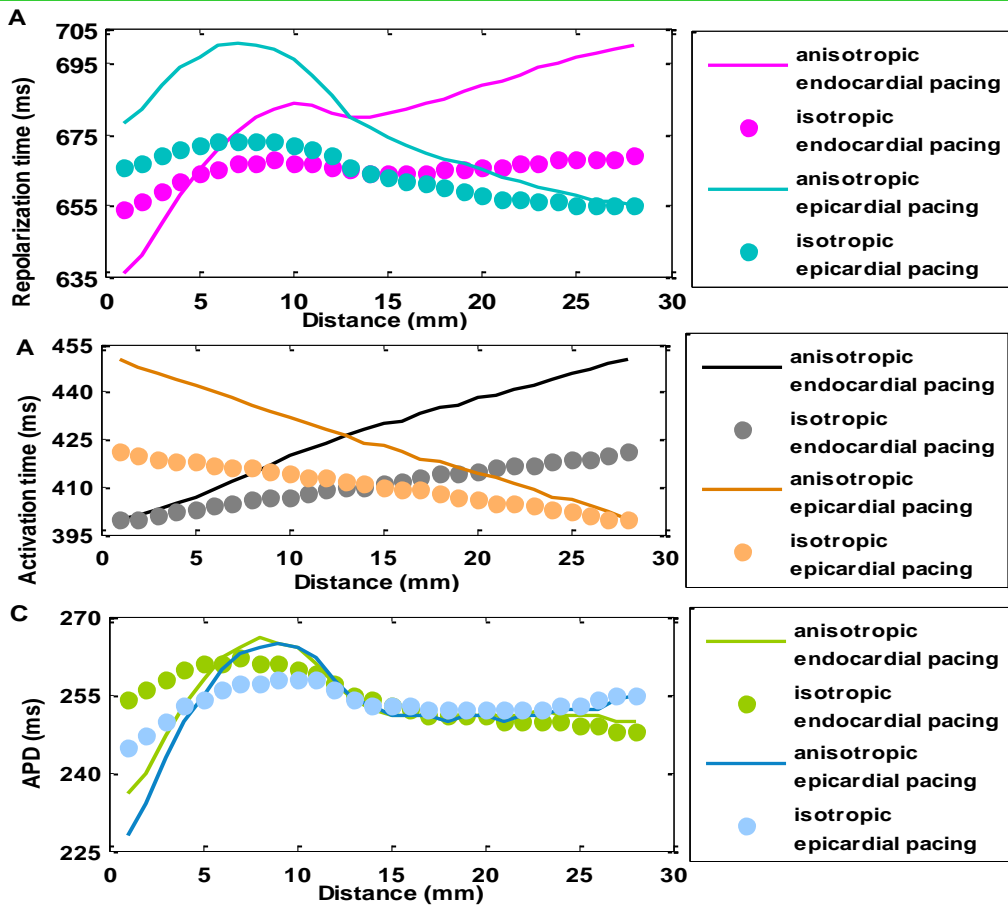


Figure 5-20: Restitution profiles of repolarization time (A); activation time (B); and APD (C)

FK4V model of isotropic & anisotropic tissue 10%Endo-30%M-60%Epi at S1S2 interval 400 ms



TP06 model of isotropic & anisotropic tissue 10%Endo-30%M-60%Epi at S1S2 interval 600 ms

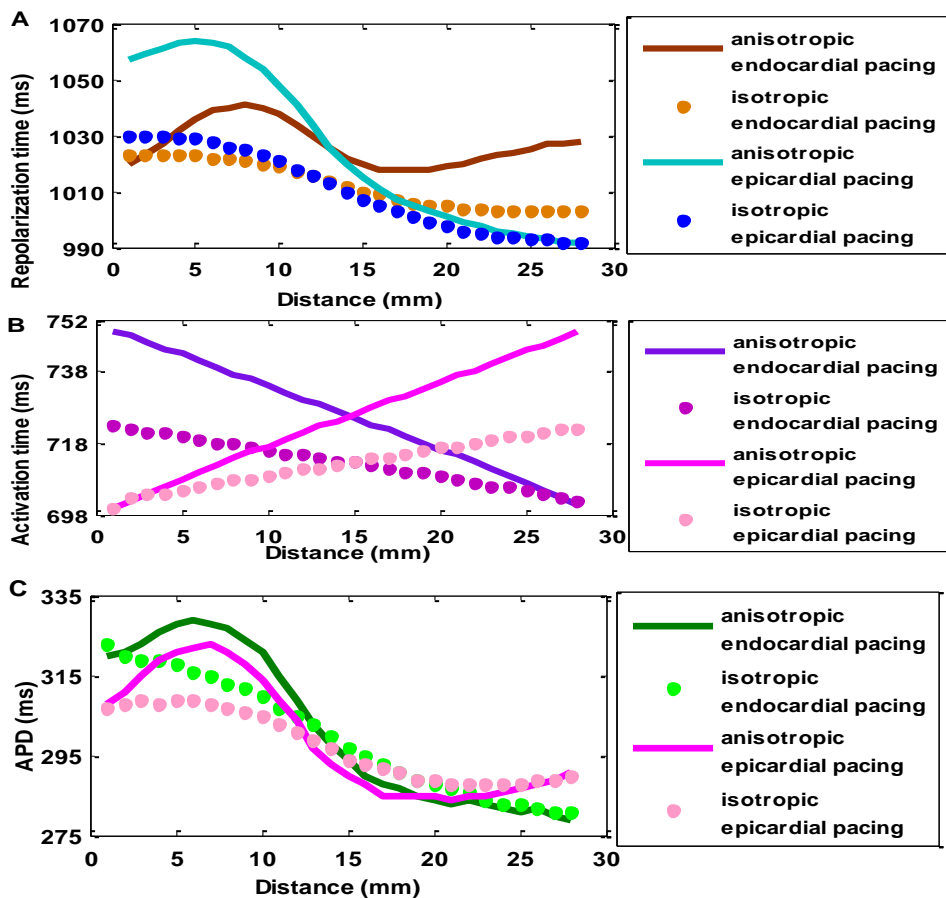
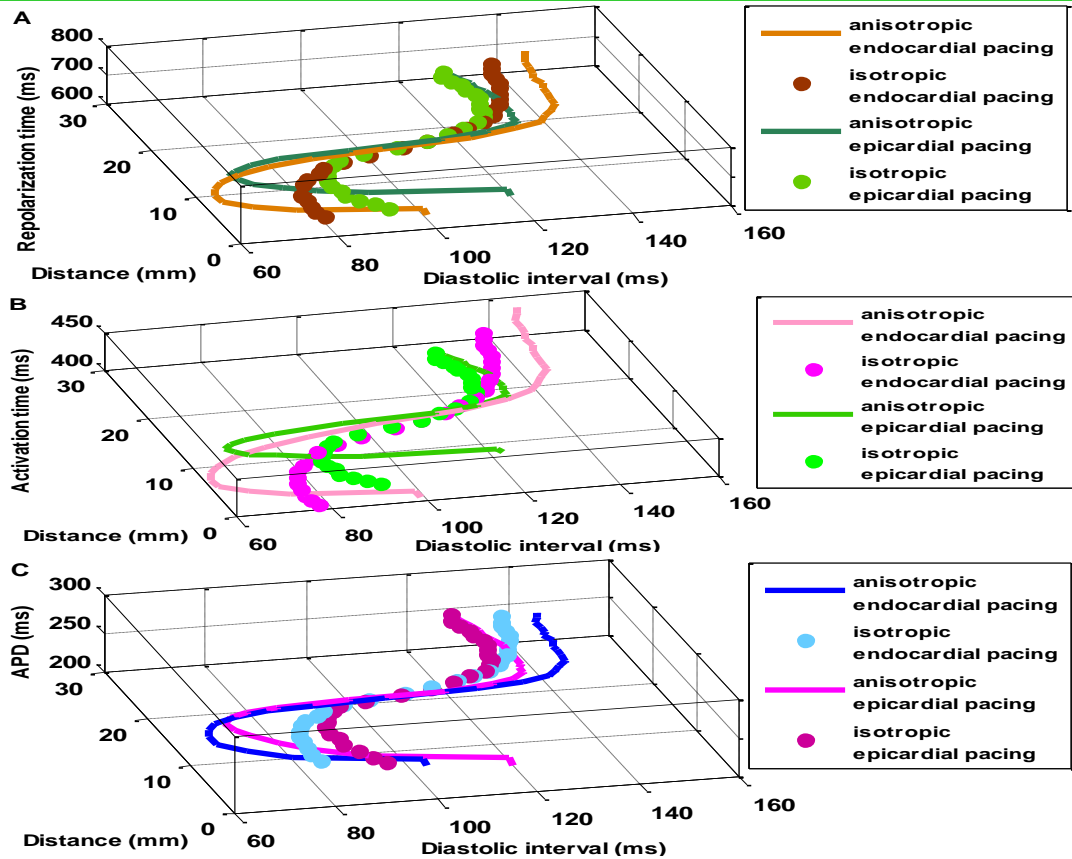


Figure 5-21: Spatial profiles of repolarization time (A); activation time (B); and APD (C)

FK4V model of isotropic & anisotropic tissue 10%Endo-30%M-60%Epi at S1S2 interval 400 ms



TP06 model of isotropic & anisotropic tissue 10%Endo-30%M-60%Epi at S1S2 interval 600 ms

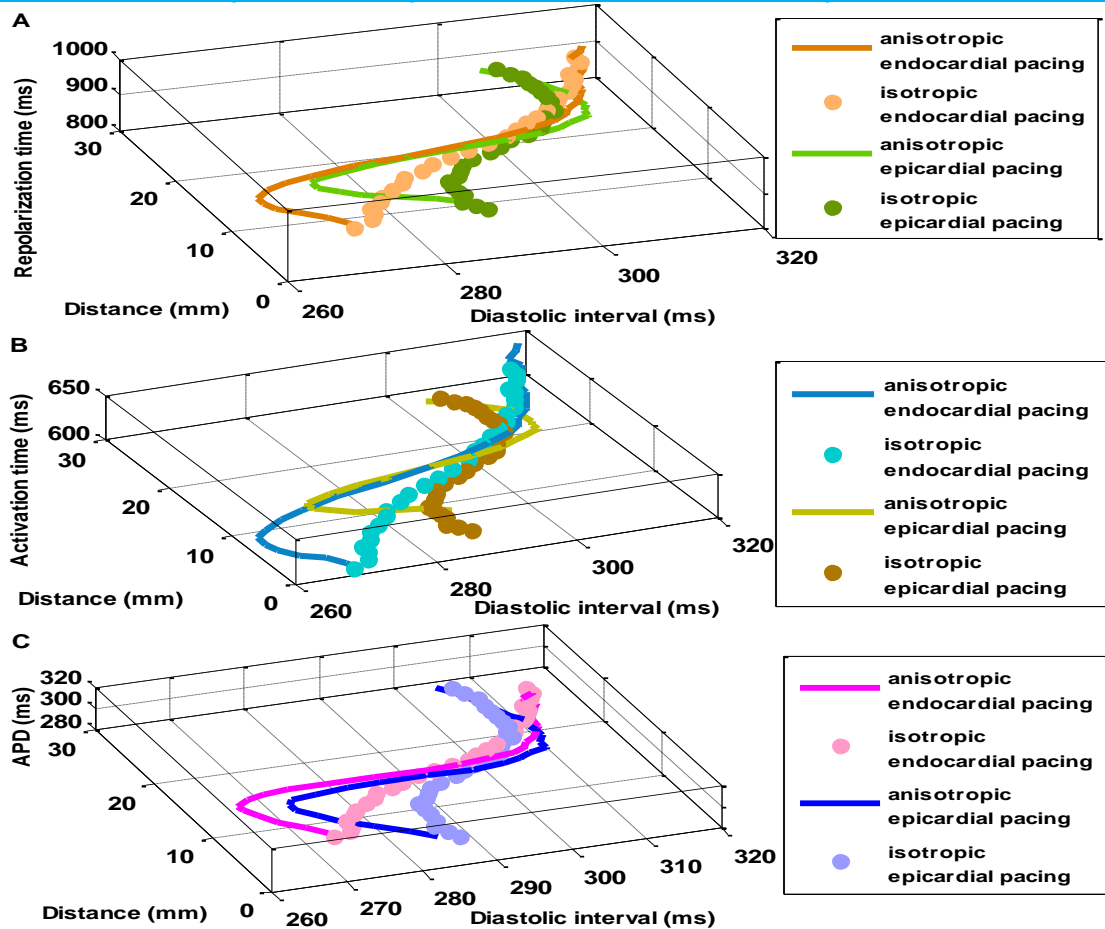


Figure 5-22: Restitution profiles of repolarization time (A); activation time (B); and APD (C)

5.2.4 Comparison with other studies

After studying the changes in spatial and restitution profiles of premature activation time, repolarization time and APD in 3D cubes of isotropic, anisotropic, and anisotropic fibrosis tissue, this part of the Chapter compares the results for premature beats in this thesis with previous experimental and simulation studies.

5.2.4-1 Quantitative comparisons

- Epicardial and endocardial properties with the TP06 model

In simulated tissues with TP06 model, APD of endocardial tissue was slightly longer than APD of epicardial tissue in agreement with many experimental studies [27]. For example, the recorded APD (at 80% repolarization) of sub-endocardial tissue by Glukhov et al. [27] was greater than APD of sub-epicardial region during diastolic intervals of 60-180 ms at slow pacing of 2000 ms in the coronary-perfused scar-free posterior-lateral left ventricular free wall wedge preparation with endocardial pacing. This was also true in the arterially perfused anterior left ventricular free wall wedge preparation in the canine heart paced from endocardial surface by Yan et al. [28] during cycle lengths of 250-2000 ms based on floating microelectrodes recording.

- Mid-myocardial properties with both models

With both FK4V and TP06 models, APD of mid-myocardial tissue was longer than APD of epicardial and endocardial tissues. This result was in agreement with experimental studies [12, 27] that provided the evidence of presence of mid-myocardial cells in the normal human hearts.

5.2.4-2 Qualitative comparisons

- A dome morphology

The mid-myocardial region of all heterogeneous tissues (isotropic, anisotropic, and anisotropic fibrosis) was characterized with a dome morphology in spatial APD profiles during a broad range of S1S2 intervals using both models similar to computational models of the human left ventricular wedge [13, 14] and a clinical and simulation study in the human hearts [29].

- Inverse relationship between activation time and APD

The inverse relationship between activation time and APD has been shown in in vivo human studies in patients with cardiomyopathy in ventricular endocardium [30], patients with preserved ventricular function without ventricular arrhythmias in the epicardial region of left ventricle (patients undergoing coronary artery bypass grafting upright T-wave) by Cowan et al. [31], patients with preserved ventricular function without ventricular arrhythmias with concordant T-wave in both epicardial and endocardial regions of left ventricle by Franz et al. [32], patients without ventricular tachycardia (positive microvolt T-wave) in the epicardial region of left ventricle and endocardial region of right ventricle by Chauhan et al. [4], and on the endocardial surfaces of normal left ventricle by Hanson et al. [33].

However, this thesis showed that this relationship is only true for homogenous tissue and for long S1S2 intervals.

In intact human hearts, the increase in APD is relatively gradual in transmural direction [34]. However, there are evidences of sharp rise in APD between ventricular layers within ventricular wall thickness in the canine wedge preparation. The spatial APD profiles for premature S2 beats in this thesis were in good agreement with a simulation study [13] (Figure 5-23) and experimental studies [35], [28], [27] (Figure 5-24).

- Example of a simulation study

Figure 5-23 show that the simulated spatial APD profiles for two anisotropic heterogeneous tissues composed of 10%Endo-30%M-60%Epi and 60%Endo-30%M-10%Epi with endocardial pacing with the FK4V model in plot A; and with the TP06 model in plot B were in agreement with APD profiles by Okada et al. [13]. They embedded the human TP06 [21] cell model into a torso model, and used an anisotropic bidomain model for propagation of excitation (explained in Chapter 3, section 3.2.3). The only difference between these curves was at the beginning and end of the curves that is possibly due to the regional difference in spatial APD profiles (explained in section 5.2.1).

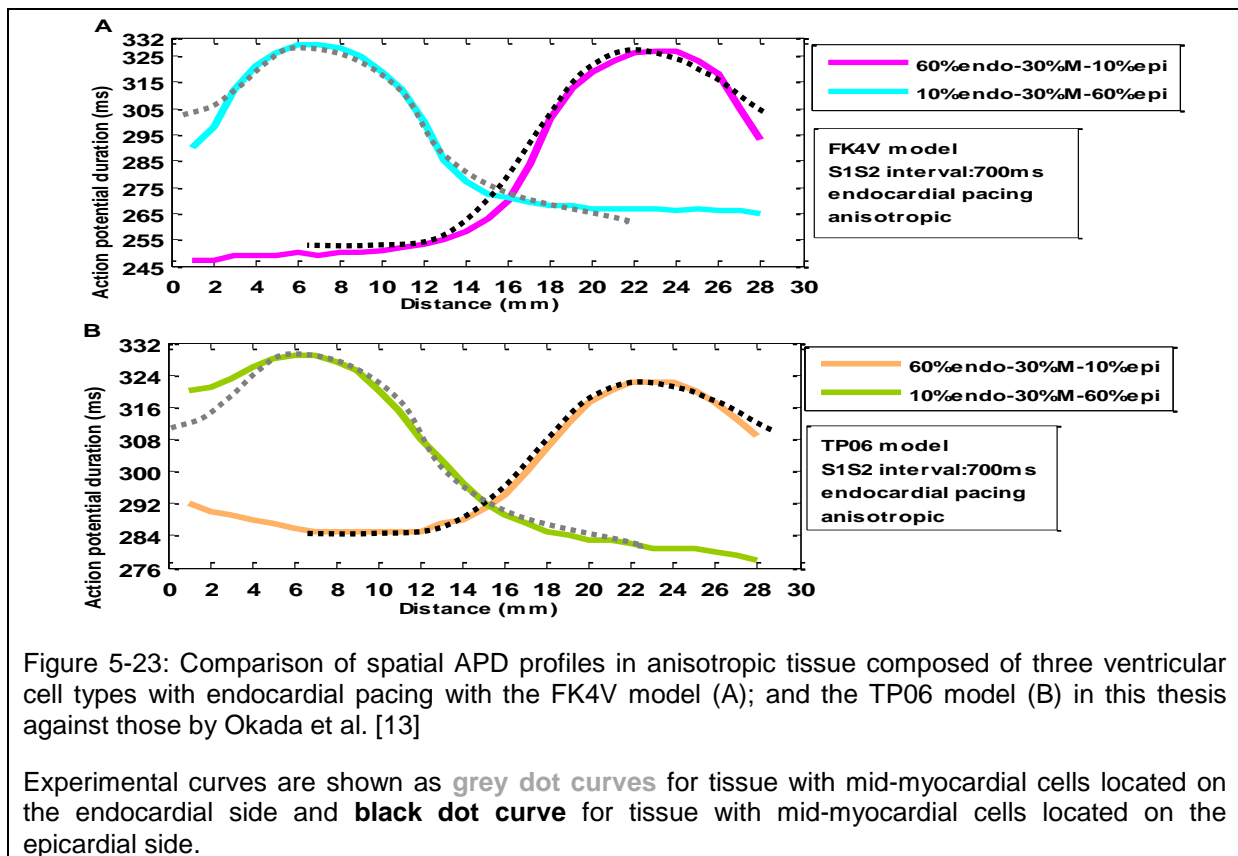


Figure 5-23: Comparison of spatial APD profiles in anisotropic tissue composed of three ventricular cell types with endocardial pacing with the FK4V model (A); and the TP06 model (B) in this thesis against those by Okada et al. [13]

Experimental curves are shown as **grey dot curves** for tissue with mid-myocardial cells located on the endocardial side and **black dot curve** for tissue with mid-myocardial cells located on the epicardial side.

- Examples of experimental studies

Increase in APD was approximately sharp between mid-myocardium and sub-epicardium in all simulated heterogonous tissues in (1) this thesis; (2) the study by Okada et al. [13]; and (3) in intact canine heart preparations by Poelzing et al. [35]. However, in arterially perfused canine left ventricular wedge preparations by Yan et al. [28], APD distribution increased sharply between the epicardium and sub-epicardium.

Figure 5-24 compares spatial APD profiles in the FK4V and the TP06 models of anisotropic tissue composed of 10%endo-30%M-60%epi with endocardial and epicardial pacing against the curve by (1) Poelzing et al. [35] at a basic cycle length 2000 ms (plots A

and C); (2) Yan et al. [28] at basic cycle length 1000 ms (plots A and C); and (3) Glukhov et al. [27] at basic cycle length 2000 ms (plots B and D).

It is important to note that the dome morphology in spatial APD profiles in the human left ventricular wedge preparation [27] corresponds to the isolated island of mid-myocardial region.

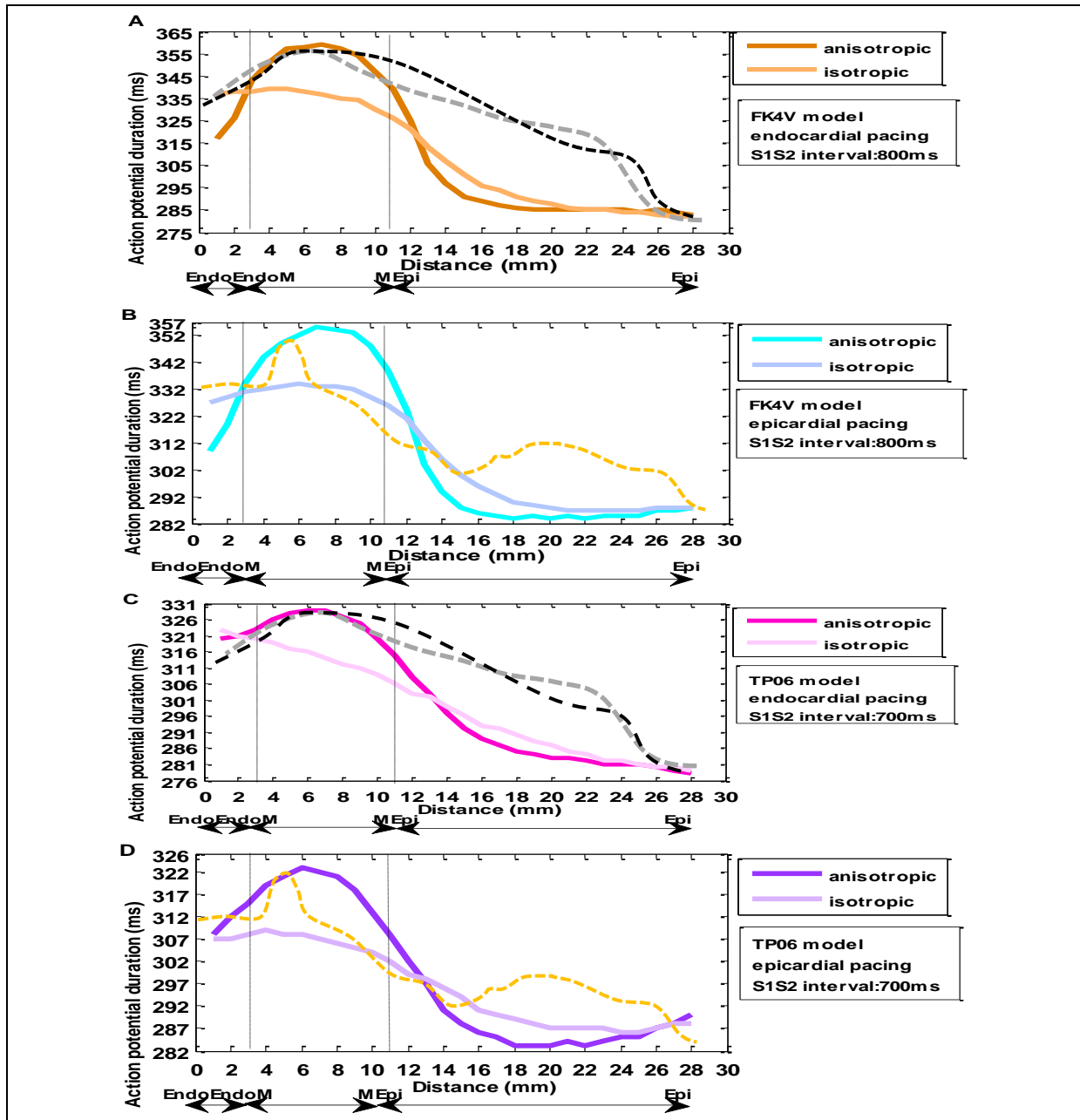


Figure 5-24: Spatial APD profiles in tissues composed of 10%Endo-30%M-60%Epi with isotropic and anisotropic diffusions with endocardial and epicardial pacing with the FK4V model (A & B); the TP06 model (C & D) in this thesis against experimental curves

Spatial APD profiles are shown as **grey dash curve** based on the Yan et al. [28] at basic cycle length of 1000 ms, as **black dash curve** based on the Poelzing et al. [35] at basic cycle length of 2000 ms, as **orange dash curve** based on the Glukhov et al. [27] at basic cycle length of 2000 ms.

5.3 Three measures of transmural dispersion

The heterogeneity in human ventricular tissue influences not only the shape but also the duration of AP during progressively decreasing S1S2 intervals. The previous section

concentrated on the changes in shape of activation time, repolarization time, and APD. This part of the Chapter evaluates three measures of dispersion in activation time, repolarization time, and APD (with precise of 1 ms) in isotropic, anisotropic, and anisotropic tissue with fibrosis. Three measures of dispersion in activation time, repolarization time, and APD in isotropic, anisotropic, and anisotropic fibrosis tissues with the FK4V and TP06 models were quantitatively different due to difference in activation time and repolarization time.

5.3.1 Dispersion in activation time

For both normal and premature beats, dispersion in activation time was the difference between the maximum and the minimum activation time at each S1S2 intervals. In homogenous tissues paced from bottom edge of tissue and heterogonous tissues with endocardial pacing, the last cell (grid point) at transmural distance had the maximum and the first cell had the minimum activation time for each S1S2 interval. For heterogeneous tissue with epicardial pacing the reverse was true. Examples of the maximum and minimum activation time in the FK4V model of anisotropic tissue composed of 50%endo-50%epi with endocardial and epicardial pacing are shown in Figure 5-25, plot A. The profiles of measures of dispersion in activation time against S1S2 interval is shown in plot B.

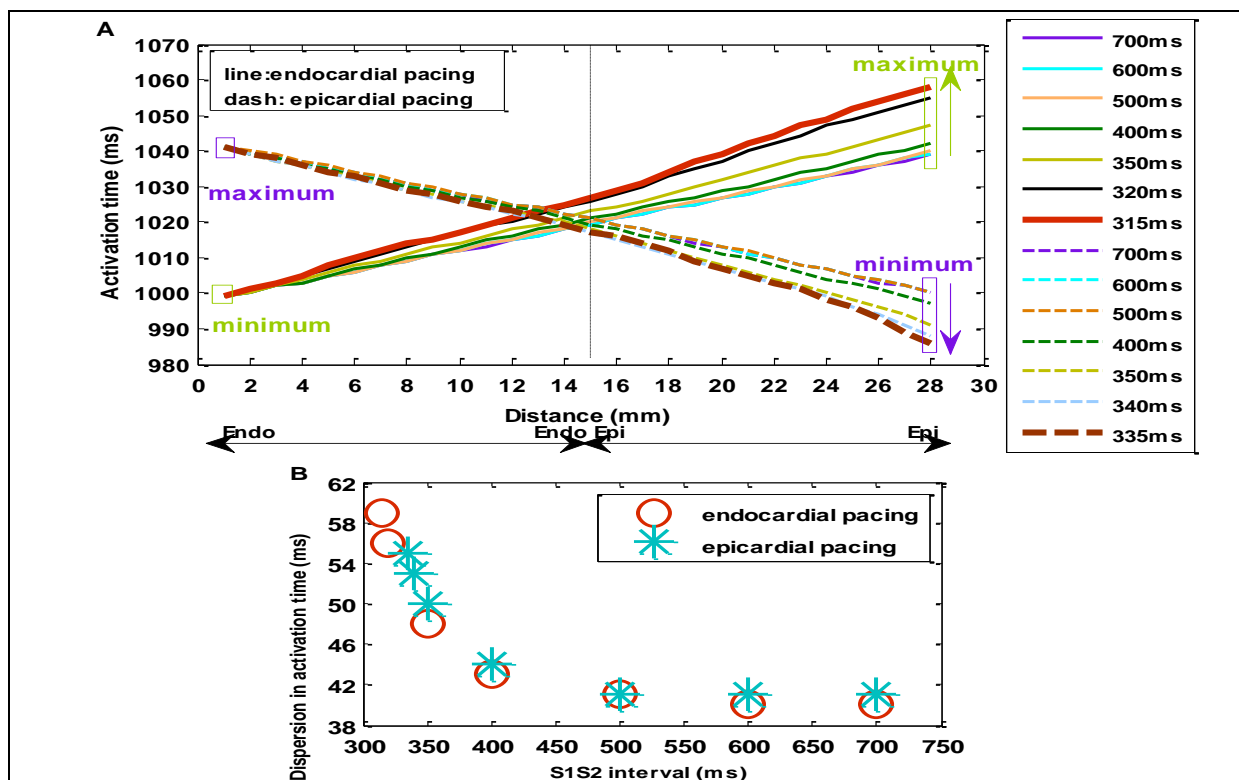


Figure 5-25: Spatial profiles of activation time (A); and profiles of dispersion in activation time against S1S2 interval (B) in the FK4V model of anisotropic tissue composed of 50%endo-50%epi with endocardial and epicardial pacing

The maximum and the minimum activation time at the last and first grid points are shown as green rectangles for endocardial pacing and violet rectangles for epicardial pacing. Arrows show that the maximum activation time increases with endocardial pacing and the minimum activation time decreases with epicardial pacing.

In plot A, the thick line and dash show the activation time that have the largest dispersion in activation time at S1S2 interval of 315 ms with endocardial pacing and S1S2 interval of 335 ms with epicardial pacing as shown in plot B.

5.3.1-1 Quantitative comparison between normal and premature beats

Measures of dispersion in activation time changed slightly around 1 ms for normal S1 beats (Table 5-1) but greatly around 1 ms to 42 ms for premature S2 beats (Table 5-2) during decreasing S1S2 intervals in all 3D cubes of tissue using the FK4V and TP06 models.

Measures of dispersion in activation time for normal S1 beats in ms in 3D cubes of tissue during decreasing S1S2 intervals (S1S2) in ms			
	Isotropic (S1S2 intervals)	Anisotropic (S1S2 intervals)	Anisotropic fibrosis (S1S2 intervals)
100%Epi Pacing from the bottom edge of tissue, FK4V model	16-17 (S1S2 700-345)	40-41 (S1S2 700-335)	37-38 (S1S2 700-340)
TP06 model	21 (S1S2 700-495)	47-48 (S1S2 700-345)	45-46 (S1S2 700-390)
100%Endo Pacing from the bottom edge of tissue, FK4V model	15-16ms (S1S2 700-315)	38-39ms (S1S2 700-315)	34-35 (S1S2 700-300)
TP06 model	21 (S1S2 700-495)	47 (S1S2 700-345)	45-46 (S1S2 700-390)
100%M Pacing from the bottom edge of tissue, FK4V model	14 (S1S2 700-460)	36-37 (S1S2 700-455)	33 (S1S2 700-475)
TP06 model	21 (S1S2 700-560)	47-48 (S1S2 700-430)	45-46 (S1S2 700-470)
50%Endo-50%Epi Endocardial pacing, FK4V model	16 (S1S2 700-310)	39-40 (S1S2 700-315)	35-36 (S1S2 700-315)
TP06 model	21 (S1S2 700-495)	47-48 (for 700-345)	45-46 (S1S2 700-390)
50%Endo-50%Epi Epicardial pacing, FK4V model	16-17 (S1S2 700-345)	40 (S1S2 700-335)	35-36 (S1S2 700-335)
TP06 model	21 (S1S2 700-495)	47-48 (S1S2 700-345)	44-45 (S1S2 700-355)
15%Endo-55%M-30%Epi Endocardial pacing, FK4V model	15 (S1S2 700-380)	37-38 (S1S2 700-420)	34-35 (S1S2 700-425)
TP06 model	21 (S1S2 700-530)	47-48 (S1S2 700-365)	45-46 (S1S2 700-415)
15%Endo-55%M-30%Epi Epicardial pacing, FK4V model	15 (S1S2 700-380)	38-39 (S1S2 700-420)	34 (S1S2 700-425)
TP06 model	21 (S1S2 700-515)	47-48 (S1S2 700-360)	44-45 (S1S2 700-355)
10%Endo-30%M-60%Epi Endocardial pacing, FK4V model	15-16 (S1S2 700-370)	38-39 (S1S2 700-390)	34 (S1S2 700-405)
TP06 model	21 (S1S2 700-540)	47-48 (S1S2 700-380)	45-46 (S1S2 700-430)
10%Endo-30%M-60%Epi Epicardial pacing, FK4V model	16-17 (S1S2 700-360)	39 (for 700-390)	34 (S1S2 700-395)
TP06 model	21 (S1S2 700-495)	47-48 (S1S2 700-345)	44-45 (S1S2 700-355)
60%Endo-30%M-10%Epi Endocardial pacing, FK4V model	15 (S1S2 700-350)	37 (for 700-390)	35-36 (S1S2 700-400)
TP06 model	21 (S1S2 700-500)	47-48 (S1S2 700-345)	45-46 (S1S2 700-390)
60%Endo-30%M-10%Epi Epicardial pacing, FK4V model	15-16 (S1S2 700-390)	38 (S1S2 700-395)	35 (S1S2 700-400)
TP06 model	21 (S1S2 700-540)	47-48 (S1S2 700-380)	44-45 (S1S2 700-400)

Table 5-1: Measures of dispersion in activation time for normal S1 beats during decreasing S1S2 intervals (S1S2) with the FK4V and the TP06 models

Measures of dispersion in activation time for premature S2 beats in ms in 3D cubes of tissue during decreasing S1S2 intervals (S1S2) in ms			
	Isotropic (S1S2 intervals)	Anisotropic (S1S2 intervals)	Anisotropic fibrosis (S1S2 intervals)
100%Epi Pacing from the bottom edge of tissue, FK4V model	17-25 (S1S2 700-345)	41-58 (S1S2 700-335)	38-60 (S1S2 700-340)
TP06 model	21-25 (S1S2 700-495)	48-72 (S1S2 700-345)	47-57 (S1S2 700-390)
100%Endo Pacing from the bottom edge of tissue, FK4V model	16-24 (S1S2 700-315)	39-51 (S1S2 700-315)	35-59 (S1S2 700-300)
TP06 model	21-23 (S1S2 700-495)	48-74 (S1S2 700-345)	47-57 (S1S2 700-390)
100%M Pacing from the bottom edge of tissue, FK4V model	15-24 (S1S2 700-460)	37-56 (S1S2 700-455)	34-52 (S1S2 700-475)
TP06 model	22-25 (S1S2 700-560)	48-72 (S1S2 700-430)	47-57 (S1S2 700-470)
50%Endo-50%Epi Endocardial pacing, FK4V model	17-31 (S1S2 700-310)	40-59 (S1S2 700-315)	36-63 (S1S2 700-315)
TP06 model	21-23 (S1S2 700-495)	48-73 (S1S2 700-345)	47-58 (S1S2 700-390)
50%Endo-50%Epi Epicardial pacing, FK4V model	17-24 (S1S2 700-345)	41-55 (S1S2 700-335)	36-56 (S1S2 700-335)
TP06 model	21-22 ms (for 700-495 ms)	48-71 (S1S2 700-345)	44-54 (S1S2 700-390) 46-49 (S1S2 385-355)
15%Endo-55%M-30%Epi Endocardial pacing, FK4V model	16-35 (S1S2 700-380)	38-53 (S1S2 700-420)	35-59 (S1S2 700-425)
TP06 model	21-23 (S1S2 700-530)	48-90 (S1S2 700-365)	47-62 (S1S2 700-415)
15%Endo-55%M-30%Epi Epicardial pacing, FK4V model	16-34 (S1S2 700-380)	39-53 (S1S2 700-420)	35-53 (S1S2 700-425)
TP06 model	21-22 (S1S2 700-515)	48-92 (S1S2 700-360)	45-66 (S1S2 700-390) 61-75 (S1S2 380-355)
10%Endo-30%M-60%Epi Endocardial pacing, FK4V model	16-32 (S1S2 700-370)	40-58 (S1S2 700-395)	36-63 (S1S2 700-405)
TP06 model	21-23 (S1S2 700-540)	48-72 (S1S2 700-380)	47-55 ms (for 700-430 ms)
10%Endo-30%M-60%Epi Epicardial pacing, FK4V model	17-36 (S1S2 700-360)	40-55 (S1S2 700-395)	36-57 (S1S2 700-395)
TP06 model	21-22 (S1S2 700-495)	48-55 (S1S2 700-420) 57-83 (S1S2 410-345)	47-57 (S1S2 700-400) 51-57 (S1S2 380-355)
60%Endo-30%M-10%Epi Endocardial pacing, FK4V model	16-24 (S1S2 700-350)	38-48 (S1S2 700-390)	35-51 (S1S2 700-400)
TP06 model	22-23 (S1S2 700-500)	48-84 (S1S2 700-345)	47-63 (S1S2 700-390)
60%Endo-30%M-10%Epi Epicardial pacing, FK4V model	16-25 (S1S2 700-390)	39-56 (S1S2 700-395)	35-65 (S1S2 700-400)
TP06 model	21-22 (S1S2 700-540)	48-55 (S1S2 700-440) 54-68 (S1S2 435-380)	44-54 (S1S2 700-430) 43-46 (S1S2 425-400)

Table 5-2: Measures of dispersion in activation time for premature S2 beats with the FK4V and the TP06 models

5.3.1-2 Profiles of dispersion in activation time for premature beats

Figure 5-26 to Figure 5-28 show that for all homogenous and heterogeneous tissues, measures of dispersion in activation time for premature S2 beats

- gradually increased during decreasing S1S2 intervals;
- with the TP06 model were greater than those with the FK4V model;
- were slightly smaller in anisotropic tissue with fibrosis than without fibrosis;
- had the smallest value for long S1S2 intervals (i.e. 700 ms) and the largest value at the shortest S1S2 interval (varied for each tissue with different cellular configuration).

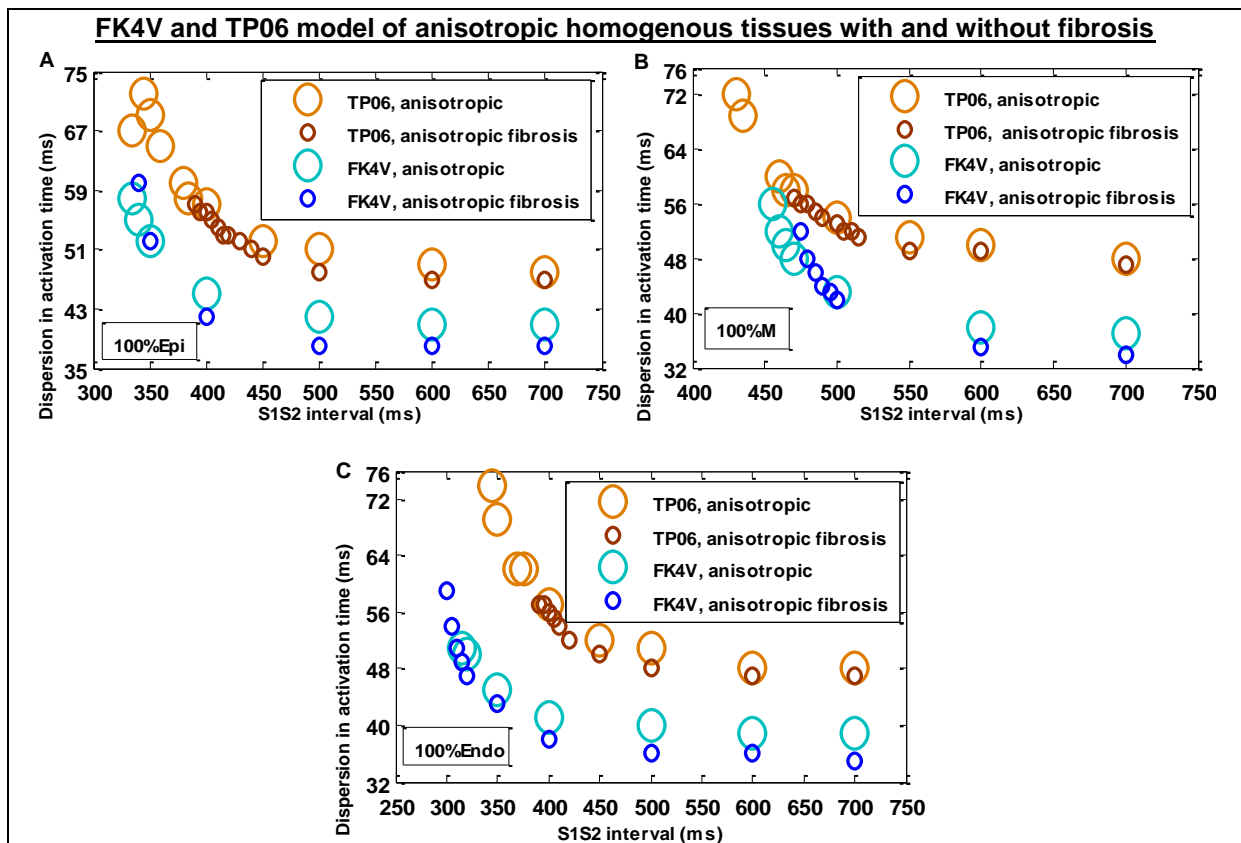


Figure 5-26: Profiles of dispersion in activation time in anisotropic homogenous epicardial (A); mid-myocardial (B); and endocardial (C) tissues with and without fibrosis with both models

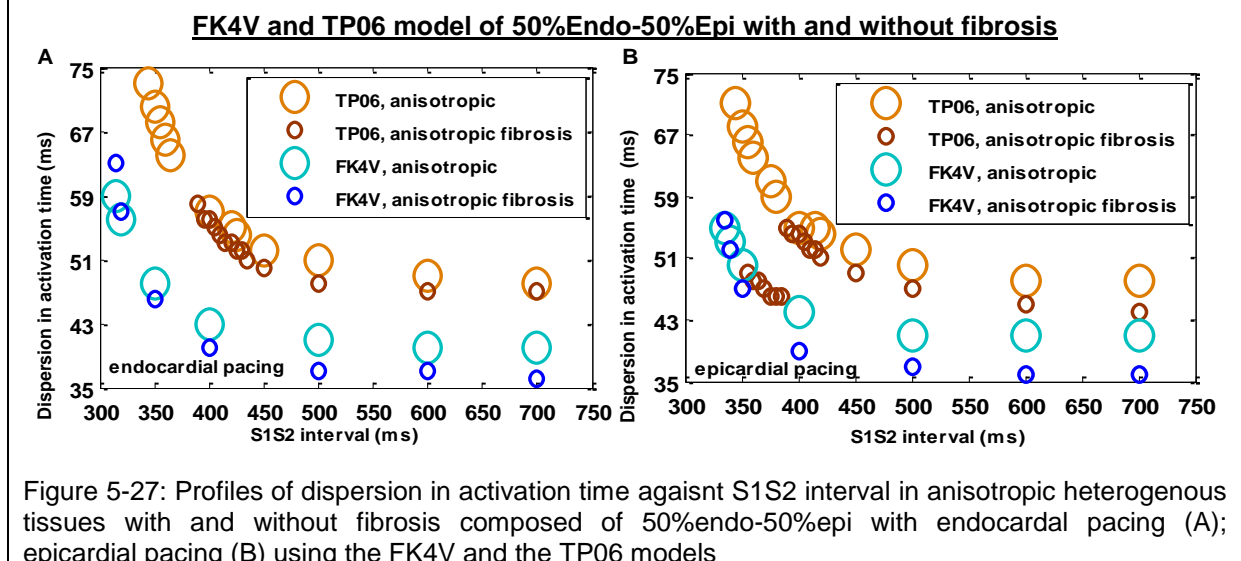
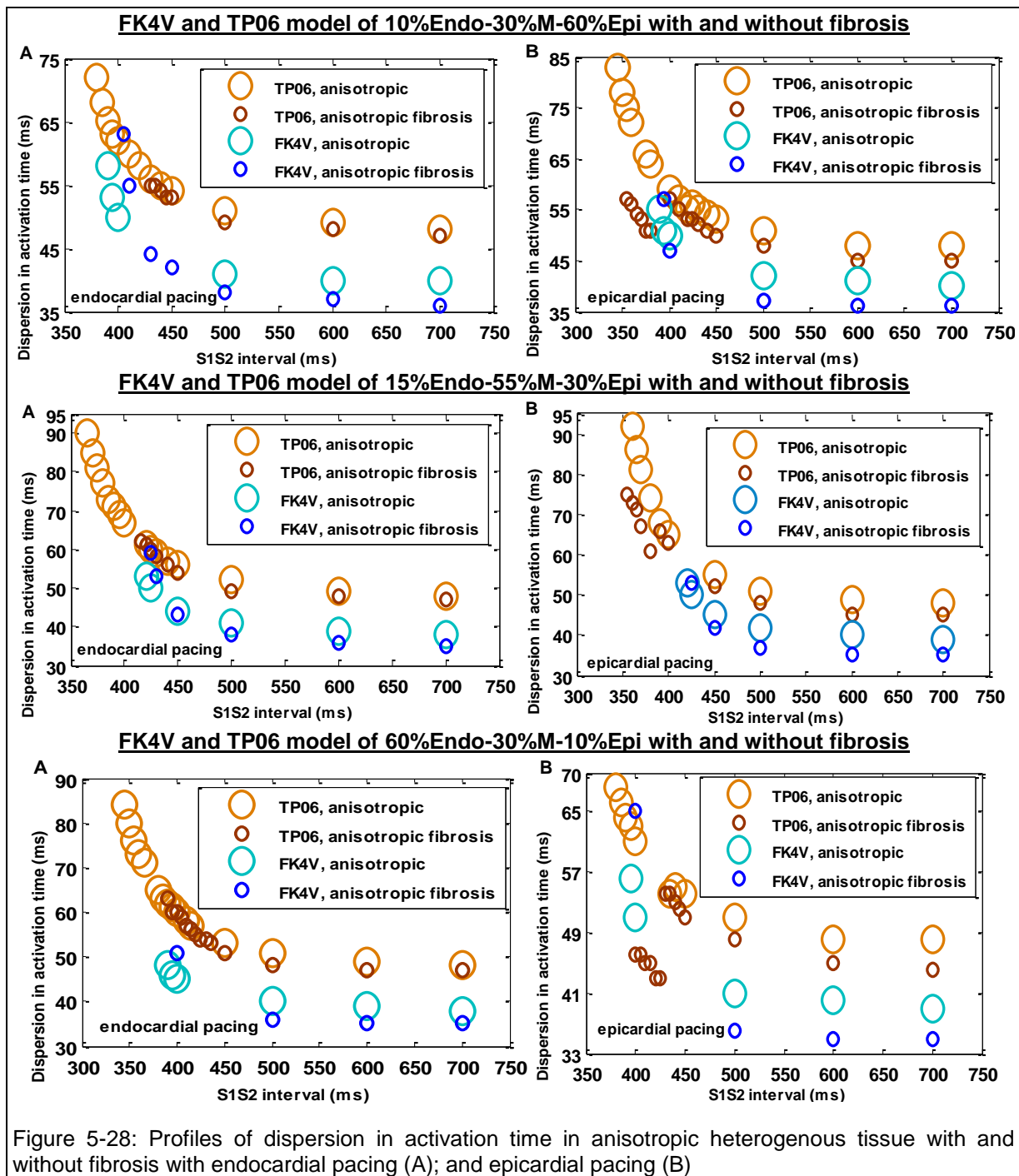


Figure 5-27: Profiles of dispersion in activation time against S1S2 interval in anisotropic heterogeneous tissues with and without fibrosis composed of 50%endo-50%epi with endocardial pacing (A); epicardial pacing (B) using the FK4V and the TP06 models



5.3.1-3 The largest and the smallest dispersion

After studying how measures of dispersion in activation time change during decreasing S1S2 intervals for both normal and premature beats, it was interesting to study the changes at the smallest and the largest measures of dispersion in activation time for premature S2 beats. Among long and short S1S2 intervals,

- the smallest dispersion in activation time was the smallest value of calculated dispersion in activation time (usually at S1S2 interval of 700 ms);
- the largest dispersion in activation time was the largest value of calculated dispersion in activation time (usually at the last S1S2 interval that was different among tissues).

Summary Figure 5-29 shows these numerical values for three groups of tissue including (1) isotropic tissues; (2) anisotropic tissues without fibrosis; and (3) anisotropic tissues with

fibrosis using the FK4V and TP06 models based on different activation dynamics. The comparison was between two groups of anisotropic and isotropic tissues as well as two groups of anisotropic tissues with and without fibrosis.

1. Anisotropic tissue compared with isotropic tissue using the FK4V model

Anisotropic diffusion compared with isotropic diffusion increased the smallest dispersion in activation time to around 18 ms to 24 ms and the largest activation time dispersion around 18 ms to 33 ms in all tissues.

For example, the largest dispersion in activation time for anisotropic epicardial tissue (58 ms) compared with isotropic epicardial tissue paced from the bottom edge of tissue (25 ms) had an increase around 33 ms, plot A.

2. Anisotropic tissue compared with isotropic tissue using the TP06 model

Anisotropic diffusion compared with isotropic diffusion increased the smallest dispersion in activation time to around 26 ms to 27 ms and the largest activation time dispersion to around 46 ms to 70 ms in all tissues.

For example, the largest dispersion in activation time for anisotropic tissue composed of 15%Endo-55%M-30%Epi with epicardial pacing (92 ms) compared with the isotropic tissue (22 ms) increased around 70 ms, plot A1.

3. Anisotropic tissue with fibrosis compared with anisotropic tissue without fibrosis using the FK4V model

Anisotropic tissue with fibrosis compared with anisotropic tissue decreased the smallest activation time dispersion to around 3 ms to 5 ms in all tissues.

On the other hand, anisotropic tissue with fibrosis compared with anisotropic tissue without fibrosis increased the largest activation time dispersion to approximately 2 ms to 9 ms in some tissues, i.e. an increase of 2 ms for homogenous epicardial tissue paced from the bottom edge of tissue. However, anisotropic mid-myocardial tissue with fibrosis (52 ms) compared with anisotropic tissue without fibrosis (56 ms) paced from the bottom edge of tissue decreased the largest value of dispersion in activation time to around 4 ms, plot A.

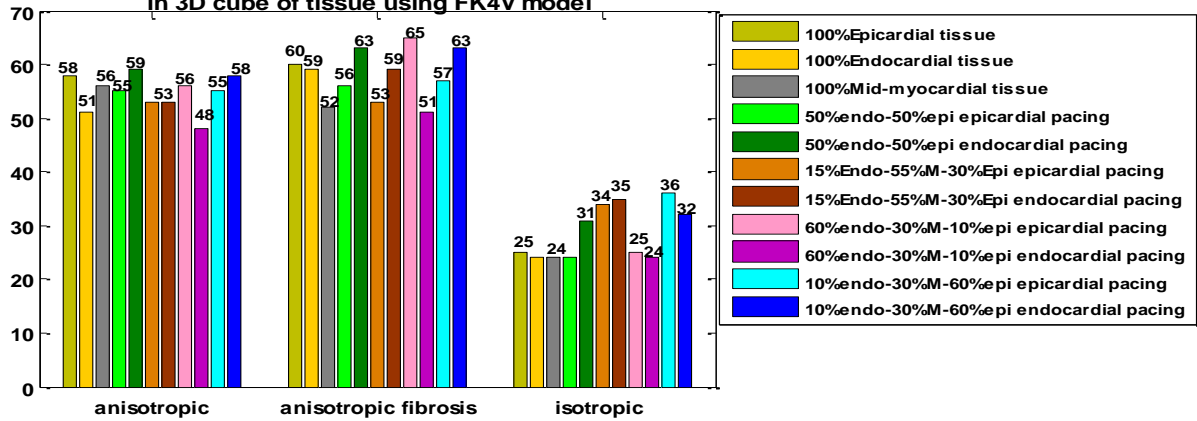
4. Anisotropic tissue with fibrosis compared with anisotropic tissue without fibrosis using the TP06 model

Anisotropic tissue with fibrosis compared with anisotropic tissue decreased the smallest activation time dispersion to around 1 ms to 5 ms and the largest activation time dispersion approximately 14 ms to 28 ms in all tissues.

For example, the largest dispersion in activation time for anisotropic fibrosis tissue composed of 15%Endo-55%M-30%Epi with endocardial pacing (62 ms) compared with anisotropic tissue without fibrosis (90 ms) had a decrease around 28 ms, plot A1.

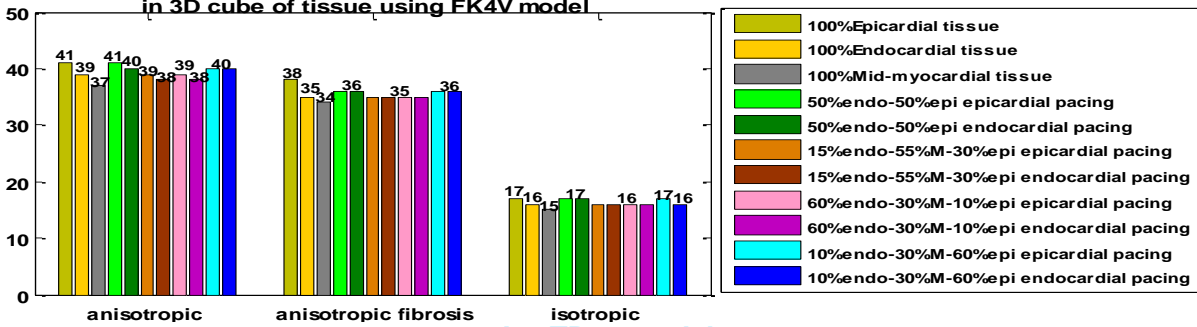
A. FK4V model

The largest value of the activation time dispersion in 3D cube of tissue using FK4V model



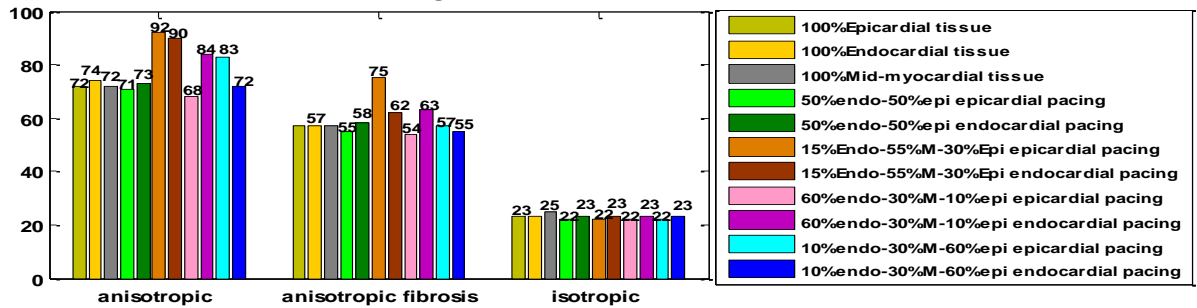
B. FK4V model

The smallest value of the activation time dispersion in 3D cube of tissue using FK4V model



A1. TP06 model

The largest value of the activation time dispersion in 3D cube of tissue using TP06 model



B1. TP06 model

The smallest value of the activation time dispersion in 3D cube of tissue using TP06 model

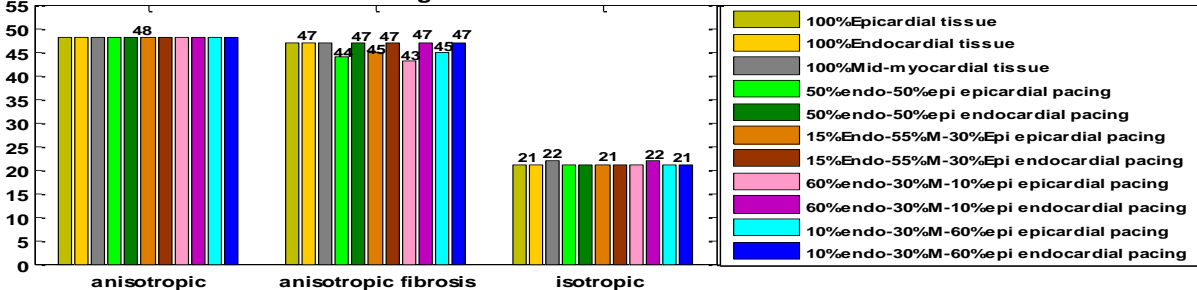


Figure 5-29: The largest and the smallest measures of dispersion in activation time for premature S2 beat in 3D cubes of isotropic, anisotropic, and anisotropic fibrosis tissue with the FK4V model (A & B); and the TP06 model (A1 & B1)

5.3.2 Dispersion in repolarization time

For normal and premature beats, dispersion in repolarization time as the difference between the maximum and the minimum repolarization time at each S1S2 interval.

5.3.2-1 Quantitative comparison

During decreasing S1S2 intervals, measures of dispersion in repolarization time changed around 1 ms to 6 ms for normal beats (Table 5-3), but 1 ms to 58 ms for premature S2 beats (Table 5-4) in isotropic, anisotropic, and anisotropic fibrosis tissues with two models.

Measures of dispersion in repolarization time for normal S1 beats in ms in 3D cubes of tissue during decreasing S1S2 intervals (S1S2) in ms			
	Isotropic (S1S2 intervals)	Anisotropic (S1S2 intervals)	Anisotropic fibrosis (S1S2 intervals)
FK4V model of 100%Epi Pacing from the bottom edge of tissue,	11 (S1S2 700-345)	34-35 (S1S2 700-335)	30 (S1S2 700-340)
TP06 model	9 (S1S2 700-495)	35-36 (S1S2 700-345)	31 (700-390)
FK4V model of 100%Endo Pacing from the bottom edge of tissue,	9 (S1S2 700-315)	30-31 (S1S2 700-315)	26 (S1S2 700-300)
TP06 model	9 (S1S2 700-495)	34-35 (S1S2 700-345)	30-31 (S1S2 700-390)
FK4V model of 100%M Pacing from the bottom edge of tissue,	7-8 (S1S2 700-460)	27-28 (S1S2 700-455)	24 (S1S2 700-475)
TP06 model	8-9 (S1S2 700-560)	33-34 (S1S2 700-430)	29-30 (S1S2 700-470)
50%Endo-50%Epi Endocardial pacing, FK4V model	21ms (S1S2 700-310)	45-46 (S1S2 700-315)	41-42 (S1S2 700-315)
TP06 model	8-9 (S1S2 700-495)	33-34 (S1S2 700-345)	29-30 (S1S2 700-390)
50%Endo-50%Epi Epicardial pacing, FK4V model	2-3 (S1S2 700-345)	19-20 (S1S2 700-335)	14-15 (S1S2 700-335)
TP06 model	10 (S1S2 700-495)	36-37 (S1S2 700-345)	32-33 (S1S2 700-355)
15%Endo-55%M-30%Epi Endocardial pacing, FK4V model	57-58 (S1S2 700-380)	108-109 (S1S2 700-420)	94-95 (S1S2 700-425)
TP06 model	23-26 (S1S2 700-530)	62-66 (S1S2 700-365)	53-5 (S1S2 700-415)
15%Endo-55%M-30%Epi Epicardial pacing, FK4V model	70 (S1S2 700-380)	117-118 (S1S2 700-420)	113-114 (S1S2 700-425)
TP06 model	38-40 (S1S2 700-515)	83-89 (S1S2 700-360)	80-84 (S1S2 700-355)
10%Endo-30%M-60%Epi Endocardial pacing, FK4V model	42-43 (S1S2 700-370)	57-58 (S1S2 700-390)	59 (S1S2 700-405)
TP06 model	24-26 (S1S2 700-540)	26-30 (S1S2 700-380)	28-32 (S1S2 700-430)
10%Endo-30%M-60%Epi Epicardial pacing, FK4V model	59-60 (S1S2 700-360)	99 (S1S2 700-390)	96 (S1S2 700-395)
TP06 model	24-26 (S1S2 700-495)	74-78 (S1S2 700-345)	71-75 (S1S2 700-355)
60%Endo-30%M-10%Epi Endocardial pacing, FK4V model	62-63 (S1S2 700-350)	108 (S1S2 700-390)	107 (S1S2 700-400)
TP06 model	39-42 (S1S2 700-500)	72-76 (S1S2 700-345)	72-76 (S1S2 700-390)
60%Endo-30%M-10%Epi Epicardial pacing, FK4V model	47 (S1S2 700-390)	66ms (S1S2 700-395)	69 (S1S2 700-400)
TP06 model	23-26 (S1S2 700-540)	25-28 (S1S2 700-380)	27-32 (S1S2 700-400)

Table 5-3: Measures of dispersion in repolarization time for normal S1 beats with both models

Measures of dispersion in repolarization time for premature S2 beats in ms in 3D cubes of tissue during decreasing S1S2 intervals (S1S2) in ms			
	Isotropic (S1S2 intervals)	Anisotropic (S1S2 intervals)	Anisotropic fibrosis (S1S2S1S2 intervals)
FK4V model of 100%Epi Pacing from the bottom edge of tissue	11-16 (S1S2 700-345)	34-52 (S1S2 700-335)	30-44 (S1S2 700-340)
TP06 model	10-11 (S1S2 700-495)	35-36 (S1S2 700-345)	31-44 (S1S2700-390)
FK4V model of 100%Endo Pacing from the bottom edge of tissue	9-13 (S1S2 700-315)	30-40 (S1S2 700-315)	26-41 (S1S2 700-300)
TP06 model	9-10 (S1S2700-495)	34-35 (S1S2 700-345)	31-44 (S1S2 700-390)
FK4V model of 100%M Pacing from the bottom edge of tissue	8-11 (S1S2 700-460)	29-42 (S1S2 700-455)	24-39 (S1S2 700-475)
TP06 model	9-10 (S1S2 700-560)	33-34 (S1S2 700-430)	30-42 (S1S2 700-470)
50%Endo-50%Epi Endocardial pacing FK4V model	24-34 (S1S2 700-400) 28-21 (S1S2 350-315)	49-60 (S1S2 700-400) 57-58 (S1S2 350-315)	45-65 (S1S2 700-315)
TP06 model	9 (S1S2 700-495)	34-60 (S1S2 700-345)	30-42 (S1S2 700-390)
50%Endo-50%Epi Epicardial pacing, FK4V model	5-12 (S1S2 700-500) 11-3 (S1S2 400-45)	16-9 (S1S2 700-500) 11-32 (S1S2 400-335)	12-9 (S1S2 700-600) 10-23 (S1S2 500-335)
TP06 model	11-12 (S1S2 700-495)	37-62 (S1S2 700-345)	32-44 (S1S2 700-390) 42-47 (S1S2 385-360)
15%Endo-55%M-30%Epi Endocardial pacing, FK4V model	47-34 (S1S2 700-500) 35-47 (S1S2 425-380)	100-70 (S1S2 700-50) 72-75 (S1S2 425-420)	84-68 (S1S2 700-450) 77-87 (S1S2 425-420)
TP06 model	19-22 (S1S2 700-530)	60-52 (S1S2 700-440) 53-83 (S1S2 430-365)	52-47 (S1S2 700-440) 49-52 (S1S2 430-415)
15%Endo-55%M-30%Epi Epicardial pacing FK4V model	60-22 (S1S2 700-420) 21-24 (S1S2 400-380)	103-45 (S1S2 700-50) 43-45 (S1S2 425-420)	93-43 (S1S2 700-450) 48 at S1S2 425
TP06 model	33-37 (S1S2 700-515)	81-82 (S1S2 700-600) 67-109 (S1S2 450-60)	77-64 (S1S2 700-450) 67-93 (S1S2 400-355)
10%Endo-30%M-60%Epi Endocardial pacing FK4V model	55-11 (S1S2 700-500) 13-22 (S1S2 400-370)	48-43 (S1S2 700-500) 64-72 (S1S2 400-390)	48-33 (S1S2 700-600) 34-69 (S1S2 500-405)
TP06 model	22-19 (S1S2 700-540)	25-21 (S1S2 700-500) 27-50 (S1S2 450-385)	27-18 (S1S2 700-450) 19-24 (S1S2 445-430)
10%Endo-30%M-60%Epi Epicardial pacing FK4V model	50-18 (S1S2 700-400) 19-25 (S1S2 395-360)	86-46 (S1S2 700-395) 48 at S1S2 390	84-45 (S1S2 700-400) 47 at S1S2 395
TP06 model	40-35 (S1S2 700-495)	72-62 (S1S2 700-400) 66-84 (S1S2 380-345)	70-59 (S1S2 700-420) 60-59 (S1S2 410-375) 61-64 (S1S2 370-355)
60%Endo-30%M-10%Epi Endocardial pacing FK4V model	58-32 (S1S2 700-350)	100-71 (S1S2 700-395) 72 at S1S2 390	99-76 (S1S2 700-400)
TP06 model	39-33 (S1S2 700-500)	71-60 (S1S2 700-410) 61-80 (S1S2 405-345)	70-57 (S1S2 700-420) 58-59 (S1S2 415-390)
60%Endo-30%M-10%Epi Epicardial pacing, FK4V model	43-17 (S1S2 700-390)	58-22 (S1S2 700-395)	62-27 (S1S2 700-400)
TP06 model	17-21 (S1S2 700-540)	23-21 (S1S2 700-500) 21-25 (S1S2 450-380)	26-17 (S1S2 700-500) 21-27 (S1S2 450-430) 21-31 (S1S2 425-405)

Table 5-4: Measures of dispersion in repolarization time for premature S2 beats with the FK4V and the TP06 models

5.3.2-2 The largest and the smallest dispersion

For comparing the smallest and the largest measures of dispersion in repolarization time for premature S2 beats in three groups of tissue including isotropic, anisotropic, and anisotropic fibrosis tissues with the FK4V and the TP06 models, summary Figure 5-30 is provided. Among long and short S1S2 intervals, the smallest dispersion in repolarization time was the smallest value of dispersion in repolarization time; and the largest dispersion in repolarization time was the largest value of dispersion in repolarization time.

Comparison between two groups of anisotropic and isotropic tissues as well as two groups of anisotropic tissues with and without fibrosis showed that:

1. Anisotropic tissue compared with isotropic tissue using the FK4V model

Anisotropic diffusion compared with isotropic diffusion increased the smallest dispersion in repolarization time to around 5 ms to 39 ms and the largest dispersion in repolarization time to around 15 ms to 53 ms in all tissues.

For example, the largest dispersion in repolarization time for anisotropic tissue composed of 15%Endo-55%M-30%Epi with endocardial pacing (100 ms) compared with isotropic tissue (47 ms) had an increase around 53 ms, red bar chart in plot A.

2. Anisotropic tissue compared with isotropic tissue using the TP06 model

Anisotropic diffusion compared with isotropic diffusion increased the smallest dispersion in repolarization time to around 2 ms to 27 ms and the largest dispersion in repolarization time to around 28 ms to 94 ms in all tissues, orange bar chart in plot A1.

For example, the largest dispersion in repolarization time for anisotropic tissue composed of 15%Endo-55%M-30%Epi with epicardial pacing (131 ms) compared with isotropic tissue (37 ms) had an increase around 94 ms.

3. Anisotropic tissue with fibrosis compared with anisotropic tissue with the FK4V model

Anisotropic fibrosis tissue compared with anisotropic tissue decreased the smallest dispersion in repolarization time to around 1 ms to 10 ms in some tissues (i.e. 10%Endo-30%M-60%Epi with epicardial and endocardial pacing) while increased this value in other tissues (i.e. 5 ms in 60%Endo-30%M-10%Epi with both epicardial and endocardial pacing).

The same was true for the largest dispersion in repolarization time. For example, the largest dispersion in repolarization time for anisotropic fibrosis tissue composed of 15%Endo-55%M-30%Epi with endocardial pacing (87 ms) compared with anisotropic tissue (100 ms) had a decrease around 13 ms, red bar chart in plot A. However, the largest dispersion in repolarization time for anisotropic fibrosis tissue composed of 50%Endo-50%Epi with endocardial pacing (65 ms) compared with anisotropic tissue (60 ms) had a rise around 5 ms, dark green bar chart in plot A.

4. Anisotropic tissue with fibrosis compared with anisotropic tissue with the TP06 model

Simulated anisotropic fibrosis compared with anisotropic tissue decreased the smallest dispersion in repolarization time to around 3 ms to 5 ms in the homogenous and most heterogeneous tissues. However, the smallest dispersion in repolarization time for anisotropic fibrosis tissue composed of 15%Endo-55%M-30%Epi with endocardial pacing (47 ms) compared with anisotropic tissue (23 ms) had a rise of 24 ms, red bar chart in B1.

Simulated anisotropic fibrosis compared with anisotropic tissue decreased the largest dispersion in repolarization time to around 10 ms to 38 ms in all tissues. For example, the largest dispersion in repolarization time for anisotropic fibrosis tissue composed of 15%Endo-55%M-30%Epi with epicardial pacing (93 ms) compared with anisotropic tissue (131 ms), had a fall around 38 ms, orange bar chart in plot A1.

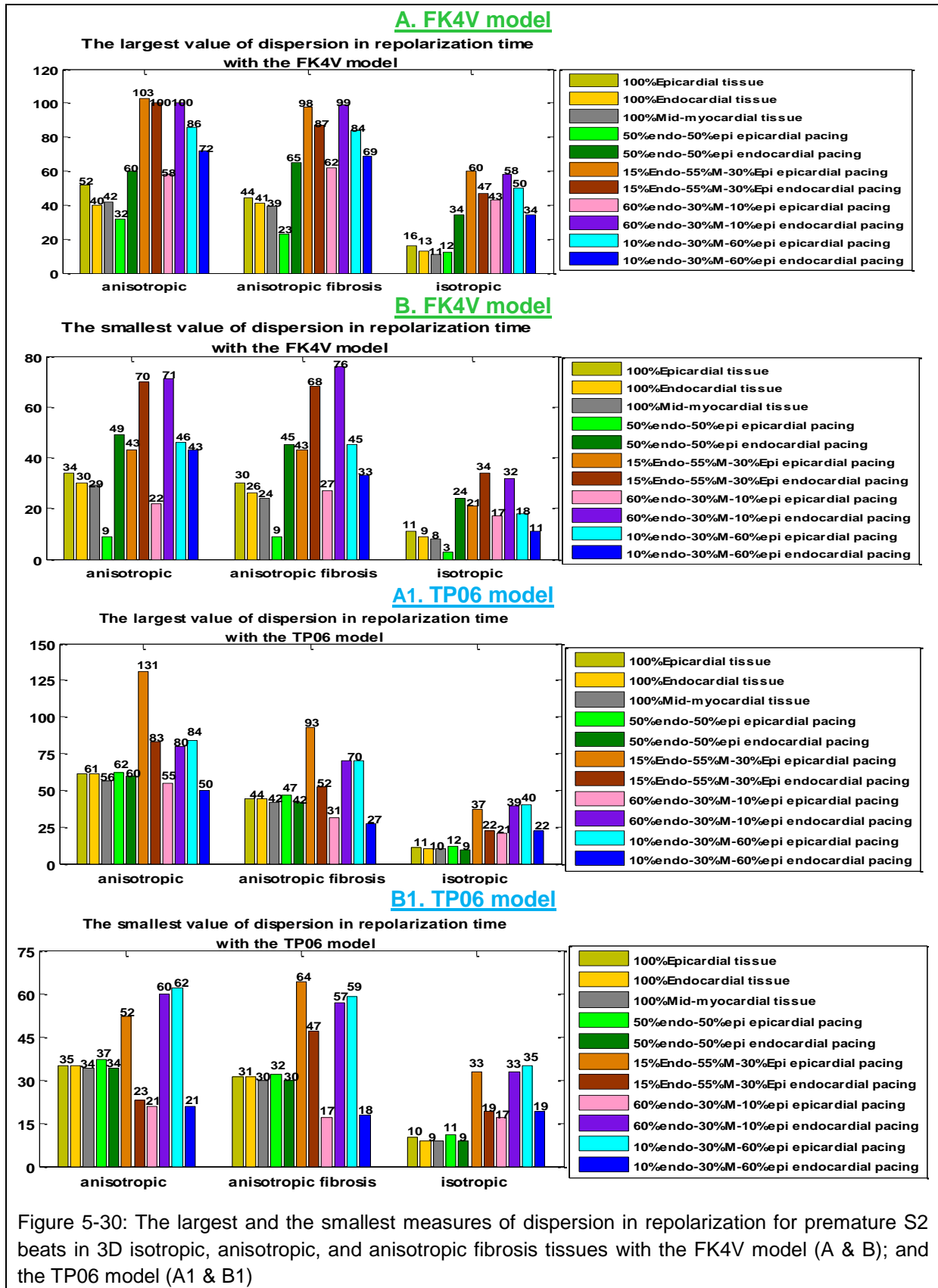


Figure 5-30: The largest and the smallest measures of dispersion in repolarization for premature S2 beats in 3D isotropic, anisotropic, and anisotropic fibrosis tissues with the FK4V model (A & B); and the TP06 model (A1 & B1)

5.3.3 Dispersion in action potential duration

After studying the changes in measures of dispersion in activation time and repolarization time for normal and premature beats, it was interesting to study how APD dispersion changes for long and short S1S2 intervals with both models.

5.3.3-1 Normal and premature beats

For both normal and premature beats The APD dispersion was the difference between the maximum and the minimum APD at each S1S2 interval. Measures of APD dispersion changed slightly around 1 ms to 2 ms for normal S1 beats (Table 5-5) and greatly around 3 ms to 41 ms for premature S2 beats (Table 5-6) during decreasing S1S2 intervals in all tissues.

Measures of dispersion in APD for normal S1 beats in ms in 3D cubes of tissue during decreasing S1S2 intervals (S1S2) in ms			
	Isotropic (S1S2 intervals)	Anisotropic (S1S2 intervals)	Anisotropic fibrosis (S1S2 intervals)
FK4V model of 100%Epi Pacing from the bottom edge of tissue	5-6 (S1S2 700-345)	6-7 (S1S2 700-335)	7-8 (S1S2 700-340)
TP06 model	12 (S1S2 700-495)	11-12 (S1S2 700-345)	14-15 (S1S2 700-390)
FK4V model of 100%Endo Pacing from the bottom edge of tissue	6-7 (S1S2 700-315)	7-9 (S1S2 700-315)	8-9 (S1S2 700-300)
TP06 model	12 (S1S2 700-495)	12-13 (S1S2 700-345)	14-16 (S1S2 700-390)
FK4V model of 100%M Pacing from the bottom edge of tissue	7 (S1S2 700-460)	9-10 (S1S2 700-455)	9 (S1S2 700-475)
TP06 model	12-13 (S1S2 700-560)	13-15 (S1S2 700-430)	15-17 (S1S2 700-470)
50%Endo-50%Epi Endocardial pacing, FK4V model	8 for 700-310	12-13 (S1S2 700-315)	13-14 (S1S2 700-315)
TP06 model	12-13 (S1S2 700-495)	13-15 (S1S2 700-345)	15-17 (S1S2 700-390)
50%Endo-50%Epi Epicardial pacing, FK4V model	17-18 (S1S2 700-345)	20-21 (S1S2 700-335)	20-22 (S1S2 700-335)
TP06 model	11 (S1S2 700-495)	11-12 (S1S2 700-345)	11-13 (S1S2 700-355)
15%Endo-55%M-30%Epi Endocardial pacing, FK4V model	67-68 (S1S2 700-380)	101 (S1S2 700-420)	99-100 (S1S2 700-425)
TP06 model	36-39 (S1S2 700-530)	64-70 (S1S2 700-365)	65-70 (S1S2 700-415)
15%Endo-55%M-30%Epi Epicardial pacing, FK4V model	61-62 (S1S2 700-380)	97-99 (S1S2 700-420)	92-93 (S1S2 700-425)
TP06 model	24-26 (S1S2 700-515)	54-60 (S1S2 700-360)	54-59 (S1S2 700-355)
10%Endo-30%M-60%Epi Endocardial pacing, FK4V model	57 (S1S2 700-370)	76-77 (S1S2 700-390)	77-79 (S1S2 700-405)
TP06 model	45-47 (S1S2 700-540)	52-57 (S1S2 700-380)	61-62 (S1S2 700-430)
10%Endo-30%M-60%Epi Epicardial pacing, FK4V model	47 (S1S2 700-360)	71 (S1S2 700-390)	71 (S1S2 700-395)
TP06 model	45-47 (S1S2 700-495)	41-45 (S1S2 700-345)	40-44 (S1S2 700-355)
60%Endo-30%M-10%Epi Endocardial pacing, FK4V model	50-51 (S1S2 700-350)	81-82 (S1S2 700-390)	84-85 (S1S2 700-400)
TP06 model	22-25 (S1S2 700-500)	39-43 (S1S2 700-345)	42-47 (S1S2 700-390)
60%Endo-30%M-10%Epi Epicardial pacing, FK4V model	61 (S1S2 700-390)	88-89 (S1S2 700-395)	90-91 (S1S2 700-400)
TP06 model	44-47 (S1S2 700-540)	52-56 (S1S2 700-380)	53-58 (S1S2 700-400)

Table 5-5: Measures of APD dispersion for normal S1 beats with the FK4V and the TP06 models

Measures of dispersion in APD for premature S2 beats in ms in 3D cubes of tissue during decreasing S1S2 intervals (S1S2) in ms			
	Isotropic (S1S2 intervals)	Anisotropic (S1S2 intervals)	Anisotropic fibrosis (S1S2 intervals)
100%Epi Pacing from the bottom edge of tissue, FK4V model	6-9 (S1S2 700-345)	7-5 (S1S2 700-340) 6 at S1S2 335	8-7 (S1S2 700-350) 16 at S1S2 340
TP06 model	11-13 (S1S2 700-495)	10-14 (S1S2 700-345)	15 at S1S2 700 16-14 (S1S2 600-440) 15-13 (S1S2 430-390)
100%Endo Pacing from the bottom edge of tissue, FK4V model	7-11 (S1S2 700-315)	8-11 (S1S2 700-315)	9-18 (S1S2 700-300)
TP06 model	11-14 (S1S2 700-495)	9-16 (S1S2 700-345)	16-13 (S1S2 700-390)
100%M Pacing from the bottom edge of tissue, FK4V model	7-13 (S1S2 700-460)	8-17 (S1S2 700-455)	9-17 (S1S2 700-475)
TP06 model	13-15 (S1S2 700-560)	11-16 (S1S2 700-430)	17-14(S1S2 700-475) 15 at S1S2 470
50%Endo-50%Epi Endocardial pacing FK4V model	10-18 (S1S2 700-500) 17-5 (S1S2 400-320) 7-9 (S1S2 315-310)	16-24 (S1S2 700-500) 23-9 (S1S2 400-315)	16-25 (S1S2 700-500) 24-14 (S1S2 400-320) 16 at S1S 315
TP06 model	13-14 (S1S2 700-530) 12-13 (S1S2 520-495)	10-16 (S1S2 700-345)	17-15 (S1S2 700-435) 16-15 (S1S2 430-395) 16 at S1S2 390
50%Endo-50%Epi Epicardial pacing FK4V model	21-30 (S1S2 700-500) 29-23 (S1S2 400-345)	25-33 (S1S2 700-400) 25-23 (S1S2 350-335)	24-33 (S1S2 700-400) 28-33 (S1S2 350-335)
TP06 model	10-11 (S1S2 700-510) 9-11 (S1S2 505-495)	8-12 (S1S2 700-345)	12-10 (S1S2 700-410) 11-4 (S1S2 405-370) 5 at S1S2 355
15%Endo-55%M-30%Epi Endocardial pacing FK4V model	57-24 (S1S2 700-385) 25 at S1S2 380	84-38 (S1S2 700-420)	83-43 (S1S2 700-450) 52 at S1S2 420
TP06 model	35-32 (S1S2 700-530)	62-21 (S1S2 700-365)	61-33 (S1S2 700-415)
15%Endo-55%M-30%Epi Epicardial pacing, FK4V model	50-31 (S1S2 700-500) 32-31 (S1S2 425-380)	66-46 (S1S2 700-420)	78-43 (S1S2 700-425)
TP06 model	23-19 (S1S2 700-515)	51-26 (S1S2 700-400) 26-37 (S1S2 380-360) 58 at S1S2 355	52-26 (S1S2 700-390) 28-33 (S1S2 380-355)
10%Endo-30%M-60%Epi Endocardial pacing FK4V model	47-13 (S1S2 700-390) 16 at S1S2 370	64-30 (S1S2 700-400) 32 at S1S2 390	66-23 (S1S2 700-430) 24-29 (S1S2 410-405)
TP06 model	44-41 (S1S2 700-540)	51-20 (S1S2 700-385) 23 at S1S2 380	55-35 (S1S2 700-430)
10%Endo-30%M-60%Epi Epicardial pacing FK4V model	38-13 (S1S2 700-395) 14-20 (S1S2 390-360)	59-35 (S1S2 700-395) 38 at S1S2 390	60-30 (S1S2 700-500) 33-38 (S1S2 400-395)
TP06 model	23-18 (S1S2 700-495)	40-25 (S1S2 700-430) 26-22 (S1S2 425-360) 25-26 (S1S2 355-345)	39-22 (S1S2 700-355)
60%Endo-30%M-10%Epi Endocardial pacing FK4V model	46-18 (S1S2 700-350)	74-40 (S1S2 700-395) 41 at S1S2 390	77-44 (S1S2 700-400)
TP06 model	22-17 (S1S2 700-500)	37-21 (S1S2 700-415) 20-22 (S1S2 410-385) 21-25 (S1S2 380-345)	41-23 (S1S2 700-390)
60%Endo-30%M-10%Epi Epicardial pacing FK4V model	57-35 (S1S2 700-395) 37 at S1S2 390	80-45 (S1S2 700-395)	82-57 (S1S2 700-400)
TP06 model	42-39 (S1S2 700-555) 40-39 (S1S2 550-540)	50-16 (S1S2 700-380)	51-29 (S1S2 700-430) 30-25 (S1S2 425-405) 26 at S1S2 400

Table 5-6: Measures of APD dispersion for premature S2 beats using the FK4V and the TP06 models

5.3.3-2 The largest and the smallest measures of dispersion

Summary Figure 5-31 compares the smallest and the largest APD dispersion for premature S2 beats among three groups of isotropic, anisotropic, and anisotropic fibrosis tissues with both models. The smallest and the largest APD dispersion was the smallest and the largest value of dispersion in APD among all S1S2 intervals.

The comparison of these values between two groups of anisotropic and isotropic tissues as well as two groups of anisotropic tissues with and without fibrosis is described here.

1. Anisotropic tissue compared with isotropic tissue with the FK4V model

Anisotropic diffusion compared with isotropic diffusion increased the smallest APD dispersion to around 1 ms to 41 ms in some tissues.

Anisotropic diffusion compared with isotropic diffusion increased the largest APD dispersion to around 3 ms to 59 ms in some tissues.

2. Anisotropic tissue compared with isotropic tissue with the TP06 model

Anisotropic diffusion compared with isotropic diffusion decreased the smallest APD dispersion to around 1 ms to 23 ms in some tissues.

On the other hand, anisotropic diffusion compared with isotropic diffusion increased the largest APD dispersion to around 1 ms to 35 ms in all tissues.

3. Anisotropic tissue with fibrosis compared with anisotropic tissue without fibrosis with the FK4V model

Simulated anisotropic tissue with fibrosis compared with anisotropic tissue increased the smallest APD dispersion to around 1 ms to 12 ms in some tissues.

Simulated anisotropic tissue with fibrosis compared with anisotropic tissue without fibrosis increased the largest APD dispersion to approximately 1 ms to 9 ms in some tissues. For example, the largest APD dispersion for anisotropic fibrosis epicardial tissue paced from the bottom edge of tissue (16 ms) compared with tissue without fibrosis (7 ms) had an increase around 9 ms, olive green bar chart in plot A.

However, anisotropic fibrosis tissue composed of 15%Endo-55%M-30%Epi with epicardial pacing compared with tissue without fibrosis decreased the largest APD dispersion to approximately 10 ms.

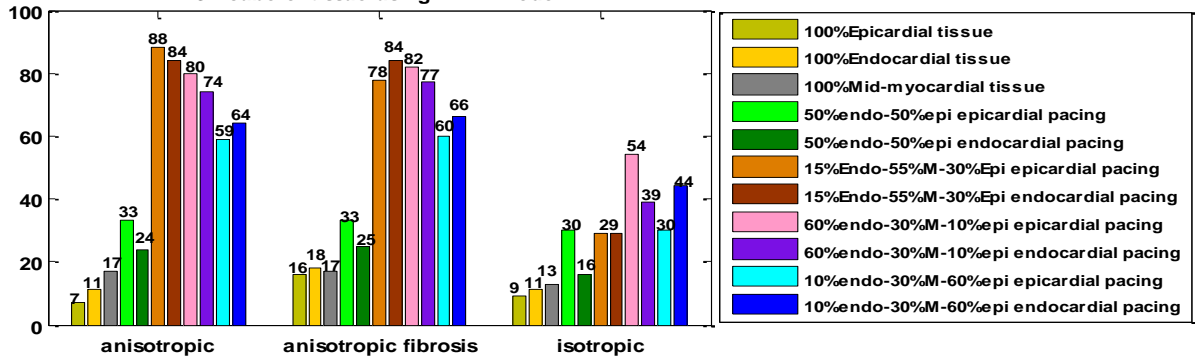
4. Anisotropic tissue with fibrosis compared with anisotropic tissue without fibrosis with the TP06 model

Simulated anisotropic tissue with fibrosis compared with anisotropic tissue increased the smallest APD dispersion to around 3 ms to 15 ms in some tissues. However, anisotropic fibrosis tissue composed of 50%Endo-50%Epi with endocardial pacing compared with tissue without fibrosis decreased the smallest APD dispersion to approximately 5 ms, dark green bar chart in plot B1.

Simulated anisotropic tissue with fibrosis compared with anisotropic tissue increased the largest APD dispersion to approximately 1 ms to 4 ms in some tissues. Whereas, anisotropic fibrosis tissue composed of 15%Endo-55%M-30%Epi with epicardial and endocardial pacing compared with tissue without fibrosis decreased the largest APD dispersion to approximately 6 ms and 1 ms respectively, orange and red bar charts in plot A1.

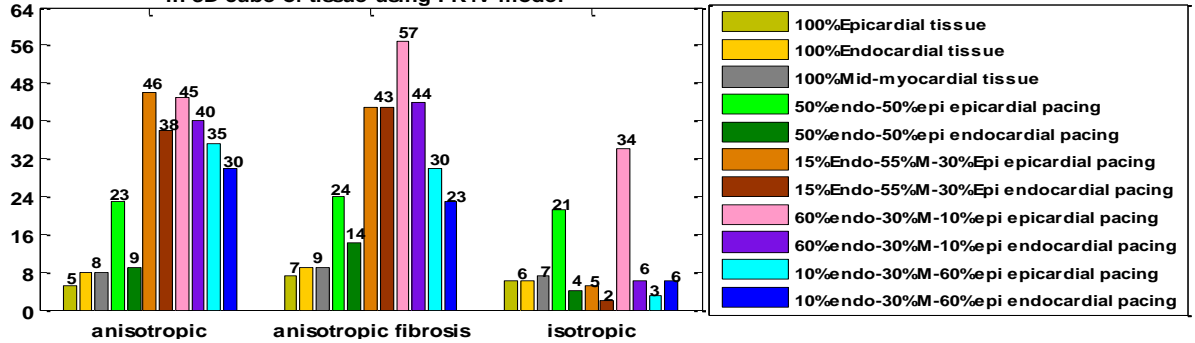
A. FK4V model

The largest value of the action potential duration dispersion in 3D cube of tissue using FK4V model



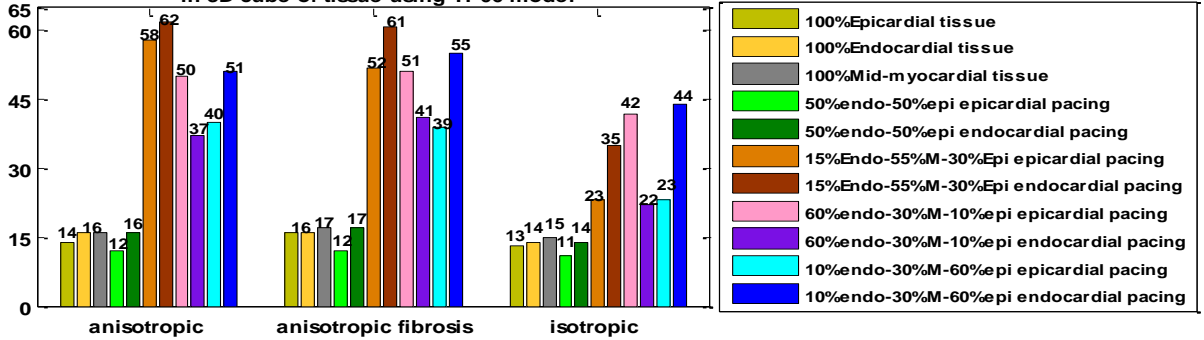
B. FK4V model

The smallest value of the action potential duration dispersion in 3D cube of tissue using FK4V model



A1. TP06 model

The largest value of action potential duration dispersion in 3D cube of tissue using TP06 model



B1. TP06 model

The smallest value of action potential duration dispersion in 3D cube of tissue using TP06 model

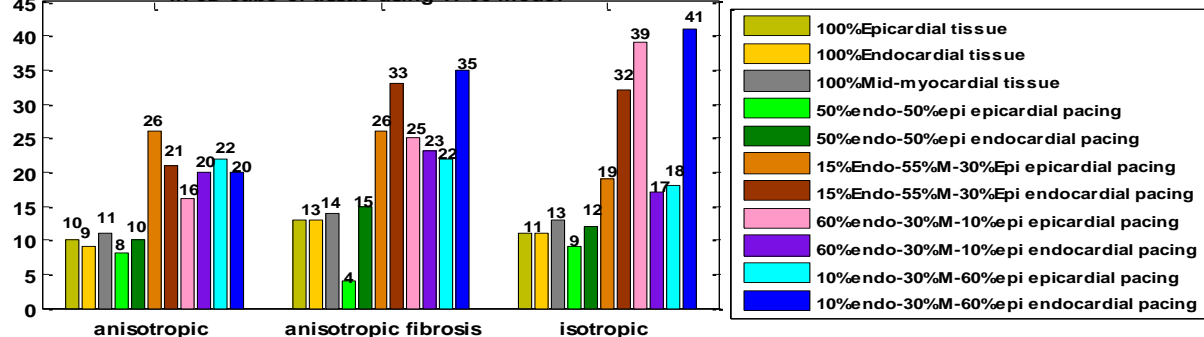


Figure 5-31: The largest and the smallest measures of APD dispersion for premature S2 beats in 3D isotropic, anisotropic, and anisotropic fibrosis tissues with the FK4V model (A & B); and the TP06 model (A1 & B1)

5.3.4 Comparison with experimental studies

After illustrating how three measures of dispersion in activation time, repolarization time and APD change during decreasing S1S2 intervals, three measures of dispersion were quantitatively compared against four human experimental studies by Cowan et al. [31], Franz et al. [32], Chauhan et al. [4], and Hanson et al. [33]. In these experimental studies, the local activation time corresponded to the interval from the onset of the earliest QRS on the ECG to local activation on the unipolar electrocardiogram, APD was duration of AP from the AP upstroke to AP downstroke, and repolarization time was the sum of local activation time and activation recovery interval. It is important to note that these data were usually limited to the epicardial or endocardial region of ventricles with atrial pacing at a constant heart rate.

5.3.4-1 Left ventricular epicardium

Cowan et al. [31] recoded monophasic APs from the epicardium of the left ventricular leads of the surface electrocardiogram using a hand held probe (7 mm in diameter) in two groups including patients undergoing coronary artery bypass grafting with upright T-wave and aortic valve replacement with inverse T-wave. This study was limited to atrial pacing at a fixed rate 10-20 beats/min in the epicardial region, and endocardium did not studied due to ethical reasons [31].

Among ten patients with upright T-wave, the average dispersion in activation time was 23 ms and the average dispersion in repolarization time was 14 ms in the epicardial region of human left ventricle [31]. These values were close to the measures of dispersion in activation time (Table 5-2) and repolarization time (Table 5-4) in this thesis for isotropic homogenous tissues paced from the bottom edge of tissue using both models.

In the right ventricular endocardium, the (average) APD dispersion was 17 ms in patients with cardiomyopathy and normal ventricular function [36, 37].

5.3.4-2 Left ventricular epicardium and endocardium

Franz et al. [32] used a contact electrode catheter to recode monophasic AP mapping in the endocardial and epicardial regions of left ventricle in patients with preserved left ventricular function undergoing bypass surgery. The monophasic AP recoding was limited to the constant sinus rhythm or right atrial pacing. They combined data from different patients with different heart rates by expressing APD and repolarization time as a percentage of the longest APD sampled in each patient. In these patients, the dispersion in repolarization time was 41 ms in the epicardial region and 26 ms in the endocardial region of left ventricle [32].

Chauhan et al. [4] measured dispersion of activation time, APD, and repolarization time during right atrial pacing at a cycle length of 550 ms in two groups with ventricular tachycardia (positive microvolt T-wave alternans) and without ventricular tachycardia (negative microvolt T-wave alternans). They used transvenous multi-electrode catheters placed along the apicobasal epicardial and endocardial surface of the anteroseptal ventricles. They [4] showed that endocardial and epicardial repolarization heterogeneity was greater in patients with ventricular tachycardia compared to those without ventricular tachycardia.

For example, dispersion of repolarization time was 51 ms along left ventricular epicardium (with repolarization time 287 ms) and 17 ms along right ventricular endocardium (with repolarization time 288 ms) in patients without ventricular tachycardia [4]. For patients

with ventricular tachycardia, dispersion of repolarization time was 66 ms along left ventricular epicardium (with repolarization time 249 ms) and 73 ms along right ventricular endocardium (with repolarization time 269 ms) [4].

It is important to note that activation time dispersion was 28 ms (with activation time 68 ms) along left ventricular epicardium and 18 ms (with activation time 38 ms) along right ventricular endocardium in patients without ventricular tachycardia [4]. For patients with ventricular tachycardia, the activation time dispersion was 25 ms (with activation time 59 ms) along left ventricular epicardium and 16 ms (with activation time 36 ms) along right ventricular endocardium [4]. These values were similar to measures of dispersion in activation time for isotropic homogenous tissues in this thesis (Table 5-2).

In this thesis, the largest dispersion of repolarization time in anisotropic homogenous epicardial tissues paced from the bottom edge of tissue using the FK4V and TP06 models (Table 5-4) was comparable with dispersion of repolarization time 51 ms, in left ventricular epicardium in patients without ventricular tachycardia [4].

5.3.4-3 Left ventricular endocardium

Hanson et al. [33] recorded activation recovery interval from the left ventricular endocardium in nine patients with normal ventricles using the reconstructed noncontact unipolar electrograms. The heart pacing was from the right ventricular apex and the coupling intervals decreased from 450 ms to the loss of capture. At long coupling interval of 450 ms, the average dispersion of repolarization time and APD among these patients was approximately 53 ms. However, for short coupling intervals (i.e. 220 ms), the average dispersion in repolarization time among all patients was greater than the average APD dispersion (75 ms and 60 ms respectively).

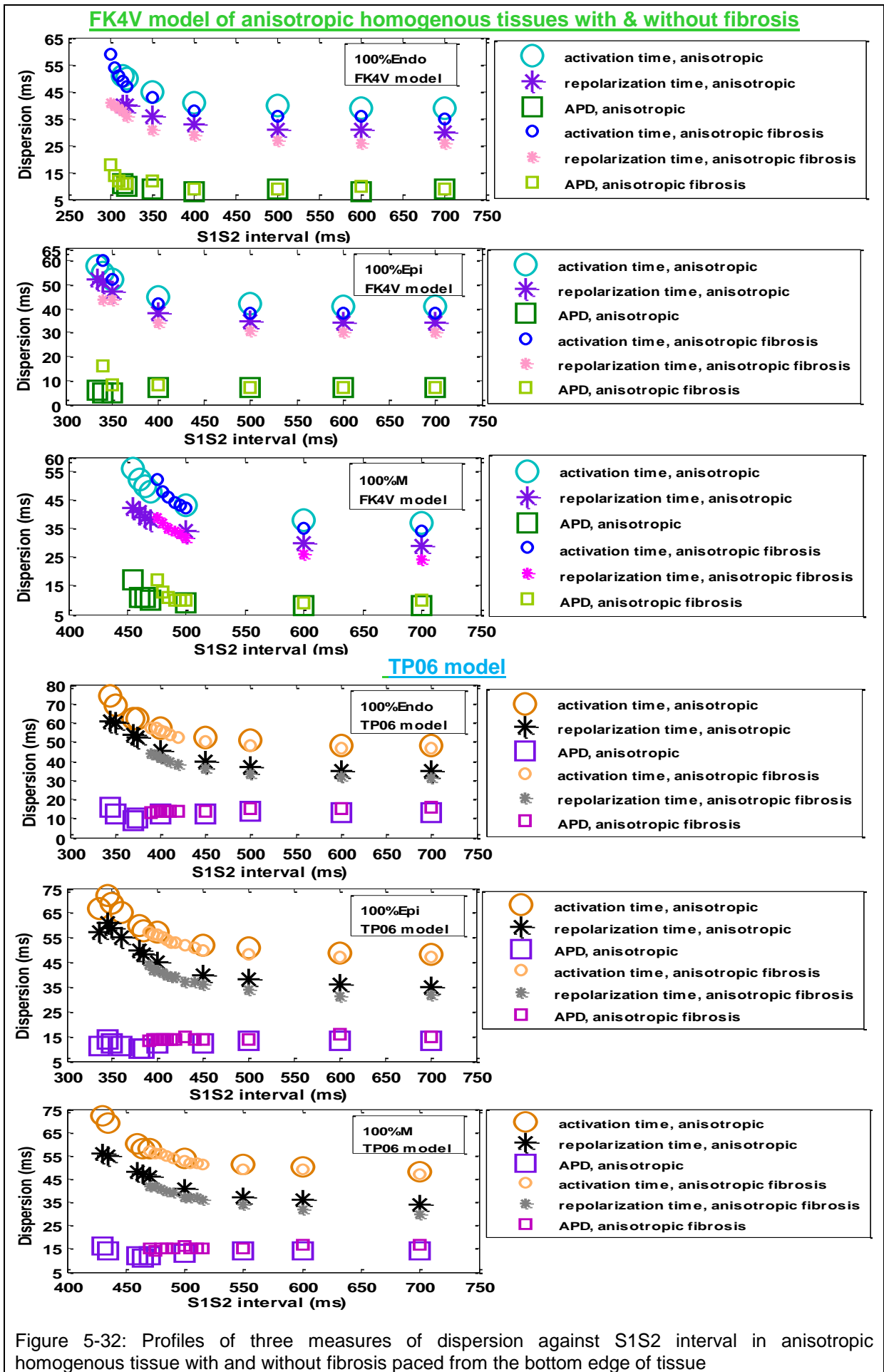
These four experimental studies reported variable dispersion in activation time, APD, and repolarization time. For reliability of comparison, one alternative approach was to find the relationship between these dispersions when restitution or rate dependency engaged. To achieve this purpose, the profiles of three measures of dispersion against diastolic interval were plotted in the same graph for premature S2 beats. This approach could distinguish homogenous and heterogeneous tissues based on relationship between three measures of dispersion. The following section describes this issue and provides a link with current evidence in experiment studies.

5.3.4-4 Relationship among three measures of dispersion in homogenous tissue

For anisotropic homogenous tissues with and without fibrosis, dispersion in both activation time and repolarization time for premature beats

- gradually increased during decreasing S1S2 intervals with both models;
- with the TP06 model were slightly greater than those with the FK4V model.

Among three measures of dispersion, measures of dispersion in activation time were the greatest and measures of APD dispersion were the smallest in three anisotropic homogenous tissues with the FK4V and the TP06 models as shown in Figures 5-32.



As explained in section 5.2.1, TP06 models of tissue composed of 50%Endo-50%Epi with both endocardial and epicardial pacing acted as a homogenous tissue due to similarities between restitution properties of epicardial and endocardial cells. Therefore, profiles of three measures of dispersion in this tissue with the TP06 model and homogenous tissues with both FK4V and TP06 models change similarly as shown in Figure 5-33.

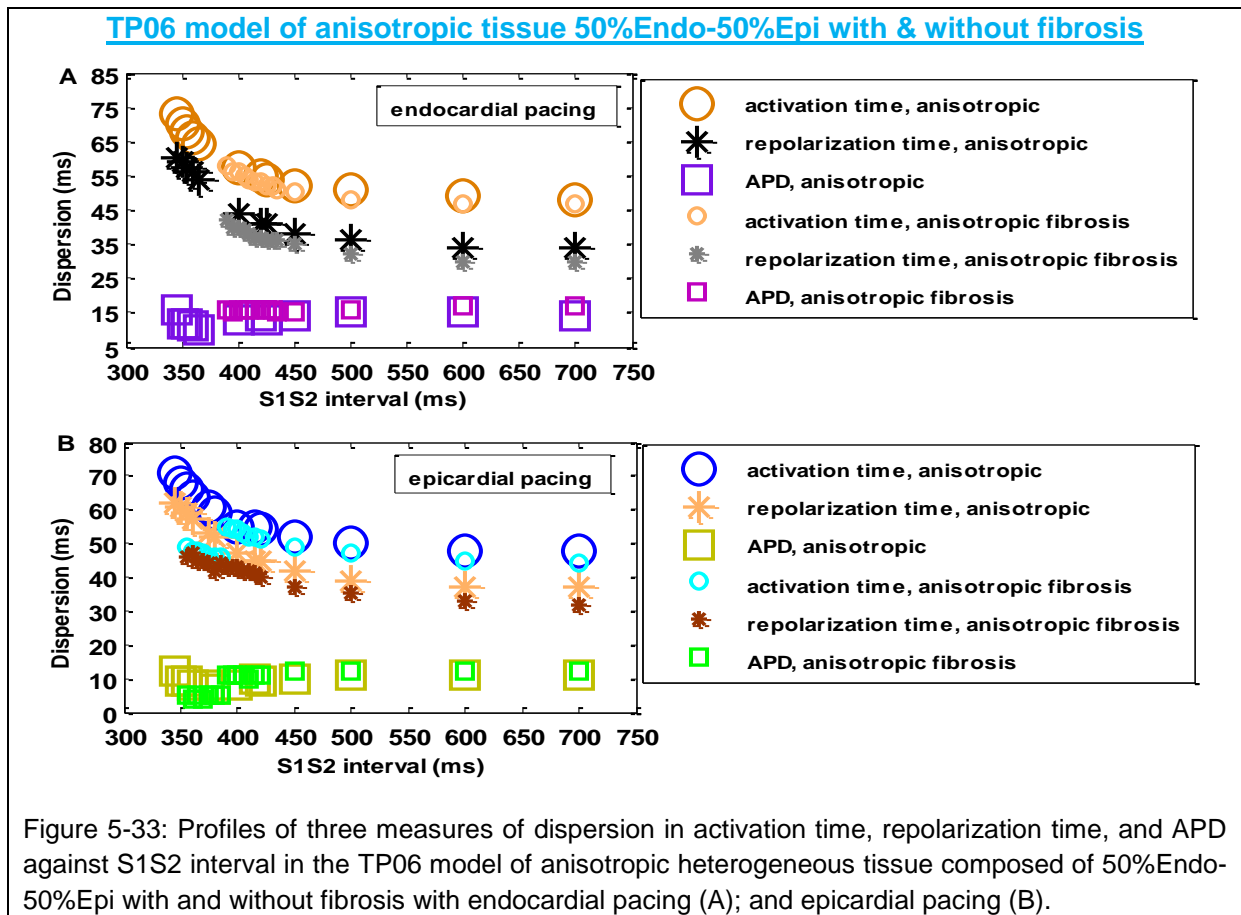


Figure 5-33: Profiles of three measures of dispersion in activation time, repolarization time, and APD against S1S2 interval in the TP06 model of anisotropic heterogeneous tissue composed of 50%Endo-50%Epi with and without fibrosis with endocardial pacing (A); and epicardial pacing (B).

One common feature among the profiles of three measures of dispersion was that these curves did not cross each other during decreasing S1S2 interval for homogenous tissue. However, this feature was not true for heterogeneous tissues that are discussed in the following section.

5.3.4-5 Relationship among three measures of dispersion in heterogeneous tissue

Before discussing about relationship among three measures of dispersion, two summary figures are provided to emphasize the involvement of additional layers of mid-myocardial cells in spatial profiles of repolarization time and APD (Figure 5-34), and spatiotemporal profiles of activation time (Figure 5-35) in heterogeneous tissues.

For three heterogeneous tissues, summary Figure 5-34 shows

1. the sharp increase in repolarization time and APD in spatial profiles of repolarization time and APD in plots A and C;
2. the vulnerable regions for wave break in the transition region from endocardial to mid-myocardial and from mid-myocardial to epicardial region in profiles of gradient in repolarization time and APD in plots B and D.

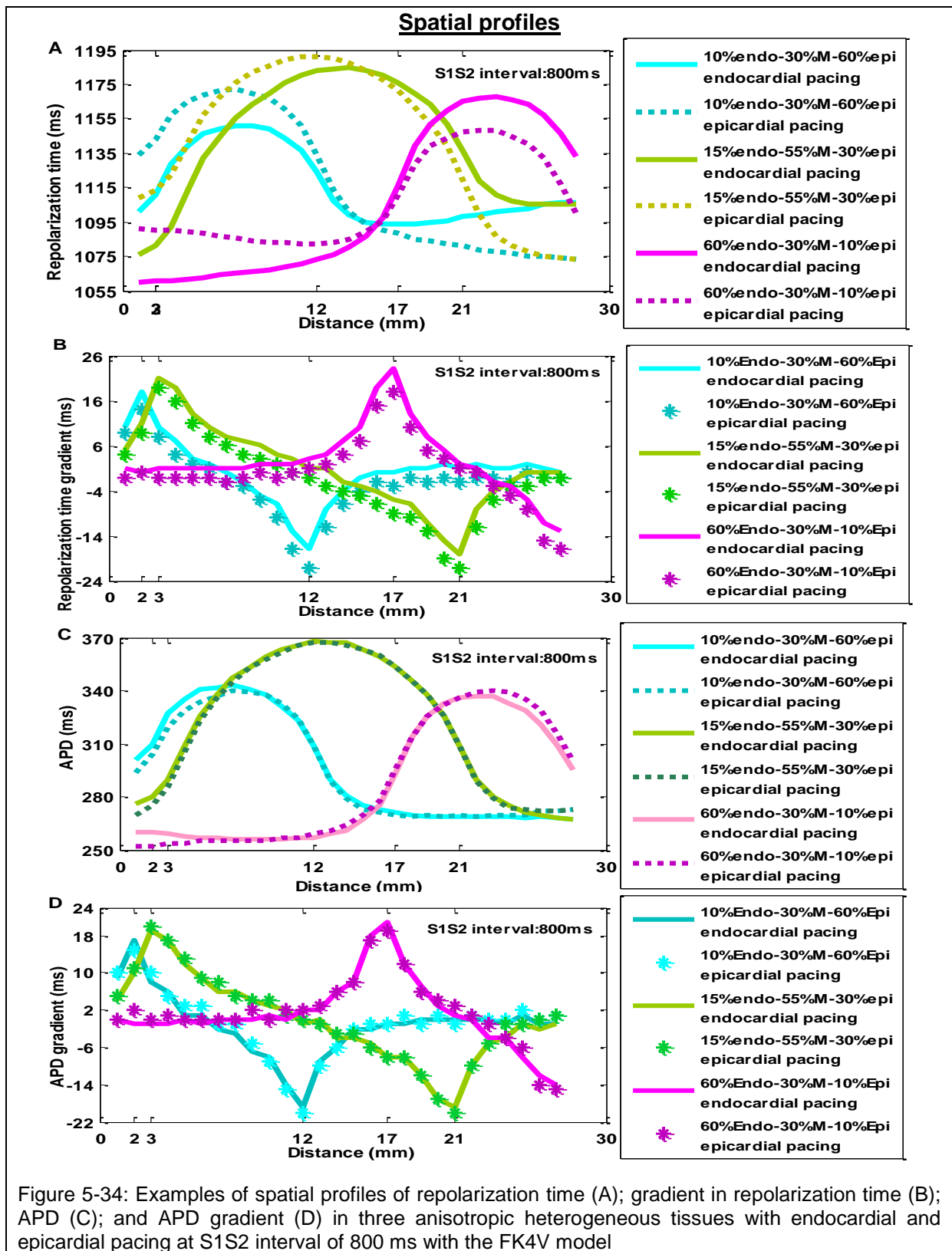
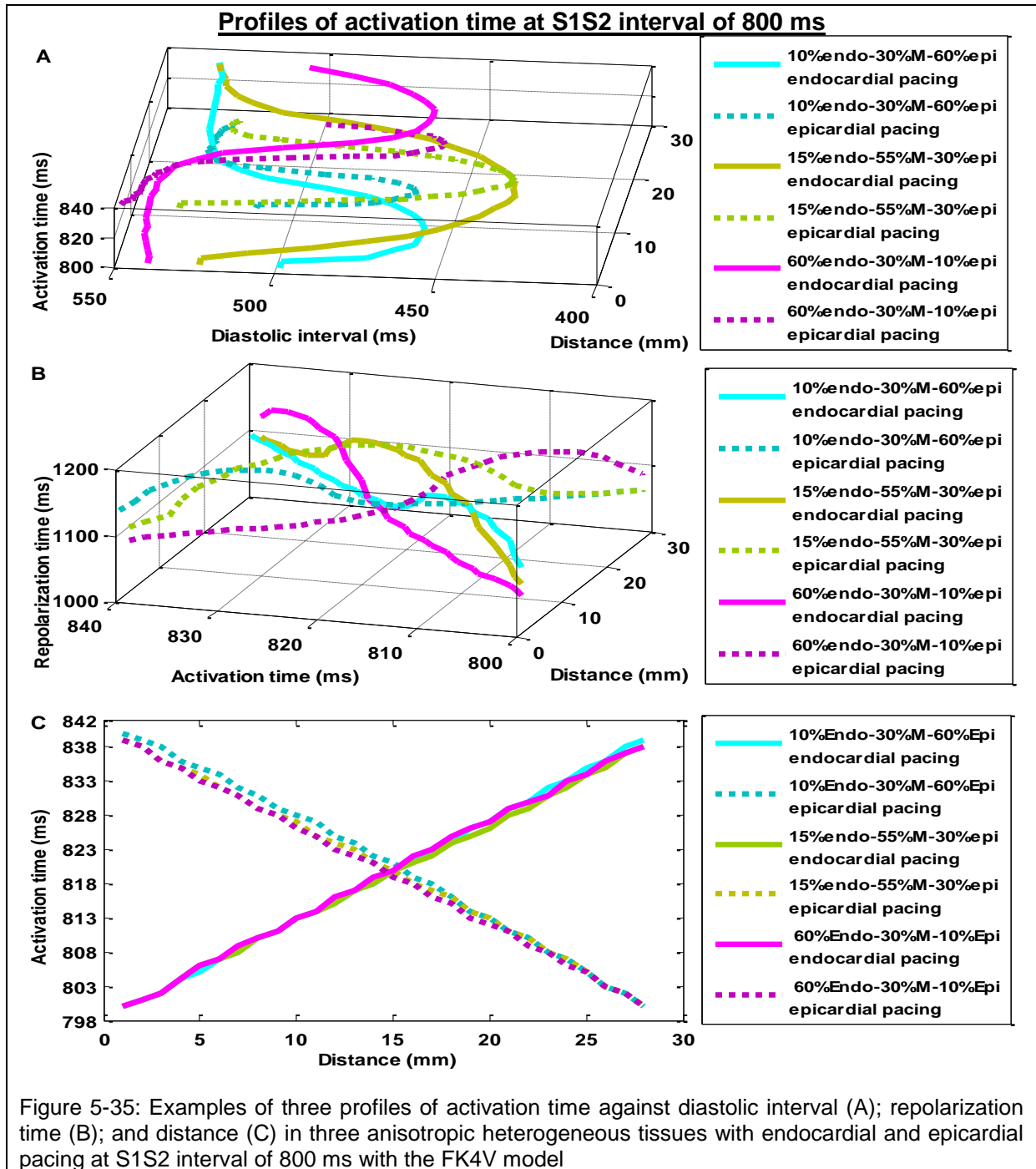


Figure 5-34: Examples of spatial profiles of repolarization time (A); gradient in repolarization time (B); APD (C); and APD gradient (D) in three anisotropic heterogeneous tissues with endocardial and epicardial pacing at S1S2 interval of 800 ms with the FK4V model

Summary Figure 5-35 highlights the involvement of mid-myocardial cells in the profile of activation time against diastolic interval (plot A) and against repolarization time (plot B) for three FK4V models of heterogeneous tissues composed of 10%Endo-30%M-60%Epi, 60%Endo-30%M-10%Epi, and 15%Endo-55%M-30%Epi with endocardial and epicardial pacing at S1S2 interval of 800 ms. However, the dome-morphology in the spatial profile of activation time is cancelled (plot C).



Consequently, the profiles of measures of dispersion in repolarization time and APD against S1S2 interval are influenced by mid-myocardial cells in the FK4V and TP06 models of three anisotropic heterogeneous tissues with and without fibrosis as shown in Figures 5-36 to 5-38.

Interestingly, non-linear relationship between activation time and APD and an increase in dispersion of repolarization has been found in patients with aortic valve replacement with T-wave inversion in the epicardial region of left ventricle by Cowan et al. [31], and in patients with ventricular tachycardia (negative microvolt T-wave) in the epicardial region of left ventricle and in the endocardial region of right ventricle by Chauhan et al. [4].

The relationship among three measures of dispersions is discussed here.

- Heterogeneous tissue composed of 10%Endo-30%M-60%Epi

For the FK4V model of anisotropic tissue without fibrosis with endocardial pacing, dispersion in repolarization time was slightly greater than dispersion in activation time during decreasing S1S2 intervals. APD dispersion was greater for long S1S2 intervals of 700-600 ms and became smaller than other measures of dispersion for short S1S2 intervals as shown in Figure 5-36. With epicardial pacing, dispersion in repolarization time was greater than other measures of dispersion for S1S2 intervals of 700-500 ms. Dispersion in activation time was smaller than other measures of dispersion for S1S2 intervals of 700-600 ms but became greater than other measures of dispersion for S1S2 interval of 400 ms.

For the TP06 model of tissues with and without fibrosis with endocardial pacing, measures of dispersion in activation time were greater than dispersion in repolarization time for all S1S2 intervals, Figure 5-36. With epicardial pacing, dispersion in repolarization time was greater and APD dispersion was smaller than other measures of dispersion.

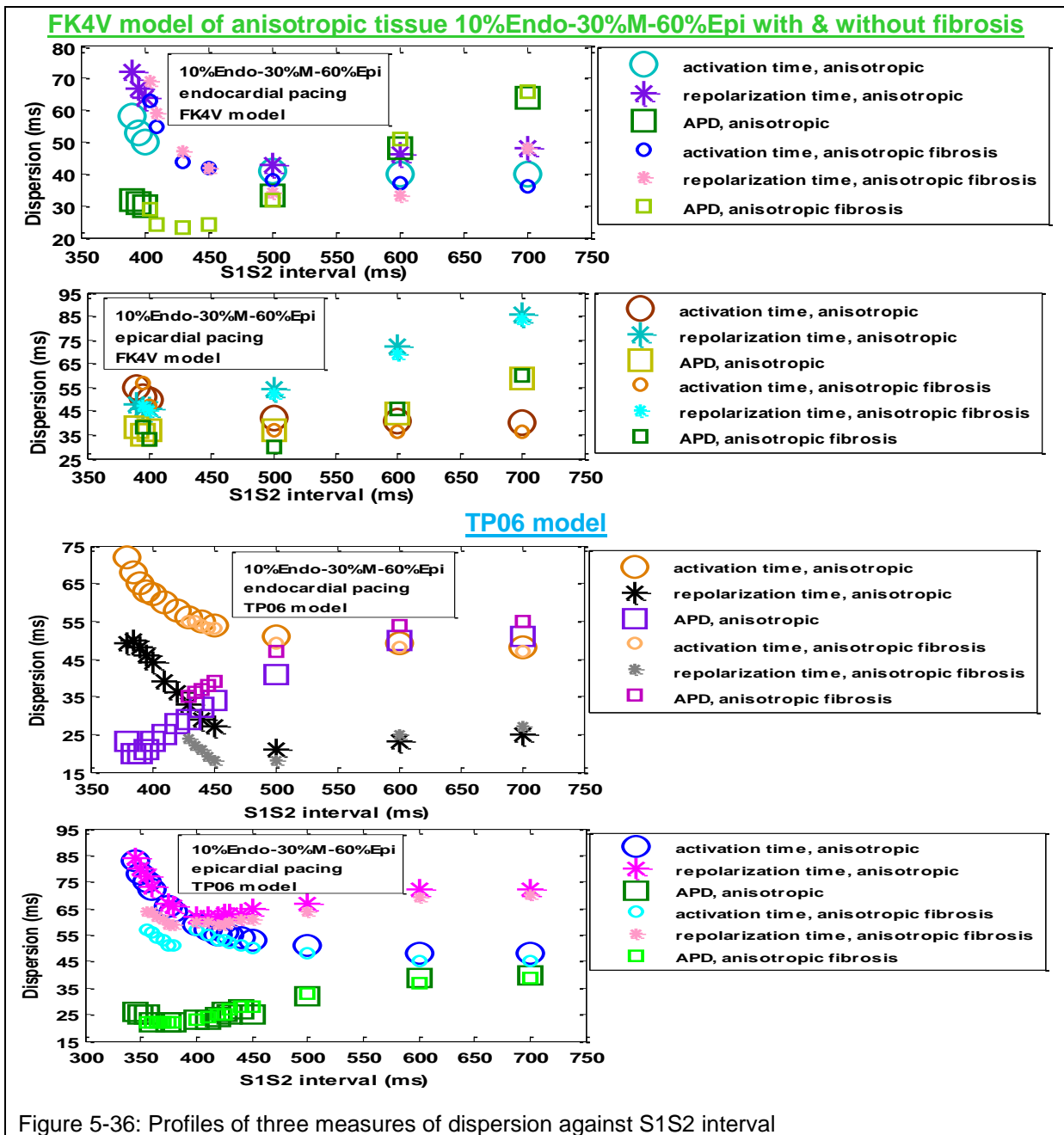


Figure 5-36: Profiles of three measures of dispersion against S1S2 interval

- Heterogeneous tissue composed of 60%Endo-30%M-10%Epi

With the FK4V model of anisotropic tissue with and without fibrosis with endocardial pacing, dispersion in repolarization time was greater than dispersion in activation time, Figure 5-37. This was only true for S1S2 intervals of 700-600 ms with epicardial pacing.

For the TP06 model of tissues with and without fibrosis with endocardial pacing, dispersion in repolarization time were greater than other measures of dispersion for S1S2 intervals of 700-400 ms as shown in Figure 5-37. With epicardial pacing, dispersion in repolarization time was smaller than other measures of dispersion for S1S2 intervals of 700-450 ms and dispersion in activation time was greater than other measures of dispersion for S1S2 intervals of 500-330 ms.

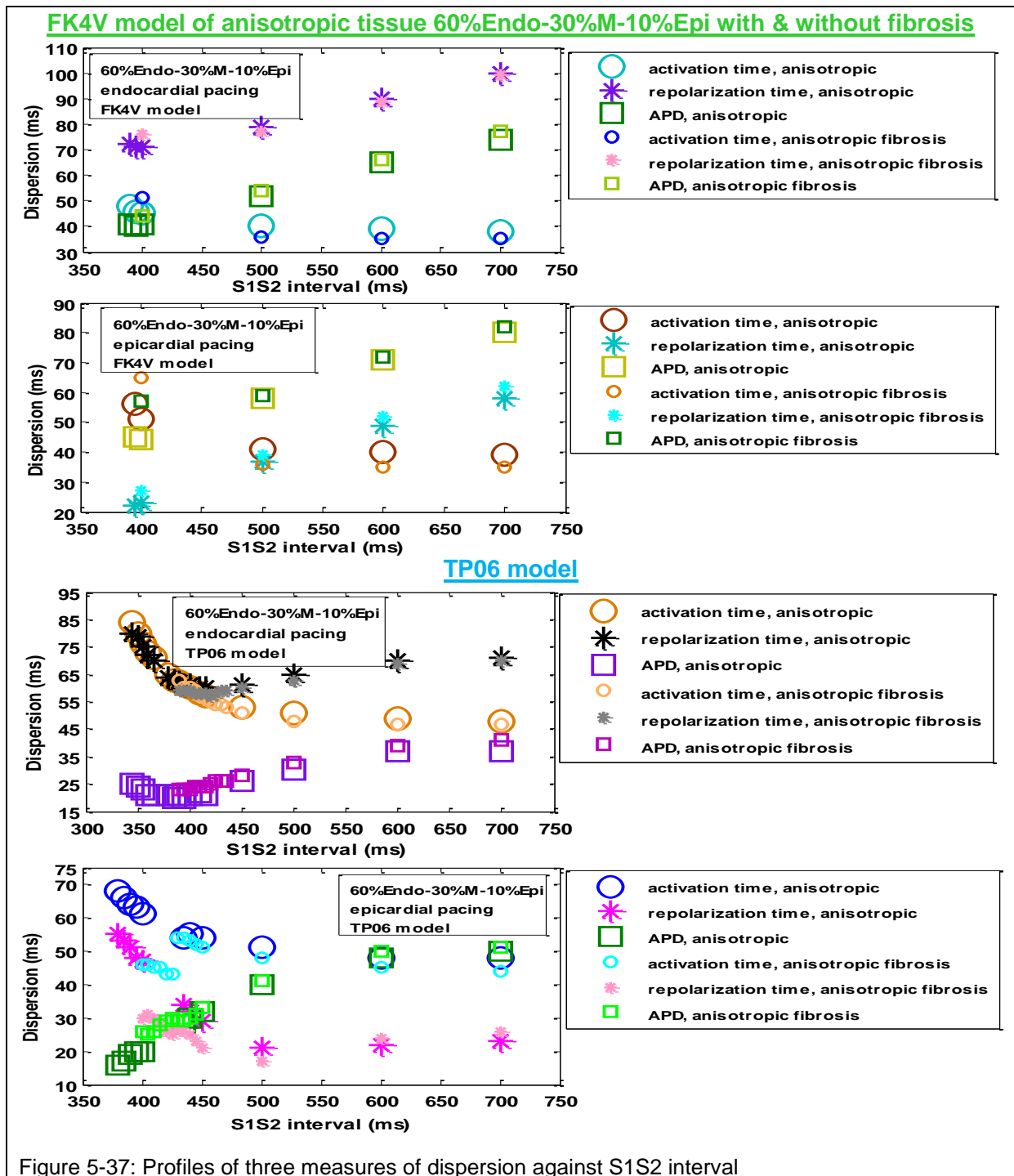


Figure 5-37: Profiles of three measures of dispersion against S1S2 interval

- Heterogeneous tissue composed of 15%Endo-55%M-30%Epi

With the FK4V model with endocardial pacing, dispersion in repolarization time was greater and dispersion in activation time was smaller than other measures of dispersion. With epicardial pacing, dispersion in repolarization time was greater than other measures of dispersion at S1S2 intervals of 700 ms and 600 ms and dispersion in the activation time was smaller than other measures of dispersion for S1S2 intervals of 700-450 ms, Figure 5-38.

With the TP06 model, with endocardial pacing dispersion in repolarization time was greater than dispersion in activation time for long S1S2 intervals of 700-500 ms while it became shorter than that for S1S2 intervals smaller than 500 ms. APD dispersion was greater than other measures of dispersion for long S1S2 intervals of 700-600 ms while became smaller than other measures of dispersion for short S1S2 intervals. With epicardial pacing, dispersion in repolarization time became greater and APD dispersion was smaller than other measures of dispersion during decreasing S1S2 intervals.

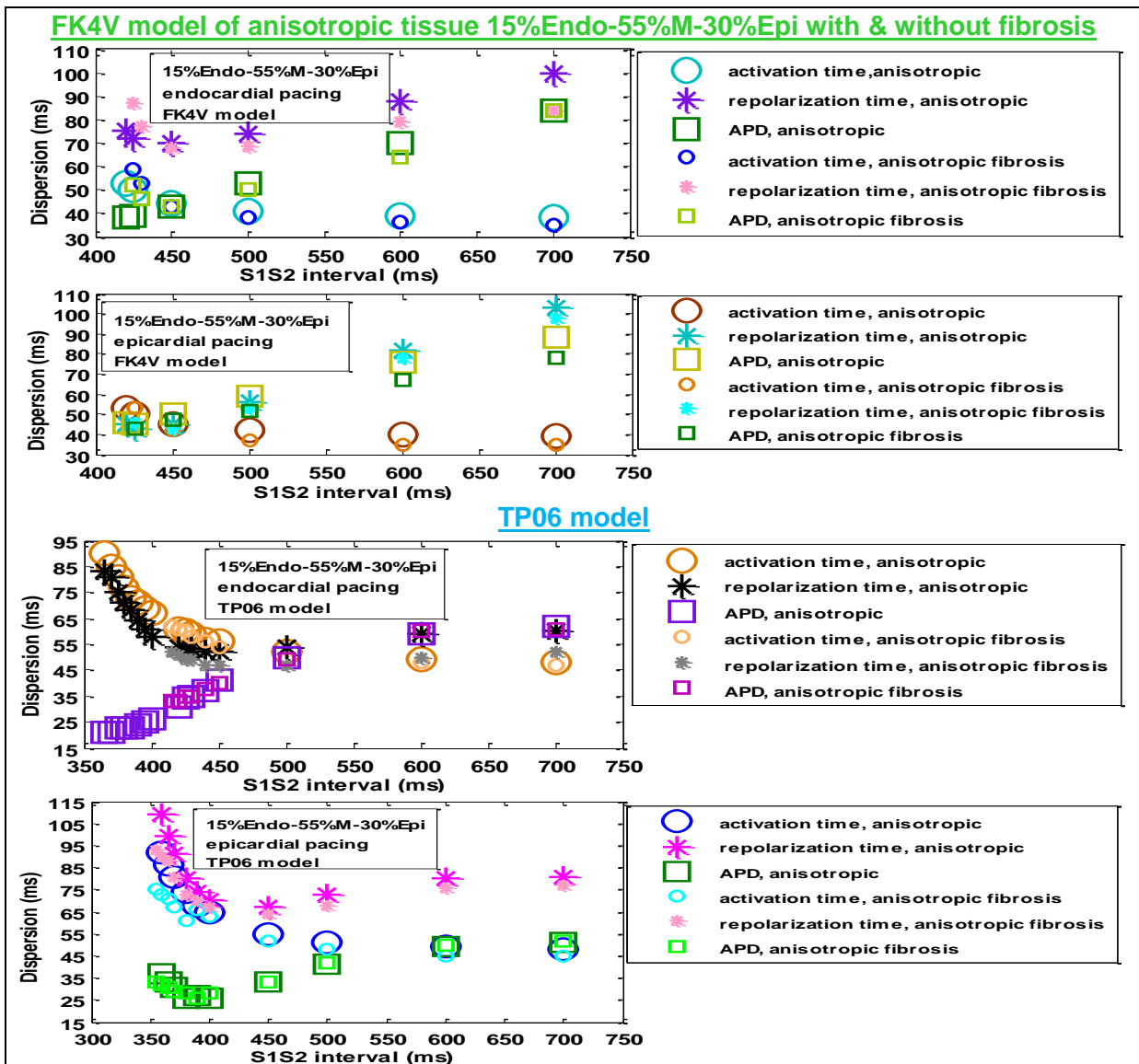


Figure 5-38: Profiles of three measures of dispersion against S1S2 interval

Note: With the TP06 model, three profiles of measures of dispersion had a sharp rise for short S1S2 intervals of 400-350 because the last S1S2 interval for the TP06 model was around 60 ms greater than FK4V model.

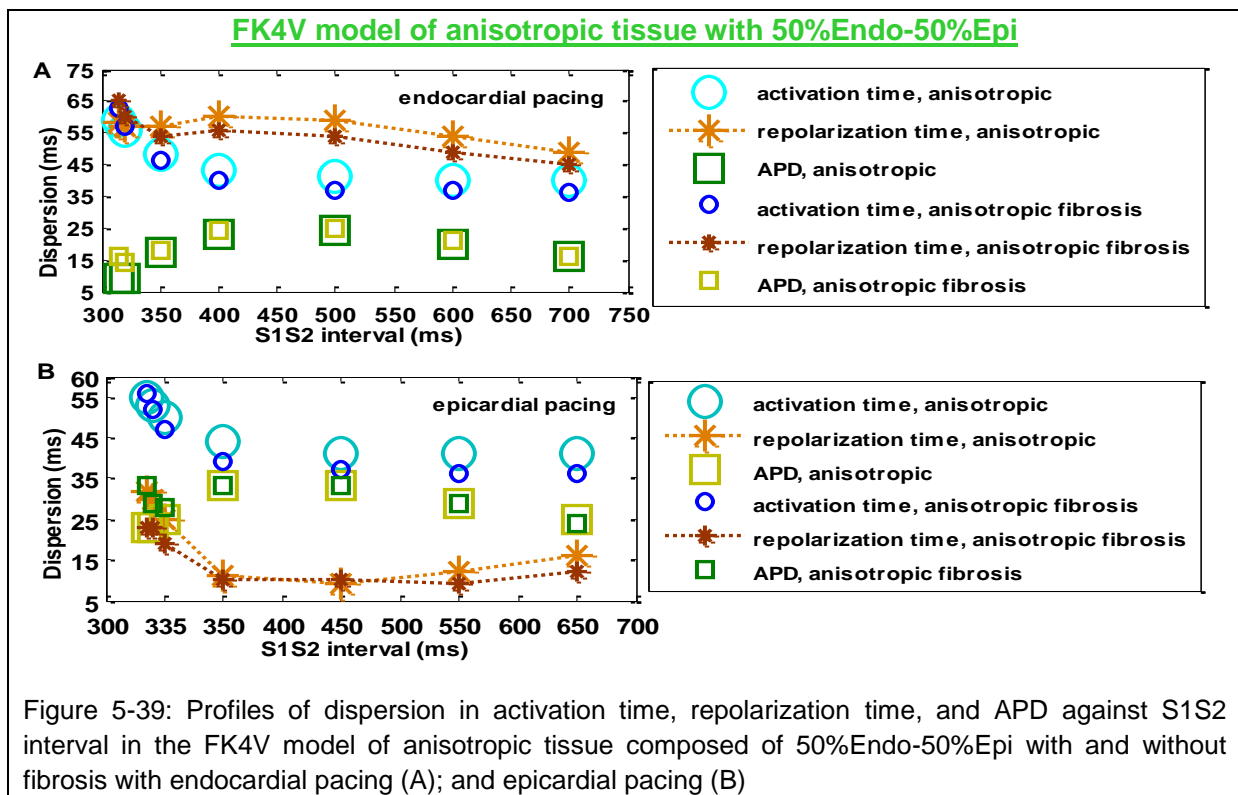
- Heterogeneous tissue composed of 50%Endo-50%Epi with the FK4V model

With endocardial pacing, dispersion in repolarization and activation time changed inversely and APD dispersion was smaller than other measures of dispersion for anisotropic tissue composed of 50%Endo-50%Epi with and without fibrosis as shown in Figure 5-39, A.

With epicardial pacing, dispersion in repolarization decreased for long S1S2 intervals and then increased for short S1S2 intervals of 350-335 ms, as shown in Figure 5-39, B. In addition, dispersion in activation time was greater and dispersion in repolarization time was smaller than other measures of dispersion.

It is important to note that among heterogenous tissue simulated with the FK4V model, anisotropic tissue composed of 50%Endo-50%Epi with and without fibrosis was the only heterogeneous tissue in which dispersion in repolarization time with endocardial pacing and APD dispersion with both endocardial and epicardial pacing initially increased for long S1S2 intervals of 700-500 ms and then decreased for short S1S2 intervals of 400-315 ms.

Furthermore, the profiles of dispersion in repolarization with endocardial and epicardial pacing were approximately symmetric about the dispersion in repolarization axis shown as star-dot in Figure 5-39.



In summary with both models,

- the relationship among three measures of dispersion during decreasing S1S2 intervals was similar for homogenous tissues but it was different for heterogeneous tissues;
- measures of dispersion in activation time gradually increased during decreasing S1S2 interval in both groups of homogenous and heterogeneous tissues in three isotropic, anisotropic, and anisotropic fibrosis tissues.

With an additional mid-myocardial layer in tissues, activation time and the speed of depolarization conduction changed in different regions of tissue particularly in anisotropic tissues with fibrosis using both models that are explained in the following sections.

5.4 Speed of depolarization conduction

Speed of depolarization conduction (conduction velocity in the literature) is important in determining the speed of AP propagation. Slow propagation is one common consequence of cardiac arrhythmia. Fibrosis after myocardial infarction may lead to cardiac conduction disturbances by forming isolating barriers and discontinuities in the real ventricular tissue [7-10].

This part of the Chapter compares the speed of depolarization conduction (1) in tissues with isotropic and anisotropic diffusions; (2) in anisotropic tissues with and without fibrosis; and (3) against experimental and simulation studies. For heterogeneous tissues, the speed of depolarization conduction was calculated in regions of different cell type to highlight the effects of the combination of anisotropy and fibrosis on the speed of depolarization conduction.

In all 3D cubes of tissues with 40×40×60 grid points and space step of 0.2 mm, the transmembrane voltage was created every other point in tissue (20×20×30 transmembrane voltage). Then, 30 transmembrane voltages were extracted from the central region of 3D cubes of tissue (Figure 5-1). In this region, the speed of depolarization conduction for premature S2 beats was calculated for a pair of points in homogenous tissues and two or three pair of points for heterogeneous tissues as follows:

- a pair of points (1, 28) with distance of 10.8 mm (the product of space step 0.2 mm and the number of grid points between these points 54) in homogenous tissues, and in the endocardial and epicardial regions of heterogeneous tissue;
- a pair of points (1, 14) in the endocardial region and (15, 28) in the epicardial region with distance of 5.2 mm for tissue composed of 50%Endo-50%Epi cells;
- a pair of points (1, 5) with distance of 1.8 mm in the endocardial region, a pair of points (6, 21) with distance of 6 mm in the mid-myocardial region, and a pair of points (22, 28) with distance of 2.4 mm in the epicardial region for tissue composed 15%Endo-55%M-30%Epi;
- a pair of points (1, 18) with distance of 6.8 mm in the endocardial region, a pair of points (19, 26) with distance of 2.8 mm in the mid-myocardial region, and a pair of points (27, 28) with distance of 0.4 mm in the epicardial region for tissue composed 60%Endo-30%M-10%Epi;
- a pair of points (1, 3) with distance of 0.8 mm in the endocardial region, a pair of points (4, 11) with distance of 2.8 mm in the mid-myocardial region, and a pair of points (12, 28) with distance of 7.2 mm in the epicardial region for tissue composed 10%Endo-30%M-60%Epi.

This thesis used the same formula for tissues with both endocardial and epicardial pacing that created positive speed of depolarization conduction for tissue with endocardial pacing and negative speed of depolarization conduction for tissues with epicardial pacing. The reason was that the activation time at grid points (cells) away from the stimulus sites was greater than activation time at grid points close to the stimulus sites.

For the FK4V and the TP06 models of isotropic and anisotropic tissues, restitution profiles of speed of depolarization conduction and spatial profiles of activation time are organized in Group Q (Figures Q1 to Q38) provided in Appendix 1. Not surprisingly, isotropic tissues with shorter activation time had faster speed of depolarization conduction compared to anisotropic tissues with longer activation time. For example, the speed of depolarization conduction in homogenous tissues with anisotropic diffusion was approximately half of that in isotropic homogenous tissue (around 0.29-0.18 m/s for anisotropic homogenous tissue with both models).

For anisotropic tissues with and without fibrosis, Figures organized in Group R (Figures R1 to R20) show (1) restitution profiles of speed of depolarization conduction; and (2) restitution profiles of activation time for heterogeneous tissues using the TP06 model. The rest of profiles for the FK4V model of heterogeneous tissues are provided in the Figures R21 to R26 in Appendix 1. These Figures show that the speed of depolarization conduction was suppressed in one or two regions of anisotropic fibrosis heterogeneous tissue that are described in the following sections.

5.4.1 Homogenous tissue: 100%Epi, 100%Endo, and 100%M

Measures of dispersion in activation time during decreasing S1S2 intervals with the TP06 model was around 5 ms to 10 ms greater than those with the FK4V model (as shown in Figure 5-26). Therefore, speed of depolarization conduction for three isotropic homogenous tissues with the TP06 model was slightly slower than that with the FK4V model as shown in Figures R1 and R2.

- With the FK4V model

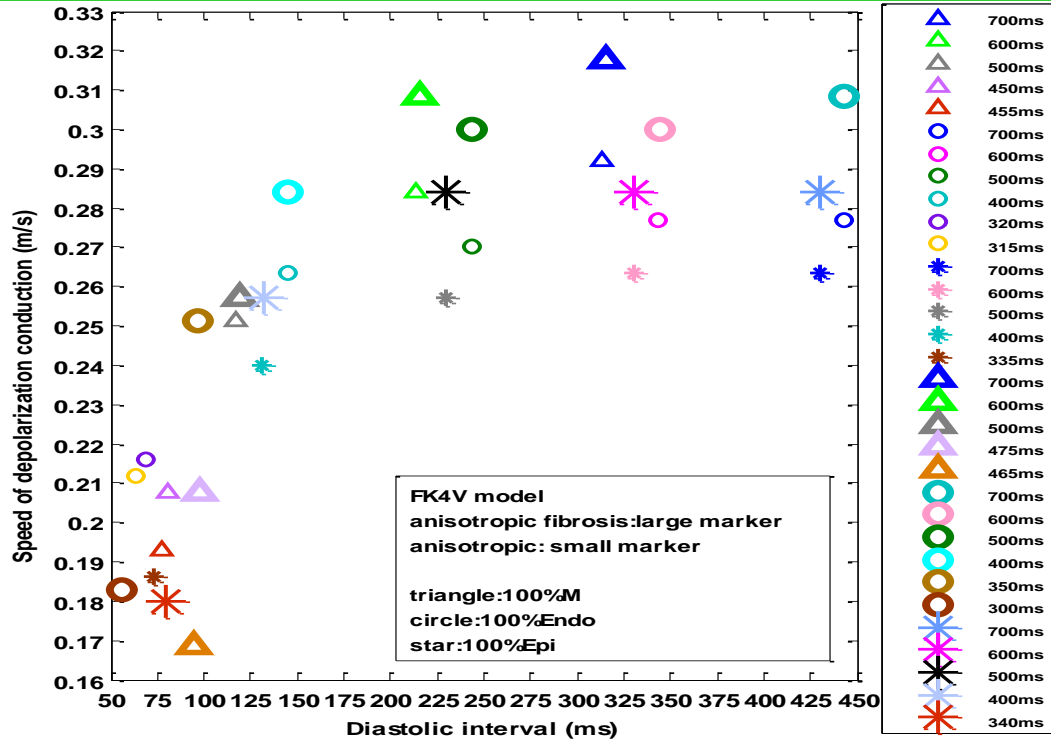
For long S1S2 intervals of 700 ms and 600 ms, the homogenous mid-myocardial tissue with shorter activation time than epicardial and endocardial tissues had the fast speed of depolarization conduction, and epicardial tissue with longer activation time than other tissues had the slowest speed of depolarization conduction.

Measures of dispersion in activation time during decreasing S1S2 intervals in anisotropic tissue with fibrosis were slightly smaller than those for anisotropic tissues without fibrosis. Therefore, the speed of depolarization conduction in tissues with fibrosis became slightly faster around 0.02-0.04 m/s than anisotropic tissue without fibrosis.

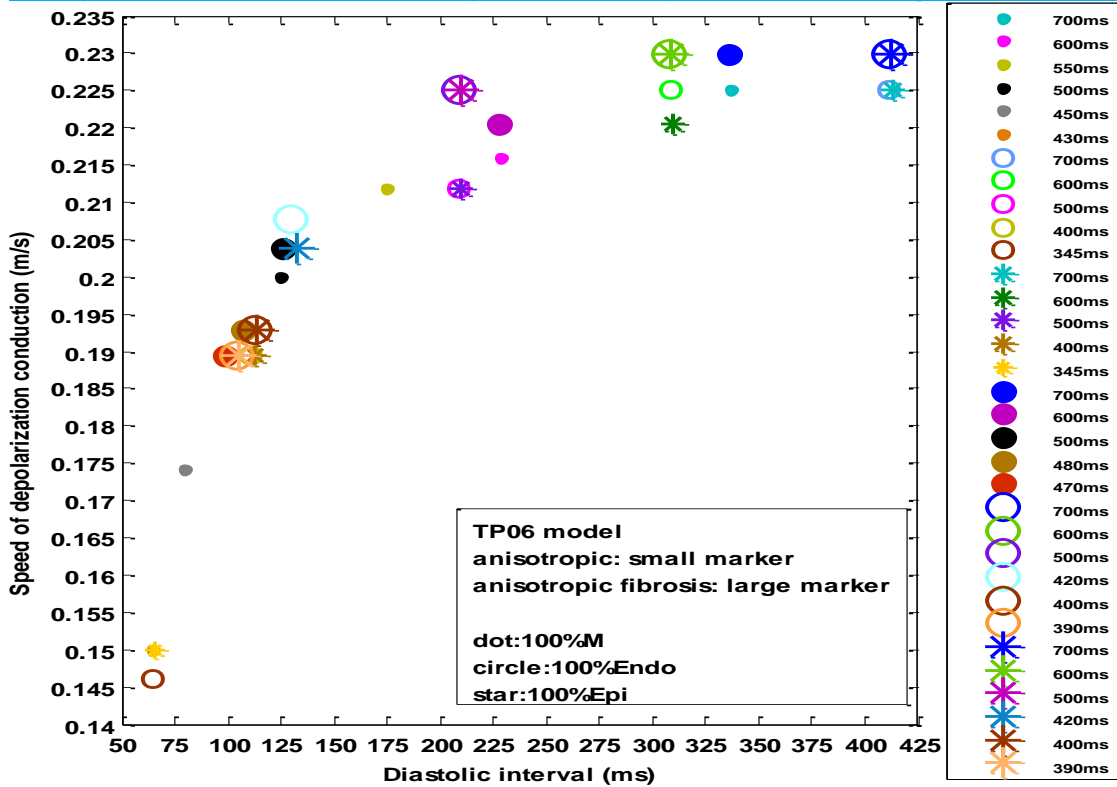
- With the TP06 model

The speed of depolarization conduction for homogenous epicardial, mid-myocardial, and endocardial tissues was fairly similar. The reason was that with the TP06 model, activation time and dispersion in activation time was approximately similar for homogenous epicardial, endocardial and mid-myocardial tissues. For example, the speed of depolarization conduction was around 0.22-0.19 m/s for S1S2 intervals of 700-390 ms in anisotropic fibrosis epicardial and endocardial tissues, and for S1S2 intervals of 700-470 ms in anisotropic fibrosis mid-myocardial tissue.

Group R: FK4V model of anisotropic & anisotropic fibrosis homogenous tissues



Group R: TP06 model of anisotropic & anisotropic fibrosis homogenous tissues



Figures R1-R2: Restitution profiles of speed of depolarization conduction in epicardial, mid-myocardial, and endocardial tissue paced from the bottom edge of tissue

With both models, speed of depolarization conduction in anisotropic fibrosis tissues was slightly faster than that in tissues without fibrosis.

For the TP06 models of three homogenous tissues, speed of depolarization conduction was approximately similar during decreasing S1S2 intervals.

5.4.2 Heterogeneous tissue: 50%Endo-50%Epi

For tissues composed of two ventricular cell types, activation time and speed of depolarization conduction changed not only across tissue but also in the endocardial and epicardial regions during decreasing S1S2 intervals as shown in Figures R3 to R8.

- With the FK4V model

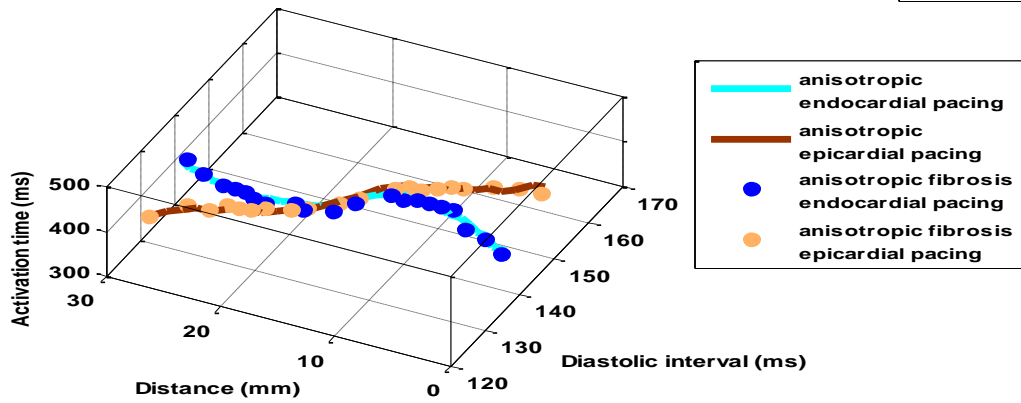
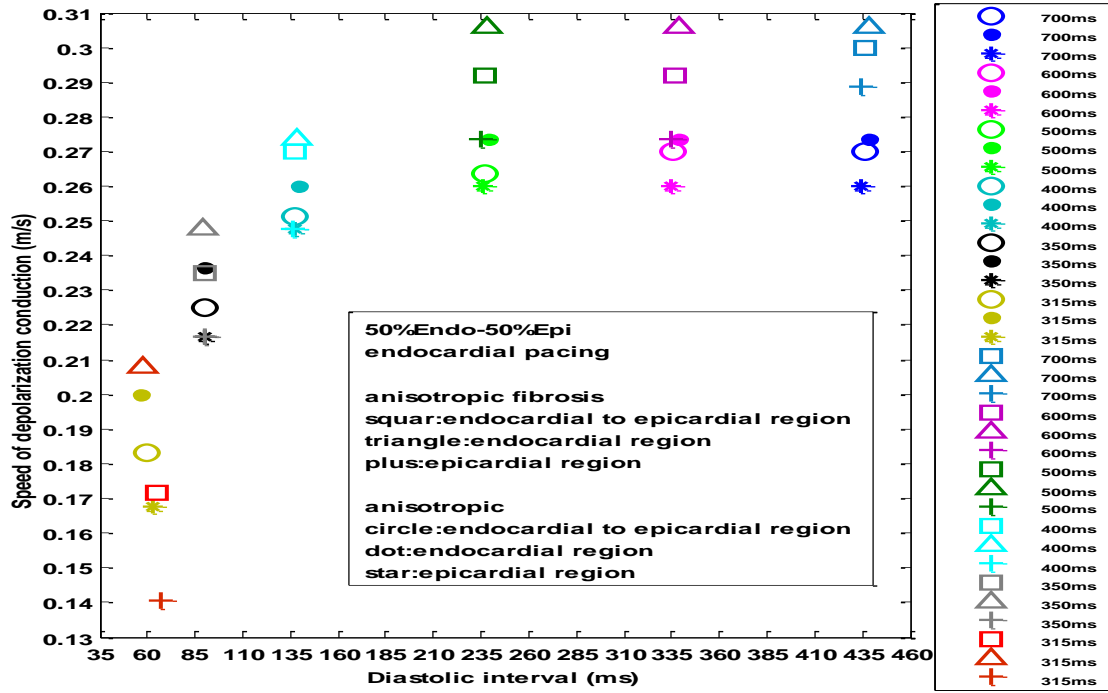
With both endocardial and epicardial pacing, the speed of depolarization conduction throughout the endocardial region was faster than the epicardial region and the region from endocardial to epicardial regions. The reason was that restitution of activation time in the endocardial region was shorter than the epicardial region (described in Section 5.2.3 shown in Figure 5-16, plot B).

The profiles of speed of depolarization conduction with endocardial and epicardial pacing was approximately symmetric about the diastolic interval axis.

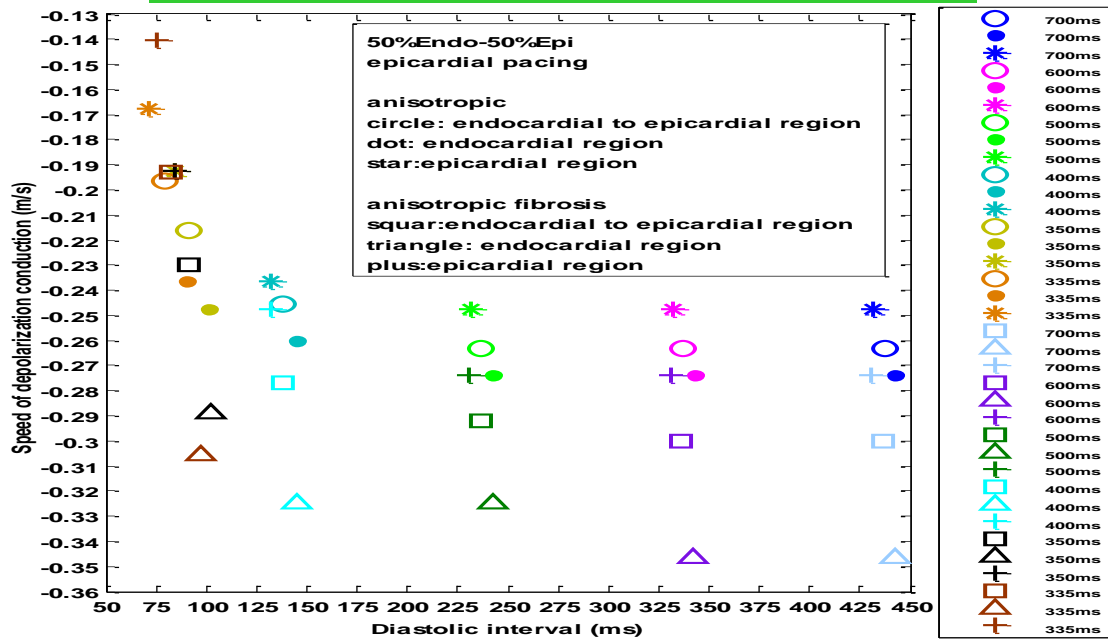
- With the TP06 model

The speed of depolarization conduction throughout epicardial region was faster than other regions for tissues with endocardial pacing while the speed of depolarization conduction was faster throughout endocardial region in tissues with epicardial pacing due to the restitution of activation time as shown in Figures R5 to R8. These results were true for isotropic, anisotropic, and anisotropic fibrosis tissues.

Group R: FK4V model of 50%Endo-50%Epi with endocardial pacing

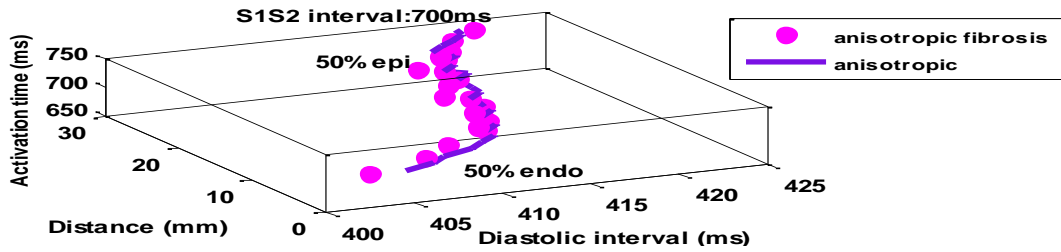
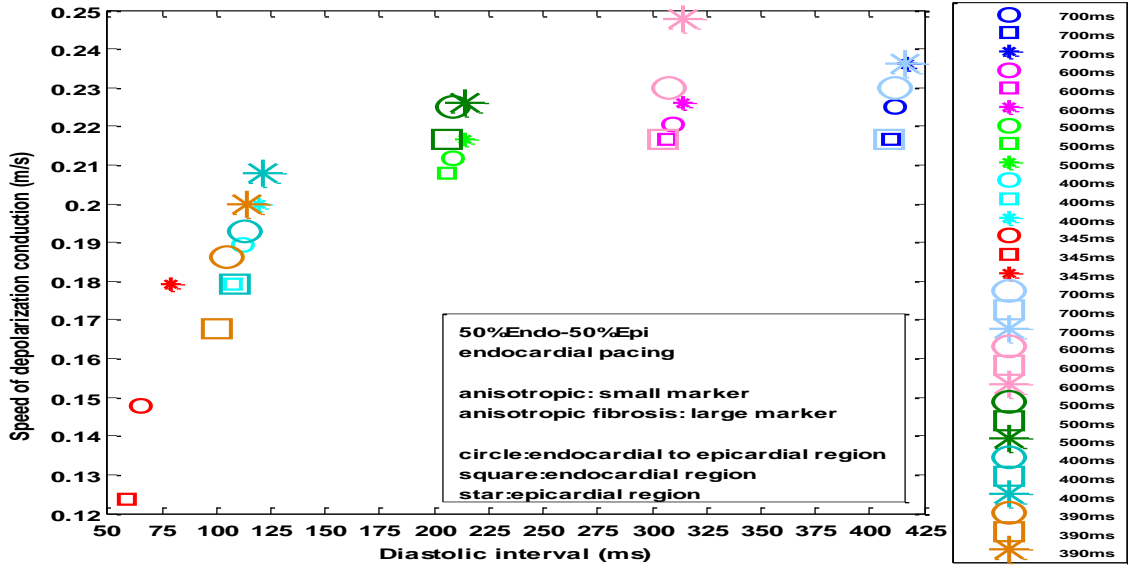


Group R: FK4V model of 50%Endo-50%Epi with epicardial pacing

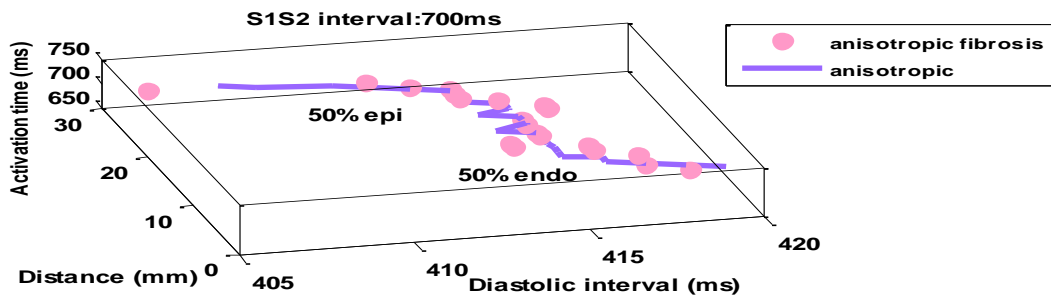
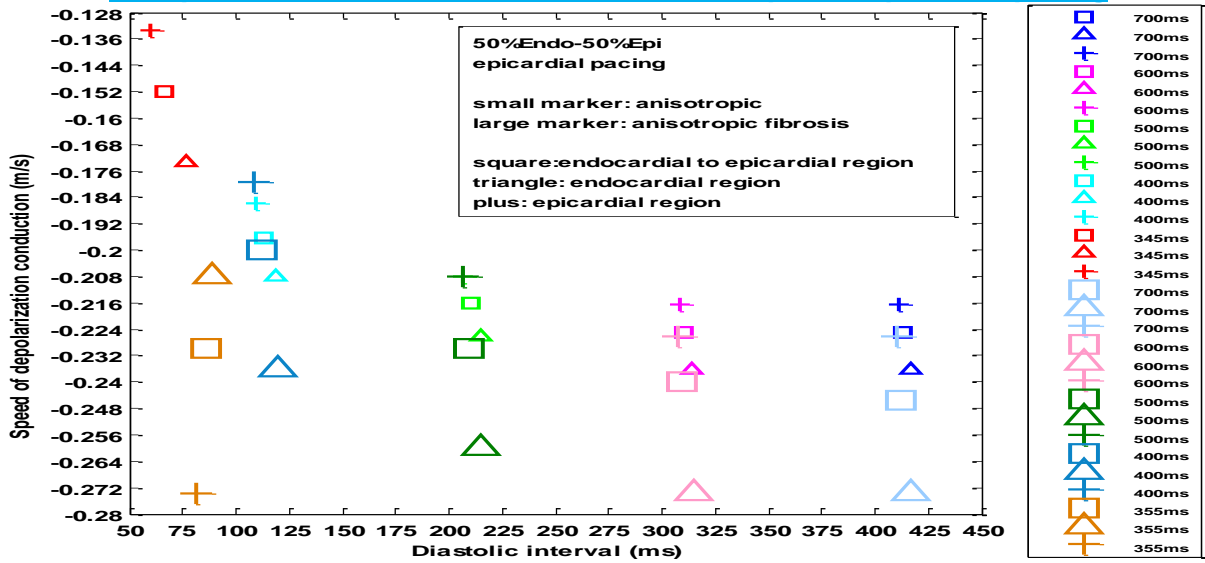


Figures R3-R4: Restitution profiles of speed of depolarization conduction

Group R: TP06 model of tissue 50%Endo-50%Epi with endocardial pacing



Group R: TP06 model of tissue 50%Endo-50%Epi with epicardial pacing



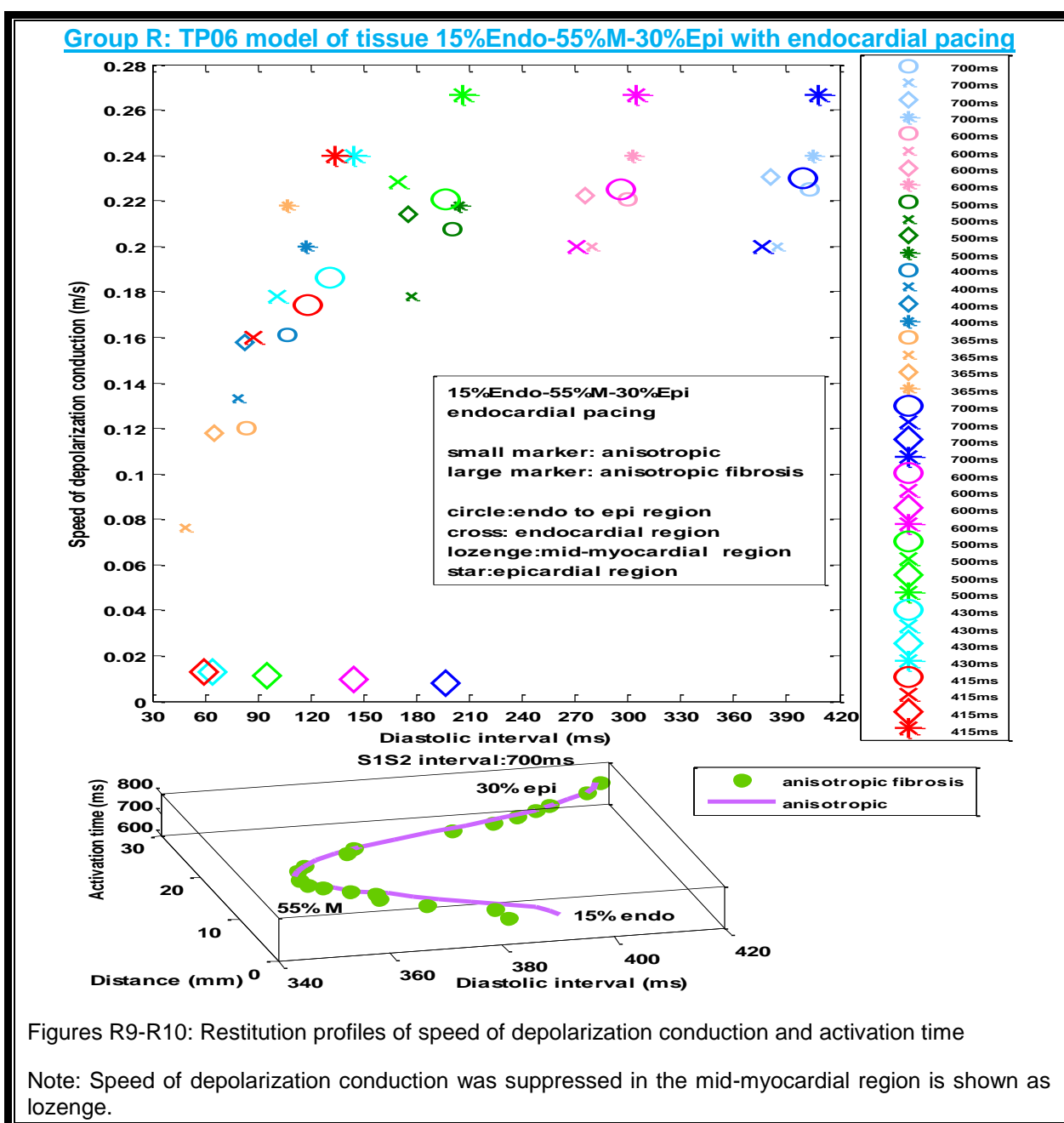
Figures R5-R8: Restitution profiles of speed of depolarization conduction and activation time

5.4.3 Heterogeneous tissue: 15%Endo-55%M-30%Epi

Figures R9 to R20 show how combined effects of anisotropy, simulated fibrosis, restitution properties, and a linear change in fibre orientation can influence restitution profiles of activation time and speed of depolarization conduction in heterogeneous tissues with additional layers of mid-myocardial cells.

Anisotropic fibrosis tissue composed of 15%Endo-55%M-30%Epi compared to tissue without fibrosis could suppress the speed of depolarization conduction throughout the mid-myocardial region with epicardial and endocardial pacing (Figure R9 and Figure R11).

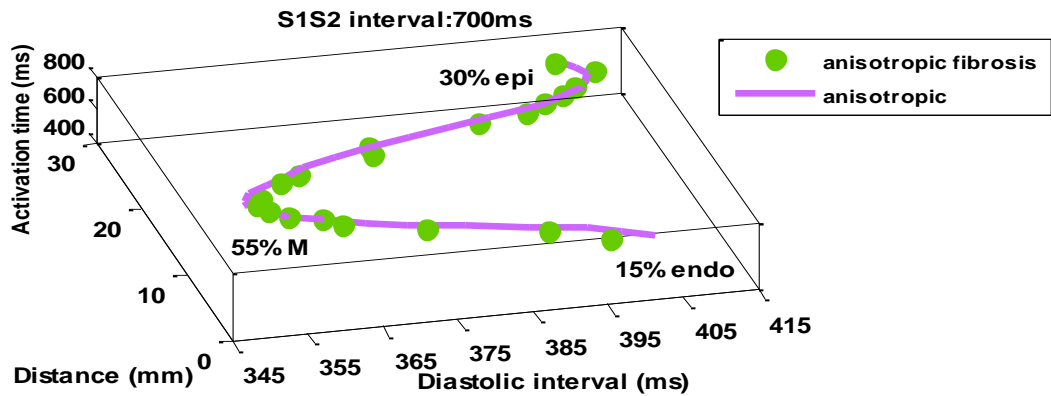
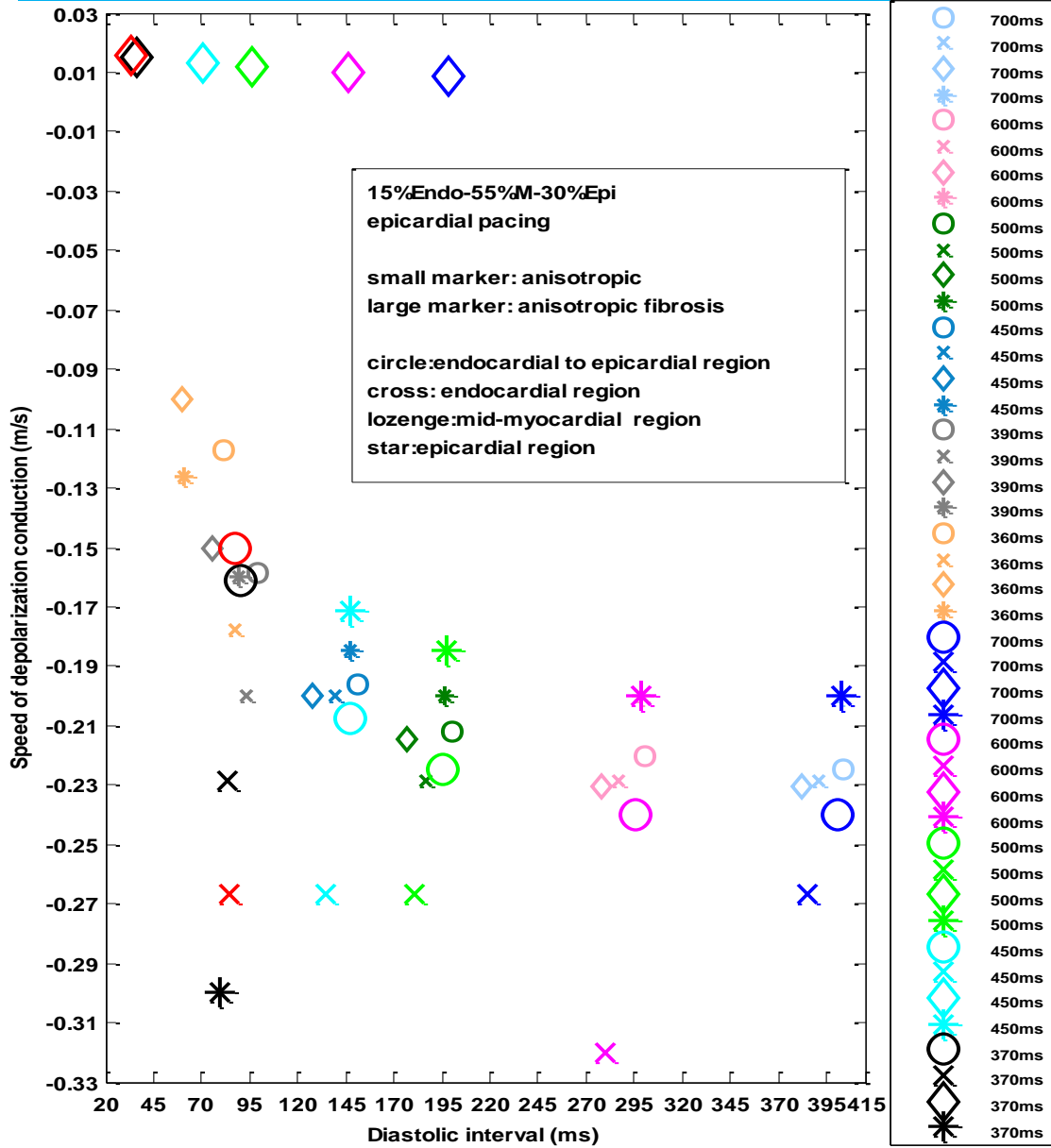
For clarity, restitution profiles of activation time for tissue with and without fibrosis at S1S2 interval of 700 ms is provided that (1) highlight the structural discontinuities due to fibrosis; (2) show the largest activation time of epicardial region that was dominant in tissue with endocardial pacing; and (3) show the largest activation time of endocardial region that was dominant with epicardial pacing compared to that in the mid-myocardial region.



Figures R9-R10: Restitution profiles of speed of depolarization conduction and activation time

Note: Speed of depolarization conduction was suppressed in the mid-myocardial region is shown as lozenge.

Group R: TP06 model of tissue 15%Endo-55%M-30%Epi with epicardial pacing

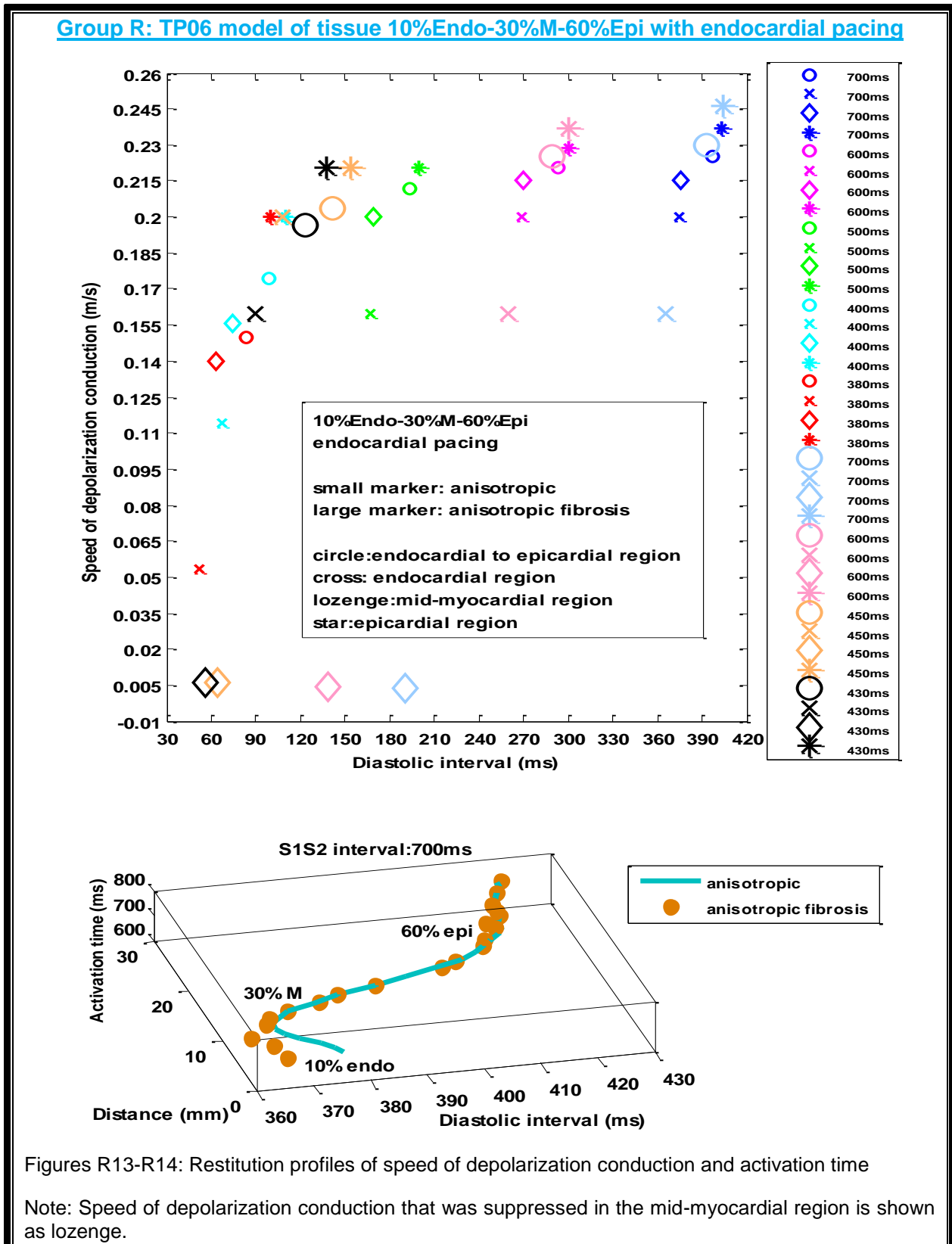


Figures R11-R12: Restitution profiles of speed of depolarization conduction and activation time

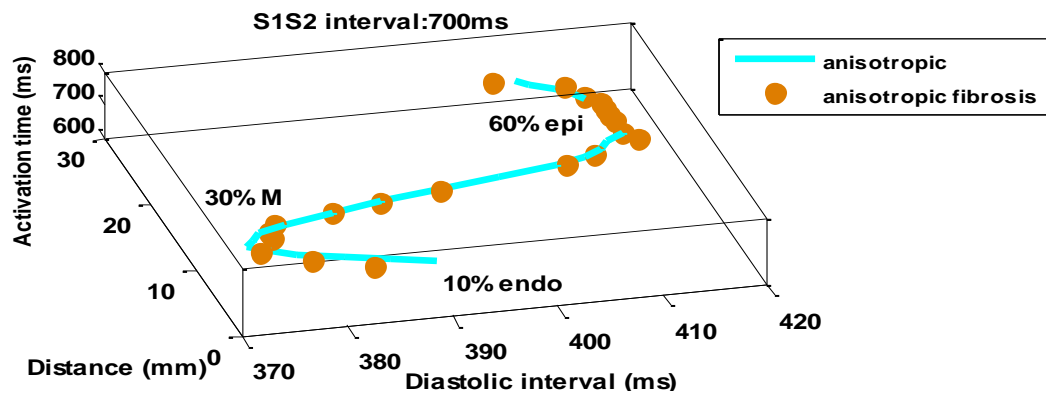
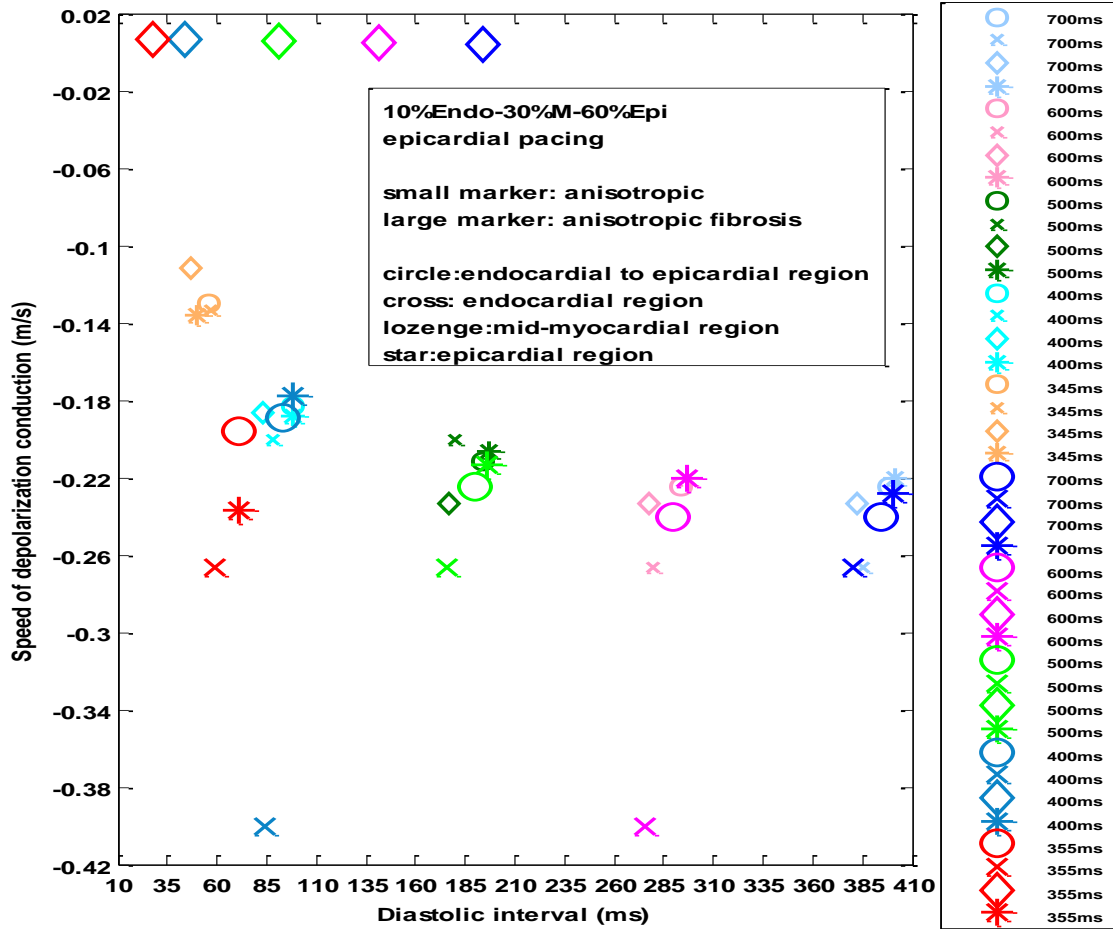
Note: Speed of depolarization conduction that was suppressed in the mid-myocardial region is shown as lozenge.

5.4.4 Heterogeneous tissue: 10%Endo-30%M-60%Epi

Similarly, the speed of depolarization conduction was suppressed throughout the mid-myocardial region in anisotropic fibrosis tissue composed of 10%Endo-30%M-60%Epi compared to tissue without fibrosis with both endocardial and epicardial pacing as shown in Figures R13 to R16.



Group R: TP06 model of tissue 10%Endo-30%M-60%Epi with epicardial pacing



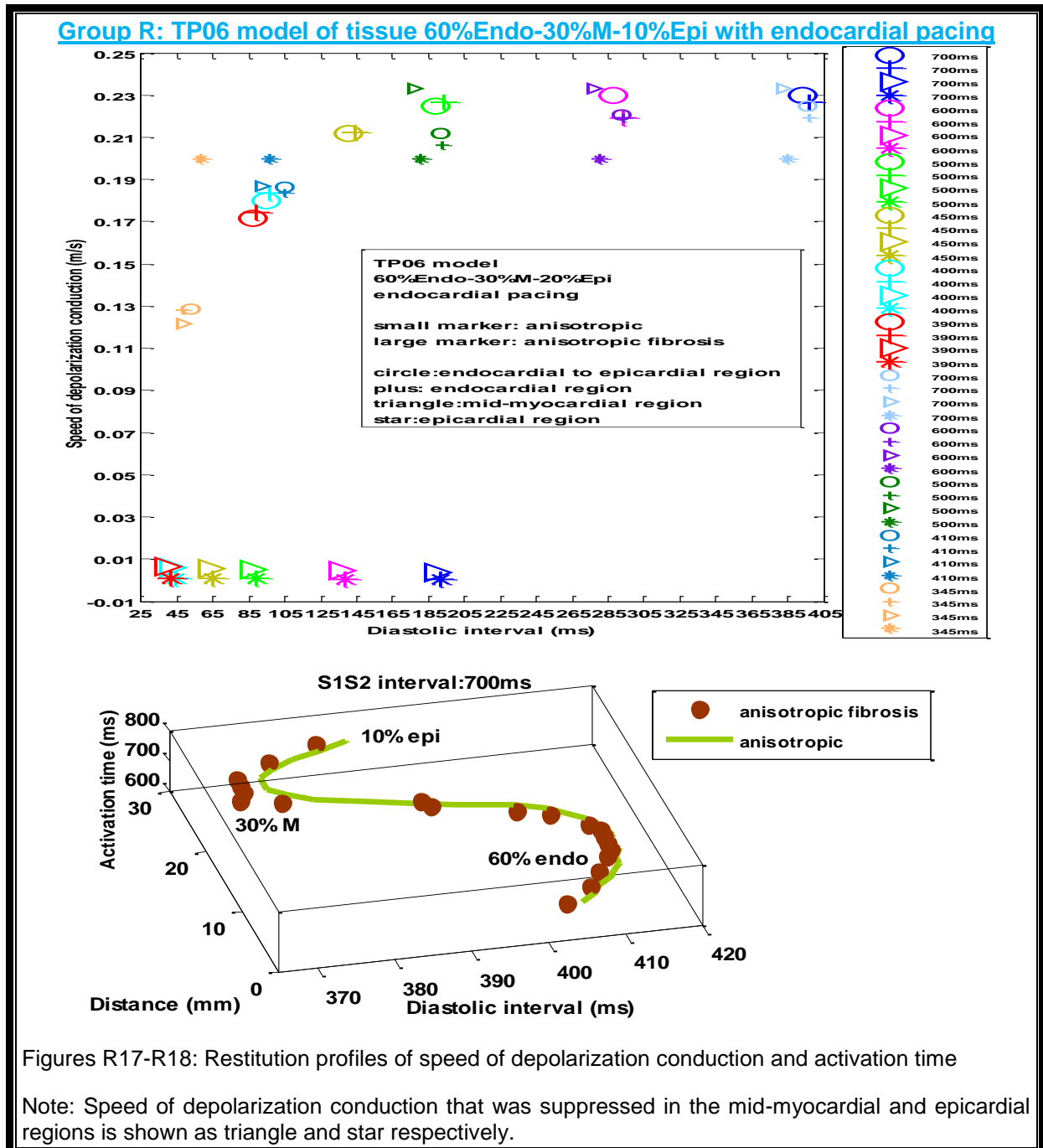
Figures R15-R16: Restitution profiles of speed of depolarization conduction and activation time

Note: Speed of depolarization conduction that was suppressed in the mid-myocardial region is shown as lozenge.

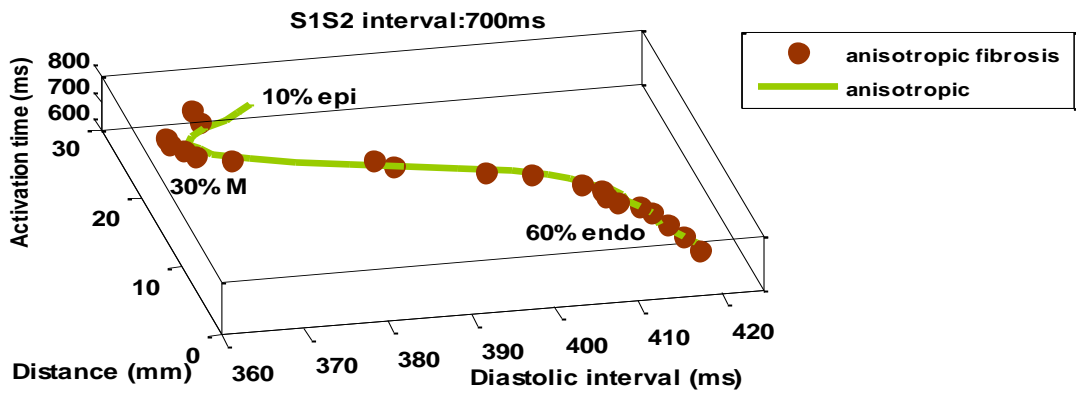
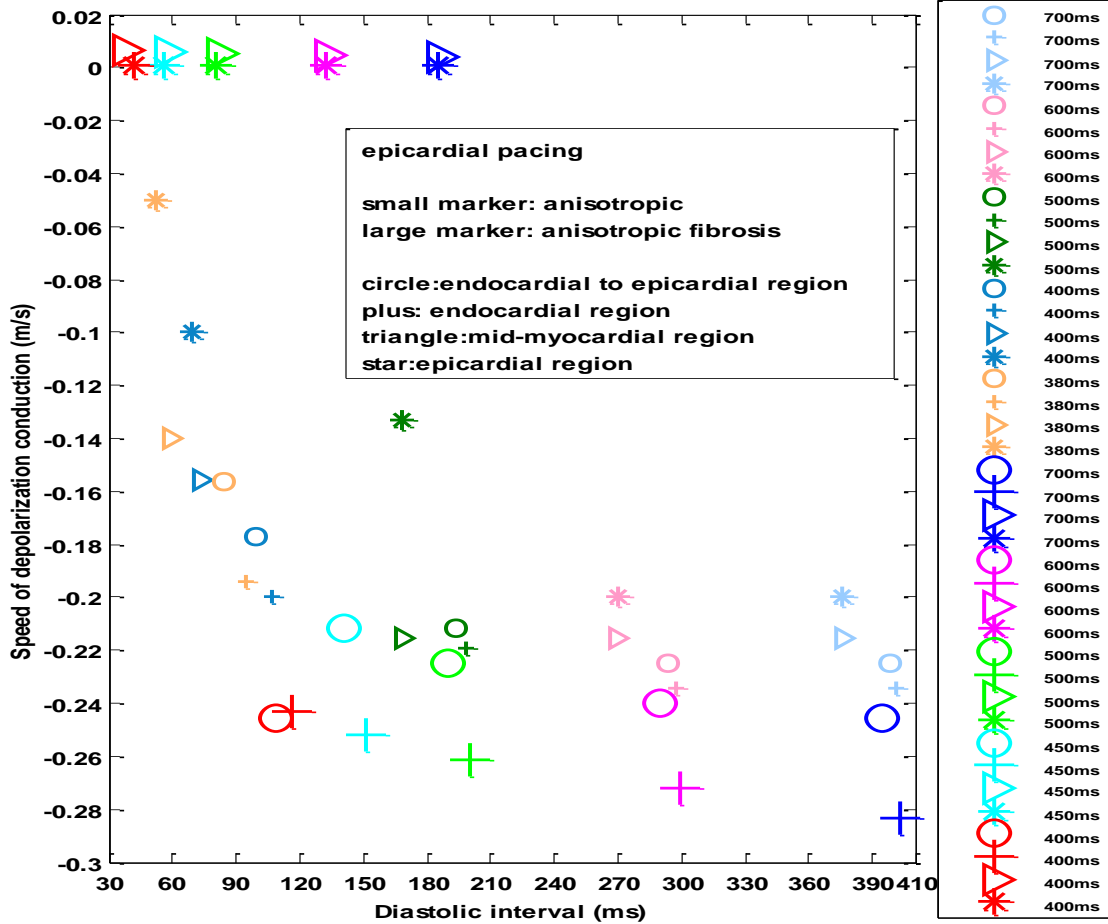
5.4.5 Heterogeneous tissue: 60%Endo-30%M-10%Epi

In anisotropic fibrosis tissue composed of 60%Endo-30%M-10%Epi, speed of depolarization conduction was suppressed throughout both mid-myocardial and epicardial regions with epicardial and endocardial pacing as shown in Figures R17 to R20.

The speed of depolarization conduction from endocardial to epicardial region was governed by the speed of depolarization conduction throughout endocardial region that was around 0.2 m/s.



Group R: TP06 model of tissue 60%Endo-30%M-10%Epi with epicardial pacing



Figures R19-R20: Restitution profiles of speed of depolarization conduction and activation time

Speed of depolarization conduction that was suppressed in the mid-myocardial and epicardial regions is shown as triangle and star respectively.

5.4.6 Summary of the speed of depolarization conduction

This part of the Chapter summarized the main findings about activation time and speed of depolarization conduction for premature S2 beats in all tissues with both models.

First, all tissues with anisotropic diffusion had longer activation time (and dispersion in activation time) and slower speed of depolarization conduction compared with tissues with isotropic diffusion. In addition, anisotropic tissues with fibrosis had smaller dispersion in activation time during decreasing S1S2 intervals and slightly faster speed of depolarization conduction than anisotropic tissues without fibrosis. The reason was that the speed of depolarization conduction had inverse relationship with the difference activation time of two cells in tissue based on the formula that was used in this thesis.

Second, with anisotropic diffusion, the speed of depolarization conduction at different S1S2 intervals depended on the differences in local restitution.

Third, in anisotropic fibrosis heterogeneous tissues composed of three ventricular cell types with both endocardial and epicardial pacing, the speed of depolarization conduction was suppressed throughout:

- mid-myocardial region in tissues composed of 15%Endo-55%M-30%Epi and 10%Endo-30%M-60%Epi;
- mid-myocardial region and epicardial regions in tissue composed of 60%Endo-30%M-10%Epi, therefore, the speed of depolarization conduction was controlled by the speed of depolarization conduction throughout endocardial region.

The possible reasons are (1) anisotropic tissue with fibrosis compared with anisotropic tissue without fibrosis decreased activation time and dispersion in activation time for long and short S1S2 intervals; and (2) combination of anisotropy, fibrosis, and restitution of activation time may decrease bulk electrical coupling and suppress the speed of depolarization conduction.

The results emphasize that the rate dependency of premature beats influences both activation time and repolarization time (as shown in Figures organized in Group T). Consequently, activation time restitution and anisotropy are two important determinants for the speed of AP propagation in heterogeneous tissue with and without simulated fibrosis.

The next section provides a general comparison between numerical values of calculated speed of depolarization conduction in this thesis and experimental and simulation studies.

5.4.7 Comparison with previous studies

In general, the variation of speed of depolarization conduction for premature S2 beats in the FK4V and the TP06 models of homogenous and heterogeneous tissues during decreasing S1S2 intervals in this thesis was in agreement with available experimental and simulation studies.

For example, in human experimental study by Taggart et al. [38], the transmural conduction velocity slowed from 0.51 to 0.26 m/s based on plunge electrode recordings in patients with coronary artery disease paced from epicardial surface at cycle length of 500 ms. In the study by Yue et al. [25], conduction velocity varied from 0.1 m/s to 0.9 m/s for short diastolic intervals in 16 segments in the endocardial region of human left ventricle without structural heart disease using noncontact mapping method. The average transmural

conduction velocity was 0.41 m/s at basic cycle length of 2000 ms in the human study by Glukhov et al. [27]. In the endocardial region of right ventricular free wall in five cardiomyopathic patients who underwent transplantation, conduction velocity varied from maximum value of 0.87 m/s to the minimum value of 0.41 m/s, Nanthakumar et al. [39].

In arterially perfused canine left ventricular wedge preparations (Yan et al. [28]), at basic cycle length of 1000 ms, the average transmural conduction time was 29.3 ms (with 12.9 mm the average wedge thick) and the average conduction velocity was 0.44 m/s comparable to that recorded in vivo [40].

For the FK4V and TP06 models of anisotropic heterogeneous tissues composed of three ventricular cell types with and without fibrosis, the speed of depolarization conduction changed approximately from 0.0002 m/s to 0.2 m/s in different regions of tissue with endocardial pacing. Similarly, a clinical and modelling study by Narayan et al. [15] showed that transmural conduction velocity did not change greater than 0.1 m/s in any region of the simulated cube of tissue with dimension of $9 \times 0.075 \times 0.075$ mm² composed of 15%Endo-55%M-30%Epi cells paced at 109 beats/min (or at cardiac cycle length of 540 ms). They used the TP06 model for describing the membrane kinetics of human ventricular cells and modelled transmural heterogeneity in ion channels expression between epicardial, mid-myocardial, and endocardial layers according to Table 1 of Weiss et al. [41]. They used a bidomain model with conductivity values to produce transmural conduction velocity of 0.4 m/s in the endocardial and mid-myocardial regions, and 0.28 m/s in the epicardial region from [35].

In the model with realistic morphology of the human torso and the heart with anisotropic diffusion (Okada et al. [13]), the transmural conduction velocity varied from 0.5 m/s to 0.62 m/s from the epicardial to endocardial region which was slightly faster than the speed of depolarization conduction in this thesis. However, the spatial APD profiles of study by Okada et al. [13] was similar to spatial APD profiles of simulated heterogeneous tissues composed of three ventricular cell type (described in section 5.2.4-2, shown in Figure 5-23). The difference in speed of propagation is possibly due to the difference in activation time or distance between two cells.

5.5 Vulnerability to ventricular arrhythmia

This part of the Chapter

1. highlights when, which S1S2 intervals, and where tissues may become vulnerable to ventricular arrhythmia;
2. suggests that spatial profiles of repolarization time and restitution profile of activation time as two useful tools can be used for studying premature beats during decreasing S1S2 intervals.

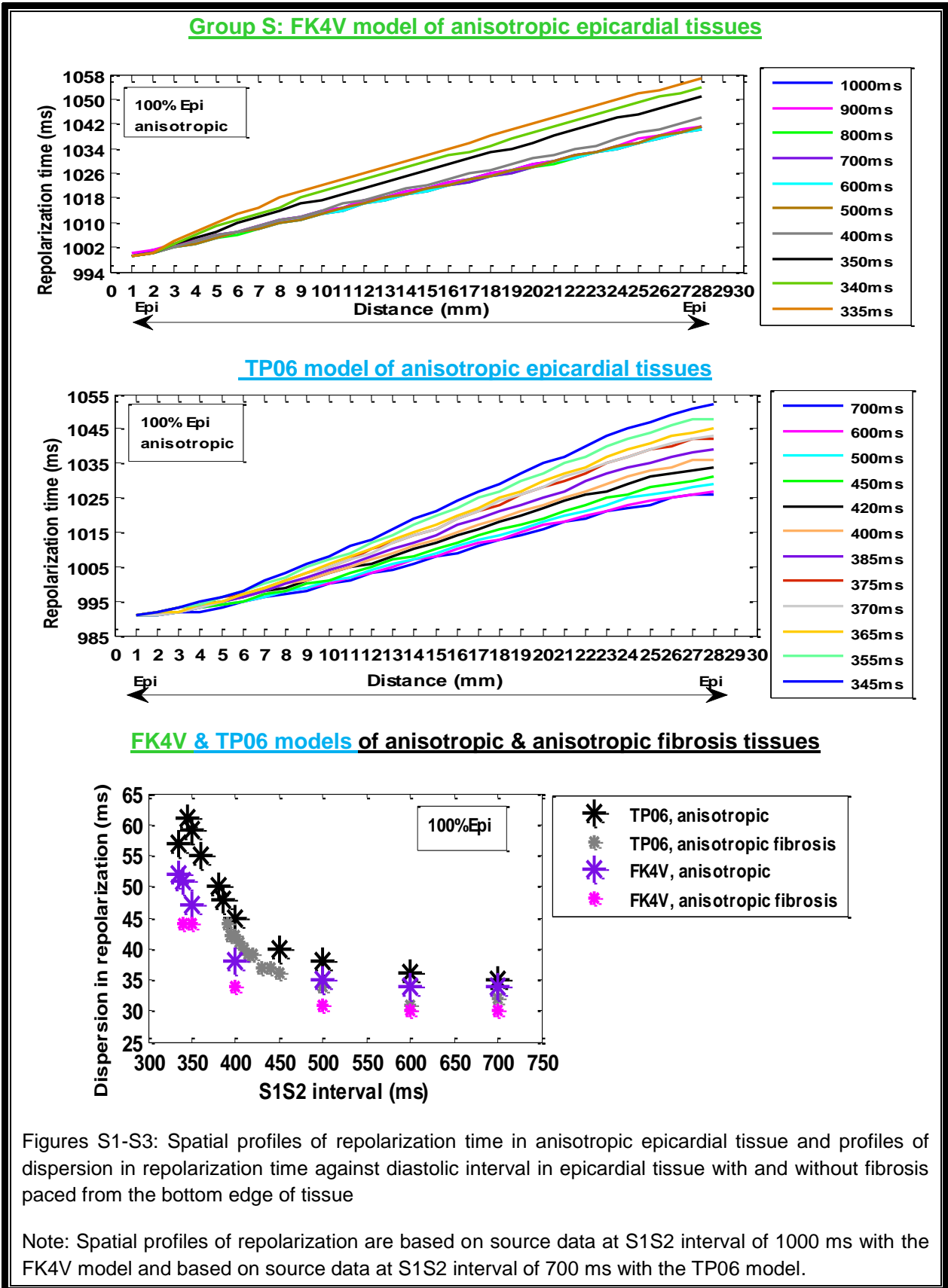
5.5.1 When

The changes in spatial profiles of repolarization time during decreasing S1S2 interval in three regions of heterogeneous tissues composed of three ventricular cell type represent clearly why dispersion in repolarization time changes for long and short S1S2 intervals as shown in Figures organized in Group S (Figures S1 to S33). Comparison between spatial profiles of repolarization time during decreasing S1S2 intervals and profiles of dispersion in repolarization time against S1S2 interval showed that:

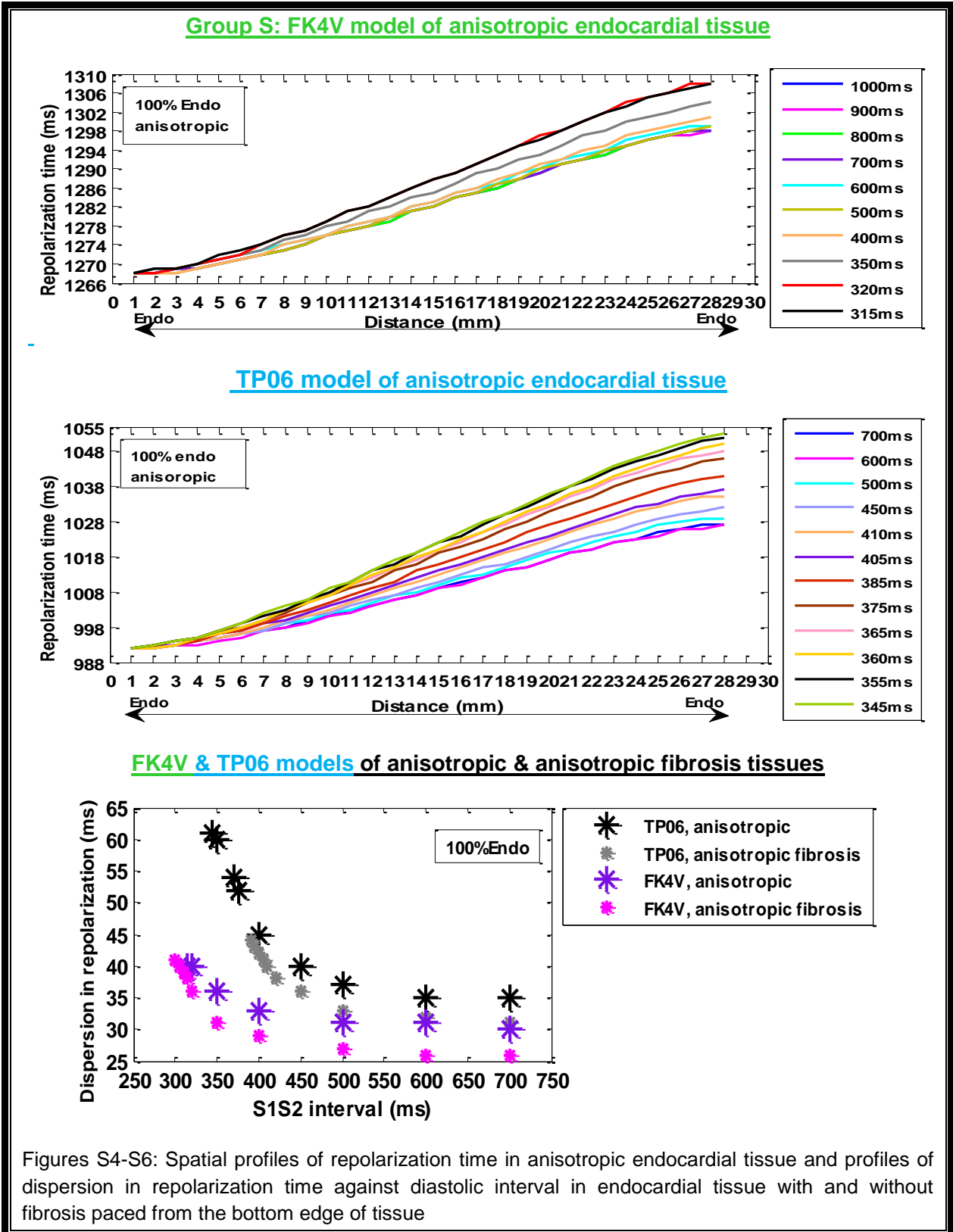
1. For homogenous epicardial tissue, dispersion in repolarization time gradually increased from long to short S1S2 intervals because repolarization time gradually increased with decreasing S1S2 intervals (Figures S1-S9).
2. For heterogeneous tissue composed of epicardial, endocardial, and additional mid-myocardial cells, dispersion in repolarization time initially decreased for long S1S2 intervals. For short S1S2 intervals, dispersion of repolarization time suddenly increased when (1) repolarization time in the epicardial region became close or greater than the largest repolarization time in mid-myocardial region with endocardial pacing; and (2) when the largest repolarization time in mid-myocardial region became close or greater than repolarization time in the endocardial region with epicardial pacing (Figure S10-S27).
3. The region where these changes occurred were the transition region between mid-myocardial and epicardial regions in tissues with endocardial pacing and between endocardial and mid-myocardial regions in tissues with epicardial pacing.
4. The only exception was for heterogeneous tissue composed of 50%Endo-50%Epi with the FK4V model. With endocardial pacing, dispersion in repolarization time initially increased for long S1S2 intervals because the largest value of repolarization time in the endocardial region was smaller than repolarization time in the epicardial region. When the largest value of repolarization time of endocardial region became close to the repolarization time of epicardial region, repolarization time of epicardial region gradually decreased for short S1S2 intervals. With epicardial pacing, dispersion in repolarization increased for S1S2 intervals of 400-335 ms when the largest repolarization time in the epicardial region became close to the repolarization time in the endocardial region (Figures S28-S33).
5. Not surprisingly, the region that was vulnerable to arrhythmia was between endocardial and epicardial regions for tissue composed of two ventricular cell type.

These changes may create conditions for re-entry and promote wave break of AP depolarization and repolarization. Moreover, these findings may explain why reversing the direction of activation in electrically heterogeneous ventricular myocardium increases the dispersion in transmural repolarization in some patients [17, 18] while decreases in others [19].

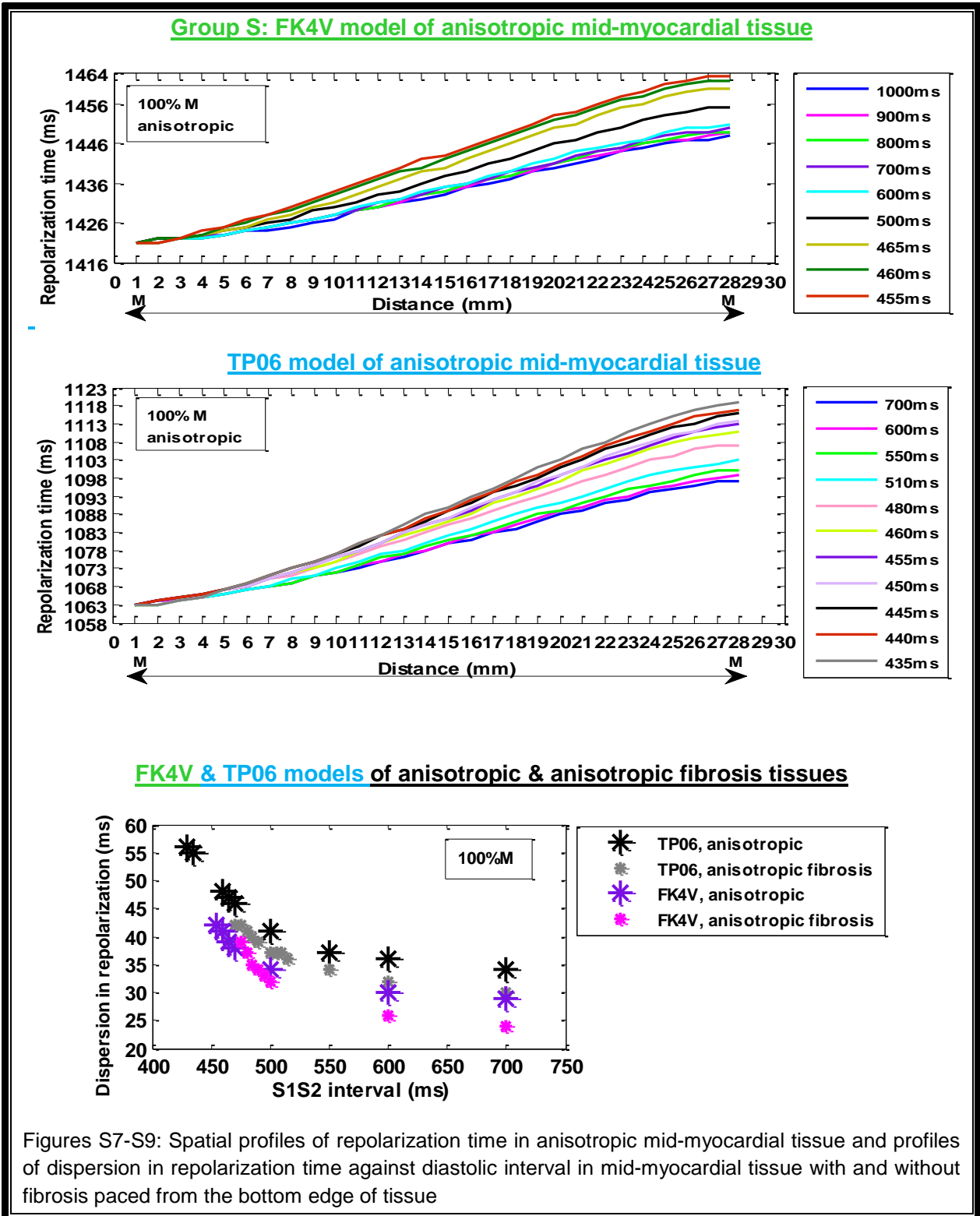
- Homogenous epicardial tissues



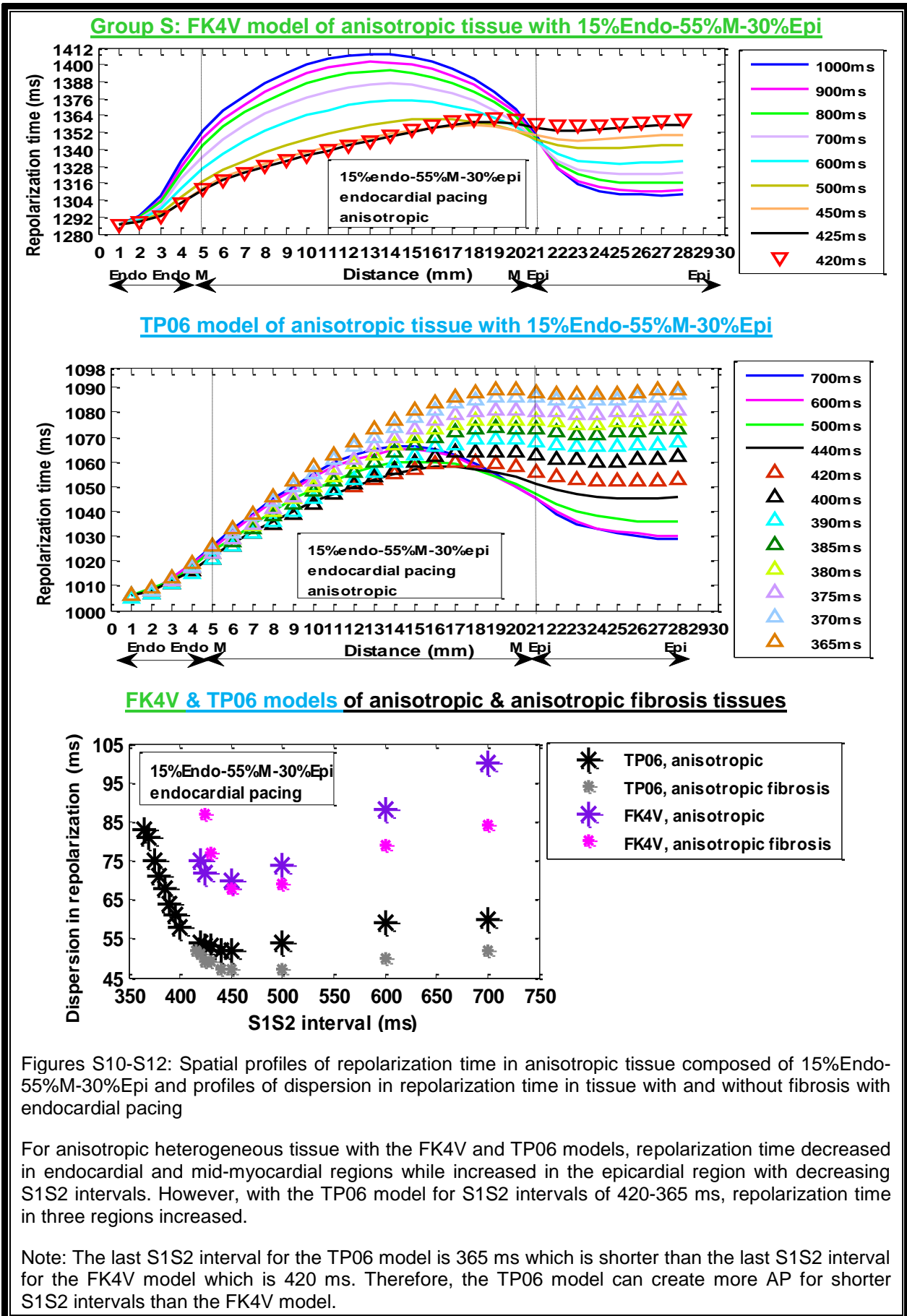
- Homogenous endocardial tissues



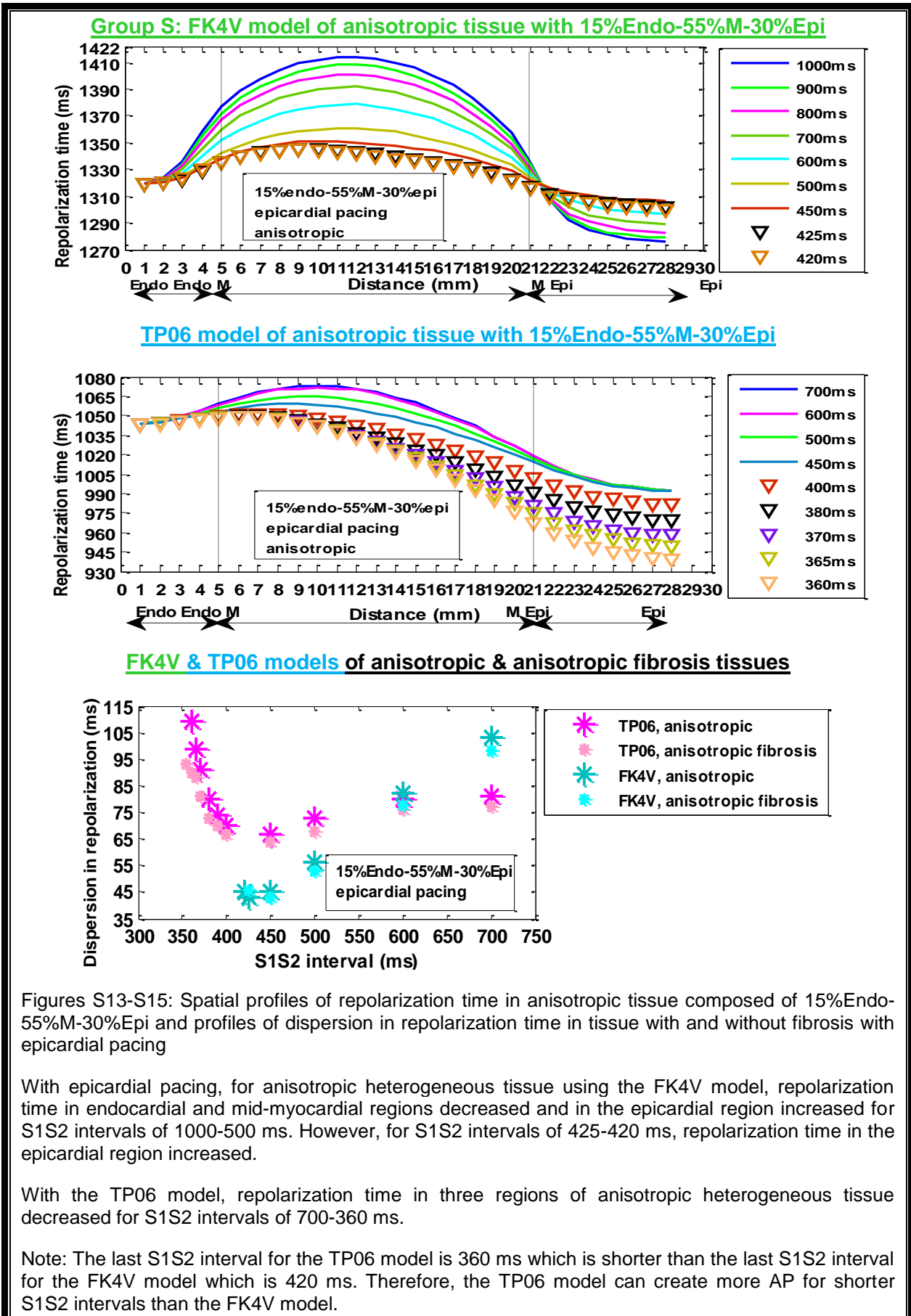
- Homogenous mid-myocardial tissues



- Tissue composed of 15%Endo-55%M-30%Epi with endocardial pacing



- Tissue composed of 15%Endo-55%M-30%Epi with epicardial pacing



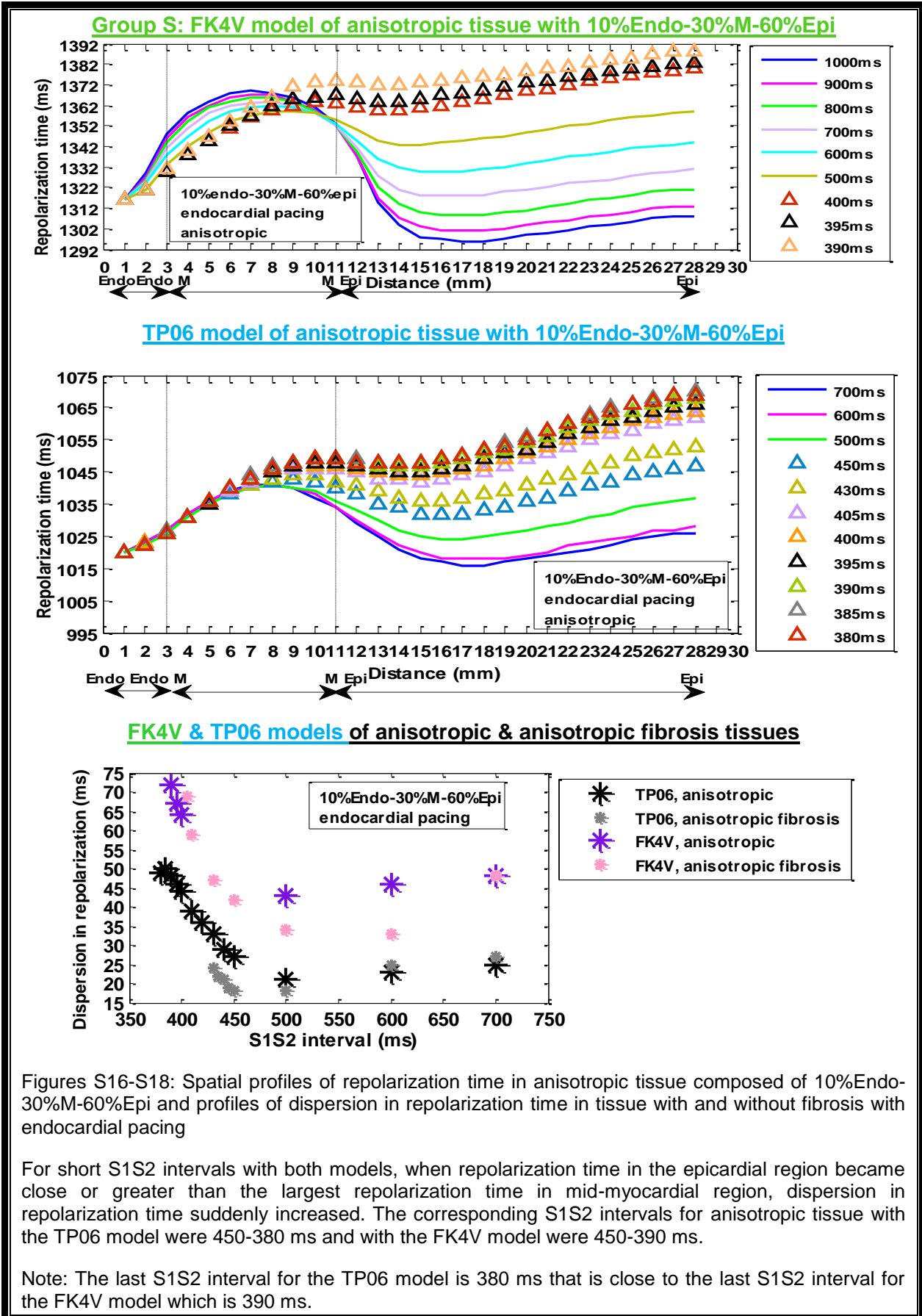
Figures S13-S15: Spatial profiles of repolarization time in anisotropic tissue composed of 15%Endo-55%M-30%Epi and profiles of dispersion in repolarization time in tissue with and without fibrosis with epicardial pacing

With epicardial pacing, for anisotropic heterogeneous tissue using the FK4V model, repolarization time in endocardial and mid-myocardial regions decreased and in the epicardial region increased for S1S2 intervals of 1000-500 ms. However, for S1S2 intervals of 425-420 ms, repolarization time in the epicardial region increased.

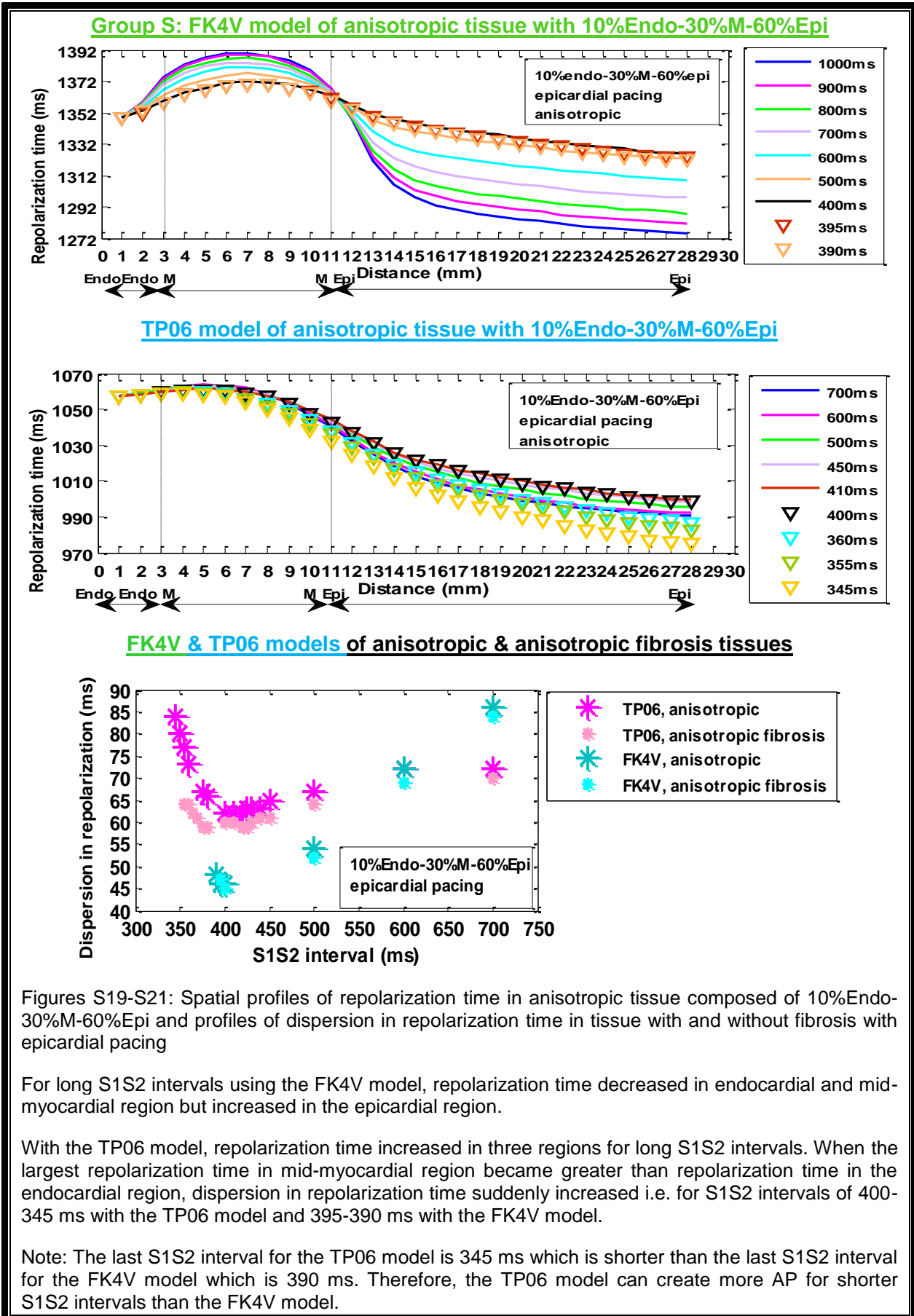
With the TP06 model, repolarization time in three regions of anisotropic heterogeneous tissue decreased for S1S2 intervals of 700-360 ms.

Note: The last S1S2 interval for the TP06 model is 360 ms which is shorter than the last S1S2 interval for the FK4V model which is 420 ms. Therefore, the TP06 model can create more AP for shorter S1S2 intervals than the FK4V model.

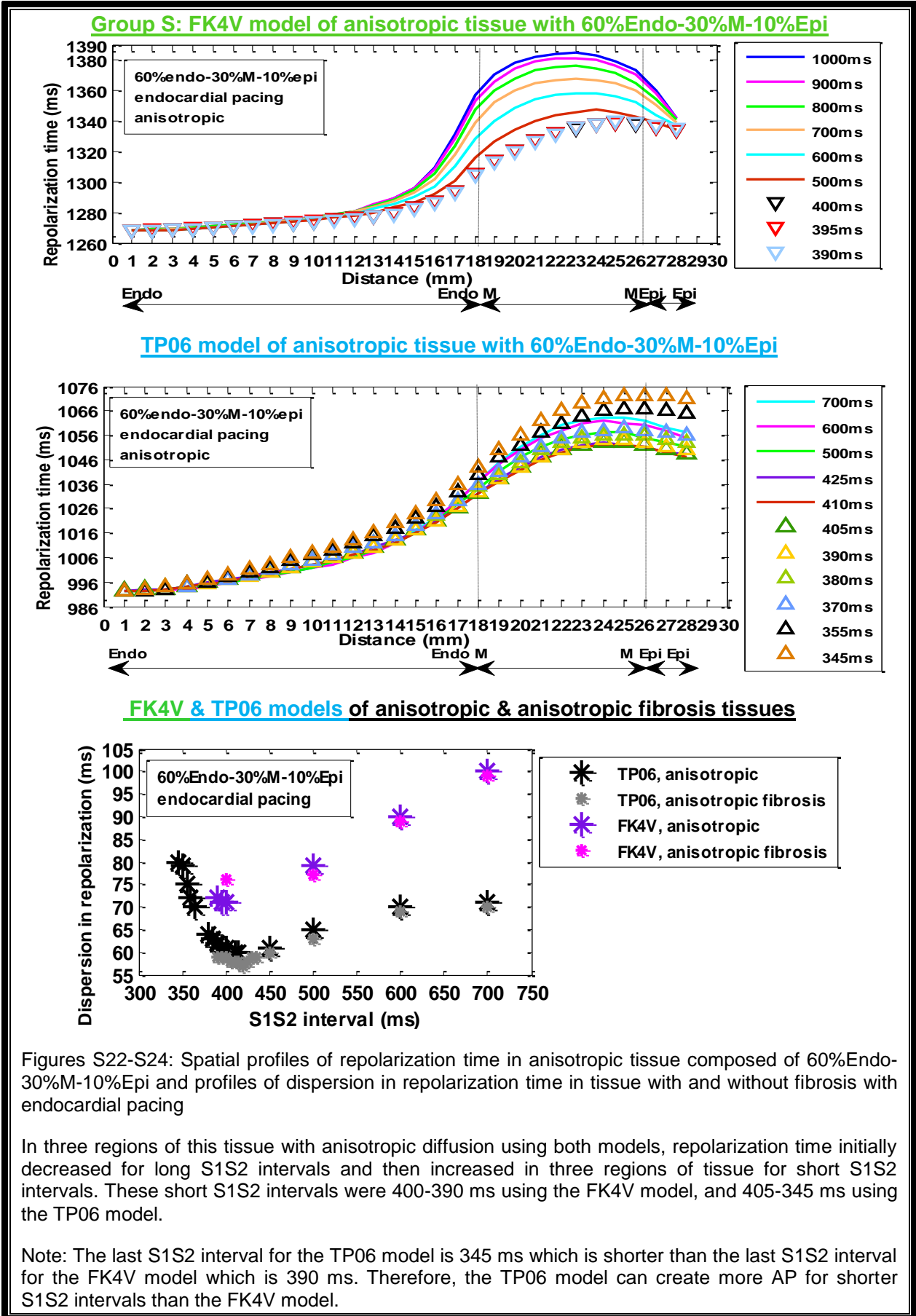
- Tissue composed of 10%Endo-30%M-60%Epi with endocardial pacing



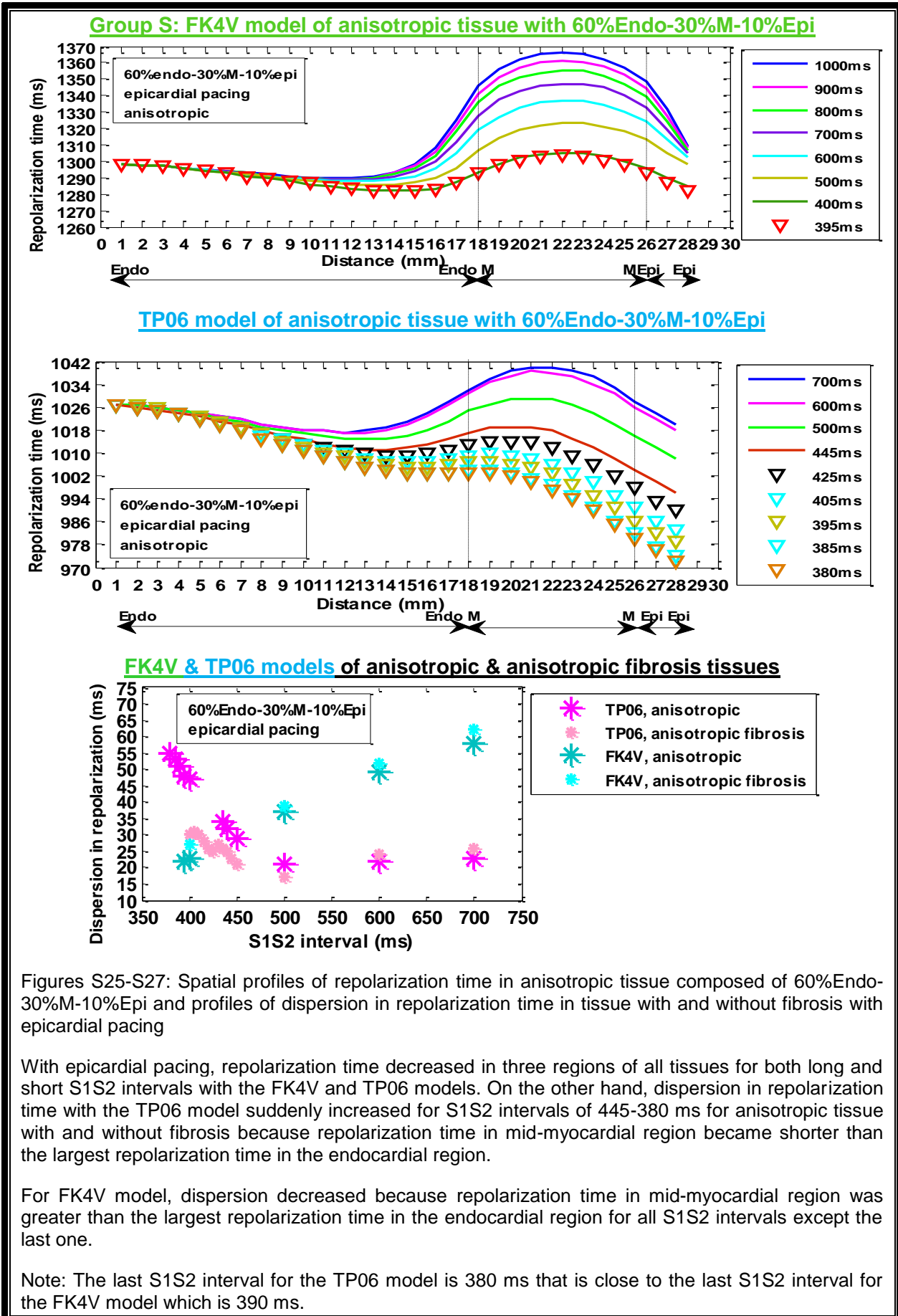
- Tissue composed of 10%Endo-30%M-60%Epi with epicardial pacing



- Tissue composed of 60%Endo-30%M-10%Epi with endocardial pacing



- Tissue composed of 60%Endo-30%M-10%Epi with epicardial pacing



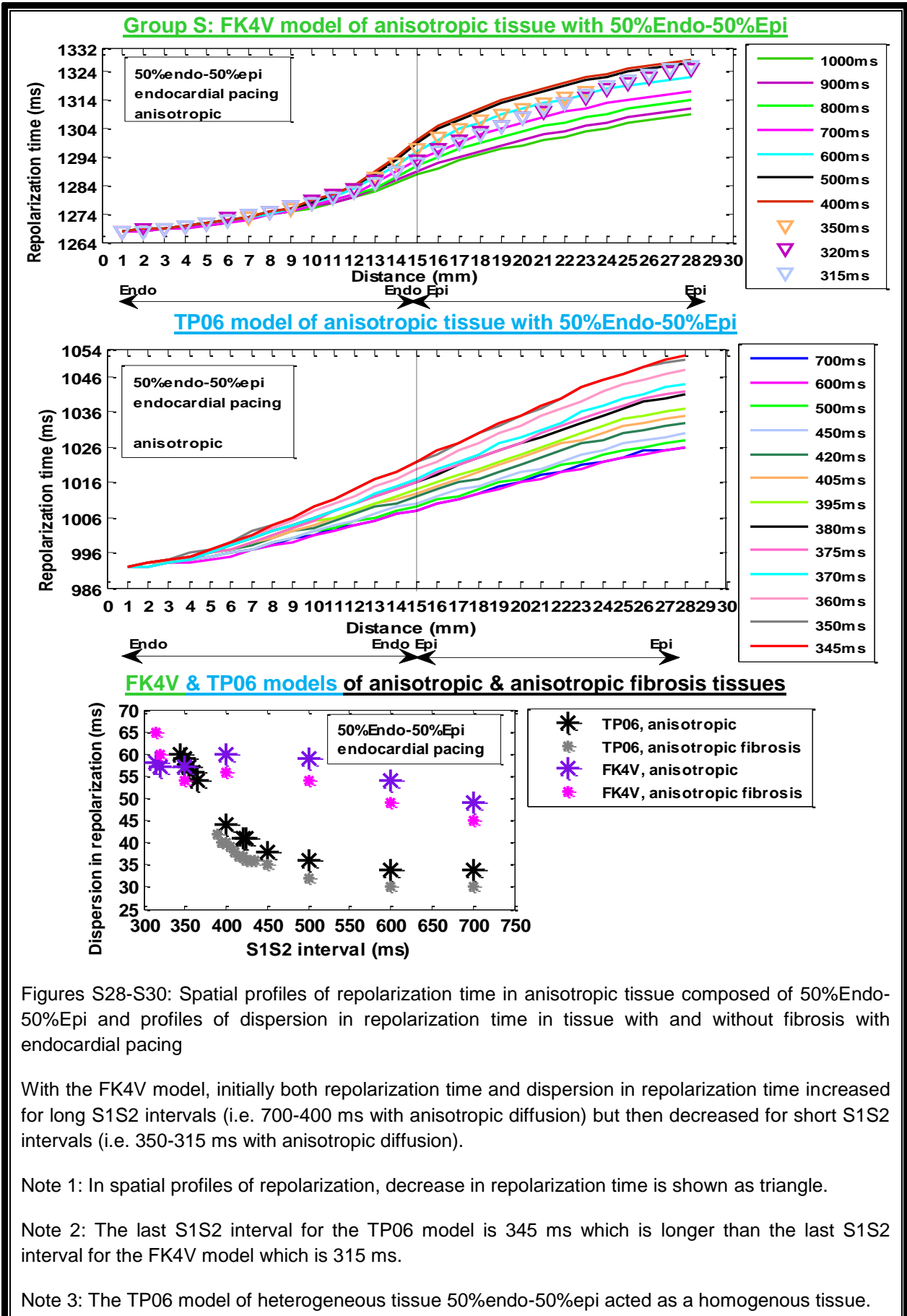
Figures S25-S27: Spatial profiles of repolarization time in anisotropic tissue composed of 60%Endo-30%M-10%Epi and profiles of dispersion in repolarization time in tissue with and without fibrosis with epicardial pacing

With epicardial pacing, repolarization time decreased in three regions of all tissues for both long and short S1S2 intervals with the FK4V and TP06 models. On the other hand, dispersion in repolarization time with the TP06 model suddenly increased for S1S2 intervals of 445-380 ms for anisotropic tissue with and without fibrosis because repolarization time in mid-myocardial region became shorter than the largest repolarization time in the endocardial region.

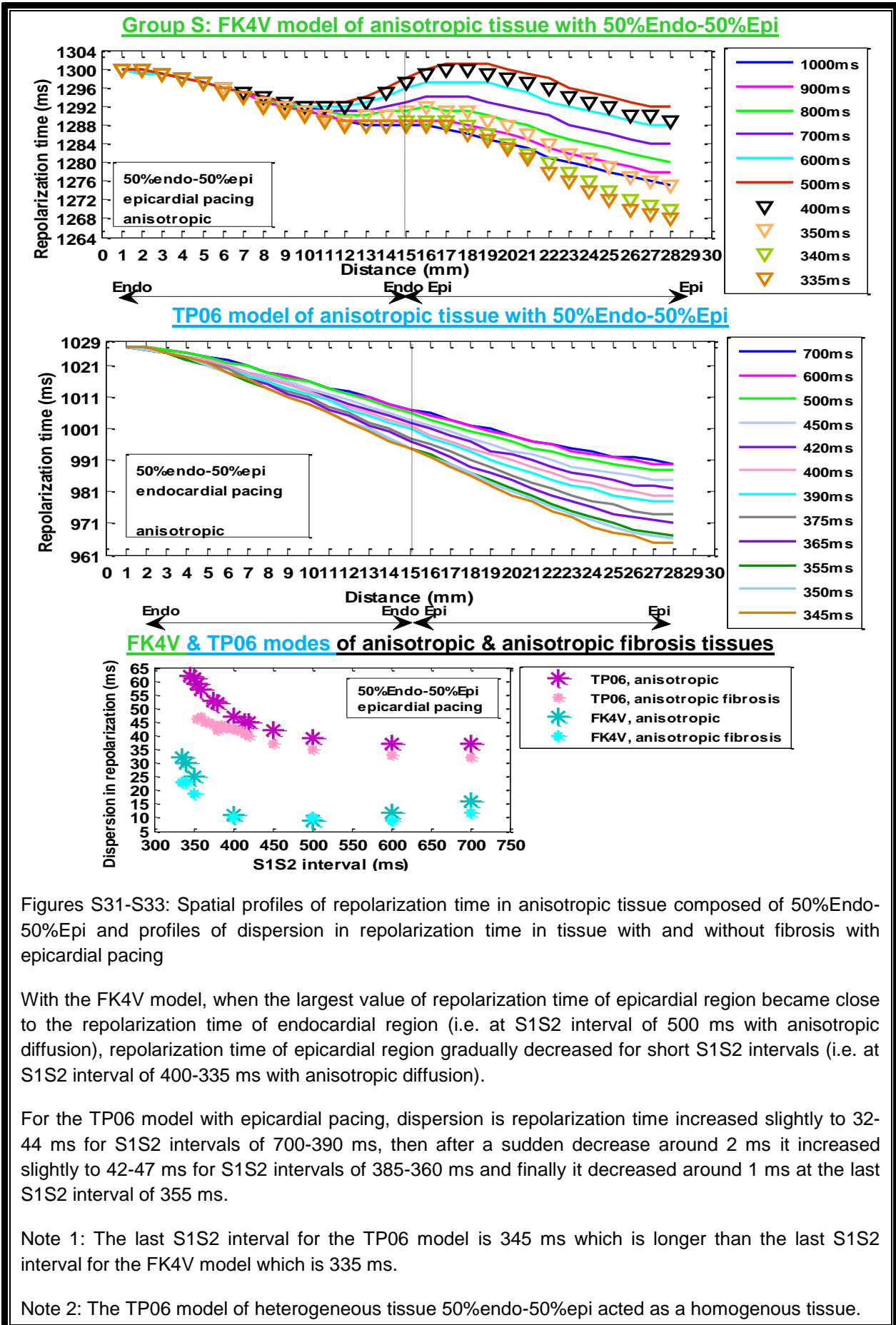
For FK4V model, dispersion decreased because repolarization time in mid-myocardial region was greater than the largest repolarization time in the endocardial region for all S1S2 intervals except the last one.

Note: The last S1S2 interval for the TP06 model is 380 ms that is close to the last S1S2 interval for the FK4V model which is 390 ms.

- Heterogeneous tissue composed of 50%Endo-50%Epi with endocardial pacing



- Heterogeneous tissue composed of 50%Endo-50%Epi with epicardial pacing



5.5.2 Which S1S2 intervals

The results suggest that profiles of dispersion in repolarization time against S1S2 interval can be used as a useful tool for highlighting changes in premature repolarization time of epicardial, mid-myocardial, and endocardial region of heterogeneous tissue in ventricular arrhythmia. For information, Table 5-7 provides the range of repolarization time and S1S2 intervals during which dispersion in repolarization time increased. For homogenous tissue, the range of repolarization time at the last S1S2 interval may increase tissue vulnerability to wave break.

Models of tissue	Anisotropic
100%Epi, paced from the bottom edge of tissue, FK4V model	573<RT<625 S1S2=495
TP06 model	559<RT<620 S1S2=345
100%Endo, paced from the bottom edge of tissue, FK4V model	538<RT<578 S1S2=315
TP06 model	562<RT<623 S1S2=495
100%M, paced from the bottom edge of tissue, FK4V model	739<RT<781ms S1S2=455
TP06 model	720<RT<776 S1S2=430
50%Endo-50%Epi Endocardial pacing, FK4V model	538<RT<691 315<S1S2<400
TP06 model	562<RT<686 345<S1S2<400
50%Endo-50%Epi Epicardial pacing, FK4V model	573<RT<669 340<S1S2<400
TP06 model	557<RT<686ms 345<S1S2<400
15%Endo-55%M-30%Epi Endocardial pacing, FK4V model	651<RT<727ms 420<S1S2<425
TP06 model	598<RT<769ms 365<S1S2<450
15%Endo-55%M-30%Epi Epicardial pacing, FK4V model	679<RT<780 420<S1S2<500
TP06 model	576<RT<777 360<S1S2<450
10%Endo-30%M-60%Epi Endocardial pacing, FK4V model	624<RT<800 390<S1S2<500
TP06 model	630<RT<694 380<S1S2<400
10%Endo-30%M-60%Epi Epicardial pacing, FK4V model	691<RT<700 390<S1S2<400
TP06 model	558<RT<716 345<S1S2<400
60%Endo-30%M-10%Epi Endocardial pacing, FK4V model	620<RT<697 390<S1S2<400
TP06 model	562<RT<702 345<S1S2<405
60%Endo-30%M-10%Epi Epicardial pacing, FK4V model	657<RT<673 S1S2=355
TP06 model	623<RT<673 380<S1S2<395

Table 5-7: Range of repolarization time for premature S2 beats in anisotropic tissues

Note: RT and S1S2 are the abbreviations of repolarization time and S1S2 intervals.

5.5.3 Vulnerable regions for wave break

Figure 5-40 to Figure 5-43 show the transition region in heterogeneous tissues composed of two or three ventricular cell types with both endocardial and epicardial pacing where the largest and the smallest dispersion in repolarization time and APD occur. These regions is characterised with a sharp increase or decrease in repolarization time and APD in transmural direction during decreasing S1S2 intervals and can be vulnerable regions for wave break during AP depolarization and AP repolarization that are discussed in section 5.9.

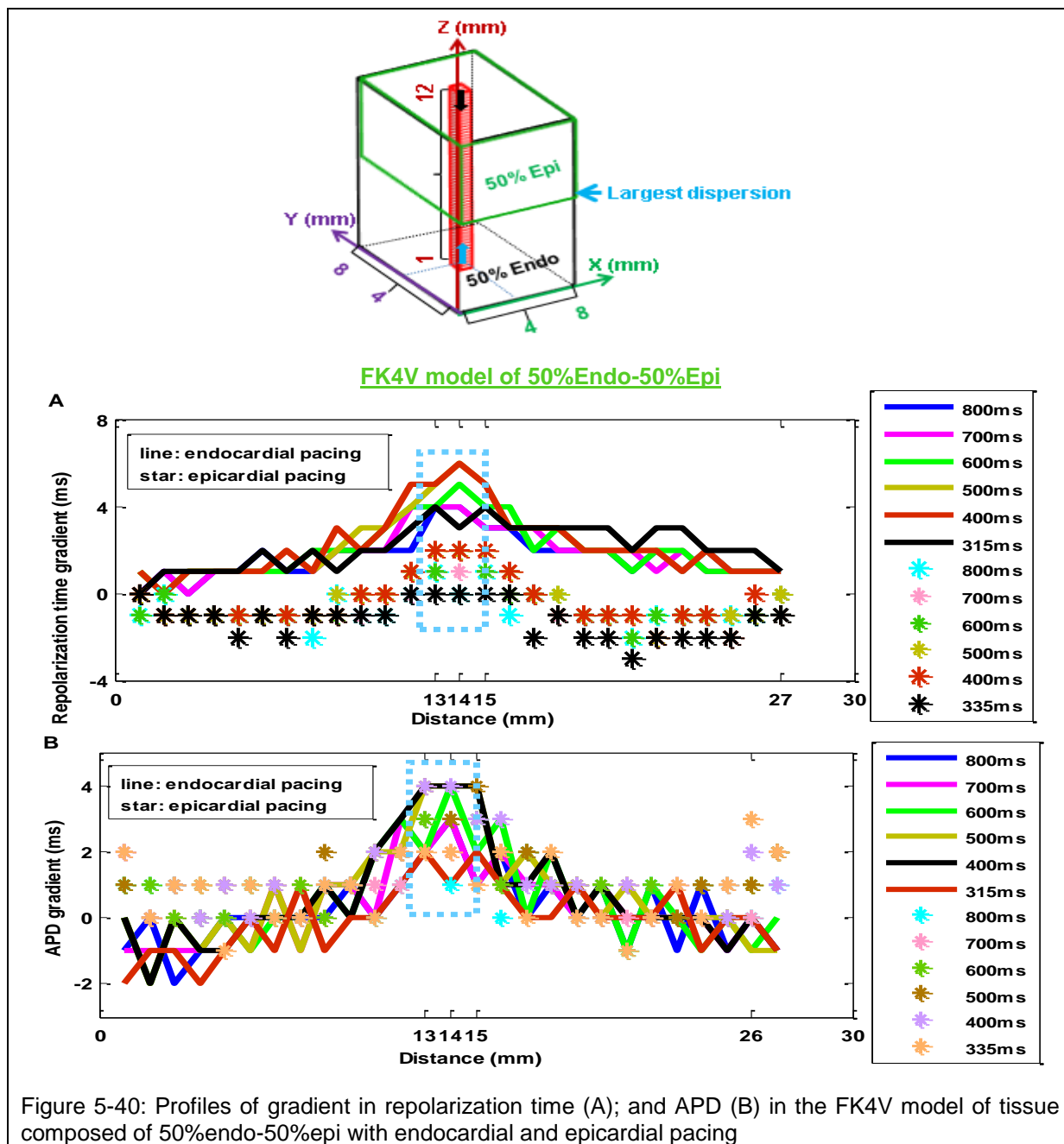


Figure 5-40: Profiles of gradient in repolarization time (A); and APD (B) in the FK4V model of tissue composed of 50%endo-50%epi with endocardial and epicardial pacing

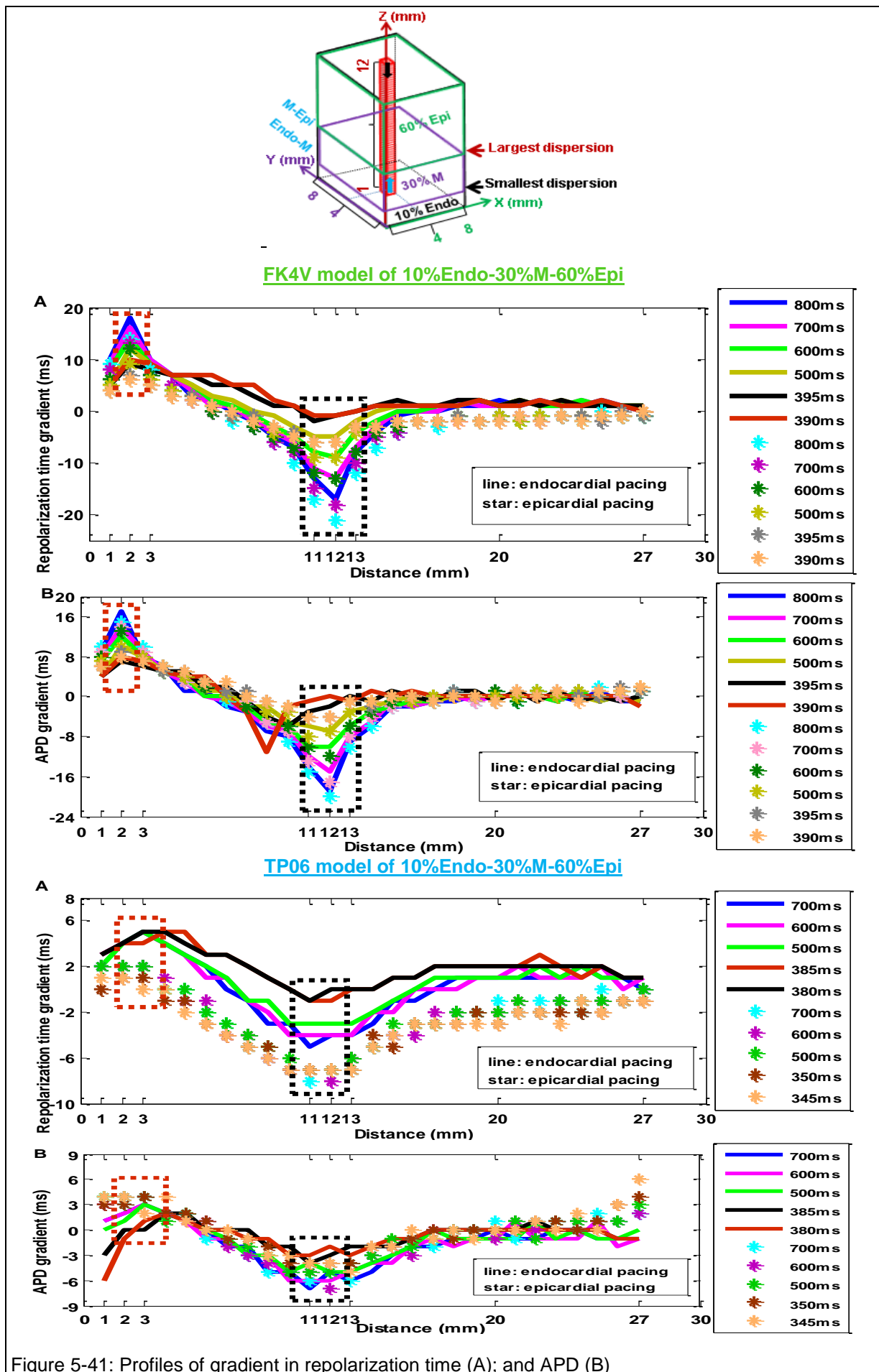


Figure 5-41: Profiles of gradient in repolarization time (A); and APD (B)

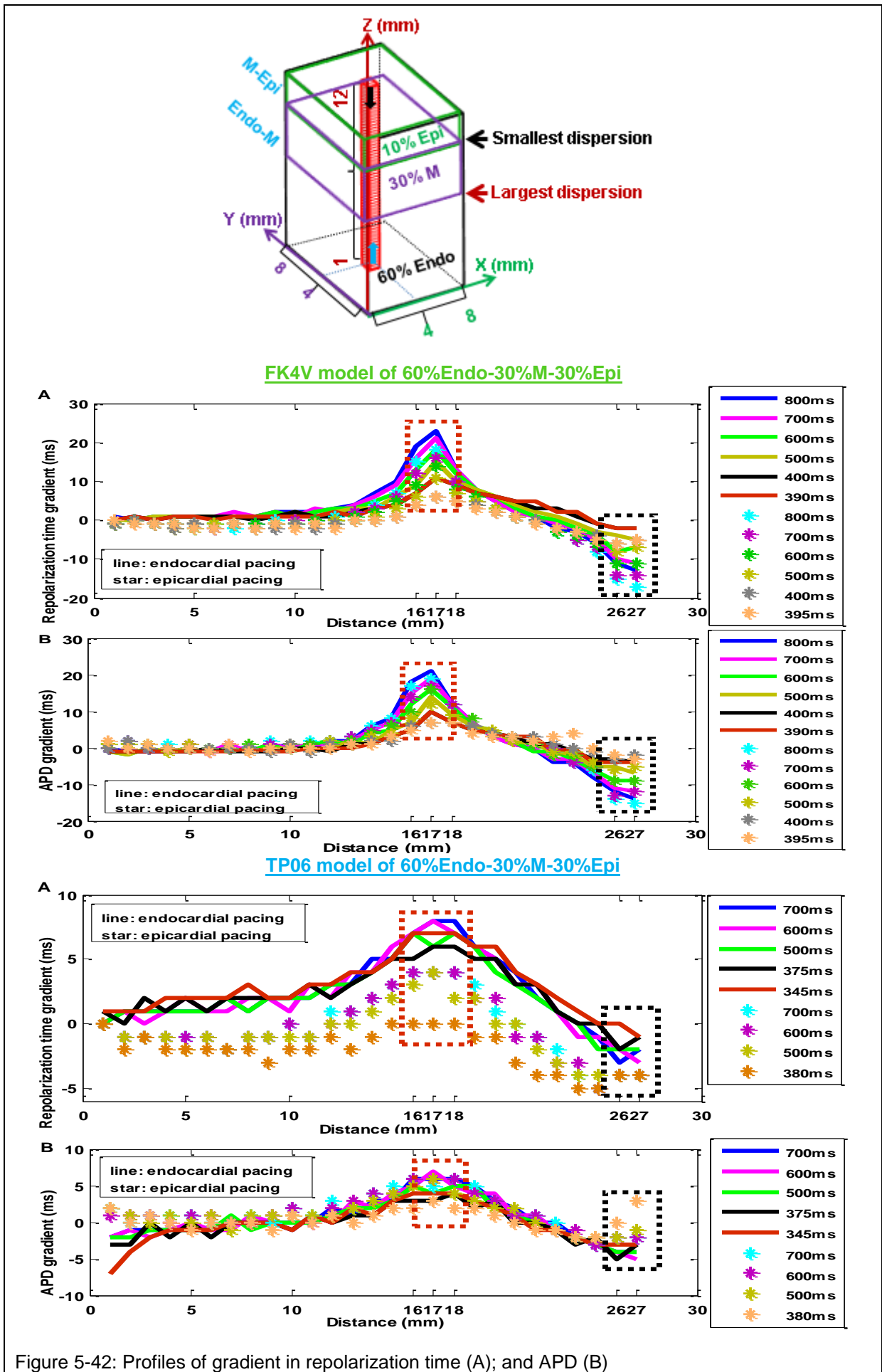
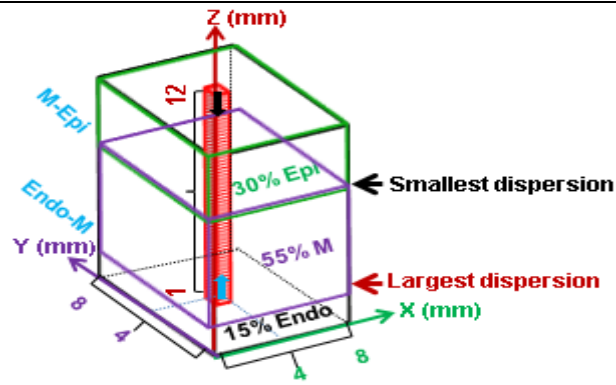
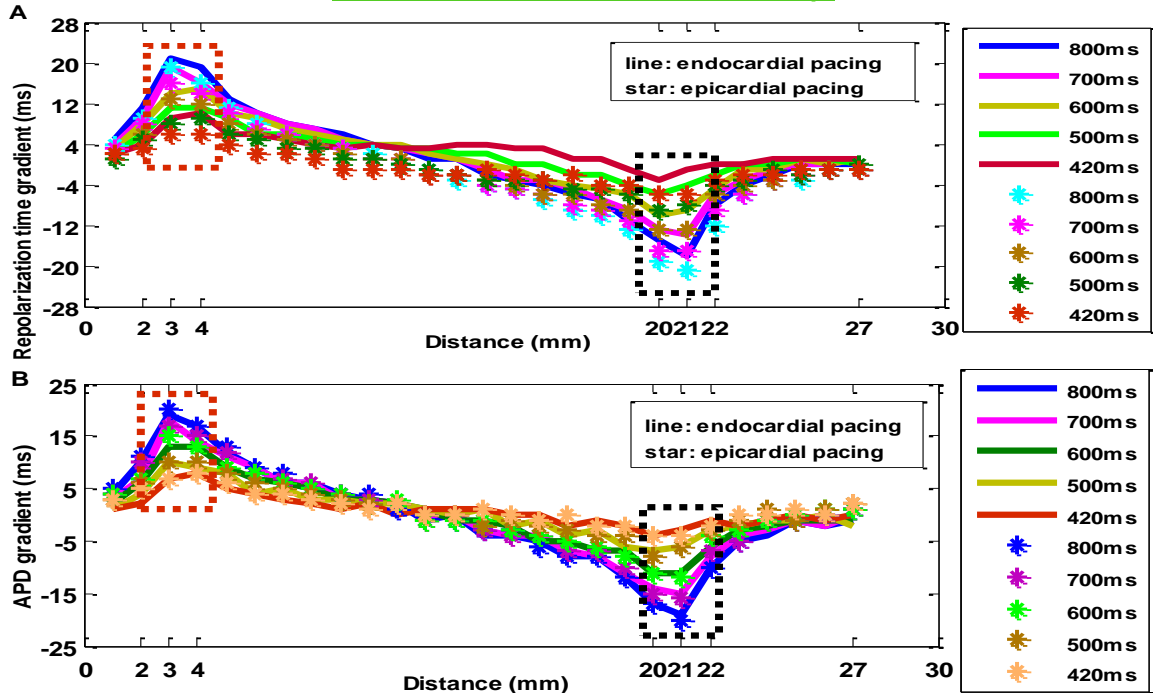


Figure 5-42: Profiles of gradient in repolarization time (A); and APD (B)



FK4V model of 15%Endo-55%M-30%Epi



TP06 model of 15%Endo-55%M-30%Epi

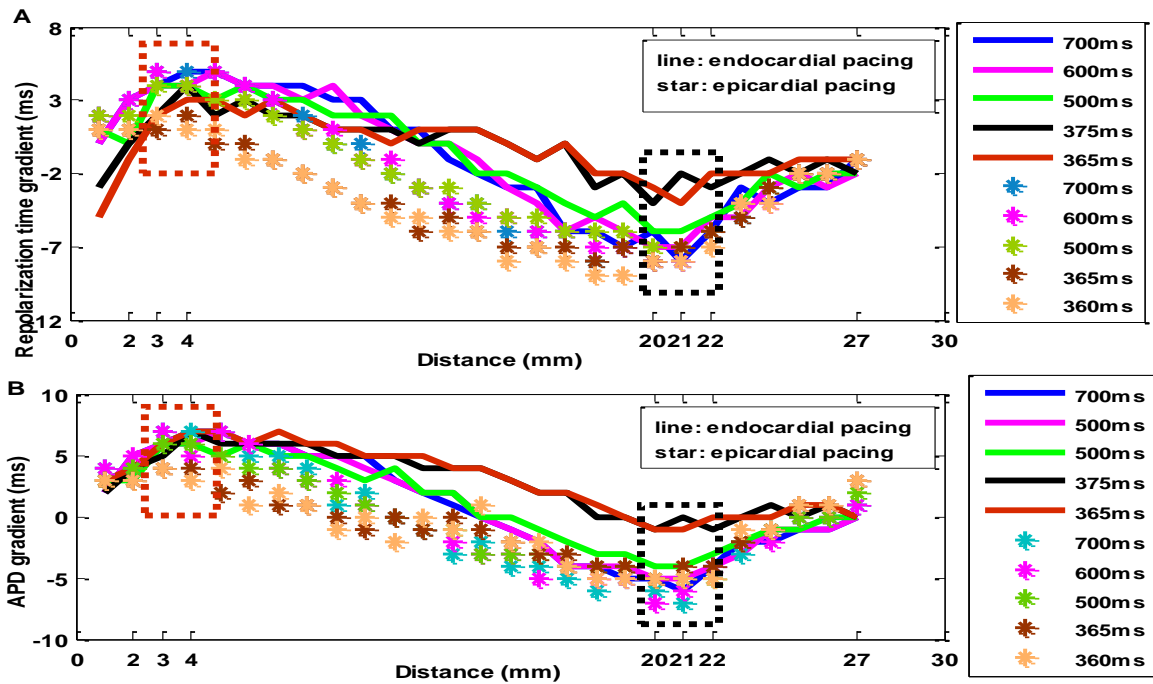


Figure 5-43: Profiles of gradient in repolarization time (A); and APD (B)

5.5.4 Which spatial profiles

Spatial and dispersion profiles of APD compared to spatial and dispersion profiles of repolarization time do not represent clearly the changes in ventricular repolarization of epicardial, mid-myocardial, and endocardial regions in heterogeneous tissues with and without fibrosis. The reason is that APD is the difference between activation time and repolarization time that can cancel some important changes in repolarization time for premature beats particularly for short S1S2 intervals. For example, in the TP06 model of heterogeneous tissue composed of 60%Endo-30%M-10%Epi with endocardial pacing, repolarization time in three regions of tissue initially decreased for long S1S2 intervals of 700-410 ms and then increased for S1S2 intervals of 405-345 ms as shown in Figure 5-44. However, spatial profiles of APD show a small increase in APD of three regions of tissue for S1S2 intervals of 395-375 ms.

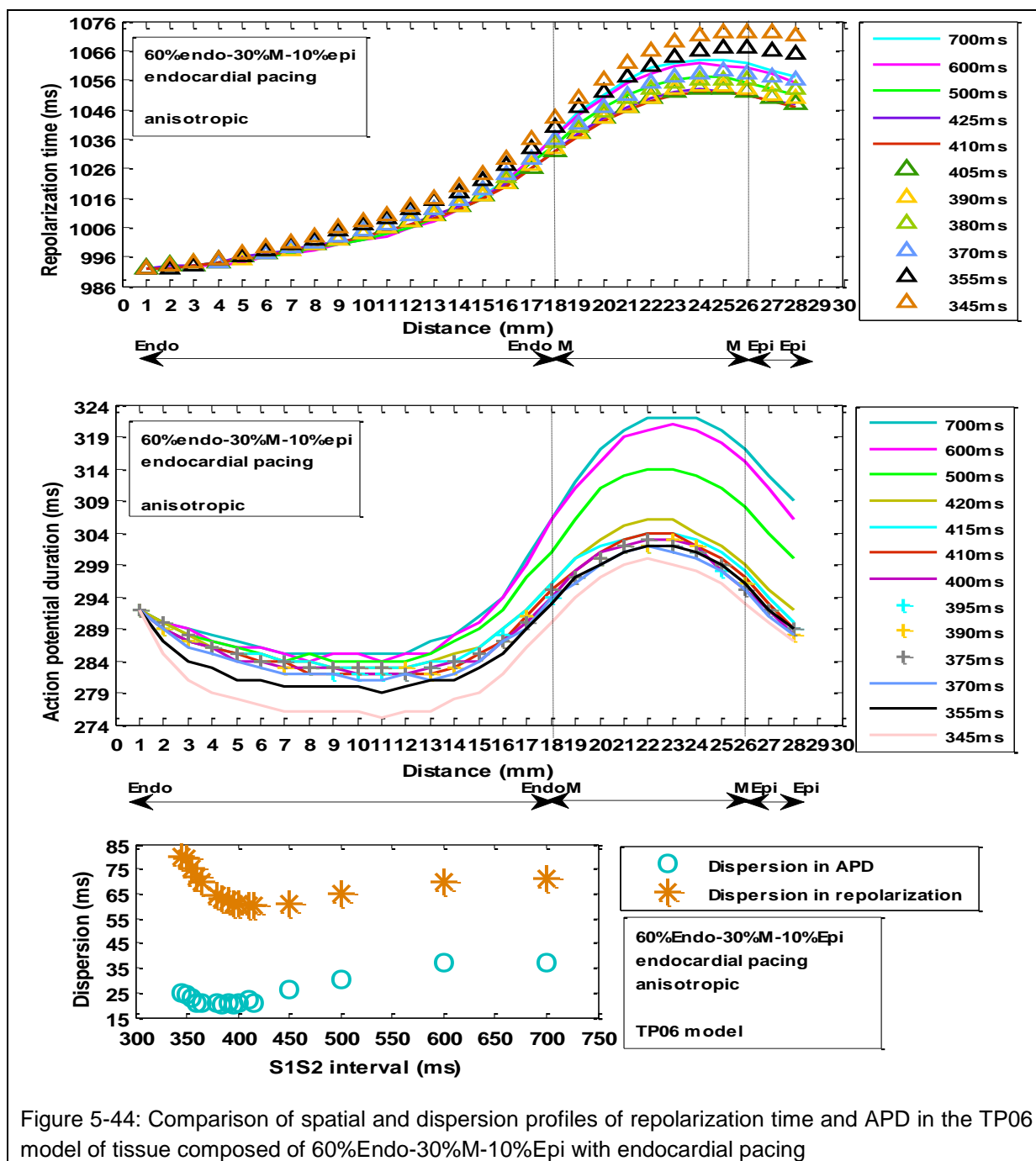


Figure 5-44: Comparison of spatial and dispersion profiles of repolarization time and APD in the TP06 model of tissue composed of 60%Endo-30%M-10%Epi with endocardial pacing

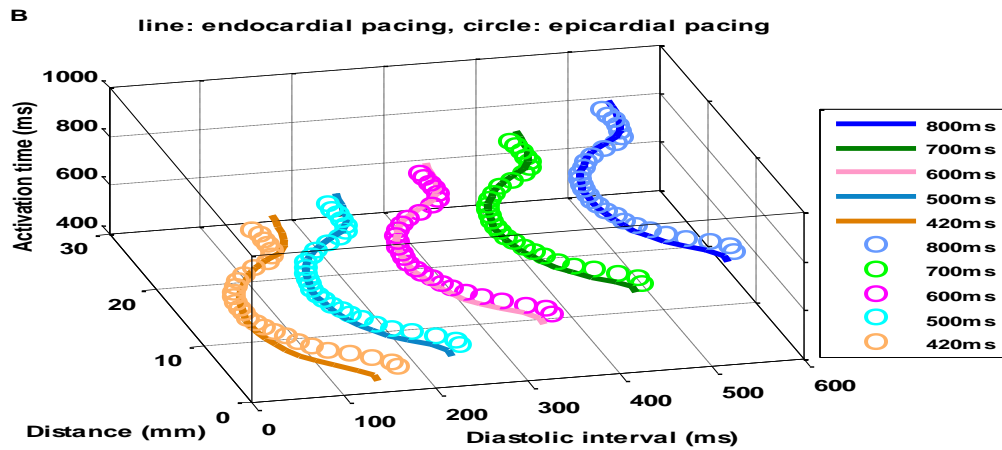
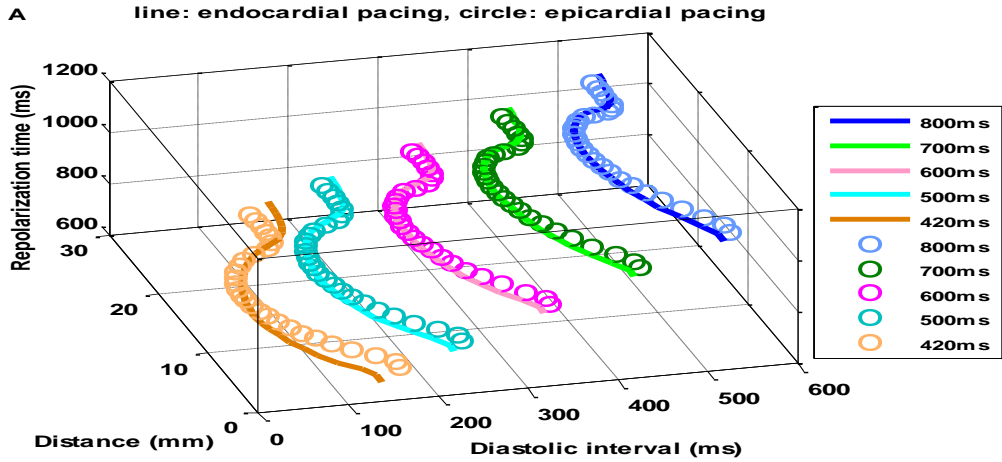
To emphasize this finding more examples are provided in Figures organized in Group U (Figures U1 to U24) in Appendix1 for (1) spatial APD profiles in anisotropic heterogeneous tissues; and (2) profiles of APD dispersion against S1S2 interval for anisotropic heterogeneous tissues with and without fibrosis with both models.

5.5.5 Restitution profiles of activation time

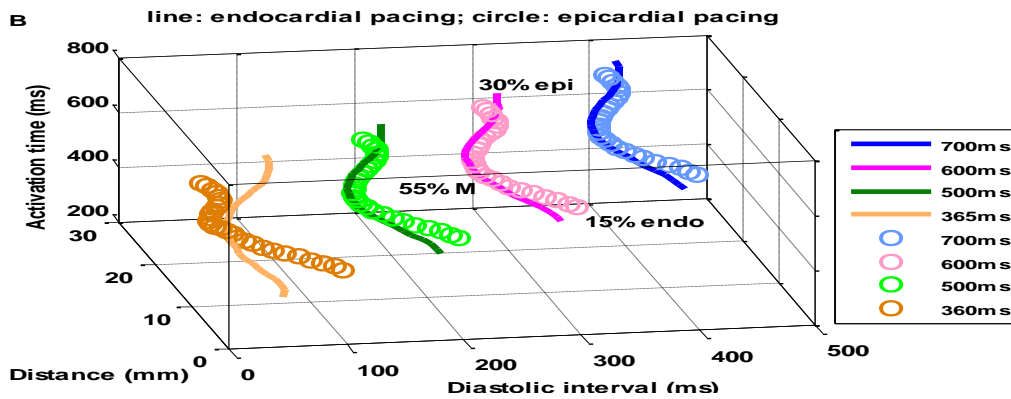
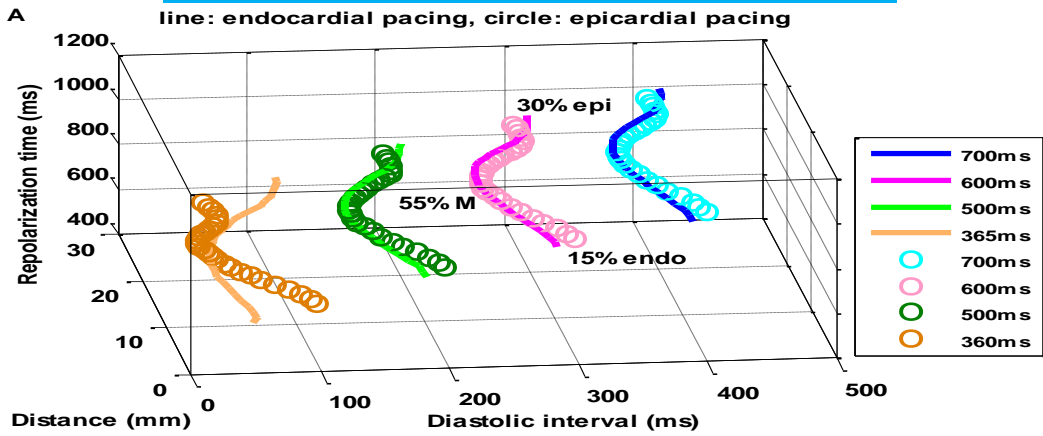
The results of speed of depolarization conduction in section 5.4 suggest that restitution profiles of activation time can be used as a useful tool to explain why the speed of depolarization conduction change in different regions of anisotropic heterogeneous tissues with and without fibrosis during decreasing S1S2 intervals.

Examples of restitution profiles of activation time and repolarization time in two examples of anisotropic heterogeneous tissue composed of 15%Endo-55%M-30%Epi and 60%Endo-30%M-10%Epi with endocardial and epicardial pacing with the FK4V and the TP06 models are shown in Figures organized in Group T (Figures T1-T8).

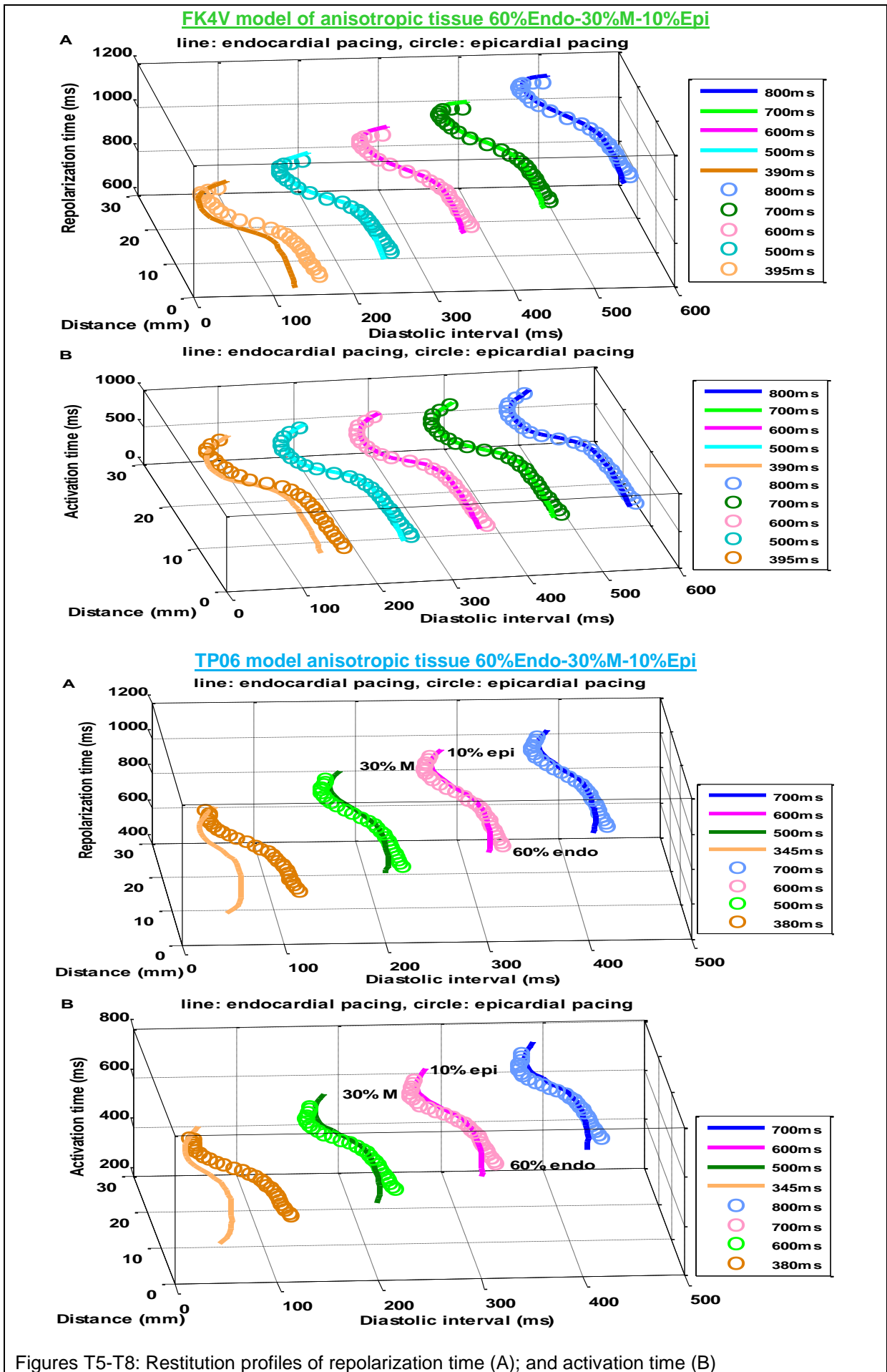
FK4V model of anisotropic tissue 15%Endo-55%M-30%Epi



TP06 model of anisotropic tissue 15%Endo-55%M-30%Epi



Figures T1-T4: Restitution profiles of repolarization time (A); and activation time (B)



5.6 Summary of results in Part I of this Chapter

Interaction between activation-repolarization coupling and restitution properties was studied for normal and premature beats during decreasing S1S2 intervals using the FK4V and TP06 models. The 3D cubes of homogenous and heterogeneous tissues were simulated in three groups of isotropic, anisotropic, and anisotropic fibrosis tissue. Heterogeneous tissues were introduced with a sharp transition between regions of different cell type based on a linear change in fibre orientation.

The main results are:

1. For normal S1 beats, three measures of dispersion in activation time, repolarization time, and APD changed slightly during decreasing S1S2 intervals compared to those for premature S2 beats in all tissues with the FK4V and TP06 models. The current results emphasize that rate dependency of normal beats is much less than that of premature beats and this finding is not model dependent.
2. The rate dependency of premature S2 beats influenced activation time, repolarization time, and APD and as a result three measures of dispersion in activation time, repolarization time, and APD changed during decreasing S1S2 intervals.
3. For premature beats in all tissues, measures of dispersion in activation time increased gradually for long S1S2 intervals and approximately sharply for short S1S2 intervals with both models. Activation time and measures of dispersion in activation time for the TP06 models of tissue were longer than the FK4V models of tissue.
4. The changes in measures of dispersion of repolarization time for premature beats were not similar in homogenous and heterogeneous tissues. For homogenous tissue, dispersion of repolarization time increased with decreasing S1S2 intervals. For heterogeneous tissues, dispersion of repolarization time initially decreased for long S1S2 intervals. For short S1S2 interval, dispersion of repolarization time increased when (1) repolarization time in the epicardial region became close or greater than the largest repolarization time in the mid-myocardial region with endocardial pacing; and (2) when the largest repolarization time in the mid-myocardial region became close or greater than repolarization time in the endocardial region with epicardial pacing.
5. The transition regions in heterogeneous tissues are where the largest and the smallest dispersion in repolarization time and APD occur (i.e. between mid-myocardial and epicardial regions with endocardial pacing and between endocardial and mid-myocardial regions in tissues with epicardial pacing).
6. Anisotropic diffusion compared with isotropic diffusion increased the smallest and the largest dispersion in repolarization using both models.
7. The combined anisotropic conductivity and fibrosis in heterogeneous tissues could suppress speed of depolarization conduction in the mid-myocardial region of tissues composed of three ventricular cell types and also in the epicardial region in tissue composed of 60%Endo-30%M-10%Epi during decreasing S1S2 intervals with both models.
8. For simulation results in all tissues, there was qualitatively agreement between the FK4V and TP06 models, without considering the differences between epicardial and endocardial restitution properties. However, there was quantitatively difference between two models.

Part II: Supplementary simulations

In 3D heterogeneous tissues composed of more than one ventricular cell type, it was assumed that there is a sharp transition between tissues with different cell type, for example between endocardial and epicardial regions. In the real human heart, this assumption may not be correct, and that instead there is a gradual transition from endocardial to epicardial region. Either, there will be transitional cells, which have an action potential that is some way between, the endocardial and epicardial regions, or the relative proportion of endocardial and epicardial cells will change as the observer moves from the endocardial to the epicardial surface. In order to implement a gradual transition, Keller et al. [42] changed cell model parameters (i.e. potassium conductance) across the ventricular wall. However, variation of model parameters using the phenomenological FK4V model [20], may produce results with no physiological interpretation.

In this thesis, the following three approaches were used to examine how a gradual transition affects the transmural spatial APD profile for premature S2 beats.

The first approach was to change the proportion of endocardial and epicardial cells in heterogeneous tissue composed of two ventricular cell type and vary the proportion of epicardial, endocardial, and mid-myocardial cells in heterogeneous tissues composed of three ventricular cell type.

Second, there is some evidence that the tissue conductance (i.e. the diffusion coefficient) is not constant across the ventricular wall [43]. This hypothesis was tested in heterogeneous tissues to find out the relative effects on the APD distribution by changing the diffusion coefficients along and across the fibre axis.

Third, the fibre organization as one important aspect of structural tissue heterogeneity was taken into account. It has been established that the fibre orientation varies as function of transmural distance in the left ventricle in animal [44] and in the human hearts [23]. However, it is still not clear whether fibre orientation change linearly or non-linearly across the ventricular wall. Streeter and Nielsen et al. [44, 45] suggested the smooth rotation of cardiac fibres from the endocardial to the epicardial region in the ventricular wall while Streeter-Bassett [46] and Vetter et al. [47] showed non-linear fibre rotation in the swine right ventricle. To address this issue, a number of heterogeneous tissues were simulated with different fibre structure to represent 3D cube of heterogeneous tissues with a non-linear change in fibre orientation within the left ventricular wall.

This part of the Chapter is a supplementary study in order to provide an outlook about how these three approaches affected spatial profiles of APD and repolarization time for premature S2 beats in heterogeneous tissues with the FK4V model. After describing the simulation results, AP propagation during depolarization and repolarization are visualized for all tissues to assess the disruption in the waves at the last S1S2 interval.

5.7 Effects of changing proportion of cells & conductivity on spatial APD profiles

The first approach focused on effects of changing the proportion of endocardial, epicardial, and mid-myocardial cells on the transmural APD profiles in heterogeneous tissues composed of more than one ventricular cell type using the FK4V model. To test this idea, the programme written in C (the file `allocate_celltype.c` described in Appendix) was

modified to calculate the probability of a particular cell being an epicardial cell using a logistic Equation (5-2) given by:

$$p = \frac{1}{1+e^{n \times m}} \quad \text{Equation (5-2)}$$

p : Probability of a cell in this layer being epicardial

n : It was set to -0.25 to change sharp distributions

m : It was set to (layer-20) assuming that layer 1 to 20 were endocardium

The aim was to allocate proportion of cell type in transition regions (i.e. between endocardial and mid-myocardial region) and avoid sharp boundaries. When each cell was allocated a cell type, a random number between 0 and 1 was calculated, and compared with the probability. The rest of the programme was modified differently based on cellular configuration.

❖ Tissue composed of 50%Endo-50%Epi

If the random number was greater than the probability that the cell was epicardial cell, then it was allocated to be endocardial cell. Otherwise it was allocated to be epicardial cell. In this tissue, layers 1 to 30 were endocardial layers and layers 31 to 60 were epicardial layers.

Figure 5-45, plot A shows how a sharp transition between endocardial and epicardial regions became a gradual transition by changing the proportion of epicardial and endocardial cells in tissue composed of 50%Endo-50%Epi with endocardial and epicardial pacing at S1S2 interval 1000 ms using the FK4V model.

Furthermore, the anisotropic conductivity was changed in this tissue by setting diffusion coefficients (in the header file described in Appendix) as provided in Table 5-8. Diffusion 1 and Diffusion 2 defined the diffusion along and across ventricular fibres. The diffusion coefficients with ratio 4:1 had been used for anisotropic tissues in Part I of this Chapter.

Diffusion1 (cm ² /ms)	Diffusion2 (cm ² /ms)	Diffusion 1: Diffusion 2
0.001	0.00025	4:1
0.001	0.0002	5:1
0.001	0.00016667	6:1
0.001	0.00014286	7:1
0.001	0.000125	8:1

Table 5-8: Diffusion coefficients along and across the fibre axis

However, the combined effect of changing conductivity and proportion of cells on spatial APD profiles in tissue composed of 50%Endo-50%Epi was negligible as shown in the second plot in Figure 5-45, plot B.

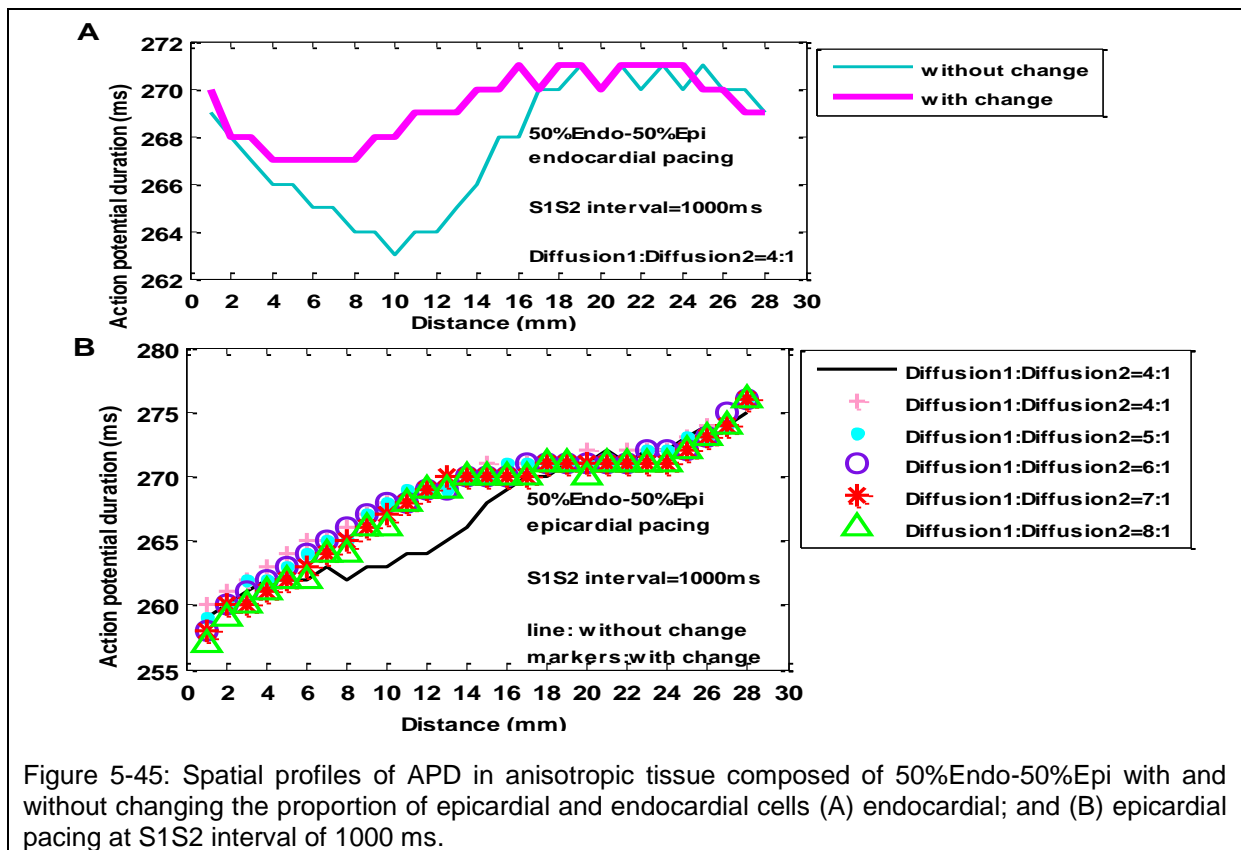


Figure 5-45: Spatial profiles of APD in anisotropic tissue composed of 50%Endo-50%Epi with and without changing the proportion of epicardial and endocardial cells (A) endocardial; and (B) epicardial pacing at S1S2 interval of 1000 ms.

❖ Tissue composed of 60%Endo-30%M-10%Epi

For tissue composed of 60%Endo-30%M-10%Epi, the programme (the file allocate_celltype.c described in Appendix) was modified to allocate cells (grid points) to be epicardial, mid-myocardial, and endocardial cells based on comparing a random number with a probability profile for each cell type. In this tissue, layers 1 to 36 were endocardial, layers 37 to 54 were mid-myocardial, and layers from 55 to 60 were epicardial layers (described in Appendix, Table 1). Accordingly, if the random number was greater than the probability that the cell was epicardial cell, then it was allocated to be endocardial cell for layer less than 36. Otherwise, it was allocated to be mid-myocardial cells for layer less than 54 and epicardial cells for the rest of layers. Next, the programs were modified for layers less than 50, 46, 40, 36, and 25.

In this approach, the dome morphology in spatial APD profiles in the mid-myocardial region shifted to the endocardial region and the APD dispersion gradually reduced by decreasing the layers in tissue. Figure 5-46 shows examples of spatial APD profiles in tissue composed of 60%Endo-30%M-10%Epi with epicardial pacing at S1S2 interval 1000 ms and diffusion coefficients with ratio of 4:1.

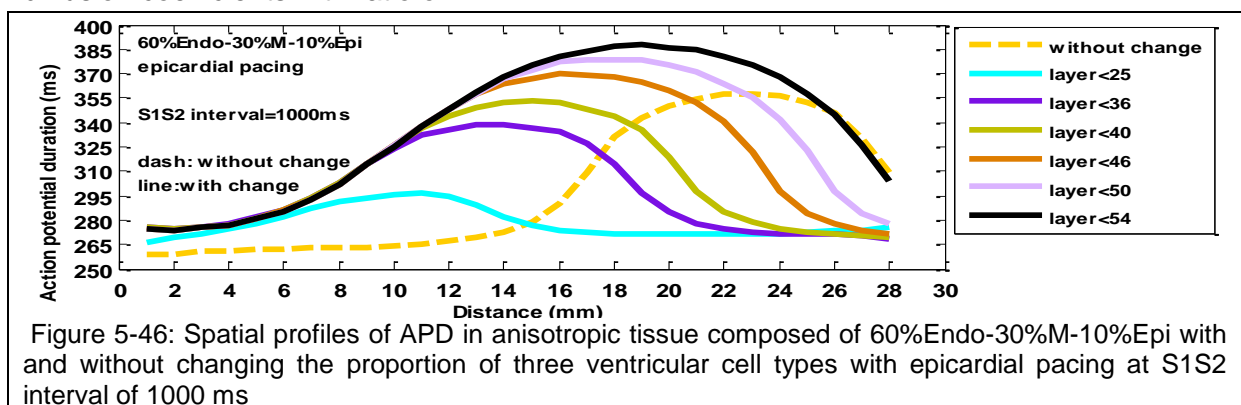
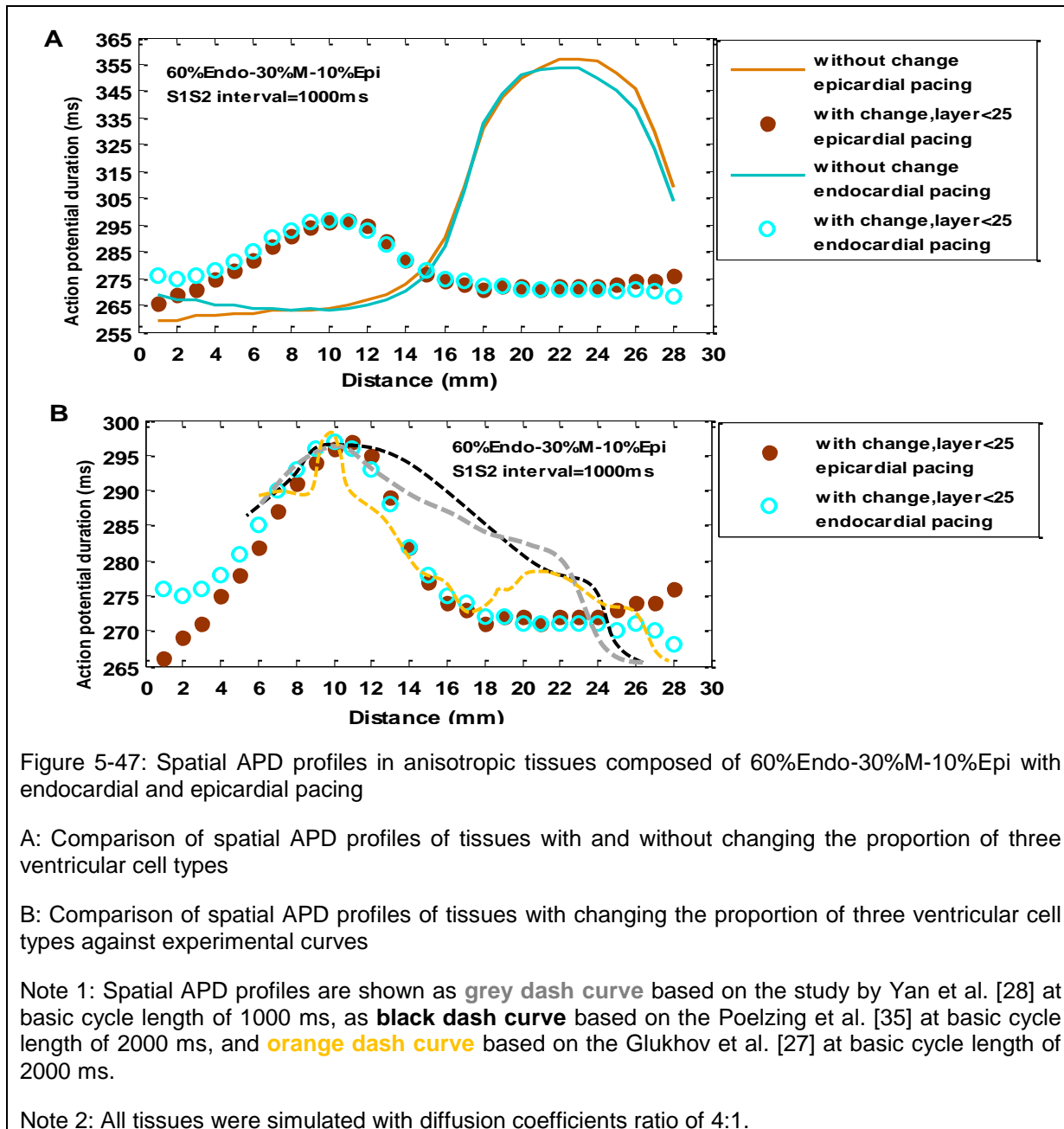


Figure 5-46: Spatial profiles of APD in anisotropic tissue composed of 60%Endo-30%M-10%Epi with and without changing the proportion of three ventricular cell types with epicardial pacing at S1S2 interval of 1000 ms

Figure 5-47 compares spatial APD profiles of tissue composed of 60%Endo-30%M-10%Epi with endocardial and epicardial pacing for layers less than 25 at S1S2 interval of 1000 ms.

As can be seen in plot B, the transition between mid-myocardial and epicardial regions in spatial profiles of APD was in broad agreement with that in the canine heart by Yan et al. [28] and Poelzing et al. [35], and in the human heart by Glukhov et al. [27].



5.8 Effects of non-linear fibre orientation on spatial APD profiles

The previous 3D simulations in this Chapter were based on a linear change in fibre orientation. It was interesting to study how spatial profiles of APD and repolarization time change with different fibre structure.

This thesis used Boltzmann Equation (5-3) that was previously used by Vetter et al. [47] for the epicardial fibre structure in swine right ventricle.

$$\theta(z) = \frac{A2-A1}{1+e^{-\frac{(z-Z_0)}{d}}} + A1 + B \times Z \quad \text{Equation (5-3)}$$

A1 was the fibre orientation after the transition, A2 was the fibre orientation at the epicardium, B was the slope at the linear part of the sigmoidal curve obtained from experimental measurements, Z_0 was the depth of the transition point where the slope of $\theta(z)$ was $S_0 = (A1-A2)/(4d)$. B and d scaled the slope at the transition point. They [47] used the total fibre rotation of 180° .

The reasons for using Boltzmann equation [47] was that the function $\theta(z)$ that determined the depth dependence of the components of the diffusion tensor could be approximated by changing parameters B and θ . The main advantage was that the 3D cubes of tissue can be simulated with different fibre structure without any change in the FK4V model parameters.

To create a geometrical model of the fibre structure, Boltzmann equation [47] was modified based on parameters in the programme as given below:

$$\theta(z) = B \times layer + \frac{\theta}{1+e^{-\frac{layer}{z}}} \quad \text{Equation (5-4)}$$

B: the variable B (degree/mm)

θ : Fibre rotation angle in degree

The following subsections initially compare the spatial APD profiles of heterogeneous tissue composed of 60%Endo-30%M-10%Epi with different fibre structure at one or two S1S2 interval with endocardial and epicardial pacing. Then, three summary figures are provided to highlight how different setting of B and fibre rotation angle θ influenced (1) the transition between regions of different cell type; (2) measures of dispersion in APD and repolarization time; and (3) the dome-morphology in spatial APD profiles. Next, four heterogeneous tissues were simulated with one geometrical model of fibre structure in which fibre orientation did not change with increasing layers in isotropic, anisotropic, and anisotropic fibrosis tissues during decreasing S1S2 intervals. Finally, a brief explanation about numerical stability is provided.

5.8.1 Tissue composed of 60%Endo-30%M-10%Epi

Initially, a number of geometrical fibre models of fibre structure were created by changing coefficient B in degree/mm and fibre rotation angle θ in degree in Equation (5-4). Among heterogeneous tissues with three ventricular cells, tissue composed of 60%Endo-30%M-10%Epi was selected because the speed of depolarization conduction in this tissue with a linear change in fibre orientation in anisotropic fibrosis tissue was suppressed in both mid-myocardial and epicardial regions for premature S2 beats during decreasing S1S2 intervals (described in section 5.4.5 Figures R17 to R20 organized in Group R). The reason is

possibly due to the effects of combination of anisotropy and fibrosis in this heterogeneous tissue. This part of the Chapter, address this issue by simulating a number of heterogeneous tissues with a non-linear change in fibre orientation. To keep consistency, these tissues were simulated at S1S2 interval 1000 ms or 800 ms with anisotropic conduction ($0.001 \text{ cm}^2/\text{ms}$ along and $0.00025 \text{ cm}^2/\text{ms}$ across the fibre axis).

To highlight the role of coefficient B and θ on the spatial APD profiles, these two parameters were changed using two approaches:

First, fibre rotation angle θ was kept as constant value (positive and negative) while coefficient B was changed. For constant value of fibre rotation angle θ , transmural APD dispersion increased by decreasing coefficient B as shown in Figure 5-48.

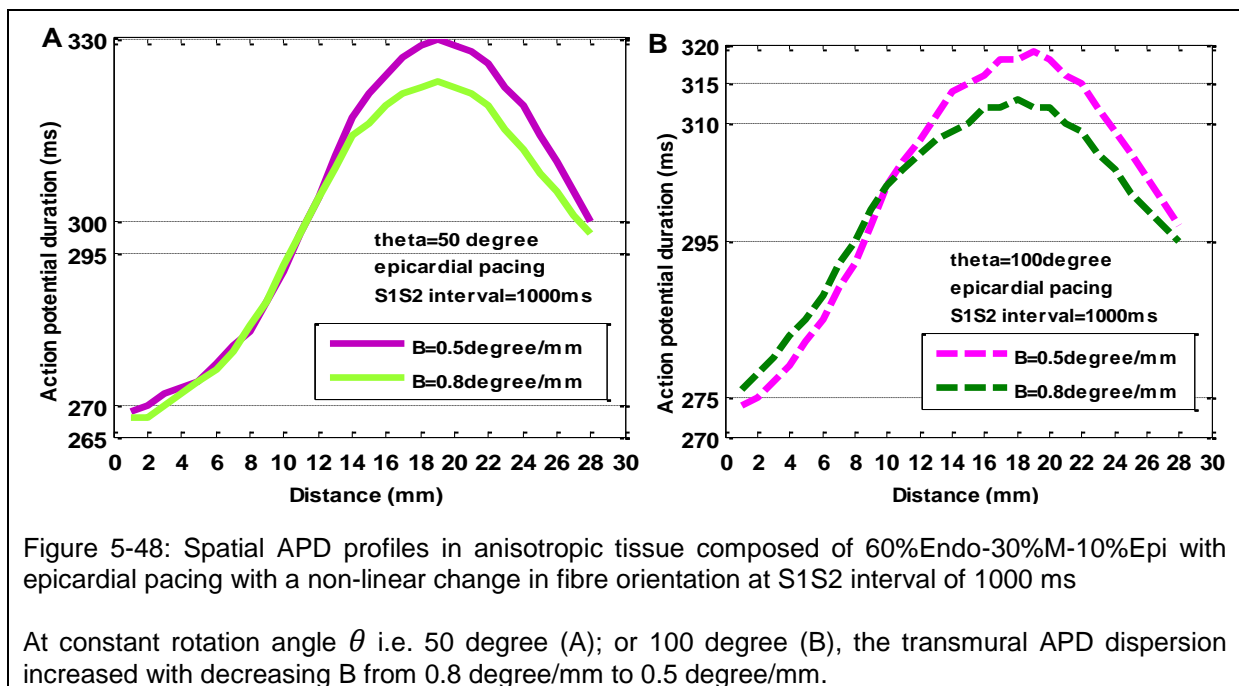


Figure 5-48: Spatial APD profiles in anisotropic tissue composed of 60%Endo-30%M-10%Epi with epicardial pacing with a non-linear change in fibre orientation at S1S2 interval of 1000 ms

At constant rotation angle θ i.e. 50 degree (A); or 100 degree (B), the transmural APD dispersion increased with decreasing B from 0.8 degree/mm to 0.5 degree/mm.

Second, B was kept as constant value (positive and negative) while rotation angle θ was changed. Figure 5-49 shows how spatial APD profiles change for the constant value of B but different values of rotation angle θ . For clarity, examples of the fibre rotation in five selected layers of the 3D cube of tissue are provided.

For a positive constant B, transmural APD dispersion decreased by increasing rotation angle θ from a negative to a positive rotation angle as shown in plot A or from a small positive to a large positive rotation angle as shown in plot B.

Furthermore, plot C shows that fibre orientation influenced the transition between regions of different cell type. For example, for some values of B and rotation angle θ , the transmural gradient in APD was reduced significantly and the dome morphology in the spatial APD profile was suppressed (i.e. with $B = 0.5$ degree/mm and $\theta = 199.8$ degree/mm).

For a negative constant B, the transmural APD dispersion decreased by decreasing rotation angle θ as shown in plot D.

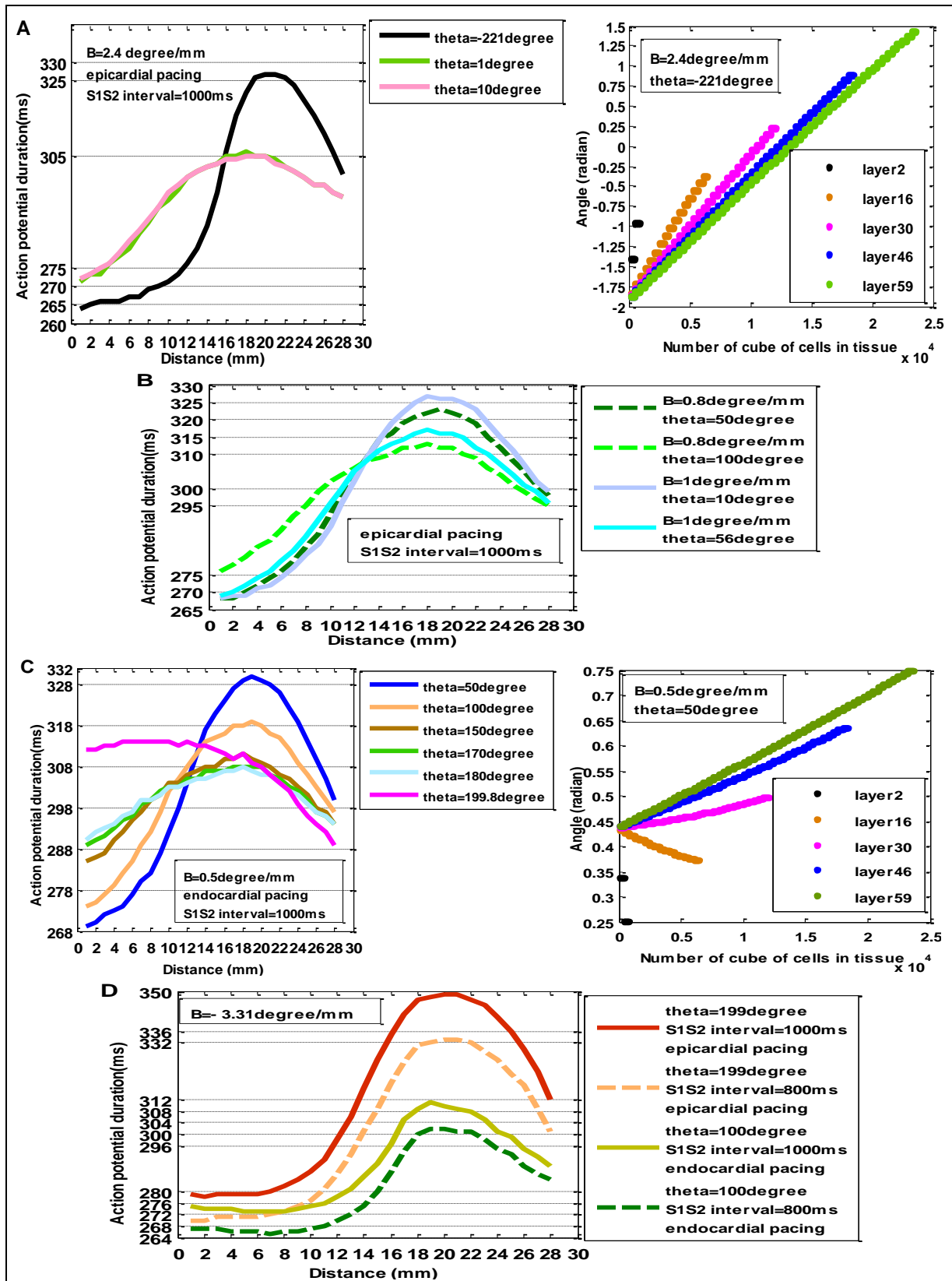


Figure 5-49: Examples of spatial APD profiles and fibre rotation in five selected layers of tissue in anisotropic tissue composed of 60%Endo-30%M-10%Epi with a non-linear change in fibre orientation

For positive constant B , if θ is changed, the transmural APD dispersion decreased with increasing θ , (A) from negative -221° to positive 10° ; (B) from small positive of 50° to large positive rotation angle of 100° at $B=0.8 \text{ degree/mm}$ or from 10° to 56° at $B=1 \text{ degree/mm}$; and (C) from $+50^\circ$ to $+199.8^\circ$.

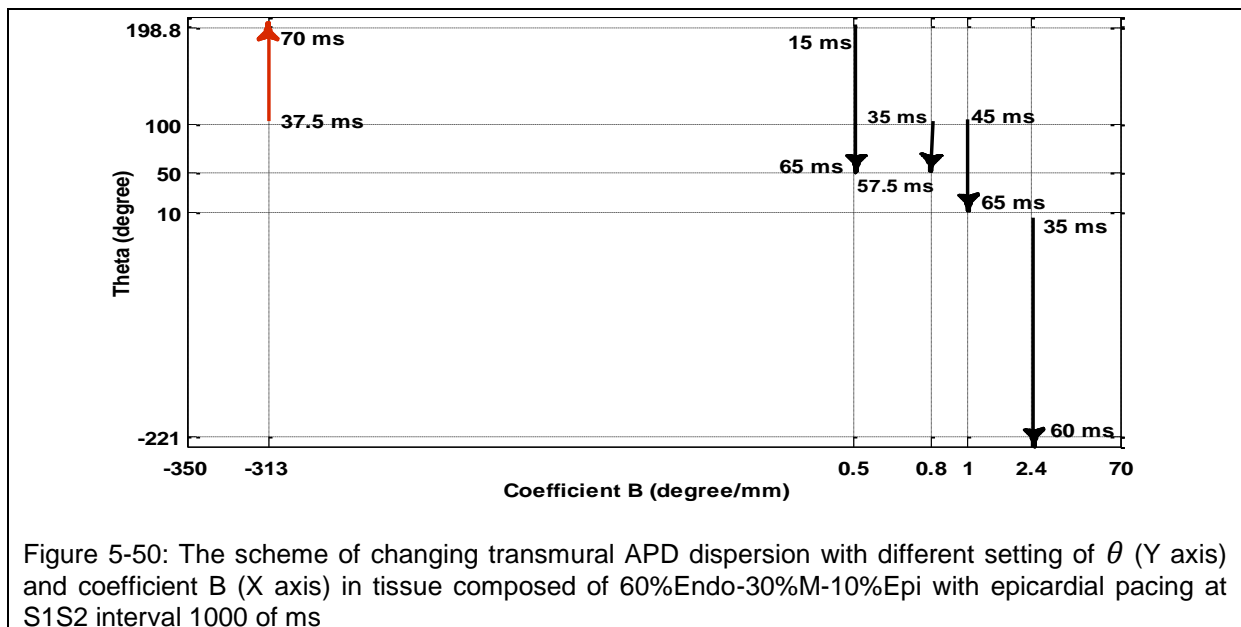
(D) For negative constant B , transmural APD dispersion decreased with reducing θ from 199° to 100° .

5.8.2 Summary figures

For tissue composed of 60%Endo-30%M-10%Epi with epicardial pacing at S1S2 interval of 1000 ms, three summary figures were provided that summarize the results with different B and rotation angle θ .

- First summary Figure

Initially, APD dispersion (difference between the maximum and the minimum APD at each S1S2 interval) was calculated to specify the role of B and rotation angle θ in increasing or decreasing the transmural APD dispersion. Summary Figure 5-50 provides a scheme of changing transmural APD dispersion with different setting of B and rotation angle θ . For the negative constant coefficient of B -3.13 degree/mm, the transmural APD dispersion increased from 37.5 ms to 70 ms by increasing rotation angle from 100° to 199.8° as shown by a red upward arrow. In contrast, for the positive constant B i.e. 0.5, 0.8, 1, and 2.4 degree/mm, transmural APD dispersion rose by decreasing rotation angle as shown by downward black arrows.



- Second summary Figure

Summary Figure 5-51 categorized spatial APD profiles in two groups based on APD dispersion (1) smaller than 55 ms; and (2) greater than 55 ms.

For measures of transmural APD dispersion smaller than roughly 55 ms, a sharp transition between regions of different cell type became more a gradual transition, i.e.

- the curve shown as green circle, for setting B=2.4 degree/mm and $\theta=10^\circ$, with APD dispersion of 35 ms;
- the curve shown as orange circle, for setting of B= 1 degree/mm and $\theta=56^\circ$, with APD dispersion of 45 ms.

Furthermore, for some setting of B and rotation angle θ , the dome-morphology in spatial APD profile in the mid-myocardial region was suppressed i.e. at B= 0.5 degree/mm and θ

=199.8° in the tissue with endocardial pacing and APD dispersion of 15 ms (the curve shown as violet cross).

For measures of transmural APD dispersion greater than 55 ms, there was a sharp transition between regions of different cell type as well as the dome-morphology in the profiles. It was important to note that these simulated values are similar to the experimentally observed transmural APD dispersion of 60 ms at basic cycle length of 1000 ms in the study by Yan et al. [28].

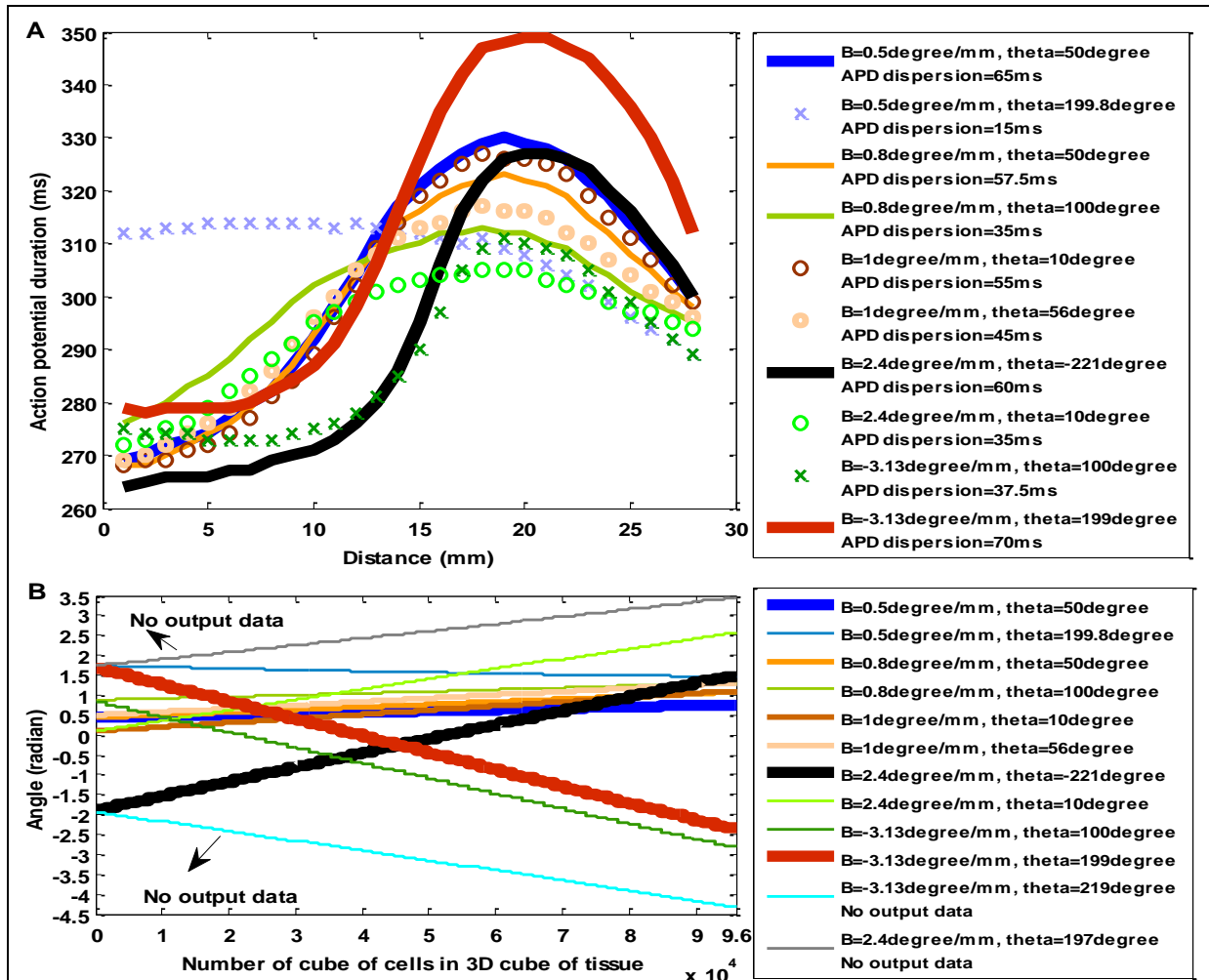


Figure 5-51: Examples of spatial APD profiles (A); and profiles of fibre rotation angle against number of cells in tissue (B) in anisotropic tissue composed of 60%Endo-30%M-10%Epi with epicardial pacing with different fibre structure at S1S2 interval of 1000 ms.

Note: Tissues with endocardial pacing are shown as violet cross with B=0.5 degree/mm and $\theta = 199.8^\circ$ and green cross with B= -3.13 degree/mm and $\theta = 100^\circ$.

- Third summary Figure

Among the geometrical fibre models that was used to create different fibre structure with different setting of B and θ , the geometrical model of fibre structure created with $\theta=89^\circ$ and B 1.7 degree/mm showed no variation in fibre orientation with increasing layers in tissue as shown in Figure 5-52, plot C for five selected layers of tissues. However, the profiles of rotation angle against number of cells did not provide any useful information in this case as shown in Figure 5-52, plot D. To find out how this particular geometrical model of fibre structure influences the spatial APD profiles, tissue composed of 60%Endo-30%M-10%Epi

was simulated with this geometrical model of fibre structure at S1S2 interval 1000 ms with epicardial pacing. As can be seen in Figure 5-52, plot A, the measure of transmural APD dispersion was 56 ms and a sharp transition between endocardial and mid-myocardial regions became a gradual transition for isotropic tissue. However, for anisotropic tissue, the dome morphology was approximately cancelled and the transmural APD dispersion became 21 ms.

As described in Part I of this Chapter, the spatial APD profiles of anisotropic tissue composed of 60%Endo-30%M-10%Epi with epicardial pacing and a linear change in fibre orientation was characterized by:

1. a dome-morphology in the mid-myocardial region;
2. a sharp transition between regions of different cell type with the transmural APD dispersion of 91 ms at S1S2 interval 1000 ms, Figure 5-52 plot A.

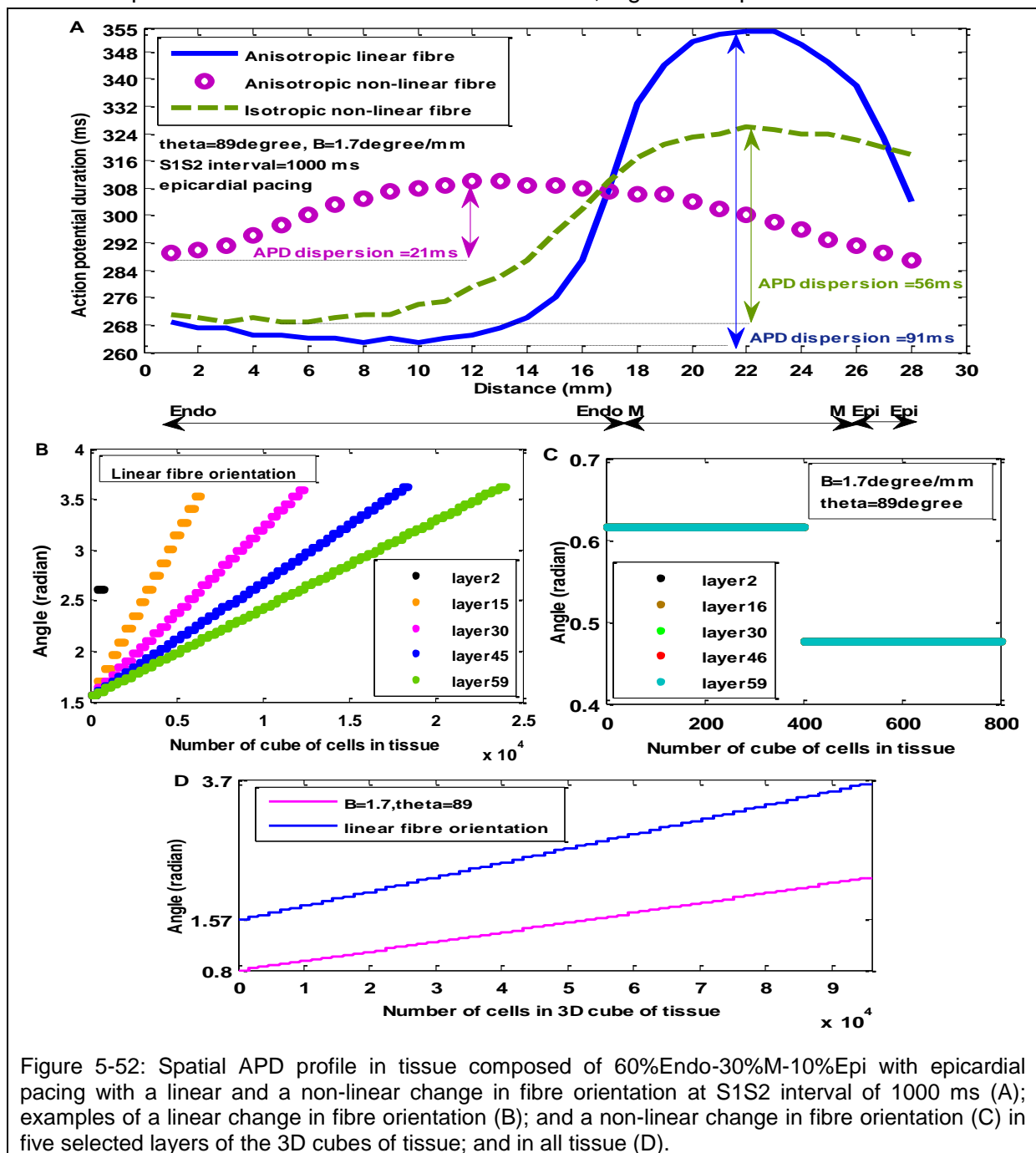


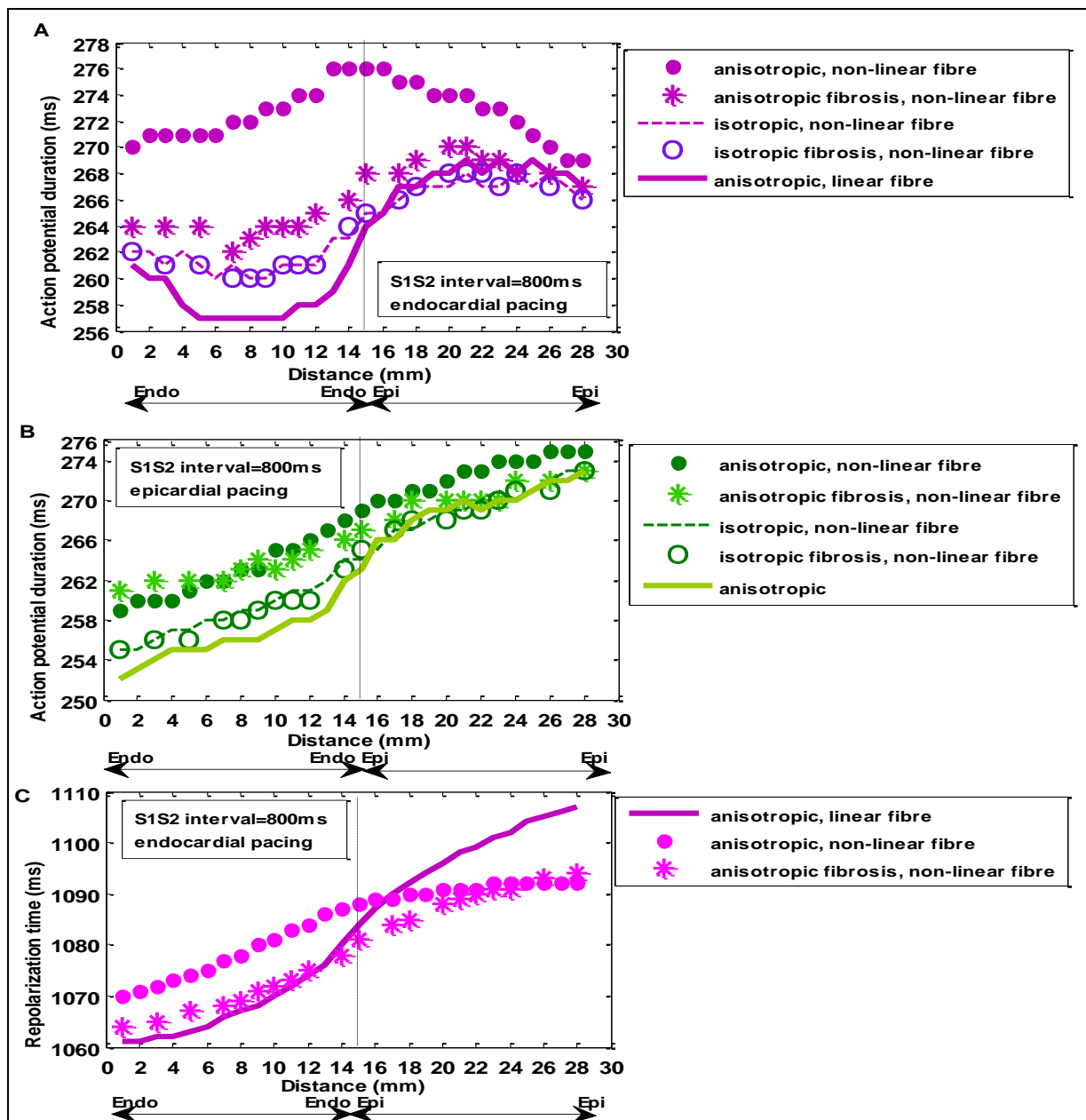
Figure 5-52: Spatial APD profile in tissue composed of 60%Endo-30%M-10%Epi with epicardial pacing with a linear and a non-linear change in fibre orientation at S1S2 interval of 1000 ms (A); examples of a linear change in fibre orientation (B); and a non-linear change in fibre orientation (C) in five selected layers of the 3D cubes of tissue; and in all tissue (D).

It was interesting to know how this particular geometrical model of fibre structure with no variation in fibre orientation with increasing layers influences spatial profiles of APD and repolarization in other heterogeneous tissues during decreasing S1S2 intervals.

These issues are illustrated in the following section.

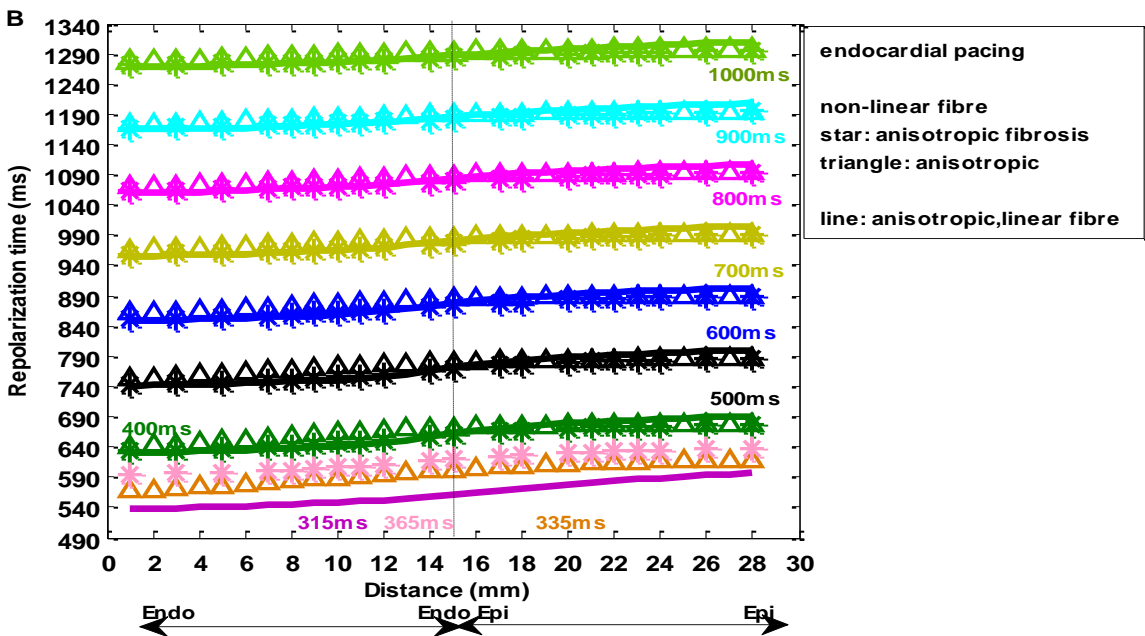
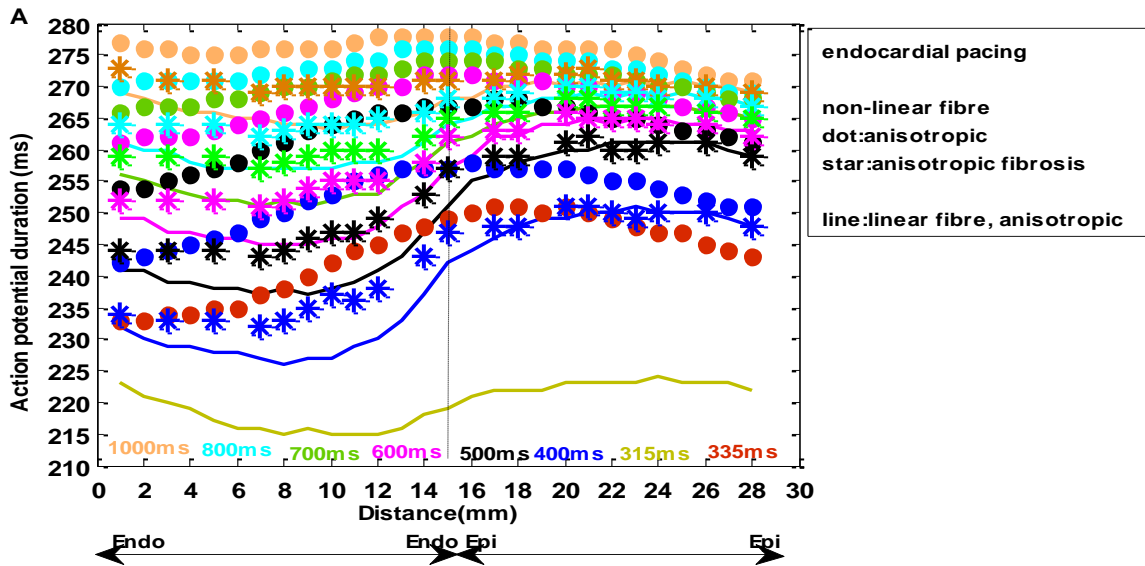
5.8.3 Four heterogeneous tissues

Figures organized in Group V (Figures V1 to V18), show examples of spatial profiles of APD and repolarization time in the FK4V models of isotropic, anisotropic, and anisotropic fibrosis heterogeneous tissues (and fibre structure with setting of $\theta=89^\circ$ and $B=1.7$ degree/mm) at one S1S2 interval and then during decreasing S1S2 intervals.

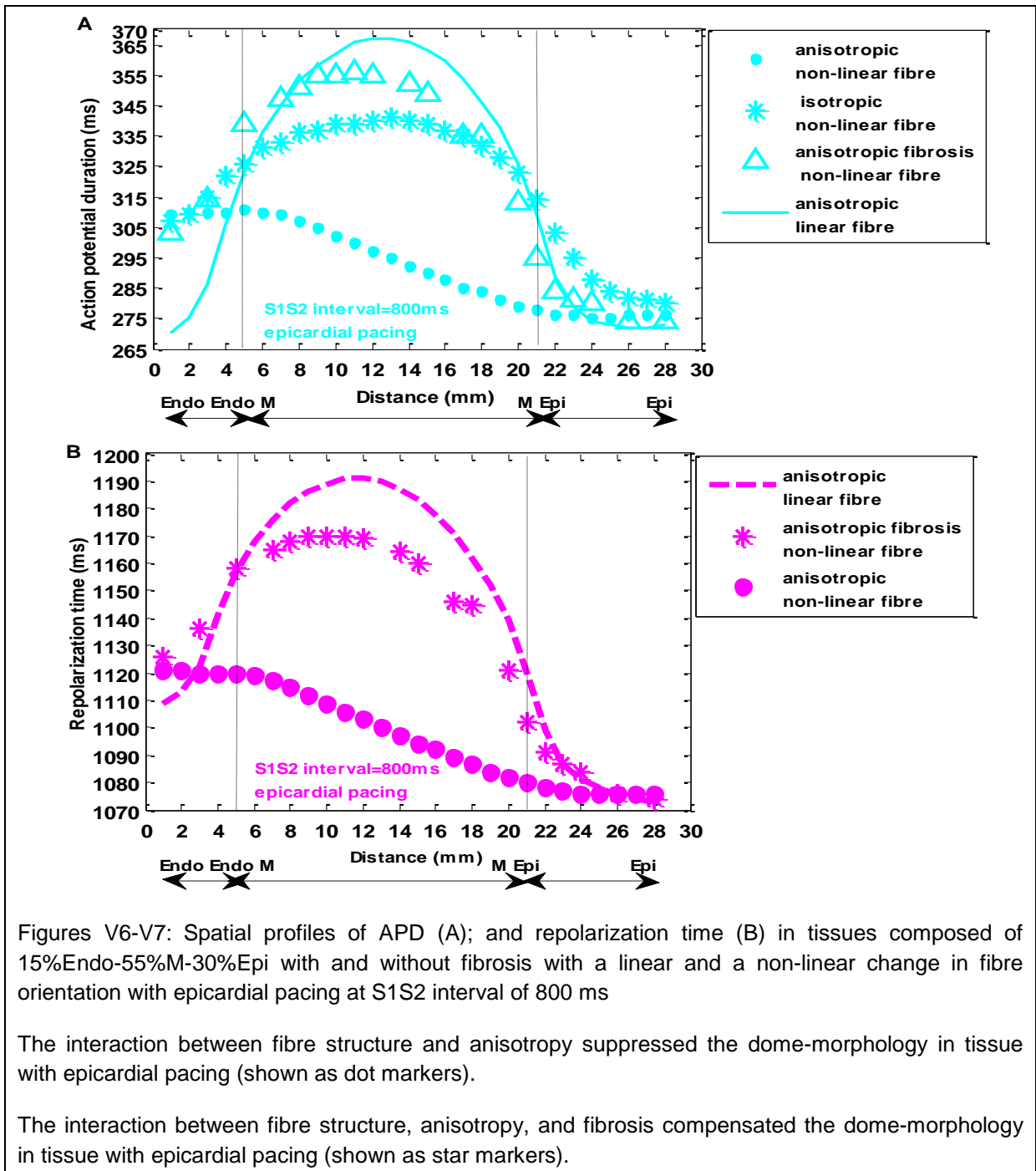


Figures V1-V3: Spatial profiles of APD with endocardial pacing (A); epicardial pacing (B); and spatial profiles of repolarization time with endocardial pacing (C) in tissues composed of 50%Endo-50%Epi with a linear and a non-linear change in fibre orientation at S1S2 interval of 800 ms

The interaction between fibre structure, anisotropy, and fibrosis compensated a sharp transition between endocardial and epicardial regions in tissue with endocardial pacing shown as star.



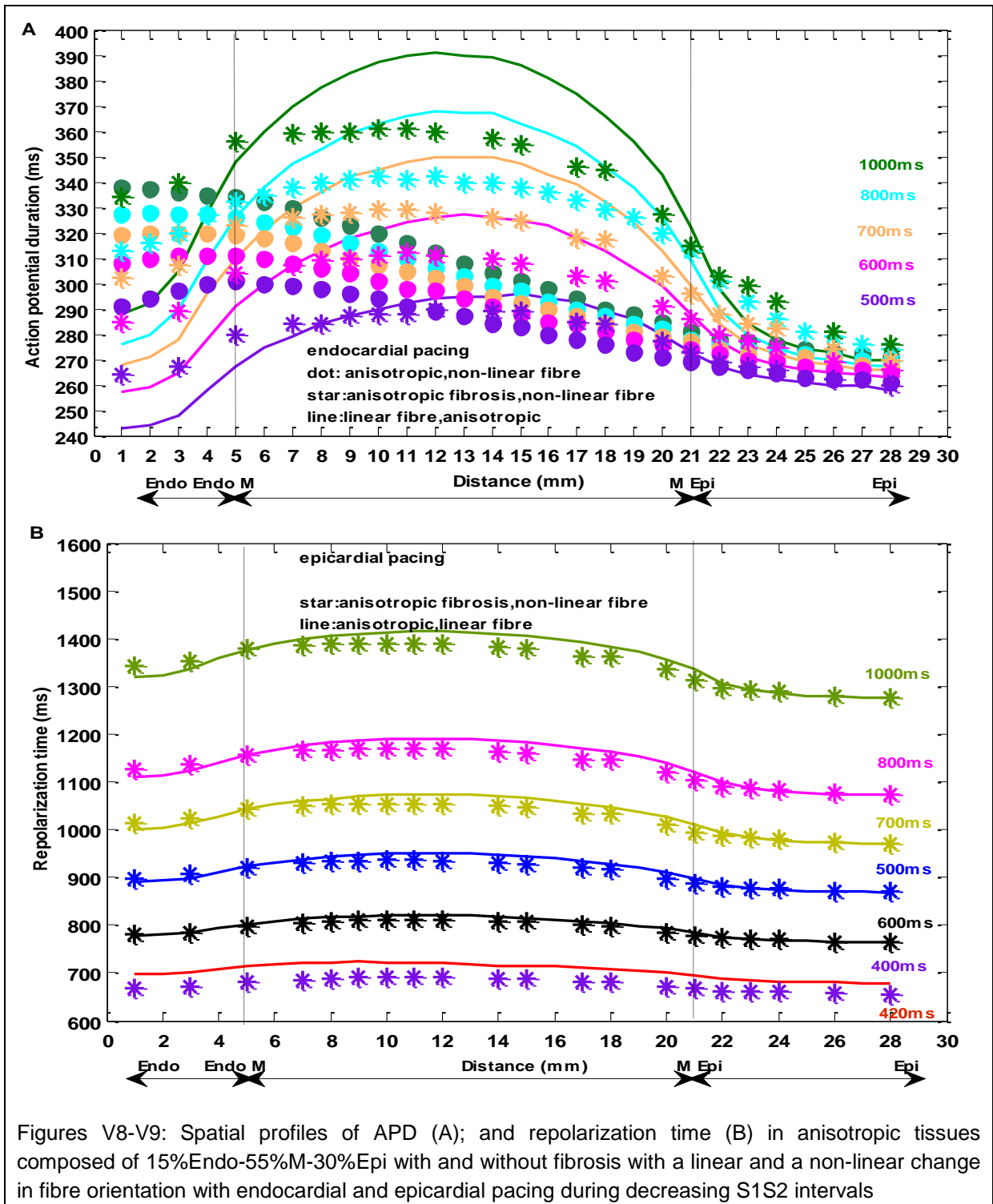
Figures V4-V5: Spatial profiles of APD (A); and repolarization time (B) in anisotropic tissues composed of 50%Endo-50%Epi with and without fibrosis with a linear and a non-linear change in fibre orientation with endocardial pacing during decreasing S1S2 intervals

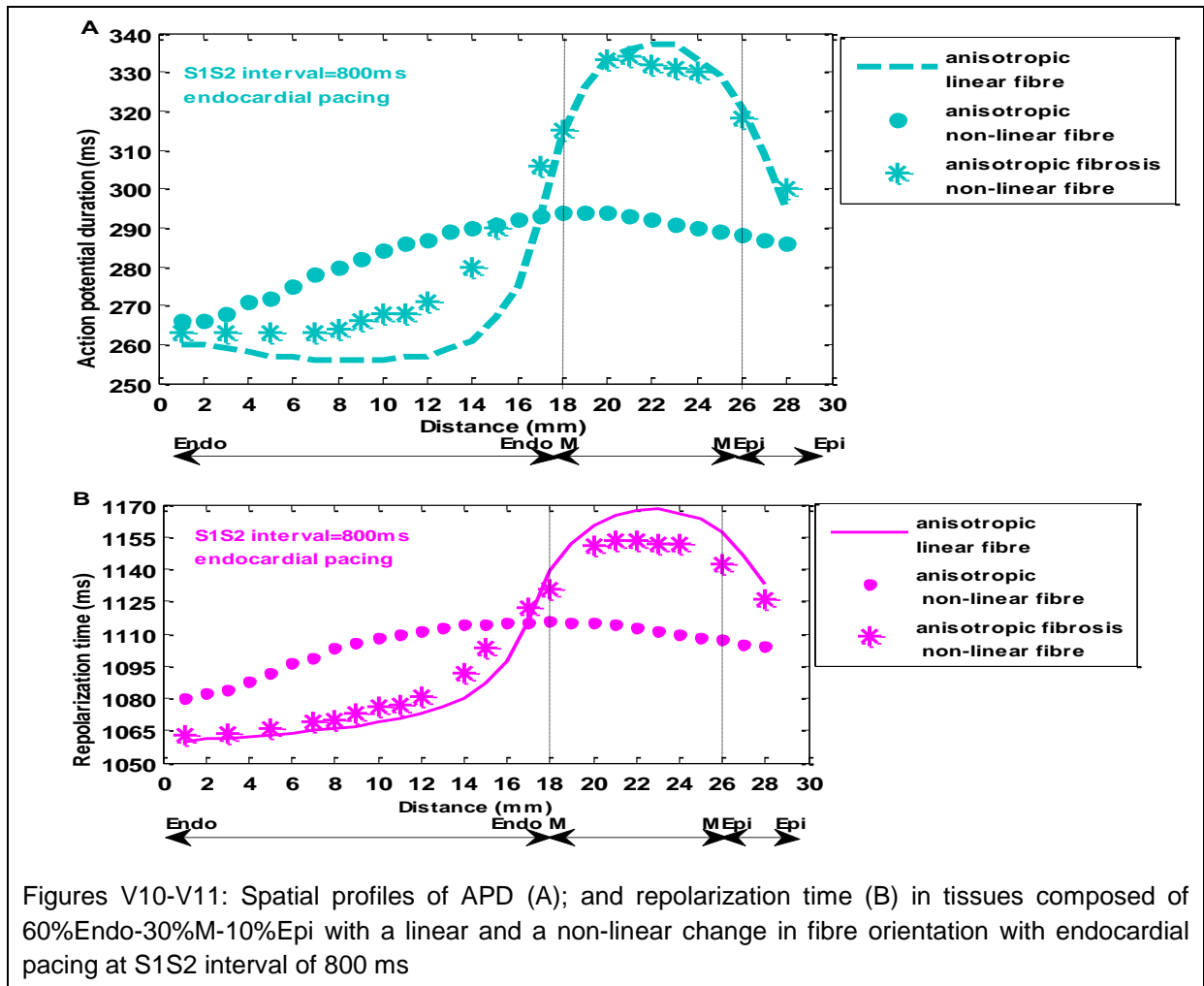


Figures V6-V7: Spatial profiles of APD (A); and repolarization time (B) in tissues composed of 15%Endo-55%M-30%Epi with and without fibrosis with a linear and a non-linear change in fibre orientation with epicardial pacing at S1S2 interval of 800 ms

The interaction between fibre structure and anisotropy suppressed the dome-morphology in tissue with epicardial pacing (shown as dot markers).

The interaction between fibre structure, anisotropy, and fibrosis compensated the dome-morphology in tissue with epicardial pacing (shown as star markers).





Figures V10-V11: Spatial profiles of APD (A); and repolarization time (B) in tissues composed of 60%Endo-30%M-10%Epi with a linear and a non-linear change in fibre orientation with endocardial pacing at S1S2 interval of 800 ms

Similar to anisotropic fibrosis tissue composed of 60%Endo-30%M-10%Epi with a linear change in fibre orientation with endocardial pacing (explained in section 5.4.5, speed of depolarization conduction was suppressed in the mid-myocardial region (but not in the epicardial region) as shown in Figure V12.

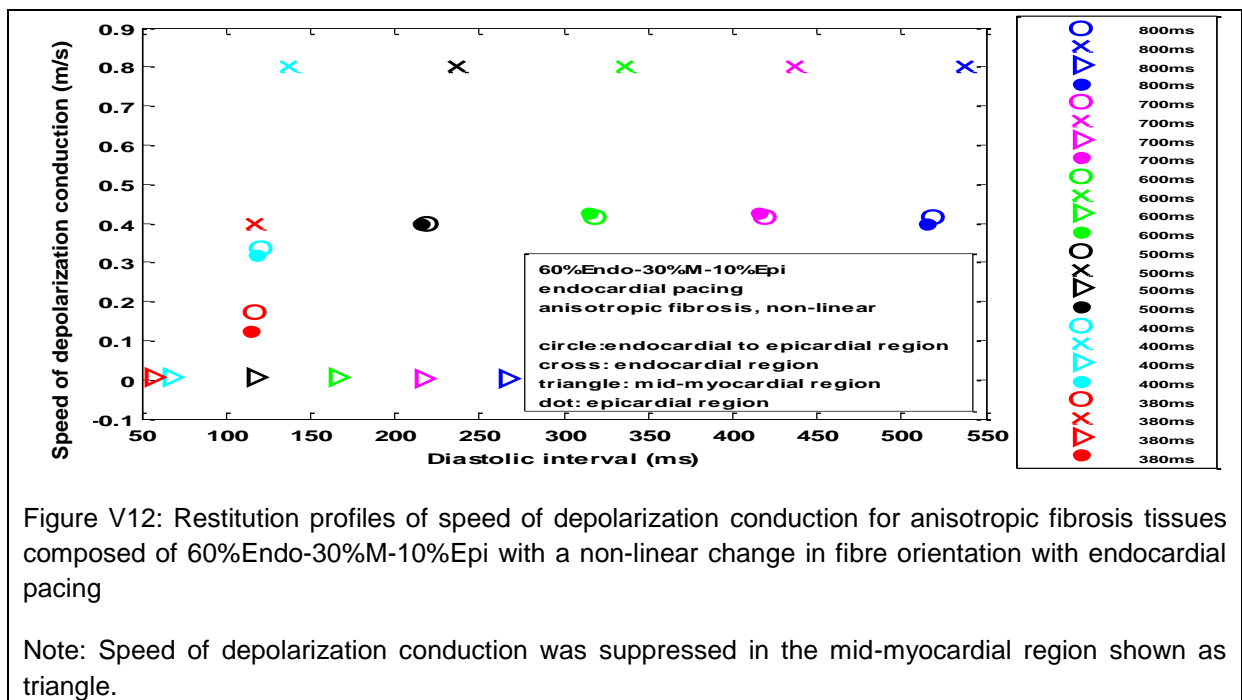
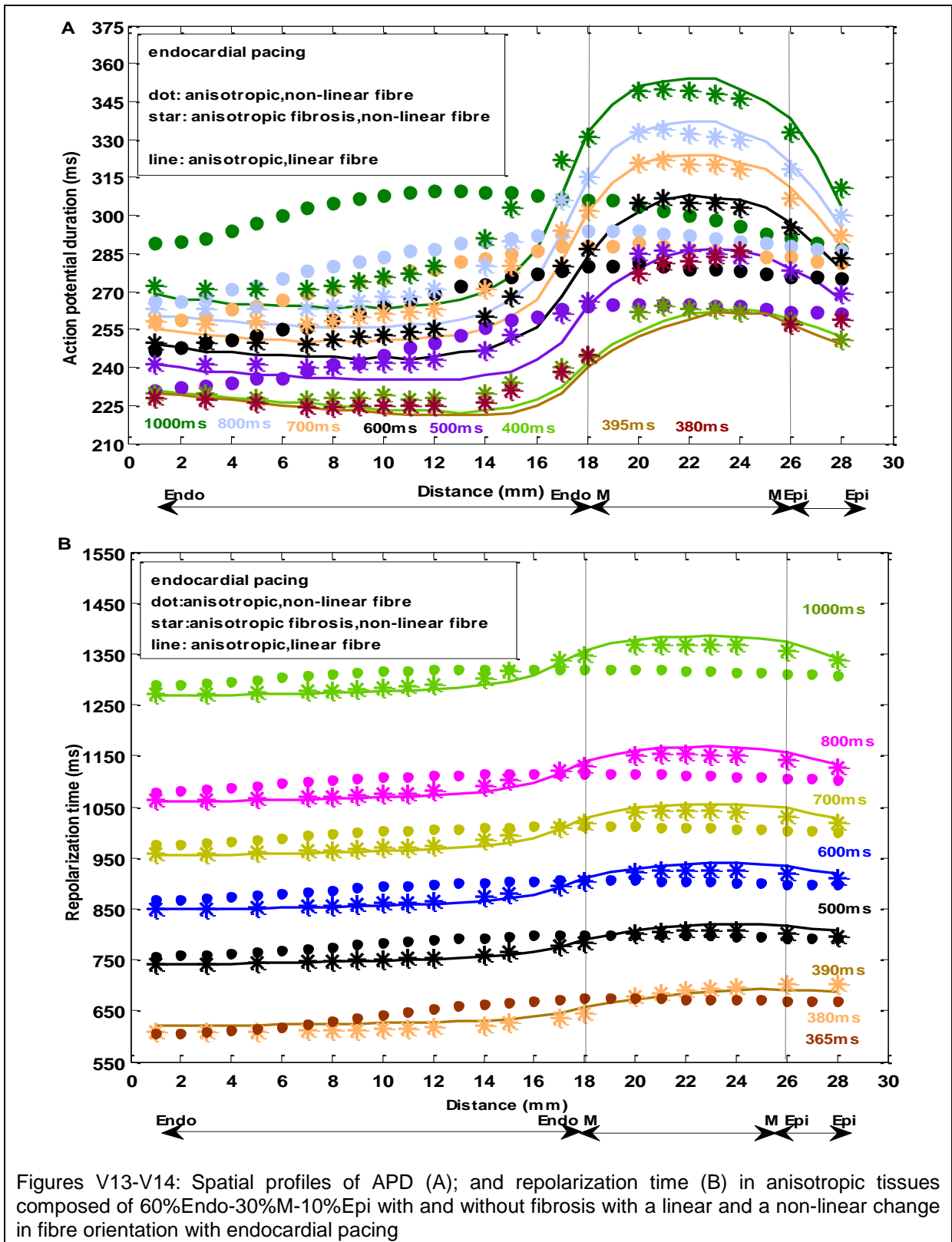
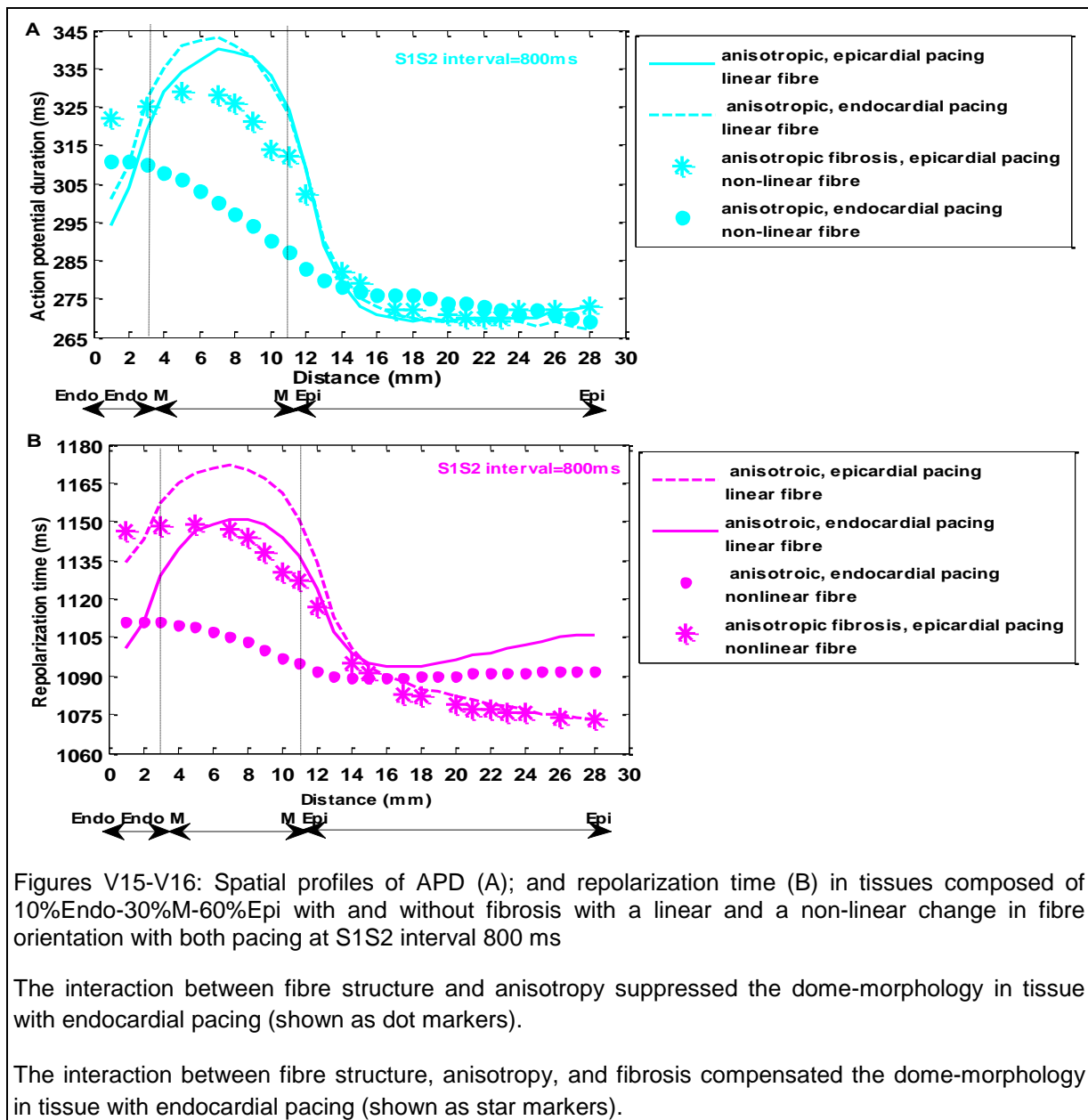


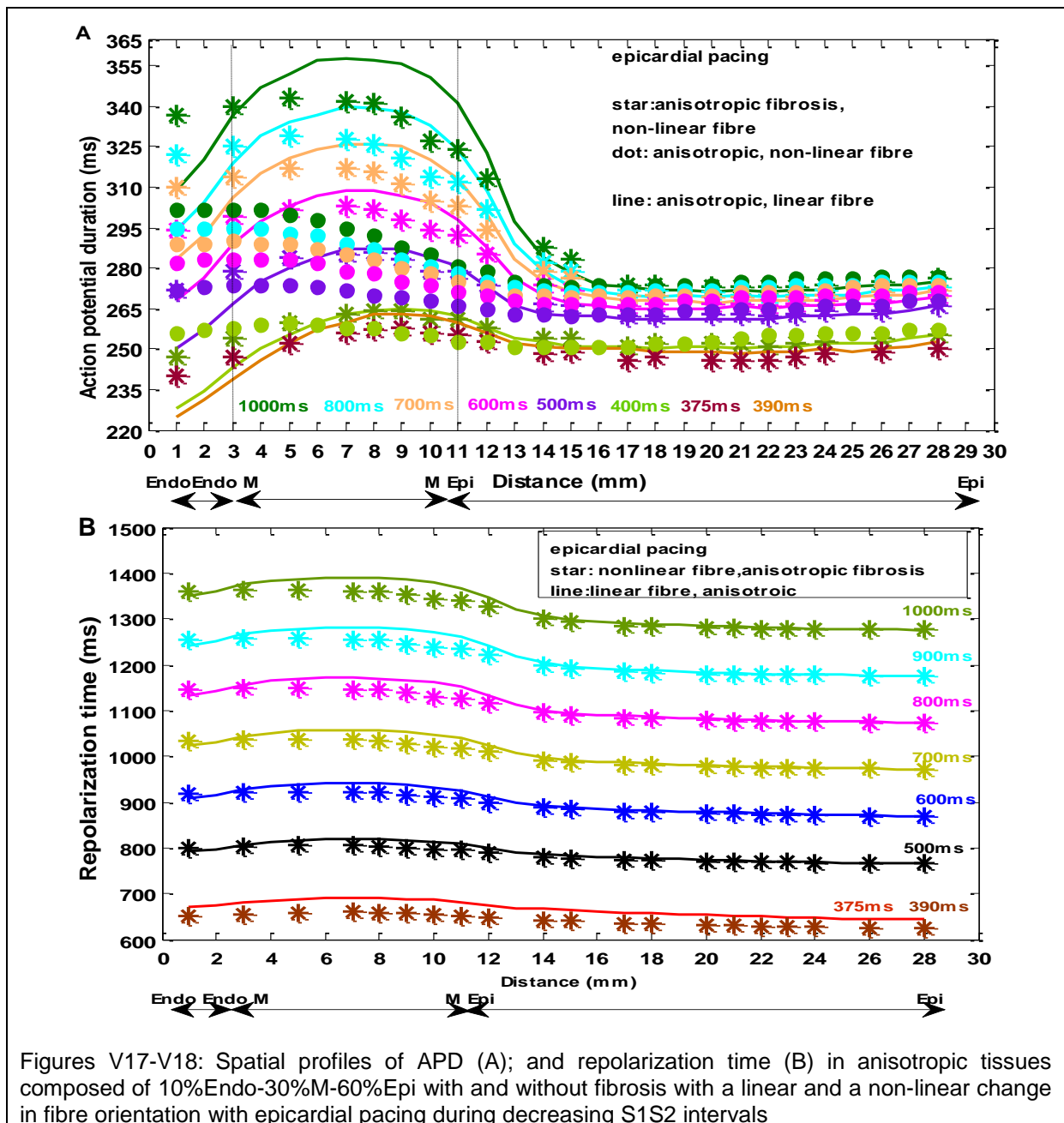
Figure V12: Restitution profiles of speed of depolarization conduction for anisotropic fibrosis tissues composed of 60%Endo-30%M-10%Epi with a non-linear change in fibre orientation with endocardial pacing

Note: Speed of depolarization conduction was suppressed in the mid-myocardial region shown as triangle.



Figures V13-V14: Spatial profiles of APD (A); and repolarization time (B) in anisotropic tissues composed of 60%Endo-30%M-10%Epi with and without fibrosis with a linear and a non-linear change in fibre orientation with endocardial pacing





During decreasing S1S2 interval, the spatial profiles of APD and repolarization time were distinguished based on interaction (1) between a non-linear change in fibre orientation (or no variation in fibre orientation) and anisotropy; and (2) between a non-linear change in fibre orientation (or no variation in fibre orientation) and anisotropic fibrosis tissue.

For heterogeneous tissue composed of 50%Endo-50%Epi, the interaction (1) could:

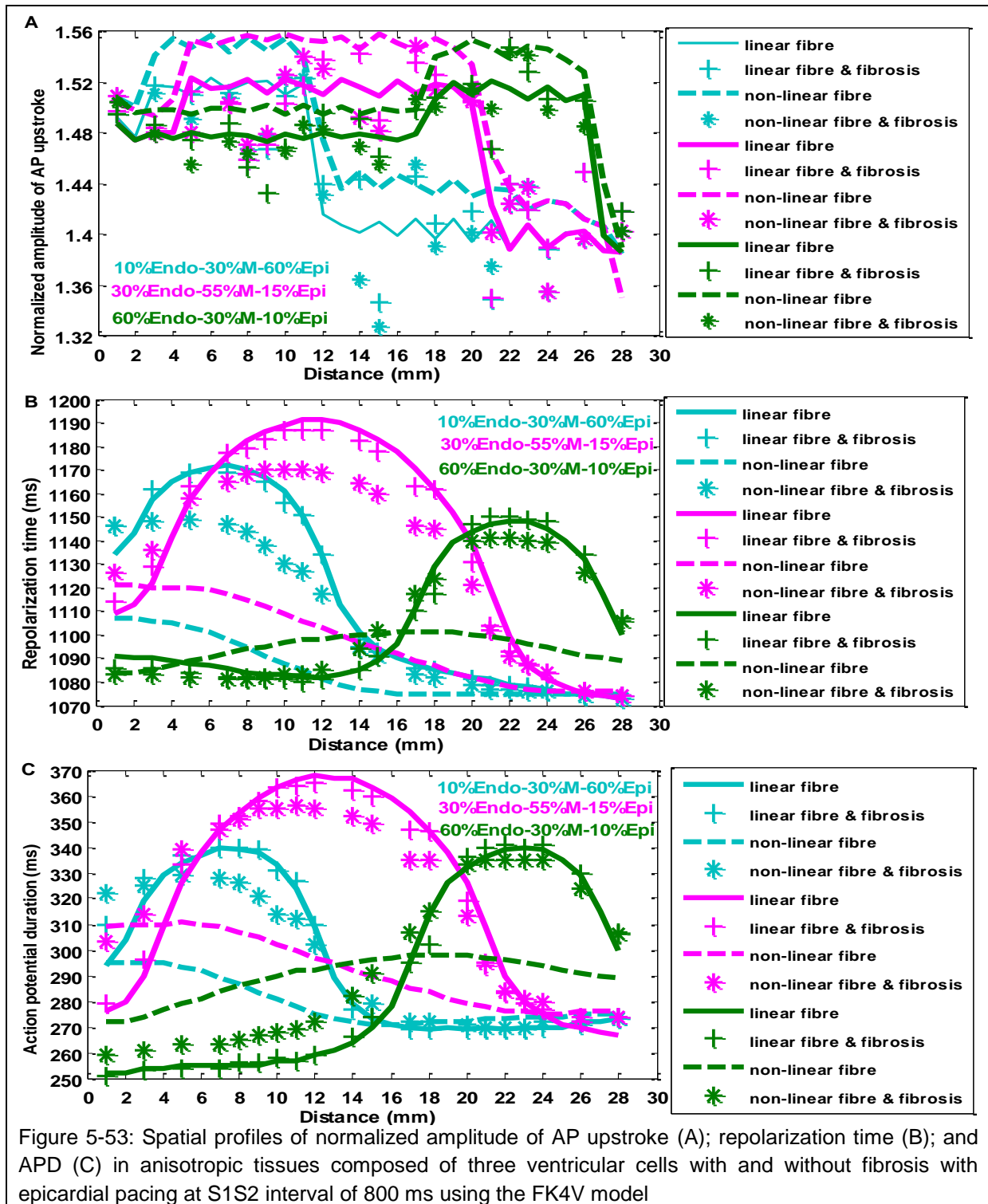
- produce a sharp transition between regions of different cell type compared to the interaction;
- suppress the dome-morphology.

On the other hand, the interaction (2) could:

- compensate the dome-morphology;
- suppress the speed of depolarization conduction in the mid-myocardial region of heterogeneous tissue.

These results were also true for the spatial profiles of the normalized amplitude of AP upstroke (or peaks of AP upstroke of premature beats as shown in Chapter 3, Figure 3-16) in anisotropic tissue with and without fibrosis. Summary Figure 5-53 shows profiles of normalized amplitude of AP upstroke (plot A); repolarization time (plot B); and APD (plots C) for three anisotropic heterogeneous tissues with and without fibrosis with epicardial pacing at S1S2 interval 800 ms. These tissues were simulated with a linear and a non-linear change in fibre orientation (at $\theta=89^\circ$ and $B=1.7$ degree/mm).

These findings emphasize the role of fibre organization and cellular configuration in AP repolarization and AP depolarization of premature beats in heterogeneous tissues.



5.8.4 Numerical stability

It is important to note that for some values of θ and B no transmembrane voltage was created in 3D cubes of anisotropic heterogeneous tissue as shown in Figure 5-51, plot B while created for isotropic heterogeneous tissues. For example, after huge number of simulations with anisotropic tissue composed of 60%Endo-30%M-10%Epi two limits were obtained: $B= 2.4$ degree/mm and $\theta =197^\circ$ for upper limit and $B= -3.13$ degree/mm and $\theta =219^\circ$ for lower limit as shown in Figure 5-51, plot B. These limits may be different in other anisotropic heterogeneous tissues with different cellular configurations. Explanations could include the following:

- this is a prediction from the model, for example in real tissue with a non-linear change in fibre orientation it would not be possible to propagate an AP;
- this results from a problem with the model and could be to do with numerical stability;
- this is a problem with the model implementation, i.e. it could be a software bug.

Obtaining no numerical values for output files for some values of rotation angle θ could be a problem with the numerical instability. It means that all simple integration schemes become unstable if the step-length is made sufficiently large for some values of rotation angle θ . Numeric instability is important as this corresponds to the limits within which these simulations are valid. If there is a numerical instability for large changes in rotation angle θ , it occurs in the codes that estimates the diffusion tensor and the maths. As a result, the geometrical models of fibre structure based on Equation (5-4) in current thesis were limited to a particular value of rotation angle θ and B.

5.8.5 Importance of fibre structure

In summary, a simple setting in the values of B and rotation angle θ in Equation (5-4) allowed controlling:

1. a sharp or a gradual transition between regions of different cell type;
2. the transmural dispersion in repolarization and APD;
3. the dome morphology in spatial APD profiles in the mid-myocardial region in anisotropic and anisotropic fibrosis tissues.

The results suggest that fibre structure with different fibre orientation may be one of the reason for no clue of significant transmural heterogeneity of repolarization or presence of mid-myocardial cells in patients in the study by Taggart et al. [48]

This part of the Chapter provided a background for simulating tissues with non-linear fibre orientation. Yet, further studies are required to assess the dispersion in activation time, repolarization time, and APD for both normal and premature S2 beats as well as speed of depolarization conduction in isotropic, anisotropic, and anisotropic fibrosis tissues.

5.9 Visualization of AP propagation

Section 5.5 showed approximately when (i.e. a range of repolarization time for short S1S2 intervals), which S1S2 intervals, and where (i.e. between epicardial and mid-myocardial regions) each simulated 3D cubes of tissue may become vulnerable for ventricular arrhythmia. This part of the Chapter tests whether wave break occurs in AP propagation during depolarization and repolarization in all tissues at the last S1S2 interval. For visualization, three programmes written in MATLAB were used (PlotStf.m, ReadStf.m, and MakeMovie3Dmpg.m described in Appendix). For the TP06 model, the voltage threshold was -65 mV and for the FK4V model the normalized voltage threshold was 0.1.

The created images of AP propagation for both normal S1 and premature S2 beats at the last S1S2 interval were organized as frames in the enclosed CD, Appendix 3 for the FK4V model and Appendix 4 for the TP06 model. Appendix 3 has four files that the first three files provide images for simulated tissues with a linear change in fibre orientation in isotropic, anisotropic, and anisotropic fibrosis tissues and the last file provides images for tissues with $\theta=89^\circ$ and $B=1.7$ degree/mm and anisotropic diffusion. Appendix 4 has two files for anisotropic tissues with and without fibrosis with a linear change in fibre orientation. The frames of AP propagation for normal and premature beats were organized based on timing of AP depolarization, AP plateau, AP repolarization, and AP rest. The main findings for tissues with a linear change in fibre orientation with both models are listed here.

For normal S1 beats, there was

- no wave break during AP depolarization and repolarization in the three homogenous epicardial, mid-myocardial, and endocardial tissues paced from the bottom edge of tissue and heterogeneous tissue composed of 50%Endo-50%Epi with both endocardial and epicardial pacing;
- the wave break during AP repolarization in three heterogeneous tissues composed of 30%Endo-55%M-15%Epi, 60%Endo-30%M-10%Epi, and 10%Endo30%M60%Epi with both endocardial and epicardial pacing.

For premature S2 beats,

- the wave break was created only during AP depolarization in three homogenous epicardial, mod-myocardial, and endocardial tissues paced from the bottom edge of tissue and tissue composed of 50%Endo-50%Epi with both endocardial and epicardial pacing;
- the break was created during both AP depolarization and AP repolarization in three heterogeneous tissues composed of 30%Endo-55%M-15%Epi, 60%Endo-30%M-10%Epi, and 10%Endo30%M60%Epi with both endocardial and epicardial pacing.

It is important to note that wave break was at the transition regions of heterogeneous tissue (i.e. between endocardial and mid-myocardial region).

For anisotropic homogenous and heterogeneous tissues with $\theta=89^\circ$ and $B=1.7$ degree/mm using the FK4V model, the wave break observed during both AP depolarization and AP repolarization.

For clarity, summary Figures in Group X (Figures X1 to X8) organized in three columns to provide examples of AP propagation (1) during AP depolarization in the first column; (2) from AP repolarization to AP rest in the second column; and (3) the profiles of transmembrane potential against time in the third column. For the FK4V model, each figure has three rows: the first two rows for simulated tissues with linear fibre orientation in anisotropic and anisotropic fibrosis tissues, and the last row for tissues with a non-linear change in fibre orientation ($\theta=89^\circ$ and $B=1.7$ degree/mm) and anisotropic diffusion. For the TP06 model, each figure has two rows for simulated anisotropic tissues with and without fibrosis with a linear change in fibre orientation. These figures correspond to premature S2 beats at the last S1S2 interval in mid-myocardial tissue, tissue composed of 50%Endo-50%Epi and 60%Endo-30%M-10%Epi.

The rest of figures are provided in organized Figures in Group X (Figures X9 to X22) in the CD, Appendix 2.

AP propagation during depolarization

AP propagation during repolarization

S2 membrane potential

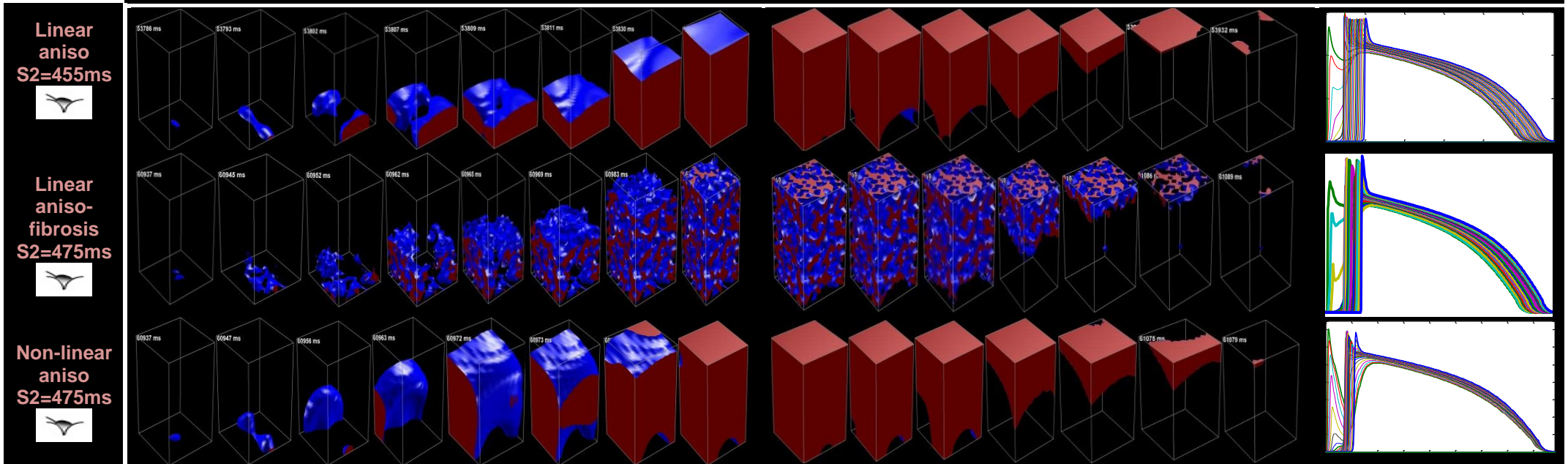


Figure X1: Examples of AP propagation from depolarization to rest in anisotropic **homogenous mid-myocardial tissue** with linear fibre orientation with and without fibrosis as well as non-linear fibre orientation without fibrosis paced from the bottom edge of tissue using the FK4V model

During AP depolarization:

- 1- one wave formed in the bottom surface of tissue
- 2- waves broke into two parts in central region of 3D cube of tissue
- 3- waves joined together in the central region of tissue and propagated till AP plateau

During AP repolarization, the observable change was on the corner and besides tissues.

The frames of tissues with non-linear change in fibre structure changed the patterns of AP propagation during depolarization.

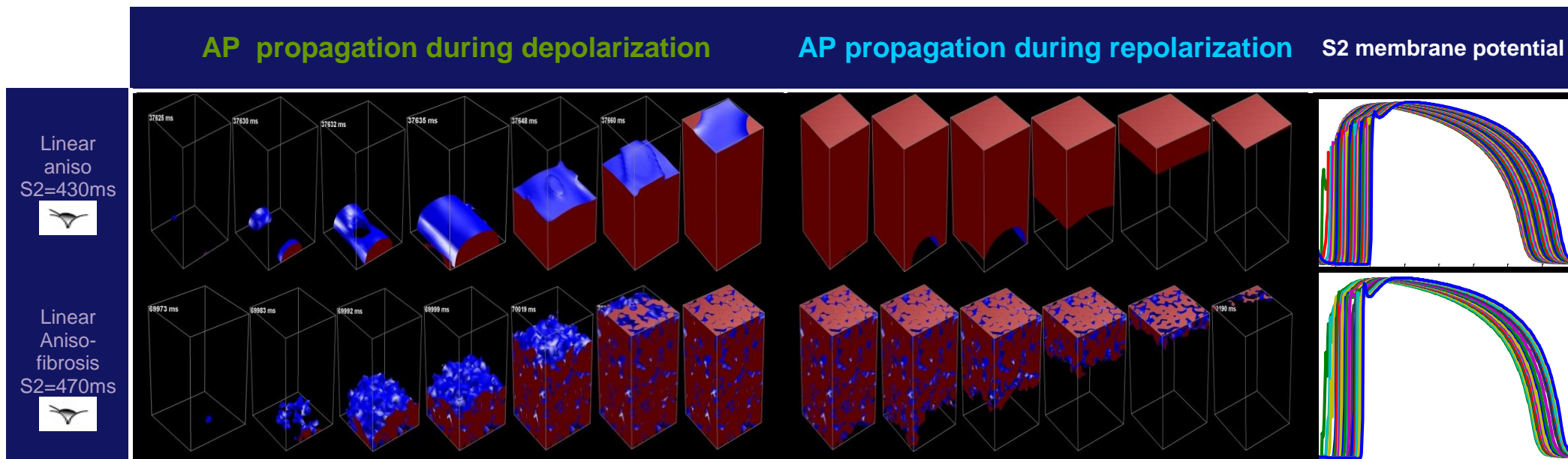


Figure X2: Examples of AP propagation from depolarization to rest in anisotropic **homogenous mid-myocardial tissue** with linear fibre orientation with and without fibrosis paced from the bottom edge of tissue using the **TP06 model**

During AP depolarization:

- 1- two waves formed besides tissue
- 2- waves joined together in the central region of tissue
- 3- the shape of the waves changed in the central region of tissue

During AP repolarization, the observable change was besides tissues.

AP propagation during depolarization

AP propagation during repolarization

S2 membrane potential

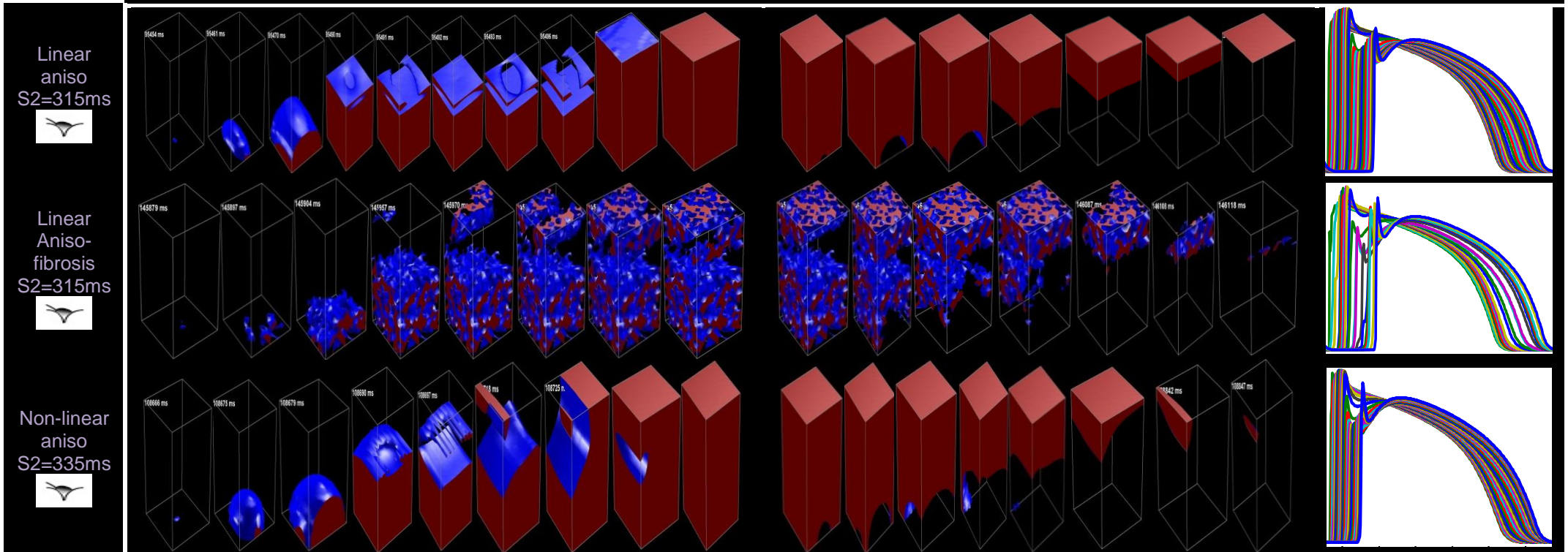


Figure X3: Examples of AP propagation from depolarization to rest in anisotropic **heterogeneous 50%Endo-50%Epi tissue with endocardial pacing** with linear fibre orientation with and without fibrosis as well as non-linear fibre orientation without fibrosis using the FK4V model

During AP depolarization

- 1- one wave formed in the bottom surface of tissue
- 2- propagated besides tissues and upward tissue
- 3- the wave broke into two parts: the top waves broke into two parts and vanished besides tissues while the bottom waves continued propagation till AP plateau

During AP repolarization, the observable change was besides tissues.

AP propagation during depolarization

AP propagation during repolarization

S2 membrane potential

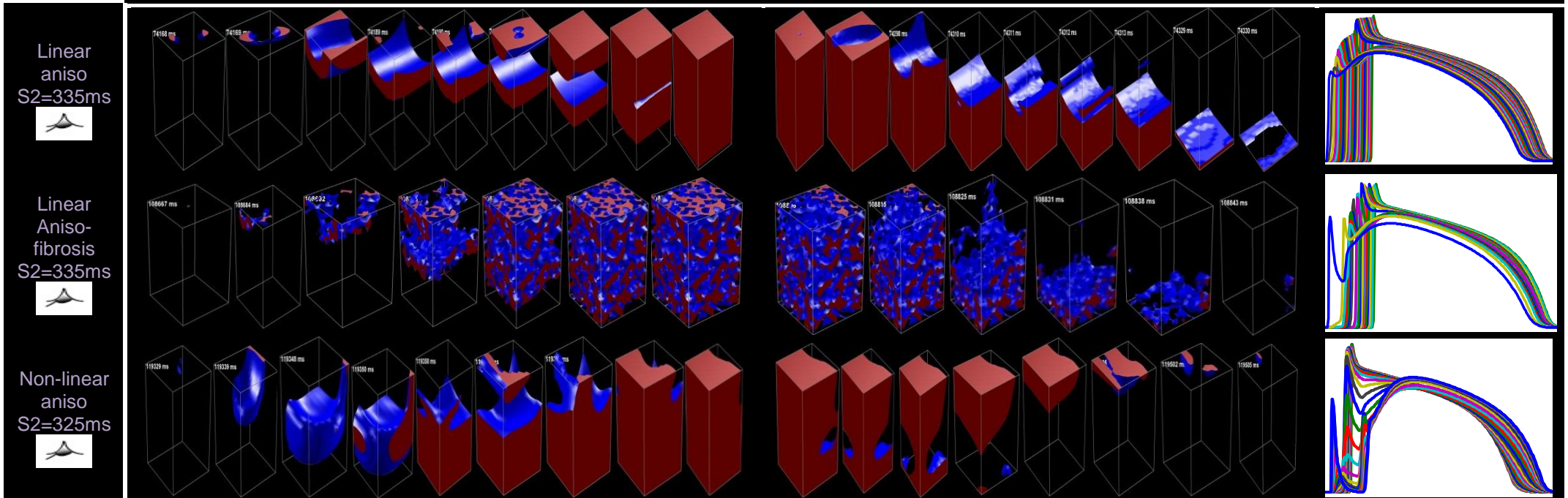


Figure X4: Examples of AP propagation from depolarization to rest in anisotropic **heterogeneous 50%Endo-50%Epi tissue with epicardial pacing** with linear fibre orientation with and without fibrosis as well as non-linear fibre orientation without fibrosis using the FK4V model

During AP depolarization:

- 1- two waves formed on the top surface of tissue and joined together not completely in the central region of tissue
- 2- another two waves formed on the top surface of tissue and joined together not completely in the central region of tissue
- 3- these two group of waves joined together and propagated toward bottom of tissue till AP plateau

During AP repolarization, the wave broke approximately in the endocardial region in two parts: the top waves broke into two parts and vanished besides tissues while the bottom waves continued propagation till AP rest

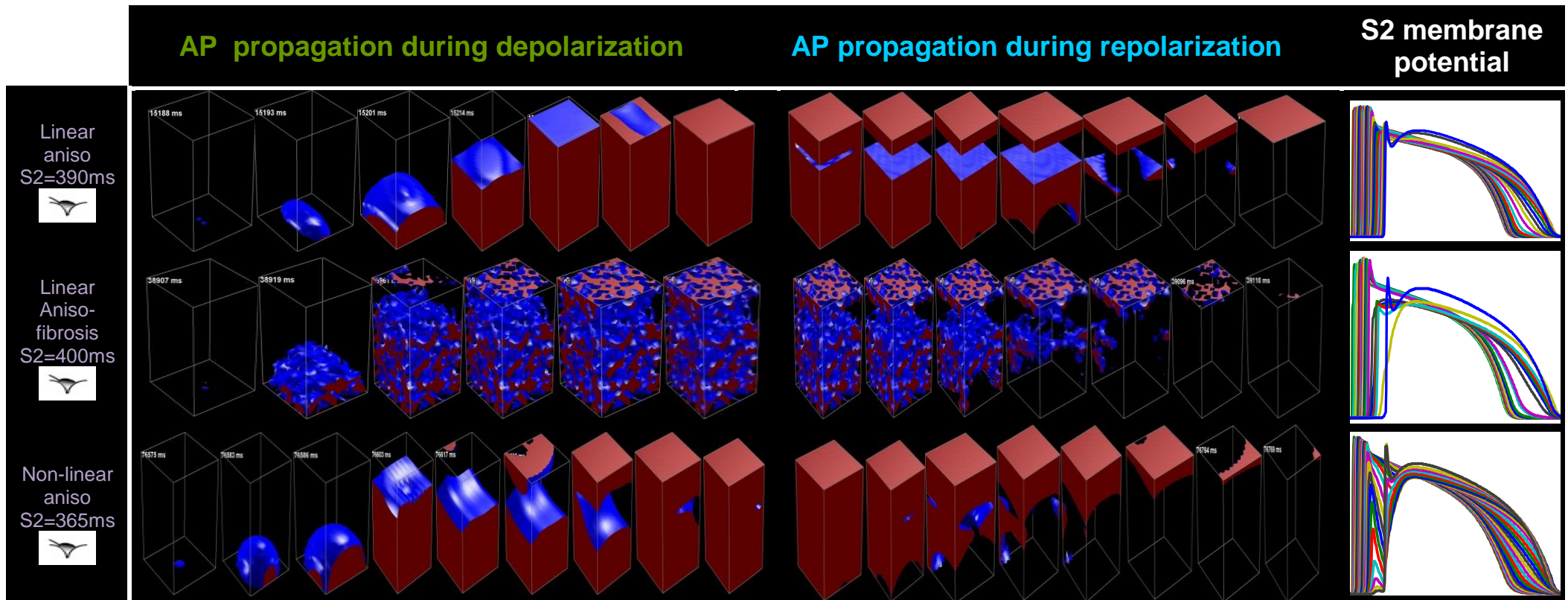


Figure X5: Examples of AP propagation from depolarization to rest in anisotropic **heterogeneous 60%Endo-30%M-10%Epi** tissue with endocardial pacing with linear fibre orientation with and without fibrosis as well as non-linear fibre orientation without fibrosis using the FK4V model

During AP depolarization:

- 1- one wave formed on the bottom surface of tissue in the endocardial region and propagated besides tissue
- 2- the wave propagated toward epicardial region before AP plateau

During AP repolarization, the wave broke into two parts approximately in region close to the mid-myocardial and epicardial regions: the bottom wave broke into two parts and vanished besides tissues while the top wave continued propagation till AP rest in the epicardial region

AP propagation during depolarization

AP propagation during repolarization

S2 membrane potential

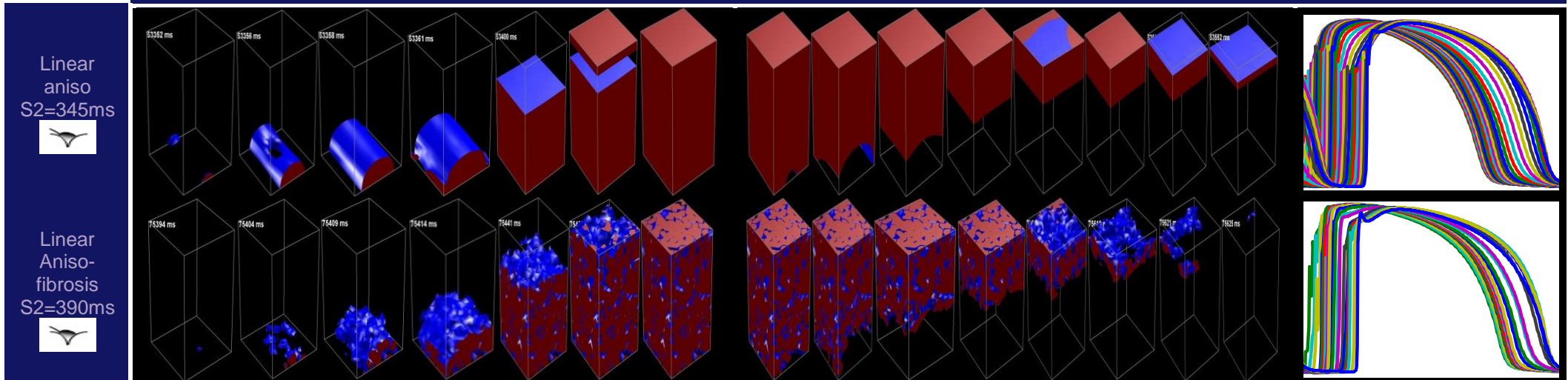


Figure X6: Examples of AP propagation from depolarization to rest in anisotropic **heterogeneous 60%Endo-30%M-10%Epi** tissue with endocardial pacing with linear fibre orientation with and without fibrosis using the **TP06 model**

During AP depolarization:

- 1- two waves formed besides tissue on the bottom surface of tissue in the endocardial region and then joined together and propagated upward
- 2- another wave formed on the top surface of tissue in the epicardial region
- 3- waves joined together close to the region between mid-myocardial and epicardial regions

During AP repolarization:

- 1- the wave propagated toward epicardial region, but then
- 2- the wave propagated downward close to the mid-myocardial region before AP rest

AP propagation during depolarization

AP propagation during repolarization

S2 membrane potential

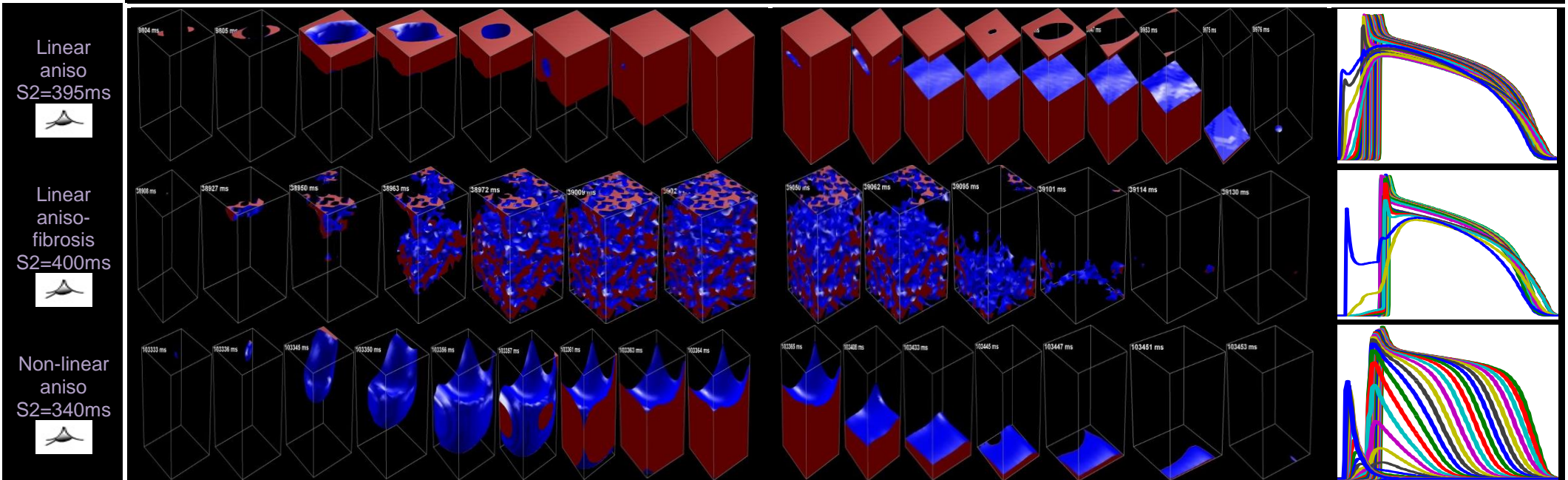


Figure X7: Examples of AP propagation from depolarization to rest in anisotropic **heterogeneous 60%Endo-30%M-10%Epi** tissue with epicardial pacing with linear fibre orientation with and without fibrosis as well as non-linear fibre orientation without fibrosis using the FK4V model

During AP depolarization:

- 1- two waves formed on the top surface of tissue in the epicardial region and only joined together beside tissue
- 2- the wave propagated toward endocardial region before AP plateau

During AP repolarization:

- 1- the wave broke into two parts close to the region between mid-myocardial and epicardial regions
- 2- the top wave broke into two parts and vanished besides tissues in the epicardial region while the bottom wave continued propagation till AP rest

AP propagation during depolarization

AP propagation during repolarization

S2 membrane potential

Linear aniso
S2=380ms



Linear aniso-fibrosis
S2=400ms

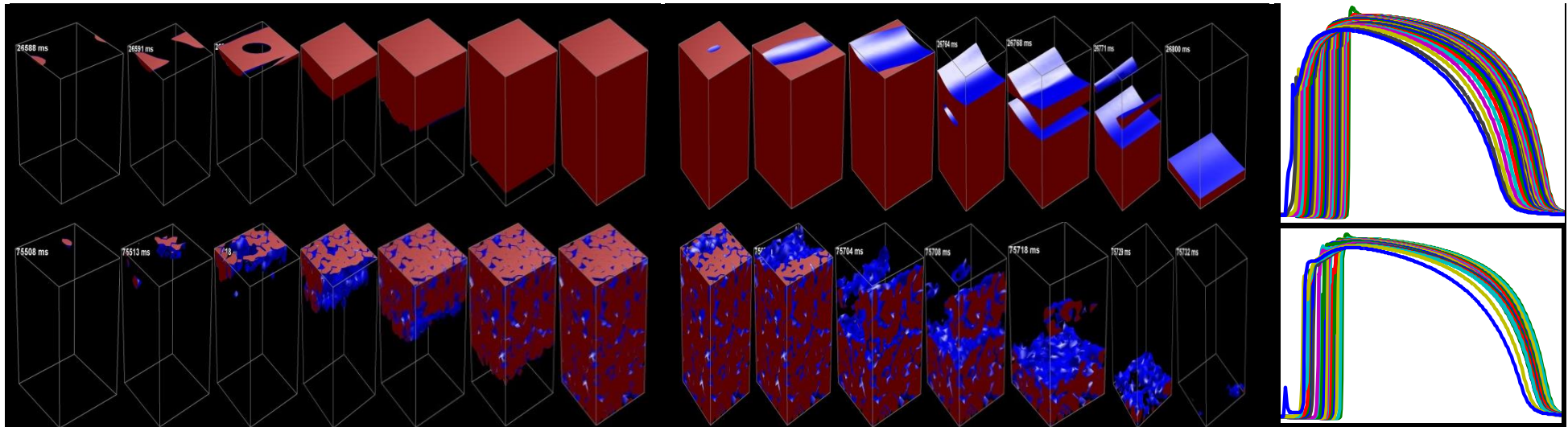


Figure X8: Examples of AP propagation from depolarization to rest in anisotropic **heterogeneous 60%Endo-30%M-10%Epi** tissue with epicardial pacing with linear fibre orientation with and without fibrosis using the [TP06 model](#)

During AP depolarization:

- 1- two waves formed besides tissue on the top surface of tissue in the epicardial region and then joined together
- 2- the wave propagated toward endocardial region before AP plateau

During AP repolarization:

- 1- the wave broke into two parts close to the region between mid-myocardial and endocardial regions
- 2- the top wave broke into two parts and vanished besides tissues in the mid-myocardial region while the bottom wave continued propagation till AP rest in the endocardial region

5.10 Summary of results

Part II introduced heterogeneous tissues with a sharp and a gradual APD transition between regions of different cell type in heterogeneous tissues. Changing the diffusion coefficients combined with changing the proportion of ventricular cells in tissue could shift the dome-morphology of spatial profiles of APD and repolarization toward endocardial or epicardial region and reduce measures of dispersion in APD and repolarization time, but did not change the sharp APD transition between regions of different cell type. Some anisotropic heterogeneous tissues simulated with a non-linear change in fibre orientation could (1) reduce the transmural dispersion in repolarization time; and (2) suppress the dome morphology in spatial profiles of repolarization time and APD. However, these changes were compensated in these tissues with simulated fibrosis. The results emphasize the importance of fibre structure in electrical activity in tissue. In summary, in heterogeneous tissues with endocardial and epicardial pacing,

- Dispersion of repolarization time decreased for long S1S2 intervals and increased for short S1S2 intervals. Because, dispersion in repolarization time depended on not only restitution properties of ventricular cells but also cellular populations, anisotropy, fibrosis, fibre structure (a linear or a non-linear change in fibre orientation), and size of tissue.
- Restitution and spatial profiles of repolarization time represent the true interaction of activation-repolarization coupling and restitution for premature beats. Whereas, spatial APD profiles may mask this interaction particularly for short S1S2 intervals. The results suggest that spatial profiles of repolarization time and profiles of measures of dispersion in repolarization time as useful tools can be used for studying premature beats.
- Visualization of AP propagation during depolarization and repolarization at the last S1S2 interval showed that the transition regions in heterogeneous tissue are where waves break and re-entry may occur. The transition regions were characterized with (1) sharp increase or decrease in APD and repolarization time; and (2) the largest or the smallest measures of dispersion in APD and repolarization time.
- Restitution profiles of premature activation time (against diastolic interval), repolarization time, and APD show qualitatively similar behaviour during decreasing S1S2 intervals.
- Speed of depolarization conduction was also depended on the differences in local restitution. Therefore, combination of anisotropy and fibrosis could suppress the speed of depolarization conduction for premature beats in regions of different cell type, in the mid-myocardial region with longer APD than other cells. The results suggest that anisotropic fibrosis heterogeneous tissue may promote tissue vulnerability to arrhythmia.

The simulation results in the left ventricular wedge model are provided next.

5.11 References

1. Han J and Moe GK, Nonuniform recovery of excitability in ventricular muscle. *Circulation Research*, 1964. **14**: p. 44-60.
2. Kuo CS and Munkata K and Reddy P and Surawicz B, Characteristics and possible mechanism of ventricular arrhythmia dependent on the dispersion of action potential durations. *Circulation*, 1983. **67**: p. 1356-1367.
3. Gough W and Mehra R and Restivo M and Zeiler R and El-Sherif N., Reentrant ventricular arrhythmias in the late myocardial infarction period in the dog: Correlation of activation and refractory maps. *Circ Res*, 1985. **57**: p. 432-442.
4. Chauhan VS and Downar E and Nanthakumar k and Parker JD and Ross HJ and Chan W and Picton P., Increased ventricular repolarization heterogeneity in patients with ventricular arrhythmia vulnerability and cardiomyopathy: a human in vivo study. *Am J Physiol Heart Circ Physiol*, 2006. **290**: p. H79-H86.

5. Sicouri S and Antzelevitch C, Drug-induced afterdepolarizations and triggered activity occur in a discrete subpopulation of ventricular muscle cells (M cells) in the canine heart: quinidine and digitalis. *J Cardiovasc Electrophysiol*, 1993. **4**: p. 48–58.
6. El-Sherif N and Caref EB and Yin H and Restivo M., The electrophysiological mechanism of ventricular arrhythmias in the long QT syndrome: tridimensional mapping of activation and recovery patterns. *Circ Res.*, 1996. **79**: p. 474–492.
7. Engelman ZJ and Trew ML and Smaill BH, Structural heterogeneity alone is a sufficient substrate for dynamic instability and altered restitution. *Circ Arrhythmia Electrophysiol*, 2010. **3**: p. 195-203.
8. de Bakker JM and Van Rijen HM, Continuous and Discontinuous Propagation in Heart Muscle: Role of Fibrosis in Discontinuous Conduction. *J Cardiovasc Electrophysiol*, 2006. **17**: p. 567-573.
9. Kawara T and Derksen R and De Groot JR and Coronel R and Tasseron S and Linnenbank AC and Hauer RNW and Kirkels H and Janse MJ and De Bakker JMT, Activation delay after premature stimulation in chronically diseased human myocardium relates to the architecture of interstitial fibrosis. *Circulation*, 2001. **104**: p. 3069-3075.
10. Wu TJ and Hwang C and Fishbein MC and Czer L and Blanche C and Kass RM and Mandel WJ and Karagueuzian HS and Chen P, Characteristics of wave fronts during ventricular fibrillation in human hearts with dilated cardiomyopathy: role of increased fibrosis in the generation of reentry. *J Am Coll Cardiol*, 1998. **32**.
11. Drouin E and Lande G and Charpentier F, Amiodarone reduces transmural heterogeneity of repolarization in the human heart. *J Am Coll Cardiol*, 1998. **32**: p. 1063-1067.
12. Drouin E and Charpentier F and Gauthier C and Laurent K and Le Marec H, Electrophysiologic characteristics of cells spanning the left ventricular wall of human heart: evidence for presence of M cells. *J Am Coll Cardiol*, 1995. **26**: p. 185-192.
13. Okada J and Washio T and Maehara A and Momomura Sh and Sugiura S and Hisada T, Transmural and apicobasal gradients in repolarization contribute to T-wave genesis in human surface ECG. *Am J Physiol Heart Circ Physiol*, 2011. **301**: p. H200-H208.
14. Dos Santos RW and Otaviano Campos F and Neumann Ciuffo L and Nygren A and Giles W and Koch H., ATX-II Effects on the Apparent Location of M Cells in a Computational Model of a Human Left Ventricular Wedg. *J Cardiovasc Electrophysiol.*, 2006. **17**: p. S86–S95.
15. Narayan SM and Bayer JD and Lalani G and Trayanova NA., Action potential dynamics explain arrhythmic vulnerability in human heart failure: a clinical and modeling study implicating abnormal calcium handling. *J Am Coll Cardiol.*, 2008. **52**: p. 1782-1792.
16. Bayer JD and Narayan SM and Lalani GG and Trayanova NA., Rate-dependent action potential alternans in human heart failure implicates abnormal intracellular calcium handling. *Heart Rhythm*, 2010. **7**: p. 1093-1101.
17. Medina-Ravell VA and Lankipalli RS and Yan GX and Antzelevitch C and Medina-Malpica NA and Medina-Malpica OA and Droogan C and Kowey PR, Effect of epicardial or biventricular pacing to prolong QT interval and increase transmural dispersion of repolarization. Does resynchronization therapy pose a risk for patients predisposed to long QT or torsade de pointes? *Circulation*, 2003. **107**: p. 740–746.
18. Fish JM and Brugada J and Antzelevitch C., Potential proarrhythmic effects of biventricular pacing. *J Am Coll Cardiol.*, 2005. **46**: p. 2340–2347.
19. Santangelo L and Ammendola E and Russo V and Cavallaro C and Vecchione F and Garofalo S and D'Onofrio A and Calabrò R., Influence of biventricular pacing on myocardial dispersion of repolarization in dilated cardiomyopathy patients. *Europace*, 2006. **8**: p. 502-5.
20. Bueno-Orovio A and Cherry EM and Fenton FH, Minimal model for human ventricular action potentials in tissue. *Journal of Theoretical Biology*, 2008. **235**: p. 544-560.
21. ten Tusscher KH and Panfilov AV, Alternans and spiral breakup in a human ventricular tissue model. *Am J Physiol Heart Circ Physiol*, 2006. **291**: p. H1088–H1100.
22. Taggart P and Sutton PM and Boyett MR and Lab M and Swanton H, Human ventricular action potential duration during short and long cycles. Rapid modulation by ischemia. *Circulation*, 1996. **94**: p. 2526–2534.
23. Greenbaum RA and Ho SY and Gibson DG and Becker AE and Anderson RH, Left ventricular fibre architecture in man. *Br Heart J* 1981. **45**: p. 248-263.
24. Hyatt CJ and Wellner M and Berenfeld O and Popp AK and Weitz DA and Jalife J and Pertsov AM, Synthesis of voltage-sensitive fluorescence signals from three-dimensional myocardial activation patterns. *Biophys J*, 2003. **85**: p. 2673-2683.
25. Yue AM and Franz R and Roberts R and Morgan JM, Global endocardial electrical restitution in human right and left ventricles determined by noncontact mapping. *J Am Coll Cardiol*, 2005. **46**.
26. Nash MP and Bradley CP and Sutton PM and Clayton RH and Kallis P and Hayward MP and Peterson DJ and Taggart P., Whole heart action potential duration restitution properties in cardiac patients: a combined clinical and modeling study. *Exp Physiol*, 2006. **91**: p. 339–354.

27. Glukhov AV and Fedorov VV and Qing L and Ravikumar VK and Kalish PW and Schuessler RB and Moazami N and Efimov IR, Transmural dispersion of repolarization in failing and nonfailing human ventricle. *Circ Res*, 2010. **106**: p. 981-991.
28. Yan GX and Shimizu W and Antzelevitch C, Characteristics and distribution of M-cells in arterially perfused canine left ventricular wedge preparations. *Circulation*, 1998. **98**: p. 1921-1927.
29. Conrath CE and Wilders R and Coronel R and De Bakker JMT and Taggart P and De Groot JR and Opthof T., Intercellular coupling through gap junctions masks M cells in the human heart. *Cardiovasc. Progress in Biophysics & Molecular Biology*, 2004a. **62**: p. 407-414.
30. Yuan S and Kongstad O and Hertvig E and Holm M and Grins E and Olsson B, Global repolarization sequence of the ventricular endocardium: monophasic action potential mapping in swine and humans. *Pacing Clin Electrophysiol*, 2001. **24**: p. 1479-1488.
31. Cowan JC and Hilton CJ and Griffiths CJ and Tansuphaswadikul S and Bourke JP and Murray A and Campbell RWF, Sequence of epicardial repolarisation and configuration of the T wave. *Eur Heart J*, 1988. **60**: p. 424-433.
32. Franz MR and Bargheer K and Rafflenbeul W and Haverich A and Lichtlen PL, Monophasic action potential mapping in human subjects with normal electrocardiograms: direct evidence for the genesis of the T wave. *Circulation*, 1987. **75**: p. 379-386.
33. Hanson B and Sutton P and Elameri N and Gray M and Critchley H and Gill JS and Taggart P., Interaction of Activation-Repolarization Coupling and Restitution Properties in Humans. *Circulation: Arrhythmia and Electrophysiology*, 2009. **2**: p. 162-170.
34. Taggart P and Sutton P and Opthof T and Coronel R and Kallis P, Electrotonic cancellation of transmural gradients in the left ventricle in man. *Biophysics and Mol Biol*, 2003. **82**: p. 243-254.
35. Poelzing S and Akar FG and Baron E and Rosenbaum DS., Heterogeneous connexin43 expression produces electrophysiological heterogeneities across ventricular wall. *Am J Physiol Heart Circ Physiol*, 2004. **286**: p. H2001-H2009.
36. Morgan J.M and Cunningham D and Rowland E, Dispersion of monophasic action potential duration: demonstrable in humans after premature ventricular extrastimulation but not in steady state. *J Am Coll Cardiol*, 1992. **19**: p. 1244-1253.
37. Vassallo JA and Cassidy DM and Kindwall KE and Marchlinski FE and Josephson ME., Nonuniform recovery of excitability in the left ventricle. *Circulation*, 1988(78): p. 1365-1372.
38. Taggart P and Sutton PMI and Opthof T and Coronel R and Trimlett R and Pugsley W and Kallis P, Inhomogeneous transmural conduction during early ischemia in patients with coronary artery disease. *J Mol Cell Cardiol*, 2000. **32**: p. 621-639.
39. Nanthakumar K and Jalife J and Massé S and Downar E and Pop M and Asta J and Ross H and Rao V and Mironov S and Dhopeswarkar R, Optical mapping of Langendorff perfused human hearts: establishing a model for the study of ventricular fibrillation in humans. *Am J Physiol*, 2007. **293**: p. H875-H880.
40. Durrer D and Van Der Tweel LH and Berreklouw S and Van Der Wey AP, Spread of activation in the left ventricular wall of the dog, IV: two and three dimensional analysis. *Am Heart J*, 1955. **50**: p. 860-882.
41. Weiss DL and Seemann G and Keller DUJ and Farina D and Sachse FB and D'ossel O., Modeling of Heterogeneous Electrophysiology in the Human Heart with Respect to ECG Genesis. *Computers in Cardiology*, 2007. **34**: p. 49-52.
42. Keller DUJ and Jarrousse O and Fritz t and Ley S and D'ossel O and Seemann G., Impact of physiological vntricular deformation on the morphology of the T-Wave: A hybrid, static-dynamic approach. *IEEE Transaction on biomedical engineering*, 2011. **58**: p. 2109-2119.
43. Gabriel S and Lau R W and Gabriel C, The dielectric properties of biological tissues: III. Parametric models for the dielectric spectrum of tissues. *Phys Med*, 1996. **41**: p. 2271-2293.
44. Streeter DDJ, Gross morphology and fiber geometry of the heart, in *Handbook of Physiology. The Cardiovascular System*, Berne RM and Sperelakis N and Greger SR, Editor. 1979, Baltimore, Maryland, Williams & Wilkins Co.
45. Nielsen PMF and LeGrice IJE and Smaill BH and Hunter PJ, Mathematical model of geometry and fibrous structure of the heart. *American Journal of Physiology (Heart and Circulatory Physiology)* 1991. **260**: p. H1365-H1378.
46. Streeter DDJ and Bassett DL, An Engineering Analysis of Myocardial Fiber Orientation in Pig's Left Ventricle in Systole. *Anat Rec*, 1966. **155**: p. 503-511.
47. Vetter FJ and Simons SB and Mironov S and Hyatt CJ and Pertsov AM, Epicardial fiber organization in swine right ventricle and its impact on propagation. *Circulation research*, 2005. **96**: p. 244-251.
48. Taggart P and Sutton PM and Opthof T and Coronel R and Trimlett R and Pugsley W and Kallis P, Transmural repolarisation in the left ventricle in humans during normoxia and ischaemia. *Cardiovasc Res*, 2001. **50**: p. 454-462.

Chapter 6

Simulation results in the left ventricular wedge model

6.1 Introduction

This Chapter highlights similarities and differences of AP depolarization and repolarization for normal and premature beats in (1) the 3D cubes of tissue; and in (2) an anatomically detailed left ventricular wedge model (including tissue and fibre geometry) composed of anisotropic homogenous and heterogeneous tissues without fibrosis. To keep consistency with simulation results in 3D cubes of anisotropic tissue, diffusion coefficient along and across the fibre axis was set to $0.001 \text{ cm}^2/\text{ms}$ and $0.00025 \text{ cm}^2/\text{ms}$ respectively.

For the left ventricular wedge model, the fibre geometry and two tissue geometries were obtained from diffusion tensor magnetic resonance imaging in the Centre for Cardiovascular Bioinformatics and Modelling at Johns Hopkins University [1]. Both tissue geometries had the same number of grid points (175 columns, 550 rows, and 300 layers) and dimensions of $3.5 \times 11.0 \times 6.0 \text{ cm}^3$ with space step 0.02 cm . In the left ventricular wedge model, to simulate

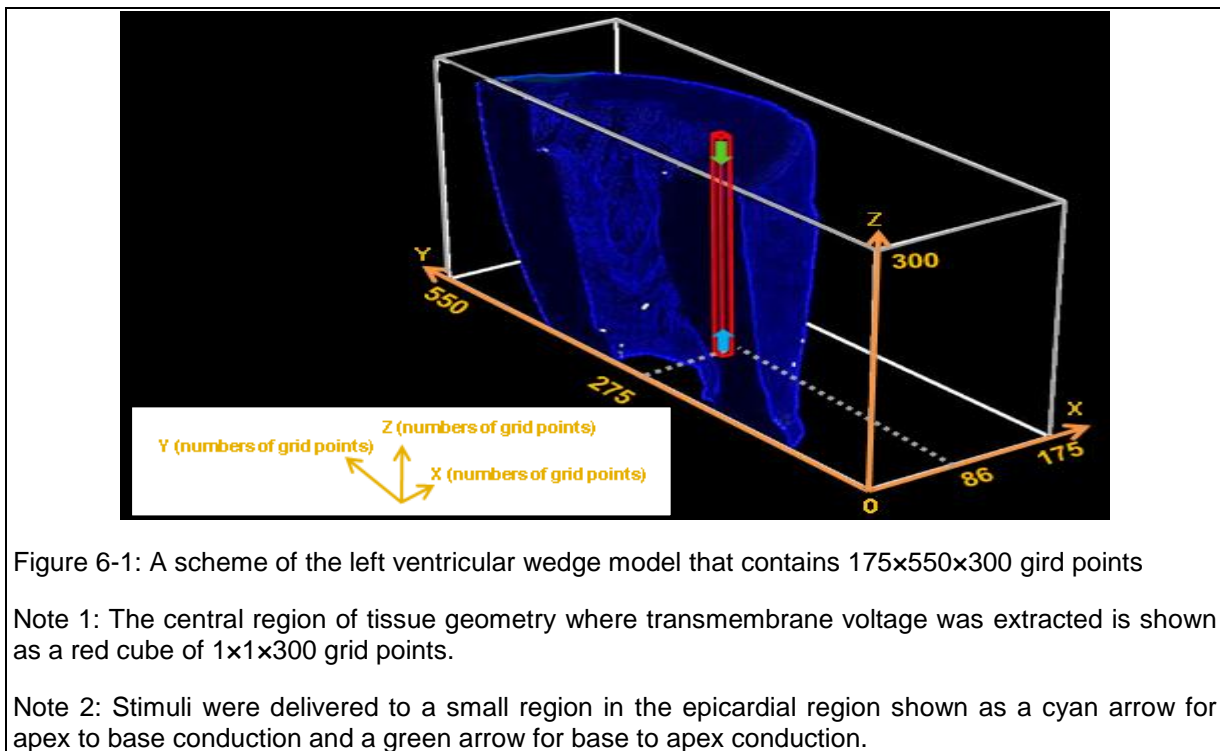
1. homogenous tissues composed of one ventricular cell type, the first tissue geometry was used that contained a left ventricular geometry, with 1s and 0s as grid points within and outside tissue, then the programme in this thesis was modified to allocate 1s to be (1) epicardial cells to represent epicardial tissue; (2) to be endocardial cells to represent endocardial tissue; and (3) to mid-myocardial cells to represent mid-myocardial tissue;
2. heterogeneous tissues composed of three ventricular cell types, the second tissue geometry was used in which the distance from the middle of the left ventricle was used to allocate ventricular cells in the tissue geometry [1]. Accordingly, 1s corresponds to epicardial cells, 2s to mid-myocardial cells, and 3 to endocardial cells. In total, this left ventricular wedge model contained 42% epicardial cells, 28% mid-myocardial cells, and 30% endocardial cells of the total number of grid points.

It is important to note that for simulations, the FK4V model was used because of long running time in the serial method for each S1S2 interval i.e. around seven days with the FK4V model and more than 10 days with the TP06 model. In addition, simulation results in 2D and 3D tissue geometries showed that the FK4V model [2] was able to produce the AP shapes and restitution of epicardial, mid-myocardial, and endocardial cells based on experimental data from the human left ventricle [3-11].

Similar to the 3D cubes of tissue, the transmembrane voltage was stored every 1 ms in the whole tissue and was sampled every other point from the central region of the wedge (from row 275, column 86 and layers from 1 to 300) as shown in Figure 6-1. In total, 150 transmembrane voltages were created.

To simulate normal and premature beats, 6 normal S1 beats at a fixed cardiac cycle length of 800 ms close to the normal human sinus rhythm and a single premature S2 beat were delivered during decreasing S1S2 intervals. For epicardial pacing,

- stimuli were delivered to the small region of epicardium (with layers 3 and 4 as the layers 1 and 2 contained 0s, rows from 273 to 277, and columns from 77 to 80) to represent epicardial pacing with apex to base conduction (bottom to the top shown as a cyan arrow in Figure 6-1).
- stimuli were delivered to the epicardial region with the same rows and columns but with layers 292 and 293 (the layers from 294 to 300 contained 0s) to represent epicardial pacing with base to apex conduction (top to bottom shown as a green arrow in Figure 6-1).



This Chapter is organized in four sections to study, (1) restitution and spatial profiles of activation time, APD, and repolarization time; (2) three measures of dispersion in activation time, repolarization time, and APD; (3) the speed of depolarization conduction; and (4) AP propagation during depolarization and repolarization in the wedge model.

6.2 Spatiotemporal profiles of normal and premature beats

This part of the Chapter focuses on rate dependency of premature AP repolarization. Then, examples of profiles in 3D cube of tissue and in the left ventricular wedge model were plotted on the same graph at one S1S2 interval, to compare the effects of tissue geometry and fibre structure on spatial and restitution profiles. Next, spatial and restitution profiles in homogenous and heterogeneous tissues in the left ventricular wedge model are described and evaluated against experimental data.

6.2.1 Rate dependent effects

Similar to findings in 2D and 3D tissue models (described in Chapters 4 and 5), shape and duration of AP for premature S2 beats changed obviously for long and short S1S2 intervals with the FK4V and the TP06 models. However, these changes for normal S1 beats were negligible due to little rate dependent effects. To emphasize this finding, Figure 6-2 shows example of spatial APD profiles for normal S1 and premature S2 beats in the same graph for the left ventricular wedge model composed of 30%endo-28%M-42%epi cells with apex to base conduction and the reverse.

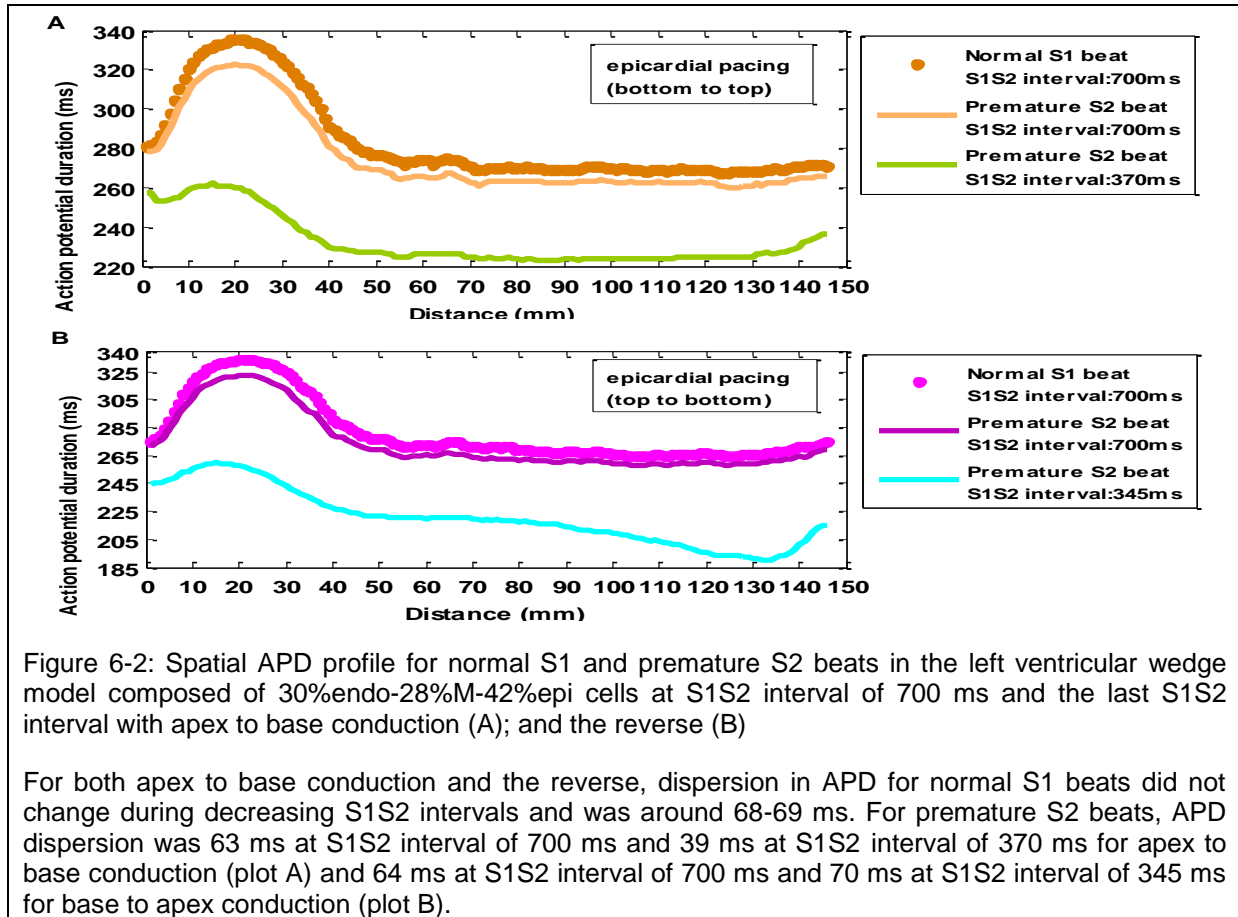


Figure 6-2: Spatial APD profile for normal S1 and premature S2 beats in the left ventricular wedge model composed of 30%endo-28%M-42%epi cells at S1S2 interval of 700 ms and the last S1S2 interval with apex to base conduction (A); and the reverse (B)

For both apex to base conduction and the reverse, dispersion in APD for normal S1 beats did not change during decreasing S1S2 intervals and was around 68-69 ms. For premature S2 beats, APD dispersion was 63 ms at S1S2 interval of 700 ms and 39 ms at S1S2 interval of 370 ms for apex to base conduction (plot A) and 64 ms at S1S2 interval of 700 ms and 70 ms at S1S2 interval of 345 ms for base to apex conduction (plot B).

6.2.2 Profiles of premature activation time, repolarization time, and APD

Initially, six plots of spatial and restitution profiles of activation time, repolarization time, and APD for premature S2 beats at S1S2 interval of 700 ms were provided for two groups of the left ventricular wedge model and 3D cubes of tissue. The comparison was based on examples of

1. heterogeneous tissues: the left ventricular wedge composed of 30%endo-28%M-42%epi cells with epicardial pacing with apex to base conduction and the reverse, and the 3D cube of tissue composed of 10%endo-30%M-60%epi cells with endocardial and epicardial pacing;
2. homogenous tissues: both left ventricular wedge model and 3D cubes of tissue were composed of 100% epicardial and 100% mid-myocardial cells.

The aim was to compare the effects of two different geometrical models of tissue and fibre with different size on the six spatial and restitution profiles for each tissue.

- Qualitative comparison

In comparison, the characteristics of spatial profiles (Figures 6-3) and restitution profiles (Figures 6-4) in the left ventricular wedge model composed of anisotropic homogenous and heterogeneous tissues were qualitatively similar to 3D cubes of tissue with a linear change in fibre orientation. Similar to 3D cubes of heterogeneous tissue, spatial and restitution profiles of repolarization time and APD as well as restitution profiles of activation time were characterized with a dome-morphology in the mid-myocardial region in the wedge model composed of three ventricular cell types.

- Quantitative comparison

Not surprisingly, the timings of AP depolarization and AP repolarization in the left ventricular wedge model with size of $3.5 \times 11.0 \times 6.0 \text{ cm}^3$ was greater than those in the 3D cubes of tissue with size of $0.8 \times 0.8 \times 1.2 \text{ cm}^3$. For example, activation time and repolarization time in the left ventricular wedge model composed of homogenous epicardial and mid-myocardial tissues were approximately 120 ms and 110 ms greater than those in 3D cubes of tissue composed of epicardial and mid-myocardial tissues respectively.

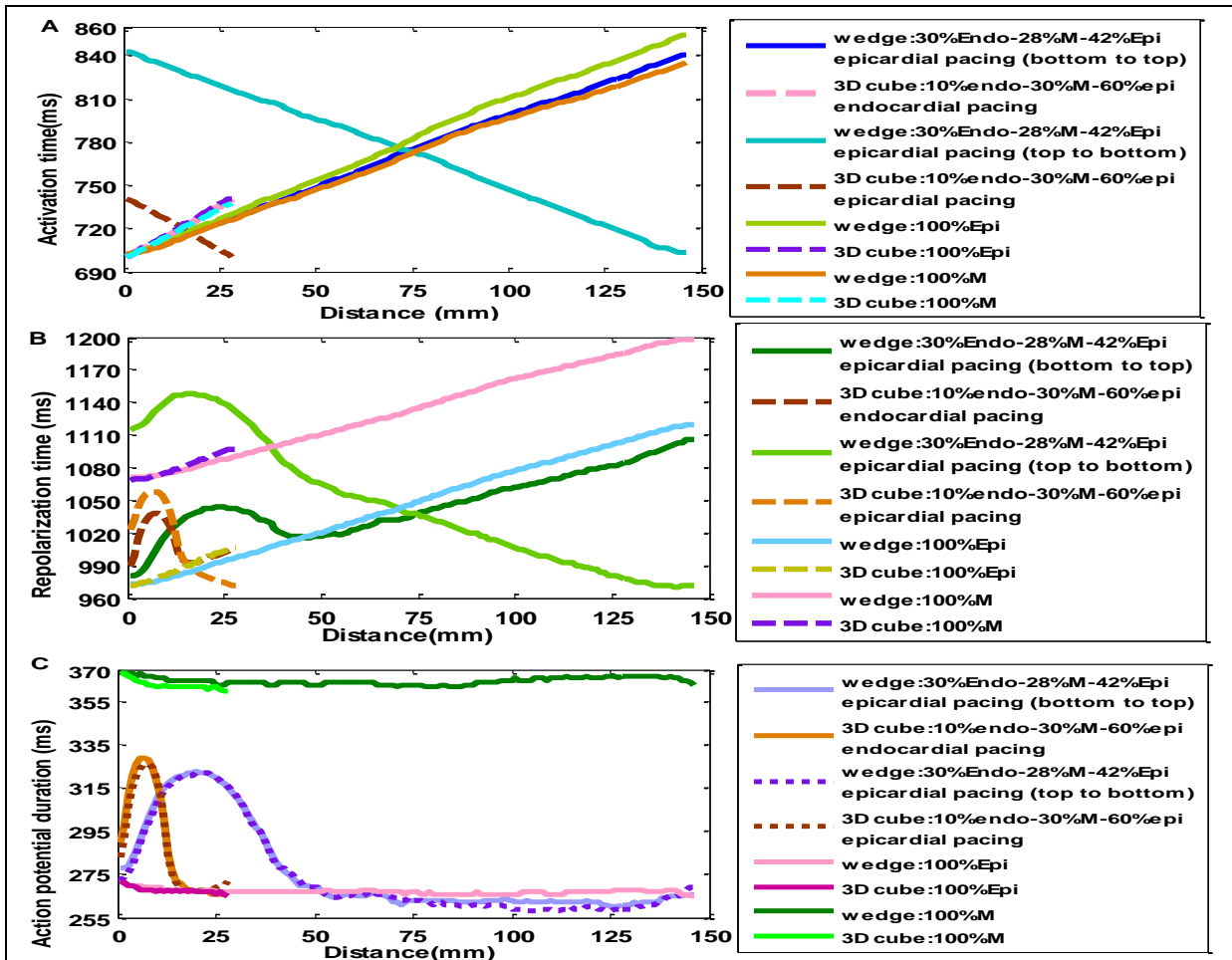


Figure 6-3: Spatial profiles of activation time (A); repolarization time (B); and APD (C) in the left ventricular wedge model and in the 3D cubes of anisotropic homogenous and heterogeneous tissue at S1S2 interval of 700 ms

Note: The number of the extracted transmembrane voltage was 150 for the wedge model and was 30 for 3D cubes of tissue. Homogenous tissues in the 3D cubes and in the wedge model were paced from the bottom edge of tissues.

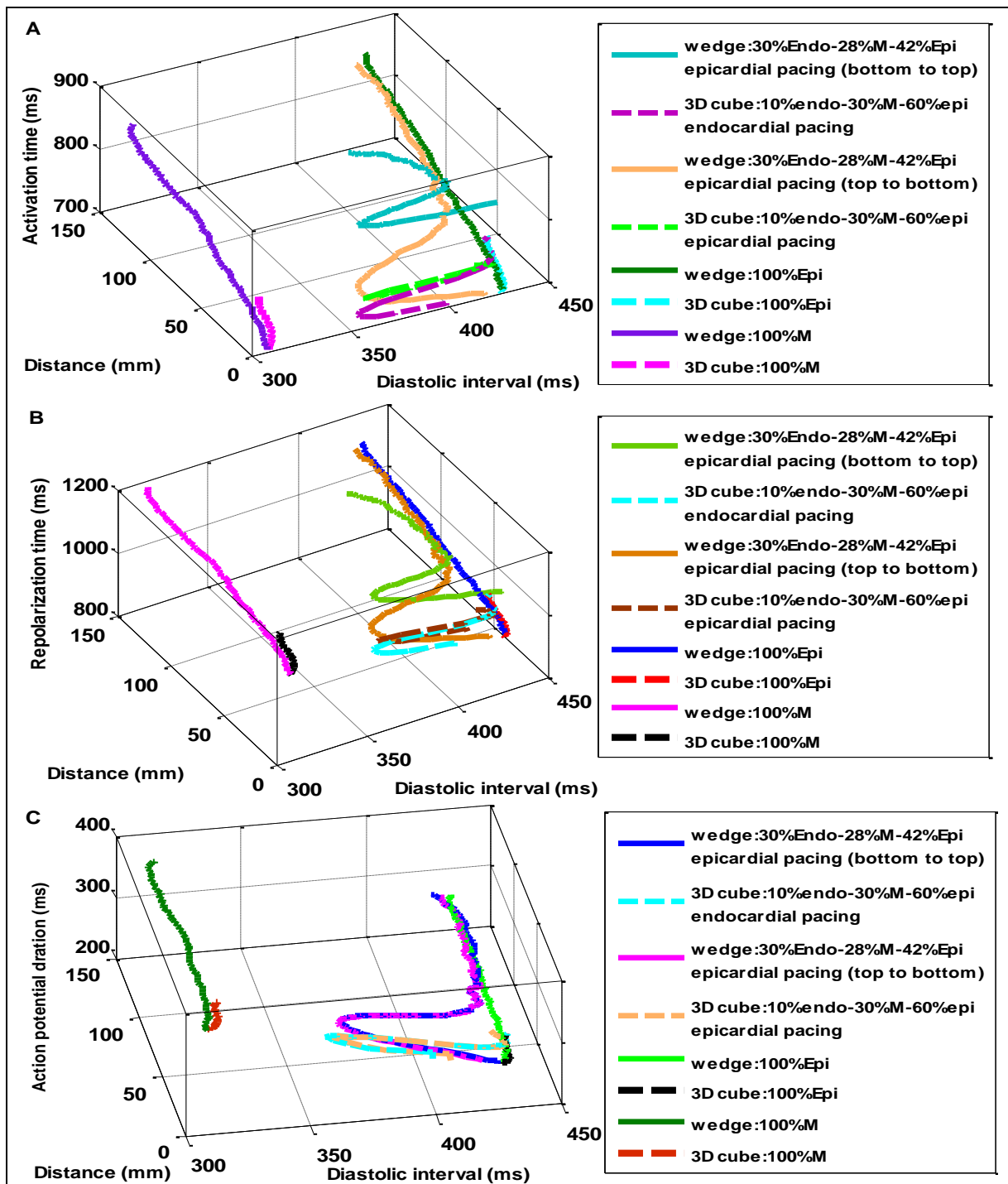


Figure 6-4: Restitution profiles of activation time (A); repolarization time (B); and APD (C) in the left ventricular wedge model and in the 3D cubes of anisotropic homogenous and heterogeneous tissue at S1S2 interval of 700 ms

Note: The number of the extracted transmembrane voltage was 150 for the wedge model and was 30 for 3D cubes of tissue. Homogenous tissues in the 3D cubes and the wedge model were paced from the bottom edge of tissues.

6.2.2-1 Left ventricular wedge composed of homogenous tissue

Spatial profiles of APD and repolarization time in three anisotropic homogenous left ventricular wedge models with apex to base conduction are shown in Figure 6-5 and Figure 6-6 based on source data at S1S2 interval of 700 ms. During decreasing S1S2 intervals,

APD increased except for short S1S2 intervals of 350 ms and 305 ms for endocardial tissue, and S1S2 intervals of 460 ms and 455 ms for mid-myocardial tissue.

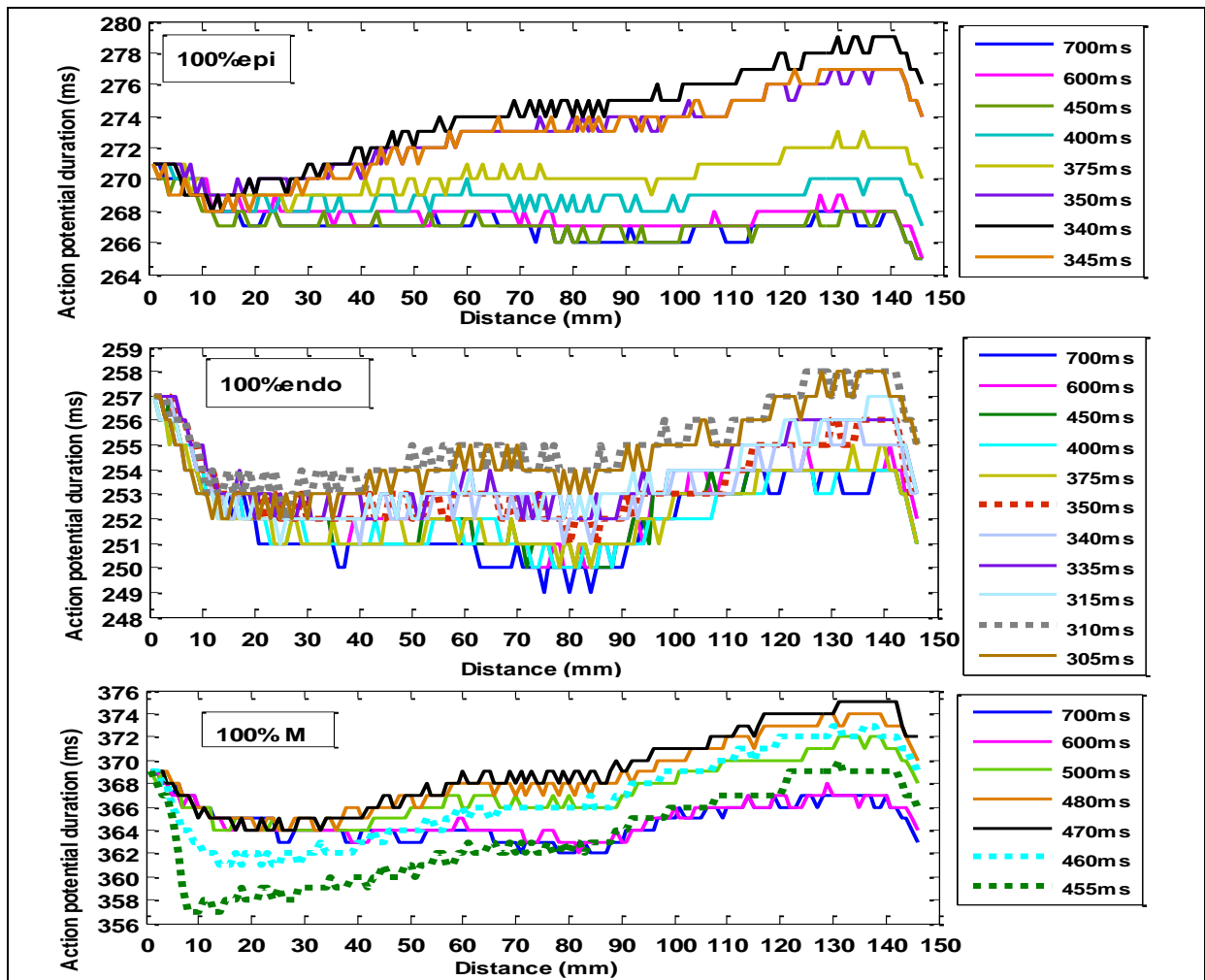


Figure 6-5: Spatial profiles of APD in three anisotropic homogenous left ventricular wedge models

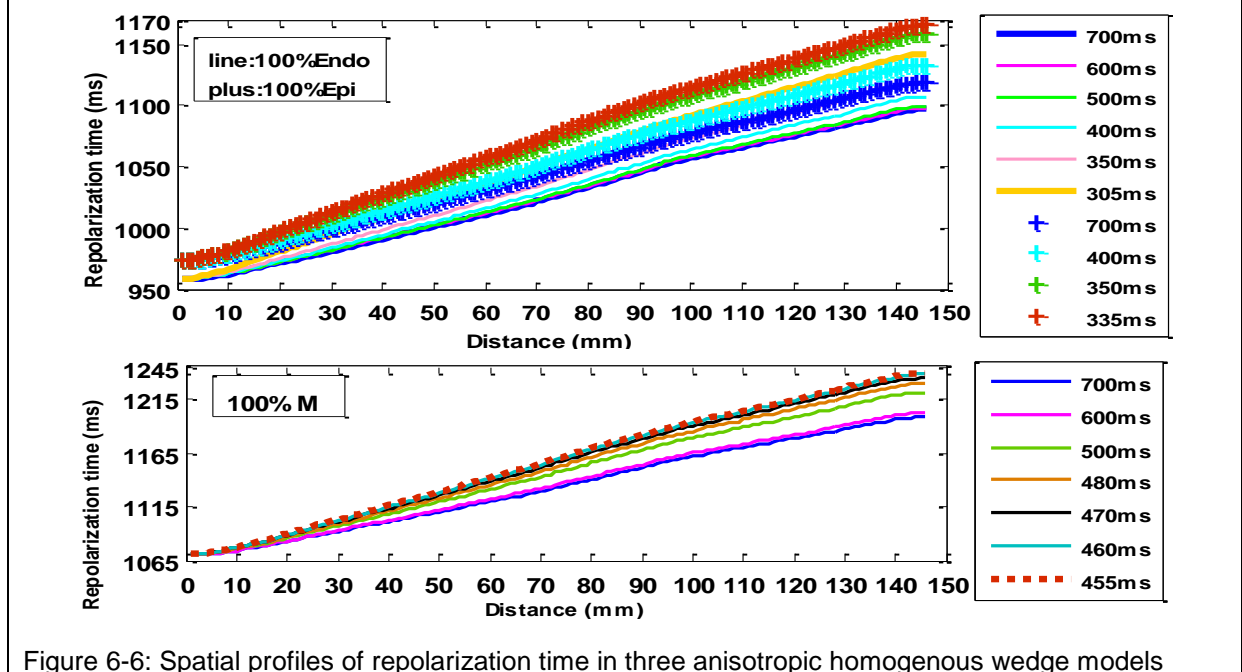
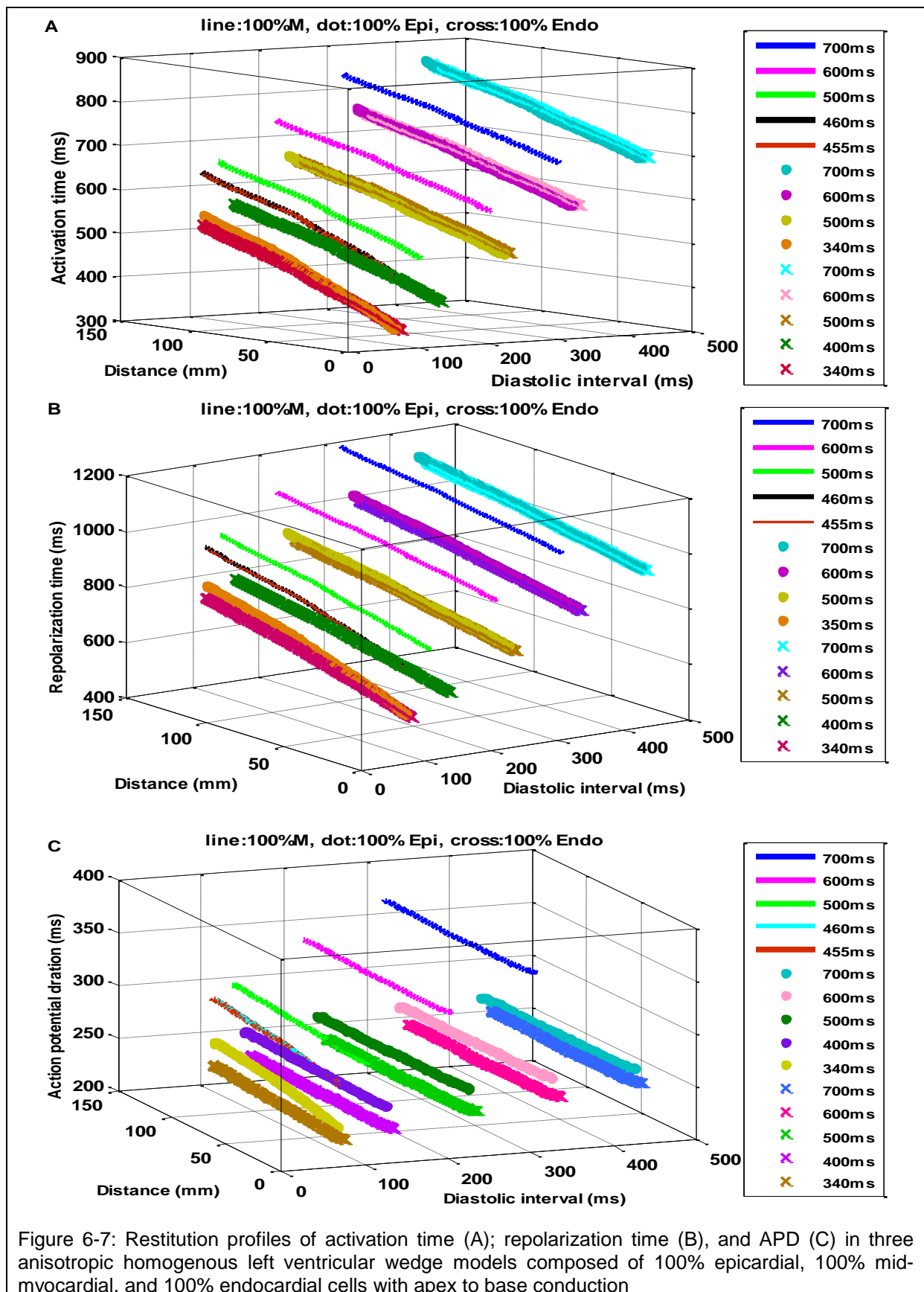


Figure 6-6: Spatial profiles of repolarization time in three anisotropic homogenous wedge models

Restitution profiles of three anisotropic homogenous left ventricular wedges were plotted in the same graph to highlight the similarities and differences during decreasing S1S2 intervals as shown in Figure 6-7. Activation time, repolarization time, and APD of mid-myocardial tissue were greater than other homogenous tissues.

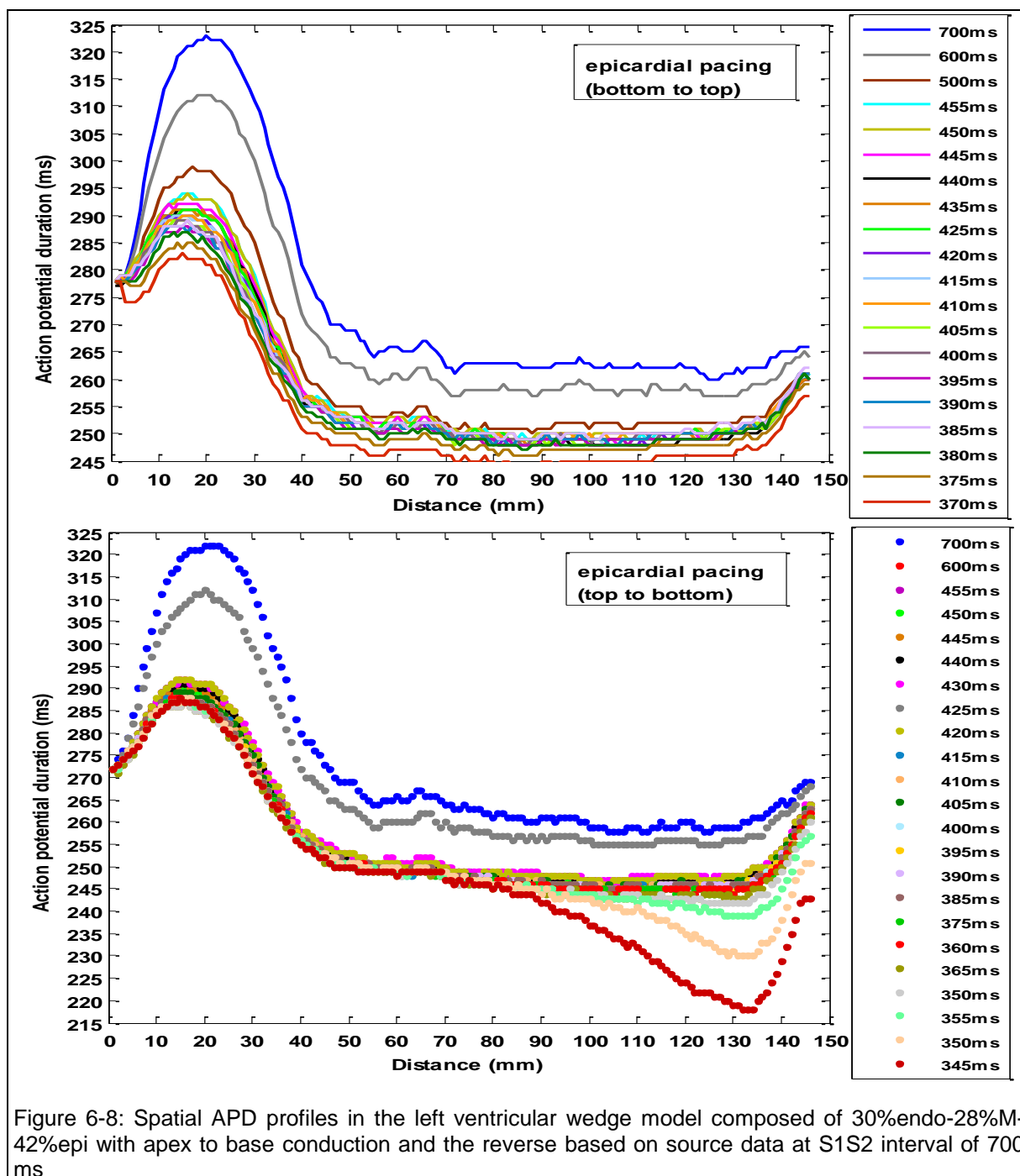


6.2.2-2 Left ventricular wedge composed of heterogeneous tissue

Figure 6-8 and Figure 6-9 show spatial profiles of APD and repolarization time for premature S2 beats during decreasing S1S2 intervals in the left ventricular wedge model composed of 30%endo-28%M-42%epi cells with anisotropic diffusion with apex to base conduction and the reverse.

It is important to note that all spatial profiles were plotted based on source data at S1S2 interval of 700 ms.

Similar to the 3D cubes of tissue composed of three ventricular cells, spatial and restitution profiles of premature S2 beats (1) change gradually with decreasing S1S2 intervals with great changes at the last S1S2 interval; and (2) were characterized with a dome morphology in the mid-myocardial region of the left ventricular wedge model.



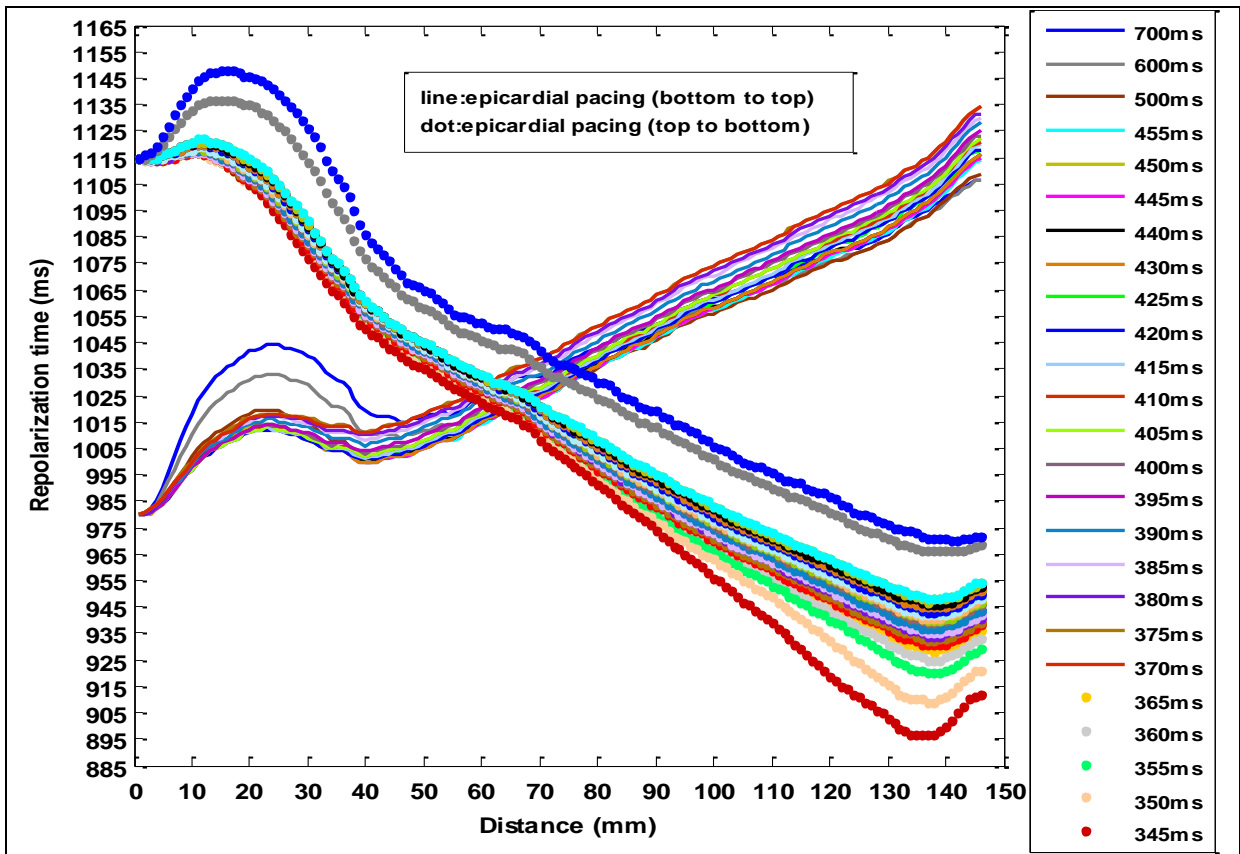


Figure 6-9: Comparison of spatial profiles of repolarization time in the left ventricular wedge model composed of 30%endo-28%M-42%epi cells with apex to base conduction and the reverse based on source data at S1S2 interval of 700 ms

Figure 6-10 supports the presence of the dome morphology in profile of APD against repolarization time in the wedge model composed of anisotropic heterogeneous tissue with apex to base conduction and the reverse during decreasing S1S2 intervals.

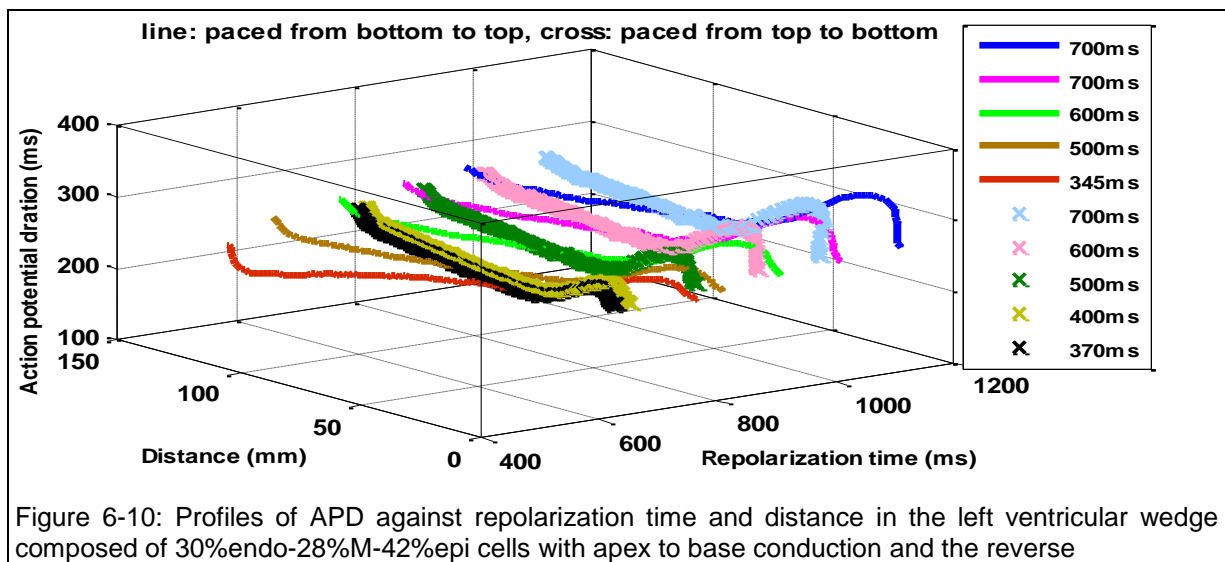


Figure 6-10: Profiles of APD against repolarization time and distance in the left ventricular wedge model composed of 30%endo-28%M-42%epi cells with apex to base conduction and the reverse

Figure 6-11 emphasizes the finding that restitution profiles of repolarization time and APD as well as restitution profiles of activation time for premature S2 beats were qualitatively similar during decreasing S1S2 intervals even for the left ventricular wedge model composed of anisotropic heterogeneous tissues with apex to base conduction and the reverse.

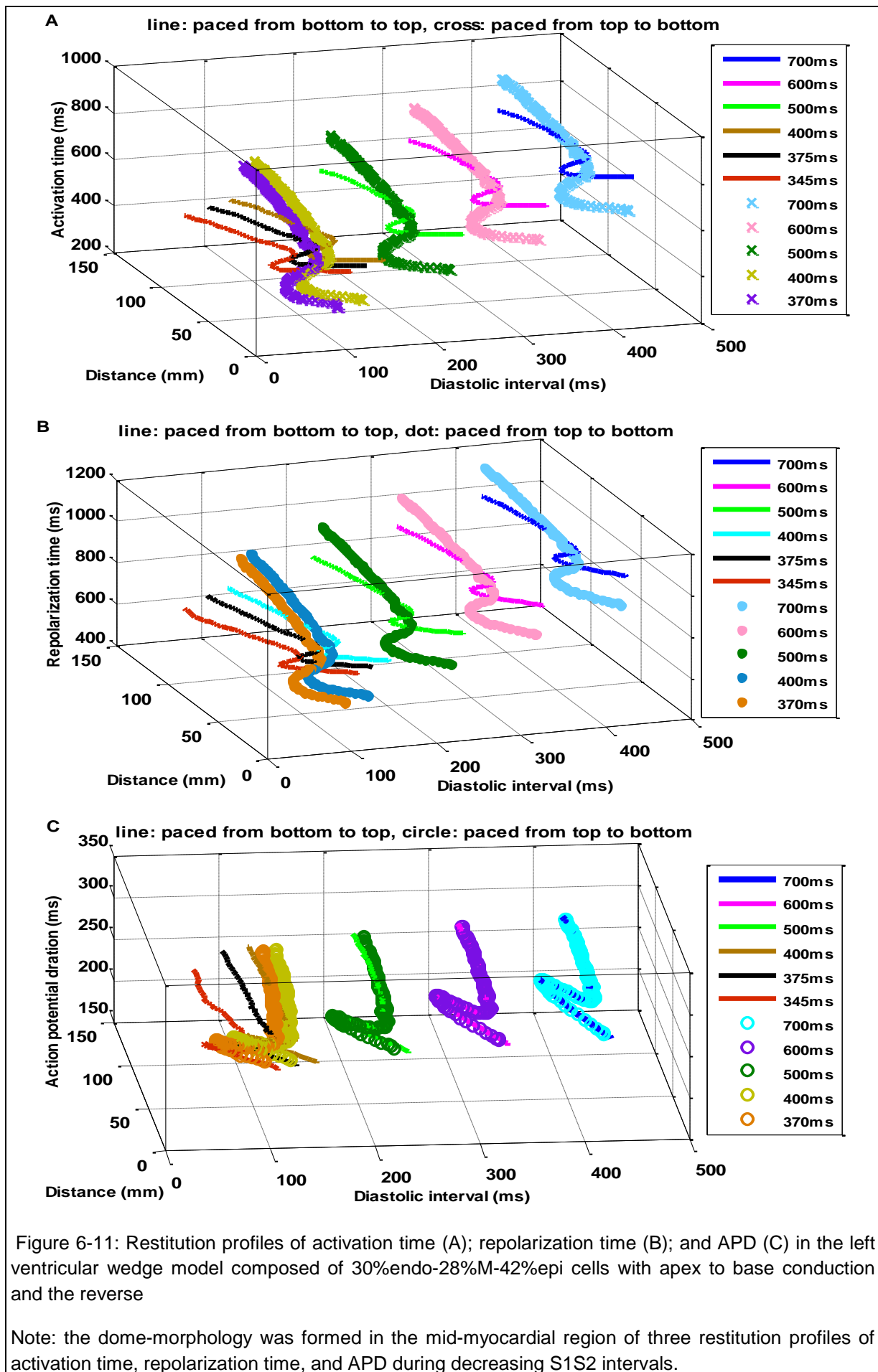


Figure 6-11: Restitution profiles of activation time (A); repolarization time (B); and APD (C) in the left ventricular wedge model composed of 30%endo-28%M-42%epi cells with apex to base conduction and the reverse

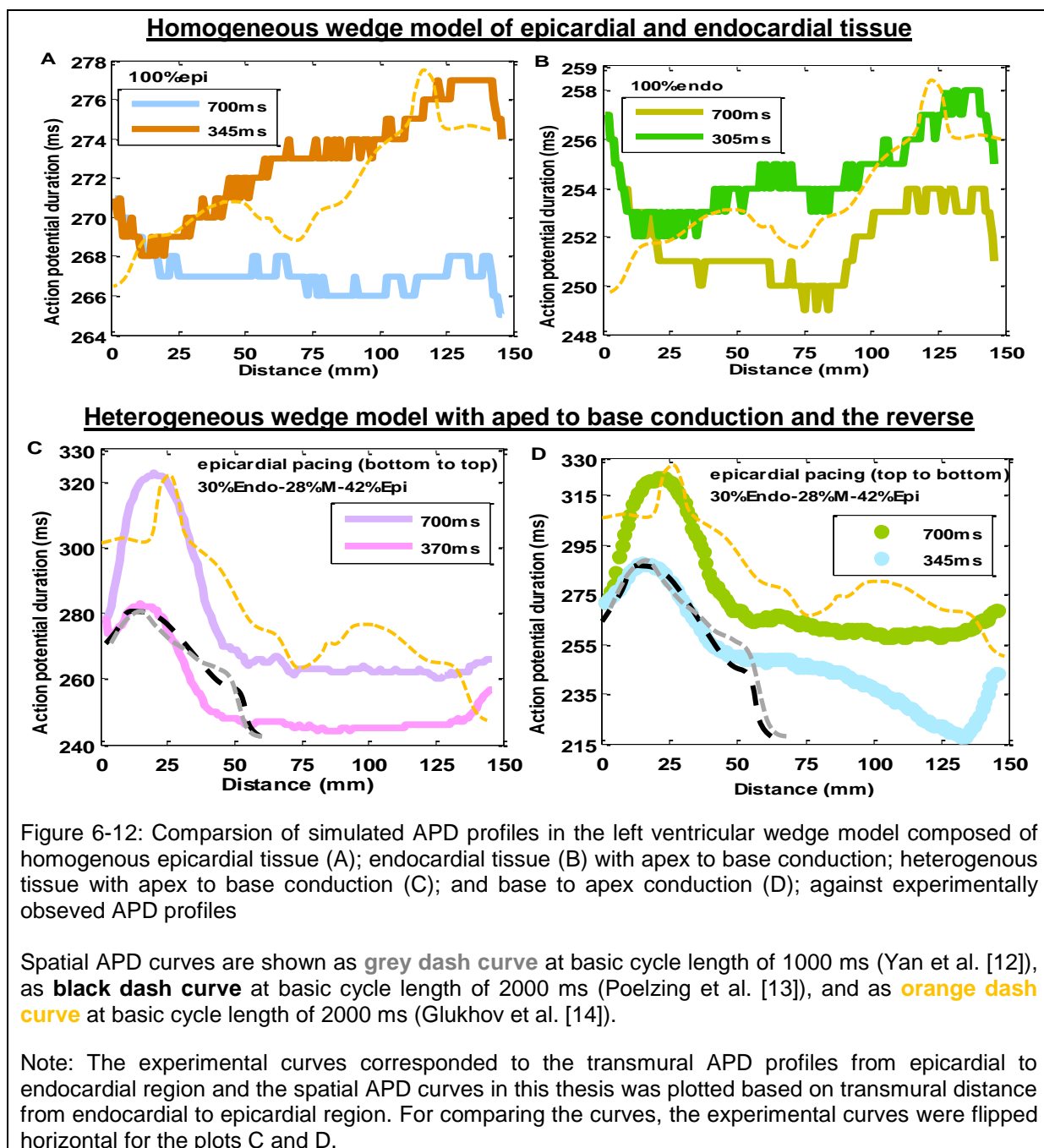
Note: the dome-morphology was formed in the mid-myocardial region of three restitution profiles of activation time, repolarization time, and APD during decreasing S1S2 intervals.

6.2.3 Qualitative comparison with experimental studies

This part of the Chapter compares the simulated APD profiles in the left ventricular wedge model composed of homogenous and heterogeneous tissues with experimentally observed APD profiles by Yan et al. [12], Poelzing et al. [13], and Glukhov et al. [14].

It is important to note these experimental curves were obtained based on different conditions i.e. different cardiac cycle lengths, tissue size and wedge preparation, fibre structure, or from the canine heart (examples of differences between the canine and human heart are described in Chapter 2, section 2.10).

Despite the current limitations, there was still broad agreement on the transition between regions of different cell type in spatial APD profiles in this thesis and experimental studies as shown in Figure 6-12.



After describing the spatial and restitution profiles for premature S2 beats in the left ventricular wedge model composed of anisotropic homogenous and heterogeneous tissues, three measures of dispersion for both normal and premature S2 beats are compared in the following section.

6.3 Three measures of dispersion

For both normal S1 and premature S2 beats at each S1S2 intervals, dispersion in activation time was the difference between the maximum and the minimum activation time; dispersion in repolarization time was the difference between the maximum and the minimum repolarization time; and dispersion in APD was the difference between the maximum and the minimum APD.

Similar to the 2D and 3D simulations for normal S1 beats, dispersion in activation time, repolarization time, and APD (with precision of 1 ms) did not change during decreasing S1S2 interval in the left ventricular wedge composed of homogenous and heterogeneous tissues, Table 6-1. For premature S2 beats compared to normal beats, dispersion in activation time increased to around 35-41 ms and dispersion in repolarization time increased approximately to 28-47 ms during decreasing S1S2 intervals in the left ventricular wedge.

Three measures of dispersion for normal S1 and premature S2 beats in ms during decreasing S1S2 intervals (S1S2) in ms			
	Activation time (ms)	Repolarization time (ms)	APD (ms)
100%Epi apex to base conduction S1S2 intervals of 700-335 ms Normal S1 beats	152	147	5
Premature S2 beats S1S2 intervals of 700-335 ms	152-192	146-193	6-4 (S1S2 700-400) 5-11 (S1S2 395-335)
100%Endo apex to base conduction S1S2 intervals of 700-305 ms Normal S1 beats	144	138	8
Premature S2 beats S1S2 intervals of 700-305 ms	144-185	138-183	8-5 (S1S2 700-335) 6 (S1S2 330-305)
100%M apex to base conduction S1S2 intervals of 700-455 ms Normal S1 beats	132	126	7
Premature S2 beats S1S2 intervals of 700-455 ms	133-171	127-168	7-13
30%endo-28%M-42%epi apex to base conduction S1S2 intervals of 700-370 ms Normal S1 beats	138	128	68
Premature S2 beats S1S2 intervals of 700-370 ms	138-175	126-154	63-39
30%endo-28%M-42%epi base to apex conduction S1S2 intervals of 700-345 ms Normal S1 beats	140	184	69
Premature S2 beats S1S2 intervals of 700-345 ms	140-175	178-170 (S1S2 700-500) 174-220 (S1S2 455-345)	43-70

Table 6-1: Three measures of dispersion in activation time, repolarization time, and APD for normal S1 and premature S2 beats in the left ventricular wedge model

6.3.1 Profiles of three measures of dispersion

Figure 6-13 and Figure 6-14 show profiles of three measures of dispersion against S1S2 interval for premature S2 beats in the left ventricular wedge model composed of anisotropic homogenous and heterogeneous tissue.

- The left ventricular wedge model composed of anisotropic homogenous tissue

Similar to the 3D cubes of homogenous tissue, for premature beats (1) measures of dispersion in activation time were slightly greater than dispersion in repolarization time during decreasing S1S2 intervals; and (2) measures of dispersion in activation time and repolarization gradually increased with decreasing S1S2 intervals.

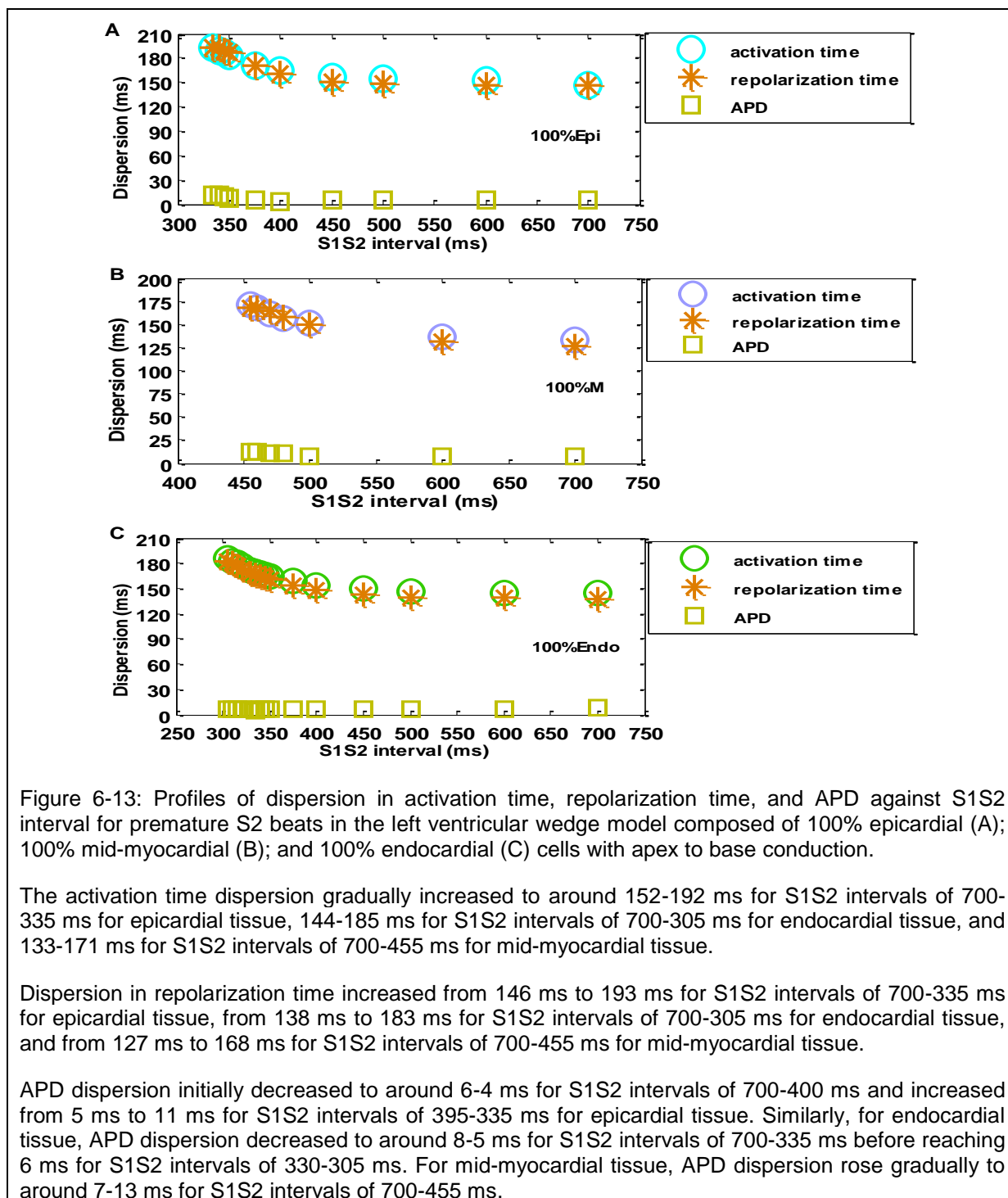


Figure 6-13: Profiles of dispersion in activation time, repolarization time, and APD against S1S2 interval for premature S2 beats in the left ventricular wedge model composed of 100% epicardial (A); 100% mid-myocardial (B); and 100% endocardial (C) cells with apex to base conduction.

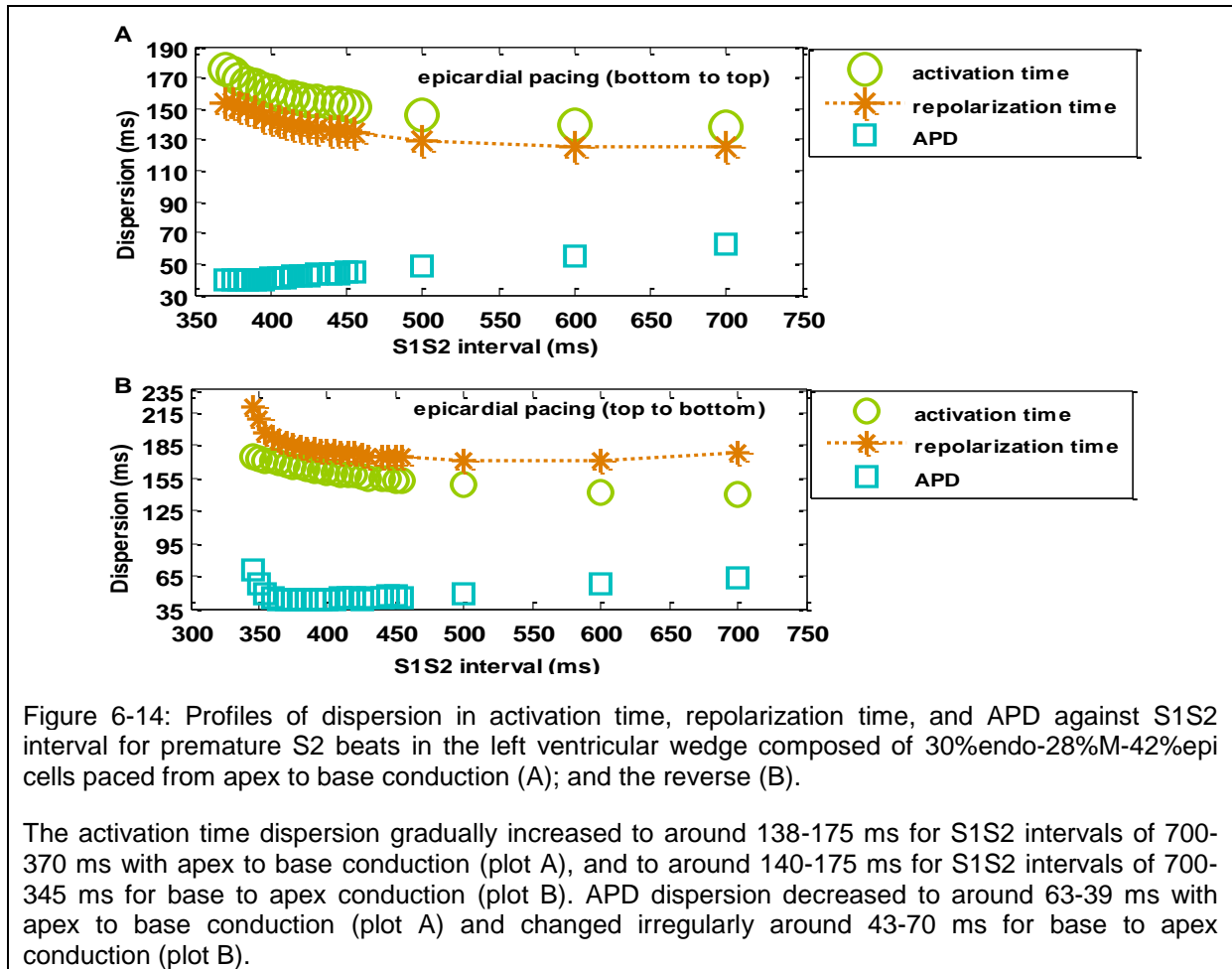
The activation time dispersion gradually increased to around 152-192 ms for S1S2 intervals of 700-335 ms for epicardial tissue, 144-185 ms for S1S2 intervals of 700-305 ms for endocardial tissue, and 133-171 ms for S1S2 intervals of 700-455 ms for mid-myocardial tissue.

Dispersion in repolarization time increased from 146 ms to 193 ms for S1S2 intervals of 700-335 ms for epicardial tissue, from 138 ms to 183 ms for S1S2 intervals of 700-305 ms for endocardial tissue, and from 127 ms to 168 ms for S1S2 intervals of 700-455 ms for mid-myocardial tissue.

APD dispersion initially decreased to around 6-4 ms for S1S2 intervals of 700-400 ms and increased from 5 ms to 11 ms for S1S2 intervals of 395-335 ms for epicardial tissue. Similarly, for endocardial tissue, APD dispersion decreased to around 8-5 ms for S1S2 intervals of 700-335 ms before reaching 6 ms for S1S2 intervals of 330-305 ms. For mid-myocardial tissue, APD dispersion rose gradually to around 7-13 ms for S1S2 intervals of 700-455 ms.

- The left ventricular wedge model composed of anisotropic heterogeneous tissue

With base to apex conduction, dispersion of activation time was greater than dispersion in repolarization time while with apex to base conduction the reverse was true during decreasing S1S2 intervals as shown in Figure 6-14.



With apex to base conduction, dispersion in repolarization time gradually increased from the smallest value of 126 ms to the largest value of 154 ms for S1S2 intervals of 700-370 ms.

With base to apex conduction, dispersion in repolarization time initially decreased to slightly around 178-170 ms for S1S2 intervals of 700-500 ms. However, dispersion in repolarization time increased around 174-220 ms for S1S2 intervals of 455-345 ms when the largest repolarization time in mid-myocardial region became close to repolarization time in the endocardial region. The same was true for 3D cubes of heterogeneous tissue when repolarization time of the mid-myocardial region became closer to the repolarization time of the endocardial or epicardial region (described in Chapter 5, section 5.5.1).

For clarity, Figure 6-15 shows examples of spatial profiles of repolarization time in the 3D cube of anisotropic tissue composed of 10%endo-30%M-60%epi with endocardial pacing and in the left ventricular wedge model composed of 30%endo-28%M-42%epi with base to apex conduction with anisotropic diffusion.

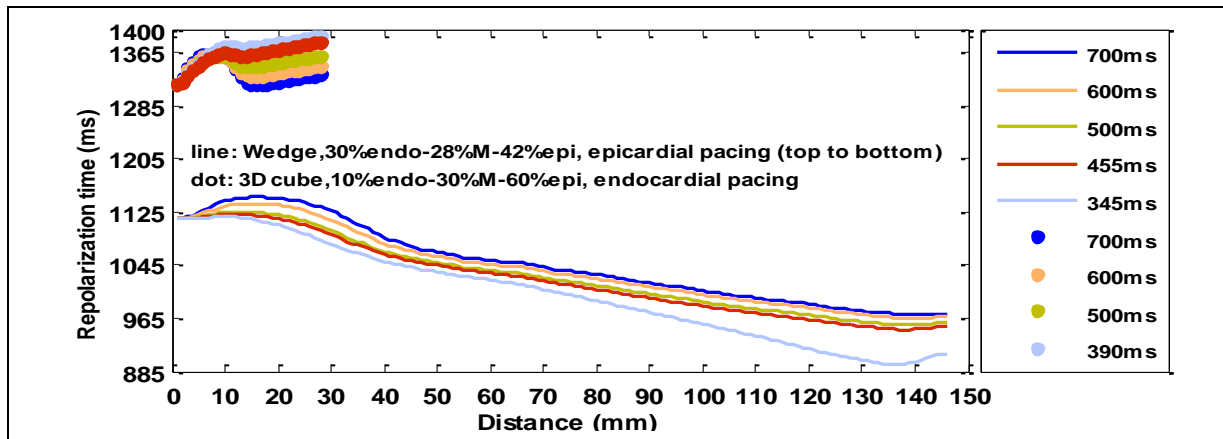


Figure 6-15: Comparison of spatial profiles of repolarization time in the 3D cube of tissue and the left ventricular wedge model with anisotropic diffusion

For the 3D cube of anisotropic tissue composed of 10%endo-30%M-60%epi with endocardial pacing, dispersion in repolarization time increased when repolarization time in the epicardial region became close or greater than the largest repolarization time in the mid-myocardial region. For the wedge model with top to bottom conduction, dispersion rose when the largest repolarization time in the mid-myocardial region became close to repolarization time in the endocardial region.

Note: The curves for the 3D cube of tissue and the wedge model were based on source data at S1S2 intervals of 1000 ms and 700 ms respectively.

6.3.2 Vulnerable regions for wave break

Similar to 3D cubes of heterogeneous tissue, the vulnerable region for wave break in heterogeneous left ventricular wedge model composed of 30%endo-28%M-42%epi may be in the transition region from endocardial to mid-myocardial region or from mid-myocardial to epicardial region as shown in Figure 6-16.

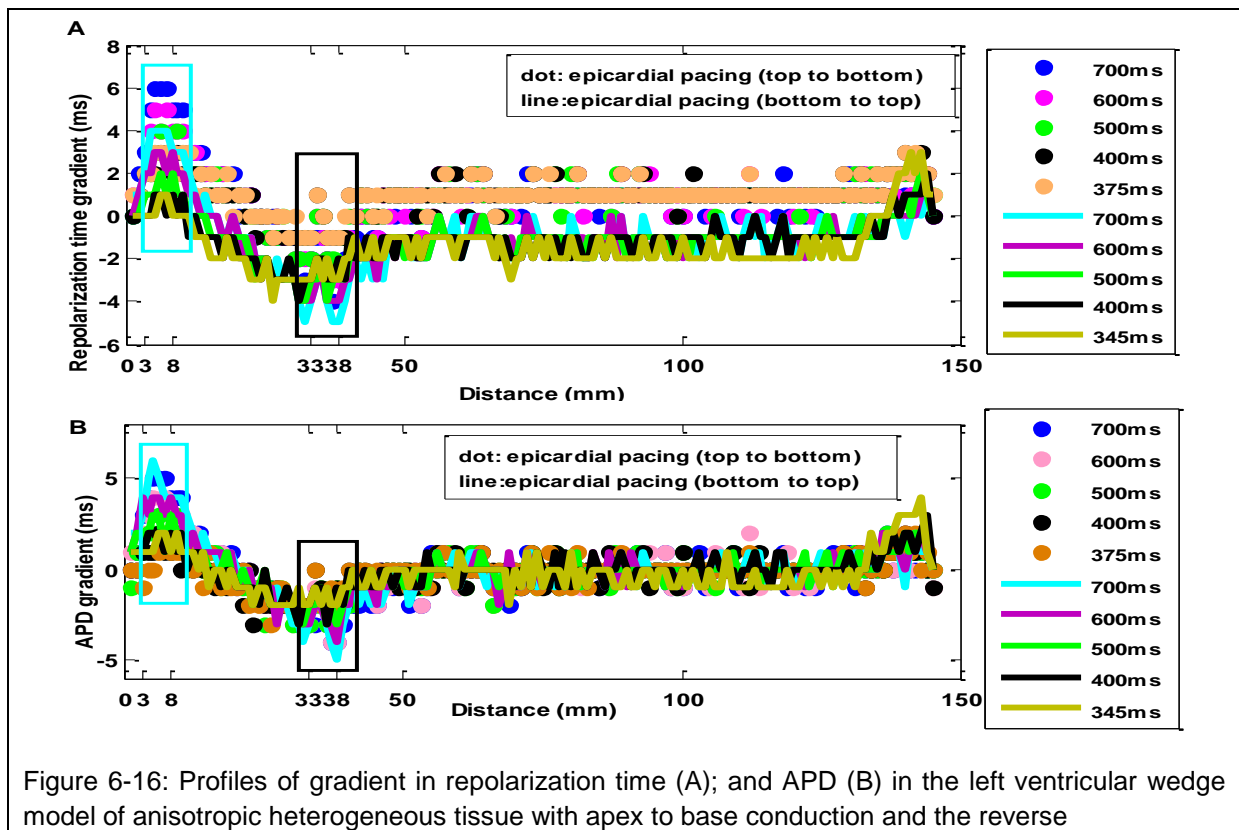


Figure 6-16: Profiles of gradient in repolarization time (A); and APD (B) in the left ventricular wedge model of anisotropic heterogeneous tissue with apex to base conduction and the reverse

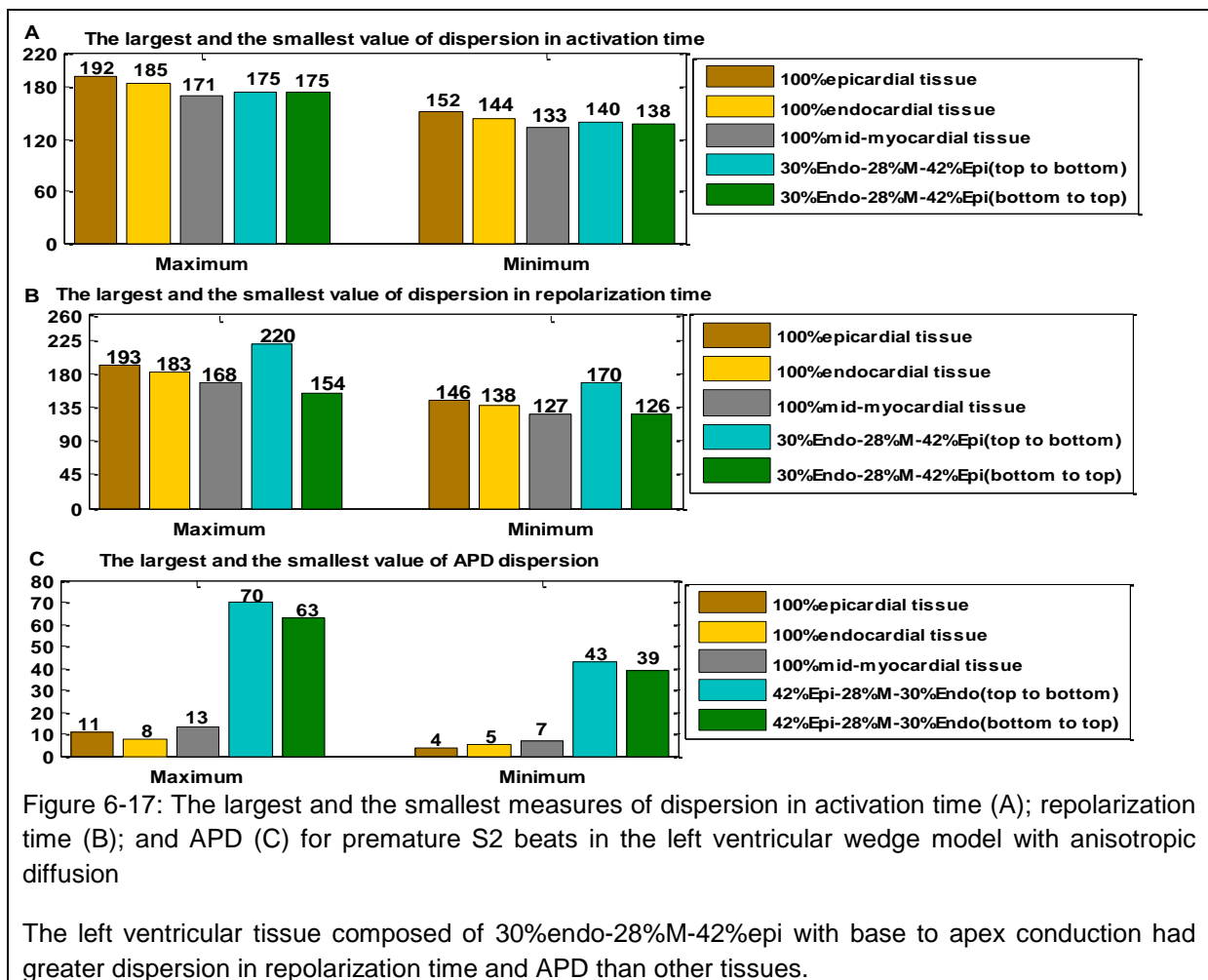
6.3.3 The smallest and the largest measures of dispersion and link to previous studies

Figure 6-17 shows the largest and the smallest dispersion in activation time, repolarization time, and APD for premature S2 beats in anisotropic homogenous and heterogeneous tissues. For premature S2 beats, the smallest dispersion in repolarization time was the smallest value of measures of dispersion in repolarization time among all S1S2 intervals; and the largest dispersion in repolarization time was the largest value of measures of dispersion in repolarization time among all S1S2 intervals.

The same was true for the largest and the smallest dispersion in activation time and APD. These values were significantly greater than those in 2D and 3D geometries due to size of wedge model. The main findings are summarized here.

Among three homogenous tissues and two heterogeneous tissues in the left ventricular wedge model,

- heterogeneous tissue composed of 30%endo-28%M-42%epi with base to apex conduction showed greater dispersion in repolarization time (170-220 ms in plot B) and APD (43-70 ms in plot C);
- homogenous mid-myocardial tissue had the smallest dispersion in activation time (133-171 ms in plot A);
- homogenous epicardial tissue had the largest dispersion in activation time (152-192 ms in plot A).



6.4 Speed of depolarization conduction

The previous two Chapters described how speed of depolarization conduction for premature S2 beats became slow during decreasing S1S2 intervals in 2D geometries and 3D cubes of tissue due to restitution of speed of depolarization conduction (conduction velocity restitution). This part of the Chapter describes how the speed of depolarization conduction changes in the left ventricular wedge model composed of homogenous and heterogeneous tissues.

As explained before, to avoid creation of a huge number of output files in the left ventricular wedge with 175 columns, 550 rows, and 300 layers, transmembrane voltage was created for every other point in tissue (275x87x150 voltages). Then, 150 transmembrane voltages were extracted from the middle region of the wedge (from row 137, column 43, and layers 1 to 150). In this region, one pair of points (1, 146) was selected with distance of 58 mm that was the product of space step 0.2 mm and the number of grid points, 290.

Figure 6-18 shows the profiles of speed of depolarization conduction against the average diastolic interval in the left ventricular wedge model composed of homogenous tissues including 100% epicardial, 100% endocardial, 100% mid-myocardial with apex to base conduction, and two heterogeneous tissue composed of 30%endo-28%M-42%epi cells with apex to base conduction and the reverse. For comparison, spatial profiles of activation time for three homogenous tissues are shown as well. There was the reverse relationship between speed of depolarization conduction at two selected points in tissue and the activation time at the same points (based on the formula that was used for calculation of speed of depolarization conduction). For example, during S1S2 intervals of 700-455 ms, the left ventricular wedge composed of 100% mid-myocardial cells had the smallest activation time (Figure 6-18, plot C) and so that the fastest speed of depolarization conduction among three homogenous tissues and two heterogenous tissues. In addition, the left ventricular wedge model composed of 100% epicardial cells with the largest activation time (Figure 6-18, plot B) had the slowest speed of depolarization conduction among all simulated tissues during S1S2 intervals of 700-335 ms.

For the left ventricular wedge composed of heterogeneous tissue, similar to the 3D simulated tissues with endocardial and epicardial pacing, the speed of depolarization conduction with apex to base conduction and base to apex conduction was positive and negative respectively as shown in Figure 6-19, plot A. The reason was that the activation time of cells away from the stimulus sites was greater than activation time of cells close to the stimulus sites. In total,

- restitution profiles of speed of depolarization conduction (plot A) and spatial profiles of activation time (plot B) with apex to base conduction and the reverse were approximately symmetric with respect to the diastolic interval axis;
- the speed of depolarization conduction in the left ventricular wedge changed approximately from 0.26 m/s to 0.2 m/s with apex to base conduction and the reverse. These values were similar to the speed of depolarization conduction in 3D cubes of anisotropic tissue composed of three ventricular cells with endocardial and epicardial pacing.

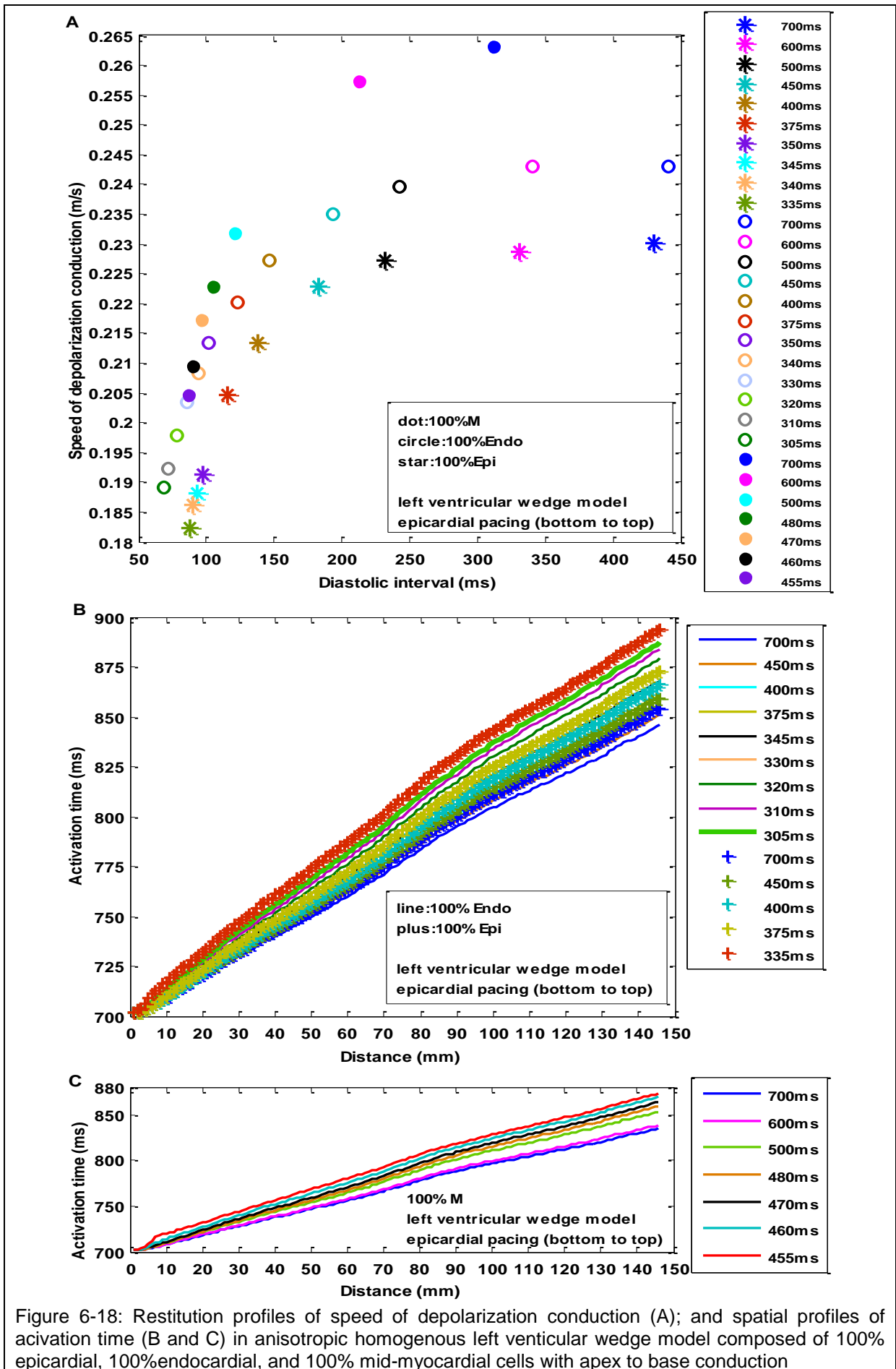


Figure 6-18: Restitution profiles of speed of depolarization conduction (A); and spatial profiles of activation time (B and C) in anisotropic homogenous left ventricular wedge model composed of 100% epicardial, 100%endocardial, and 100% mid-myocardial cells with apex to base conduction

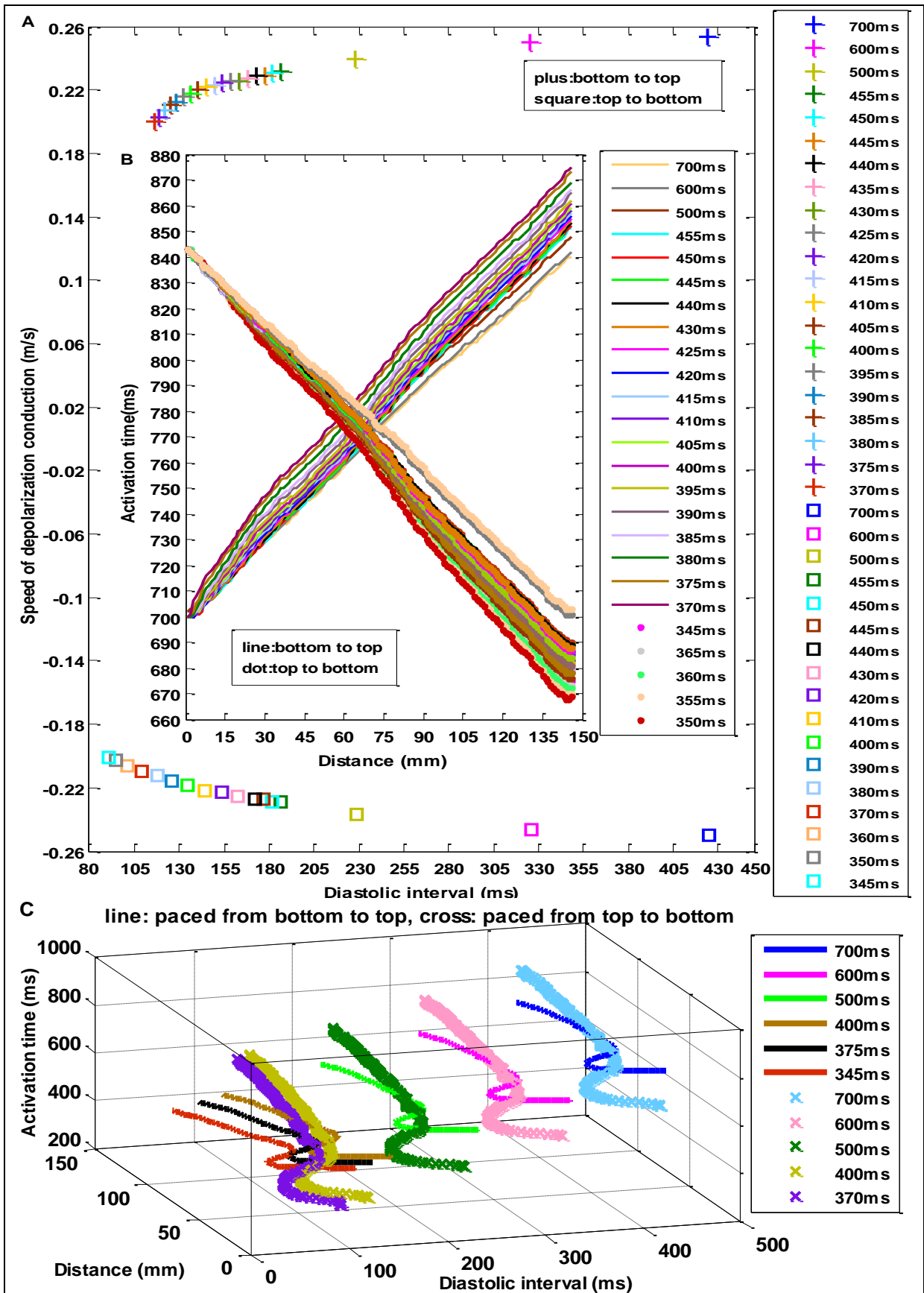


Figure 6-19: Spatial profiles of activation time (A); speed of depolarization conduction (B); and restitution profiles of activation time (C) in anisotropic heterogeneous left ventricular wedge model composed of 30%endo-28%M-42%epi cells with apex to base conduction and the reverse

Note: Restitution profiles of activation time in plot C (not spatial profiles in plot B) highlights the presence of mid-myocardial cells.

The following section compares AP propagation in 3D cubes of tissue and in the left ventricular wedge model at the last S1S2 intervals.

6.5 Visualization of AP propagation

For both apex to base and the reverse conduction, AP propagation was visualized for both normal S1 and premature S2 beats at the last S1S2 interval. The created images were organized as frames in the enclosed CD, Appendix 5. These frames were organized based on timing of AP depolarization, AP plateau, AP repolarization, and AP rest for normal and premature beats.

Figure 6-20 to Figure 6-23 provide examples of AP propagation during AP depolarization and AP repolarization for both normal S1 and premature S2 beats at the last S1S2 interval with the FK4V model. The main findings are summarized below.

- Normal S1 beats

No wave break was formed during AP depolarization and AP repolarization in the left ventricular wedge composed of anisotropic homogenous epicardial, mid-myocardial, and endocardial tissues with apex to base conduction and anisotropic heterogeneous tissue composed of 30%endo-28%M-42%epi with apex to base conduction and the reverse.

In comparison, for 3D cubes of anisotropic heterogeneous tissue composed of three ventricular cell types, there was wave break during AP repolarization with both endocardial and epicardial pacing for normal beats.

- Premature S2 beats

No wave break was created during AP depolarization and AP repolarization in the left ventricular wedge composed of anisotropic homogenous tissues.

For the left ventricular wedge composed of 30%endo-28%M-42%epi, there was electrical disturbance in the waves during AP propagation with apex to base conduction and wave break during AP depolarization and AP repolarization with base to apex conduction.

However, for 3D cubes of tissue, wave break occurred during AP depolarization for homogenous tissue and during AP depolarization and repolarization for heterogeneous tissue with endocardial and epicardial pacing.

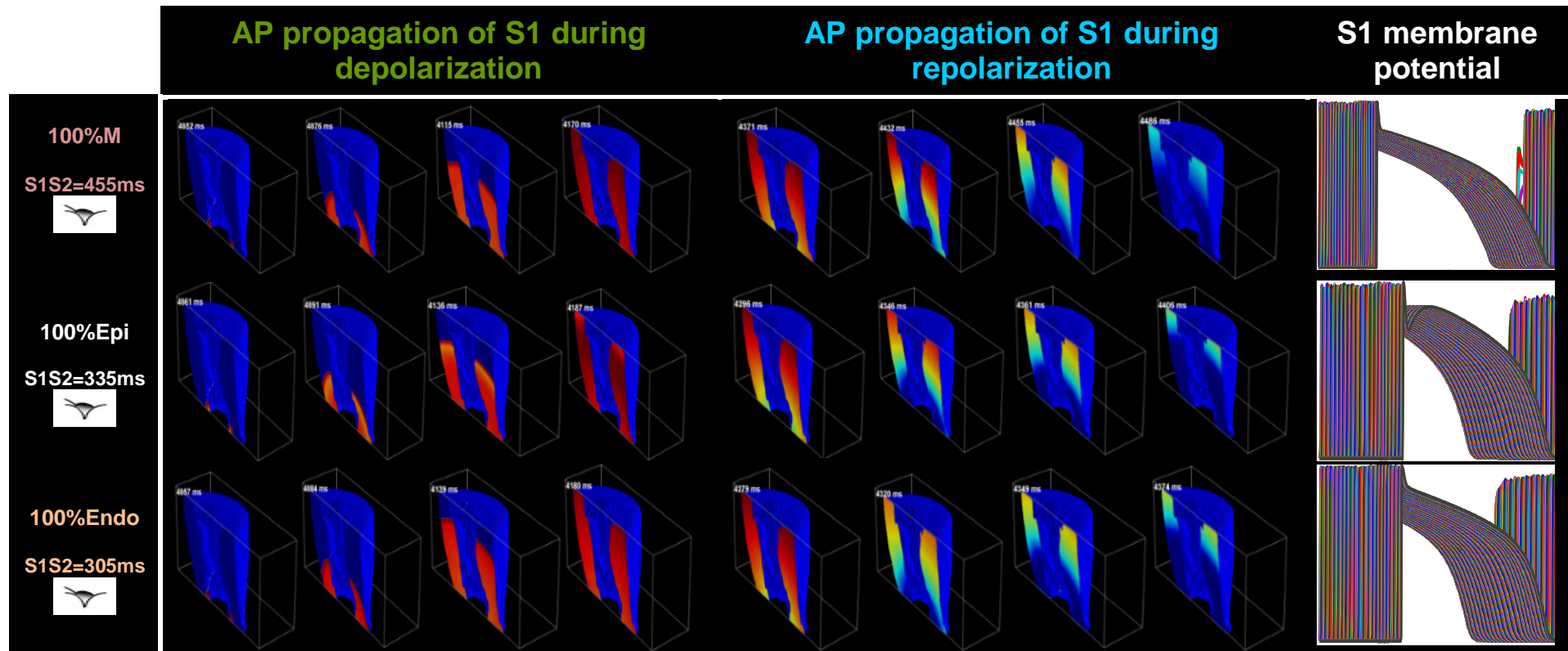


Figure 6-20: Examples of AP propagation from depolarization to rest for normal S1 beats in the left ventricular wedge composed of 100% mid-myocardial, 100% epicardial and 100% endocardial cells with epicardial pacing with apex to base conduction with anisotropic diffusion

During both AP depolarization and AP repolarization, AP propagation initiated from two corners of tissue in the bottom surface of tissue and propagated upward with no wave break.

AP propagation of S2 during depolarization

AP propagation of S2 during repolarization

S2 membrane potential

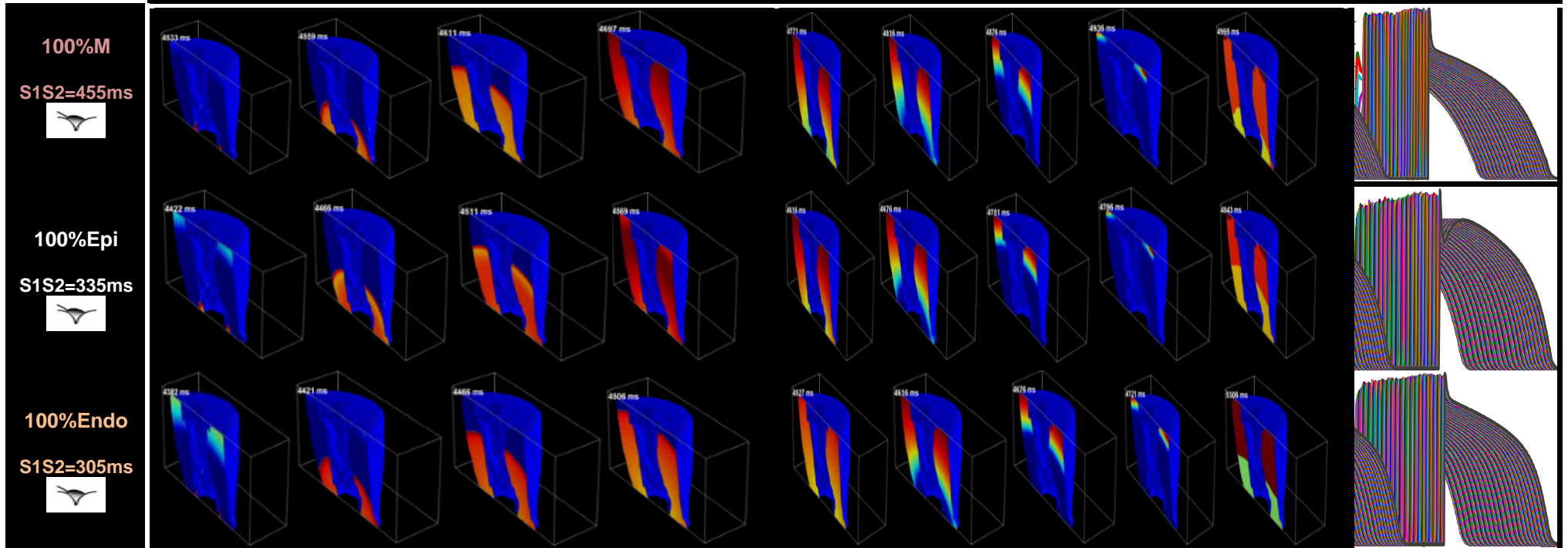


Figure 6-21: Examples of AP propagation from depolarization to rest for premature S2 beats in the left ventricular wedge composed of 100% mid-myocardial, 100% epicardial and 100% endocardial cells with epicardial pacing with apex to base conduction with anisotropic diffusion

No wave break was observed during AP depolarization and AP repolarization.

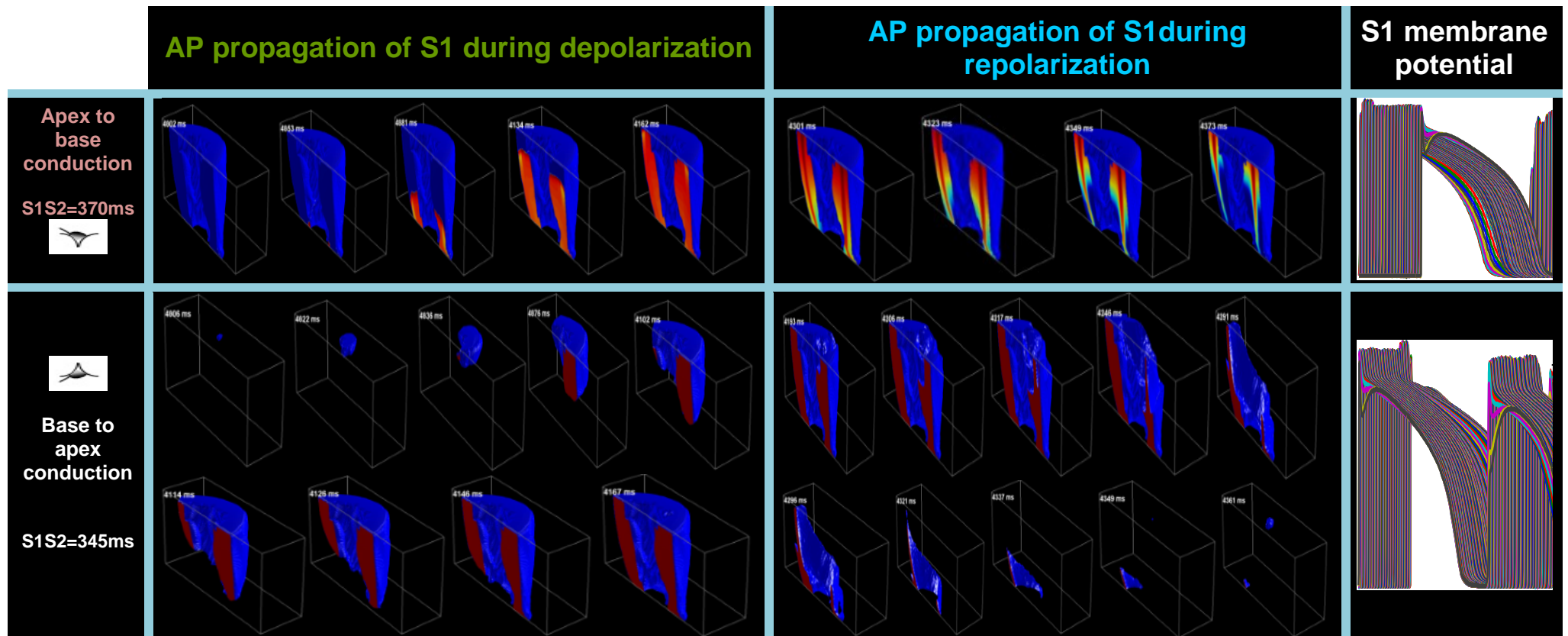


Figure 6-22: Examples of AP propagation from depolarization to rest for **normal S1 beats** in the left ventricular wedge composed of 30%endo-28%M-42%epi with epicardial pacing with apex to base conduction and the reverse with anisotropic conduction

With apex to base conduction, depolarization wave initiated from two corners of tissue in the bottom of the wedge and propagated upward. AP propagation during repolarization changed in the mid-myocardial region of the wedge highlighted as the red column.

With base to apex conduction, electrical disturbance was observed in AP propagation during depolarization and repolarization.

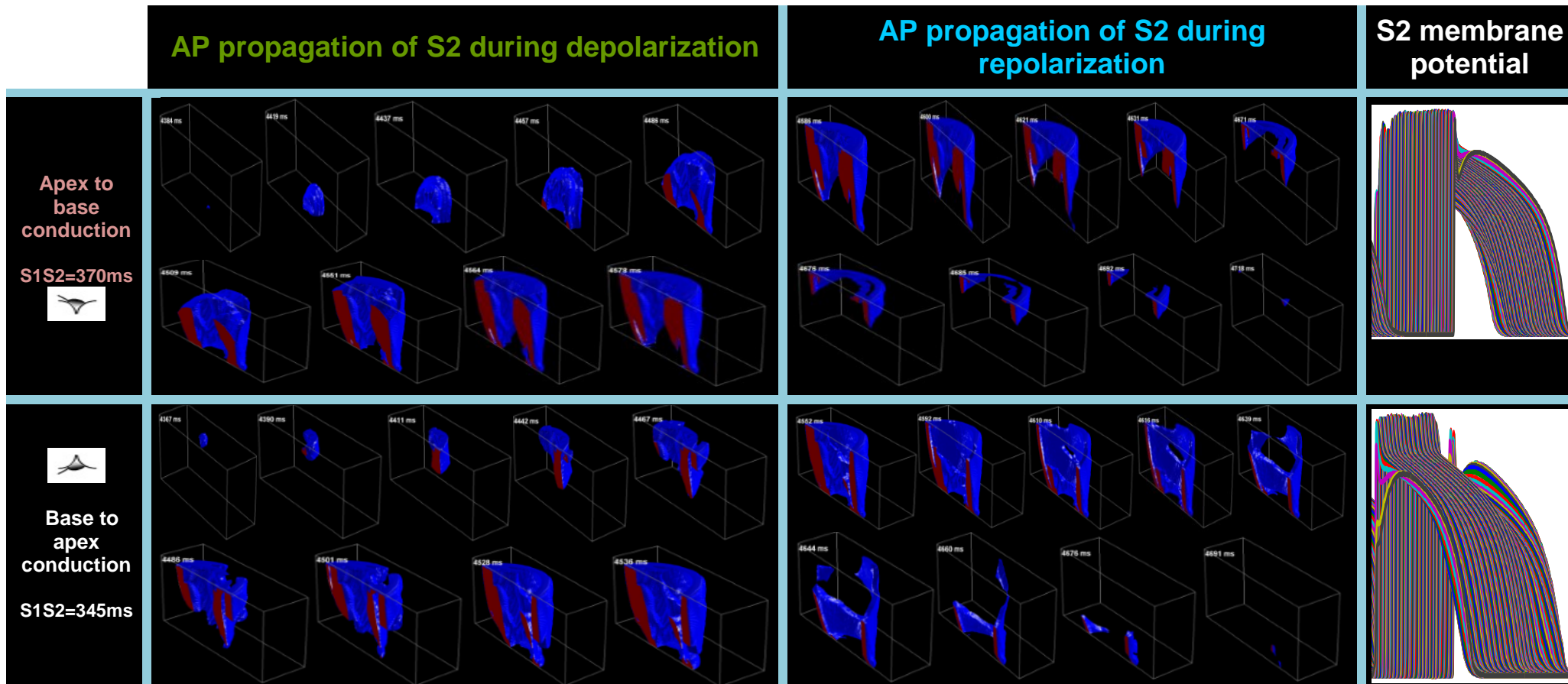


Figure 6-23: Examples of AP propagation from depolarization to rest for **premature S2 beats** in the left ventricular wedge composed of 30%endo-28%M-42%epi with epicardial pacing with apex to base conduction and the reverse with anisotropic conduction

With apex to base conduction, depolarization wave started from the bottom of the wedge and gradually formed while propagating upward. Repolarization wave gradually vanished from the bottom of the wedge and broke in the mid-myocardial region and then became into two parts.

With base to apex conduction, depolarization wave formed on the top of the wedge and gradually formed but not completely in mid-myocardial region while propagating downward. Repolarization wave gradually vanished and broke into two parts while propagating downward.

6.6 Summary of results

A wedge model including an anatomically detailed left ventricular tissue geometry and fibre geometry was introduced composed of anisotropic homogenous and heterogeneous tissue paced from the epicardial region with apex to base conduction and the reverse.

Comparison between 3D cubes of tissue and the wedge model showed (1) qualitatively similar changes in spatial and restitution profiles of activation time, repolarization time, and APD for premature beats; (2) greater measures of dispersion in activation time and repolarization time in the wedge model than 3D cubes due to size of the wedge model.

For the heterogeneous left ventricular wedge model with base to apex conduction, the transition regions with different cell types were the regions (1) with abnormal increase in measures of dispersion in repolarization time for short S1S2 intervals of 455-345 ms; and (2) where wave break in AP propagation occurred during AP depolarization and AP repolarization at the last S1S2 interval. This region may increase tissue vulnerability to ventricular arrhythmia.

Next Chapter provides a brief discussion, and describes limitations and future studies.

6.7 References

1. The centre for cardiovascular bioinformatics and modelling of the Johns Hopkins University (CCBM). Available from: <http://www.ccbm.jhu.edu/reacerch>.
2. Bueno-Orovio A and Cherry EM and Fenton FH, Minimal model for human ventricular action potentials in tissue. *Journal of Theoretical Biology*, 2008. **235**: p. 544-560.
3. Morgan J.M and Cunningham D and Rowland E, Dispersion of monophasic action potential duration: demonstrable in humans after premature ventricular extrastimulation but not in steady state. *J Am Coll Cardiol*, 1992. **19**: p. 1244–1253.
4. Sakakibara Y and Furukawa T and Singer DH and Jia H and Backer CL and Arentzen CE and Wasserstrom JA, Sodium current in isolated human ventricular myocytes. *Am J Physiol*, 1993. **265**: p. H1301–H1309.
5. Drouin E and Charpentier Fand Gauthier C and Laurent K and Le Marec H, Electrophysiologic characteristics of cells spanning the left ventricular wall of human heart: evidence for presence of M cells. *J Am Coll Cardiol*, 1995. **26**: p. 185-192.
6. Drouin E and Lande G and Charpentier F, Amiodarone reduces transmural heterogeneity of repolarization in the human heart. *J Am Coll Cardiol*, 1998. **32**: p. 1063-1067.
7. Nabauer M and Beuckelmann DJ and Uberfuhr Pand Steinbeck G, Regional differences in current density and rate-dependent properties of the transient outward current in subepicardial and subendocardial myocytes of human left ventricle. *Circulation*, 1996. **93**: p. 168–177.
8. Li GR and Feng J and Yue L and Carrier M, Transmural heterogeneity of action potentials and Ito1 in myocytes isolated from the human right ventricle. *Am J Physiol*, 1998. **275**: p. H369–H377.
9. Perea Y and Demolombe S and Baro I and Drouin E and Charpentier Fand Escande D, Differential expression of KvLQT1 isoforms across the human ventricular wall. *Am J Physiol Heart Circ Physiol*, 2000. **278**: p. H1908– H1915.
10. Pak HN and Hong SG and Hwang GS and Lee HS and Park SW and Ahn JC and Moo Ro Y and Kim YH, Spatial dispersion of action potential duration restitution kinetics is associated with induction of ventricular tachycardia/fibrillation in humans. *J Cardiovasc Electrophysiol*, 2004. **15**: p. 1357–1363.
11. Koller ML and Maier SKG and Gelzer AR and Bauer WR and Meesmann M and Gilmour RF, Altered dynamics of action potential restitution and alternans in humans with structural heart disease. *Circulation*, 2005. **112**: p. 1542-1548.
12. Yan GX and Shimizu W and Antzelevitch C, Characteristics and distribution of M-cells in arterially perfused canine left ventricular wedge preparations. *Circulation*, 1998. **98**: p. 1921-1927.
13. Poelzing S and Akar FG and Baron E and Rosenbaum DS., Heterogeneous connexin43 expression produces electrophysiological heterogeneities across ventricular wall. *Am J Physiol Heart Circ Physiol*, 2004. **286**: p. H2001-H2009.
14. Glukhov AV and Fedorov VV and Qing L and Ravikumar VK and Kalish PW and Schuessler RB and Moazami N and Efimov IR, Transmural dispersion of repolarization in failing and nonfailing human ventricle. *Circ Res*, 2010. **106**: p. 981-991.

Chapter 7

Discussions, future studies, and conclusions

7.1 Introduction

In this thesis, a simple [1] and a biophysically detailed [2] models of human ventricular cells, a traditional monodomain tissue model, and geometrical models were used to study the interaction of activation-repolarization coupling and restitution properties in cardiac ventricular tissues with the normal and reversed activation sequences. The simulation results were based on seven timings including six timings for normal S1 and premature S2 beats (activation time from indices of AP depolarization, repolarization time from indices of AP repolarization, and APD as the difference between activation time and repolarization time) and one timing of diastolic interval (between indices of AP downstroke of the 6th normal S1 beat and indices of AP upstroke of premature S2 beat).

These data were evaluated in the form of (1) spatial and restitution profiles; (2) profiles of three measures of dispersion; (3) restitution profiles of speed of depolarization conduction; and (4) profiles of AP propagation during depolarization and repolarization. Comparing these profiles during progressively decreasing S1S2 intervals in the same study with two different ventricular human models could increase current understanding about dynamics of depolarization and repolarization in the small scale of the heart (i.e. 2D slabs, 3D cubes, and the left ventricular wedge model).

This Chapter is organized in three sections to provide explanations to the relative research questions, a brief description of limitations in this thesis, future studies, and conclusions.

7.2 Some research questions and answers

The simulation results in this thesis showed that premature S2 beats act to change AP depolarization and AP repolarization profiles with the FK4V and the TP06 models.

For premature AP depolarization in the 2D, 3D, and wedge model of tissue,

1. activation time rose with increasing distance;
2. profiles of activation time against diastolic interval qualitatively changed similar to restitution profiles of repolarization time and APD based on restitution properties of ventricular cells in heterogeneous tissues
3. profiles of amplitude of AP depolarization against transmural distance was influenced by restitution properties of ventricular cells in heterogeneous tissues
4. dispersion in activation time gradually increased while speed of depolarization conduction became slow during decreasing S1S2 intervals;
5. wave break occurred during AP depolarization at the last S1S2 interval at the transition regions composed of different ventricular cell types under some conditions.

However, for premature AP repolarization, its spatial and restitution profiles of repolarization time, measures of dispersion in repolarization time, and heterogeneous recovery (wave break during AP repolarization described for 3D cubes of heterogeneous tissue in Chapter 5, section 5.9; and for left ventricular wedge model of heterogeneous tissue in Chapter 6, section 6.5) were less dependent on the type of cell model but significantly dependent on:

1. S1S2 intervals;
2. cellular configurations;
3. direction of activation;
4. geometrical models including tissue and fibre structure.

These issues are discussed here.

Is repolarization across the ventricular wall uniform or heterogeneous?

Whether repolarization across the ventricular wall is uniform or heterogeneous is still a matter of controversy [3-8]. There is evidence that the increase in APD is relatively gradual in transmural direction [9] in the human heart while there is sharp increase in APD between the epicardium and sub-epicardium in the canine hearts [10-12]. The latter may be due to an increase in tissue resistivity in this region [10, 11]. In the human heart, Drouin et al. [13] suggested the spatial geometric orientation of epicardial layers perpendicular to sub-epicardial layers with AP characteristics of mid-myocardial cells may explain the poor intercellular coupling between epicardial and sub-epicardial layers. The other animal studies suggested this may be related to a sharp transition in fibre orientation and reduced expression of connexin 43 [12, 14], which is responsible for intracellular communication in the ventricular myocardium. In 2005, Antzelevitch [15] suggested that both degree of electrotonic coupling and intrinsic APD contribute to the expression of electrical heterogeneity in the ventricular myocardium. An important factor is whether the heart is intact and beating, or cut and isolated as in a wedge preparation.

This thesis showed how different fibre structure can change the transmural gradient in repolarization and APD in 3D cubes of anisotropic heterogeneous tissue. The results emphasize the existence of strong interaction among fibre organization, activation-repolarization coupling, anisotropy, and restitution properties that are responsible for the dynamics of depolarization and repolarization in the human heart. Therefore, variation in fibre orientation may be one of the reasons for

1. a sharp or gradual transition between regions of different cell type (i.e. between epicardium and endocardium);
2. variable reported dispersion in activation time and repolarization in the normal and diseased hearts.

For example, Taggart et al. in 2001 [5] failed to identify the transmural heterogeneity of repolarization or the presence of mid-myocardial cells in patients undergoing coronary artery bypass surgery. It may be due to not only tools and method of measurement i.e. the unipolar plunge electrodes and location of the epicardial electrode as suggested by Antzelevitch [6] (explained in Chapter 2, section 2.7) but also due to the specific arrangement of fibre organization in the injured myocardial region. Moreover, the interaction between electrical activity and fibre structure may explain why Laurita and Girouard [16] measured considerably larger APD differences in the epicardial surface compared to APD differences measured by Kanai and Salama [17] between epicardium and endocardium in the guinea pig heart.

Is there an inverse relationship between APD and activation time?

An inverse relationship between APD (activation-recovery) and activation time has been shown in a number of in vivo studies in animal [18] and human [19-23] hearts. Most of these studies were limited to the epicardial or endocardial region of ventricles or some S1S2 intervals. The simulation results in this thesis showed that inverse relationship between APD and activation time is only true during long S1S2 intervals and for homogenous epicardial, mid-myocardial, and endocardial tissues. With decreasing S1S2 intervals, spatial profiles of APD and repolarization time changed and there was no linear relationship between APD and activation time particularly for short S1S2 intervals. This finding was true in 2D tissue geometries in the absence of a geometrical model of fibre structure with isotropic diffusion coefficients, 3D cubes of tissue with different fibre structure in isotropic, anisotropic, and anisotropic fibrosis tissues, and the left ventricular wedge model composed of anisotropic homogenous and heterogeneous tissues paced from apex to base conduction and the reverse.

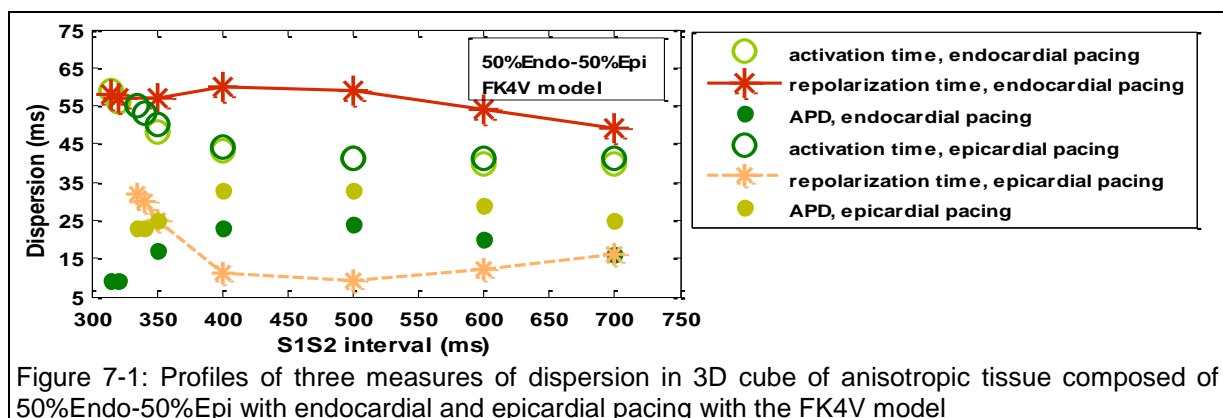
Is transmural heterogeneity of repolarization amplified as a consequence of reversal of the normal activation sequence?

Reversing the direction of activation in electrically heterogeneous ventricular myocardium prolongs the QT interval and rises the dispersion in transmural repolarization based on clinical studies in human heart with heart failure [24, 25] and arterially perfused canine left ventricle wedge preparations [26]. On the other hand, there is evidence that reversing the direction of activation reduced ventricular heterogeneity of repolarization and has an electrophysiological anti-arrhythmic effect on the arrhythmogenic substrate of dilated cardiomyopathy in a human study [27].

This thesis showed that increase or decrease of dispersion in repolarization time as a consequence of reversing the direction of activation during decreasing S1S2 intervals depends on the cellular configuration within left ventricular thickness and restitution properties of ventricular cells. Figures 7-1 to 7-5 emphasize this finding by plotting profiles of dispersions of activation time, repolarization time, and APD against S1S2 interval for anisotropic heterogeneous tissues with both normal and reverse activation sequence in 3D cubes of tissue and in the left ventricular wedge models.

- Tissue composed of 50%Endo-50%Epi

In the FK4V model of 3D cube of tissue composed of 50%Endo-50%Epi with the FK4V model, dispersion in repolarization time with endocardial pacing was amplified as shown in Figure 7-1.



- Tissue composed of 10%Endo-30%M-60%Epi

For the FK4V and the TP06 models 3D cube of tissue composed of 10%Endo-30%M-60%Epi, measures of dispersion in repolarization time with epicardial pacing were greater than those with endocardial pacing (except for short S1S2 intervals with the FK4V model), Figure 7-2.

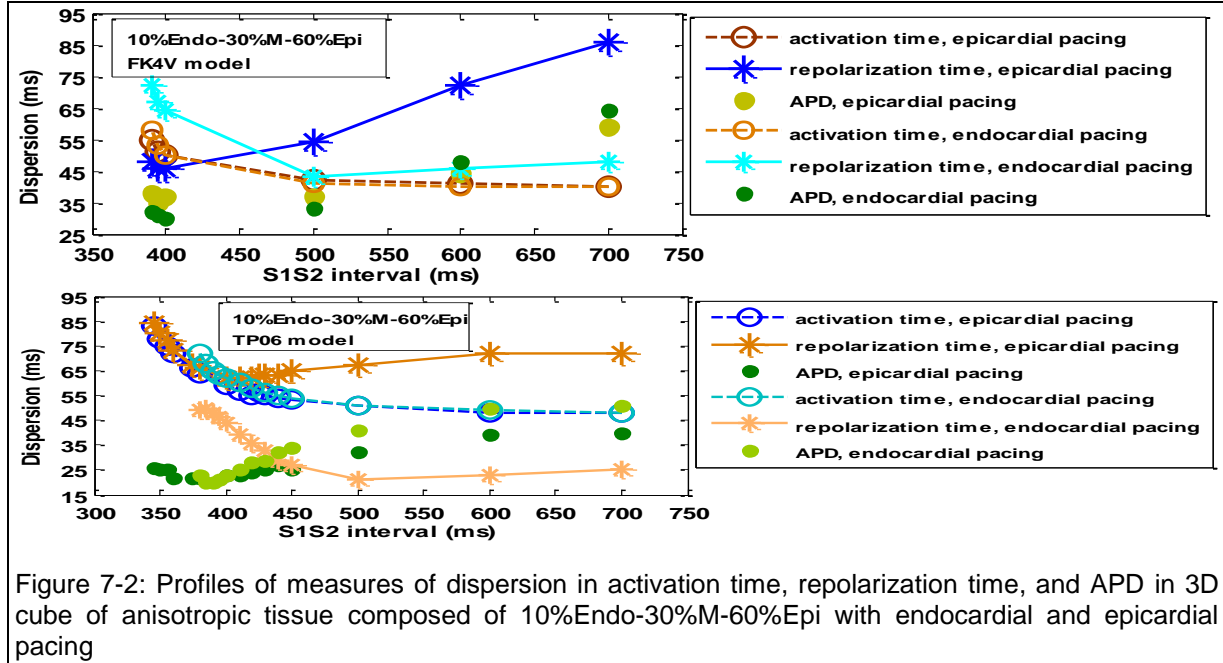


Figure 7-2: Profiles of measures of dispersion in activation time, repolarization time, and APD in 3D cube of anisotropic tissue composed of 10%Endo-30%M-60%Epi with endocardial and epicardial pacing

- Tissue composed of 60%Endo-30%M-10%Epi

For the 3D cube of tissue composed of 60%Endo-30%M-10%Epi, measures of dispersion in repolarization time with endocardial pacing were amplified compared to epicardial pacing with both FK4V and TP06 models as shown in Figure 7-3.

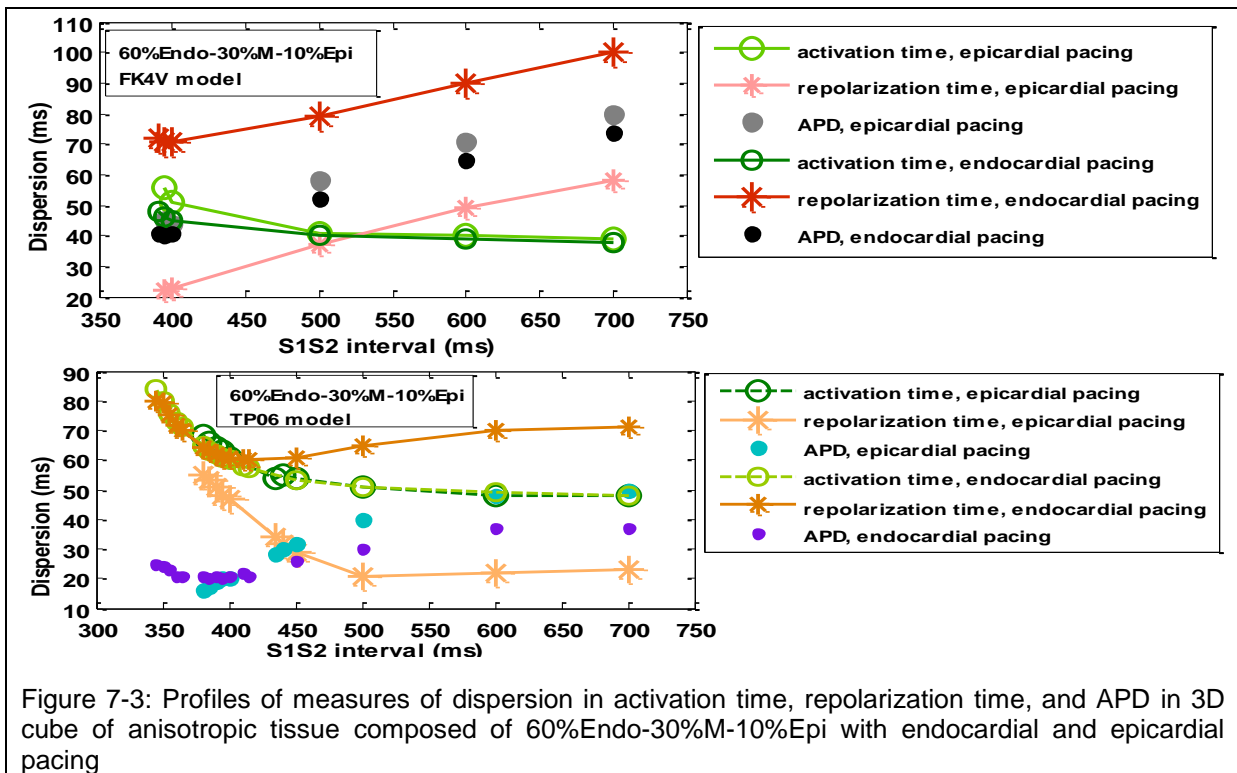
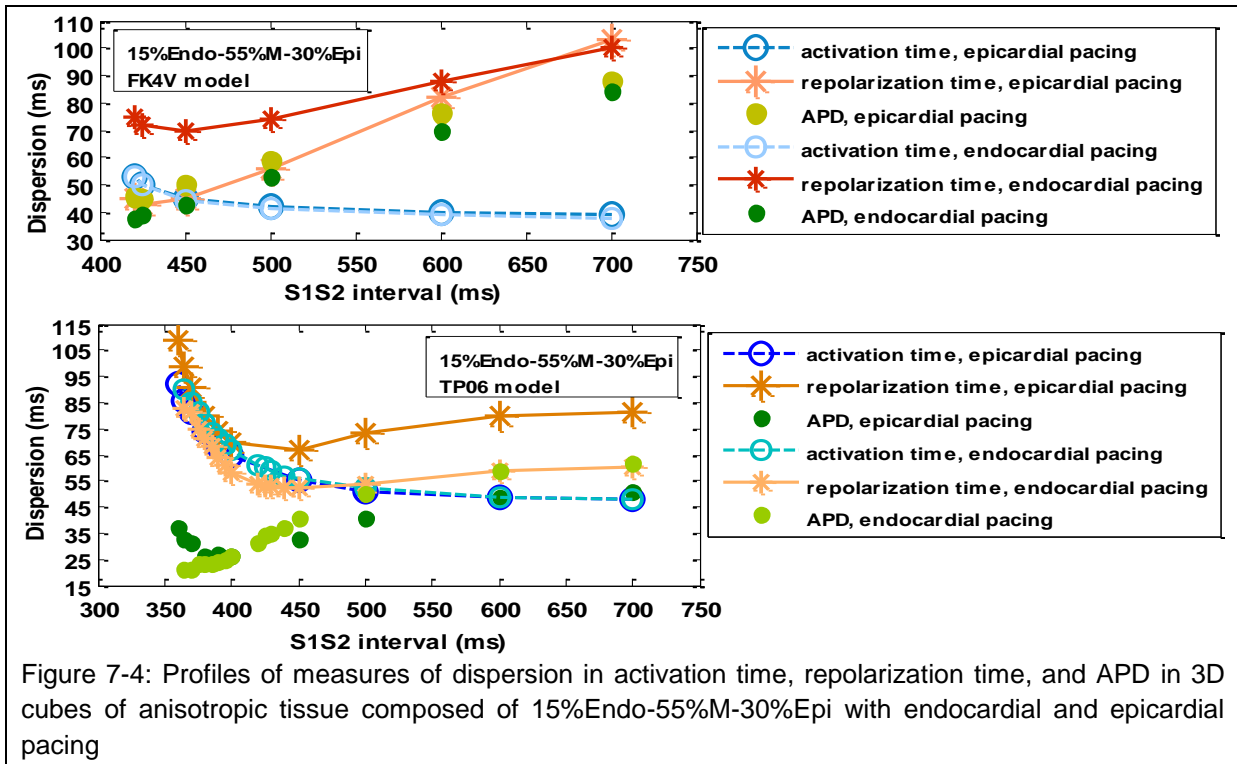


Figure 7-3: Profiles of measures of dispersion in activation time, repolarization time, and APD in 3D cube of anisotropic tissue composed of 60%Endo-30%M-10%Epi with endocardial and epicardial pacing

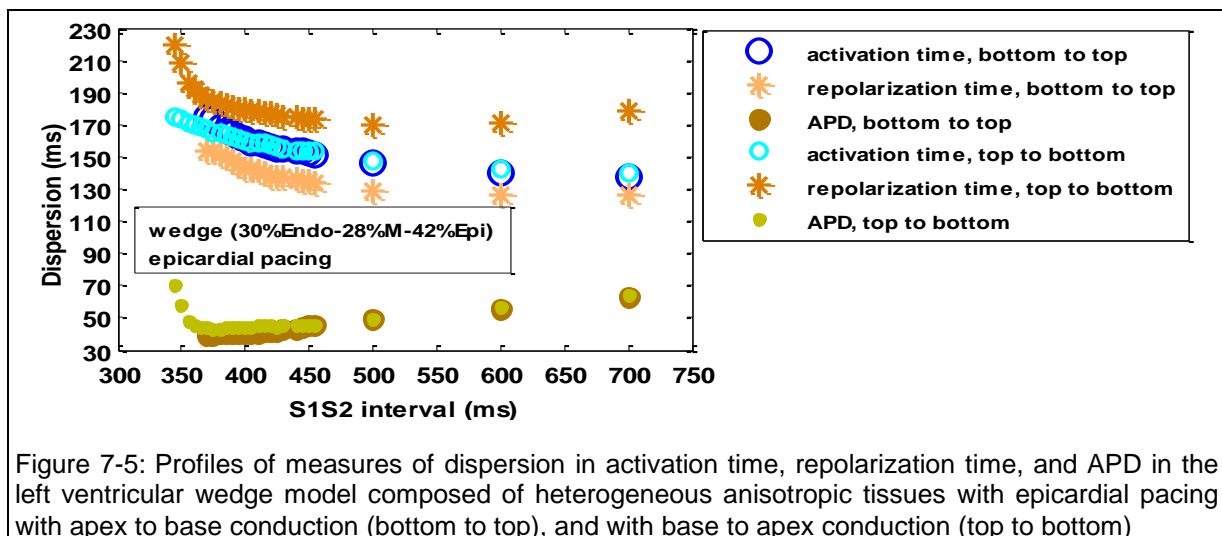
- Tissue composed of 15%Endo-55%M-30%Epi

For the 3D cube of tissue composed of 15%Endo-55%M-30%Epi, measures of dispersion in repolarization time with endocardial pacing were amplified compared to epicardial pacing with the FK4V model while the reverse was true with the TP06 model, Figure 7-4.



- Heterogeneous left ventricular wedge model

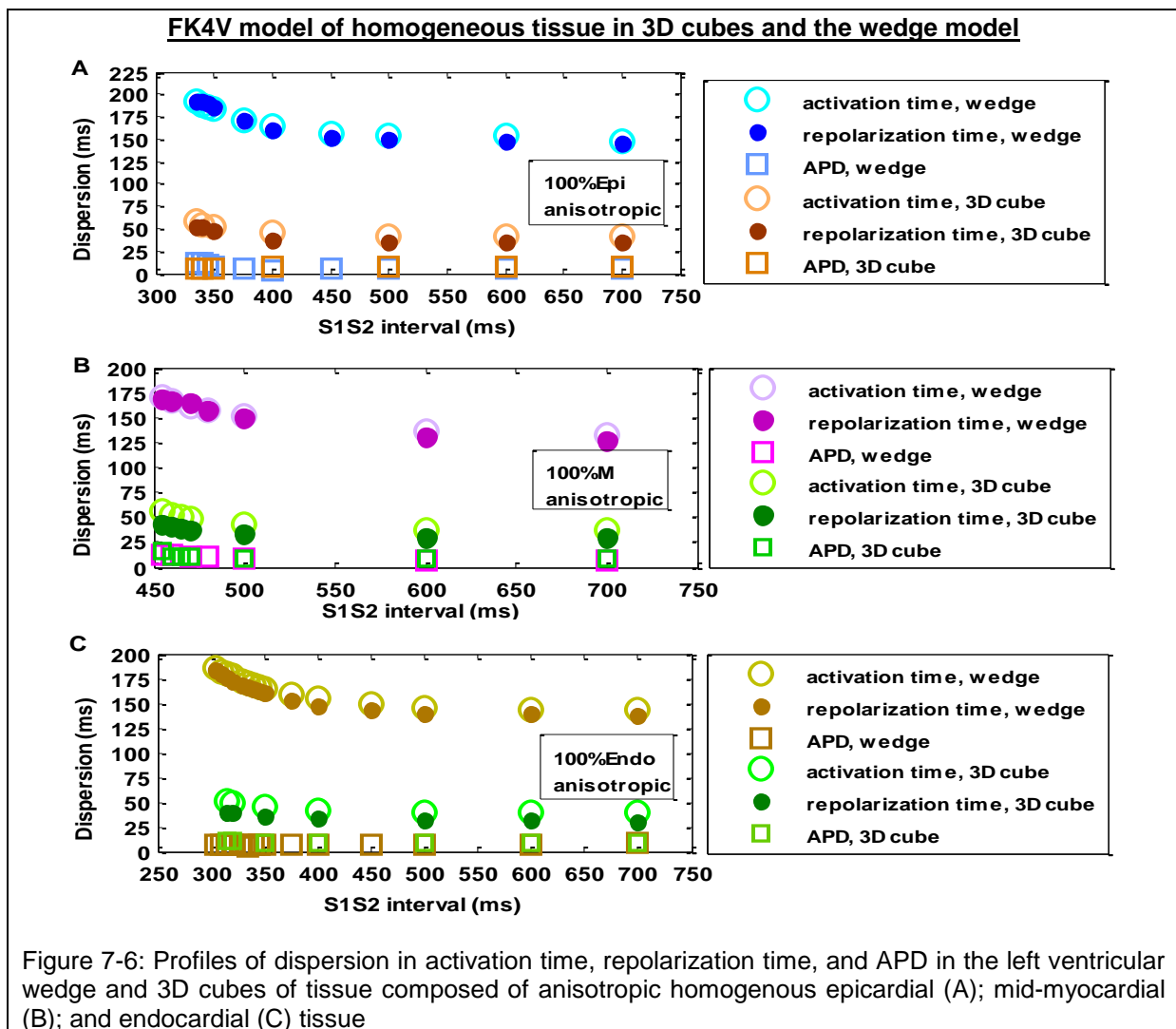
In the left ventricular wedge model composed of anisotropic heterogeneous tissue with 30%Endo-28%M-42%Epi cells, measures of dispersion in repolarization time were amplified with epicardial pacing with base to apex conduction compared to the apex to base conduction with the FK4V model as shown in Figure 7-5.



What is the reason for significantly decrease in dispersion of repolarization time and APD in the ventricular wall thickness compared with those in the wedge preparation?

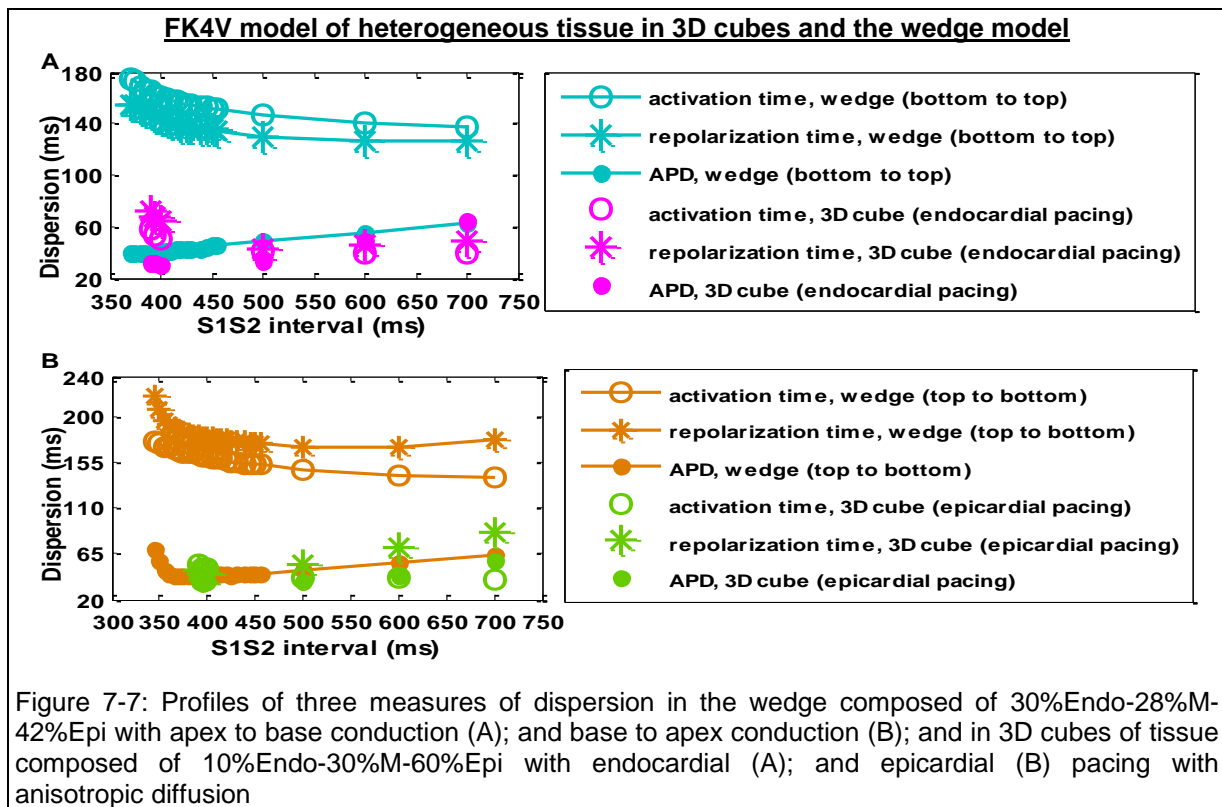
Yet, the true reason for variant dispersion in APD and repolarization reported by animal and human studies is not clear and may be due to the different pathophysiology and dimension of the area of assessment.

For anisotropic homogenous tissues in this thesis, measures of dispersion in activation time and repolarization time increased with increasing size of geometrical tissue models. For example, dispersion in activation time and repolarization time were approximately tripled in the left ventricular wedge model with size of 3.5×11.0×6.0 cm³ compared to the 3D cube of tissue with size of 0.8× 0.8×1.2 cm³ for three homogenous tissues as shown in Figure 7-6.



For heterogeneous tissues in this thesis, measures of dispersion in activation time and repolarization time increased to around 100 ms during decreasing S1S2 intervals i.e. in the left ventricular wedge composed of 30%Endo-28%M-42%Epi with apex to base conduction and the reverse compared to the 3D cube of tissue composed of 10%Endo-30%M-60%Epi with endocardial and epicardial pacing as shown in Figure 7-7.

Interestingly, measures of APD dispersion in both 3D cubes and the left ventricular wedge were approximately similar in homogenous and heterogeneous tissues during decreasing S1S2 intervals.



Is increase in dispersion of repolarization time pre-requisite for re-entry?

Ghanem et al. [28] suggested that dispersion of repolarization creates conditions for the formation of unidirectional block and re-entry due to asymmetry of excitability properties. Consequently, the myocardial regions with large repolarization heterogeneities constitute an arrhythmogenic substrate with the potential for developing arrhythmias. Chauhan et al. [22] suggested that increase in heterogeneity of transmural ventricular repolarization in the human heart may provide the substrate for ventricular arrhythmia, however, this finding may not be applied to the whole heart. A simulation study by Benson et al. [29] concluded that simple cuboid models with rule-based architecture do not accurately reproduce the complex geometry and architecture of the human ventricles.

Simulation results in this thesis showed that an increase in dispersion of repolarization can promote the wave break during AP depolarization and AP repolarization and may provide conditions for re-entry under particular conditions. For the former,

- In anisotropic homogenous and heterogeneous tissues, dispersion in activation time and repolarization time in the left ventricular wedge was greater than 3D cubes of tissue with a linear change in fibre orientation. However, for homogenous anisotropic tissues, depolarization wave broke in 3D cube of tissue and un-broke in the left ventricular wedge even at the last S1S2 interval.
- In anisotropic heterogeneous tissues, depolarization wave and repolarization wave broke in both 3D cubes of tissue and in the left ventricular wedge with apex to based conduction and the reverse. In these tissues, a sharp APD in the transition regions with different cell type may provide conditions for wave break.

The findings in this thesis suggest that 3D cube of tissues with a linear change in fibre organization may be more vulnerable for re-entry than the wedge model with greater dispersion in repolarization (due to the size of wedge model). Still, further studies are required to test this hypothesis that is not the scope of this thesis.

Does large dispersion in repolarization time facilitate the development of the conduction delay?

An animal study in dogs by Kuo et al. [30] showed that the large dispersion in repolarization facilitates the development of a conduction delay necessary to induce sustained arrhythmia by an early premature stimulus applied at the site with a short monophasic AP.

This thesis has showed that large dispersion of repolarization can slow conduction during decreasing S1S2 intervals under variety of conditions. For example,

- 2D isotropic tissues with structural discontinuities compared to tissues without structural discontinuities (1) increased dispersion in activation time and repolarization time around 1 to 7 ms; (2) slowed speed of depolarization conduction between two structural discontinuities in tissues;
- 3D cubes of anisotropic fibrosis heterogenous tissues compared to tissues without fibrosis simulated with a linear change in fibre orientation (1) decreased measures of dispersion in repolarization time for long S1S2 intervals and increased measures of dispersion in repolarization time for short S1S2 intervals; (2) suppressed speed of depolarization conduction in the mid-myocardial region;
- combined effect of anisotropy, fibrosis, and a non-linear change in fibre orientation (or with no variation) could compensate the speed of depolarization conduction in the mid-myocardial region of 3D cubes of heterogenous tissues.

These findings suggest that decreasing or increasing measures of dispersion in repolarization time are influenced by anisotropy, fibrosis, fibre structure, and cellular configurations in heterogenous tissues.

Whether reducing dispersion in repolarization time is considered as a protective mechanism?

Cowan et al. [19] in the epicardial region of human left ventricular suggested an inverse relationship between APD and activation time may decrease dispersion in repolarization time. These measurements were made in patients undergoing coronary artery bypass grafting, and were used as evidence for the presence of an upright T-wave on the ECG (Electrocardiogram). If it is assumed that reducing dispersion in repolarization time is a protective mechanism, this relationship may provide an intrinsic anti-arrhythmic property of ventricular tissue [19]. They showed this relationship was not true in patients with aortic valve replacement (with T wave inversion on the ECG) and the dispersion of repolarization increased [19]. Hanson et al. [23] suggested that strong activation-repolarization coupling may be protective at the basic cycle length by limiting dispersion in repolarization time, but that the situation may become complex at short coupling intervals attributable to interaction with restitution.

In this thesis, for homogenous tissues in the 3D cubes of tissue and the left ventricular wedge, dispersion in repolarization time increased gradually with decreasing S1S2 intervals. On the other hand, for heterogeneous tissue composed of three ventricular cells, dispersion in repolarization time initially decreased for long S1S2 intervals (i.e. 700-500 ms) while increased for S1S2 intervals shorter than approximately 450 ms. Therefore, decrease in dispersion of repolarization may be protective in particular conditions i.e. isotropic or anisotropic heterogeneous tissues with no fibrosis for long S1S2 intervals. However,

anisotropic fibrosis heterogeneous tissues composed of three ventricular cell types could suppress the speed of depolarization conduction even for long S1S2 intervals when dispersion in repolarization decreased.

Which cell model is more efficient?

The TP06 model [2] is able to reproduce calcium-driven alternans [31, 32] which is an additional source of instability that may lead to ventricular fibrillation, one of the most dangerous life-threatening ventricular arrhythmia. The FK4V [1] model can estimate the dynamic concentration changes of calcium ion. However, Clayton et al. [33] suggested that the choice of cellular electrophysiology model can influence tissue level behaviour such as re-entry.

This thesis showed the similarities and differences between simulation results with the FK4V [1] and TP06 [2] models. For example, the TP06 model [2] was able to produce membrane voltage at a shorter S1S2 interval i.e. around 350 ms while the last S1S2 interval with the FK4V model was around 400 ms for anisotropic heterogeneous tissues composed of three ventricular cells. However, with isotropic diffusion, the last S1S2 interval with the FK4V model was greater than the TP06 model. In total, both models showed similar behaviour in tissues with isotropic, anisotropic, and anisotropic fibrosis in 3D cubes of tissue and in 2D isotropic tissue with and without structural discontinuities. However, for the wedge model, the TP06 model is computationally expensive due to more running time for simulations.

7.3 Limitations and future studies

This part of the Chapter summarizes the limitations in this thesis.

First, simulation results in 2D, 3D, and left ventricular wedge model were based on membrane voltage extracted from the central region of geometrical tissue models in which changes in the spatial profiles of APD and repolarization time were more than other regions. A supplementary study is required to evaluate data from the other regions of tissue.

Second, in the left ventricular wedge model, tissue was paced from a small region in epicardium with apex to base conduction and the reverse. Still, more simulations are required to pace tissue from the endocardial region with apex to base conduction and the reverse in order to compare the results with results of epicardial pacing. In addition, it would be interesting to study the effect of structural discontinuities and fibrosis in the left ventricular wedge model.

Third, AP propagation was visualized at the last S1S2 interval that was more likely for wave break. However, it would be interesting to study the pattern of AP propagation for other S1S2 intervals.

Fourth, Part II of Chapter 5 simulated some 3D heterogeneous tissues with different fibre structure. Further studies are required to compare simulation results of tissues with a linear and non-linear change in fibre orientation during decreasing S1S2 intervals in detail to provide a frame work for studying the effects of fibre structure on AP depolarization and repolarization in the normal and diseased heart.

Fifth, the most important missing part of this thesis was to estimate a pseudo ECG resulting from propagation of normal S1 beat and premature S2 beats in tissues. Because it

could provide information about how direction of T-wave change in each simulated tissues and it's relevant to ventricular arrhythmia.

There are many other ambiguities that still have remained important research questions. The following subsections provide a brief discussion of these issues.

7.3.1 Fibre-sheet structure and orthotropic conductivities

There is evidence that the spread of electric activation in ventricular myocardium is not axially anisotropic but is orthotropic. The evidence came from a histological study in the canine heart [34] and in the ventricular wall of the pig heart [35]. Caldwell et al. [35] suggested that non-uniform laminar myocardial architecture and associated electric orthotropic should be included in future models of initiation and maintenance of ventricular arrhythmia. It is important to know that the detailed information about sheet orientation has still not provided in the human and are limited to the animal studies.

To test this idea, the programme that was used in this thesis could be modified based on monodomain equation. To create orthotropic anisotropy of cardiac tissue within left ventricular wedge model, and therefore to create fibre and fibre sheet structure in the tissue, the ventricular conductivity tensor at any spatial point can be described by Equation 7-1 and Equation 7-2 (used by Colli Franzone et al. [36]).

$D_{ij} = A\tilde{D}A^T$	Equation 7-1
$D_{ij} = D_1ff^T + D_2ss^T + D_3nn^T$	Equation 7-2
$\tilde{D} = \begin{pmatrix} D_1 & 0 & 0 \\ 0 & D_2 & 0 \\ 0 & 0 & D_3 \end{pmatrix}$: diffusion matrix in which D_x, D_y, D_z are diffusion tensor elements that represent the characteristic values or eigenvalue of the matrix, longitudinal to fibres, normal to fibres in the sheet plane, and normal to both fibres and sheets f, s, n : are unit vectors in orthogonal direction defined as a fibre direction parallel to the local fibre direction (f), a sheet direction (s), and a sheet normal direction (n) are tangent and orthogonal to the radial laminae and transversal to the fibre axis respectively	

For orthotropic conductivity in the left ventricle, the ratio of diffusion coefficients would be set based on the Caldwell [35] study i.e. 4:1.8:1 to obtain the maximum conduction velocity of 0.67 m/s aligned to the myocyte axis, 0.30 m/s parallel to the myocyte layers, and 0.17 m/s normal to them. In addition it would be interesting to allocate different set of diffusion coefficients to epicardial, mid-myocardial, and endocardial regions in 3D cubes of tissue and in the left ventricular wedge. Because the simulation results in this thesis showed that speed of depolarization conduction in epicardial, mid-myocardial and endocardial regions varied during decreasing S1S2 intervals in 3D cubes of tissue and in the wedge model composed of heterogeneous tissues. Table 7-1 shows examples of diffusion coefficients that can be allocated to epicardial, mid-myocardial, and endocardial regions.

	Diffusion1 (cm ² /ms)	Diffusion2 (cm ² /ms)	ratio
Epicardial region	0.001	0.00025	4:1:2
	0.001	0.0002	5:1:2
Endocardial region	0.001	0.00016667	6:1:2
Mid-myocardial region	0.001	0.00014286	7:1:2
	0.001	0.000125	8:1:2

Table 7-1: Examples of numerical values of the diffusion coefficients in orthogonal directions

It is important to note that the available estimated physiological range for conductance are between 3 and 12 μ S from data in the human ventricle [37].

7.3.2 Fibroblasts

The heart muscle is composed of several cell types including cardiomyocytes, fibroblast, endothelial cells, and vascular smooth muscle cells [38, 39], and in diseased heart there may be scar tissues from earlier damage. Fibroblasts are highly concentrated in scarred human tissue [40, 41] where synthesis and deposition of collagen promote scar formation and fibrosis [40]. The fibroblasts contain interconnected cellular processes that form a network of cells within the collagen network [42]. Increased levels of collagen may disturb electrophysiological communication between cardiomyocytes [43]. There are different distributions of fibroblast throughout the heart and the number of fibroblast varies with physiological conditions [44] in the animal hearts. Fibroblasts communicate with cardiomyocytes, other fibroblast and endothelial cells. There is evidence that direct interactions between cardiomyocytes and fibroblasts occur via gap junctional connexins to function in electrical conduction in the heart [38, 39]. Gap junctions are transmembrane channels between neighbouring cells that are important in maintaining a normal heartbeat by providing electrical coupling between cells and electrotonic interaction in tissue. Some studies suggested that the effect of the intracellular coupling through gap junctions may cancel the transmural gradients and mid-myocardial cells in the human left ventricle [9, 45].

It is important to note that electrical coupling between cardiac fibroblasts and myocytes was found in the cell cultures by Kohl et al. [46], but it has not been established in human in vivo. In 2010, Petrov et al. [47] showed that the fibroblasts with different resting potentials may change the restitution properties of tissue and may cause a spiral wave break-up in 2D sheets. They used the 3D monodomain tissue model and the Luo-Rudy phase I model [48] for describing cardiac cell. To simulate fibroblast, a model of Sachse et al. [49] was used that involved three ionic currents to describe the voltage of a single cell (inward potassium rectifier current, voltage and time dependent potassium current, and the background current) as well as seven dynamical variables and the seven non-linear ordinary differential equations. The values of conductivities in the extracellular space were 0.05 S/m^3 , the conductance along the fibre axis was twice of transverse to the axis, and 0.1 S/m^3 for fibroblasts.

Furthermore, an experimental study [50] showed that fibroblasts may slow down the impulse conduction and reduce the largest upstroke velocity. Combination of ventricular cell types with fibroblast and gap junctions into mathematical models may provide new insights into better understanding of the sequence of AP depolarization and repolarization in the normal and diseased heart. To achieve this purpose, the programme that was used in this thesis could be modified to simulate heterogeneous tissues composed of three ventricular cells and fibroblast with the FK4V [1] and the TP06 [2] models.

7.3.3 Mechanics

Repolarization occurs during systole when the ventricular myocardium is mechanically contracting. The muscular contractile activity depends on the predominant direction and spatial arrangement of constitutive muscular fibres [51, 52]. During isometric contraction and ejection phase, an active force is generated in the left ventricle. A human simulation study [53] showed that the simulation results about the effects of muscle active force and fibre orientation on the ventricular contraction were sensitive to the fibre orientation and magnitude of the active force. The other human simulation study [54] emphasized the importance of fibre structure in carrying out force pattern analysis in systole since the force

was more dependent on the direction of fibres and tissue geometry for stress analysis in diastole due to the lower stress when more anatomically realistic fibre structure was used.

Since electrical repolarization occurs at the same time as force generation in cardiac cells, the effect of cardiac mechanics on susceptibility to re-entry is one important research question. An electromechanical study in tissue by Nash and Panfilov [55] showed that mechanics influence the behaviour of re-entrant wave. In addition, stretch activated channels in the cell membrane can increase vulnerability to re-entry if the cardiac tissue is stretched during AP repolarization [56].

This thesis did not consider mechanics because (1) the current mechanics model is usually based on animal experimental contraction data such as a study by Keldermann et al. [57] based on an electromechanical model of the human left ventricle; (2) the lack of data about the sheet structure and sheet angles in the human heart that may change transverse shear deformations, or the strains near the apex and base [58]. In addition, to represent active contractile tension, it is needed to change model parameters such as the intracellular calcium concentration which may produce results with no physiological interpretation with the FK4V model [1]. Moreover, combining mechanic to the simulated tissues in current thesis could increase the complexity of results with no explanation. However, the simulation results in this thesis in the absence of mechanic could answer some important research questions and provide a foundation for future studies. For example, cardiac models can include tension development to consider the ventricular contraction on the sequence of AP depolarization and repolarization and study the combined effect of cardiac electro-mechanics on susceptibility to re-entry.

7.3.4 Speed of depolarization conduction and speed of repolarization conduction

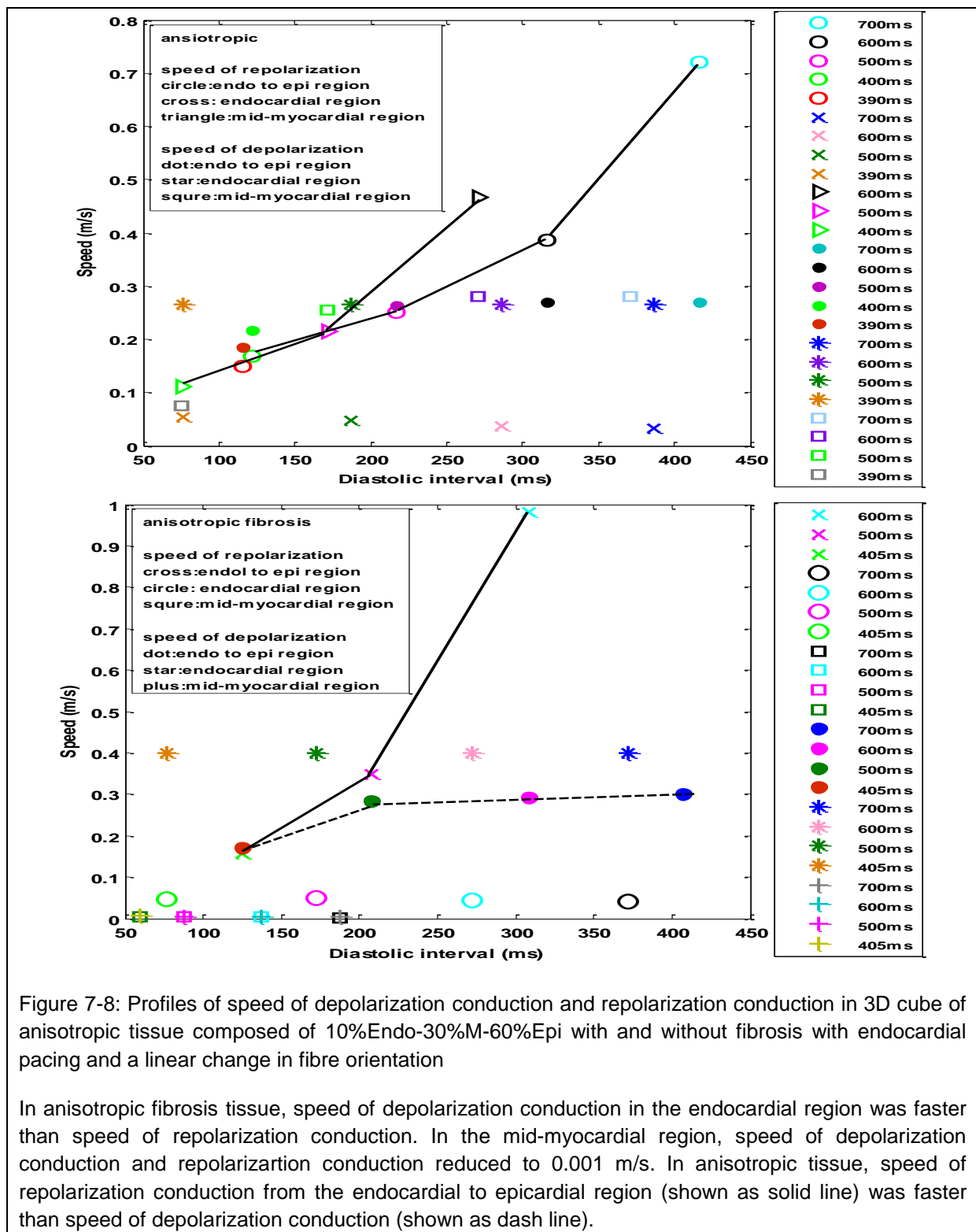
During AP depolarization and AP final repolarization several dynamic processes are engaged such as conduction velocity and restitution, Boyett-Jewel [59] and Qu et al. [60] in mammalian ventricles. This thesis suggests that besides these factors, speed of repolarization conduction may be also involved and should be included in the future studies.

This thesis calculated speed of depolarization conduction (conduction velocity) based on activation time from AP upstroke. In addition, the other speed was calculated based on repolarization time from AP downstroke and was called the speed of repolarization. Figure 7-8 shows examples of speed of depolarization conduction and speed of repolarization conduction in 3D cube of anisotropic tissues composed of 10%Endo-30%M-60%Epi with and without fibrosis with endocardial pacing and a linear change in fibre orientation. In both tissues with and without fibrosis, the speed of repolarization from the endocardial to epicardial regions changed in two stages: initially rapid for long S1S2 intervals, and then slow for short S1S2 intervals. Moreover, the speed of repolarization conduction similar to the speed of depolarization conduction

- (1) changed in the epicardial, mid-myocardial, and endocardial regions;
- (2) was suppressed in the mid-myocardial region in anisotropic fibrosis tissue.

Investigating speed of AP propagation based on activation time and repolarization time is particularly important in heterogenous tissues. This thesis showed that the speed of depolarization conduction changed not only across tissue but also in the epicardial, mid-myocardial, and endocardial regions. Therefore, comparing speed of AP propagation based

on timing of AP upstroke and AP downstroke may provide useful information about (1) the differences between speed of depolarization conduction and repolarization conduction particularly in anisotropic fibrosis tissues; and (2) whether modification of speed of repolarization conduction may prevent spiral wave break in simulated cardiac tissue.



7.4 Conclusions

It is concluded that dispersion in repolarization (not APD) could be used clinically for estimating arrhythmia risk if it is addressed from a variety different angles including whether an increase or decrease in dispersion of repolarization time is due to:

- fibre structure with a linear or non-linear change in fibre orientation
- short or long S1S2 intervals
- structural discontinuities in tissue geometries or fibrosis
- cellular configurations with and without mid-myocardial cells
- anisotropic or orthotropic conduction
- endocardial and epicardial pacing in transvers direction, or in apico-basal direction

Without knowing the reason for increasing or decreasing dispersion in repolarization time, it is not easy to reduce pro-arrhythmic risk in drug development for diseased heart.

7.5 References

1. Bueno-Orovio A and Cherry EM and Fenton FH, Minimal model for human ventricular action potentials in tissue. *Journal of Theoretical Biology*, 2008. **235**: p. 544-560.
2. ten Tusscher KH and Panfilov AV, Alternans and spiral breakup in a human ventricular tissue model. *Am J Physiol Heart Circ Physiol*, 2006. **291**: p. H1088–H1100.
3. Antzelevitch C and Shimizu W and Yan GX and Sicouri S and Weissenburger J and Nesterenko VV and Burashnikov A and Di Diego JM and Saffitz J and Thomas GP, The M cell: its contribution to the ECG and to normal and abnormal electrical function of the heart. *J Cardiovasc Electrophysiol.*, 1999. **10**: p. 1124–1152.
4. Anyukhovskiy EP and Sosunov EA and Gainullin RZ and Rosen MR, The controversial M cell. *J Cardiovasc Electrophysiol*, 1999. **10**: p. 244–260.
5. Taggart P and Sutton PM and Opthof T and Coronel R and Trimlett R and Pugsley W and Kallis P, Transmural repolarisation in the left ventricle in humans during normoxia and ischaemia. *Cardiovasc Res*, 2001. **50**: p. 454–462.
6. Antzelevitch C., Transmural dispersion of repolarization and the T wave. *Cardiovasc Res.*, 2001. **50**: p. 426-431.
7. Opthof T and Coronel R and Janse MJ, Controversies in Arrhythmia and Electrophysiology. Is there a significant transmural gradient in repolarization time in the intact heart? Repolarization Gradients in the Intact Heart. *Circulation: Arrhythmia and Electrophysiology*, 2009. **2**: p. 89-96.
8. Patel C and Burke JF and Patel H and Gupta P and Kowey PR and Antzelevitch C and Yan G., Is there a significant transmural gradient in repolarization time in the intact heart? Cellular Basis of the T Wave: A Century of Controversy. *Circ Arrhythm Electrophysiol.*, 2009. **2**: p. 80–88.
9. Taggart P and Sutton P and Opthof T and Coronel R and Kallis P, Electrotonic cancellation of transmural gradients in the left ventricle in man. *Biophysics and Mol Biol*, 2003. **82**: p. 243-254.
10. El-Sherif N and Caref EB and Yin H and Restivo M., The electrophysiological mechanism of ventricular arrhythmias in the long QT syndrome: tridimensional mapping of activation and recovery patterns. *Circ Res.*, 1996. **79**: p. 474–492.
11. Yan GX and Shimizu W and Antzelevitch C, Characteristics and distribution of M-cells in arterially perfused canine left ventricular wedge preparations. *Circulation*, 1998. **98**: p. 1921-1927.
12. Poelzing S and Akar FG and Baron E and Rosenbaum DS., Heterogeneous connexin43 expression produces electrophysiological heterogeneities across ventricular wall. *Am J Physiol Heart Circ Physiol*, 2004. **286**: p. H2001-H2009.
13. Drouin E and Charpentier F and Gauthier C and Laurent K and Le Marec H, Electrophysiologic characteristics of cells spanning the left ventricular wall of human heart: evidence for presence of M cells. *J Am Coll Cardiol*, 1995. **26**: p. 185-192.
14. Yamada KA and Kanter EM and Green KG and Saffitz JE, Transmural distribution of connexins in rodent hearts. *J Cardiovasc Electrophysiol*, 2004. **15**: p. 710-715.

15. Antzelevitch C., Cardiac repolarization. The long and short of it. *Oxford Journal*, 2005. **7**: p. S2-S9.
16. Laurita KR and Girouard SD., Modulation of ventricular repolarization by a premature stimulus. Role of epicardial dispersion of repolarization kinetics demonstrated by optical mapping of the intact guinea pig heart. *Circ Res*, 1996. **79**: p. 493–503.
17. Kanai A and Salama G., Optical mapping reveals that repolarization spreads anisotropically and is guided by fiber orientation in guinea pig hearts. *Circ Res*, 1995. **77**: p. 784-802.
18. Burgess MJ and Green LS and Millar K and Wyatt R and Abildskov JA, The sequence of normal ventricular recovery. *Am Heart J*, 1972. **84**: p. 669–678.
19. Cowan JC and Hilton CJ and Griffiths CJ and Tansuphaswadikul S and Bourke JP and Murray A and Campbell RWF, Sequence of epicardial repolarisation and configuration of the T wave. *Eur Heart J*, 1988. **60**: p. 424–433.
20. Franz MR and Swerdlow CD and Liem LB and Schaefer J, Cycle length dependence of human action potential duration in vivo. *J Clin Invest*, 1988. **82**: p. 972–979.
21. Yuan S and Kongstad O and Hertervig E and Holm M and Grins E and Olsson B, Global repolarization sequence of the ventricular endocardium: monophasic action potential mapping in swine and humans. *Pacing Clin Electrophysiol*, 2001. **24**: p. 1479–1488.
22. Chauhan VS and Downar E and Nanthakumar k and Parker JD and Ross HJ and Chan W and Picton P., Increased ventricular repolarization heterogeneity in patients with ventricular arrhythmia vulnerability and cardiomyopathy: a human in vivo study. *Am J Physiol Heart Circ Physiol*, 2006. **290**: p. H79-H86.
23. Hanson B and Sutton P and Elameri N and Gray M and Critchley H and Gill JS and Taggart P., Interaction of Activation–Repolarization Coupling and Restitution Properties in Humans. *Circulation: Arrhythmia and Electrophysiology*, 2009. **2**: p. 162-170.
24. Medina-Ravell VA and Lankipalli RS and Yan GX and Antzelevitch C and Medina-Malpica NA and Medina-Malpica OA and Droogan C and Kowey PR, Effect of epicardial or biventricular pacing to prolong QT interval and increase transmural dispersion of repolarization. Does resynchronization therapy pose a risk for patients predisposed to long QT or torsade de pointes? *Circulation*, 2003. **107**: p. 740–746.
25. Fish JM and Brugada J and Antzelevitch C., Potential proarrhythmic effects of biventricular pacing. *J Am Coll Cardiol.*, 2005. **46**: p. 2340–2347.
26. Fish JW and Di Diego JM and Nesterenko VV and Antzelevitch C., Epicardial activation of left ventricular wall prolongs QT interval and transmural dispersion of repolarization implications for biventricular pacing. *Circulation*, 2004. **109**: p. 2136–2142.
27. Santangelo L and Ammendola E and Russo V and Cavallaro C and Vecchione F and Garofalo S and D'Onofrio A and Calabrò R., Influence of biventricular pacing on myocardial dispersion of repolarization in dilated cardiomyopathy patients. *Europace*, 2006. **8**: p. 502-5.
28. Ghanem RN and Burnes JE and Waldo AL and Rudy Y, Imaging dispersion of myocardial repolarization, II: noninvasive reconstruction of epicardial measures. *Circulation*, 2001. **104**: p. 1306–1312.
29. Benson AP and Ries ME and Holden AV, Effects of geometry and architecture on re-entrant scroll wave dynamics in human virtual ventricular tissues, in *Functional Imaging and Modeling of the Heart*, Sachse FB and Seemann G, Editor. 2007, Springer.
30. Kuo CS and Munkata K and Reddy P and Surawicz B, Characteristics and possible mechanism of ventricular arrhythmia dependent on the dispersion of action potential durations. *Circulation*, 1983. **67**: p. 1356-1367.
31. Pruvot RP and Katra EJ and Rosenbaum DS and Kaurita KR., Role of calcium cycling versus restitution in the mechanism of repolarization alternans. *Circ Res*, 2004. **94**: p. 1083–1090.
32. Shiferaw Y and Watanabe MA and Garfinkel A and Weiss JN and Karma A., Model of intracellular calcium cycling in ventricular myocytes. *Biophys J*, 2003(85): p. 3666–3686.
33. Clayton RH and Bernus O and Cherry EM and Dierckx H and Fenton FH and Mirabella L and Panfilov AV and Sachse FB and Seemann G and Zhang H., Models of cardiac tissue electrophysiology: Progress, challenges and open questions. *Progress in Biophysics and Molecular Biology*, 2010. **104**: p. 22-48.
34. LeGrice IJ and Smaill BH and Chai LZ and Edgar SG and Gavin JB and Hunter PJ, Laminar structure of the heart: ventricular myocyte arrangement and connective tissue architecture in the dog. *Am J Physiology.*, 1995. **269**: p. H571-H582.
35. Caldwell BJ and Trew ML and Sands GB and Hooks DA and LeGrice IJ and Smaill BH., Three distinct directions of intramural activation reveal nonuniform side-to-side electrical coupling of ventricular myocytes. *Circ Arrhythmia Electrophysiol*, 2009. **2**.

36. Colli Franzone P and Pavarino L and Taccardi B, Simulating patterns of excitation, repolarization and action potential duration with cardiac Bidomain and Monodomain models. *Mathematical Biosciences*, 2005. **197**: p. 35-66.
37. Jongsma HJ and Wilders R, Gap junctions in cardiovascular disease. *Circ Res*, 2000. **86**: p. 1193–1197.
38. Camelliti P and Borg TK and Kohl P., Structural and functional characterization of cardiac fibroblasts. *Cardiovasc Res*, 2005. **65**: p. 40–51.
39. Baudino TA and Carver W and Giles W and Borg TK., Cardiac fibroblasts: friend or foe? *Am J Physiol Heart Circ Physiol*, 2006. **291**: p. H1015–H1026.
40. Sun Y and Weber KT., Infarct scar: a dynamic tissue. *Cardiovasc Res*, 2000. **46**: p. 250–256.
41. Willems IE and Havenith MG and DeMey JG and Daemen MJ., The alpha-smooth muscle actin-positive cells in healing human myocardial scars. *Am J Pathol*, 1994. **145**: p. 868–875.
42. Souders CA and Bowers SL and Baudino TA., Cardiac Fibroblast: The Renaissance Cell. *Cardiovasc Res*, 2009. **105**: p. 1164-1176.
43. Kohl P., Heterogeneous cell coupling in the heart: an electrophysiological role for fibroblasts. *Circ Res*, 2003. **93**: p. 381–383.
44. Goldsmith EC and Hoffman A and Morales MO and Potts JD and Price RL and McFadden A and Rice M and Borg TK., Organization of fibroblasts in the heart. *Dev. Dyn*, 2004. **230**: p. 787–794.
45. Conrath CE and Wilders R and Coronel R and De Bakker JMT and Taggart Pand De Groot JR and Ophhof T., Intercellular coupling through gap junctions masks M cells in the human heart. *Cardiovasc. Progress in Biophysics & Molecular Biology*, 2004a. **62**: p. 407–414.
46. Kohl P and Camelliti P and Burton FL and Smith GL, Electrical coupling of fibroblasts and myocytes: relevance for cardiac propagation. *Journal of Electrocardiology* 2005. **38**: p. 45-50.
47. Petrov VS and Osipov GV and Kurths J, Fibroblasts alter spiral wave stability. *Chaos*, 2010. **20**: p. 1-8.
48. Luo CH and Rudy Y., A Model of the ventricular cardiac action potential: depolarisation, repolarisation and their Interaction. *Circulation Research*, 1991. **68**: p. 1501-1526.
49. Sachse FB and Moreno AP and Abildskov JA., Electrophysiological modeling of fibroblasts and their interaction with myocytes. *Ann.Biomed. Eng*, 2008. **36**.
50. Miragoli M and Gaudesius G and Rohr S, Electrotonic modulation of cardiac impulse conduction by myofibroblasts. *Circ Res*, 2006. **98**: p. 801–810.
51. Torrent-Guasp F and Ballester M and Buckberg GD and Carreras F and Flotats A and Carrio I and Ferreira A and Samuels LE and Narula J, Spatial orientation of the ventricular muscle band: physiologic contribution and surgical implications. *J Thorac Cardiovasc Surg*, 2001. **122**: p. 389-392.
52. Torrent-Guasp F and Buckberg GD and Clemente C and Cox JL and Coghlan HC and Gharib M, The structure and function of the helical heart and its buttress wrapping. I. The normal macroscopic structure of the heart. *Sem Thor Cardiovasc Surg*, 2001(13): p. 301–319.
53. Hassan MA and Ahmad AD Sarhan and Amano A, Effect of Muscle Active Force and Fiber Orientation on the Left Ventricle Mechanics of the Human Heart. *Proceedings of the World Congress on Engineering*, 2011.
54. Yettram AL and Vinson CA and Gibson DG, Effect of myocardial fibre architecture on the behavior of the human left ventricle in diastole. *J Biomed Eng*, 1988. **5**: p. 321-328.
55. Nash MP and Panfilov AV, Electromechanical model of excitable tissue to study reentrant cardiac arrhythmias. *Biophysics and Molecular Biology*, 2004. **85**: p. 501-522.
56. Garny A and Kohl P., Mechanical induction of arrhythmias during ventricular repolarization: modeling cellular mechanisms and their interaction in two dimensions. *Ann N Y Acad Sci.*, 2004. **1015**: p. 133-143.
57. Keldermann RH and Nash MP and Gelderblom H and Wang VY and Panfilov AV, Electromechanical wavebreak in a model of the human left ventricle. *Am J Physiol Heart Circ Physiol*, 2010. **299**: p. H134-H143.
58. Geerts L and Bovendeerd PH and Nicolay K and Arts T, Characterization of normal cardiac myofiber field in goat measured with MR-diffusion tensor imaging. *Am J Physiol Heart Circ Physiol*, 2002. **283**: p. H139-H145.
59. Boyett MR and Jewell BR, A study of the factors responsible for rate-dependent shortening of the action potential in mammalian ventricular muscle. *J Physiol*, 1978. **285**: p. 359–380.
60. Qu Z and Weiss JN and Garfinkel A, Cardiac electrical restitution properties and stability of re-entrant spiral waves: a simulation study. *Am J Physiol Heart Circ Physiol*, 1999. **276**: p. H269–H283.